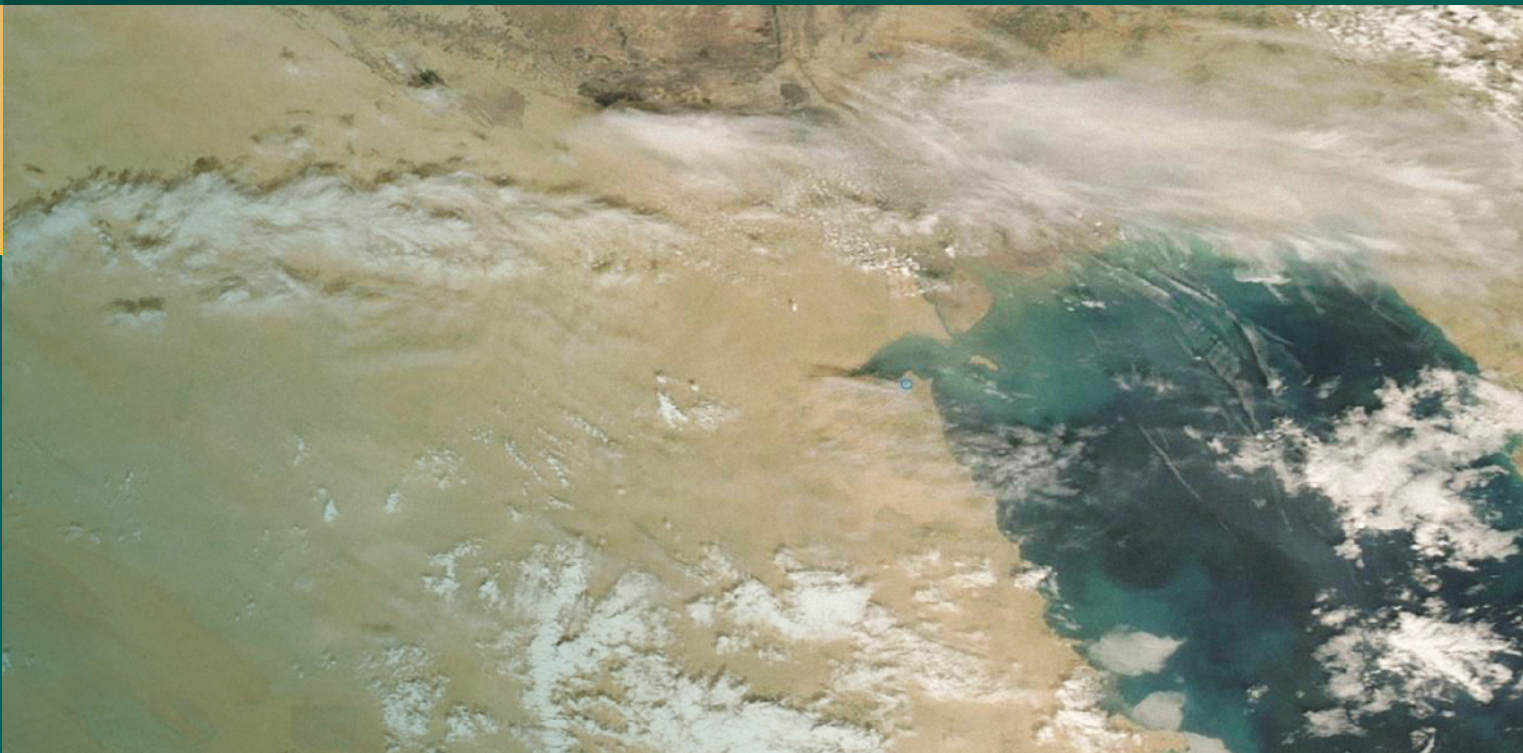


Ali Al-Dousari
Editor

Atlas of Fallen Dust in Kuwait



OPEN ACCESS

 Springer

Atlas of Fallen Dust in Kuwait

Ali Al-Dousari
Editor

Atlas of Fallen Dust in Kuwait

 Springer

Editor

Ali Al-Dousari
Environment and Life Sciences Research
Center (ELSRC)
Kuwait Institute for Scientific Research (KISR)
Kuwait City, Kuwait



ISBN 978-3-030-66976-8 ISBN 978-3-030-66977-5 (eBook)
<https://doi.org/10.1007/978-3-030-66977-5>

© The Editor(s) (if applicable) and The Author(s) 2021. This book is an open access publication.

Open Access This book is licensed under the terms of the Creative Commons Attribution 4.0 International License (<http://creativecommons.org/licenses/by/4.0/>), which permits use, sharing, adaptation, distribution and reproduction in any medium or format, as long as you give appropriate credit to the original author(s) and the source, provide a link to the Creative Commons licence and indicate if changes were made.

The images or other third party material in this book are included in the book's Creative Commons licence, unless indicated otherwise in a credit line to the material. If material is not included in the book's Creative Commons licence and your intended use is not permitted by statutory regulation or exceeds the permitted use, you will need to obtain permission directly from the copyright holder.

The use of general descriptive names, registered names, trademarks, service marks, etc. in this publication does not imply, even in the absence of a specific statement, that such names are exempt from the relevant protective laws and regulations and therefore free for general use.

The publisher, the authors and the editors are safe to assume that the advice and information in this book are believed to be true and accurate at the date of publication. Neither the publisher nor the authors or the editors give a warranty, expressed or implied, with respect to the material contained herein or for any errors or omissions that may have been made. The publisher remains neutral with regard to jurisdictional claims in published maps and institutional affiliations.

This Springer imprint is published by the registered company Springer Nature Switzerland AG
The registered company address is: Gewerbestrasse 11, 6330 Cham, Switzerland

Preface

Kuwait is located within a desert region characterized by active eolian activities. Land degradation and extended drought periods act as major activators of Sand and Dust Storms (SDS) in deserts. There are substantial levels of dust grains that may be driven thousands of kilometers from their origin. Reducing the adverse effects of eolian sand and dust in Kuwait and its surrounding regions is a challenge that requires a full understanding of dust phenomena, both chemically and physically, to improve future effective control measures. In desert regions, some environmental challenges have the potential to reduce solar energy production. These challenges are aerosols and the formation of thinly crusted carbonates and/or mud coatings on the solar panel surfaces that form from fallen dust. These challenges greatly affect wind turbines and photovoltaic panel surfaces in Kuwait. The dust has a negative effect on health, aviation, agricultural production, and the economy. Most recent studies have documented eolian SDS as environmental and economic threats in the region. On the other hand, few studies have focused on these threats as part of the ecological system in desert areas. Mobile sand and dust are a major source of native plant-seed dispersion in the region. The depositional characteristics of radionuclides ^7Be , ^{210}Pb , ^{40}K , and ^{137}Cs indicate that most of the deposited dust in dust traps is a result of re-suspension in Kuwaiti dust. The only thing that can prevent this re-suspension is the presence of dense native vegetation in the area. The environmental and economic importance of native plants and green belts in controlling mobile sand and dust hazards has been addressed by a few studies in the Middle East region. On the other hand, eolian deposits, including dust, play a significant role in the rehabilitation of degraded areas, as they act as a major healing factor because of their content of seeds and organic matter.

The benefits of mobile sand and dust are as follows:

1. They both act as a major source of native plant seeds in the region, and they are two major healing factors in the rehabilitation of degraded areas.
2. The maximum percentages of organic material reach up to 4.85% and 9% in mobile sands and dust, respectively, in Kuwait.
3. The mobile sand and dust accumulate around native plants forming a sand body (nabkha or coppice dune) around each perennial plant. These eolian accumulations are incredibly beneficial to native plants. The eolian sands act as follows:
 - a. a protective shield from sandblasting
 - b. a source of nutrients
 - c. for water storage obtained during rain and flood seasons.
4. There is a negative relationship between native plants, density, and eolian activities. The plantation of about 110,000 native plants reduces the percentages of deposited dust and mobile sand by 33.2% and 34.5%, respectively.

This atlas includes most of the information, if not all, related to dust phenomena, such as dust particle size, mineralogy, trace elements, radionuclides, physical properties (particle size and surface area), and associated pollen, organic matter, and pollutants.

Kuwait City, Kuwait

Ali Al-Dousari

Acknowledgments

The authors express their gratitude to the following entities:

1. The Kuwait Institute for Scientific Research (KISR) for partially funding Project EC063C and the following:
 - a. Project ECO41K (Dust Fallout Monitoring and Analysis in Jahra City and its Surroundings)
 - b. General Activity EC055G (Particle-Size Analysis of Seasonal Dust in Kuwait)
 - c. General Activity EC058G (Seasonal Color Spectrophotometric Variations of Dust Samples within Kuwait).
2. The Kuwait Foundation for the Advancement of Science (KFAS) for the partial funding of Project EC063C, grant number (2008-1401-01), and for funding the open access cost.

Thanks are extended also to all contributors and to Sayed Ahmed, Mamdouh Khadhayrah, Abu Nour Muhamad, and Khaleq Beg, Teena William for their help with the sample collection and analysis and to Soumya Kannappassen for editing and proofreading.

Contents

1 Dust Storm Satellite Images	1
Meshari Al-Obed, Sief Uddin, and Ashraf Ramadhan	
2 Deposited Dust	47
Ali Al-Dousari and Noor Al-Dousari	
3 Dust Particle Size and Statistical Parameters	57
Noor Al-Dousari, Modi Ahmed, Ali Al-Dousari, Musaad Al-Daihani, and Murahib Al-Elaj	
4 Mineralogy (XRD)	95
Ali Al-Dousari and Muntha Bahbahani	
5 Inductively Coupled Plasma (ICP)	121
Ali Al-Dousari, Fatin Al-Mutawaa, Hanan Al-Mansour, and Badreya Mandekar	
6 Deposited Rates of Radionuclides	141
Abdulaziz Aba, Anfal Ismaeel, Aisha Al-Boloushi, Hanadi Al-Shimary, and Omar Al-Boloushi	
7 Pollen in Dust	177
Mohamed Ismail Ibrahim, Ali Al-Dousari, and Abeer Hassan Al-Saleh	
8 Other Properties (BET Surface Area, Conductivity, Organic Matter, and pH)	199
Modi Ahmed and Khaliq Beg	
9 Spectro Absorption	207
Safaa Al-Awadhi and Mustafa Al-Shemali	
Summary	247
Index	249

About the Editor

Prof. Ali Al-Dousari Kuwait Institute for Scientific Research, Environmental and Life Science Research Center, Safat, Kuwait.

He is a professor in the Kuwait Institute for Scientific Research Center, Kuwait where he conducts scientific projects and do researches tackling Land degradation and rehabilitation Flood management, Aeolian and fluvial landforms and dust fallout, Mobile sand control measures, water harvesting techniques soil sealing and compaction. He has received many awards and recognitions for his research activities. He won encouraging prizes and awards (The Wildlife Award from the Arabian Gulf Cooperation Council; the Abdul Hameed Shoman Award for Best Arab researchers, the State Incentive Award, the Best Arab Book Award in the field of environment) and acts as Kuwait representation active member within Committee of Science and Technology (CST) in United Nation Committee for Compacting Desertification-UNCCD (2016–2019) and member in many local, regional and global scientific committees. Al-Dousari now is acting as referee and editor in many scientific journals. Al-Dousari receives his Ph.D. in geology from Royal Holloway University of London and Master degree from Kuwait University.



Dust Storm Satellite Images

1

Meshari Al-Obed, Sief Uddin, and Ashraf Ramadhan

Abstract

- DATA of Aerosol Robotic Network (Aeronet) stations and Ozone Monitoring Instrument (OMI) were obtained to get valuable and reliable information about the occurrence of dust events. In addition to Total Ozone Mapping Spectrometer (TOMS) provide informative and long dust events record.
 - To analyze the dust time series, monthly, annual and seasonal linear trends are applied to the dust time series. This is achieved by summing the total number of dusty hours for each month and then the total number of dusty days for the month is calculated.
 - Dust trend analysis includes; annual, winter, spring, summer and autumn with the rate of change.
 - Dust frequency of seasons in days/season before and after sorting in a descending manner from 1984 to 2013.
 - Satellite images use for PM_{2.5} Estimation and concentrations
 - Remote sensing-based measurements
 - Calibration of Field and Laboratory Equipment.
 - Particle concentrations in different size ranges and the total suspended particulate matter in the air in Kuwait.
 - Dust deposition rates were monitored and analyzed in Kuwait at the northern Arabian Gulf to estimate quantities of fallen dust within major eight dust trajectories in the Arabian Gulf.
 - Kuwait is surrounded by five major sources of dust rather than intermediate dust source areas that are listed.
- Satellite images from 2000 to 2010 were used to identify major dust trajectories within seven major deserts in the world.

Introduction

Dust is a common phenomenon in Kuwait. Therefore, understanding dust is a significant step toward adapting control measures in the area to minimize its adverse socioeconomic effects. Dust, traveling long distances, is commonly very fine, with the predominant sizes being between 0.068 mm and 0.02 mm (Walker and Costin 1971). Significant quantities of dust may be blown thousands of kilometers from their source (Meng and Lu 2007; Al-Dabbas et al. 2011; Awadh 2012; Al-Awadhi and Al-Dousari 2013; Al-Dousari and Al-Hazza 2013), and it has been estimated that windblown dust derived from soil erosion contributes approximately 500×10^6 tons of particulate matter to the atmosphere each year (Peterson and Junge 1971). Northwesterly winds are prevalent in Kuwait, with 18 km/h as the average wind speed (Al-Ghadban et al. 2008; Al-Dousari et al. 2017). Al-Dousari (2009) listed Kuwait as having one of the highest dust precipitation rates in the world. Safar (1980) states that the annual average number of dusty days of dust storms, or rising dust, or suspended dust in Kuwait is 255.4. Al-Dousari and Al-Awadhi (2012) identified five major sources of dust: (1) southwestern desert of Iraq; (2) the Mesopotamian Floodplain in Iraq; (3) the northeastern desert of Saudi Arabia; (4) the drained marshes (Ahwar) area in southern Iraq; and (5) sabkhas, dry marshes, and abandoned farms in Iran, especially in the northern coastal area of the Arabian Gulf (Fig. 1.1). This atlas covers the physical (particle size, particle surface area) and chemical (mineralogy, trace element percentages, and radionuclide contents) characteristics, as well as the pollen contents within

M. Al-Obed (✉)

Meteorological Unit, Kuwait National Guard, P.O. Box: 17010
72451 Khaldiya, Kuwait
e-mail: Dr.Aeolian@gmail.com

S. Uddin · A. Ramadhan

Environmental Pollution and Climate Program (EPCP),
Environment and Life Sciences Research Center (ELSRC),
Kuwait Institute for Scientific Research (KISR), P.O. Box: 24885
13109 Safat, Kuwait

© The Author(s) 2021

A. Al-Dousari (ed.), *Atlas of Fallen Dust in Kuwait*,
https://doi.org/10.1007/978-3-030-66977-5_1

1

deposited dust to identify its origin and to adapt to such common phenomena in the area, as well as to determine the distribution pattern of the dust fallout.

The dust fallout in Kuwait was monitored continuously to attain the following objectives:

- To assess the physical (morphometry of the grains) and chemical (trace elements percentages) characteristics of dust fallout to identify its origin.
- To identify the potential local sources and distribution pattern of the dust fallout in Kuwait.
- To test and environmentally evaluate many varieties of effective control measures.
- To identify the pollen distribution in dust samples.
- To establish a geographical information system (GIS) database on dust and pollen in Kuwait.

The dust fallout in Kuwait was monitored, and the monthly dust fallout data were recorded. Then, samples were analyzed to study the fallout. Maps were generated to understand the dust fallout distribution, statistical parameters, mineralogy, etc.

Data

State-of-the-art instruments such as Aerosol Robotic Network (AERONET) stations and the Ozone Monitoring Instrument (OMI) can provide valuable and reliable information about the occurrence of dust events (Al-Dousari et al. 2018a). However, such instruments do not offer lengthy records as monitoring AERONET stations and OMIs have been installed and operational only since 2000. Other

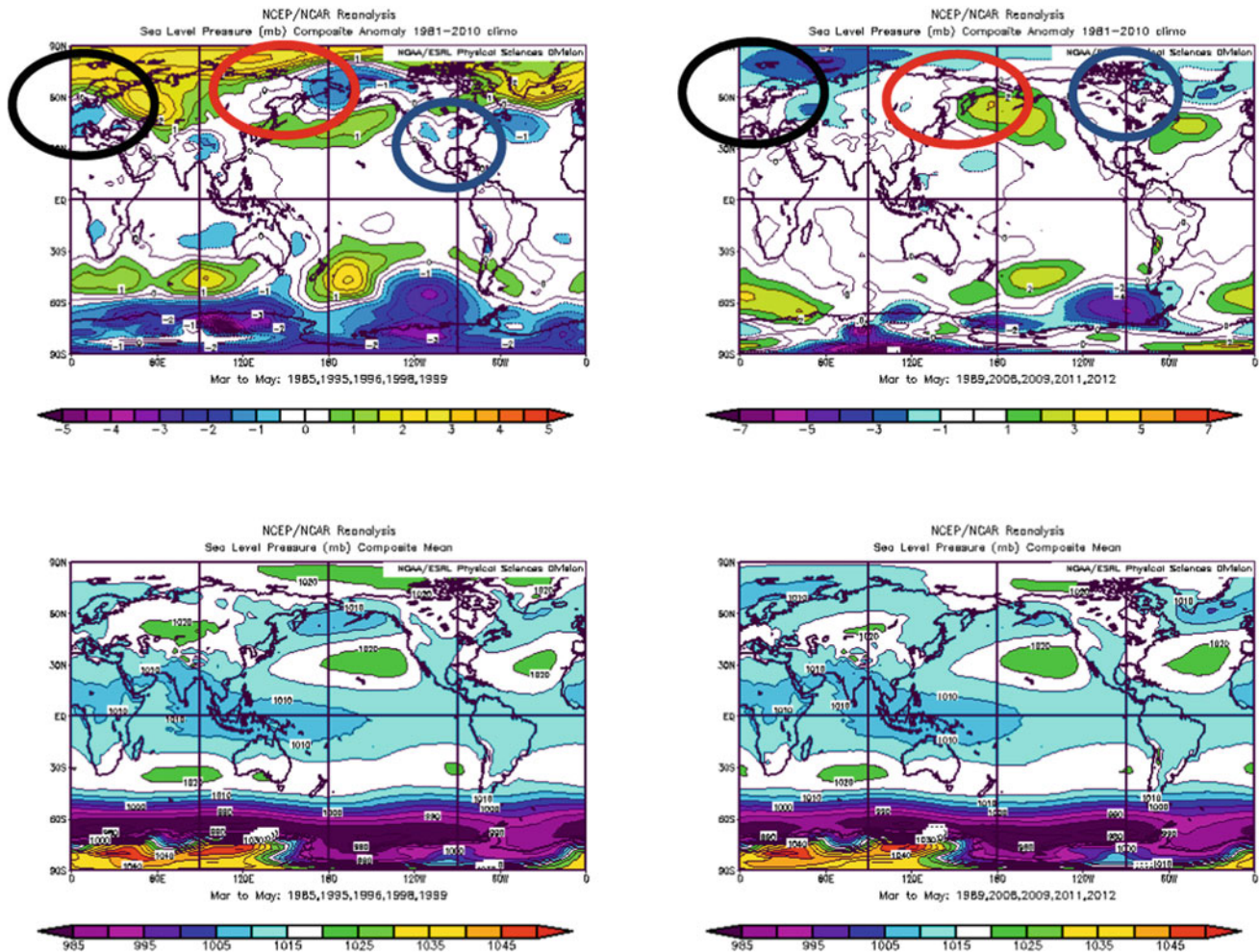


Fig. 1.1 Top left (bottom left) anomalies (mean) of sea level pressure during the minimum spring frequency; top right (bottom left) anomalies (mean) of sea level pressure during the maximum spring frequency.

The images show also the areas of Aleutian low pressure, Azores high pressure, and the western flank of the Siberian high pressure, which are encircled in red, blue, and black, respectively

Aerosol Optical Depth recorders, such as the Total Ozone Mapping Spectrometer (TOMS), provide informative and long dust-event records. Nevertheless, due to the limitations of remote sensing instruments, dust events within the planetary boundary layer cannot be easily detected (Prospero et al. 2002). In addition, the presence of cloud can obscure low-level dust detection. Therefore, 30 years of hourly climate data (recorded between 1983 and 2013) from the Kuwait International Airport weather station (WMO# 40,582 located at 29.22 N, 047.96 E) were used to determine dust-event outbreaks in Kuwait. Within the climate data, a report summarizing the daily weather is included. This summary provides additional information about the occurrence of any weather phenomena, such as dust, haze, or fog. However, most of the daily reports are missing or inaccurate, especially prior to 2004.

Therefore, in this study, dusty conditions are extrapolated from other climate variables, such as visibility, wind speed, and relative humidity (RH). Certain criteria were selected to filter out hourly dust conditions: in Kuwait, the minimum wind speed required to lift dust is between 5.5 and 6 m/s (Wilkerson 1991; Al-Dousari et al. 2018b). In this study, 7.7 m/s is the minimum threshold for wind speeds. This wind speed is the minimum threshold for initiating sandstorms (Wilkerson 1991). Furthermore, RH during dust events ranges from 5 to 45% in the summer and winter, respectively (Al-Dousari et al. 2008). While there is no specific research for this region that states at what particular visibility range dust substantially influences life patterns, the authors, who have local knowledge of the area, conclude that dust events that reduce visibility ranges to less than 4 km affect life patterns. This distance is due to the local deposition of dust in the area, which can cause severe consequences for life patterns. Thus, only hours that recorded visibility less than and equal to 4 km, RH less than and equal to 45%, and wind speeds greater than 7.7 m/s were selected for Kuwait dust storm frequency analysis.

Methodology

At least one dust event occurs every month in Kuwait. To analyze the dust time series, monthly, annual, and seasonal linear trends are applied. This approach is achieved by

summing the total number of dusty hours for each month, and then the total number of dusty days for the month is calculated. For example, if the number of dusty hours in December 1990 is 240, then $240/24 = 10$ dusty days for December. Then, the monthly, annual, and seasonal total numbers of dusty days are calculated. Subsequently, linear trends are fitted to each of the mentioned time series above to investigate any increase in Kuwait dust frequency. However, this research considers only slopes of linear trends that have 95% confidence interval and above. Boyles and Raman (2003) used the same method when analyzing climate trends in North Carolina.

After obtaining the time scales at which dust conditions have significantly changed over the period of study, the data from only significant time series were sorted in a descending manner. Subsequently, the top and bottom 15th percentile of the selected time scale were chosen. Plots of global pressure anomalies for the selected period of maximum and minimum frequency were produced, which assisted with the investigation of any possible effect caused by the change in global pressure systems on Kuwait dust frequency. For example, if dust-event frequency has significantly increased in the spring season, then the top and bottom five years for the 30-year record of spring are selected. Then, the reanalysis plots of global pressure anomalies of the same years and season are obtained from NCEP/NCAR. The reanalysis plots of the five years that experienced the highest frequency and the five years that experienced the lowest frequency are compared and carefully examined to determine whether there is a possible relationship between any of the global climate indices and the dust frequency. After that, if a potential relationship is detected in the anomaly plots, the correlation between the Kuwait dust index and the selected pressure index is investigated (Table 1.1).

Results and Discussion

As is evident in the table above, only the spring dust trend is significant for the period of study (significant at 95%). Other than that, dust frequency appears not to have changed in the past 30 years. Therefore, only the spring season data are sorted in a descending manner, and the top and bottom 15th percentiles were selected. The maximum and minimum

Table 1.1 Dust trend analysis results

Timescale	Dust trends	Significance	Rate of change
Annual	9.77	Not Significant	0.039 days/years
Winter	0.68	Not Significant	0.007 days/season
Spring	1.1	Significant at 95% Confidence Interval	0.075 days/season
Summer	0.69	Not Significant	0.0078 days/season
Autumn	1.1	Not Significant	0.075 days/season

Table 1.2 Dust frequency of the spring season in days/season before and after sorting in a descending manner

Years	Days in spring season	Years	Days in spring season
1984	2.63	2012	6.71
1985	0.38	1989	5.58
1986	0.96	2008	5.29
1987	2.67	2011	4.42
1988	2.79	2009	3.92
1989	5.58	2000	3.50
1990	1.38	2003	3.50
1991	1.25	2010	3.13
1992	1.50	1988	2.79
1993	1.50	2013	2.71
1994	2.00	1987	2.67
1995	0.29	1984	2.63
1996	0.33	2007	2.33
1997	0.96	1994	2.00
1998	0.17	2006	1.54
1999	0.92	1992	1.50
2000	3.50	1993	1.50
2001	1.08	1990	1.38
2002	1.25	2005	1.38
2003	3.50	1991	1.25
2004	1.17	2002	1.25
2005	1.38	2004	1.17
2006	1.54	2001	1.08
2007	2.33	1986	0.96
2008	5.29	1997	0.96
2009	3.92	1999	0.92
2010	3.13	1985	0.38
2011	4.42	1996	0.33
2012	6.71	1995	0.29
2013	2.71	1998	0.17

frequencies of the spring season occurred in 1989, 2008, 2009, 2011, and 2012, and 1985, 1995, 1996, 1998, and 1999, respectively, as displayed in Table 1.2. A plot of global pressure anomalies for 1989, 2008, 2009, 2011, and 2012 is shown in the bottom left (mean pressure for the same period below it), and the plot of global pressure anomalies 1985, 1995, 1996, 1998, and 1999 is shown in the bottom right (mean pressure for the same period below it).

The global pressure anomaly plots reveal that the Azores high-pressure, Siberian high-pressure, and the Aleutian and Icelandic low-pressure systems behave in the opposite mode between the years of maximum and minimum spring season dust frequencies. During the peaks, positive anomalies are observed for the Aleutian low-pressure and Azores high-pressure areas. Meanwhile, negative anomalies were

found for the western flank of the Siberian high-pressure and the Icelandic low-pressure areas. During the minimum, the anomalies of the previously mentioned systems are the opposite.

The spring dust frequency is correlated with the Azores high-pressure index, the Icelandic and Aleutian low-pressure indices, and the western flank of the Siberian high-pressure index. These correlation scores are not significant at lag (0, 1, 2, and 3) (not shown). Since the area between the latitudes of 30° and 65° N seems to be displaying different modes between the maximum and minimum spring dust frequencies, the NPI*, which covers the same area, is correlated with the dust index on different time scales. The NPI is significantly correlated (at 95% confidence interval) with dust frequency on an annual time scale, and the spring dust

frequency is significantly correlated (at 95% confidence interval) with the winter means NPI (see Table 1.3 for the correlations results).

As there is a possible influence of the NPI on Kuwait dust frequency, further investigation of this factor and regional dust frequency is needed. In addition, Trenberth and Hurrell, James and the National Center for Atmospheric Research Staff postulated that Pacific sea surface temperatures (SSTs), which govern the NPI area, are influenced by tropical SSTs. Thus, the relationship between Kuwait and regional dust frequency and the tropical SST and El Niño Southern Oscillation (ENSO) should be explored.

*As mentioned by Trenberth and Hurrell (1994), the NPI is the area-weighted sea level pressure over the region 30°N–65°N, 160°E–140°W. The NPI measures interannual to decadal variations in the atmospheric circulation. The

dominant atmosphere–ocean relation in the North Pacific is one in which atmospheric changes lead to changes in SSTs by one to two months. However, strong ties exist with events in the tropical Pacific, with changes in tropical Pacific SSTs leading SSTs in the North Pacific by three months.

(<https://climatedataguide.ucar.edu/climate-data/north-pacific-np-index-trenberth-and-hurrell-monthly-and-winter>).

Satellite Images Use for PM_{2.5} Estimation

Dust storm episodes are among the most critical weather phenomena in arid countries worldwide (Al-Awadhi 2005; Chi et al. 2008; Garrison et al. 2006). These episodes are caused by high-energy winds eroding the topsoil in regions with minimal vegetation cover. Kuwait and other countries

Table 1.3 On the left is the annual mean values of dust frequency in days and the North Pacific Index (NPI) with the correlation and t-test value; on the right is the correlation between winter mean NPI values and spring dust frequency values in days

Year	NPI annual means	Annual dust freq.	Year	NPI winter means	Spring dust freq.
1984	1011.6	20.3	1984	1007.12	2.63
1985	1014.2	13.1	1985	1008.33	0.38
1986	1010.8	11.2	1986	1001.25	0.96
1987	1010.9	17.0	1987	1003.22	2.67
1988	1011.9	11.2	1988	1006.36	2.79
1989	1014.6	23.0	1989	1011.80	5.58
1990	1013.8	7.0	1990	1010.11	1.38
1991	1012.3	6.0	1991	1007.45	1.25
1992	1011.4	5.7	1992	1004.54	1.50
1993	1012.2	5.6	1993	1008.79	1.50
1994	1013.4	9.7	1994	1008.51	2.00
1995	1011.5	3.6	1995	1004.73	0.29
1996	1012.2	1.6	1996	1005.32	0.33
1997	1011.5	9.5	1997	1005.36	0.96
1998	1011.7	0.6	1998	1003.10	0.17
1999	1013.2	4.1	1999	1008.74	0.92
2000	1012.4	12.6	2000	1008.33	3.50
2001	1011.9	4.2	2001	1004.90	1.08
2002	1012.3	4.5	2002	1008.24	1.25
2003	1011.9	11.8	2003	1003.45	3.50
2004	1011.4	6.0	2004	1003.56	1.17
2005	1012.1	9.2	2005	1007.10	1.38
2006	1013.6	8.2	2006	1007.29	1.54
2007	1011.8	7.9	2007	1007.21	2.33
2008	1013.3	22.8	2008	1008.58	5.29
2009	1014.2	16.6	2009	1013.04	3.92
2010	1011.9	9.6	2010	1003.13	3.13
2011	1013.2	18.7	2011	1010.83	4.42
2012	1013.3	18.7	2012	1007.75	6.71
2013	1013.4	11.5	2013	1008.45	2.71
	C = 0.38	2.15		C = 0.423	2.475

in the Middle East experience some of the worst dust storm episodes in the world. Kuwait is particularly susceptible to dust storms because of its low topography, scant vegetative cover, and strong, turbulent winds that occur mainly in the summer months (Al-Awadhi 2005; Ahmed and Al-Dousari 2013; Al-Awadhi et al. 2014). The rates of dust fallout in Kuwait have been reported as being among the highest in the world (Foda et al. 1985), with mean monthly concentrations as high as $1400 \mu\text{g m}^{-3}$.

It is possible to trace the origin of dust and its transport pathway from the nature of the particulate matter (PM). The frequency of dust activity can be related to long- and short-term climate changes (Prasad and Singh 2007). Climatic processes can also be affected by dust events (Boucher and Haywood 2001). Air temperatures, for example, may be altered by dust as a result of the scattering and absorption of solar radiation (Li et al. 1996; Moulin et al. 1997; Alpert et al. 1998; Miller and Tegen 1998; Goudie and Middleton 2001). Suspended dust modifies the short-wave solar radiation transmitted through to the earth and long-wave infrared radiation emitted into space (Goudie and Middleton 2001). Moreover, the size and type of aerosol have a major influence on radiation, in addition to cloud cover and surface albedo. Massive dust storms have been reported to result in the lowering of ocean temperatures, which may affect the primary productivity of seas and oceans (Pierson et al. 2003) and impact carbon dioxide sequestration (Ridgwell 2002). This study utilized satellite data to estimate atmospheric aerosol, especially $\text{PM}_{2.5}$, which has been reported to have a significant effect on human health (Dockery et al. 1993; Pope and Dockery 2006; Pope et al. 2002) and on the regional and global climatic changes (Hansen et al. 1998; Hurtado et al. 1996; Ramanathan et al. 2007; Hu et al. 2010). Several reports have indicated that dust serves as a vehicle for the long-range transport of associated contaminants, including viruses (Griffin 2007; Reynolds and Pepper 2000; Williamson et al. 2003; Yates and Yates 1988), pathogens (Garrison et al. 2006; Griffin 2007; Griffin et al. 2002), trace metals (Di-Lella et al. 2006), and organic pollutants (Di-Lella et al. 2006; Gevaio et al. 2011).

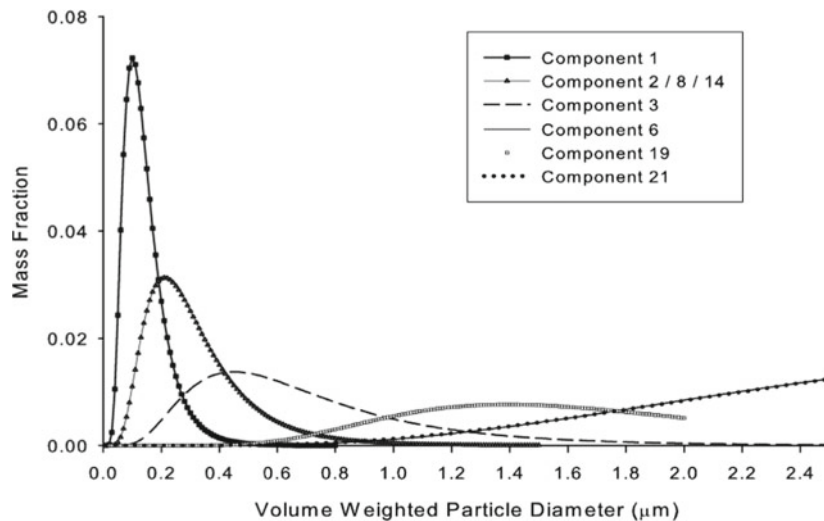
Remote Sensing-Based Measurements

Remote sensing measurements, by virtue of their synoptic monitoring capabilities, can be used to quantify dust on a large spatiotemporal scale. Currently, the Multiangle Imaging Spectro Radio Meter (MISR), which can determine AERONET's observations in desert regions (AOD) over land and ocean surfaces through observing visible and infrared wavelengths (King et al. 1992, 1999; Kaufman et al. 1997; Diner et al. 1998, 2002; Kahn et al. 1998, 2005a, b; Liu et al. 2004, 2005, 2007, 2009; Hu et al. 2010), was used. Images over

Kuwait and adjacent areas were procured from the National Aeronautics and Space Administration (NASA). The relationship between MISR AOD and surface $\text{PM}_{2.5}$ was established. The $\text{PM}_{2.5}$ data were correlated using in situ measurements at two calibration sites: one in Abdalli and the other at the KISR Shuwaikh. A high degree of correlation was observed between the MISR AOD and the $\text{PM}_{2.5}$ estimates. However, the relationship is empirical due to the complicated dependence on multiple factors, including aerosol chemistry, particulate size distribution, aerosol profile, and, most importantly, the atmospheric conditions. The Moderate Resolution Imaging Spectroradiometer (MODIS) has fewer and poorer retrievals over Kuwait because of high surface albedo. However, with the Collection 6 data, the problem was solved, and now MODIS is a more useful sensor for PM retrieval. The satellite-based measurements used AOD as a quantitative measure of PM abundance in the atmospheric column. AOD is dominated by near-surface emission sources and can be used to track long-range dust transport pathways caused by a storm event (Seinfeld and Pandis 1998). AOD retrieved at visible wavelengths is sensitive to $0.1\text{--}2 \mu\text{m}$ particle sizes (Kahn and Braverman 1998) and is not affected by gaseous co-pollutants, providing a noisy measurement of fine PM loading over large spatial areas.

The methodology proposed by Liu et al. (2004) for PM estimation using MISR data was used. The method demonstrates the validity of the MISR AOT with standard ground-level aerosol optical thickness (AOT) measurement from the AERONET. The sensitivity of the MISR AOT measurements from 0.05 to $2.0 \mu\text{m}$ has also been reported (Kahn et al. 2001; Liu et al. 2005; Hu et al. 2010). Field validation of the $\text{PM}_{2.5}$ retrievals from the satellite datasets was carried out at Abdalli and KISR's Shuwaikh campus on a weekly basis over the past 36 months. The samples were collected using a high-volume air sampler (HVAS) fitted with a six-stage cascade impactor. The metrological parameters, such as mixing height, RH, air temperature, and wind speed, which could affect $\text{PM}_{2.5}$ retrievals using AOD, were also accounted for. The rapid update cycle (RUC) model of the Earth System Research (ERS) group was used to integrate the various metrological data sources.

The MISR's aerosol retrieval algorithms do not depend on explicit radiometric surface properties (Martonchik et al. 2004, 16,102—pp. 1–4, American Geophysical Union). Therefore, the MISR can retrieve aerosol properties over a variety of terrain conditions, including highly reflective surfaces such as found in Kuwait. Observing continuously at nine distinct zenith angles and in four narrow spectral bands centered at 446, 558, 672, and 866 nm The MISR repeats its measurements every 16 days in a tropical region. Version 22 MISR aerosol data were used, which have a spatial resolution of 17.6 km. "In this dataset, there are 74 different aerosol mixtures that are constructed from up to three of the eight



Note that Components 8 and 14 have the same mass distributions by size as Component 2, and the distributions of Components 6 and 21 are nearly identical in the plotted size range (Fig. 1.2).

Fig. 1.2 Mass size distribution for the MISR aerosol components (source <https://edg.larc.nasa.gov/>)

pre-defined aerosol components (i.e., Components 1, 2, 3, 6, 8, 14, 19, and 21)” (Liu et al. 2009, IEEE, p. 177) (Fig. 1.2).

Each MISR aerosol component is defined by size distribution, shape, and single scattering albedo, of which two (Components 19 and 21) are designed for dust particles. “A detailed discussion of MISR data structure, the aerosol components used to construct the aerosol models and the percentage contribution of each component to total AOD as given elsewhere” (Liu et al. 2009, IEEE, 177). The MISR aerosol data covering Kuwait and the surrounding areas from 2008 to 2014 were processed. The data were downloaded from the NASA Langley Research Center (LARC) Atmospheric Sciences Data Center.

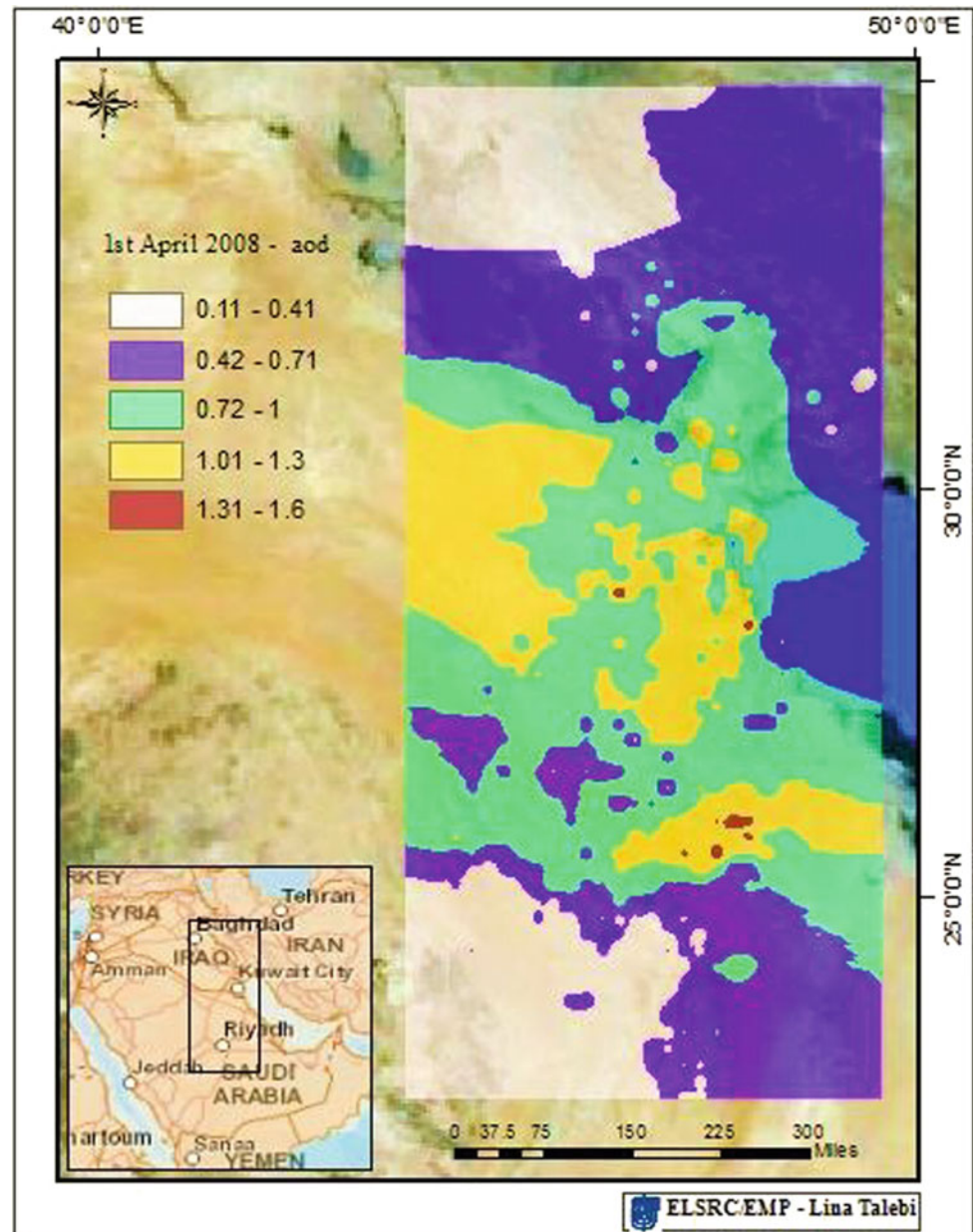
MISR AOD Validation in the Gulf Region. It has been demonstrated that MISR AOD compares well with AERONET’s observations in desert regions (Martonchik et al. 2004). We conducted a more comprehensive validation of MISR AOD in the region. The following AERONET sites (Abu Al Bukhoosh, Bahrain, Abu Dhabi, Dhadnah, Hamim, Kuwait University, Mezaira, Mussafa, Solar Village) were identified in the study region with at least one year of operation time. These AERONET data were downloaded from the NASA Goddard Space Flight Center (<https://aeronet.gsfc.nasa.gov/>). MISR AOD maps were generated for the area (Figs. 1.3 and 1.4).

Sampling and Particulate Quantification

The sampling campaign was initiated in April 2012. Size-segregated aerosol samples were collected using a six-stage high-volume cascade impactor (Tisch Environmental, Inc) on the premises of the KISR (29° 20.227 N; 47° 54.208 E) and Abdalli (30° 02.312 N; 47° 49.589E). The sampler was located about 2 m above the ground. Over each 24 h sampling period, approximately $815 \pm 5 \text{ m}^3$ of air was drawn through the cascade impactor at a constant flow rate of $0.855 \text{ m}^3/\text{min}$ to trap various aerodynamic particles on different filters. The particles were separated into the aerodynamic diameter (D_p) size ranges, such as the following: < 0.39 (backup high-volume filter), 0.39 to 0.69 , 0.69 to 1.3 , 1.3 to 2.1 , 2.1 to 4.2 , 4.2 to 10.2 , and $>10.2 \text{ }\mu\text{m}$. In addition to the weekly sampling, the samples were also collected on all dusty days to capture the spatiotemporal variations in the PM concentrations.

In addition to the in situ HVAS sampling, a noninvasive infrared (IR)-based measurement was conducted for both the particulate count and the particulate mass determination using a Metone AEROCET 531 particle mass profiler and counter, which takes hourly measurements and logs the data in the built-in data logger.

Fig. 1.3 AOD map for the study area corresponding to 01 April 2008



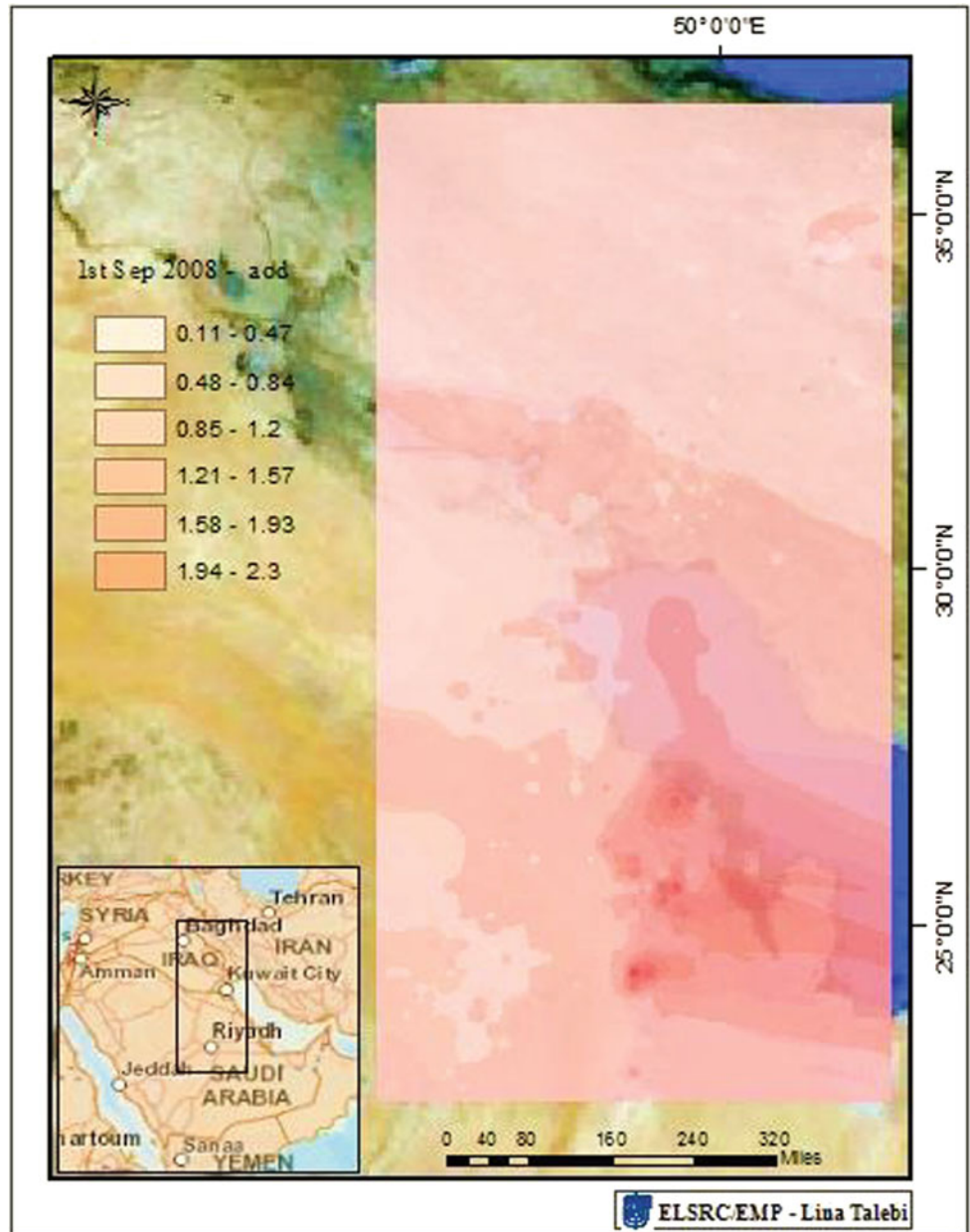
Calibration of Field and Laboratory Equipment

Air volumes for each sample collected were determined using a flowmeter with a flow tantalizer, in addition to a Magnehelic gauge (Tisch Environmental, Inc.). Calibrations were done in accordance with the manufacturer's guidelines. The calibrations were performed upon the installation of the sampler, and at least once every quarter.

Model Development for PM_{2.5} Estimation

Given the scarcity of ground-level PM_{2.5} measurements in the study region, a technique that can estimate regional PM_{2.5} concentrations without ground data support becomes an important tool. The MISR has eight aerosol components that are indicative of different contributions to ground-level PM_{2.5} concentrations: total MISR column AOD was

Fig. 1.4 AOD map for the study area corresponding to 01 September 2008



deconstructed into species-related fractions using the AOD value associated with, and the three aerosol components defined by, each of the 74 aerosol mixtures (Eq. 1.1). The fractional AOD of an MISR aerosol component is defined as the average contribution of this component to total AOD. For example, if the MISR does not observe the presence of any dust particles in a 17.6-km pixel, the fractional AODs for dust components (i.e., 19 and 21) would be zero. By definition, the sum of all the significant fractional AODs is equal to the total column AOD.

$$\text{Fractional AOD}_{i(i=1,8)} = \frac{\sum_{j=1}^{74} \text{AOD}_{\text{mixture}_j} \times \text{Fraction}_{\text{component } i \text{ in mixture }_j}}{\text{No. of Successful Mixtures}} \quad (1.1)$$

Then, the simulated AOD and $\text{PM}_{2.5}$ concentrations from the GEOS-Chem model were used to define a physically consistent relationship between AOD and surface level $\text{PM}_{2.5}$ concentrations (Eq. 1.2). GC surface $[\text{PM}_{2.5}]$ in Eq. 1.2 refers to the sum of GEOS-Chem fine particle species concentrations within 1 km from the surface, and GC

column dust AOD refers to the sum of GEOS-Chem total AOD in all 35 layers. A similar analysis for dust particles was performed.

$$\begin{aligned} [\text{PM}_{2.5}] &= \frac{\text{GC Surface} [\text{PM}_{2.5}]}{\text{GC Column AOD}} \times \text{MISR AOD} \\ [\text{Dust}] &= \frac{\text{GC Surface} [\text{Dust}]}{\text{GC Column Dust AOD}} \times \text{MISR dust AOD} \end{aligned} \quad (1.2)$$

This technique has been demonstrated previously using the early-version MISR and GEOS-Chem data in the United States (US) (Liu et al. 2004) and was successfully utilized in this present study. The annual MISR $\text{PM}_{2.5}$ concentrations exhibited an improved agreement with the ground measurements regarding the spatial pattern when compared with simulated $\text{PM}_{2.5}$ concentrations. The annual average MISR $\text{PM}_{2.5}$ concentrations had a good linear relationship with ground measurements ($r = 0.69$, linear regression slope = 0.87), and the estimated intercept was insignificant ($p = 0.81$).

High-resolution spatial statistical models were developed using ground $\text{PM}_{2.5}$ measurements from the two sites in the study region and Collection 6 MODIS 10-km AOD data. Given the limited ground data support (one site in Abdalli, KISR, and Wafra each), a linear mixed effects model was developed similar to, but more advanced. This random intercept, random slope model is expressed as follows:

$$\begin{aligned} [\text{PM}_{2.5}]_{i,j} &= (\alpha + u_j) + (\beta_1 + v_j) \\ &\quad \times \text{MODIS AOD}_{i,j} + (\beta_2 + \omega_j) \\ &\quad \times \text{MODIS AOD}_{i,j-1} + \varepsilon_{i,j} \end{aligned} \quad (1.3)$$

where $[\text{PM}_{2.5}]_{i,j}$ is the daily $\text{PM}_{2.5}$ concentration at monitoring site i on day j ; $\text{MODIS AOD}_{i,j}$ is the average of Collection 6 Terra and Aqua MODIS AOD in the 10 km 10 km grid cell corresponding to monitoring site i on day j ; α and u_j are the fixed and random intercepts, respectively; β_1 and v_j are the fixed and random slopes on same day AOD, respectively; β_2 and ω_j are the fixed and random slopes on previous day AOD, respectively; $\varepsilon_{i,j} \sim N(0, \sigma^2)$ is the error term at site i and on day j . In this statistical model, the AOD fixed effect represents the average effect of AOD on $\text{PM}_{2.5}$ for all study days. The AOD random effects explain the daily variability in the $\text{PM}_{2.5}$ -AOD relationship. Given the limited number of monitoring sites, a random intercept was not included for the site.

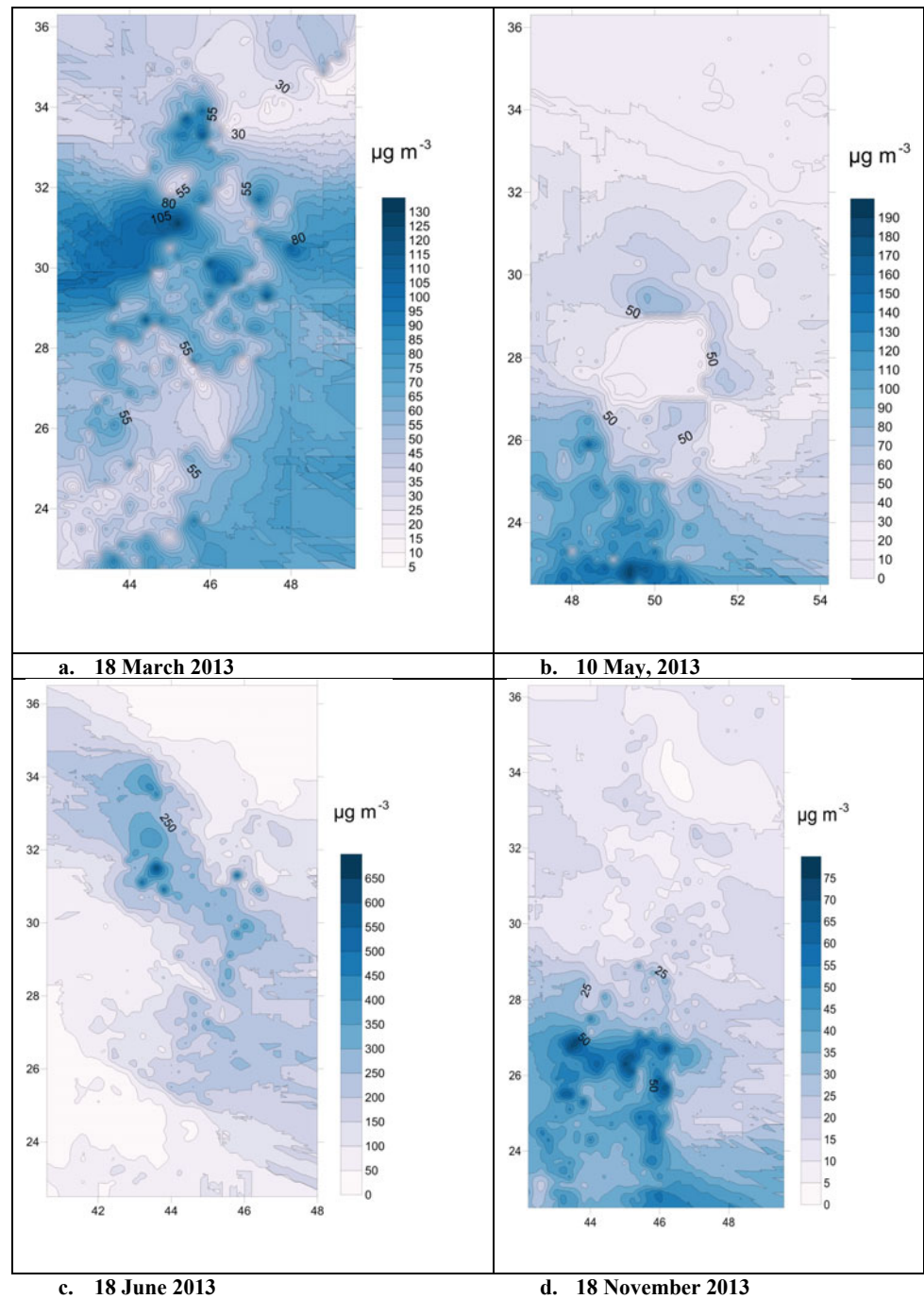
Since no previous studies have been conducted on desert regions, another statistical model format was explored. A generalized additive model (Liu et al. 2009) was tried also (Eq. 1.4):

$$\text{PM}_{2.5} = N \left(\begin{aligned} &\mu + f_{\text{AOD}}(\text{AOD}) + f_{\text{AOD}_2}(\text{AOD}_{\text{lag}}) + f_{\text{RH}}(\text{RH}) + f_{\text{TEMP}}(\text{TEMP}) \\ &+ \beta_1 \times \text{precip} + \beta_2 \times \text{precip}_{\text{lag}} + \beta_3 \times \text{weekend} \end{aligned} \right) \quad (1.4)$$

where all the covariates on the right-hand side of Eq. (1.3) are averaged spatially and, therefore, only vary with time; μ is the model intercept; $f_{\text{AOD}}(\text{AOD})$ is the smooth regression term describing the association between AOD and $\text{PM}_{2.5}$; $f_{\text{AOD}_2}(\text{AOD}_{\text{lag}})$ is the smooth regression term describing the association between mean AOD of the previous two days and $\text{PM}_{2.5}$; $f_{\text{RH}}(\text{RH})$ and $f_{\text{TEMP}}(\text{TEMP})$ are smooth regression terms describing the impact of domain-averaged RH and surface air temperature (TEMP) on the AOD- $\text{PM}_{2.5}$ association, respectively. The inclusion of the lag AOD term reflects the fact that urban aerosol has a general lifetime of a few days without major scavenging events. Precipitation on a given day (precip) and precipitation on the previous day (precip_lag) are both modeled as a binary variable (0 = no rain, 1 = rain). The weekend effect is reflected here as a binary variable (weekend = 1 if Friday and Saturday, = 0 otherwise).

The $\text{PM}_{2.5}$ concentrations were estimated using the models developed (Fig. 1.5), which indicated a high correlation with the point measurements. The total suspended PM in each size fraction measured at the sampling site at the KISR between April and October 2012 are displayed in Fig. 1.6, whereas the time series plot of the total suspended particulate matter (TSP) over the same period is expressed in Fig. 1.7. A summary of the particle-size distribution for the entire study period, expressed as the average particle concentration in each size range, is in Fig. 1.8. The mean (and range) in TSP concentrations for the entire study period was 1400 (140–8500) $\mu\text{g}/\text{m}^3$. If the concentrations measured on the 6th of March are excluded, as this sample was collected during a major dust storm episode in Kuwait, the mean (and range) in TSP that is typical for this site would be 1040 (140–2750) $\mu\text{g}/\text{m}^3$. The TSP concentrations in this study were higher than those reported in Chicago (27.7 $\mu\text{g}/\text{m}^3$) and Lake Michigan in the USA (Offenberg and Baker 1999); Mumbai (119–216 $\mu\text{g}/\text{m}^3$), (Venkataraman et al. 1999); rural Taiwan (182–238 $\mu\text{g}/\text{m}^3$) (Wu et al. 2006); Thessaloniki in Greece (243 $\mu\text{g}/\text{m}^3$) (Chrysikou et al. 2009); and in Hamilton, Ontario Canada (58–121 $\mu\text{g}/\text{m}^3$) (Katz and Chan 1980). These high TSP values measured in Kuwait may be due, in part, to the fact that Kuwait is a desert country where high-energy winds often result in localized or regional dust storms. The rates of dust fallout in Kuwait have been reported as one of the highest in the world (Foda et al. 1985). The particle-size distribution was bimodal, with the major peak located in the $<0.63\text{-}\mu\text{m}$ fraction, constituting about 85% (range 44–94%) of the PM in the air. Another small but distinct peak occurred in the particle-size fraction $>10\text{ }\mu\text{m}$. Particles smaller than $3.0\text{ }\mu\text{m}$ are easily transported through the respiratory tract into the bronchioles and alveoli of the lungs and are, thus, a human health risk.

Fig. 1.5 PM_{2.5} concentrations using satellite datasets



One of the most important indicators of air quality in most industrialized countries in the world, according to the World Health Organization (WHO), is the concentration of PM in the air (WHO 2005). These standards, however, often ignore the concentrations of toxic compounds, such as polycyclic aromatic hydrocarbons (PAHs), trace metals, and other contaminants, some of which are carcinogens, that are associated with these particles. This ignoring may be due to inadequate information on the concentrations of the

associated contaminants that are required for risk assessments. Several studies have found that an inverse relationship exists between particle size and pollutant concentration (Lewis et al. 1999). The inhalable ($<10 \mu\text{m}$) and respirable ($<2.5 \mu\text{m}$) fractions of PM, which remain suspended in the air the longest, are thought to be the most essential fractions associated with respiratory illnesses. Many studies have linked long-term exposure to PM with adverse health effects, such as cardiovascular disease, chronic respiratory illnesses,

Fig. 1.6 Atmospheric concentrations of particles in different impactor size range in the air at the KISR in Kuwait City between April and August 2012

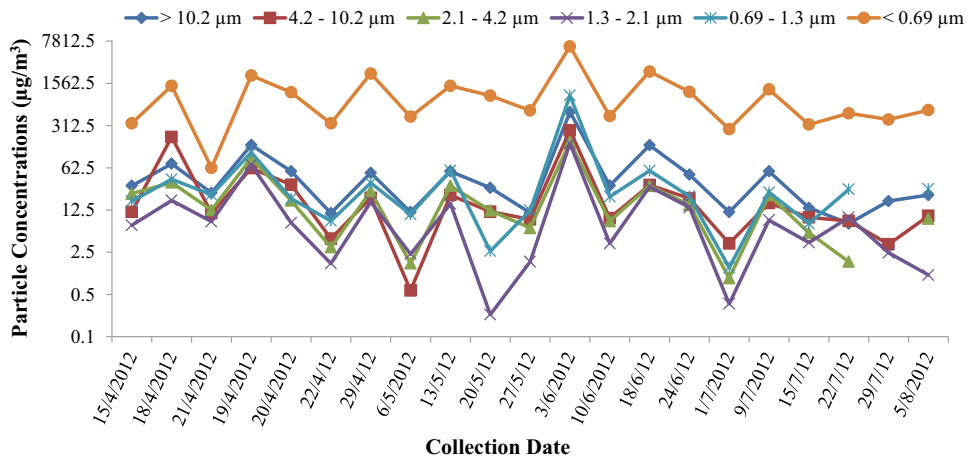


Fig. 1.7 Total suspended particle concentrations in different impactor size ranges in the air at the KISR in Kuwait City between April and August 2012

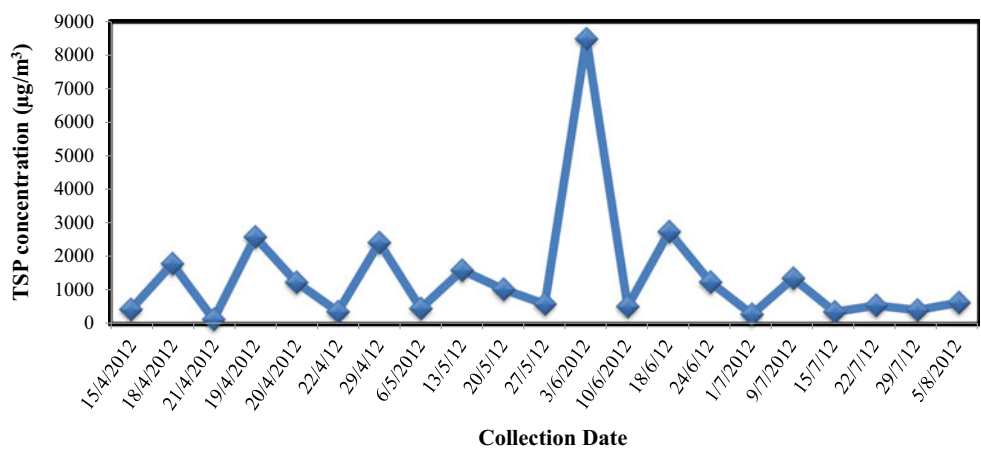
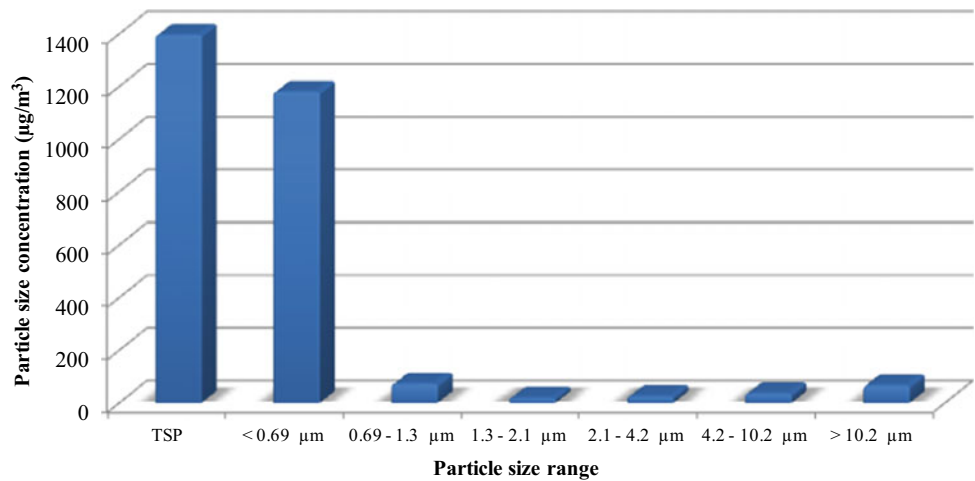


Fig. 1.8 Average particle concentrations in different size ranges and the TSP matter in the air at the KISR in Kuwait City between April and August 2012



and cancer. To comprehend better the risks posed by particle inhalation, it is important to understand the distribution of pollutants in various size fractions.

This study developed a basic model framework and setup that can be populated by continuous data collection using both an HVAS and an AEROCET particle counter. The

accuracy of the MISR revealed a systematic underestimate, which, using additional data, can be integrated into the model. The calibration of Collection 6 for MODIS also provides an additional opportunity to use MODIS as a reliable satellite for PM estimation. The PM_{2.5} concentrations from the satellite images correlated well with the measured

data, both from the IR mass and particle counter and the HVAS. The accuracy of the MISR determination was close to 68 and 62% for MODIS. There is currently a systematic underestimation of PM using both the MISR and the MODIS data, possibly due to very high backscatter. Nevertheless, these sensors provide a very reasonable estimate of PM_{2.5} concentrations on a large spatiotemporal scale.

Dust Storm Trajectories

Dust deposition rates were monitored and analyzed in Kuwait in the northern Arabian Gulf to estimate quantities of fallen dust within major dust trajectories in the Gulf. Eight major dust storm trajectories around the Gulf were detected using satellite images (2000–2010) and weather data. The Arabian Gulf receives about 120 tons.km² annually of fallen dust. The amount of fallen dust from these major trajectories into the Gulf is estimated at 30 million tons. yr⁻¹, by water volume. There are 4886 tons in each cubic kilometer. In comparison with other seas and oceans, the amount of dust

deposited in the Gulf in reference to water body volume is the highest. The particle-size distribution of coastal dust is trimodal, with a dominance of coarse silt (19%), medium silt (18%), fine silt (16%), and clay (21%), with a minor amount of very coarse silt (9%), very fine silt (6%), and sand (11%). Mineralogically, the dust is composed mainly of carbonates (41%) and quartz (29%), with an appreciable amount of feldspars (11%). The mineralogical composition and particle surface area illustrate slight physical and mineralogical variations between dust fallout samples in the Arabian Gulf (Fig. 1.9).

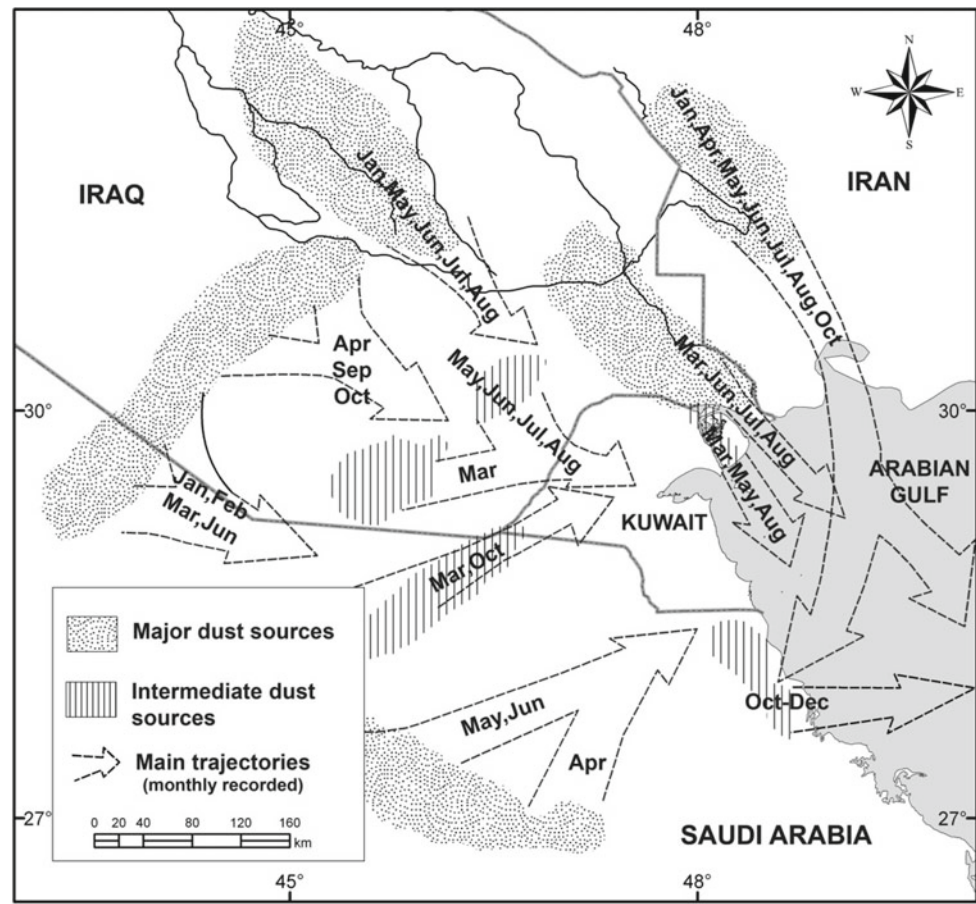
Dust Storms

Kuwait is surrounded by major, rather than intermediate, dust source areas. In this study, these regional sources of dust were identified, and satellite-derived data were used to identify temporal and spatial variations in their emission intensities. These five major sources of dust are



Fig. 1.9 Directions and timing of major dust trajectories with sampling sites in the Arabian Gulf

Fig. 1.10 Major and intermediate source areas of dust storms and trajectories for the northwestern areas of the Arabian Gulf, including the study area in reference to dust storm days in Kuwait and satellite images from 2000 to 2010



1. Southwestern desert of Iraq;
2. The Mesopotamian Floodplain in Iraq;
3. Northeastern desert of Saudi Arabia;
4. Drained marshes (Ahwar) area in southern Iraq;
5. Sabkhas, dry marshes, and abandoned farms in Iran at the northern coastal area of Arabian Gulf .

Furthermore, four intermediate sources of dust storm trajectories (covering areas of less than 3000 km²) were identified as follows:

1. Bubiyan and Warba islands (sabkhas) in Kuwait;
2. The drainage systems in the tri-border area between Kuwait, Saudi Arabia, and Iraq;
3. The playas and drainage basins in the southwestern desert of Iraq close to Kuwait;
4. The coastal sabkha in Saudi Arabia, near southern Kuwaiti borders.

Dust Zone Areas

Satellite images from 2000 to 2010 were used to identify major dust trajectories in seven major deserts worldwide. The fallen dust from these trajectories was collected and analyzed. Fallen dust rates tend to be lower downwind. The average samples of the world's fallen dust are negatively skewed, trimodal, and with a dominance of silt size fractions (61%). Most of the fallen dust within major dust trajectories is fining downwind. The fallen dust from the eastern zones (Taklimakan, Gobi, and Australian deserts) are characterized by higher percentages of feldspars and clay minerals, and low carbonate content and grain surface area in comparison with the western zones (Sahara and Arabian deserts). The Western Sahara Desert dust has the highest depositional rates and average quartz percentage (66%). The dust samples in this zone contain low carbonates and grain surface area

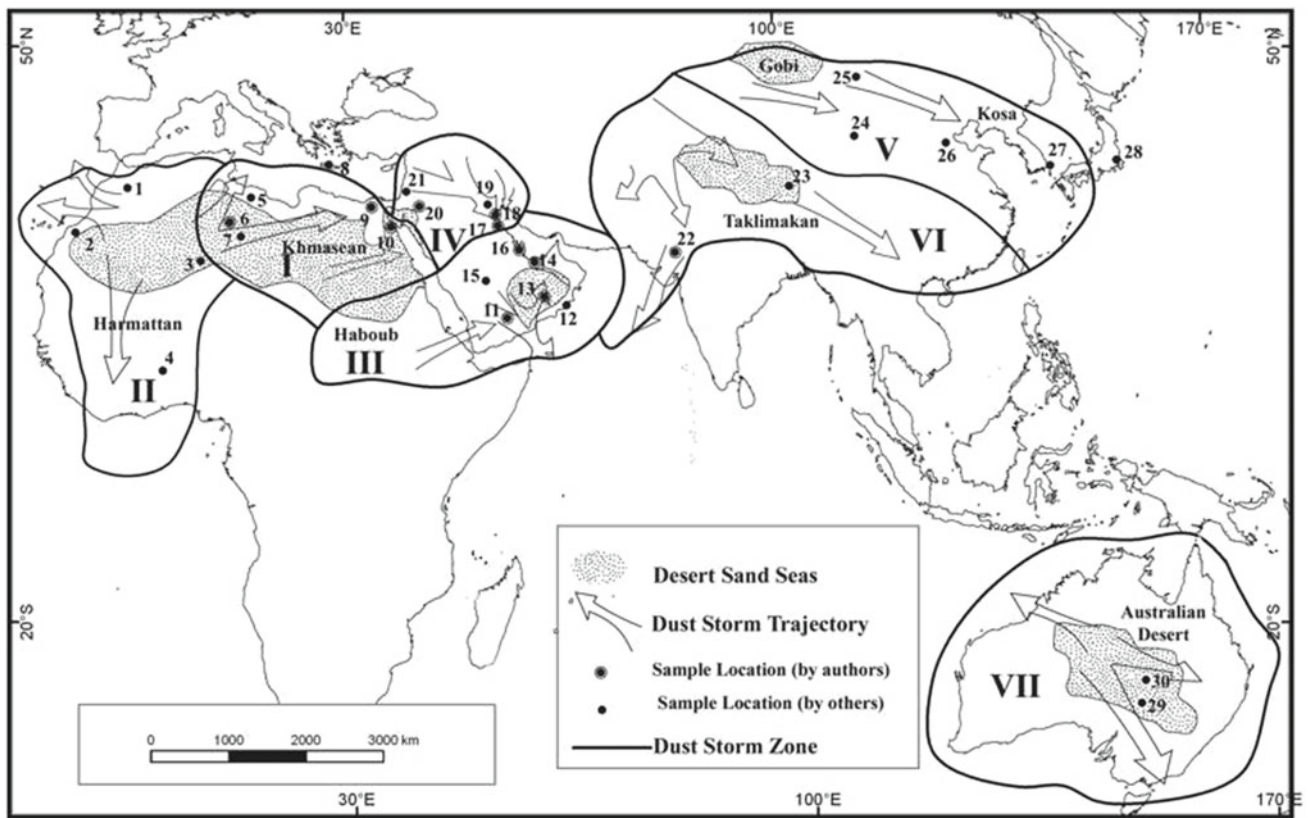


Fig. 1.11 Major dust storm trajectories within the seven zones, showing the desert sand seas, major dust trajectories, and sample locations. (1: Sous Masa, 2: Biougra, 3: Diarmena, 4: Bawku, 5: Tripoli, 6 & 7 south Tripoli, 8: Crete, 9: Cairo, 10: Hurghada, 11: Wadi

Dawasir, 12: Fahal, 13: Ain, 14: Dubai, 15: Riyadh, 16: Manama, 17 and 18: Kuwait, 19: Um Qasr, 20: Amman, 21: Dead Sea, 22: Lahore, 23: Taklimakan, 24: Ejin, 25: Shapotou, 26: Beijing, 27: Andong, 28: Tokyo, 29 and 30: Bald Hill)

when compared with dust from the Eastern Sahara Desert. The dust samples within the Northern Arabia and the Ethiopian-South Arabia zones contain the highest average amounts of carbonate and grain surface area (Fig. 1.11).

Satellite Images

An exotic occasion of the coalition of two dust storms to form a bidirectional dust storm, one blowing from northern Arabia and the Western Desert of Iraq toward Kuwait, and the second from the southern Mesopotamian Floodplain toward the Arabian Gulf on the 11th of February 2009. These types of dust storm trajectories take a wider form, with the area covered by the storm being more than 3000 km². The northwestern dust storm has large trajectories that normally blow in January, February, March, April, June, September, and October. Furthermore, moderate dust storm trajectories that cover an area less than 3000 km² are familiar in March, May, June, July, and August. In the northwesterly trajectories, fallen dust is brighter in color,

coarser in size fraction, with more sand particles (diameter ranges between 0.063 and 2 mm), contains more quartz and feldspars, but has fewer carbonates and clay minerals, lower particle surface area, and less iron and organic matter in comparison with trajectories from the Iranian side and the Mesopotamian Floodplain. On the other hand, dust from the northern and northeastern trajectories is finer, darker in color, contains less quartz and feldspars, is higher content in carbonates, heavy and clay minerals, is lower in surface area, and provides more organic matter compared with other trajectories around Kuwait. These dust storm trajectories normally occur in January, April, May, June, July, August, and, rarely, in February. The following weather data were recorded for 11th February 2009 (Fig. 1.12):

- Heavy cloud covers obscured the area of concern.
- The prevailing wind direction: northwest, west-northwest, west.
- The northwest, west-northwest, and west wind directions represent 21.4%, 41.7%, and 22.4%, respectively, of the total hourly wind count for that day.

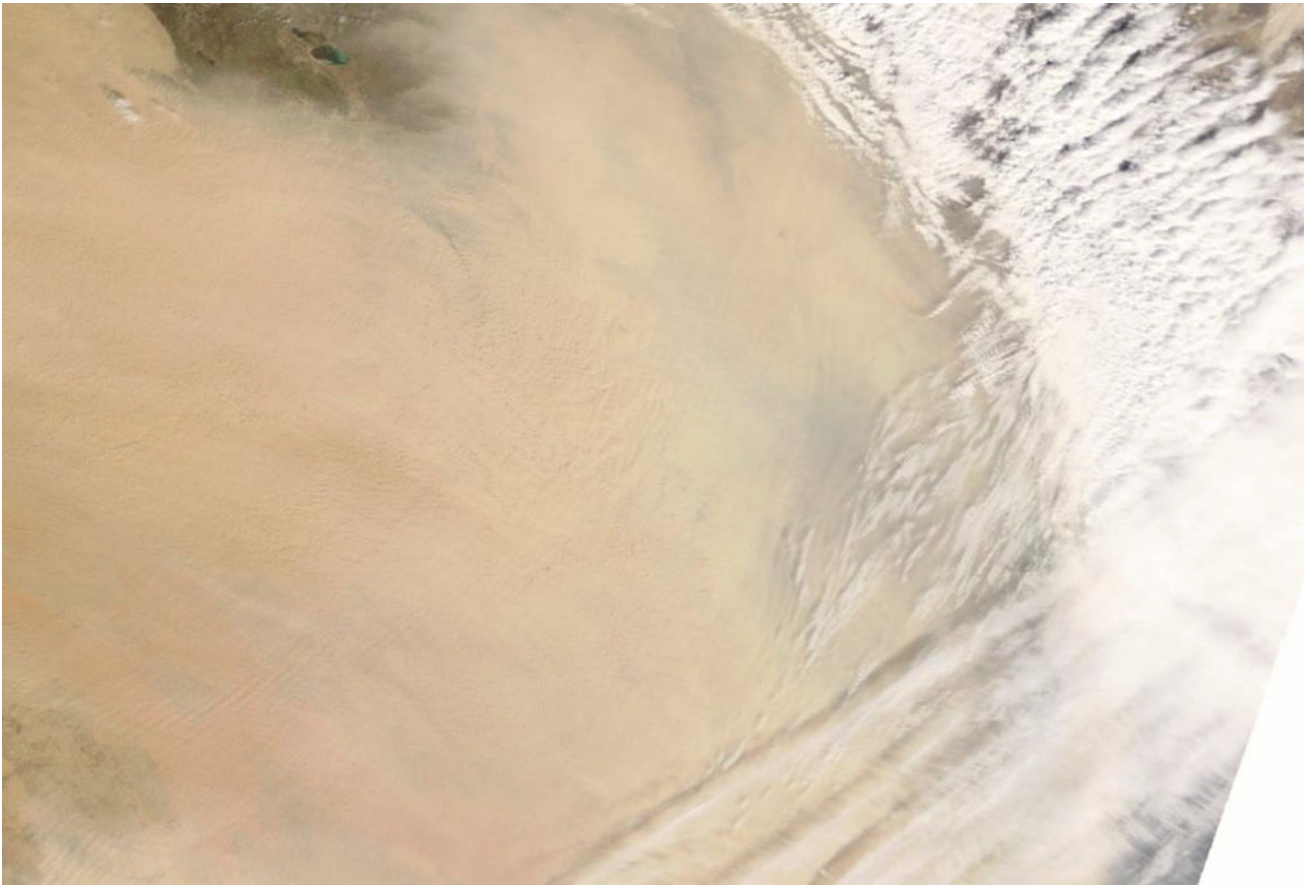


Fig. 1.12 MODIS image of dust storm that originated from the Western Desert of Iraq, covering southern Iraq, Kuwait, and northern Arabian Gulf on 11th February 2009

Satellite Images

The southeast, east-southeast, and east wind directions unidirectional dust storm blowing toward northeastern Arabia, including Kuwait and the northern Arabian Gulf on the 17th February 2009 from intermediate dust sources. This type of dust storm trajectory has moderate wind speed and forms in source areas with a short distance, is covered by a trajectory that is less than 3000 km² in size, and the level of suspended dust particles is not as dense as in storms from the Arabian deserts. This type of dust storm trajectory normally blows in March, April, May, June, and October. The fallen dust from this type of trajectory is deposited more quickly than normal as it contains more quartz and feldspars but fewer carbonates and clay minerals, has a lower particle surface area, and lower iron and organic matter content that is brighter and coarser in size fraction, and sand particles are more than in trajectories from the Mesopotamian Floodplain. The following weather data were recorded for 17th February 2009 (Fig. 1.13):

- Heavy cloud cover obscured the area of concern.
- Prevailing wind direction: southeast, east-southeast, east, with a strong northwest component.
- The southeast, east-southeast, east wind directions represent 15.6%, 13.5%, and 12.0%, respectively, of the total hourly wind count for that day. The northwest component represented 16.7%.

Satellite Images

Tridirectional dust storm: northwest, west-northwest, and west wind directions toward Kuwait from Western Desert of Iraq on 28th February 2009 toward the Arabian Gulf. This type of storm takes the broad form of dust storm trajectories in which the area covered is more than 3000 km². This form is also associated with storm clouds. The northwest, northwest-west, and west dust storm large trajectories normally blow in January, February, March, April, June, September, and October. Furthermore, intermediate dust

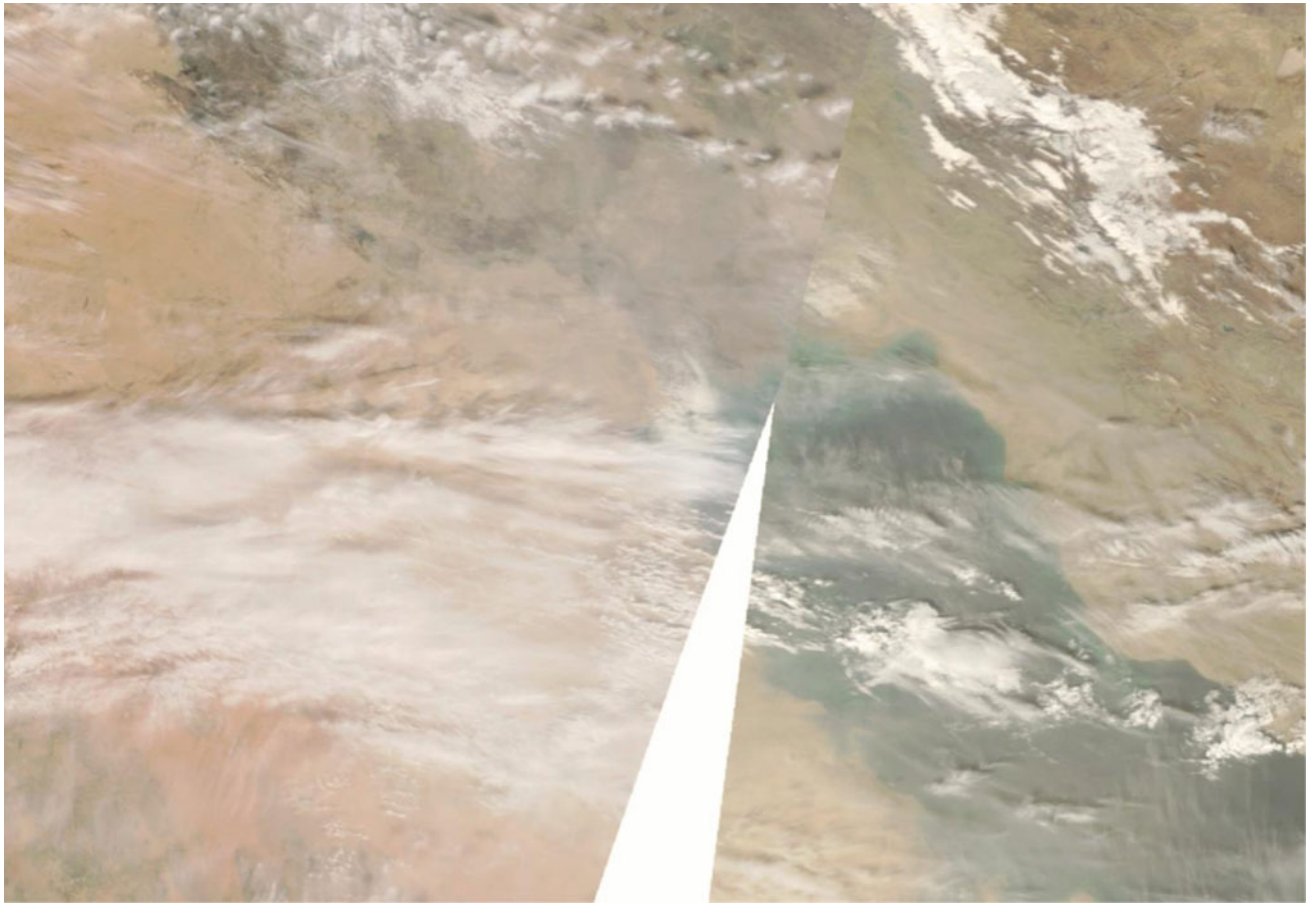


Fig. 1.13 MODIS image of dust storm that originated from the Western Desert of Iraq, covering southern Iraq, Kuwait and northern Arabian Gulf on 17th February 2009

storm trajectories are familiar in March, May, June, July, and August. With the northwesterly trajectories, fallen dust is brighter in color, coarser in mean size fraction sand particles (diameter more than 0.063 mm), and contains more quartz and feldspars, but has fewer carbonates and clay minerals, a lower particle surface area, and less iron and organic matter than trajectories from the Mesopotamian Floodplain. The following weather data were recorded on 28th February 2009 (Fig. 1.14):

- Heavy cloud cover obscured the area of concern.
- The local prevailing wind direction: northwest, west-northwest, west.
- The northwest, west-northwest, and west wind directions represent 32.1%, 35.1%, and 14.9%, respectively, of the total hourly wind count for that day.

Satellite Images

A unidirectional dust storm blew from northern Arabia and the Western Desert of Iraq toward Kuwait on 2nd March 2009. This type of dust storm trajectory takes a wider form, covering an area of 3000 km², but sometimes it occurs on a smaller scale and is seasonally known as Subag Sarayat, which extends from early March until the 28th April. The large trajectories of the northwestern dust storm normally blow in January, February, March, April, June, September, and October. Furthermore, moderate dust storm trajectories that cover an area of less than 3000 km² are familiar in March, May, June, July, and August. Fallen dust of the northwesterly trajectories is brighter in color and coarser in size fraction, with more sand particles, more quartz and



Fig. 1.14 MODIS image of dust storm that originated from the Western Desert of Iraq covering southern Iraq, Kuwait, and northern Arabian Gulf on 28th February 2009

feldspars, but fewer carbonates and clay minerals, lower particle surface area, and less iron and organic matter than trajectories from the Mesopotamian Floodplain or those coming from marches in Iraq and Iran. This trajectory is also expected to have fewer microorganisms. The following weather data were recorded for 2nd March 2009 (Fig. 1.15):

- Heavy cloud cover obscured the area of concern.
- The local prevailing wind direction: west-northwest, west.
- The west-northwest and west wind directions represent 49.4% and 22.6%, respectively, of the total hourly wind count for that day.

Satellite Images

Bidirectional dust storms: one blowing from southern Iraq toward the Arabian Gulf in an arrow-shaped dust storm trajectory on 10th March 2009, while the second is blowing from the northeast. The trajectory diverted its direction from

above the Arabian Gulf toward Arabia. This type of dust storm trajectory takes the wider form and is part of the Subg Sarayat season that extends from early March until 28th April. The northwestern dust storm large trajectories usually blow in January, February, March, April, May, June, July, August, September, and October. The northeastern trajectories' fallen dust is darker in color, finer in size fraction, with fewer sand particles, and contains more clay and carbonates but has fewer quartz and feldspar minerals, as well as larger values of particle surface area, and higher percentages of iron and organic matter than other trajectories. Weather data collected on 10th March 2009 were as follows (Fig. 1.16):

- The local prevailing wind direction (northwest, west-northwest) agrees with that deduced from the image. Note that there is a huge south-southeast wind component.
- The northwest and west-northwest wind directions represent 29.2% and 23.4%, respectively, of the total hourly wind count for that day. The south-southeast component represents 22.4%.

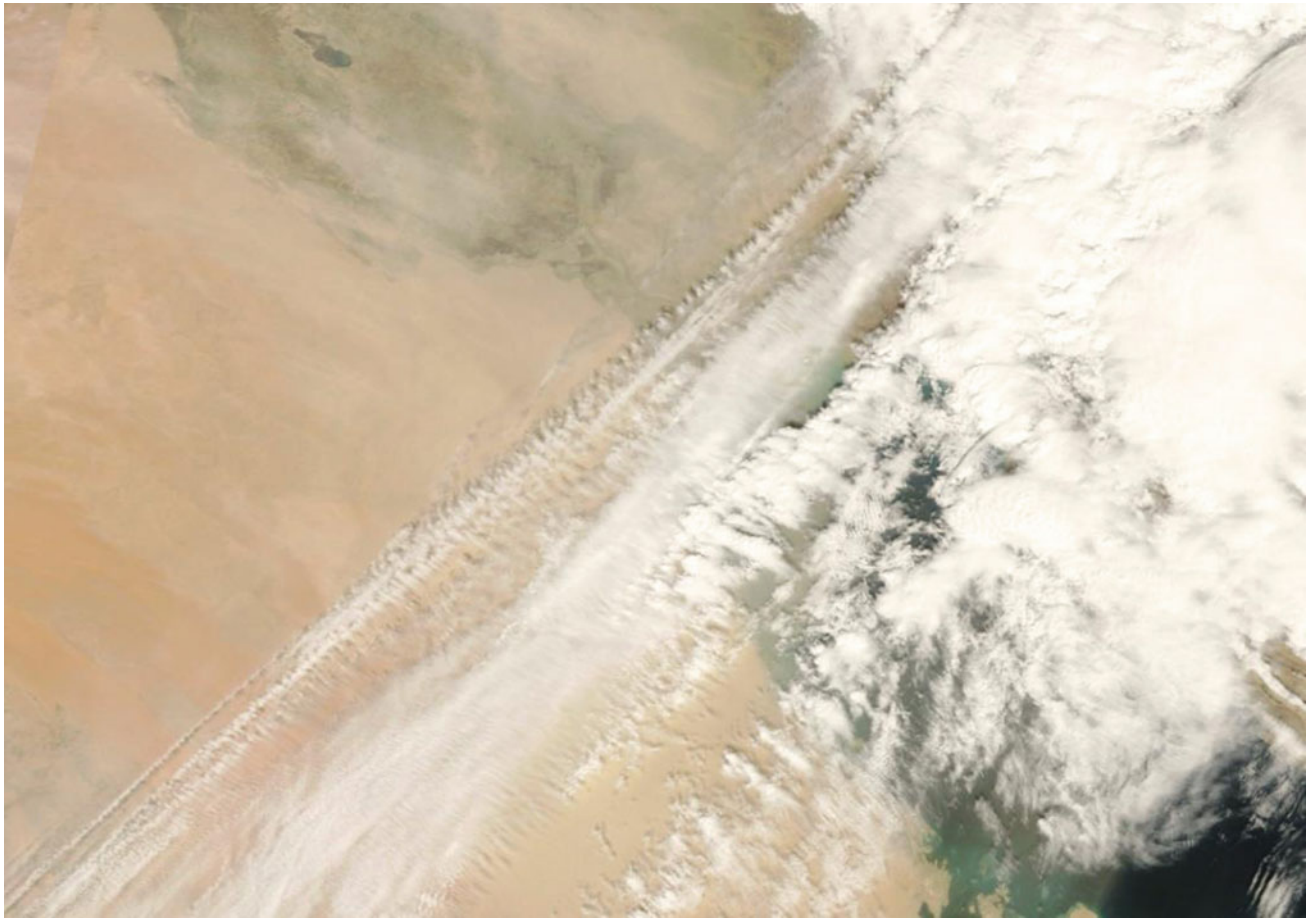


Fig. 1.15 MODIS image of dust storm that originated from the Western Desert of Iraq covering southern Iraq, Kuwait, and northern Arabian Gulf on 2 March 2009

Satellite Images

This unidirectional dust storm blew from the northern Arabian Gulf toward Kuwait on the 13th March 2009. This type of dust storm trajectory takes the wider form with a low wind speed. These northern dust storm large trajectories blow normally in January, March, April, May, June, July, August, and October. The northern trajectories' fallen dust contains higher percentages of iron and organic matter than other trajectories. Weather data collected on 13th March 2009 were as follows (Fig. 1.17):

- The local prevailing wind direction (west-northwest, northwest, north) agrees with that deduced from the image.
- The west-northwest, northwest, and north wind directions represent 19.4%, 21.1%, and 15.4%, respectively, of the total hourly wind count for that day.

Satellite Images

This unidirectional dust storm blew from northern Arabia and the Western Desert of Iraq toward Kuwait on 14th May 2009. This type of dust storm trajectory takes the wider form and blows normally in January, February, March, April, June, September, and October. Furthermore, moderate dust storm trajectories are familiar in March, May, June, July, and August. The northwesterly trajectories' fallen dust is coarser in size fraction, with sand particles (diameter more than 0.063 mm) containing more quartz and feldspars minerals, a smaller particle surface area, and less iron and organic matter than trajectories from the Mesopotamian Floodplain. Weather data collected on 14th May 2009 were as follows (Fig. 1.18):

- Heavy cloud cover obscured the area of concern.
- The prevailing wind direction: northwest, west-northwest, west.

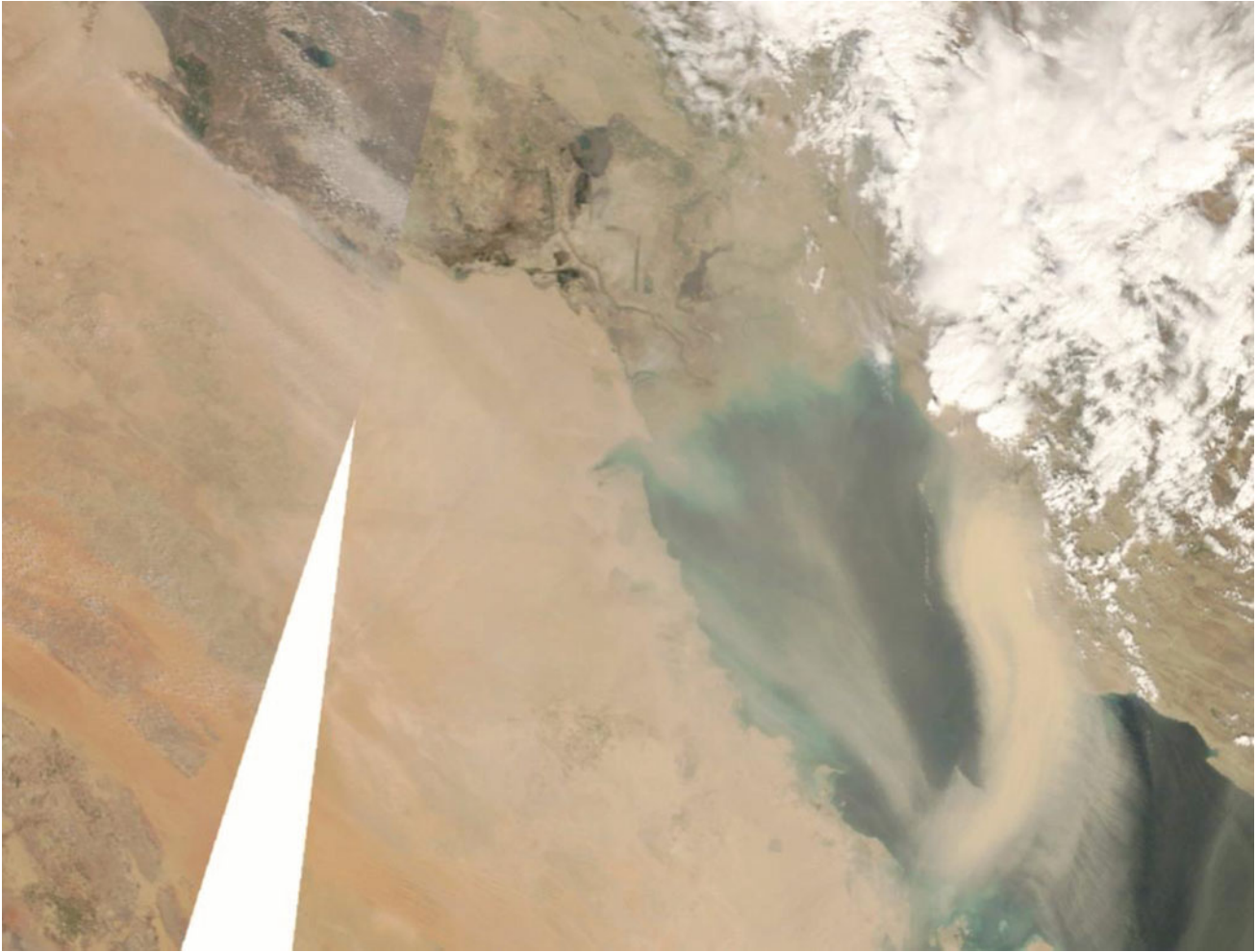


Fig. 1.16 MODIS image of dust storm that originated from the Western desert of Iraq, covering southern Iraq, Kuwait, and northern Arabian Gulf on 10th March 2009

- The northwest, west-northwest, and west wind directions represent 17.3%, 31.5%, and 15.5%, respectively, of the total hourly wind count for that day.

Satellite Images

Moderate wind speed caused a unidirectional dust storm blowing from northern Arabia and the Western Desert of Iraq toward Kuwait on 15th May 2009. The northwestern dust storm large trajectories are affected by wind from the southwest. Moderate dust storm trajectories that cover less than 3000 km² of the area are most likely in March, May, June, July, and August. The northwesterly trajectories' fallen dust is brighter in color, coarser in size fraction, with sand particles (diameter more than 0.063 mm) containing more

quartz and feldspars but fewer carbonates and clay minerals, with a lower particle surface area, and less iron and organic matter than north and northeastern trajectories. The associated pollen with these types of dust trajectories originates mainly from *Haloxylon sp.* and *Cyperus sp.*, native plants that were transferred a short distance from regional source areas. Weather data collected on the 15th May 2009 were as follows (Fig. 1.19):

- Cloud cover obscured the area of concern.
- Prevailing wind direction (west-southwest, west, west-northwest, with strong north-northwest component) agrees with that deduced from the image.
- The west-southwest, west, and west-northwest wind directions represent 14.3%, 23.8%, and 16.7%, respectively, of the total hourly wind count for that day.

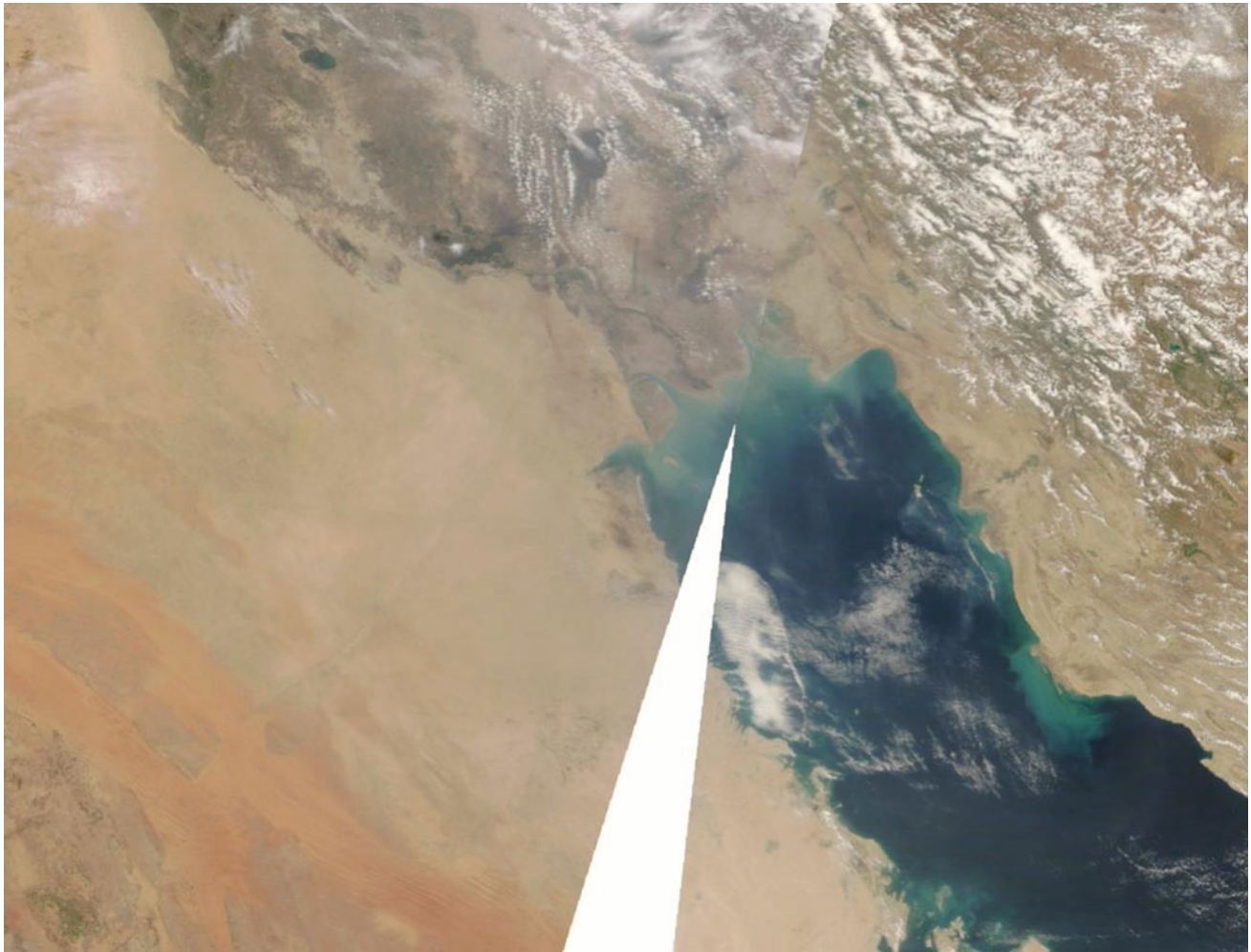


Fig. 1.17 MODIS image of dust storm that originated from the Western Desert of Iraq, covering southern Iraq, Kuwait and northern Arabian Gulf on 13th March 2009

Satellite Images

This unidirectional dust storm blew from the southwest toward Kuwait in the on 16th May 2009. This type of dust storm trajectory takes the wider form and normally blows in March, April, May, June, and October. Fallen dust from the southwesterly trajectories is brighter in color, coarser in size fraction, with more sand particles, causing dust deposits to accumulate quickly. Such dust contains more quartz and feldspars but fewer carbonates and clay minerals, a lower particle surface area, and a smaller percentage of iron and organic matter than other trajectories. Weather data collected on 16th May 2009 were as follows (Fig. 1.20):

- Heavy cloud cover obscured the area of concern.
- The prevailing wind direction was southwest, west-southwest, and west.

- The southwest, west-southwest, and west wind directions represent 12.1%, 19.1%, and 31.8%, respectively, of the total hourly wind count for that day.

Satellite Images

A small unidirectional dust storm with an arrow shape blowing from the Mesopotamian Floodplain, particularly from the Samawa region in Iraq, toward Kuwait on 2nd July 2009. This type of dust storm trajectory has a moderate size form that covers an area less than 3000 km² and is familiar in March, May, June, July, and August. The northwesterly trajectories' fallen dust is darker in color, smaller in size fraction, with fewer sand particles that contain more carbonates and clay minerals but less quartz and feldspars, has a larger the particle surface area, and higher percentages of

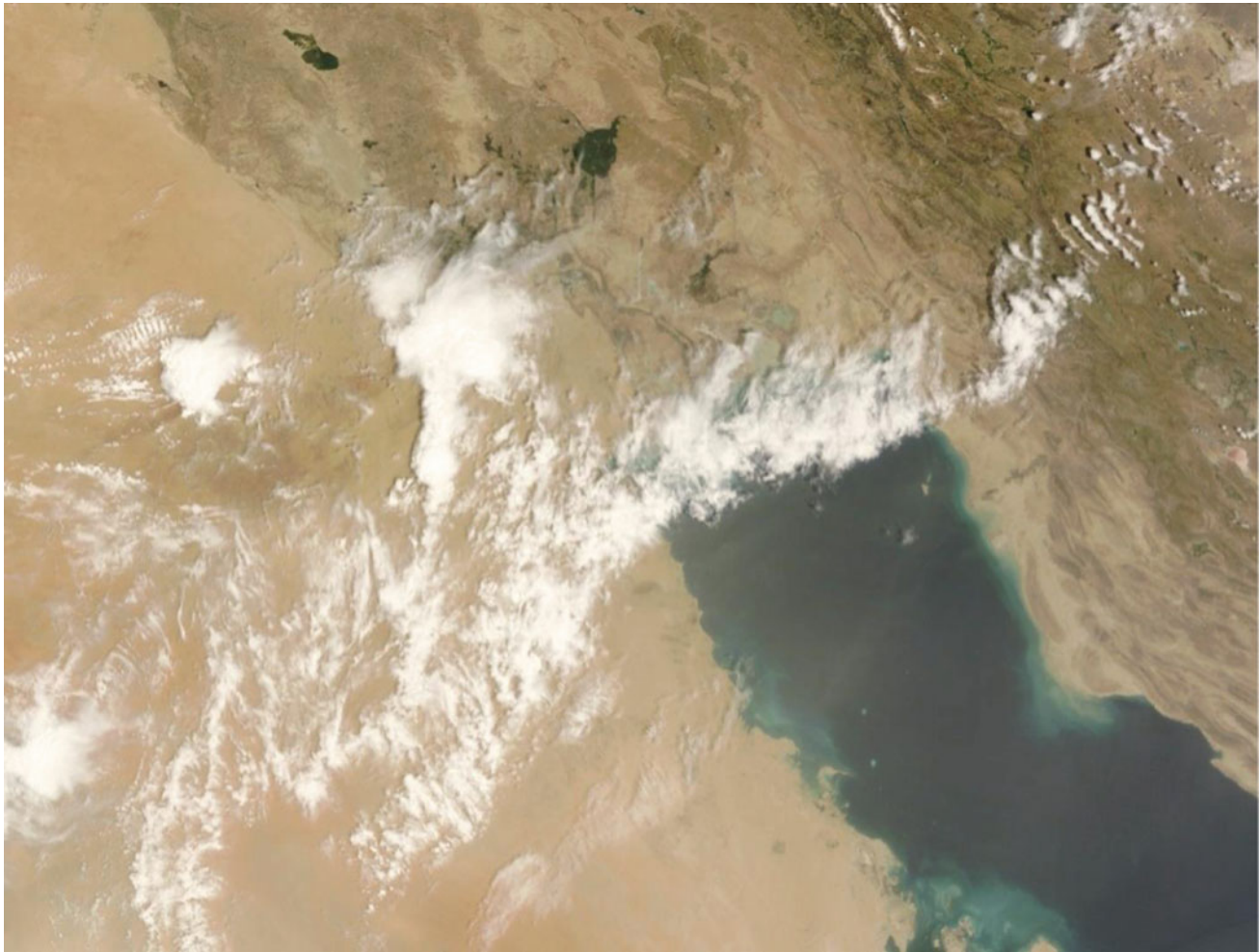


Fig. 1.18 MODIS image of dust storm that originated from the Western Desert of Iraq, covering southern Iraq, Kuwait, and the northern Arabian Gulf on 14th May 2009

iron and organic matter than other trajectories. Weather data obtained on 2nd July 2009 were as follows (Fig. 1.21):

- The local prevailing wind direction (northwest, west-northwest) agreed with that deduced from the image over the area of the State of Kuwait;
- The northwest and west-northwest wind directions represent 30.4% and 47.3%, respectively, of the total hourly wind count for that day.

Satellite Images

The same dust storm that blew on 2nd July continued for a second day but at a higher wind speed. The storm took the form of an arrow shape, was unidirectional, and covered small areas. It blew from the Mesopotamian Floodplain,

particularly from the Samawa region in Iraq, Bubiyan Island, and Sabiya in Kuwait, toward the Arabian Gulf on 3rd July 2009. This type of dust storm trajectory has a moderate size, covers an area of less than 3000 km², and is familiar in March, May, June, July, and August. The northwesterly trajectories' fallen dust is darker in color, smaller in size fraction, with fewer sand particles, contains more carbonates and clay minerals, has a larger particle surface area, and high percentages of iron and organic matter compared with the other trajectories. The weather data collected on 3rd July 2009 were as follows (Fig. 1.22):

- The local prevailing wind direction (northwest, west-northwest, west) agreed with that deduced from the image over the area in Kuwait;
- The northwest, west-northwest, and west wind directions represent 33.3%, 36.9%, and 20.8%, respectively, of the total hourly wind count for that day.

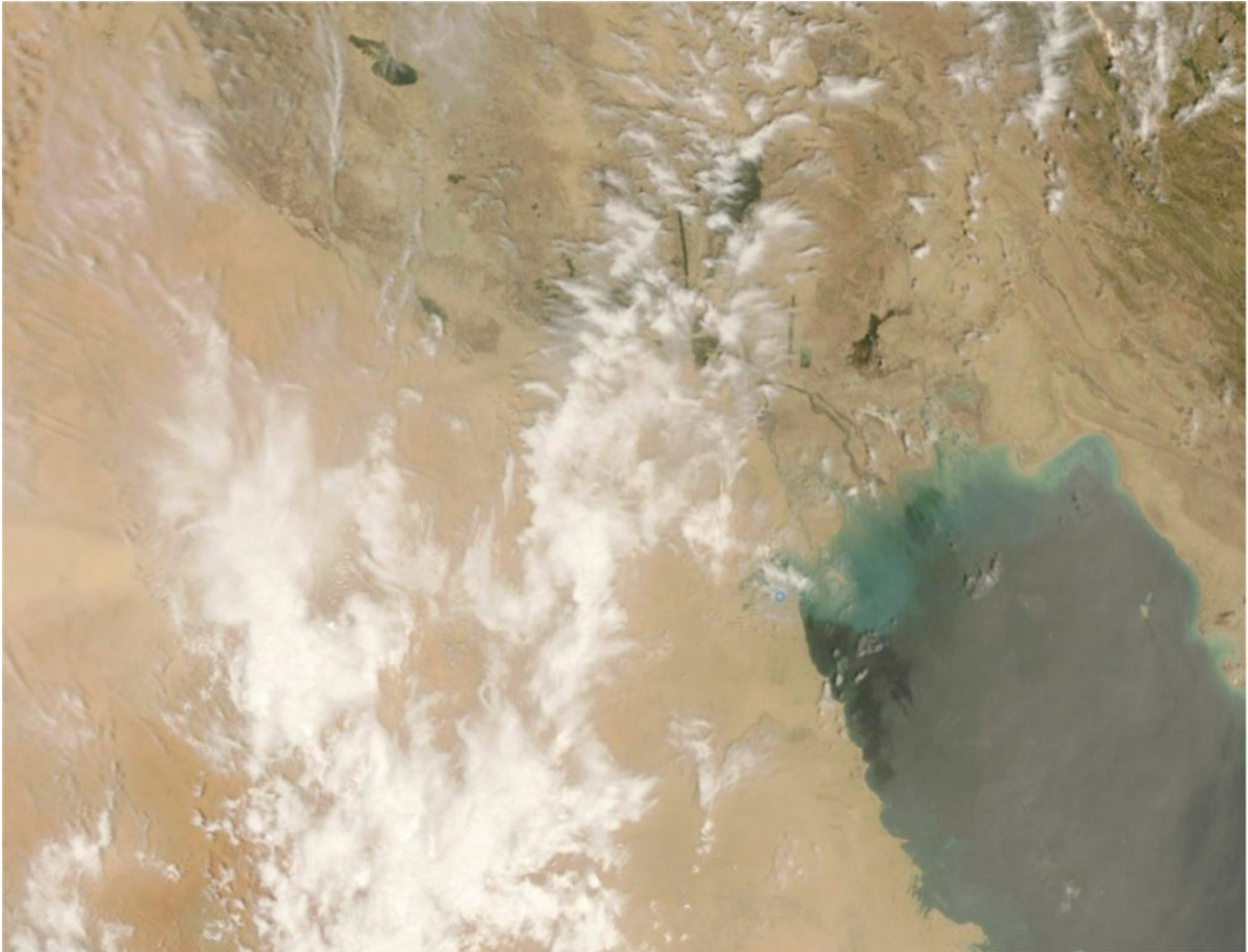


Fig. 1.19 MODIS image of dust storm that originated from the Western Desert of Iraq, covering southern Iraq, Kuwait, and the northern Arabian Gulf on 15th May 2009

Satellite Images

A transition zone of an intermediate dust storm into a wide dust storm form that covers an area of more than 3000 km² blowing from the Mesopotamian Floodplain, mainly from the Samawa and Ahwar regions in Iraq, toward Kuwait and the Arabian Gulf on 29th July 2009. This type of dust storm trajectory is familiar in March, May, June, July, and August. The northwesterly trajectories' fallen dust is darker in color, smaller in size fraction, with fewer sand particles, contains more carbonates and clay minerals, has a larger particle surface area, and a high percentage of iron and organic matter when compared with other trajectories. The following weather data were recorded for 29th July 2009 (Fig. 1.23):

- The local prevailing wind direction (northwest, west-northwest, west) agreed with that deduced from the image over the area of the State of Kuwait;

- The northwest, west-northwest, and west wind directions represent 22.9%, 37.5%, and 27.1%, respectively, of the total hourly wind count for that day.

Satellite Images

Two dust storm trajectories taking the form of arrow-shapes, indicating high wind speed. This form is a moderate size that covers an area of less than 3000 km² and predominantly occurs in July but is familiar in March, May, June, and August. It is a unidirectional form blowing from the Mesopotamian Floodplain, particularly from the Samawa and Hur Suwaiga regions in Iraq, Bubiyan Island, and Subiyah in Kuwait, toward the Arabian Gulf on 15th August 2009. The northwesterly trajectories' fallen dust is characterized by more carbonates and higher clay mineral percentages, is

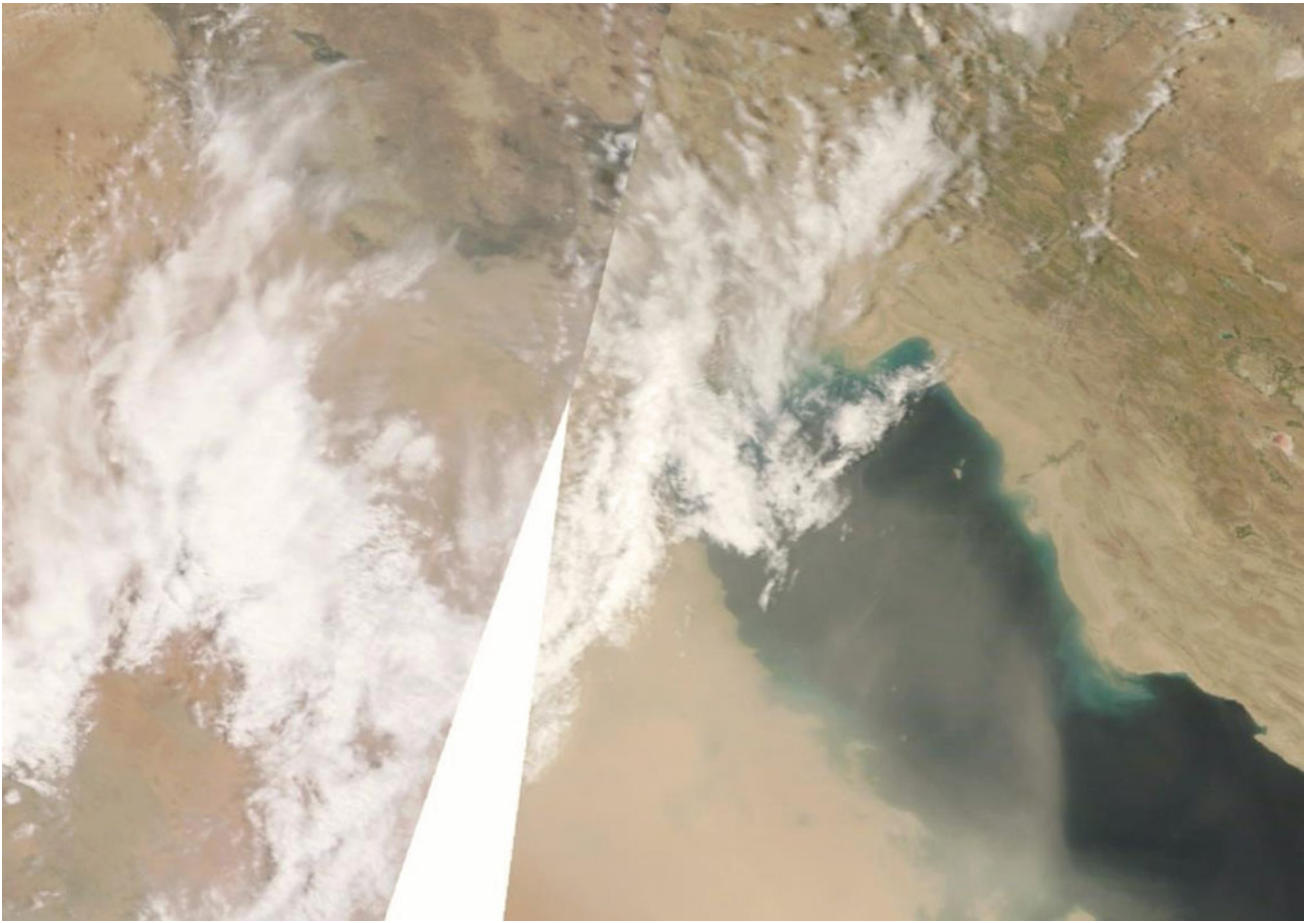


Fig. 1.20 MODIS image of dust storm that originated from the Western Desert of Iraq, covering southern Iraq, Kuwait, and the northern Arabian Gulf on 16th May 2009

darker in color, smaller in size fraction, with more mud particles, larger in particle surface area, and has high percentages of iron and organic matter in comparison with other trajectories. The following weather data were recorded on 15th August 2009 (Fig. 1.24):

- The local prevailing wind directions (west-northwest, northwest) over the entire Kuwait agreed with that deduced from the image.
- The west-northwest and northwest wind directions represent 45.9% and 43.8%, respectively, of the total hourly wind count for that day.

Satellite Images

This image shows that no dust storm has occurred, which indicates that visibility is not a good indicator for dust storms, as visibility can be low due to fog, rain, smog, and humidity, rather than dust. Ordinarily, when visibility is less

than 1000 m, it is considered a clear indicator of dust storms. This day showed low visibility (less than 1000 m) despite the non-occurrence of dust, which indicates that depending only on visibility as an indicator of dust storms is incorrect. The following weather data were recorded on 6th January 2010 (Fig. 1.25):

- The local prevailing wind direction was west-northwest, northwest, north-northwest over the whole area of Kuwait.
- The west-northwest, northwest, and north-northwest wind directions represent 49.0%, 31.8%, and 12.0%, respectively, of the total hourly wind count for that day.

Satellite Images

A massive dust storm blowing from the Sahara Desert in northern Africa, passing through Palestine, Jordan, northern Arabia, and the Western Desert of Iraq toward western

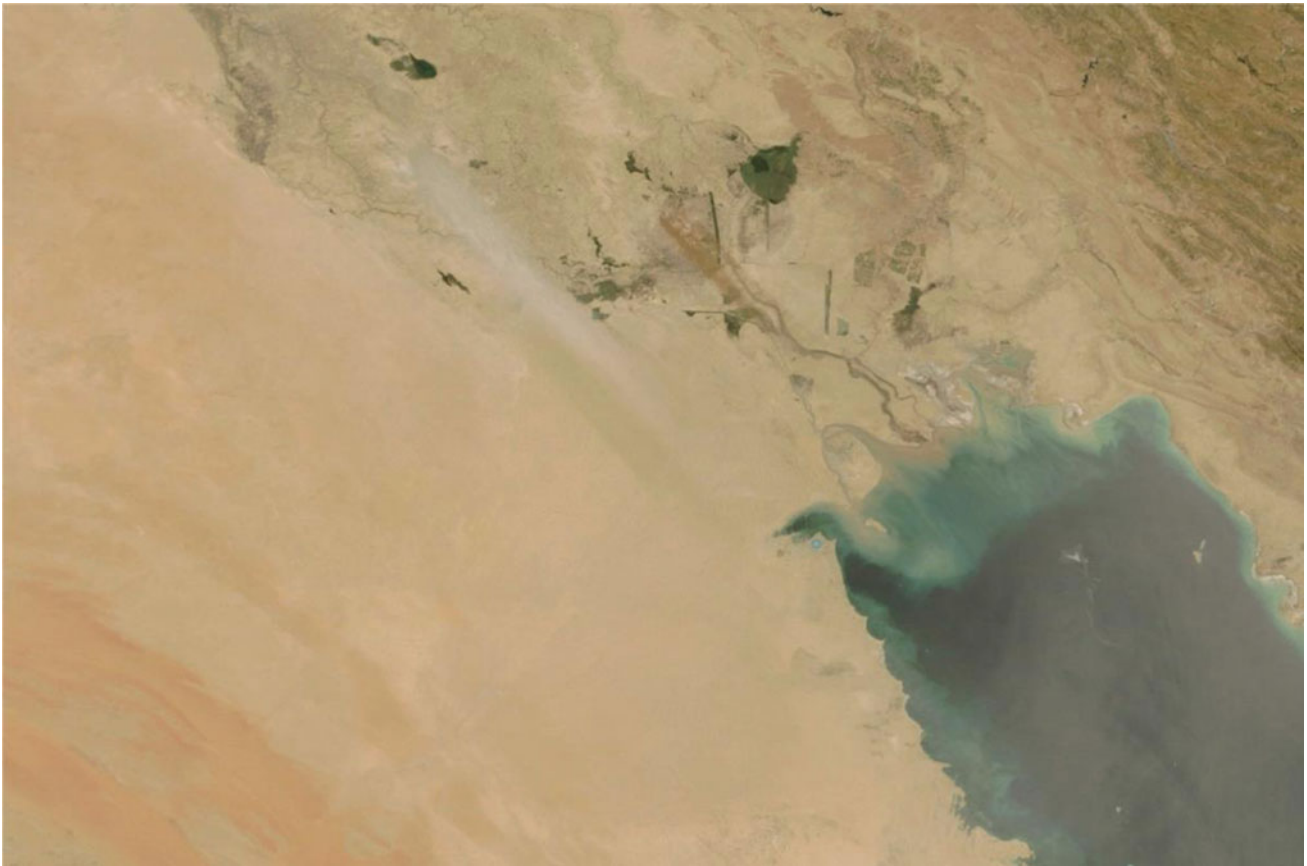


Fig. 1.21 MODIS image of dust storm that originated from the Western Desert of Iraq, covering southern Iraq, Kuwait, and the northern Arabian Gulf on 2nd July 2009

Kuwait on 25th January 2010. These types of unidirectional dust storm trajectories take the wider form of covering the Western Desert of Iraq, where the Mesopotamian Floodplain is not affected. These northwestern dust storms' large trajectories blow normally in January, February, March, April, June, September, and October. The northwesterly trajectories' fallen dust that passes only through the Western Desert of Iraq is brighter in color, coarser in size fraction, with more sand particles, and contains more quartz and feldspars but fewer carbonates and clay minerals, with a lower particle surface area, and less iron and organic matter in comparison with the trajectories from the Mesopotamian Floodplain. The following weather data were recorded on 25th January 2010 (Fig. 1.26):

- The local prevailing wind directions (west, west-northwest, northwest, and some southeast, south-southeast components) agree with those deduced from the image.
- The northwest, west-northwest, and west wind directions represent 12.5%, 22.9%, and 14.1%, respectively, of the total hourly wind count for that day

Satellite Images

A small and unidirectional dust storm blowing from the southeast toward Kuwait on 31st January 2010. The southeastern dust storms' small trajectories normally blow in October and December, and rarely in January and February. The southeastern trajectories' fallen dust is brighter in color, coarser in size fraction, with more sand particles, and contains more quartz and feldspars but fewer carbonates and clay minerals, with a lower particle surface area, and less content of iron and organic matter when compared with the trajectories from the north and northwest. On the other hand, the dust deposited from this trajectory is characterized by smaller particle size, less quartz, and contains more organic matter than trajectories from the southwest. The following weather data were recorded on 31st January 2010 (Fig. 1.27):

- Heavy cloud cover obscured the area of concern.
- Prevailing wind direction: east, east-southeast. The wind passing over the Arabian Sea became laden with water vapor, explaining the clouds.

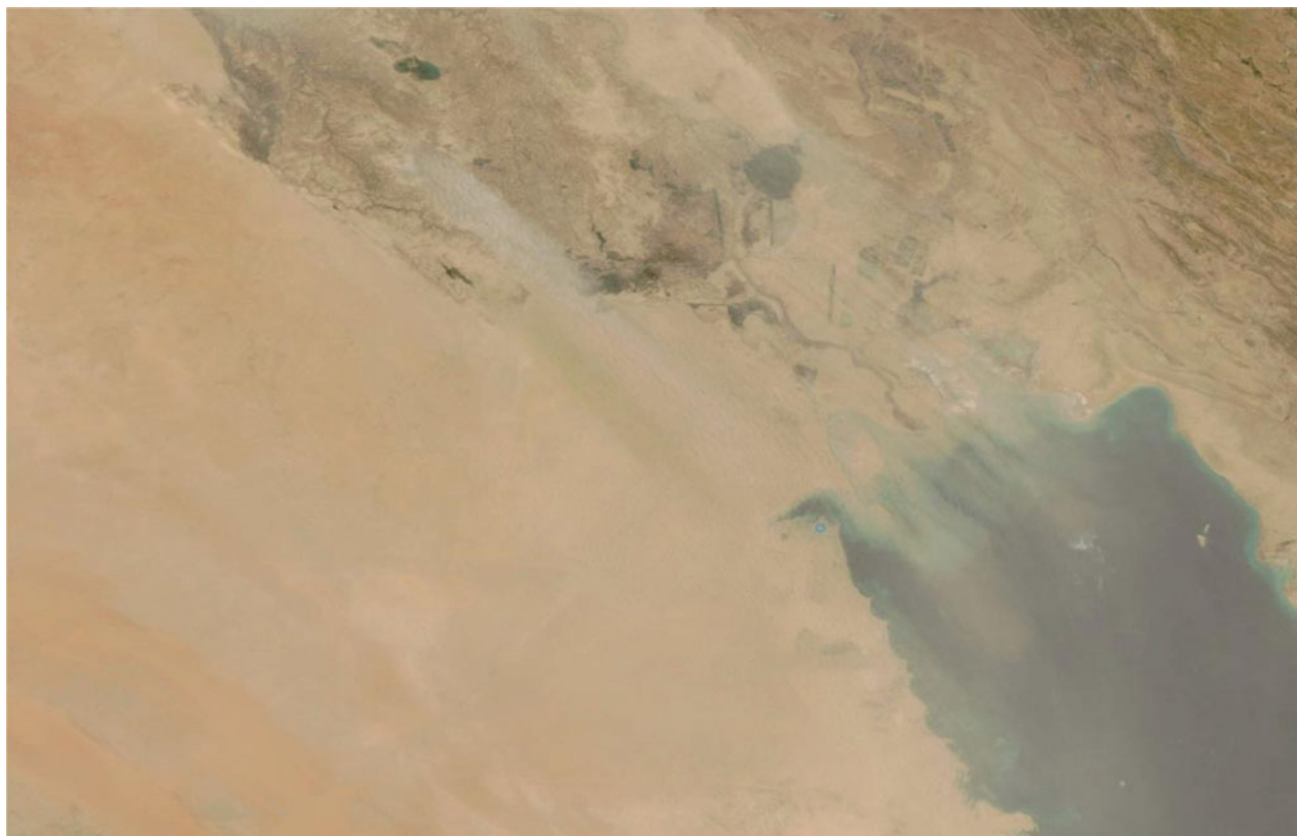


Fig. 1.22 MODIS image of dust storm that originated from the Western Desert of Iraq, covering southern Iraq, Kuwait, and the northern Arabian Gulf on 3rd July 2009

- The east and east-southeast wind directions represent 20.8% and 25.5%, respectively, of the total hourly wind count for that day.

Satellite Images

A dust storm blew from the southeast toward Kuwait on 1st February 2010. The southeastern dust storm small trajectories usually blow in October and December, and occasionally in February. The wind passing over the Arabian Gulf becomes laden with water vapor, which causes the rapid deposition of dust. The fallen dust within southeastern trajectories is brighter in color, coarser in size fraction, with more sand particles, and contains more quartz and feldspars but fewer carbonates and clay minerals, with a lower particle surface area, and less content of iron and organic matter in comparison with trajectories from the north and northwest. On the other hand, the deposited dust from this trajectory is characterized by smaller particle size, less quartz, and contains more organic matter when compared with trajectories

from the southwest. Weather data collected on 1st February 2010 were as follows (Fig. 1.28):

- Heavy cloud cover obscured the area of concern.
- Prevailing wind direction: east-southeast, southeast, south-southeast, south. The wind passing over the Arabian Gulf became laden with water vapor, which could explain the clouds.

Satellite Images

Coalescence of two wind directions from the southeast and southwest caused a dust storm blowing mainly from local sources within Kuwait on 3rd February 2010. This type of dust storm trajectory is a moderate form in which the area covered is less than 3000 km². The southeasterly trajectories' fallen dust's physical and chemical properties are fully described in previous images from the same direction. The following weather data were recorded on 3rd February 2010 (Fig. 1.29):

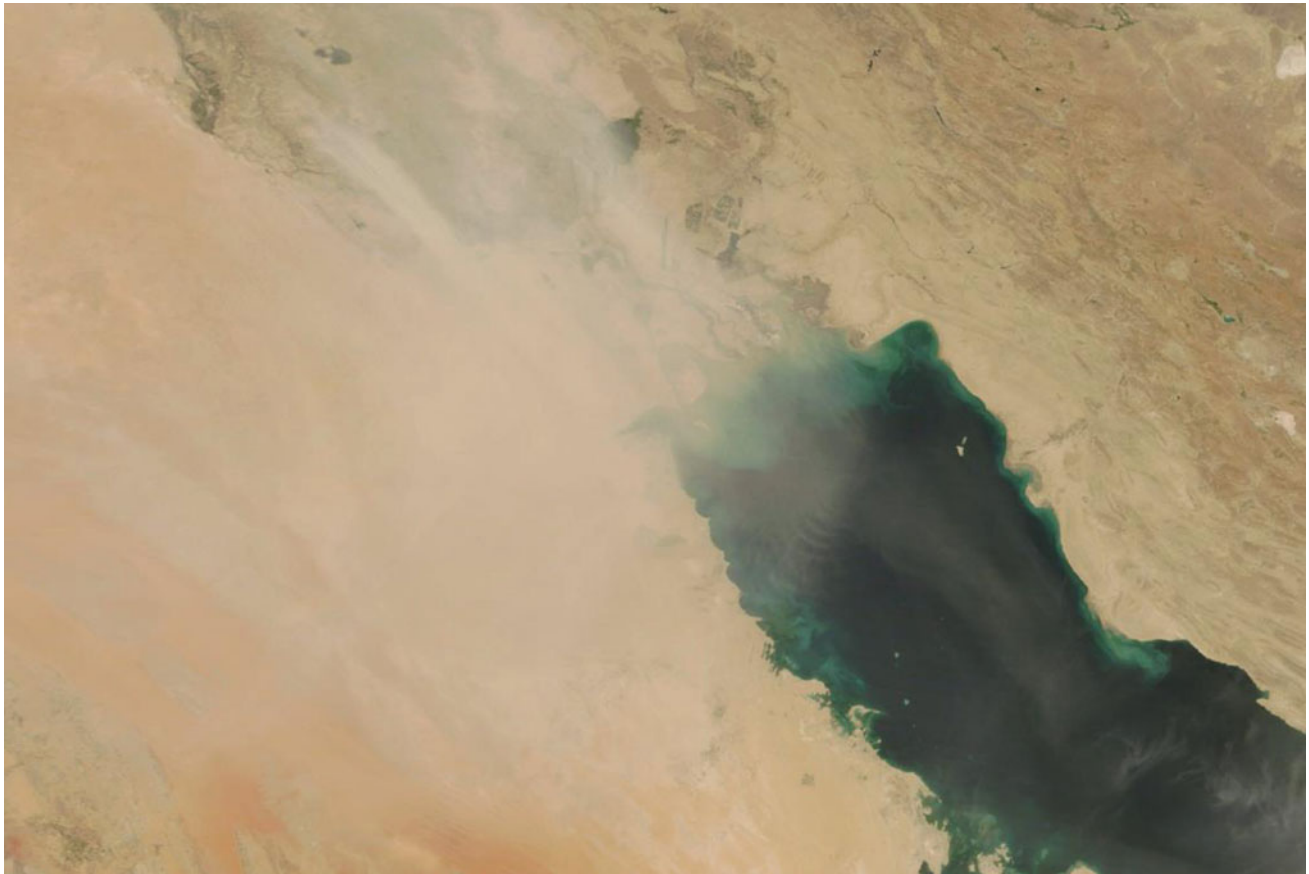


Fig. 1.23 MODIS image of dust storm that originated from the Western Desert of Iraq, covering southern Iraq, Kuwait, and the northern Arabian Gulf on 29th July 2009

- Heavy cloud cover obscured the area of concern.
- Prevailing wind direction: southeast, south-southeast. The wind passing over the Arabian Gulf became laden with water vapor, which explains the clouds.
- The southeast and south-southeast wind directions represent 25.5% and 22.9%, respectively, of the total hourly wind count for that day.
- Cloud cover obscured the area of concern.
- Prevailing wind direction: east-southeast, southeast, south-southeast. The wind passing over the Arabian Sea became laden with water vapor, which explains the clouds.
- The east-southeast, southeast, and south-southeast wind directions represent 22.9%, 17.7%, and 14.6%, respectively, of the total hourly wind count for that day.

Satellite Images

A two-wind direction from the southeast and west-northwest facing each other in northern Kuwait caused a small unidirectional dust storm blowing mainly from local and close regional sources toward Kuwait on 13th February 2010. This type of dust storm trajectory is a moderate form and lasts only for a short period. The southeasterly trajectory's fallen dust physical and chemical properties are fully described in previous images from the same direction. The following weather data were recorded on 13th February 2010 (Fig. 1.30):

Satellite Images

A broad and unidirectional dust storm blew from northern Arabia and the Western Desert of Iraq toward Kuwait on 23rd February 2011. These types of dust storm trajectories take a wider form but have a low wind speed. Normally, the northwest trajectory has a high wind speed but, on this rare occasion, was only moderate, causing the movement of mud-sized particles. In this case, the dust contains more nutrients, organic matter, and pollen, and is characterized by a higher content of clay minerals and carbonates than

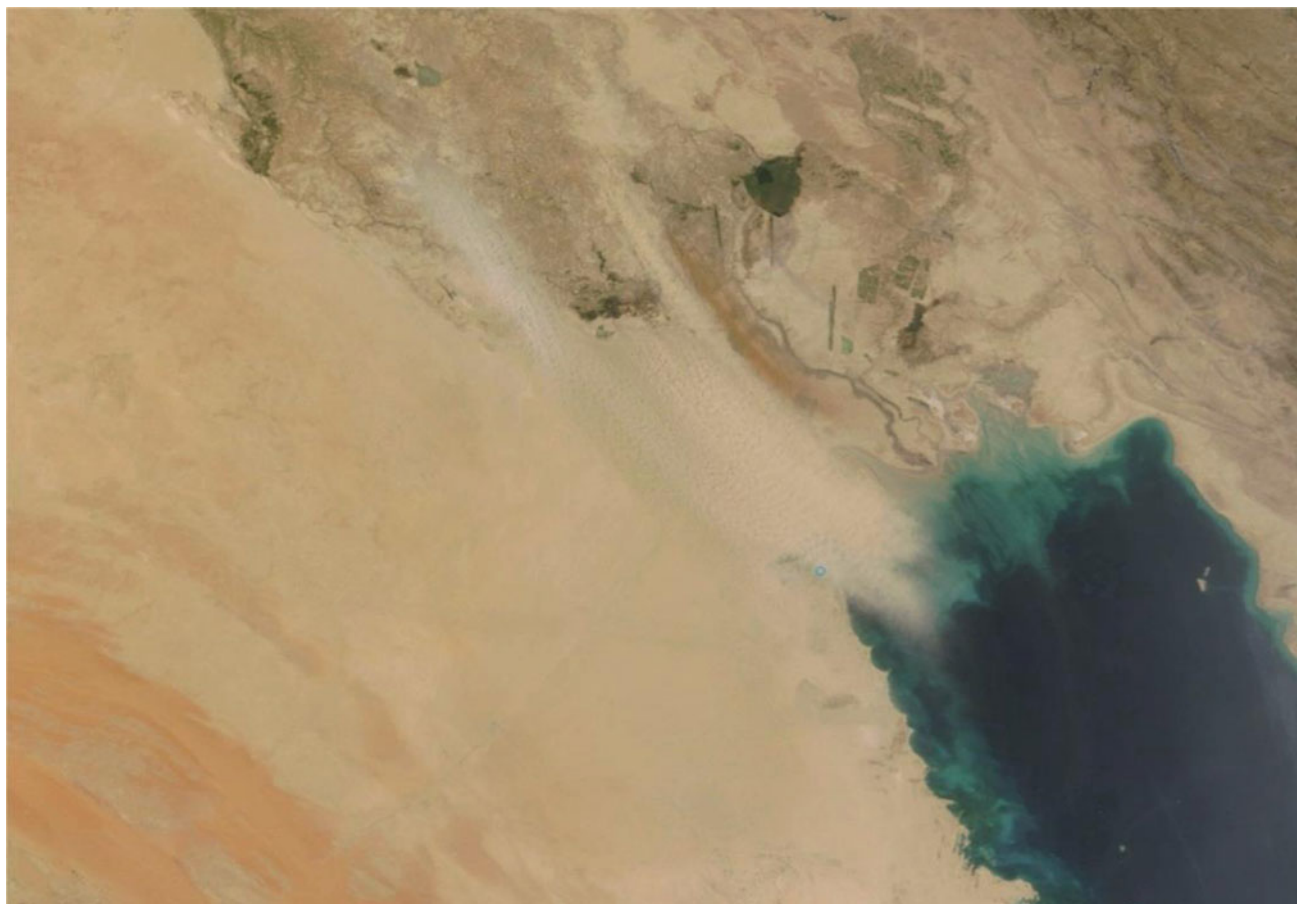


Fig. 1.24 Satellite image (MODIS) of dust storm on 15th August 2009 that blew from Diwaniyah and Ahwar in the Mesopotamian Floodplain in southern Iraq, passing through northern Kuwait toward the Arabian Gulf

normal. The following weather data were recorded on 23rd February 2010 (Fig. 1.31):

- Heavy cloud cover obscured the area of concern.
- Prevailing wind direction: north, north-northwest.
- The north and north-northwest wind directions represent 30.2% and 30.7%, respectively, of the total hourly wind count for that day.

Satellite Images

A moderate, unidirectional dust storm blowing from northern Arabia and the Western Desert of Iraq toward Kuwait on 26th February 2010. This type of dust storm trajectory takes a small arrow shape form, in which the area covered by the trajectory is less than 3000 km². These moderate, north-westerly large trajectories are familiar in March, but this one was at the end of February. The northwesterly trajectories' fallen dust contains more quartz and feldspars but fewer

carbonates and clay minerals, with a lower particle surface area, and less iron and organic matter when compared with trajectories from the Mesopotamian Floodplain, but much more when compared with other trajectories. The following weather data were recorded on 26th February 2010 (Fig. 1.32):

- Heavy cloud cover obscured the area of concern.
- Prevailing wind direction: west, west-northwest, with south and east components.
- The west and west-northwest wind directions represent 15.6% each of the total hourly wind count for that day.

Satellite Images

Massive and strong unidirectional dust storm formed in northern Arabia and the Western Desert of Iraq blowing toward Kuwait on 4th March 2010. This type of dust storm trajectory took the wider form, in which the area covered is

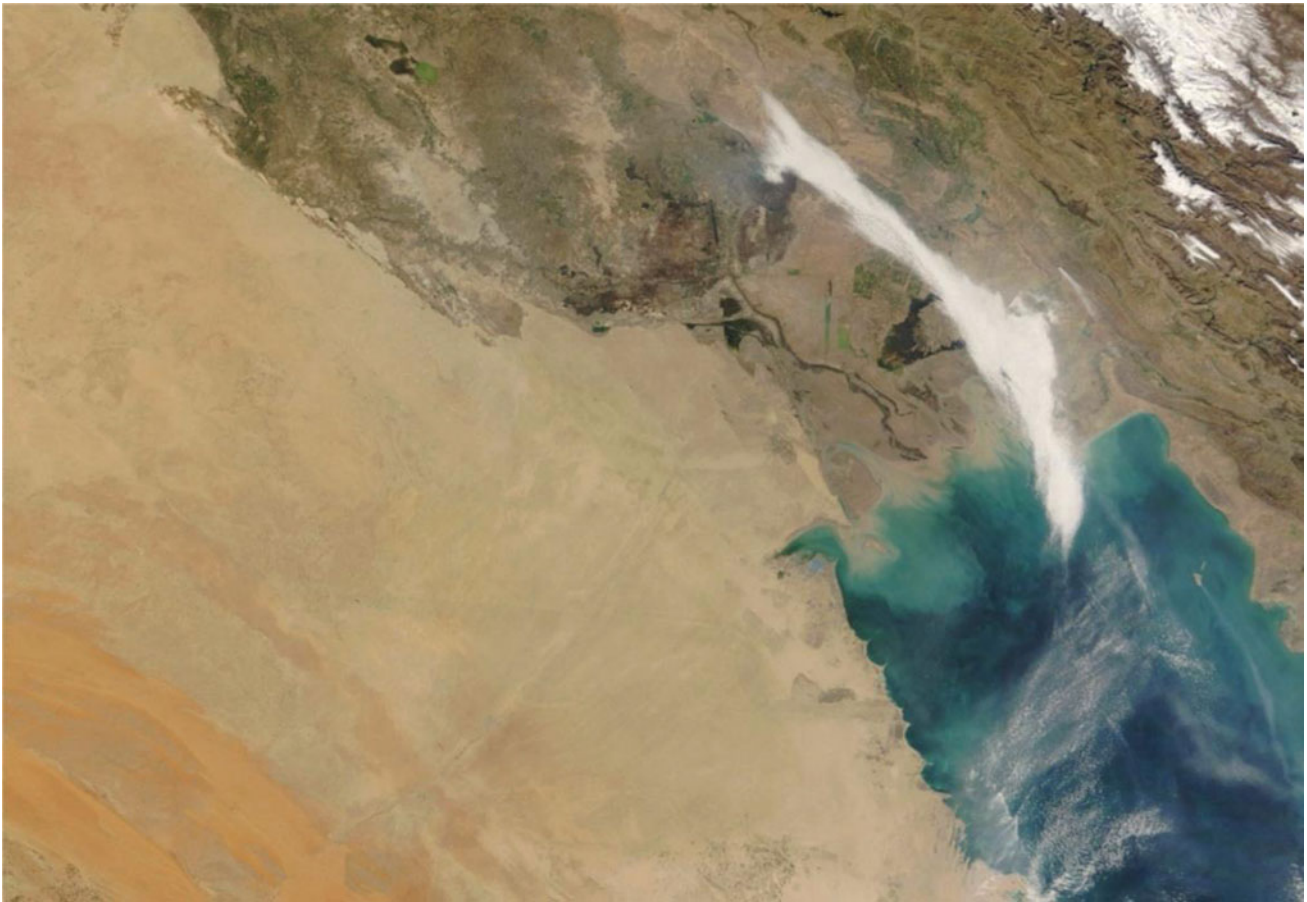


Fig. 1.25 MODIS image of dust storm that originated from the Western Desert of Iraq, covering southern Iraq, Kuwait, and the northern Arabian Gulf on 6th January 2010

more than 3000 km². The northwestern large trajectories blow normally in January, February, March, April, June, September, and October. Fallen dust of the northwesterly trajectories is brighter in color, coarser in size fraction, with more sand particles, and contains more quartz and feldspars but fewer carbonates and clay minerals, with a lower particle surface area, and less iron and organic matter when compared with the trajectories from the Mesopotamian Floodplain, but is higher when compared with the other trajectories. The following weather data were recorded on 4th March 2010 (Fig. 1.33):

- The local prevailing wind direction (northwest, west-northwest) agrees with the outcome deduced from the image. Note there is a huge south-southeast wind component.
- The northwest and west-northwest wind directions represent 22.9% and 26.0%, respectively, of the total hourly wind count for that day. The south-southeast component represents 17.2%.

Satellite Images

A northwesterly unidirectional dust storm covering the northern part of the Arabian Gulf coming from the Western Desert of Iraq toward Kuwait on 5th March 2010. This type of dust storm trajectory takes the wider form. The northwestern dust storm has large trajectories that blow normally in January, February, March, April, June, September, and October. The fallen dust during these trajectories is brighter in color, coarser in size fraction, with more sand particles, contains more quartz and feldspars but fewer carbonates and clay minerals, with a lower particle surface area, and less iron and organic matter than trajectories from the Mesopotamian Floodplain but more than other trajectories. The following weather data were recorded on 5th March 2010 (Fig. 1.34):

- The local prevailing wind direction (northwest, west-northwest) agrees with that deduced from the image.

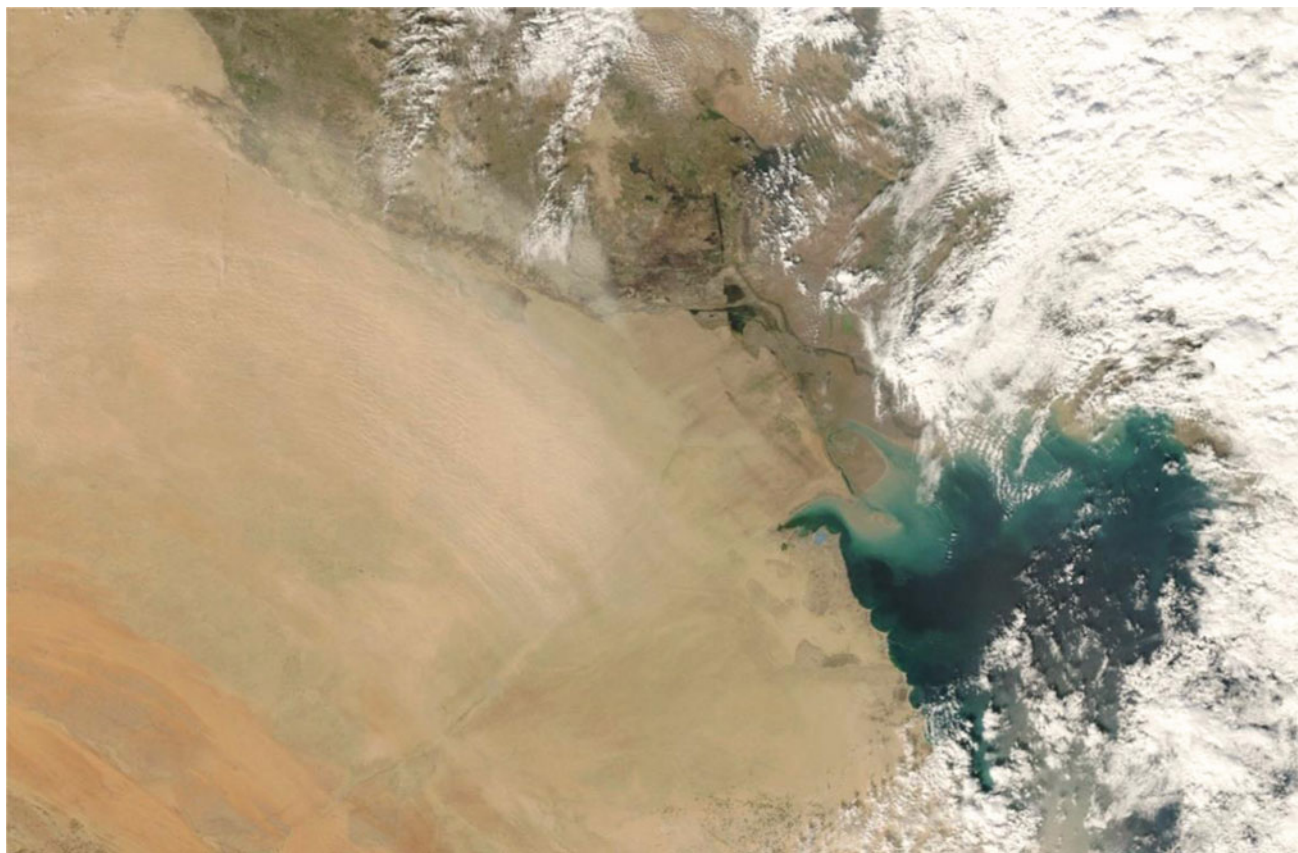


Fig. 1.26 MODIS image of dust storm that originated from the Western Desert of Iraq, covering southern Iraq, Kuwait, and the northern Arabian Gulf on 25th January 2010

- The northwest and west-northwest wind directions represent 36.5% and 41.7%, respectively, of the total hourly wind count for that day.
- The northwest and north-northwest wind directions represent 40.1% and 39.6%, respectively, of the total hourly wind count for that day.

Satellite Images

A unidirectional dust storm blowing with moderate wind speed from the northern Arabian Gulf toward Kuwait on 19th March 2010. The northwestern dust storm has large trajectories that blow normally in January, February, March, April, June, September, and October. The fallen dust of the trajectories is brighter in color, finer in size fraction, with very few sand particles, contains more carbonates and clay minerals but less quartz and feldspars, with higher particle surface area, and is high in iron content and organic matter when compared with all other trajectories. The following weather data were recorded on 19th March 2010 (Fig. 1.35):

- The local prevailing wind direction (northwest, north-northwest) agrees with that deduced from the image.

Satellite Images

A dust storm of about 250 km width blowing from the southeast toward the northern Arabian Gulf, Bahrain, Qatar, and Kuwait on 27th March 2010. The southwestern large trajectories' fallen dust is brighter in color, coarser in size fraction, and contains more quartz and feldspars but has fewer carbonates and clay minerals, with a lower particle surface area, and less iron and organic matter in comparison with trajectories from the north and northwest. The following weather data were recorded on 27th March 2010 (Fig. 1.36):

- The local prevailing wind direction: west, west-northwest. There was also a north component. This direction agrees with that deduced from the image over the area of Kuwait.

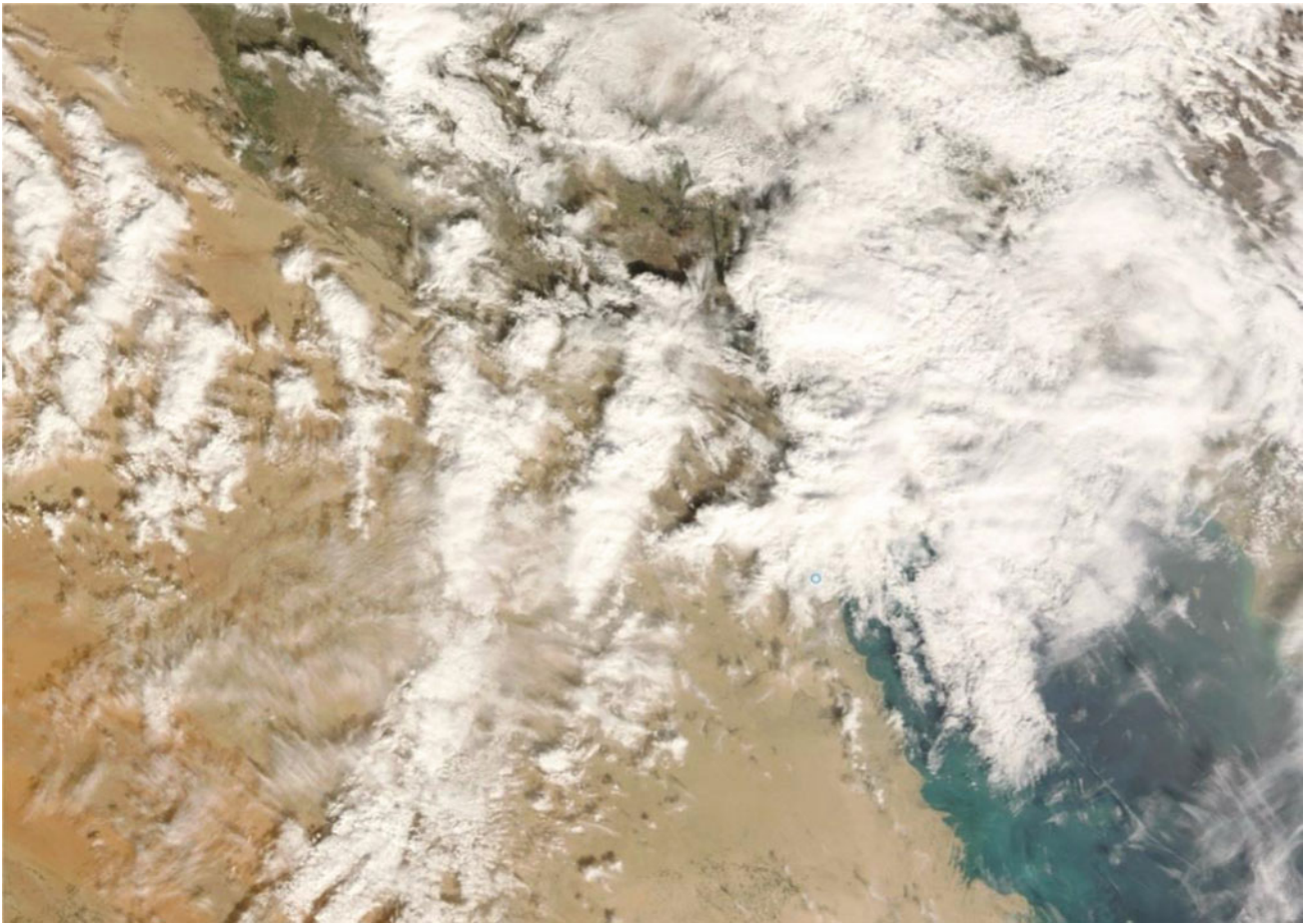


Fig. 1.27 MODIS image of dust storm that originated from the Western Desert of Iraq, covering southern Iraq, Kuwait, and the northern Arabian Gulf on 31st January 2010

- The west-northwest and west wind directions represent 16.1% each of the total hourly wind count for that day.
- The local prevailing wind direction (northwest, west-northwest) agrees with that deduced from the image over the area of the State of Kuwait.
- The northwest and west-northwest wind directions represent 35.9% and 32.2%, respectively, of the total hourly wind count for that day.

Satellite Images

A substantial unidirectional dust storm blowing from the northern Mesopotamian Floodplain and the Western Desert of Iraq toward Kuwait on 7th June 2010. This type of dust storm trajectory takes the wider form, covering more than 3000 km². The northwestern large trajectories blow normally in January, February, March, April, June, September, and October. The northwesterly trajectories' fallen dust is brighter in color, coarser in size fraction, with mud particles, contains more carbonates and clay but less quartz and feldspar minerals, has a higher particle surface area, and a high content of iron and organic matter compared with other trajectories toward Kuwait. The following weather data were recorded on 7th June 2010 (Fig. 1.37):

Satellite Images

A unidirectional dust storm blowing from northern Arabia and the Western Desert of Iraq toward Kuwait on 20th June 2010. This type of dust storm trajectory takes the wider form, covering more than 3000 km². The northwestern dust storm large trajectories blow normally in January, February, March, April, June, September, and October. Furthermore, moderate dust storm trajectories that cover an area of less than 3000 km² are familiar in March, May, June, July, and August. The northwesterly trajectories' fallen dust is brighter

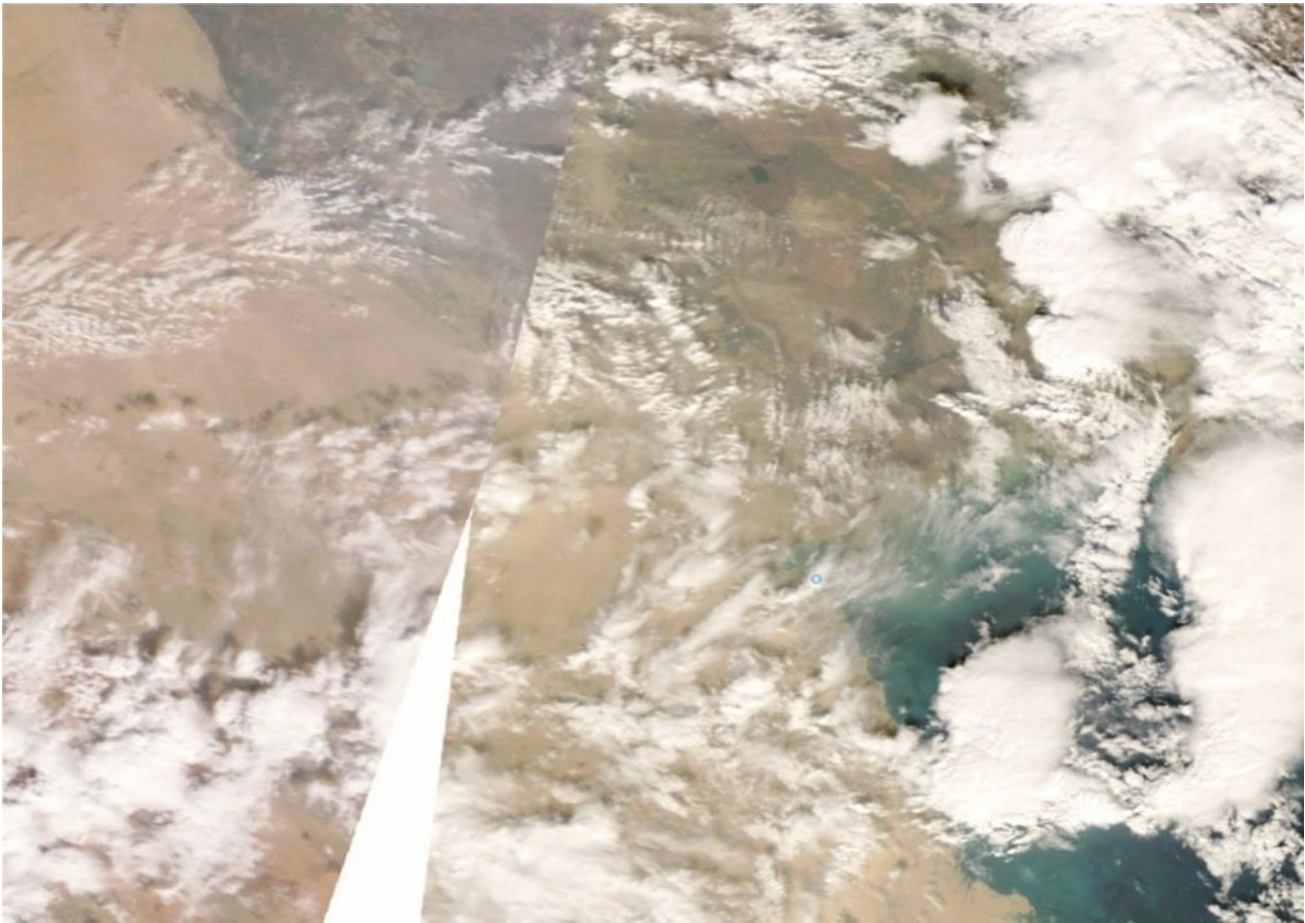


Fig. 1.28 MODIS image of dust storm that originated from the Western Desert of Iraq, covering southern Iraq, Kuwait, and the northern Arabian Gulf on 1st February 2010

in color, coarser in fraction size, with more sand particles, and contains more quartz and feldspars but fewer carbonates and clay minerals, has a lower particle surface area, and has less iron and organic matter compared with trajectories from the Mesopotamian Floodplain. The following weather data were recorded on 20th June 2010 (Fig. 1.38):

- Cloud cover obscured the area of concern.
- Prevailing wind direction: southeast-east, east, northeast-east.
- The southeast-east, east, and northeast-east wind directions represent 9.9%, 19.8%, and 13.5%, respectively, of the total hourly wind count for that day.

Satellite Images

A strong unidirectional dust storm blowing from northern Arabia and the Western Desert of Iraq toward Kuwait on 23rd July 2010. This type of dust storm trajectory takes the

wider form, covering more than 3000 km². The northwestern large trajectories blow normally in January, February, March, April, June, September, and October. Furthermore, moderate dust storm trajectories that cover an area of less than 3000 km² are familiar in March, May, June, July, and August. The northwesterly trajectories' fallen dust is brighter in color, coarser in fraction size, with more sand particles, contains more quartz and feldspars but fewer carbonates and clay minerals, has a lower particle surface area and less iron and organic matter in comparison with trajectories from the Mesopotamian Floodplain. The following weather data were recorded on 28th July 2010 (Fig. 1.39):

- Local prevailing wind direction (west, southwest-west) agrees with that deduced from the image. Note that there is a north wind component too.
- The west and southwest-west wind directions represent 21.9% and 21.3%, respectively, of the total hourly wind count for that day. The north component represents 9.9%.

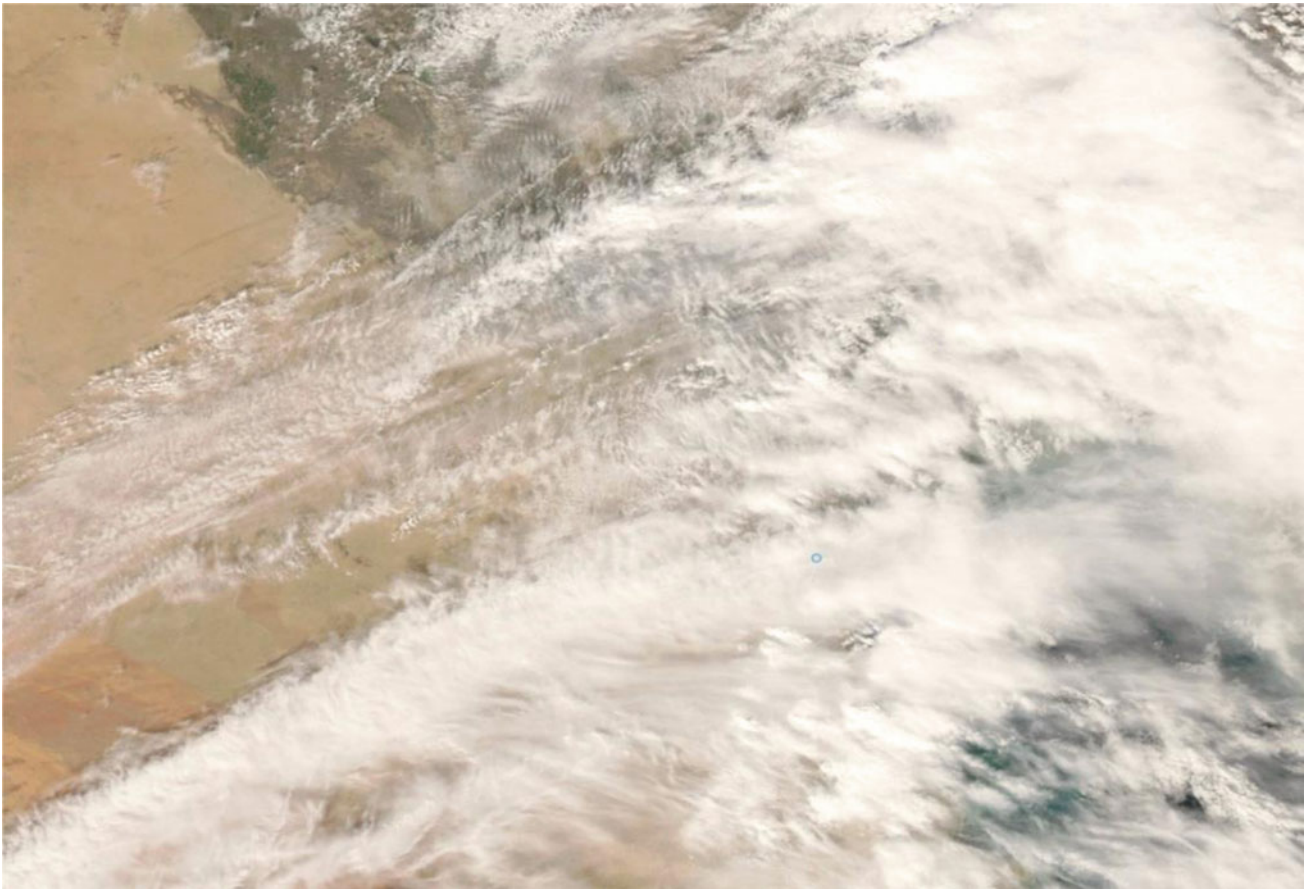


Fig. 1.29 MODIS image of dust storm that originated from the Western Desert of Iraq, covering southern Iraq, Kuwait, and the northern Arabian Gulf on 3rd February 2010

Satellite Images

A spiral multidirectional dust storm blowing from the southwest toward Kuwait on 29th July 2010. This type of dust storm trajectory is uncommon in the area. The trajectory takes the wider form, covering more than 3,000 km² and normally blows in January, February, March, April, June, September, and October. The northwesterly trajectories' fallen dust is brighter in color, coarser in fraction size, with more sand particles (diameter more than 0.063 mm), contains more quartz and feldspars but fewer carbonates and clay minerals, has a lower particle surface area, and less iron and organic matter when compared with trajectories from the Mesopotamian Floodplain. The following weather data were recorded on 29th July 2010 (Fig. 1.40):

- The local prevailing wind direction (south-southeast, southeast, east-southeast) agrees with that deduced from the image. Note that there is a huge west-southwest wind component.
- The south-southeast, southeast, and east-southeast wind directions represent 11.5%, 16.1%, and 14.1%, respectively, of the total hourly wind count for that day. The west-southwest component represents 14.6%.

Satellite Images

A small, unidirectional dust storm on 10th August 2010 that originated in southeastern Kuwait. The storm has a smaller trajectory, covering the southern area of Kuwait, but

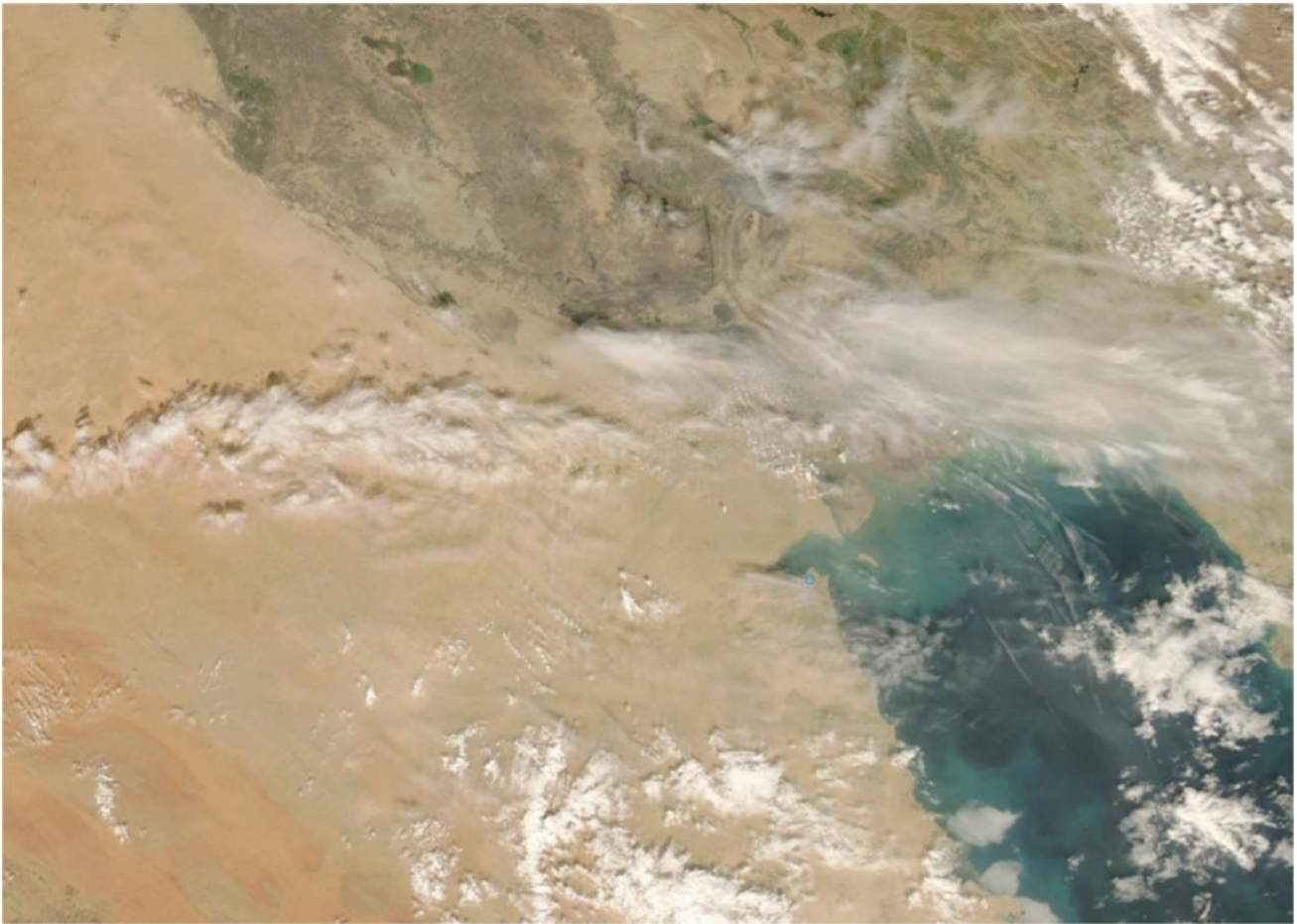


Fig. 1.30 MODIS image of dust storm that originated from the Western Desert of Iraq, covering southern Iraq, Kuwait, and the northern Arabian Gulf on 13th February 2010

contains the largest particles of dust, which have the highest quartz content and the smallest surface area compared with other trajectories. This type of trajectory is not in a straight line but is curved because of the wind from the sea. The settlement time is quick, as it contains large particles, mainly sand and coarse silt (Fig. 1.41).

The following weather data were recorded on 10th August 2010:

- The local prevailing wind direction: east, east-southeast, southeast. The skies reflect this direction (i.e., the wind is clear of sand), and this agrees with that deduced from the image. There is a northwest wind component.
- The southeast, east-southeast, east wind directions represent 13.0%, 13.0%, and 10.4%, respectively, of the total hourly wind count for that day. The northwest component represents 9.4%.

Satellite Images

A small dust storm that originated from a regional but short distance and local source areas of dust. This type of dust is brighter in color, has coarse size particles that contain more quartz but fewer carbonates and a lower surface area than from dust storms from the north and northeast. The following weather data were recorded on 31st August 2010 (Fig. 1.42):

- The local prevailing wind direction: west-northwest, west. The dominant wind speed category is 3.6–5.7 m/s; hence, not much dust is evident in the image.
- The west-northwest and west wind directions represent 30.2% and 26.0%, respectively, of the total hourly wind count for that day.

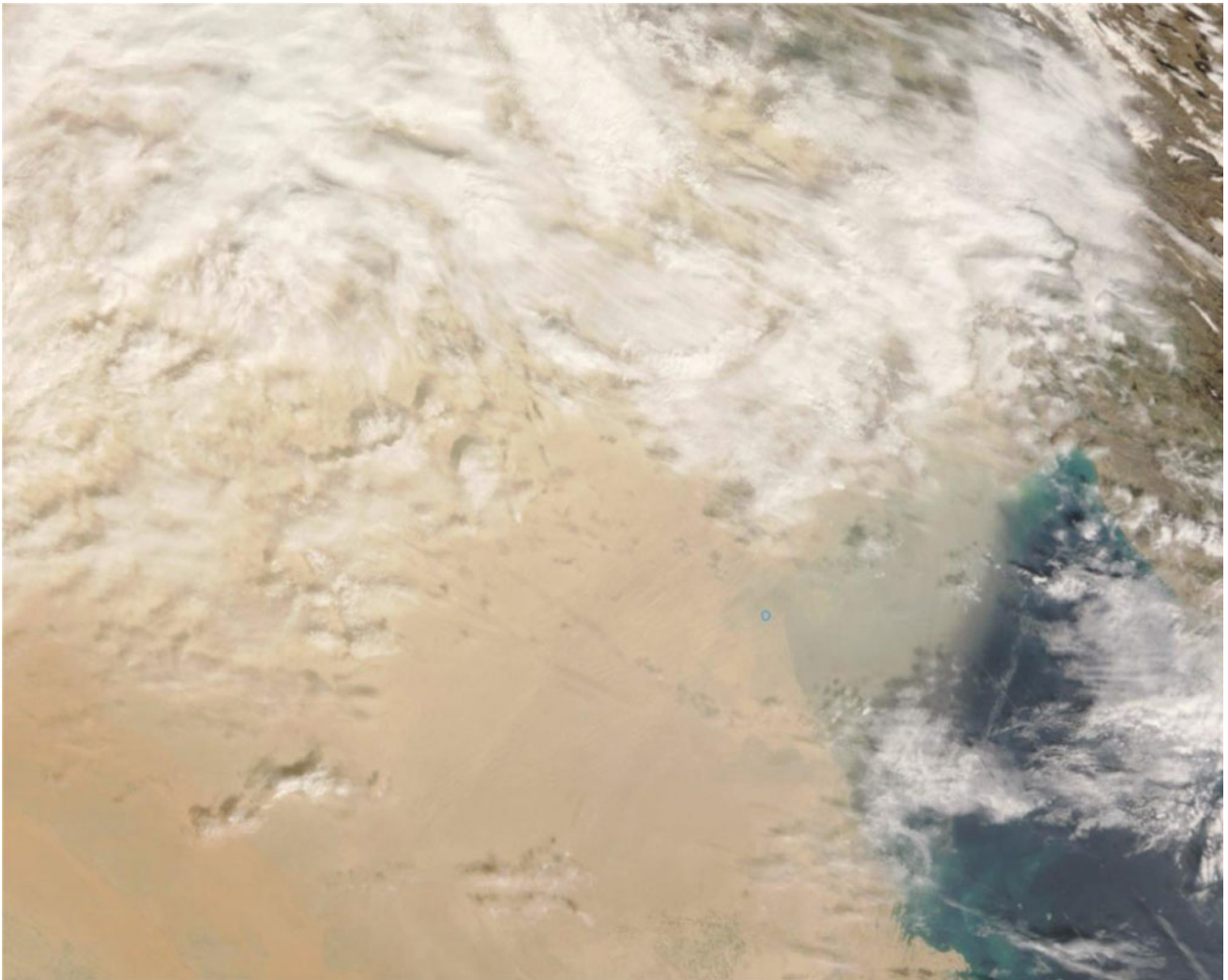


Fig. 1.31 MODIS image of dust storm that originated from the Western Desert of Iraq, covering southern Iraq, Kuwait, and the northern Arabian Gulf on 23rd February 2010

Satellite Images

A small dust storm blowing from the northwest, covering small areas less than 3000 km². This type of dust storm forms commonly from intermediate regional and local

source areas. This type of dust contains more quartz, fewer carbonates and heavy minerals, larger particles, has a smaller surface area and quicker settling time in comparison with broader scale dust storms from the same direction. The following weather data were recorded on 10th October 2010 (Fig. 1.43):

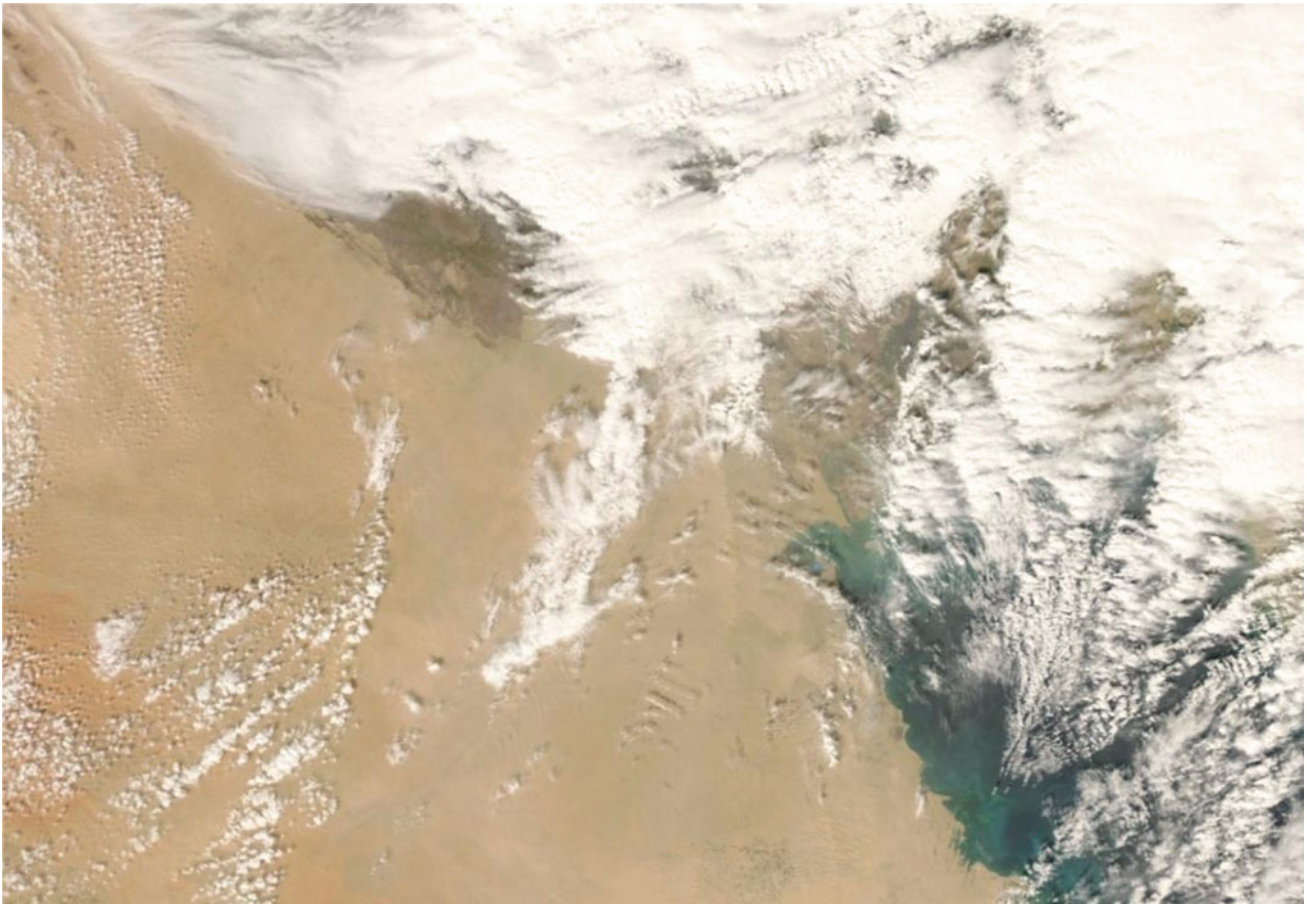


Fig. 1.32 MODIS image of dust storm that originated from the Western Desert of Iraq, covering southern Iraq, Kuwait, and the northern Arabian Gulf on 26th February 2010

- The local prevailing wind direction: northwest, north-northwest, north.
- The northwest, north-northwest, and north wind directions represent 19.3%, 22.9%, and 21.4%, respectively, of the total hourly wind count for that day.

Satellite Images

A strong unidirectional dust storm blowing from northern Arabia and the Western Desert of Iraq toward Kuwait and the Arabian Gulf on 13th December 2010. This type of dust

storm trajectory takes the wider form, covering more than 3,000 km² (Fig. 1.44).

The following weather data were recorded on 13th December 2010:

- The local prevailing wind direction (northwest, west-northwest) agrees with that deduced from the image. Note that there is a huge south-southeast wind component.
- The northwest and west-northwest wind directions represent 24.5% and 30.7%, respectively, of the total hourly wind count for that day. The south-southeast component represents 17.7%.

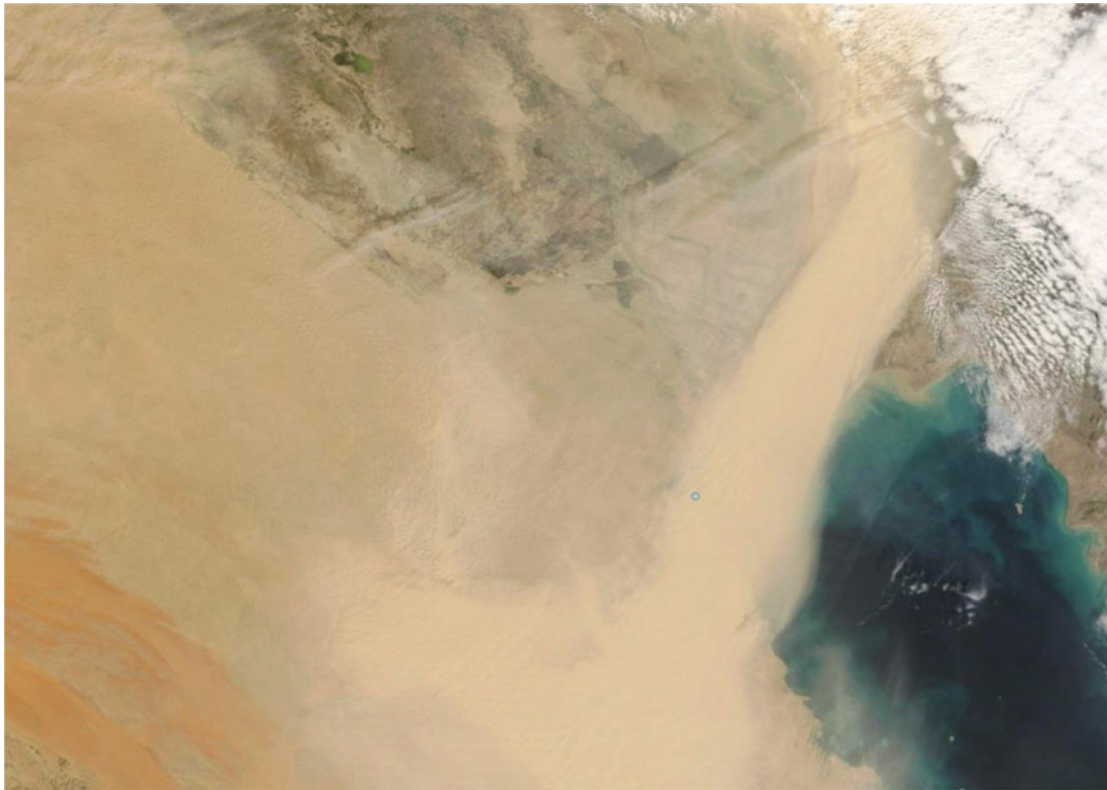


Fig. 1.33 MODIS image of dust storm that originated from the Western Desert of Iraq, covering southern Iraq, Kuwait, and the northern Arabian Gulf on 4th March 2010

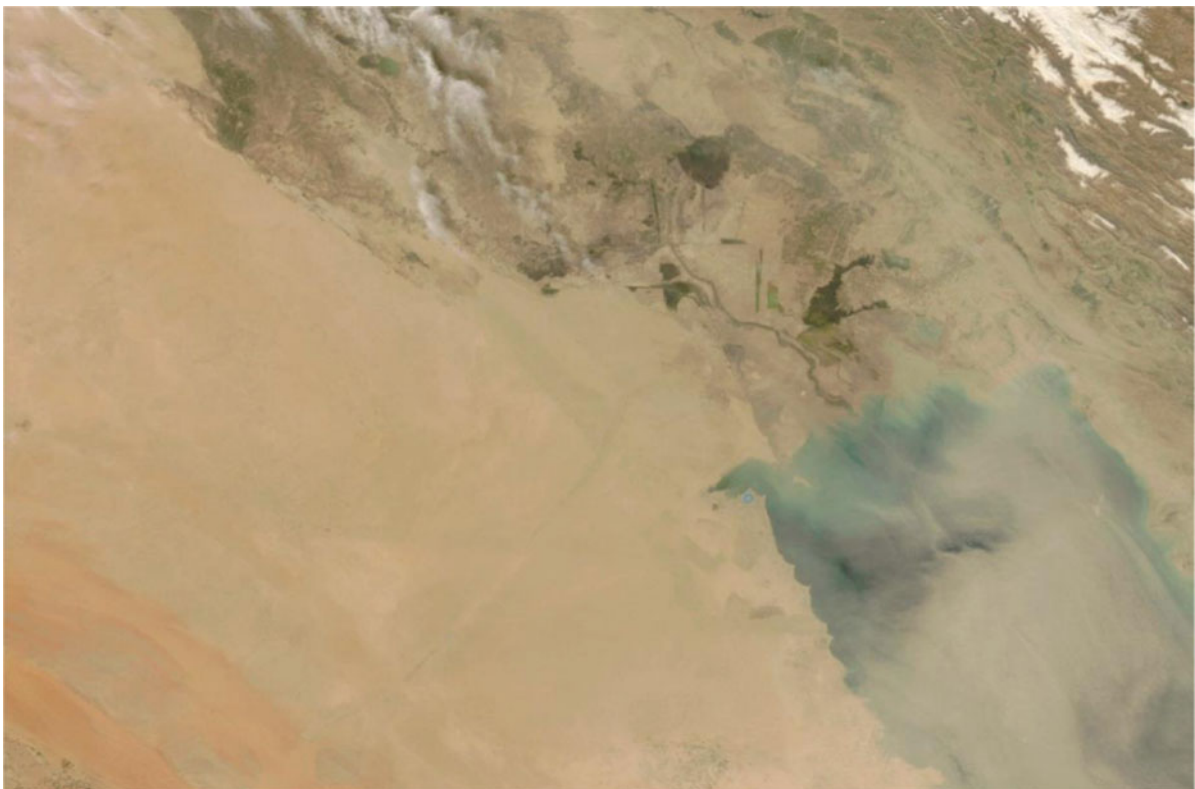


Fig. 1.34 MODIS image of dust storm that originated from the Western Desert of Iraq, covering southern Iraq, Kuwait, and the northern Arabian Gulf on 5th March 2010

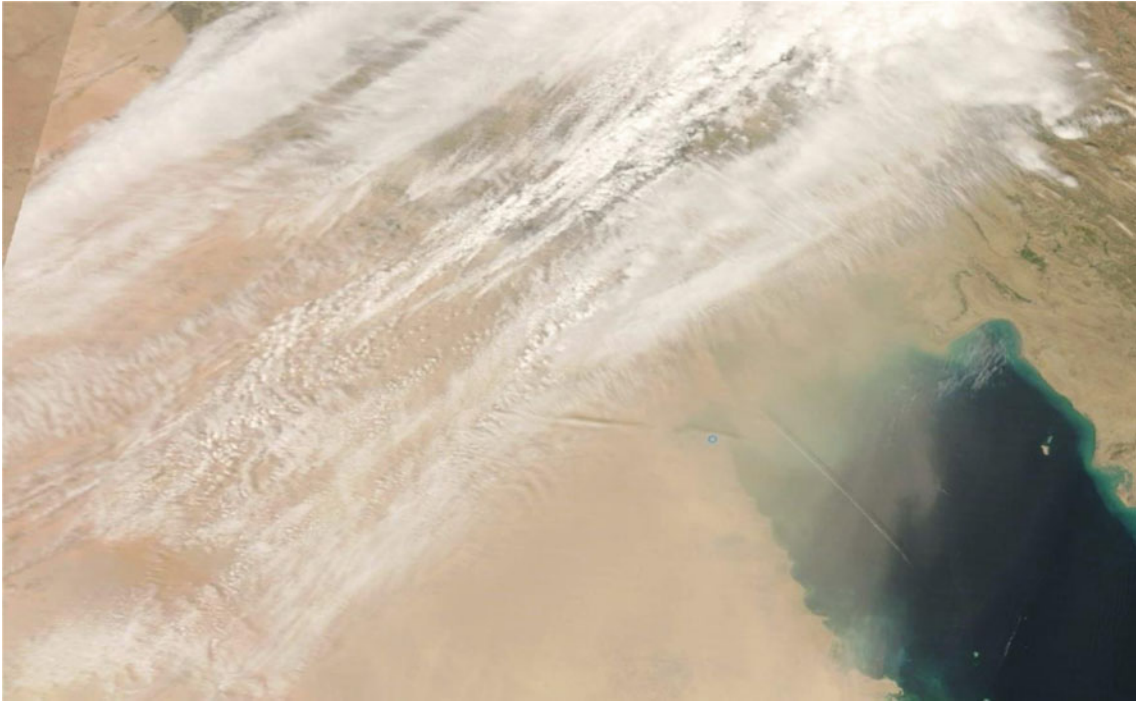


Fig. 1.35 MODIS image of dust storm that originated from the Western Desert of Iraq, covering southern Iraq, Kuwait, and the northern Arabian Gulf on 19th March 2010

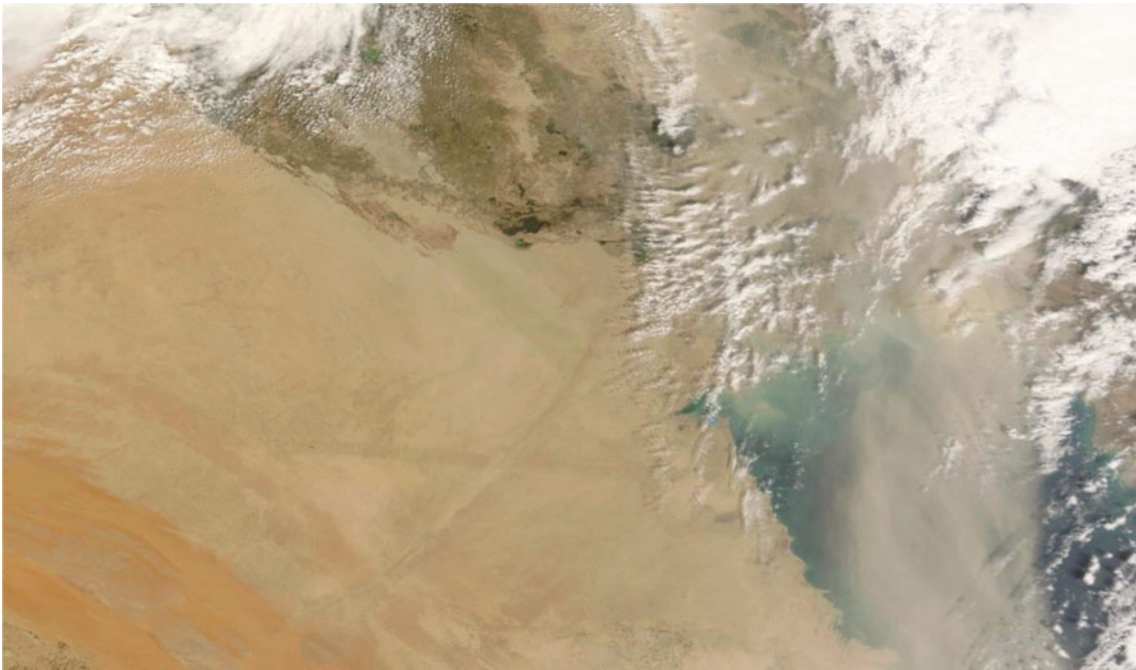


Fig. 1.36 MODIS image of dust storm that originated from the Western Desert of Iraq, covering southern Iraq, Kuwait, and the northern Arabian Gulf on 27th March 2010



Fig. 1.37 MODIS image of dust storm that originated from the Western Desert of Iraq, covering southern Iraq, Kuwait, and the northern Arabian Gulf on 7th June 2010

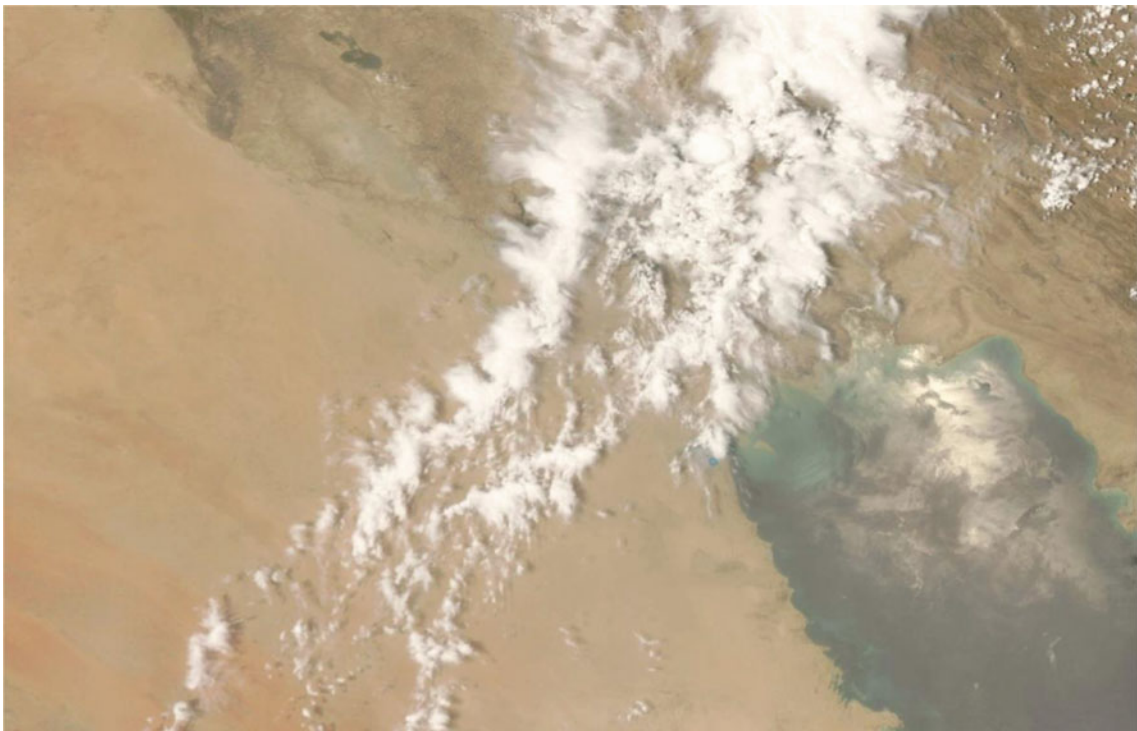


Fig. 1.38 MODIS image of dust storm that originated from the Western Desert of Iraq, covering southern Iraq, Kuwait, and the northern Arabian Gulf on 20th June 2010



Fig. 1.39 MODIS image of dust storm that originated from the Western Desert of Iraq, covering southern Iraq, Kuwait, and the northern Arabian Gulf on 28th July 2010

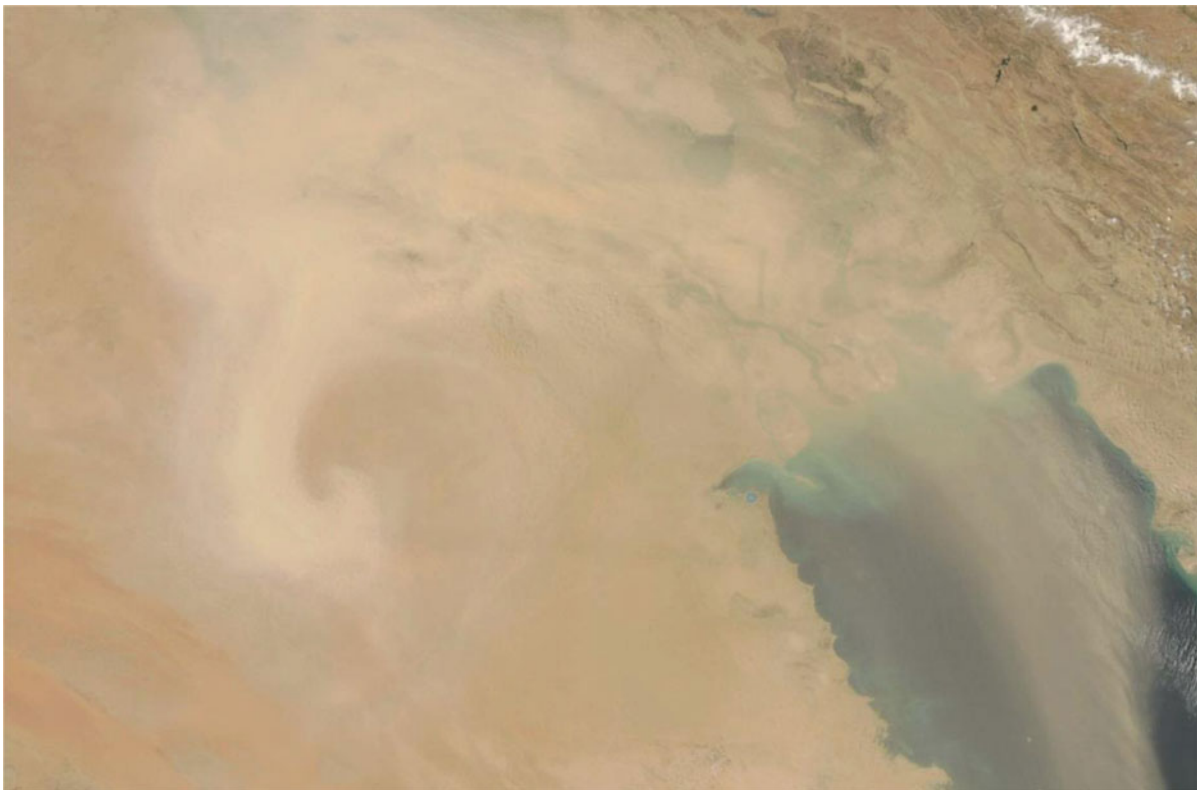


Fig. 1.40 MODIS image of dust storm that originated from the Western Desert of Iraq, covering southern Iraq, Kuwait, and the northern Arabian Gulf on 29th July 2010

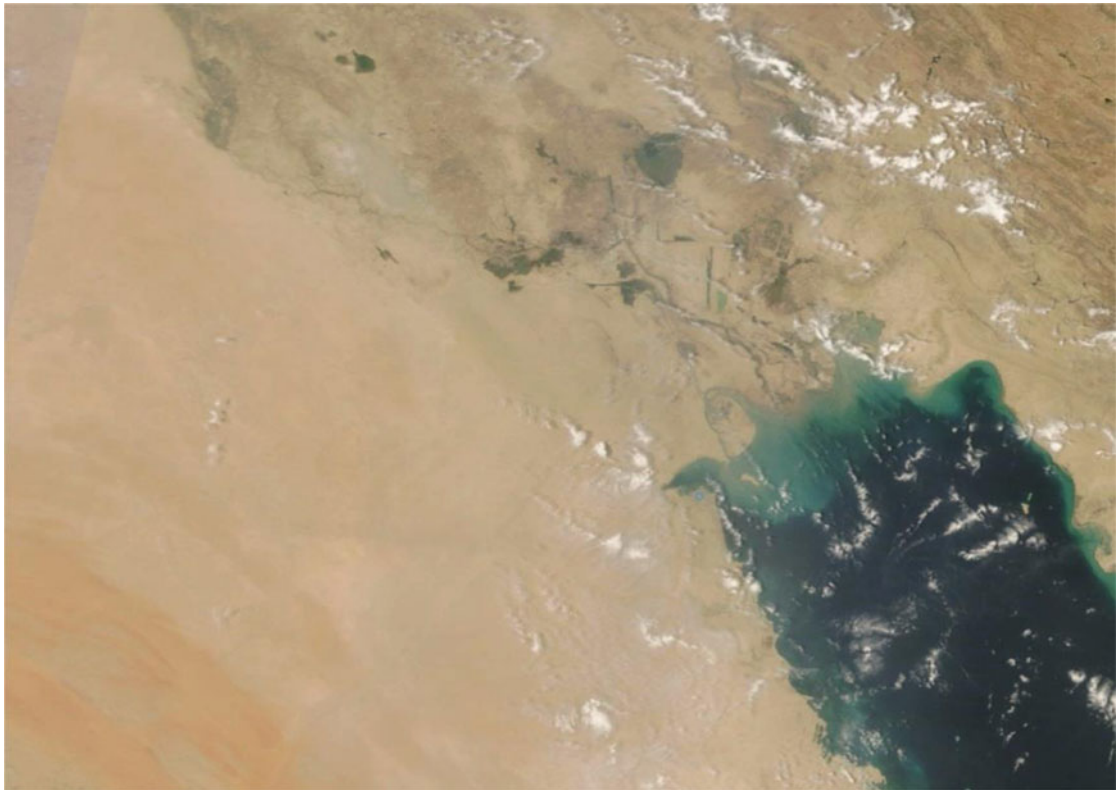


Fig. 1.41 Satellite image showing the State of Kuwait and surroundings—taken on 10th August 2010



Fig. 1.42 Satellite image showing the State of Kuwait and surroundings—taken on 31st August 2010

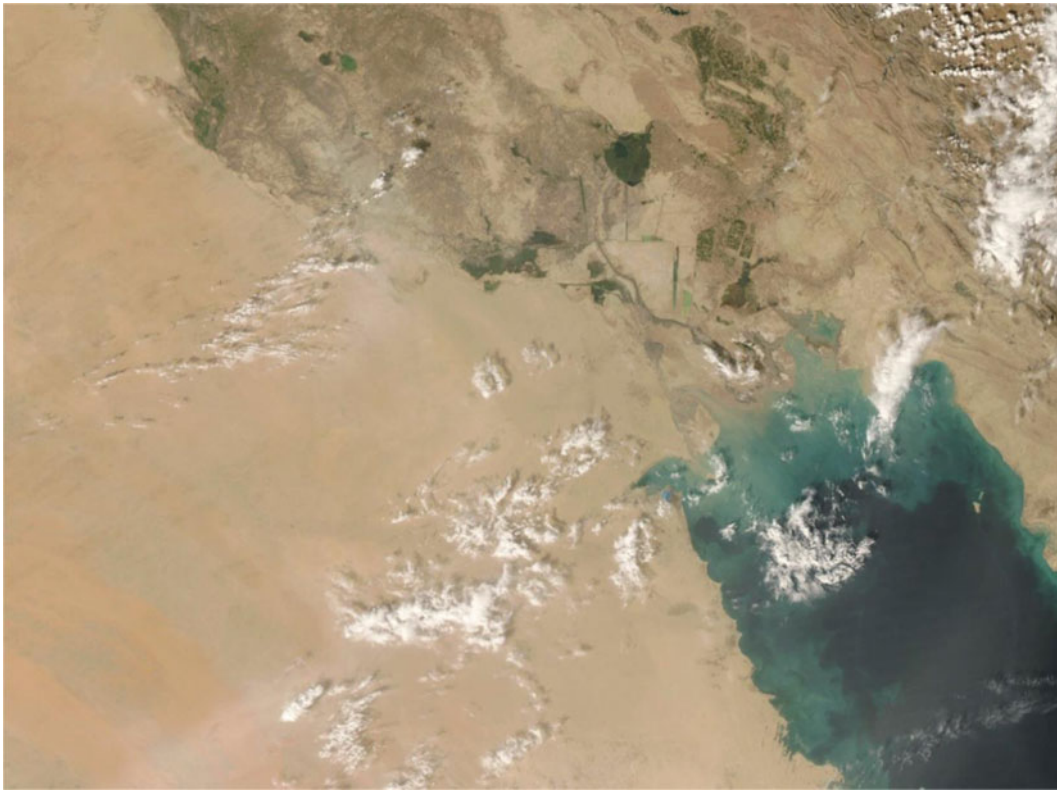


Fig. 1.43 Satellite image showing the State of Kuwait and surroundings—taken on 10th October 2010

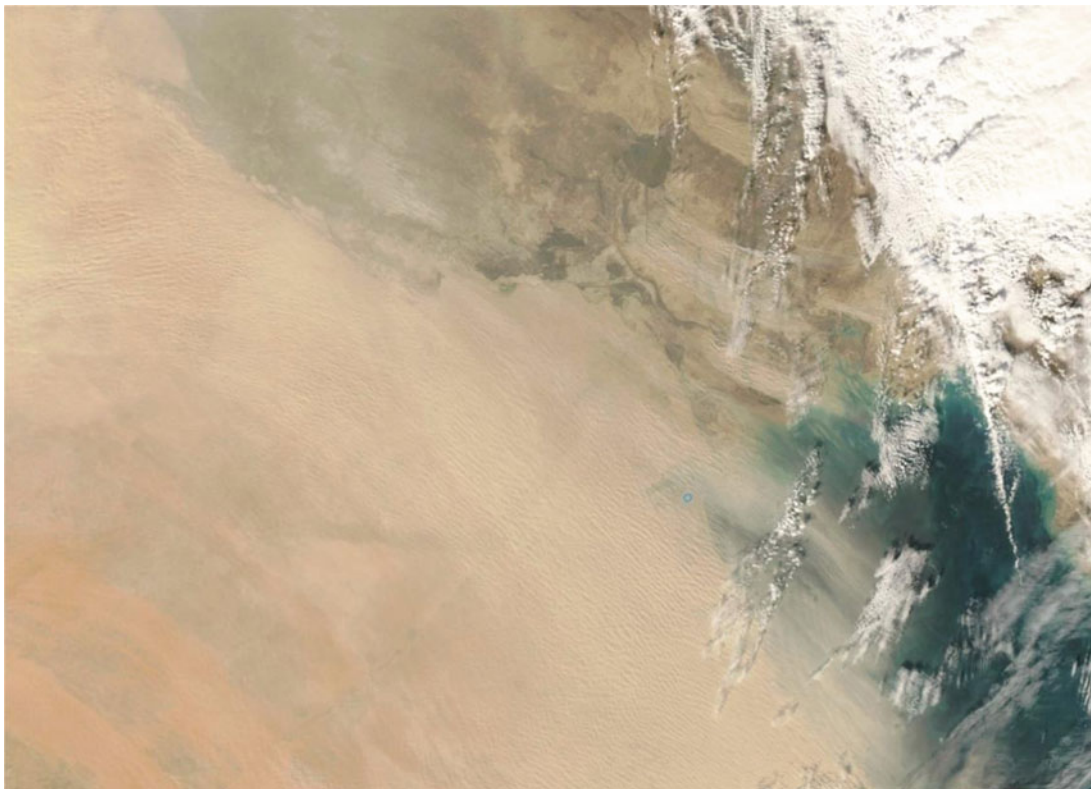


Fig. 1.44 Satellite image showing the State of Kuwait and surroundings—taken on 13th December 2010

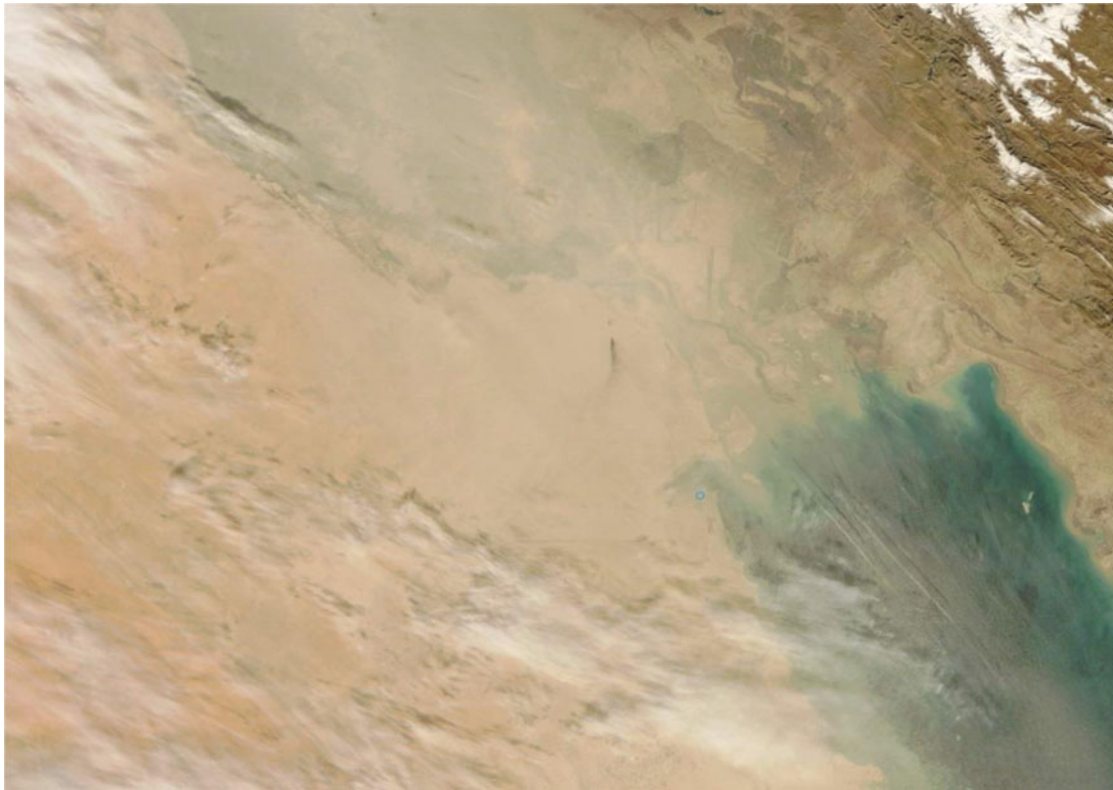


Fig. 1.45 Satellite image showing the State of Kuwait and surroundings—taken on 14th December 2010

Satellite Images

A unidirectional dust storm blowing from northern Arabia and the Western Desert of Iraq toward Kuwait on 14th December 2010. This dust storm trajectory takes the wider form and blows normally in January, February, March, April, June, September, and October. Additionally, moderate trajectories are common in March, May, June, July, and August. The dust in these trajectories is brighter in color, coarser in fraction size, with more sand particles, contains more quartz and feldspars but fewer carbonates and clay minerals, has a lower particle surface area, and less iron and organic matter when compared with trajectories from the Mesopotamian Floodplain. The following weather data were recorded on 14th December 2010 (Fig. 1.45):

- The local prevailing wind direction (west-northwest, northwest, north-northwest) agrees with that deduced from the image.
- The west-northwest, northwest, and north-northwest wind directions represent 29.7%, 29.2%, and 19.8%, respectively, of the total hourly wind count for that day.

References

- Ahmed, M., & Al-Dousari, A. (2013). Geomorphological characteristics of the Um-Rimam depression in northern Kuwait. *Kuwait Journal of Science*, 40(1), 165–178.
- Al-Awadhi, J. (2005). Dust fallout characteristics in Kuwait: A case study. *Kuwait Journal of Science and Engineering*, 32(2), 135–152. ISSN: 1024–8684.
- Al-Awadhi, J. M., & Al-Dousari, A. M. (2013). Morphological characteristics and development of coastal nabkhas, north-east Kuwait. *International Journal of Earth Sciences*, 102(3), 949–958. <https://doi.org/10.1007/s00531-012-0833-9>.
- Al-Awadhi, J. M., Al-Dousari, A. M., & Khalaf, F. I. (2014). Influence of land degradation on the local rate of dust fallout in Kuwait. *Atmospheric and Climate Sciences*, 4(03), 437–446. <https://doi.org/10.4236/acs.2014.43042>.
- Al-Dabbas, M., Abbas, M. A., & Al-Khafaji, R. (2011). The mineralogical and micro-organisms effects of regional dust storms over Middle East region. *International Journal of Water Resources and Arid Environments* 1.2 (2011), 129–141. ISSN 2079-7079
- Al-Dousari, A. M., Al-Enezi, A., & Al-Awadhi, J. M. (2008). Textural variations within different representative types of dunes in Kuwait. *Arabian Journal of Geosciences*, 1, 17–31. <https://doi.org/10.1007/s12517-008-0002-4>.
- Al-Dousari, A., & Al-Hazza, A. (2013). Physical properties of aeolian sediments within major dune corridor in Kuwait. *Arabian Journal of Geosciences*, 6(2), 519–527. <https://doi.org/10.1007/s12517-011-0353-0>.

- Al-Dousari, A., Doronzo, D., & Ahmed, M. (2017). Types, indications and impact evaluation of sand and dust storms trajectories in the Arabian Gulf. *Sustainability*, 9(9), 1526. <https://doi.org/10.3390/su9091526>.
- Al-Dousari, A. M., Ahmed, N.-D., & Al-Awadhi, S. (2018). Native plants in Kuwait: environmental and economic perspective. *Journal of the Gulf and Arabian Peninsula Studies*, 44(168), 277–310.
- Al-Dousari, A. M., M. I. Ibrahim, Al-Dousari, N., Ahmed, M., & Al-Awadhi, S. (2018b). Pollen in aeolian dust with relation to allergy and asthma in Kuwait. *Aerobiologia*, 1–12. <https://doi.org/10.1007/s10453-018-9516-8>.
- Al-Dousari, A. M., & Al-Awadhi, J. (2012). Dust fallout in northern Kuwait: Major sources and characteristics. *Kuwait Journal of Science*, 39, 171–187.
- Al-Dousari, A. M. (2009). Section III: Recent studies on dust fallout within preserved and open areas in Kuwait. In N.R. Bhat, A.Y. Al-Nasser, & S. Omar (Eds.), *Desertification in Arid lands: Causes, consequences and mitigation* (pp. 137–148). Kuwait: Kuwait Institute for Scientific Research.
- Al-Ghadban, A. N., Uddin, S., Beg, M. U., Al-Dousari, A. M., Gevao, B., & Al-Yamani, F. (2008). Ecological consequences of river manipulations and drainage of Mesopotamian marshes on the Arabian Gulf ecosystem: Investigations on changes in sedimentology and environmental quality, with special reference to Kuwait Bay. *Kuwait Institute for Scientific Research (KISR)*, 9362, 1–141. <https://doi.org/10.13140/RG.2.2.10969.62562>.
- Alpert, P., Kaufman, Y. J., El-Shay, Y., Tanre, D., da Silva, A., Schubert, S., & Joseph, J. H. (1998). Quantification of dust-forced heating of the lower troposphere. *Nature*, 394, 367–370. <https://doi.org/10.1038/26456>.
- Awadh, S. M. (2012). Geochemistry and mineralogical composition of the airborne particles of sand dunes and dust storms settled in Iraq and their environmental impacts. *Environmental Earth Sciences*, 66(8), 2247–2256. <https://doi.org/10.1007/s12665-011-1445-6>.
- Boucher, O., & Haywood, J. (2001). On summing the components of radiative forcing of climate change. *Climate Dynamics*, 18, 297–302. <https://doi.org/10.1007/s003820100185>.
- Boyles, R. P., & Raman, S. (2003). Analysis of climate trends in North Carolina (1949–1998). *Environment International*, 29(2003), 263–275. [https://doi.org/10.1016/S0160-4120\(02\)00185-X](https://doi.org/10.1016/S0160-4120(02)00185-X).
- Chi, K. H., Hsu, S. C., Wang, S. H., & Chang, M. B. (2008). Increases in ambient PCDD/F and PCB concentrations in Northern Taiwan during an Asian dust storm episode. *Science of the Total Environment*, 401(1–3), 100–108. <https://doi.org/10.1016/j.scitotenv.2008.03.041>.
- Chrysikou, L. P., Gemenetzi, P. G., & Samara, C. A. (2009). Wintertime size distribution of polycyclic aromatic hydrocarbons (PAHs), polychlorinated biphenyls (PCBs) and organochlorine pesticides (OCP) in the urban environment: Street—vs rooftop-level measurements. *Environmental Pollution*, 43, 290–300. <https://doi.org/10.1016/j.atmosenv.2008.09.048>.
- Di-Iella, L., Protano, G., Loppi, S., & Riccobono, F. (2006). Toxic trace elements and organic compounds in the ambient air of Kabul, Afghanistan. *Atmospheric Environment*, 40(2), 225–237. <https://doi.org/10.1016/j.atmosenv.2005.09.052>.
- Diner, D., Beckert, J., Reilly, T. H., Bruegge, C., Conel, J. E., Kahn, R. A., et al. (1998). Multi-angle Imaging SpectroRadiometer (MISR) Instrument Description and experiment overview. *IEEE Transactions Geoscience Remote Sensing*, 36, 1072–1087. <https://doi.org/10.1109/36.700992>.
- Diner, D., Martonchik, J. J., Kahn, R. A., Verstraete, M., & Pinty, B. (2002). Characterization of tropospheric aerosols: new insights from MISR on Terra. *AGU fall meeting Abstracts*.
- Dockery, D. W., Pope, C. A., Xiping, X., Spengler, J. D., Ware, J. H., Fay, M. E., et al. (1993). An association between air pollution and mortality in six US cities. *The New England Journal of Medicine*, 329, 1753–1759. <https://doi.org/10.1056/NEJM199312093292401>.
- Foda, M. A., Khalaf, F. I., & Al-Kadi, A. S. (1985). Estimation of dust fallout rates in the northern Arabian Gulf. *Sedimentology*, 32, 595–603. <https://doi.org/10.1111/j.1365-3091.1985.tb00473.x>.
- Garrison, V. H., Foreman, W. T., Genualdi, S., Griffin, D. W., Kellogg, C. A., Majewski, M. S., et al. (2006). Sahara dust—A carrier of persistent organic pollutants, metals and microbes to the Caribbean. *International Journal of Tropical Biology and Conservation*, 54 (Supplement 3), 9–21. <https://doi.org/10.15517/rbt.v54i3.26867>.
- Gevao, B., Al-Ghadban, A. N., Uddin, S., Jaward, F. M., Bahloul, M., & Zafar, J. (2011). Polybrominated diphenyl ethers (PBDEs) in soils along a rural-urban-rural transect: Sources, concentration gradients, and profiles. *Environmental Pollution*, 159, 3666–3672. <https://doi.org/10.1016/j.envpol.2011.07.021>.
- Goudie, A. S., & Middleton, N. J. (2001). Saharan dust storms: Nature and consequences. *Earth-Science Reviews*, 56, 179–204. [https://doi.org/10.1016/S0012-8252\(01\)00067-8](https://doi.org/10.1016/S0012-8252(01)00067-8).
- Griffin, D. W. (2007). Atmospheric movement of microorganisms in clouds of desert dust and implications for human health. *Clinical Microbiology Reviews*, 20(3), 459–477. <https://doi.org/10.1128/CMR.00039-06>.
- Griffin, D. W., Kellogg, C. A., Garrison, V. H., & Shinn, E. A. (2002). The global transport of dust. *American Scientist*, 90, 228–235. <https://doi.org/10.1511/2002.3.228>.
- Hansen, J., Sato, M., Lacis, A., Ruedy, R., Tegen, I., & Mathews, E. (1998). Climate forcings in the industrial era. *Proceedings National Academy of Science*, 95, 12753–12758. <https://doi.org/10.1073/pnas.95.22.12753>.
- Hu, D., Qiao, L., Chen, J., Ye, X., Yang, X., Cheng, T., & Fang, W. (2010). Hygroscopicity of inorganic aerosols: Size and relative humidity effects on the growth factor. *Aerosol and Air Quality Research*, 10, 255–264. <https://doi.org/10.4209/aaqr.2009.12.0076>.
- Hurtado, E., Vidal, A., & Caselles, V. (1996). Comparison of two atmospheric correction methods for Landsat TM thermal band. *International Journal of Remote Sensing*, 17, 237–247. <https://doi.org/10.1080/01431169608949002>.
- Kahn, R., & Braverman, A. (1998). What shall we do with the data we are expecting from upcoming earth observation satellites? *Journal of Computational and Graphical Statistics*, 8. <https://doi.org/10.1080/10618600.1999.10474834>.
- Kahn, R. A., Gaitley, B. J., Martonchik, J. V., Diner, D. J., Crean, K. A., & Holben, B. (2005a). MISR global aerosol optical depth validation based on two years of coincident Aeronet observations. *Journal Geophysical Research*, 110, D10S04. <https://doi.org/10.1029/2004JD004706>.
- Kahn, R., Banerjee, P., & McDonald, D. (2001). The sensitivity of Multiangle Imaging to natural mixtures of aerosols over ocean. *Journal Geophysical Research*, 106, 18219–18238. <https://doi.org/10.1029/2000JD900497>.
- Kahn, R., Banerjee, P., McDonald, D., & Diner, D. (1998). Sensitivity of multiangle imaging to aerosol optical depth, and to pure-particle size distribution and composition over ocean. *Journal of Geophysical Research*, 103(D24), 32195–32213. <https://doi.org/10.1029/98JD01752>.
- Kahn, R., Li, W.-H., Martonchik, J., Bruegge, C., Diner, D., Gaitley, B., et al. (2005). MISR low-light-level calibration, and implications for aerosol retrieval over dark water. *Journal of Atmospheric Sciences*, 62, 1032–1062. <https://doi.org/10.1175/JAS3390.1>.
- Katz, M., & Chan, C. (1980). Comparative distribution of eight polycyclic aromatic hydrocarbons in airborne particulates collected by conventional high-volume sampling and by size fractionation. *Environmental Science and Technology*, 14, 838–843. <https://doi.org/10.1021/es60167a010>.

- Kaufman, Y. J., Tanré, D., Remer, L., Vermote, E. F., Chu, A., & Holben, B. N. (1997). Operational remote sensing of tropospheric aerosol over the land from EOS-MODIS. *Journal of Geophysical Research*, *102*, 17051–17068. <https://doi.org/10.1029/96JD03988>.
- King, M. D., Menzel, W. P., & Tanré, D. (1992). Remote sensing of cloud, aerosol, and water vapor properties from the Moderate Resolution Imaging Spectrometer (MODIS). *IEEE Transactions on Geoscience and Remote Sensing*, *30*, 2–27. <https://doi.org/10.1109/36.124212>.
- King, M. D., Kaufman, Y. J., Tanré, D. A., & Nakajima, T. (1999). Remote sensing of tropospheric aerosols from space: Past, present, and future. *Bulletin of the American Meteorological Society*, *80*(11), 2229–2259. [https://doi.org/10.1175/1520-0477\(1999\)080%3c2229:RSOTAF%3e2.0.CO;2](https://doi.org/10.1175/1520-0477(1999)080%3c2229:RSOTAF%3e2.0.CO;2).
- Lewis, R. G., Fortune, C. R., Willis, R. D., Camann, D. E., & Antley, J. T. (1999). Distribution of pesticides and polycyclic aromatic hydrocarbons in house dust as a function of particle size. *Environmental Health Perspective*, *107*, 721–726. <https://doi.org/10.1289/ehp.99107721>.
- Li, X., Maring, H., Savoie, D., Voss, K., & Prospero, J. M. (1996). Dominance of mineral dust in aerosol light-scattering in the North Atlantic trade winds. *Nature*, *380*, 416–419. <https://doi.org/10.1038/380416a0>.
- Liu, Y., Sarnat, J., Kilaru, V., Jacob, D., & Koutrakis, P. (2005). Estimating ground-level PM_{2.5} in the eastern United States using satellite remote sensing. *Environment Science and Technology*, *39* (9), 3269–3278. <https://doi.org/10.1021/es049352m>.
- Liu, Y., Kahn, R. A., Chaloulakou, A., & Koutrakis, P. (2009). Analysis of the impact of the forest fires in August 2007 on air quality of Athens using multi-sensor aerosol remote sensing data, meteorology and surface observations. *Atmospheric Environment*, *43*(21), 3310–3318. <https://doi.org/10.1016/j.atmosenv.2009.04.010>.
- Liu, Y., Kahn, R., & Koutrakis, P. (2007). Estimating PM_{2.5} component concentrations and size distributions using satellite retrieved fractional aerosol optical depth: Part I—Method development. *Journal of the Air and Waste Management Association*, *57* (11), 1351–1359. <https://doi.org/10.3155/1047-3289.57.11.1351>.
- Liu, Y., Park, R. J., Jacob, D. J., Li, Q. B., Kilaru, V., & Sarnat, J. A. (2004). Mapping annual mean ground-level PM_{2.5} concentrations using Multiangle Imaging Spectroradiometer aerosol optical thickness over the contiguous United States. *Journal of Geophysical Research: Atmospheres*, *109*(D22): Art. No. D22206. <https://doi.org/10.1029/2004jd005025>.
- Martonchik, J., Diner, D., Kahn, R., Gaitley, B., & Holben, B. (2004). Comparison of MISR and AERONET aerosol optical depths over desert sites. *Geophysical Research Letters*, *31*(16): Art. No. L16. <https://doi.org/10.1029/2004GL019807>.
- Meng and Lu. (2007). Dust events as a risk factor for daily hospitalization for respiratory and cardiovascular diseases in Minqin, China. *Atmospheric Environment*, *41*, 7048–7058. <https://doi.org/10.1016/j.atmosenv.2007.05.006>.
- Miller, R. L., & Tegen, I. (1998). Climate response to soil dust aerosols. *Journal of Climate*, *11*, 3247–3267. [https://doi.org/10.1175/1520-0442\(1998\)011%3C3247:CRTSDA%3E2.0.CO;2](https://doi.org/10.1175/1520-0442(1998)011%3C3247:CRTSDA%3E2.0.CO;2).
- Moulin, C., Lambert, C. E., Dulac, F., & Dayan, U. (1997). Control of atmospheric export of dust by North Atlantic oscillation. *Nature*, *387*, 691–694. <https://doi.org/10.1038/42679>.
- Offenberg, J. H., & Baker, J. E. (1999). Aerosol size distributions of polycyclic aromatic hydrocarbons in urban and over-water atmospheres. *Environment Science and Technology*, *33*, 3324–3331. <https://doi.org/10.1021/es990089c>.
- Peterson, S. T., & Junge, C. E. (1971). Sources of particulate matter in the atmosphere. In W. W. Kellogg & G. D. Robinson (Eds.), *Man's Impact on the Climate* (pp. 310–320). MIT Press.
- Pierson, D. C., Markensten, H., & Strömbeck, N. (2003). Long and short term variations in suspended particulate material: The influence on light available to the phytoplankton community. *Hydrobiologia*, *494*, 299–304. <https://doi.org/10.1023/A:1025455424972>.
- Pope, C. A., III., & Dockery, D. W. (2006). Health effects of fine particulate air pollution: Lines that connect. *Journal of the Air and Waste Management Association*, *56*, 709–742. <https://doi.org/10.1080/10473289.2006.10464485>.
- Pope, C. A., Burnett, R. T., Thun, M. J., Calle, E. E., Krewski, D., Ito, K., & Thurston, G. D. (2002). Lung cancer, cardiopulmonary mortality, and long-term exposure to fine particulate air pollution. *Journal of the American Medical Association*, *287*, 1132–1141. <https://doi.org/10.1001/jama.287.9.1132>.
- Prasad, A. K., & Singh, R. P. (2007). Comparison of MISR-MODIS aerosol optical depth over the Indo-Gangetic basin during the winter and summer seasons (2000–2005). *Remote Sensing of Environment*, *107*, 109–119. <https://doi.org/10.1016/j.rse.2006.09.026>.
- Prospero, J. M., Ginoux, P., Torres, O., Sharon E. Nicholson, S. E., & Gill, T. E. (2002). Environmental characteristics of global sources of atmospheric soil dust identified with the Nimbus 7 Total Ozone Mapping Spectrometer (TOMS) absorbing aerosol product. *Reviews of Geophysics*, *40*, February 1, 2002. <https://doi.org/10.1029/2000RG000095>.
- Ramanathan, V., Ramana, M. V., Roberts, G., Kim, D., Corrigan, C., Chung, C., & Winker, D. (2007). Warming trends in Asia amplified by brown cloud solar absorption. *Nature*, *448*, 575–578. <https://doi.org/10.1038/nature06019>.
- Reynolds, K. A., & Pepper, I. L. (2000). *Microorganisms in the environment*. San Diego, CA: Academic Press.
- Ridgwell, A. J. (2002). Dust in Earth system: The biogeochemical linking of land, air and sea. *Philosophical Transactions of Royal Society London*, *360*, 2905–2924. <https://doi.org/10.1098/rsta.2002.1096>.
- Safar, M. I. (1980). *Frequency of dust in day-time summer in Kuwait*. Kuwait: Directorate General of Civil Aviation.
- Seinfeld, J. H., & Pandis, S. N. (1998). *Atmospheric chemistry and physics: From air pollution to global change*. New York: Wiley.
- Trenberth, K., & Hurrell, J. W. (1994). Decadal atmosphere-ocean variations in the Pacific. *Climate Dynamics*, *9*, 303–319. <https://doi.org/10.1007/BF00204745>.
- Venkataraman, C., Thomas, S., & Kulkarni, P. (1999). Size distributions of polycyclic aromatic hydrocarbons gas/particle partitioning to urban aerosols. *Journal of Aerosol Science*, *30*, 759–770. [https://doi.org/10.1016/S0021-8502\(98\)00761-7](https://doi.org/10.1016/S0021-8502(98)00761-7).
- Walker, P. H., & Costin, A. B. (1971). Atmospheric dust accession in south-eastern Australia. *Australian Journal of Soil Research*, *9*, 1–5. <https://doi.org/10.1071/SR9710001>.
- WHO. (2005). Air quality guidelines for particulate matter, ozone, nitrogen dioxide and sulfur dioxide. Global update 2005. World Health Organization, Geneva, Switzerland.
- Wilkerson, W. D. (1991). Dust and sand forecasting in Iraq and adjoining countries. USAF Environmental Technical Applications Center, 72 pp.
- Williamson, K. E., Wommack, K. E., & Radosevich, M. (2003). Sampling natural viral communities from soil for culture-independent analyses. *Applied Environmental Microbiology*, *69*, 6628–6633. <https://doi.org/10.1128/AEM.69.11.6628-6633.2003>.
- Wu, S. P., Tao, S., & Liu, W. X. (2006). Particle size distributions of polycyclic aromatic hydrocarbons in rural and urban atmosphere of Tianjin, China. *Chemosphere*, *62*, 357–367. <https://doi.org/10.1016/j.chemosphere.2005.04.101>.
- Yates, M. V., & Yates, S. R. (1988). Modeling microbial fate in the subsurface environment. *CRC Critical Reviews in Environmental Control*, *17*, 307–344. <https://doi.org/10.1080/10643388809388339>.

Open Access This chapter is licensed under the terms of the Creative Commons Attribution 4.0 International License (<http://creativecommons.org/licenses/by/4.0/>), which permits use, sharing, adaptation, distribution and reproduction in any medium or format, as long as you give appropriate credit to the original author(s) and the source, provide a link to the Creative Commons licence and indicate if changes were made.

The images or other third party material in this chapter are included in the chapter's Creative Commons licence, unless indicated otherwise in a credit line to the material. If material is not included in the chapter's Creative Commons licence and your intended use is not permitted by statutory regulation or exceeds the permitted use, you will need to obtain permission directly from the copyright holder.



Abstract

A dust storm is meteorologically defined whenever visibility is less than 1,000 meters (Al-Kulaib 1990). Al-Dousari (2009) lists Kuwait as having one of the highest dust precipitation rates in the world. Safar (1980) states that the annual average number of dusty days due to dust storms or rising dust or suspended dust in Kuwait is 255.4. Forty-seven sampling sites representing all the geomorphological and sedimentological provinces in Kuwait were selected for the installation of dust traps to measure the average annual amount of deposited dust during 2009–2010 and 2010–2011 in tons.km⁻².

- To test and environmentally evaluate many varieties of effective control measures.
- To identify the pollen distribution in dust samples.
- To establish a GIS database on dust and pollen in Kuwait.

Deposited Dust

Introduction

Wind is the most active agent in the desert ecosystem. It can remove sand, silt, and clay-sized particles from the surface and blow them, as dust and sandstorms, over great distances (Al-Dousari 2009). Al-Dousari (2009) lists Kuwait as having one of the highest dust precipitation rates in the world. Safar (1980) states that the annual average number of dusty days due to dust storms or rising dust or suspended dust in Kuwait is 255.4 (Al-Dousari 2009). Data on the frequency and rates of dust deposition suggest that the rates of aeolian accumulation may be of a similar order of magnitude as rates of fluvial erosion (Goudie 1978; Wells et al. 2007). Although dust is a result of soil erosion from some areas, it is also a major contributor to soil in other areas, as noted in the dust deposition in Oman (Badawy et al. 1992); Riyadh (Al-Tayeb and Jarrar 1993); Australia, New Zealand (Marx et al. 2005); Canary Islands (Moreno et al. 2006); Florida, Bahamas, Barbados (Muhs et al. 2007); and Spain (Querol et al. 2007). “Desert areas are important sources of mineral dust to the atmosphere, which upon deposition, can influence oceanic and terrestrial biochemical cycles and affect forest productivity” (Avila and Penuelas 1999). Dust traveling long distances is commonly very fine, with sizes predominantly between 0.068 and 0.02 mm (Walker and Costin 1971). Significant quantities of dust may be blown thousands of kilometers from their source (Meng and Lu 2007), and it has been estimated that windblown dust derived from soil erosion contributes approximately 500×10^6 t of the PM to the atmosphere each year (Peterson and Junge 1971).

Sample Location

Forty-seven sampling sites representing all the geomorphological and sedimentological provinces in Kuwait were selected for the installation of dust traps (Fig. 2.1). The sites included the largest island in Kuwait, coastal areas, desert ecosystems, and the Kuwaiti boundaries with Saudi Arabia and Iraq. The dust fallout in Kuwait was monitored continuously to attain the following objectives:

- To assess the physical (morphometry of the grains) and chemical (trace element percentages) characteristics of dust fallout to identify its origin.
- To identify the potential local sources and distribution pattern of the dust fallout in Kuwait.

A. Al-Dousari (✉) · N. Al-Dousari
 Crisis Descision Supports Program (CDS), Environment and Life Sciences Research Center (ELSRC), Kuwait Institute for Scientific Research (KISR), P.O. Box 24885 13109 Safat, Kuwait
 e-mail: adousari@kISR.edu.kw

N. Al-Dousari
 e-mail: ndousari@kISR.edu.kw

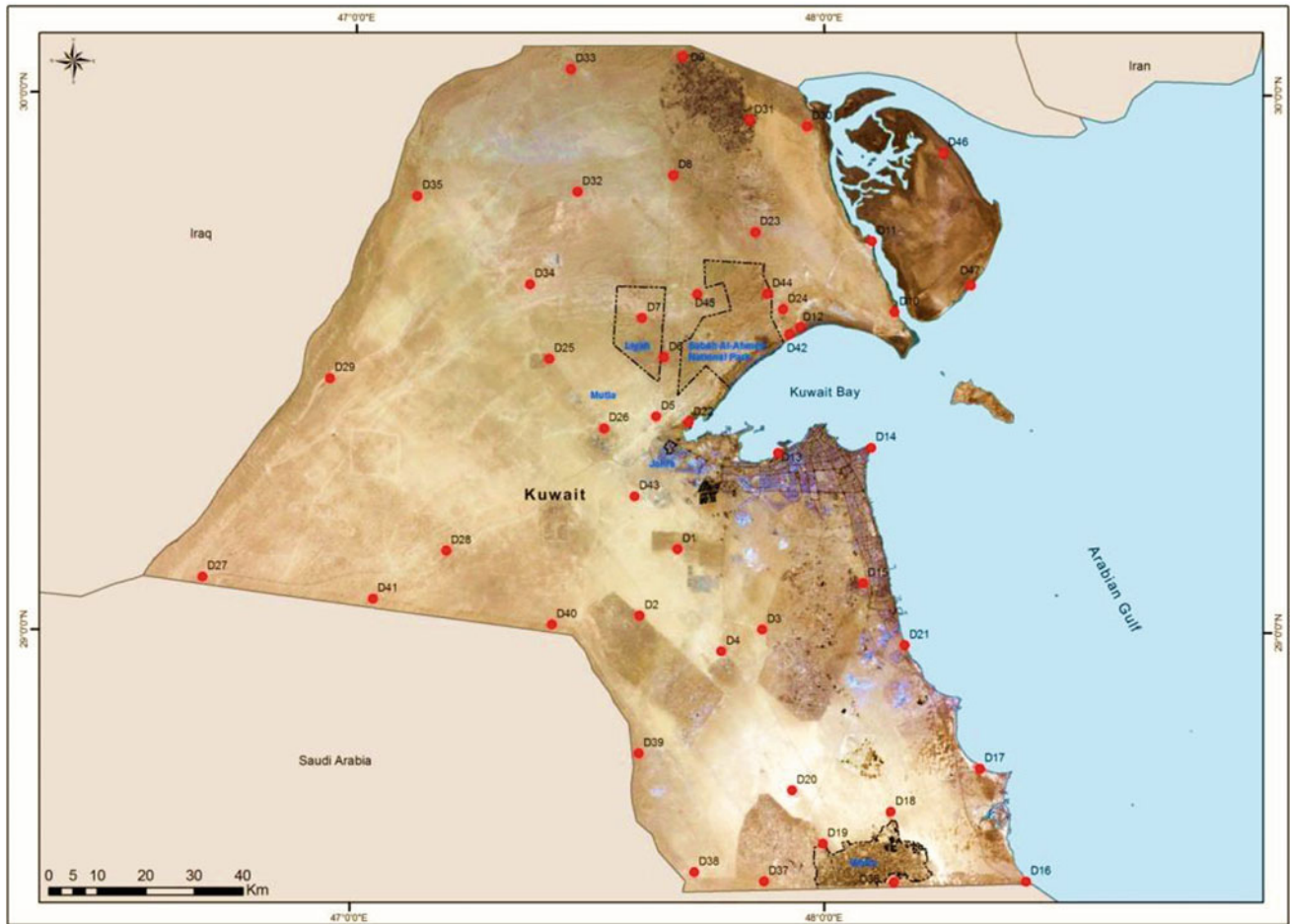


Fig. 2.1 Dust traps sampling locations among Kuwait

Methodology

A dust storm is meteorologically defined whenever visibility is less than 1000 m (Al-Kulaib 1990). In the first decade of this century (July 2000–March 2010), dust storm days were counted in Kuwait using airport meteorological data. Low-resolution images such as METEOSAT (visible and infrared images), MODIS (bands 3, 4, and 7), TOMS, AVHRR, and SeaWiFS were collected within the same period to locate the dust storm primary, intermediate, regional, and local sources and trajectories. Dust storm images were obtained from the satellites' free websites. A map was produced by locating the significant trajectories showing the trajectory direction and duration. The trajectories were classified into two types according to surface area covered by the dust storm that was detected using meteorological data and satellite images: major (greater than or equal to 3000 km²) and intermediate (less than 3000 km²) trajectories.

Modified dust traps were manufactured following the design of Al-Awadhi (2005). Modifications included thermal insulation on the sides and the bottom of the dust containers. The dust traps were installed at 47 sites, at 240 cm above the ground surface, and were chosen to represent the prevailing environmental conditions of Kuwait (Fig. 2.2). The traps were

fixed in fields at least 50 m away from any infrastructure. The fallen dust rates were monitored monthly, from September 1, 2009, to August 31, 2011. The collected data and samples were compared with those from the Kuwait Environment Public Authority (KEPA) and regional and global literature.

Initially, the characteristics of the dust were examined and interpreted using a series of analytical tools. Grain-size parameters were determined using standard sieve analysis and the Centrifugal Particle Analyzer (Shimadzu, SA-CP3) for all dust fallout samples in January and October 2010. The Brunauer, Emmett, and Teller (BET) surface area is expressed as the value of a specific weight of loose sand in terms of m²/g measured by using isotherm plot diagrams of volume against pressure and the BET equation. The whole components of the dust samples were gently powdered and analyzed using Philips PW-1830 X-ray Diffraction (XRD). Semi-quantitative analysis was carried out for the Bubiyan (D07), Warba (D09), Sabiya (S-3), and National Park (RD4) samples, and the results were compared with regional and global dust collection by the authors or others from the literature. Furthermore, a scanning electron microscope (SEM) was used to analyze the Bubiyan and Al-Liyah dust samples (L18 and D-08) with a magnification ranging from 600 to 2700X.



Fig. 2.2 Dust trap in Al-Liyah newly preserved area (2009)

Annual Deposited Dust

The average annual amount of deposited dust during 2009–2010 was 220 tons km⁻². The northern coastal areas and the western areas of Kuwait had the highest amount of deposited dust. The preserved areas and southern coastal areas had the lowest amount. The preserved areas around Jahra, with dense vegetation cover compared with the open desert areas, had less deposited dust, which is attributed to the capability of native vegetation preventing the movement (re-suspension) of dust particles after the initial deposition (Fig. 2.3).

Areas of high deposited dust concentration	Areas of low deposited dust concentration
Bubiyah Island	Um Eish
Abdulli	Doha
Salmi	Um Qudayr
Shuwaikh	Khur Fawaris
Kabd	Shuaiba

The annual dust deposited rate in Kuwait during 2010–2011 was 373 tons km⁻², which is higher than in 2009/2010 by 33.2% (220 tons km⁻²). The areas of lower and higher concentrations of dust were nearly the same as in 2009–2010. It is evident from the slight variation in the distribution of dust fallout over the two years that there is an appreciable amount of dust fallout contribution from local sources. This knowledge guides us for planning future urban areas such as the Sabiyah and Bubiyah Island, which suffer from a high concentration of dust fallout as they are rich in mud size particles. Spatial and temporal variations in dust fallout

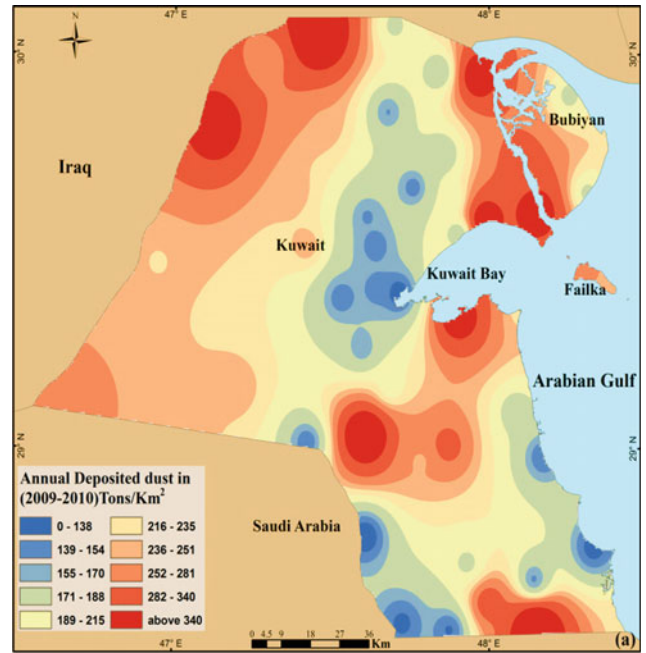


Fig. 2.3 Annual deposited dust for 2009–2010

fluxes within Kuwait are shown in the attached Figs. 2.4, 2.5, 2.6, 2.7, 2.8, 2.9 and 2.10.

Areas of high deposited dust concentration	Areas of low deposited dust concentration
Ratqah	Ras Ezur
Bubiyah Island	Qurain
Abdulli	Gudhi
Kabd	Jal Al-Liyah
Salmi	Rwdatayn

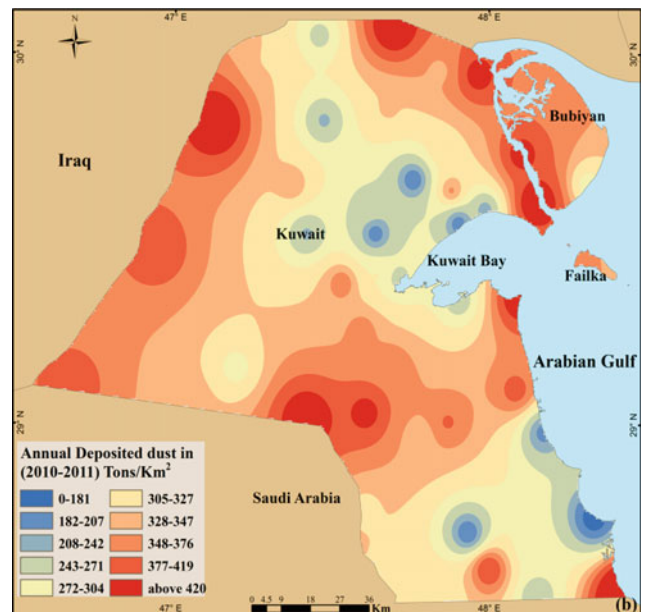


Fig. 2.4 Annual deposited dust for 2010–2011

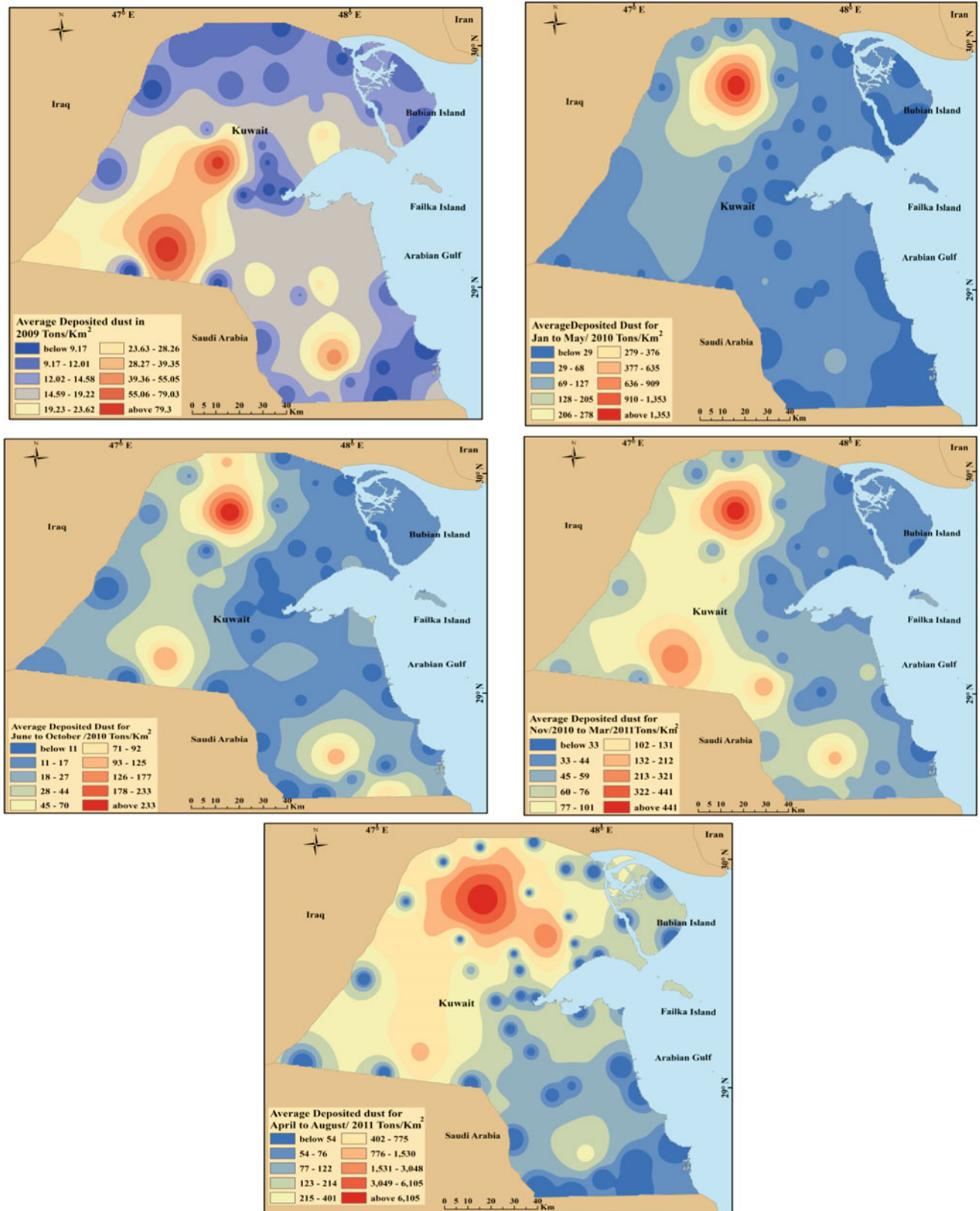


Fig. 2.5 Deposited dust

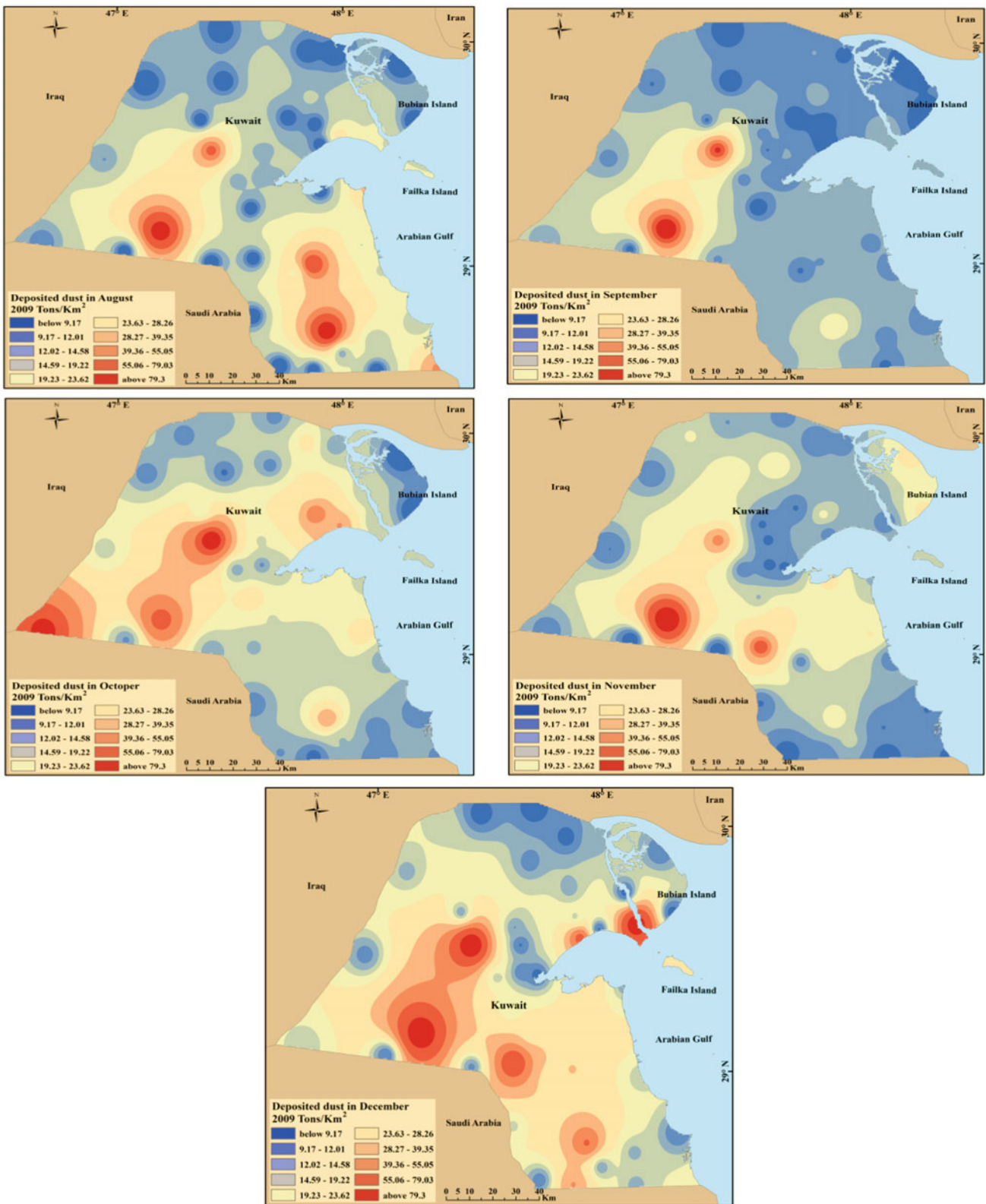


Fig. 2.6 Deposited dust for August 2009–December 2009

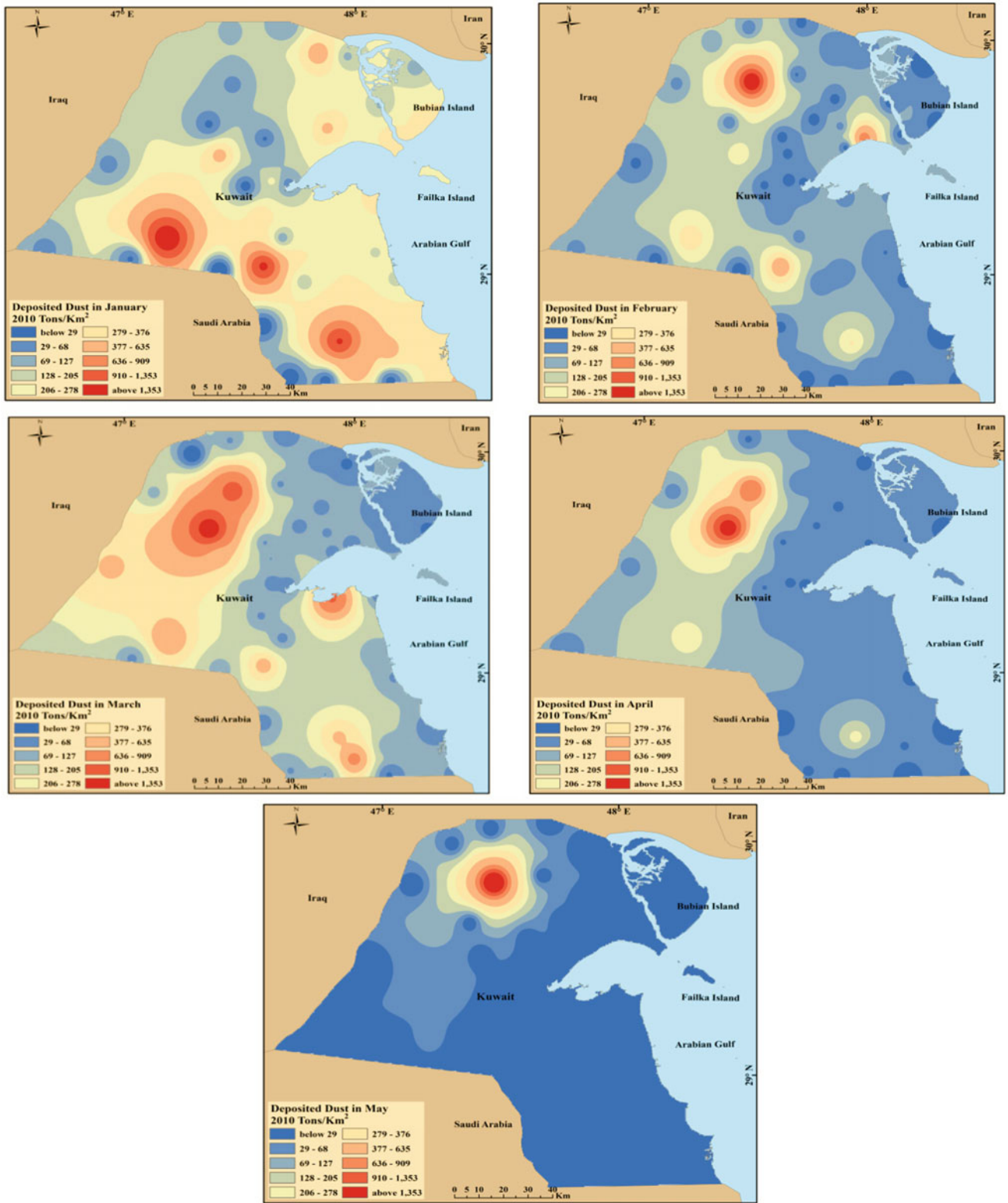


Fig. 2.7 Deposited dust for January 2010–May 2010

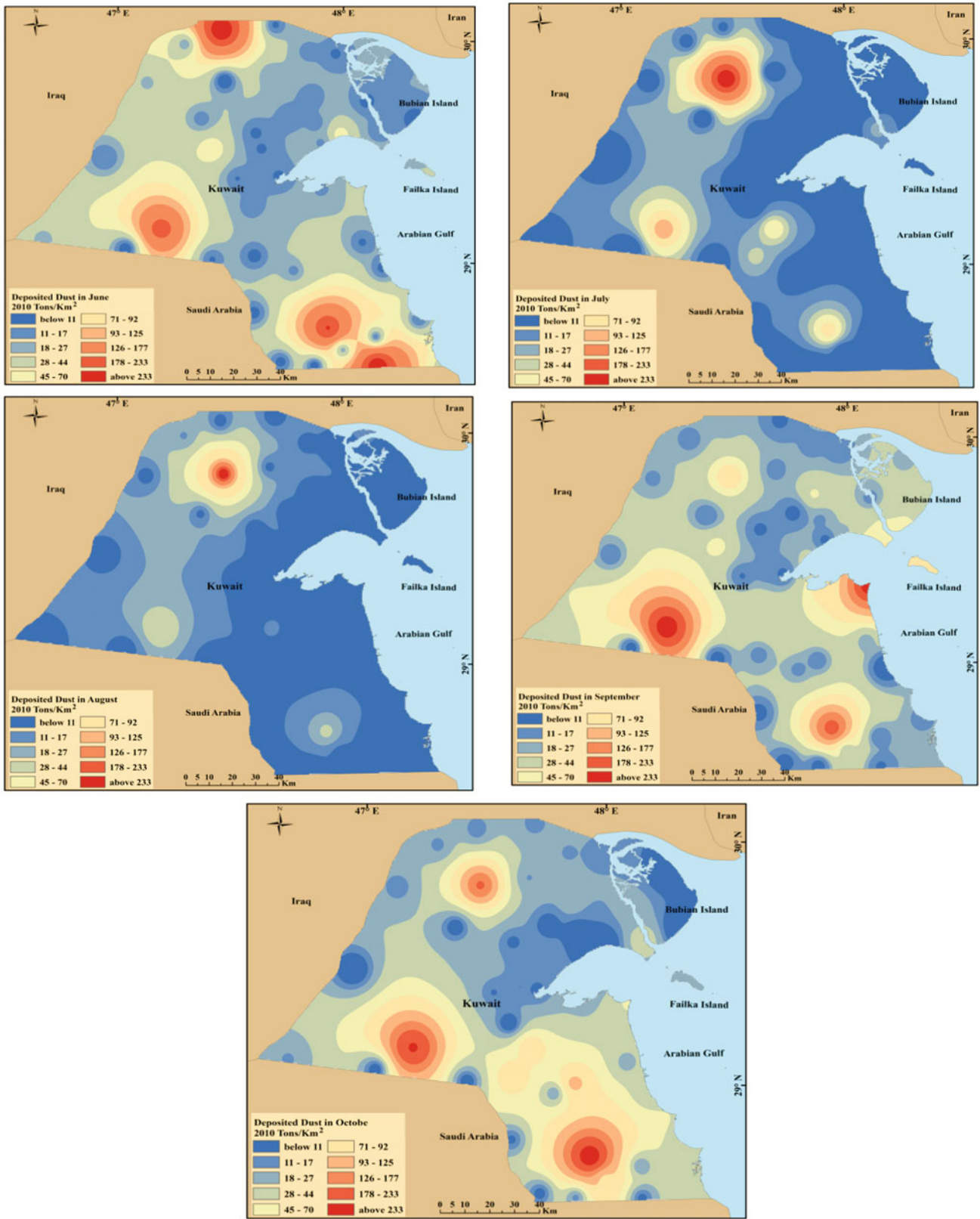


Fig. 2.8 Deposited dust for June 2010–October 2010

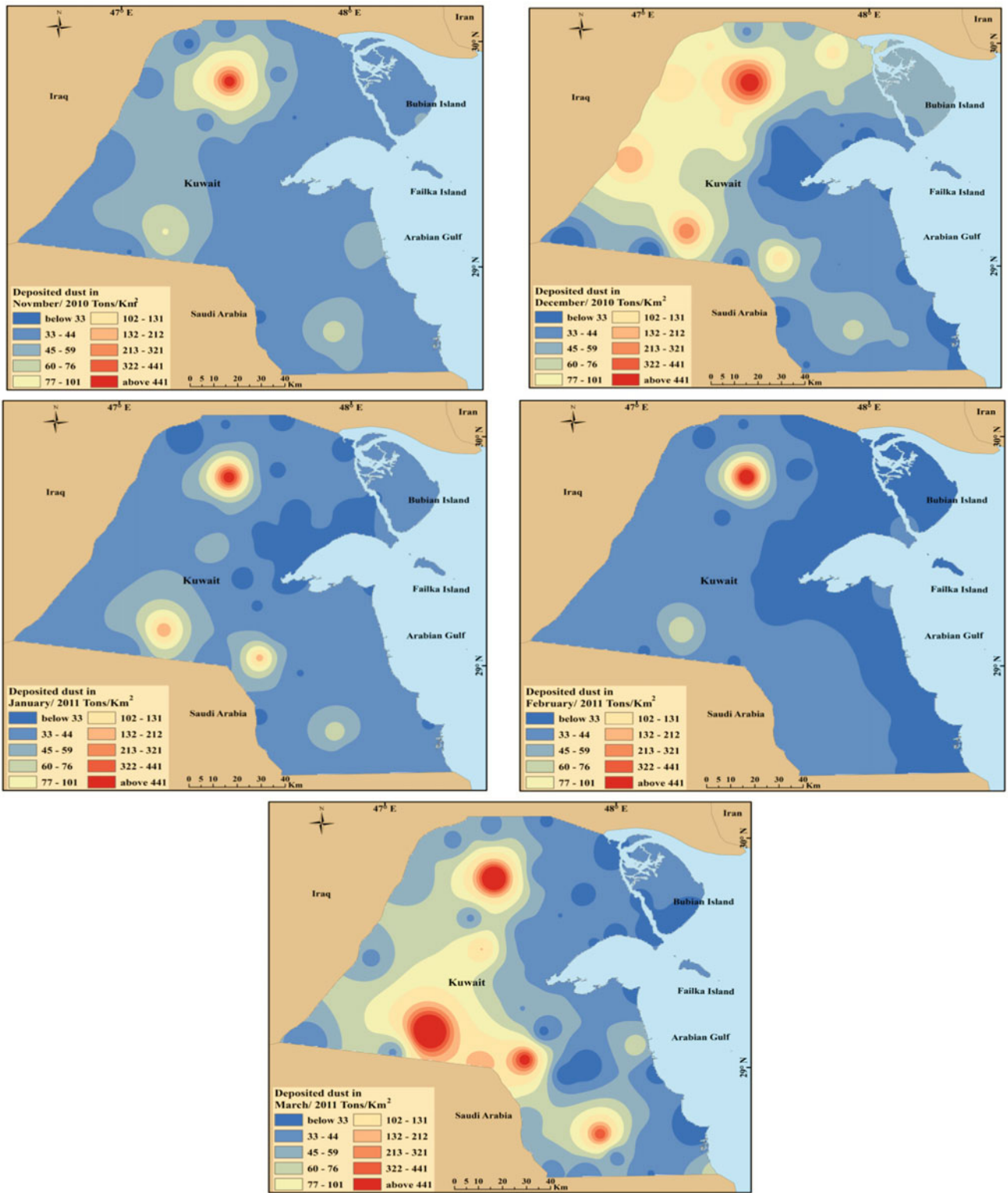


Fig. 2.9 Deposited dust for November 2010–March 2011

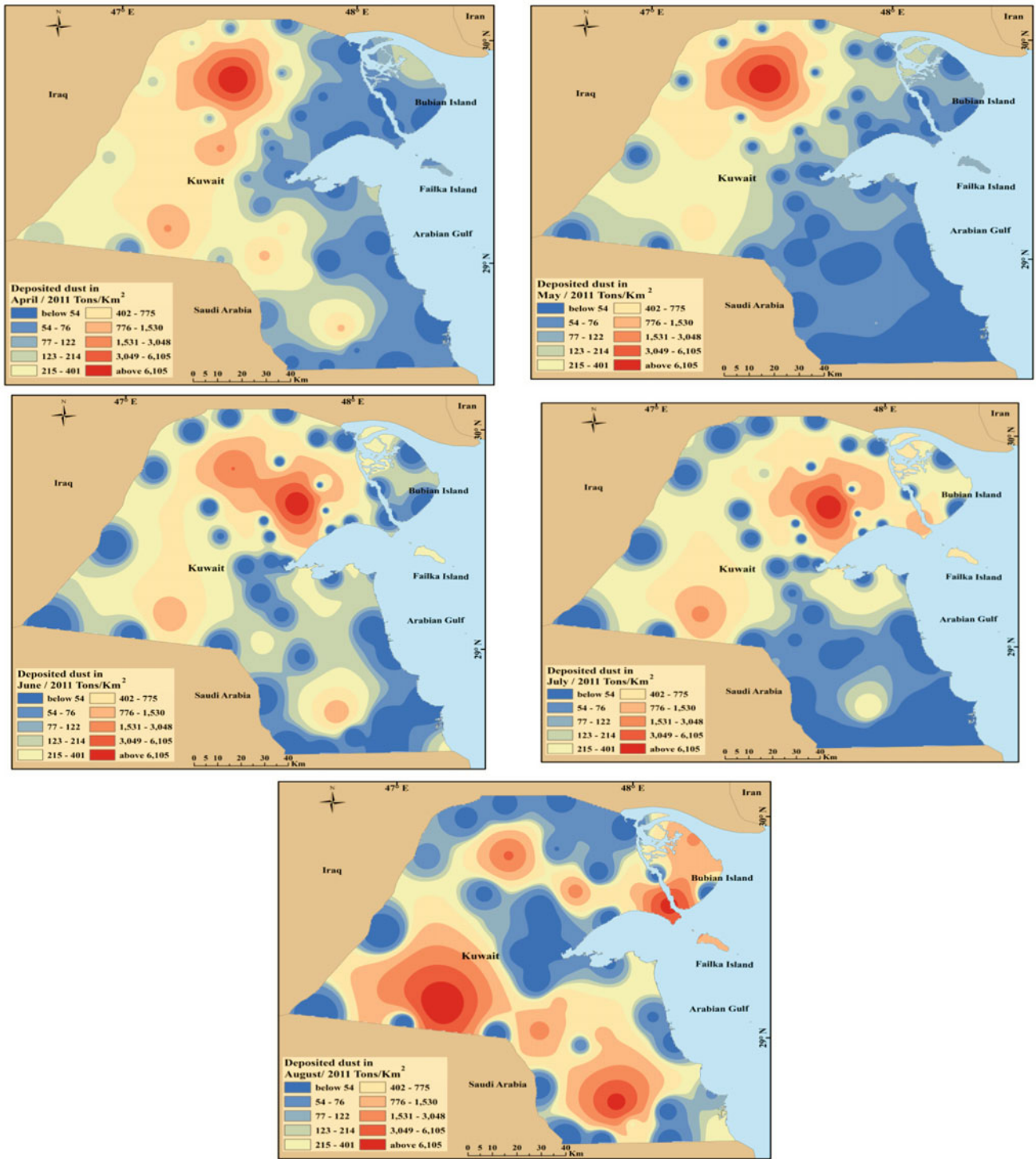


Fig. 2.10 Deposited dust for April 2011–August 2011

References

- Al-Dousari. (2009). Section III: Recent studies on dust fallout within preserved and open areas in Kuwait. In N. R. Bhat, A. Y. Al-Nasser, & S. Omar (Eds.), *desertification in arid lands: Causes, consequences and mitigation* (pp: 137–148). Kuwait: Kuwait Institute for Scientific Research.
- Al-Awadhi, J. (2005). Dust fallout characteristics in Kuwait: a case study. *Kuwait Journal of Science and Engineering*, 32(2), 135–152. ISSN: 1024–8684.
- Al-Kulaib, A.A. (1990). *Climate of Arabian Gulf*., Kuwait: That Alsalsail Press.
- Al-Tayeb, N. T., & Jarrar, B. M. (1993). Dust fall in the city of Riyadh. In *Proceedings of the Industrial Air Pollution Symposium*, Riyadh, 15–17 November 1993, Saudi Arabia, pp. 66–74.
- Avila, A., & Peñuelas, J. (1999). Increasing frequency of Saharan rains over northeastern Spain and its ecological consequences. *the Science of the Total Environment*, 228, 153–156. [https://doi.org/10.1016/S0048-9697\(99\)00041-8](https://doi.org/10.1016/S0048-9697(99)00041-8).
- Badawy, M. I., Hernandez, M. D., & Al-Harthy, F. (1992). Sources of pollution at Mina al Fahal coastal area. *Bulletin of Environmental Contamination and Toxicology*, 49, 813–820. <https://doi.org/10.1007/BF00203152>.
- Goudie A. (1978). Arid geomorphology. *Progress in Physical Geography: Earth and Environment*, 2(2):333–338. <https://doi.org/10.1177/030913337800200207>
- Marx, S. K., Kamber, S. B., & McGowan Hamish, A. (2005). Estimates of Australian dust flux into New Zealand: Quantifying the eastern Australian dust plume pathway using trace element calibrated 210Pb as a monitor. *Earth and Planetary Science Letters*, 239(3–4), 336–351. <https://doi.org/10.1016/j.epsl.2005.09.002>.
- Meng and Lu. (2007). Dust events as a risk factor for daily hospitalization for respiratory and cardiovascular diseases in Minqin, China. *Atmospheric Environment*, 41, 7048–7058. <https://doi.org/10.1016/j.atmosenv.2007.05.006>.
- Moreno, T., Querol, X., Castillo, S., Alastuey, A., Cuevas, E., Herrmann, L., Mounkaila, M., Ivira, J., & Gibbons, W. (2006). Geochemical variations in Aeolian mineral particles from the Sahara-Saheldust corridor. *Chemosphere*, 65, 261–270. <https://doi.org/10.1016/j.chemosphere.2006.02.052>.
- Muhs, D. R., Budahn, J., Reheis, M., Bean, J., Skipp, G., & Fisher, E. (2007). Airborne dust transport to the eastern Pacific Ocean off southern California: Evidence from San Clemente Island. *Journal of Geophysical Research*, 112. <https://doi.org/10.1029/2006JD007577>.
- Peterson, S. T., & Junge, C. E. (1971). Sources of particulate matter in the atmosphere. In W. W. Kellogg & G. D. Robinson (Eds.), *Man's impact on the climate* (pp. 310–320). MIT Press.
- Querol, X., Viana, M., Alastuey, A., Amato, F., Moreno, T., Castillo, S., Pey, J., De La Rosa, J., Sanchez De La Campa, A., Artinano, B., Salvador, P., García, Dos Santos, S., Fernández-Patier, R., Moreno-Grau, S., Negral, L., Minguillón, M. C., Monfort, E., Gil, J. I., Inza, A., Ortega, L. A., Santamaria, J. M., & Zabalza, J. (2007). Source origin of trace elements in PM from regional background, urban and industrial sites of Spain, Atmos. *Environ*, 41, 7219–7231. <https://doi.org/10.1016/j.atmosenv.>
- Safar, M. I. (1980). *Frequency of dust in day-time summer in Kuwait*. Kuwait: Directorate General of Civil Aviation.
- Walker, P. H., & Costin, A. B. (1971). Atmospheric dust accession in South-Eastern Australia. *Australian Journal of Soil Research*, 9, 1–5. <https://doi.org/10.1071/SR9710001>.
- Wells, K. C., Witek, M., Flatau, P., Kreidenweis, S. M., & Westphal, D. L. (2007). An analysis of seasonal surface dust aerosol concentrations in the western US (2001–2004): Observations and model predictions. *Atmospheric Environment*, 41(31), 6585–6597. <https://doi.org/10.1016/j.atmosenv.2007.04.034>.

Open Access This chapter is licensed under the terms of the Creative Commons Attribution 4.0 International License (<http://creativecommons.org/licenses/by/4.0/>), which permits use, sharing, adaptation, distribution and reproduction in any medium or format, as long as you give appropriate credit to the original author(s) and the source, provide a link to the Creative Commons licence and indicate if changes were made.



The images or other third party material in this chapter are included in the chapter's Creative Commons licence, unless indicated otherwise in a credit line to the material. If material is not included in the chapter's Creative Commons licence and your intended use is not permitted by statutory regulation or exceeds the permitted use, you will need to obtain permission directly from the copyright holder.



Noor Al-Dousari, Modi Ahmed, Ali Al-Dousari, Musaad Al-Daihani,
and Murahib Al-Elaj

Abstract

Grain 'size' can be specified and measured in several different ways. All methods of grain size determination have blemishes, and the choice of the most appropriate method is governed by the nature of the sample and the use to which the data are placed. Four main methods are currently used for size analysis of sands: (a) sieving; (b) settling tube analysis; (c) electro-optical methods, including Coulter Counter analysis and laser granulometry; and (d) computerized image analysis. The classification of the particle size distribution of Kuwait dust was mapped according to the parameters proposed by Folk And Ward (1957) which were widely used for quantitative comparisons between natural grain size distribution and the lognormal that shows better sorted sediments have lower values of σ . Maps of the distribution of dust in Kuwait were obtained that included: fine sand (F.S.), Coarse sand (C.S), Medium Sand (M.S), Very Fine Sand (V.F.S), Very Coarse Silt (V.C.Silt), Coarse Silt (C.Silt), Medium Silt (M.Silt), Fine Silt (F.Silt), Very Fine Silt (V.

F.Silt), in addition to that, the deposition percentage of Clay, Sand, mud (silt plus clay) and silt were provided.

Introduction

Dust suspended over long distances consists of mud particles that predominantly originate from regional sources such as the Western Desert of Iraq and the Mesopotamian Floodplain, in addition to local dust deposition that produces relatively coarse saltated dust material greater than 63 μ m grain-size fractions. The former type represents 63% of the dust, and the latter, 37%. Generally, the distribution of particle size is trimodal and displays slight variation over time. The sand particles, being heavier than mud, move in the form of saltation, are transported for short distances, and predominantly originate from local sources. The grain-size percentages of dust collected in the open desert and coastal areas, such as Bubiyan, vary. Bubiyan dust is negatively skewed, trimodal with clay dominance coarse, and with fine silt size fractions. The trimodal of the distribution curves indicates multiple sources.

Liyah dust (i.e. open desert) is negatively skewed and unimodal with the dominance of very coarse sand size fraction. There is a trend of a coarsening of the mean size fraction toward the west. Furthermore, the dust particles collected from the western side of the study area are larger and smoother than those from the eastern side. Bubiyan dust is finer and contains more adhering particles, mainly gypsum ($\text{CaSO}_4 \cdot 2\text{H}_2\text{O}$) and bassanite ($\text{CaSO}_4 \cdot 1/2\text{H}_2\text{O}$). The average percentages for clay, very fine silt, very coarse silt, and very fine sand in the dust reveal the dominance of clay along the sides of the dunes corridor (Huwaimiliyah-Wafra), Um Umara, north and east Bubiyan, and Bahrat Hushan.

Dust storms cause serious health hazards.

N. Al-Dousari (✉) · M. Ahmed · A. Al-Dousari
Crisis Decision Supports Program (CDS), Environment & Life
Sciences Research Center (ELSRC), Kuwait Institute for Scientific
Research (KISR), P.O. Box. 24885 Safat, 13109, Kuwait
e-mail: ndousari@kISR.edu.kw

M. Ahmed
e-mail: mmahmed@kISR.edu.kw

A. Al-Dousari
e-mail: adousari@kISR.edu.kw

M. Al-Daihani
Construction & Production Department, Kuwait Oil Company
(KOC), P.O. Box. 9758 Ahmadi, 61008, Kuwait
e-mail: mdaihani@kockw.com

M. Al-Elaj
Environment & Life Sciences Research Center (ELSRC), Kuwait
Institute for Scientific Research (KISR), P.O. Box. 24885 Safat,
13109, Kuwait
e-mail: marahib@protonmail.com

Methodology

Grain movement is influenced by the characteristics of individual grains from the source, such as size, shape, and density, but also by the characteristics of the sediment bulk, which include the grain-size distribution (sorting), orientation, packing arrangement, porosity, and cohesion. During transport, grains are sorted according to size and shape due to inter-particle collisions or contact with the bed.

Grain 'size' can be specified and measured in several different ways. All methods of grain-size determination have issues, and the choice of the most appropriate method is governed by the nature of the sample and the use to which the data are made. Four main methods are currently used for the size analysis of sands: (a) sieving; (b) settling tube analysis; (c) electro-optical methods, including Coulter

Counter analysis and laser granulometry; and (d) computerized image analysis.

However, the most widely used method is dry sieving, in which a sand sample is shaken through a nest of successively finer mesh sieves. Conventionally, the weight of the sand retained on each sieve is converted to a percentage of the total sample. Several studies have shown that particle shape can significantly impact the sieve data (Komar and Cui 1984; Kennedy et al. 1985). All the difficulties may be experienced when samples contain a mixture of quartz and parts of the platy crusts (Carter 1982). The deposit particle sizes range from several meters to less than 1 μm , (Udden 1914; Wentworth 1922). Table 1 presents a graphical representation and statistical manipulation of grain-size frequency data. Krumbein (1934) proposes that the grade boundaries should be logarithmically transformed into phi (ϕ) values.

Table 1 Size scales of Udden (1914) and Wentworth (1922), with class terminology modifications proposed by Friedman and Sanders (1978)

Size mm	μm	phi	Sediment size class terminology of Wentworth (1922)	Sediment size class terminology of Friedman and Sanders (1978)	
2048		-11	Cobbles	very large boulders	gravel
1024		-10		very large boulders	
512		-9		large boulders	
256		-8		medium boulders	
128		-7		small boulders	
64		-6		large cobbles	
32		-5		small cobbles	
16		-4	Pebbles	very coarse pebbles	
8		-3		coarse pebbles	
4		-2		medium pebbles	
2	2000	-1		fine pebbles	
1	1000	0	Granules	very fine pebbles	sand
0.5	500	1	Very coarse sand	very coarse sand	
0.25	250	2	Coarse sand	coarse sand	
0.125	125	3	Medium sand	medium sand	
0.063	63	4	Fine sand	fine sand	
0.031	31	5	Very fine sand	very fine sand	
0.016	16	6	Silt	very coarse silt	
0.008	8	7		coarse silt	
0.004	4	8		medium silt	
0.002	2	9		fine silt	
			Clay	very fine silt clay	clay

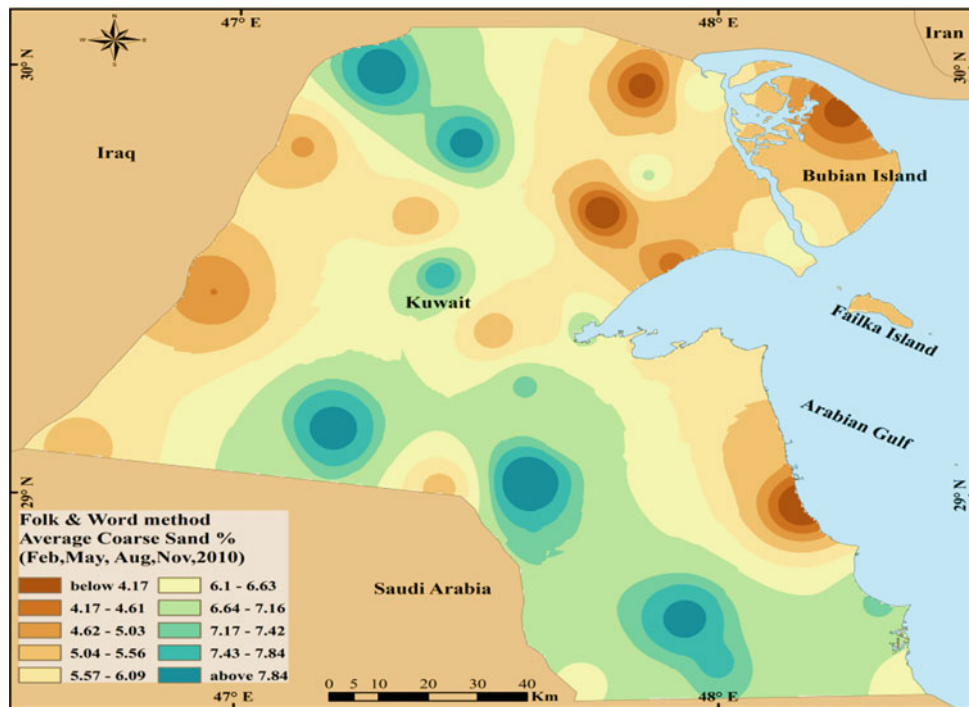


Fig. 3.1 Average percentages of coarse sand in the deposited dust (February, May, August, November 2010)

Coarse sand (C.S.) ranges in size between 0.5 and 1 mm (1-0 phi). The fallen dust in the northeastern and coastal area of Kuwait had the lowest C.S. percentage. In contrast, Wafra, the southwestern areas of Kuwait, and the Ratqah had the highest C.S. percentage. Although the C.S. percentages are less than 10% in general, they could indicate size behavior of fallen dust both temporarily and spatially. The highest rates were noted in February.

Areas with high particle size concentration	Areas with low particle size concentration
Ratqah	Bubiyan Island
Dibdibah	Shuaiba
Um qudayr	Um Rimam
Wafra	Ubayriq

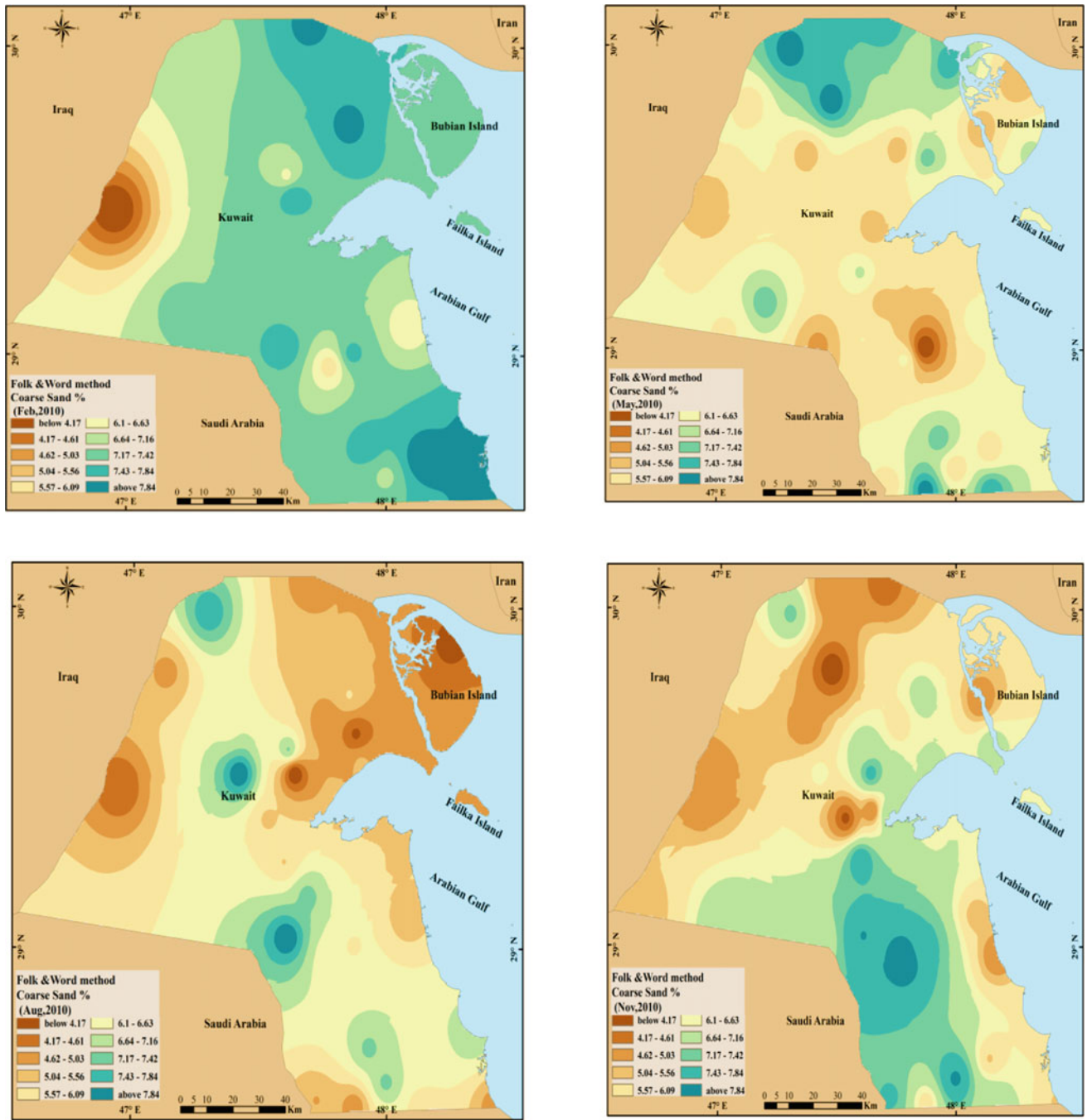


Fig. 3.2 Coarse sand size fractions percentages in Feb, May, Aug, Nov 2010

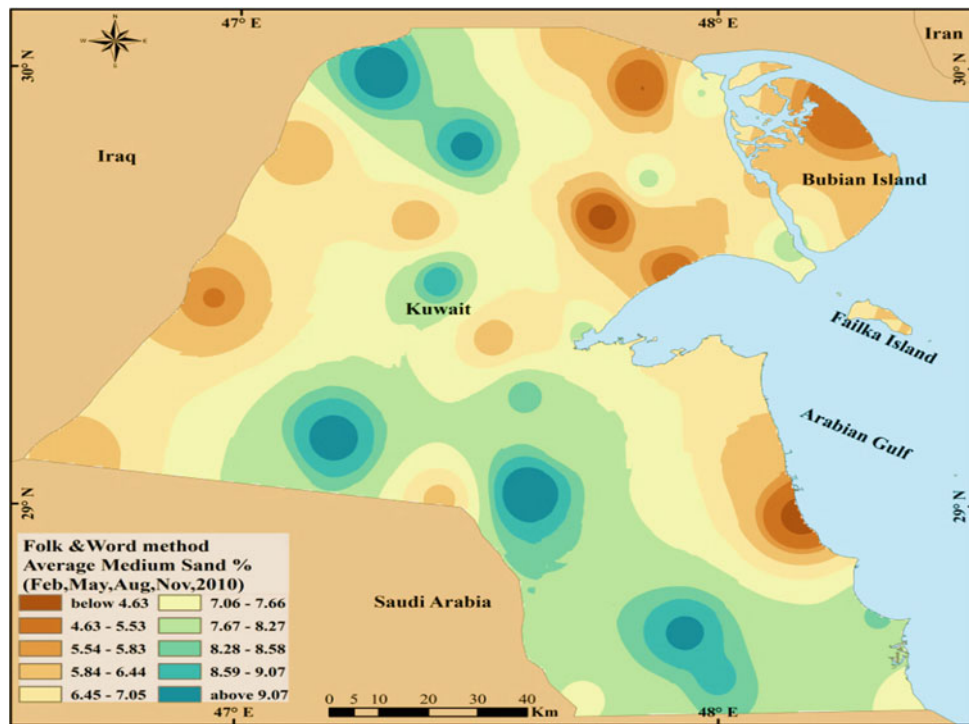


Fig. 3.3 Average percentages of medium sand in the deposited dust (February, May, August, November 2010)

Medium sand (M.S.) ranges in size between 0.25 and 0.5 mm (2–1 phi). It had a similar distribution to C.S. Furthermore, February’s fallen dust had the highest percentages. It has always been noted that the southern areas of Kuwait are characterized by sandy dust more than most other areas in the country, as they experience the highest aeolian accumulation. On the other hand, the northern and northeastern areas of Kuwait have the lowest percentages of M.S. size fraction. In August, the M.S. had a higher percentage within the major wind or dune corridor in Kuwait.

Areas with high particle size concentration	Areas with low particle size concentration
Ratqah	Bubiyan Island
Dibdibah	Gudhi
Kabd	Shuaiba
Wafra Farms	Ubayriq

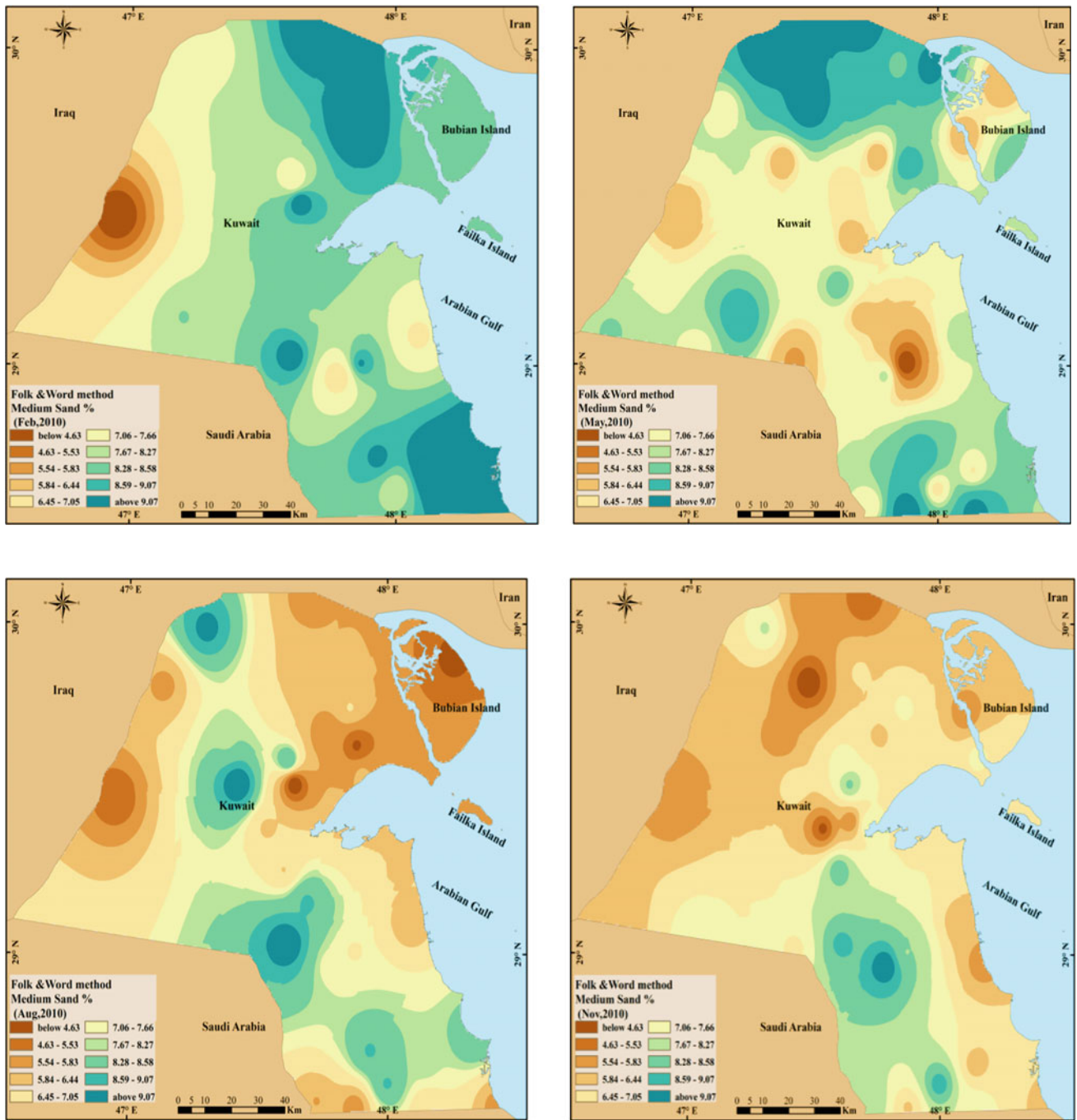


Fig. 3.4 Medium sand size fraction percentages in Feb, May, Aug, Nov 2010

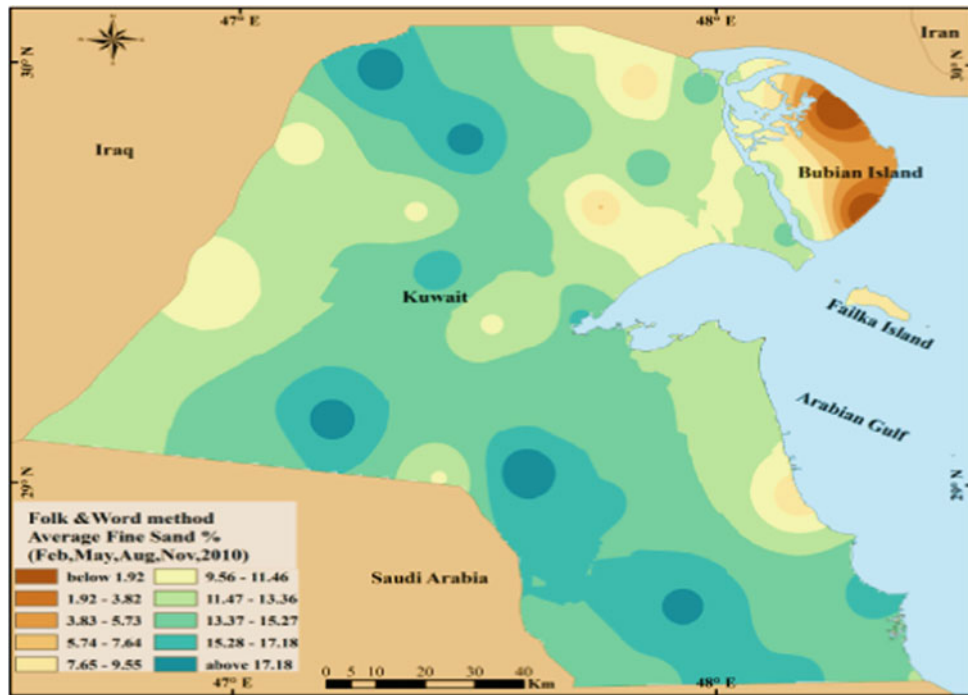


Fig. 3.5 Average percentages of fine sand in the deposited dust (February, May, August, November 2010)

Fine sand (F.S.) ranges in size between 0.125 and 0.25 mm (3–2 phi). It had a similar trend of distribution to C.S. and M.S., but the percentages are about twice of those. The highest rates were recorded in February. The highest percentages were in a corridor that extends from the Retqah toward the Wafra in Kuwait. On the other hand, the lowest rates of M.S. size fraction were noted on Bubiyan Island and the northeastern areas of Kuwait.

Areas with high particle size concentration	Areas with low particle size concentration
Ratqah	Bubiyan Island
Dibdibah	Failaka Island
Kabd	Gudhi
Wafra Farms	Abdulli

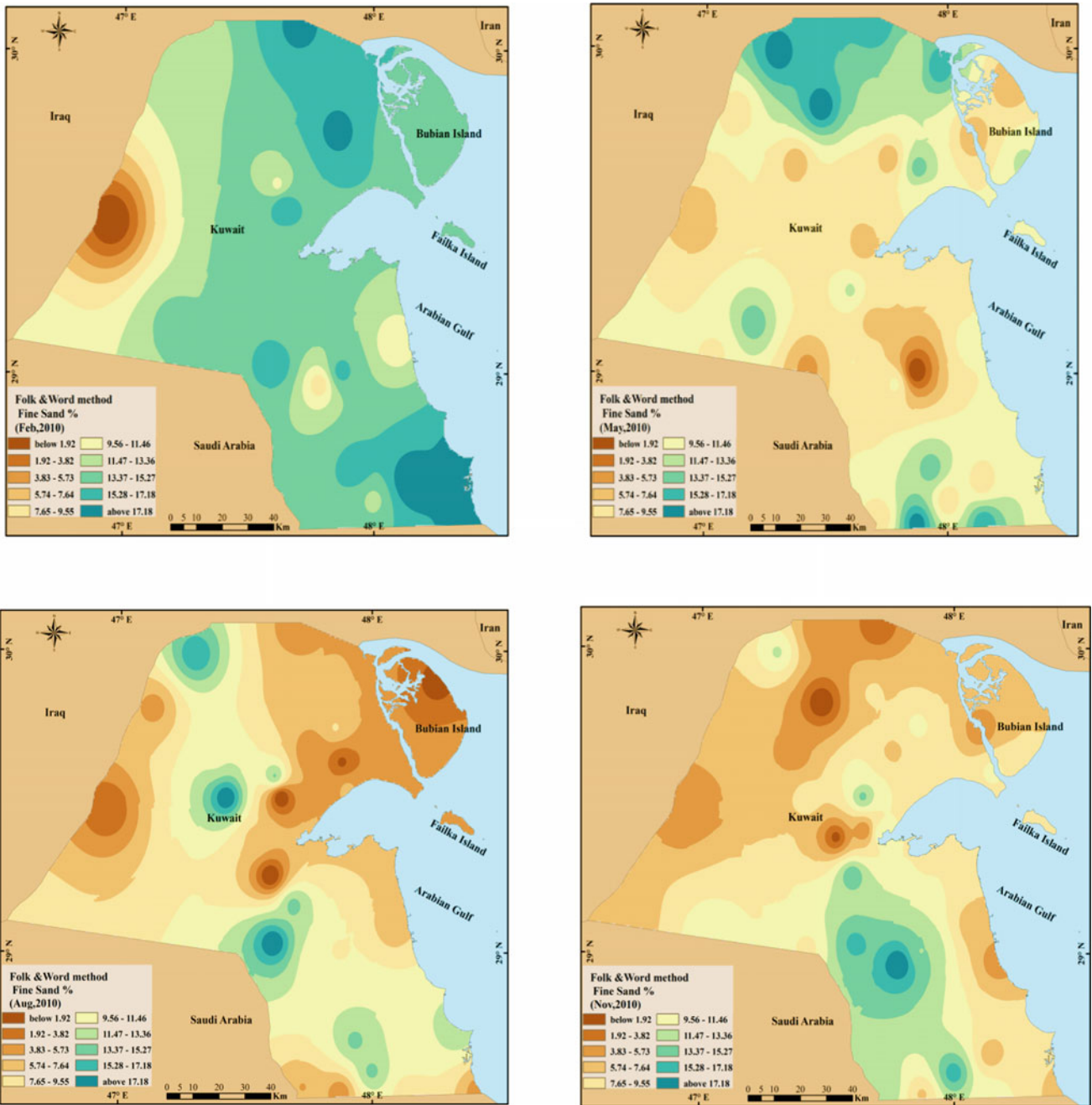


Fig. 3.6 Fine sand size fractions percentages in Feb, May, Aug, Nov 2010

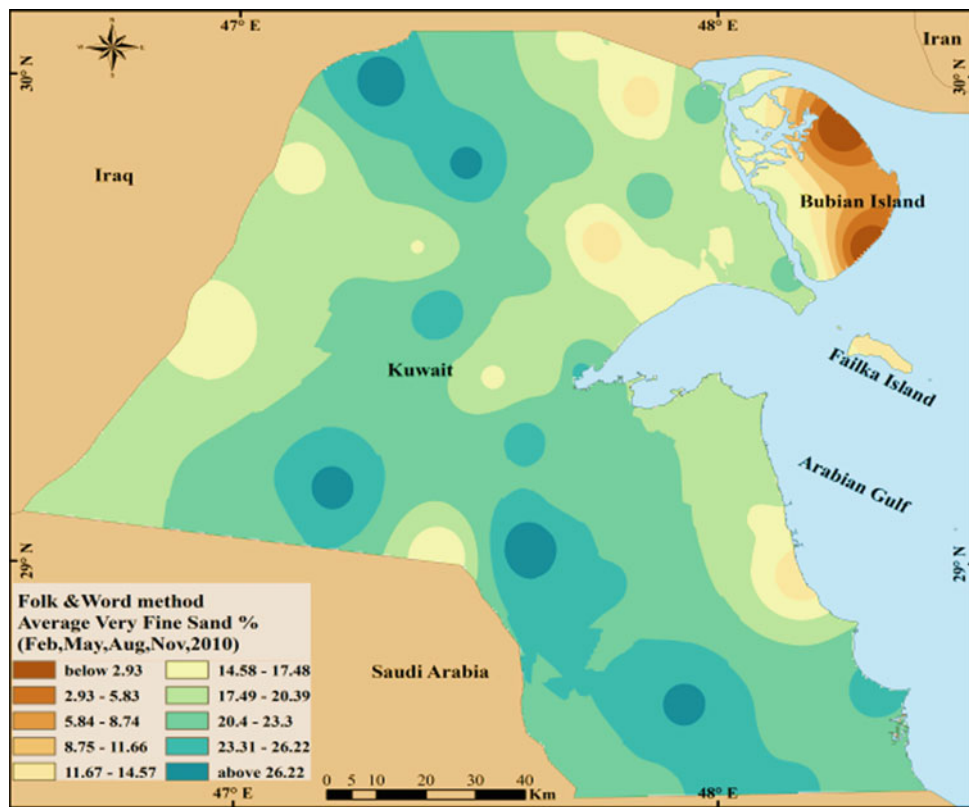


Fig. 3.7 Average percentages of very fine sand in the deposited dust (February, May, August, November 2010)

Very fine sand (V.F.S.) ranges in size between 0.063 and 0.125 mm (4–3 phi). It had a similar trend of distribution to C.S. and M.S., but the percentages were much more than twice the amount. The highest percentage rates were noted in February. The highest percentages were in a corridor that extends from the Retqah area toward the Wafra area in Kuwait. On the other hand, the lowest percentage rates of V. F.S. were recorded on Bubiyan Island and in the northeastern areas of Kuwait.

Areas with high particle size concentration	Areas with low particle size concentration
Ratqah	Bubiyan Island
Dibdibah	Failaka Island
Kabd	Gudhi
Wafra Farms	Abdulli

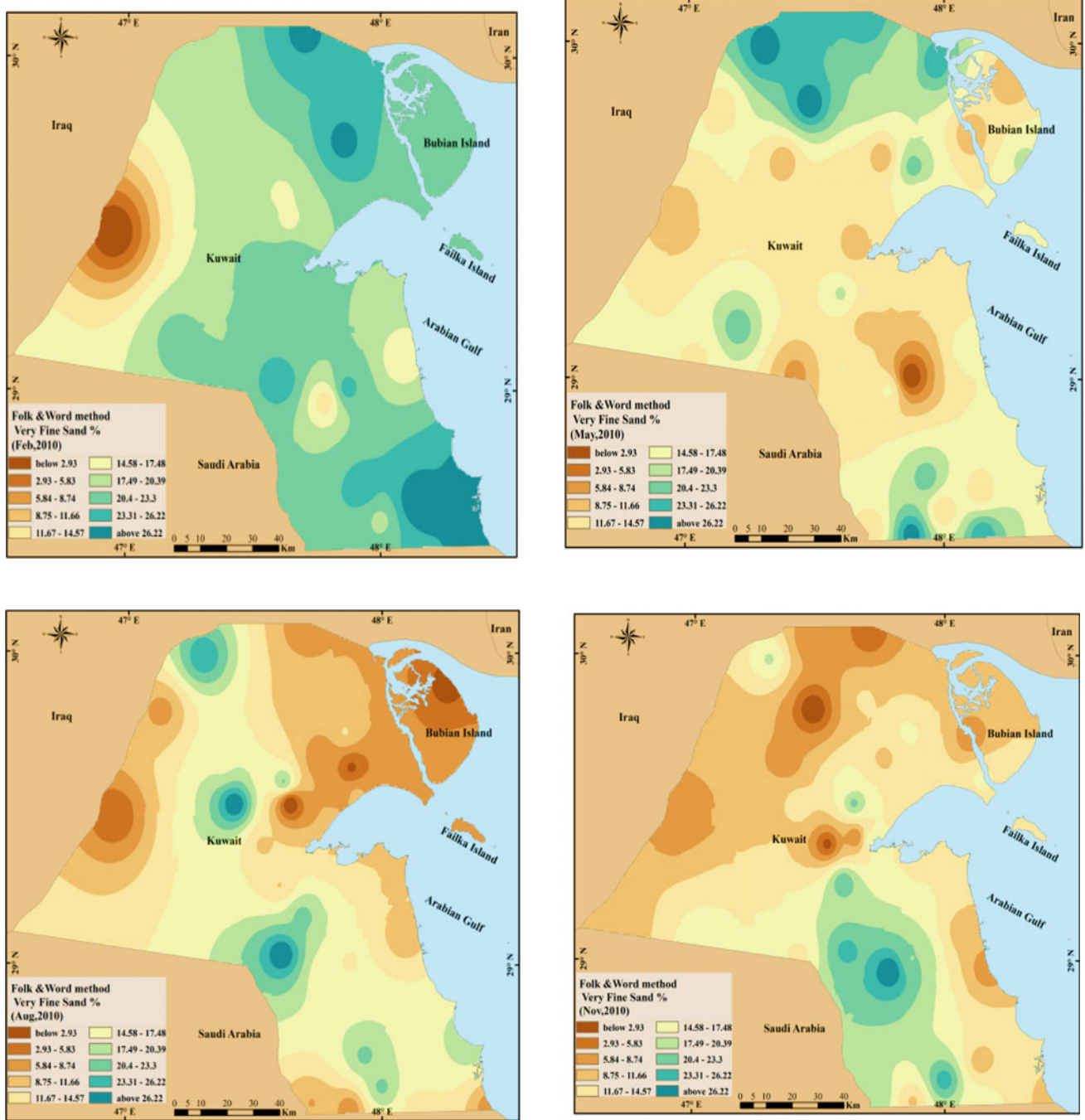


Fig. 3.8 Very fine sand size fractions percentages in Feb, May, Aug, Nov 2010

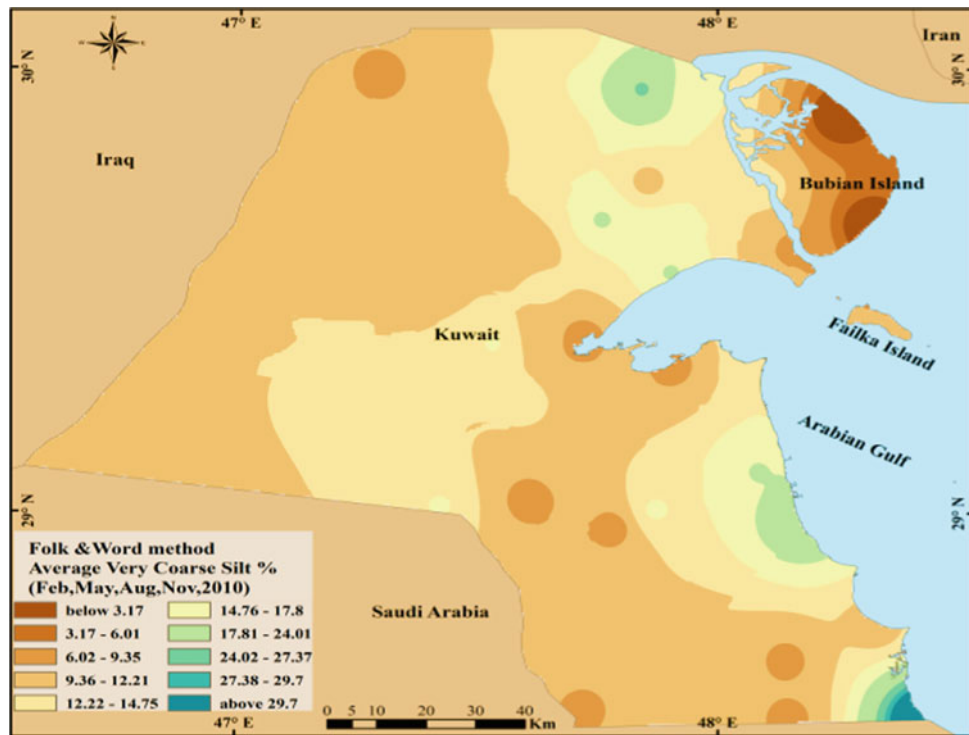


Fig. 3.9 Average percentages of very coarse silt in the deposited dust (February, May, August, November 2010)

Very coarse silt (V.C. Silt) ranges in size between 0.031 and 0.063 mm (4–5 phi). V.C. Silt was present in higher percentages toward the coastal areas of Kuwait. The lowest percentages were in May. The V.C. Silt and the C. Silt had lower rates within the major wind or dune corridor in Kuwait during August. The lowest percentages were recorded in the eastern part of Bubiyan Island in all months except August.

Areas with high particle size concentration	Areas with low particle size concentration
Khiran	Bubiyan Island
Shuaiba	Subiyah
Abdulli	Ratqah
Gudhi	Mutla

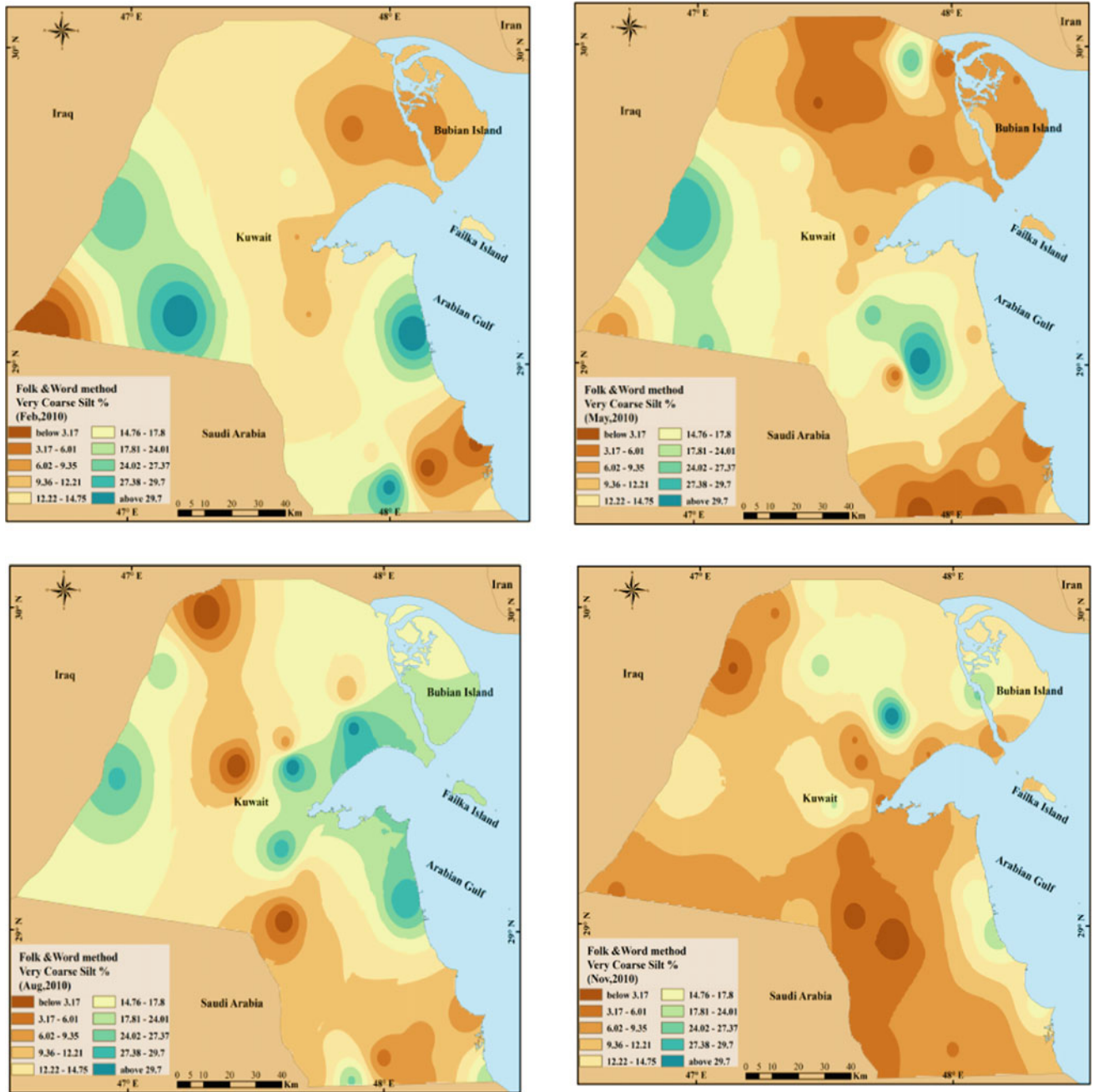


Fig. 3.10 Very coarse silt size fractions percentages in Feb, May, Aug, Nov 2010

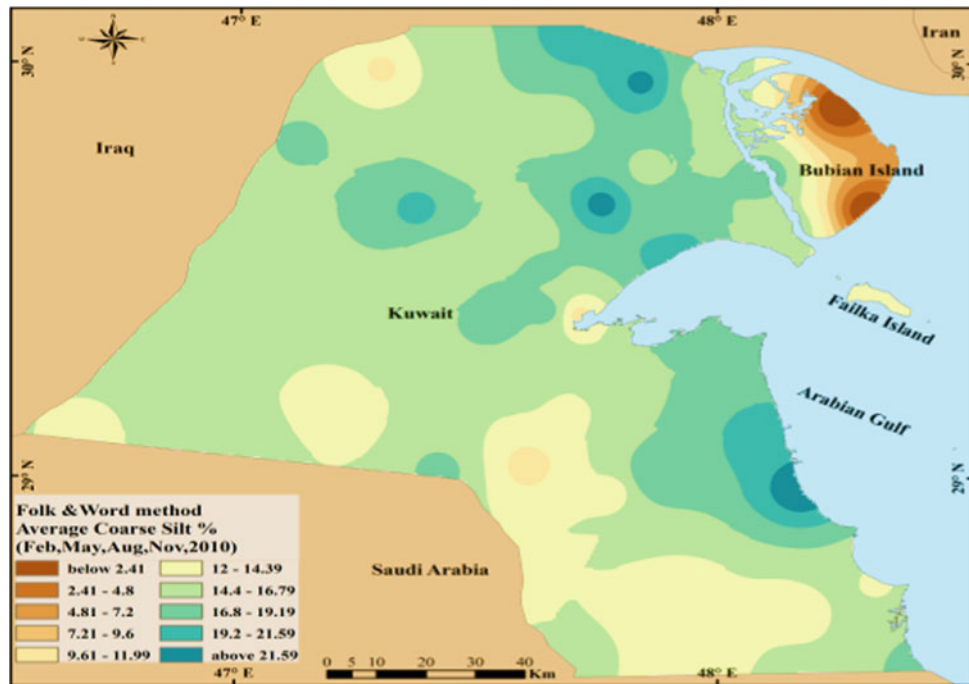


Fig. 3.11 Average percentages of coarse silt in the deposited dust (February, May, August, November 2010)

Coarse silt (C.Silt) ranges in size between 0.031 mm and 0.016 mm (6–5 phi). The silt size fractions act as the main component of fallen dust. C.silt was present in higher percentages in the northeastern sector of Kuwait. The lowest percentages were seen during May. The lowest rates were observed in the east of Bubiyan Island.

Areas with high particle size concentration	Areas with low particle size concentration
Abdulli	Bubiyan Island
Gudhi	Failaka Island
Shuaiba	Dibdibah
Huwaymilyah	Wafra Farms

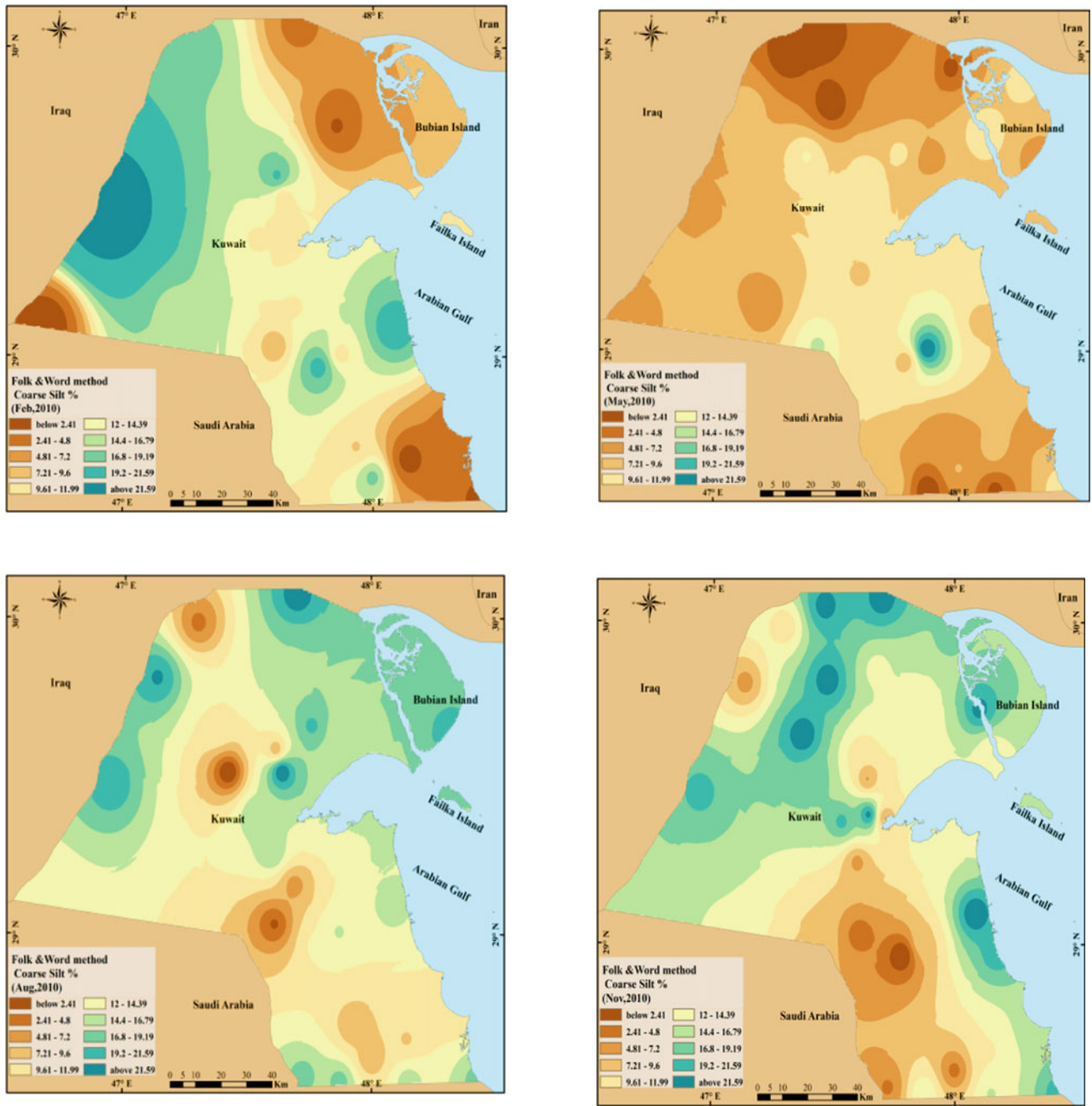


Fig. 3.12 Coarse silt size fractions percentages in Feb, May, Aug, Nov 2010

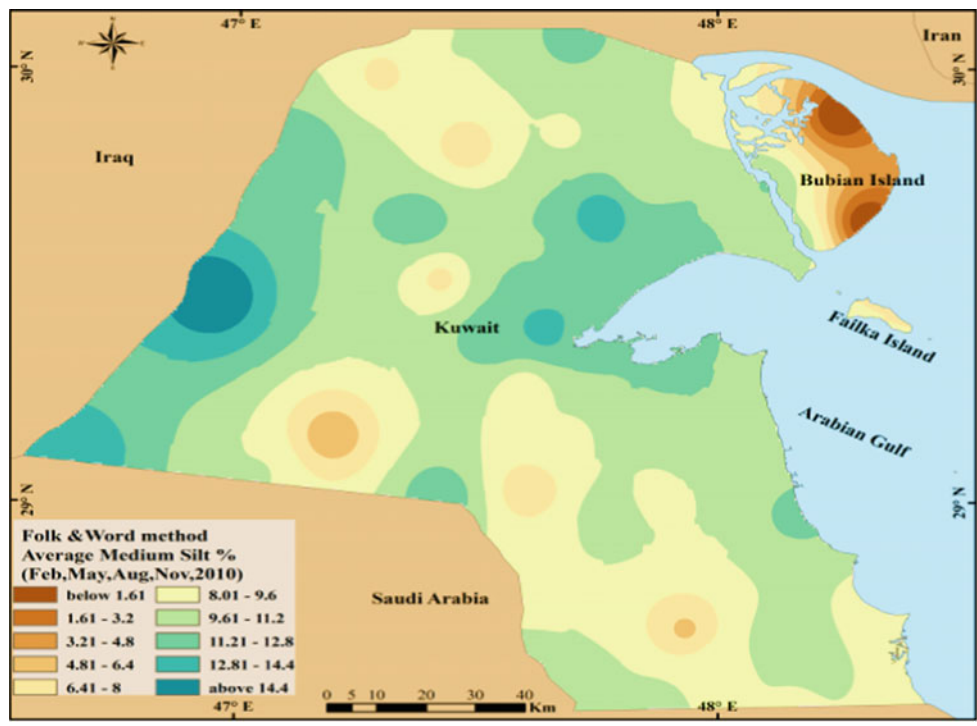


Fig. 3.13 Average percentages of medium silt in the deposited dust (February, May, August, November 2010)

Medium silt (M. Silt) ranges in size between 0.008 mm and 0.016 mm (6-7 phi). M.Silt was present in higher percentages around Kuwait Bay and Wadi Al-Batin at the western borders of Kuwait. The lowest percentages were recorded in February, while the highest were observed in May. Preserved areas (Liyah, around Kuwait Bay, and the fenced border zone) had the highest percentages of M. Silt. The lowest M. Silt percentages were on Bubiyan Island. The second lowest M. Silt percentages were observed in a corridor that extends from Retqah toward Wafra in Kuwait.

Areas with high particle size concentration	Areas with low particle size concentration
Salmi	Bubiyan Island
Ubayriq	Dibdibah
Gudhi	Um qudayr
Mutla	Um Al Madfi'

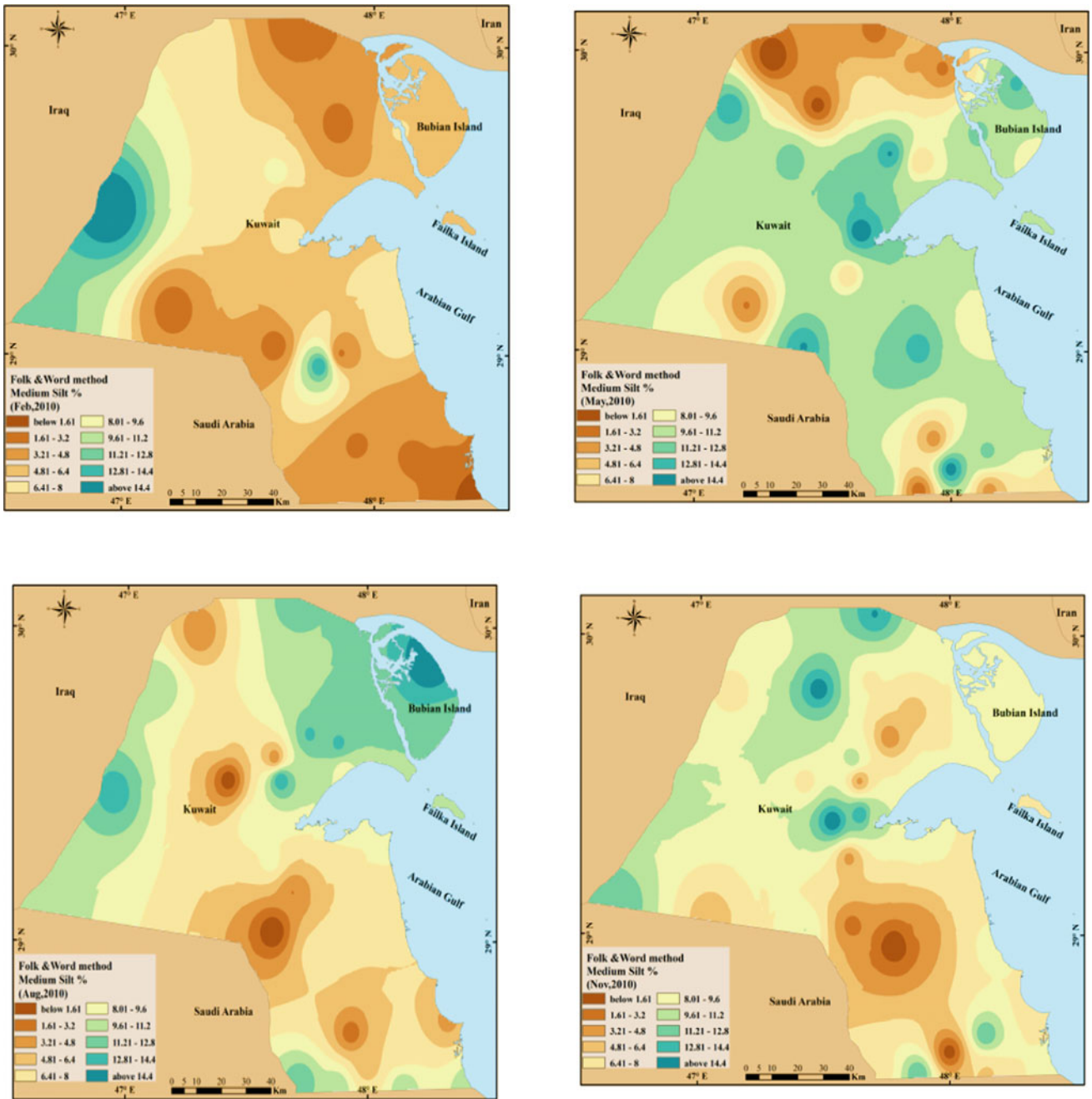


Fig. 3.14 Medium silt size fractions percentages in Feb, May, Aug, Nov 2010

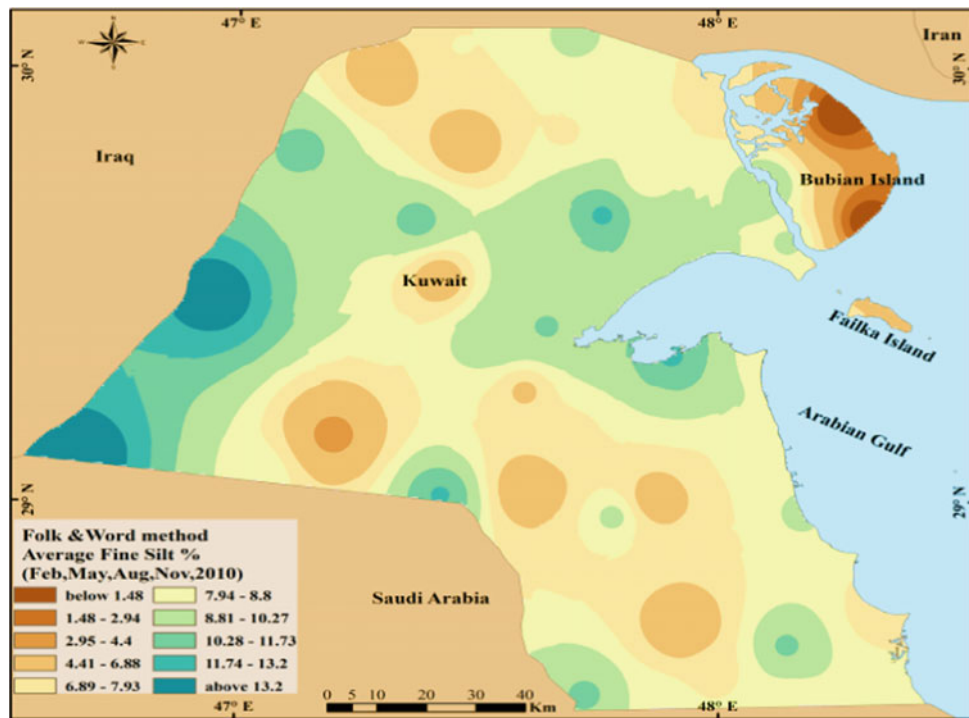


Fig. 3.15 Average percentages of fine silt in the deposited dust (February, May, August, November 2010)

Fine silt (F. Silt) ranges in size between 0.004 mm and 0.008 mm (7–8 phi). Similar to M. Silt, F. Silt was present in higher percentages around Kuwait Bay and Wadi Al-Batin at the western borders of Kuwait. The lowest percentages were recorded during February. During active aeolian processes in August, the lowest percentage rates were noted in a corridor that extends from Retqah toward Wafra in Kuwait. Bubiyan Island had low M. Silt percentages during winter, in February and November, but high percentage rates during summertime in May and August.

Areas with high particle size concentration	Areas with low particle size concentration
Ubayriq	Bubiyan Island
Salmi	Dibdibah
Gudhi	Um Al Madfi'
Um Rimam	Qurani

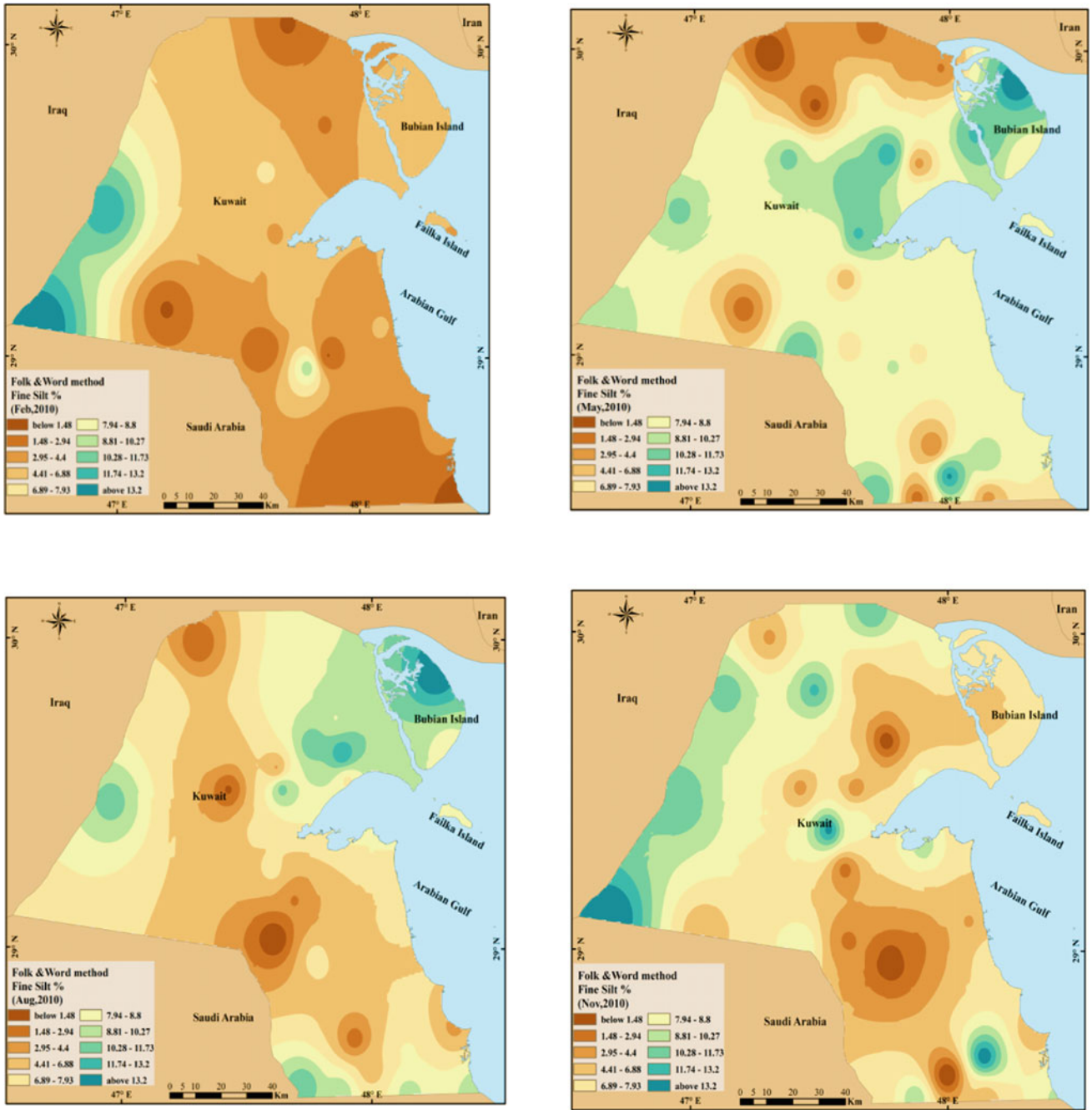


Fig. 3.16 Fine Silt size fractions percentages in Feb, May, Aug, Nov 2010

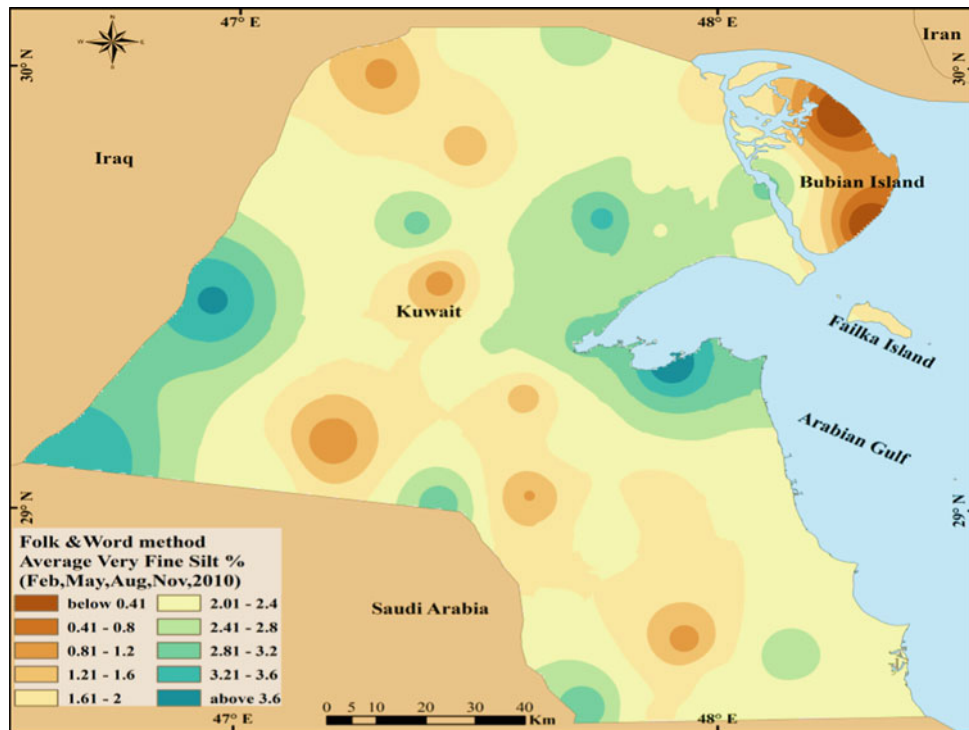


Fig. 3.17 Average percentages of very fine silt in the deposited dust (February, May, August, November 2010)

Very fine silt (V.F. Silt) ranges in size between 0.002 mm and 0.004 mm (8–9 phi). Similar to all the other silt size fractions, it was present in higher percentages around Kuwait Bay and Wadi Al-Batin at the western borders of Kuwait. The lowest percentages were noted during February and August. The lowest percentages of V.F. Silt were in a corridor that extends from the Retqah toward Wafra during August. Bubiyan Island had low V.F. Silt percentages during wintertime but high percentages during summertime.

Areas with high particle size concentration	Areas with low particle size concentration
Shuwaikh	Bubiyan Island
Salmi	Jreshan
Ubayriq	Dibdibah
Khur Fawaris	Qurain

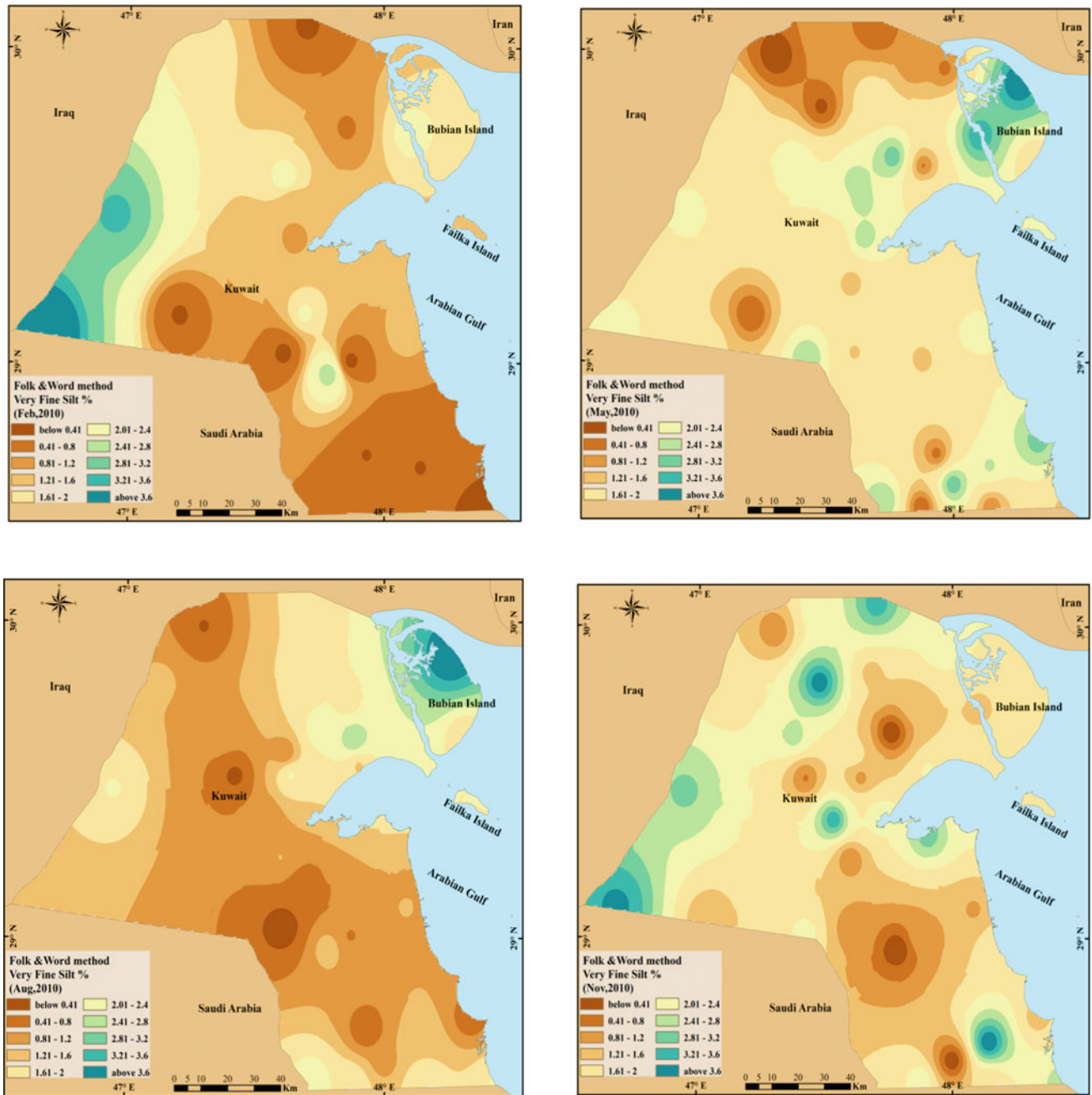


Fig. 3.18 Very fine silt size fractions percentages in Feb, May, Aug, Nov 2010

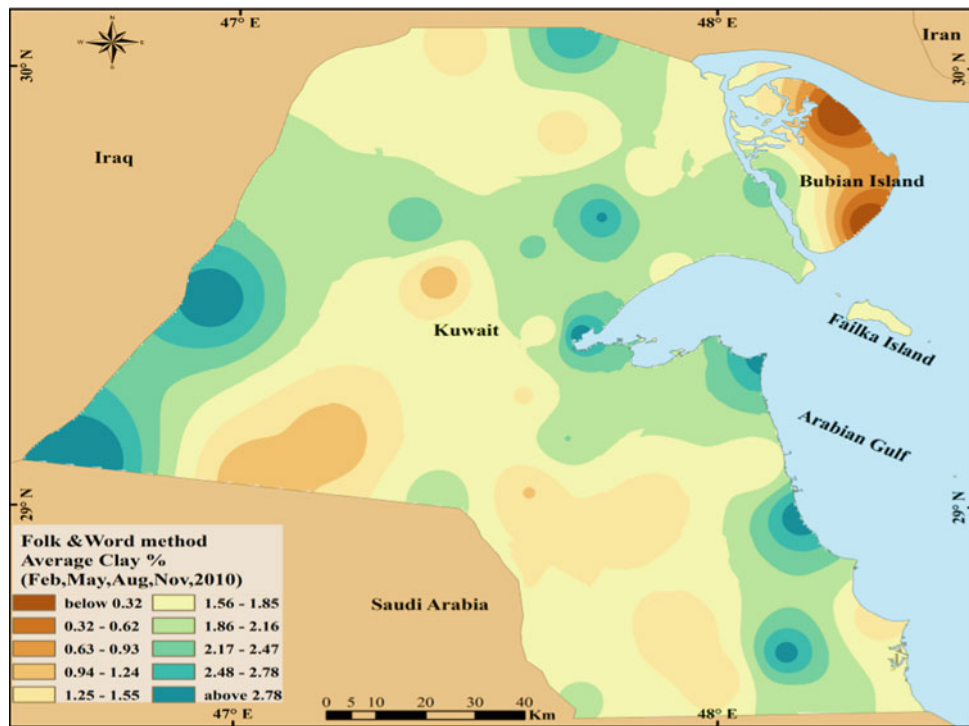


Fig. 3.19 Average percentages of clay in the deposited dust (February, May, August, November 2010)

Clay particle size is less than 0.002 mm (9 phi) and represents a small percentage of fallen dust in Kuwait. Clay presented higher percentage rates around coastal areas, preserved areas, and the Wadi Al-Batin at the western borders of Kuwait. The lowest percentages were during February. Coastal and preserved areas had the highest rates of clay. The western Bubiyan Island contained more clay than the eastern side of the island.

Areas with high particle size concentration	Areas with low particle size concentration
Salmi	Bubiyan Island
Ubayriq	Dibdibah
Abdulli	Kabd
Shuaiba	Qurain

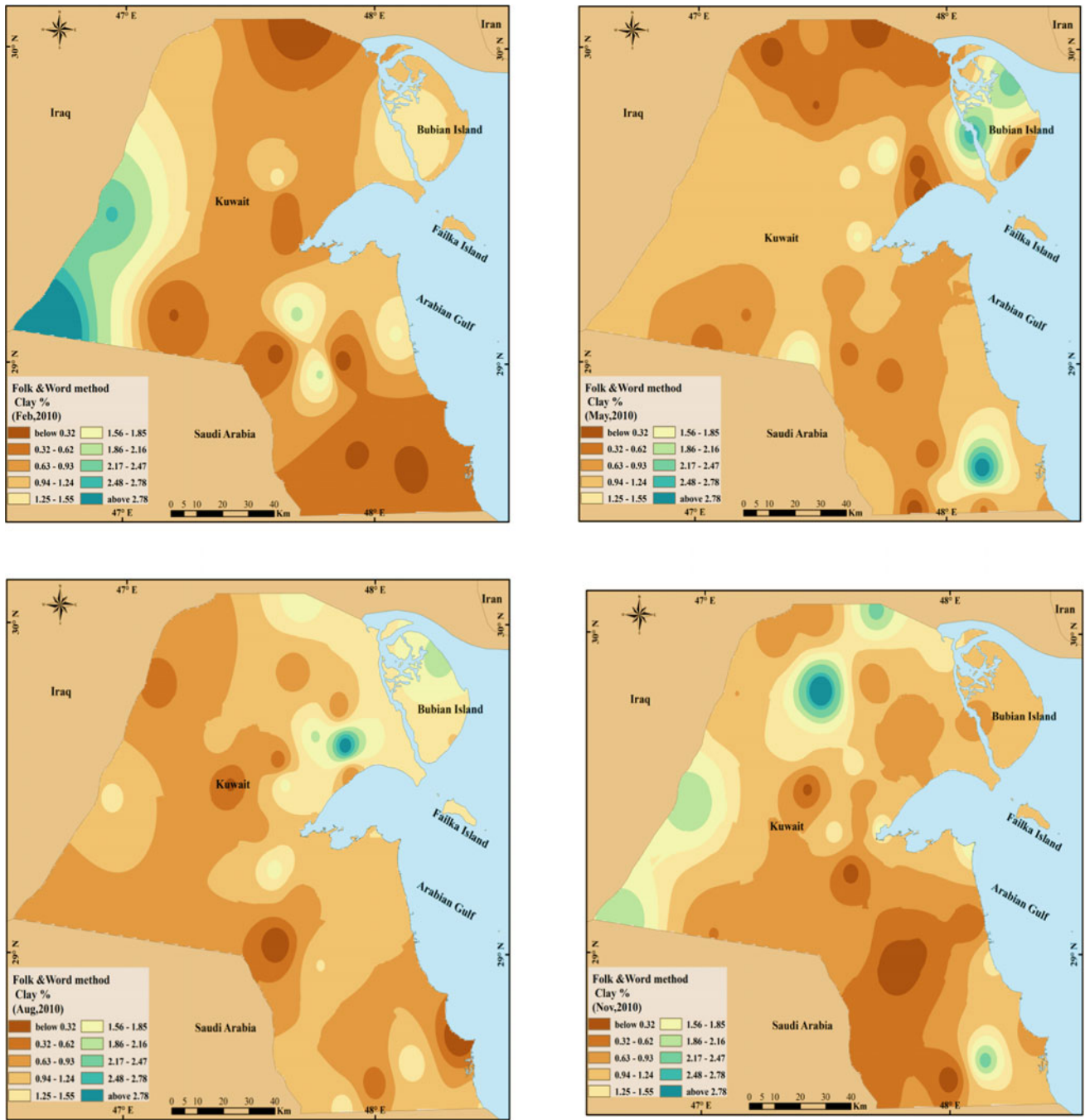


Fig. 3.20 Clay size fraction percentages in Feb, May, Aug, Nov 2010

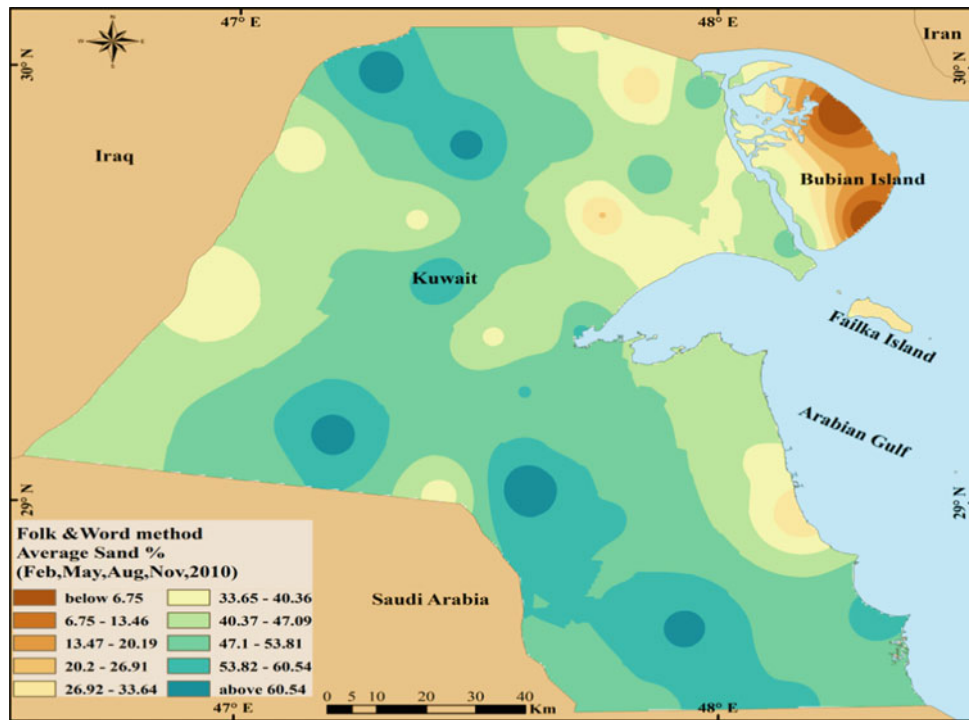


Fig. 3.21 Average percentages of sand in the deposited dust (February, May, August, November 2010)

Sand particles range in size between 2 mm and 0.063 mm (4–2 phi). February had the highest percentages of sand. Furthermore, the highest percentages were noted within a corridor that extends from the Retqah toward Wafra, as these areas experienced the highest aeolian accumulation in Kuwait.

Areas with high particle size concentration	Areas with low particle size concentration
Huwaymilyah	Bubiyan Island
Dibdibah	Failaka Island
Kabd	Shuaiba
Qurain	Abdulli

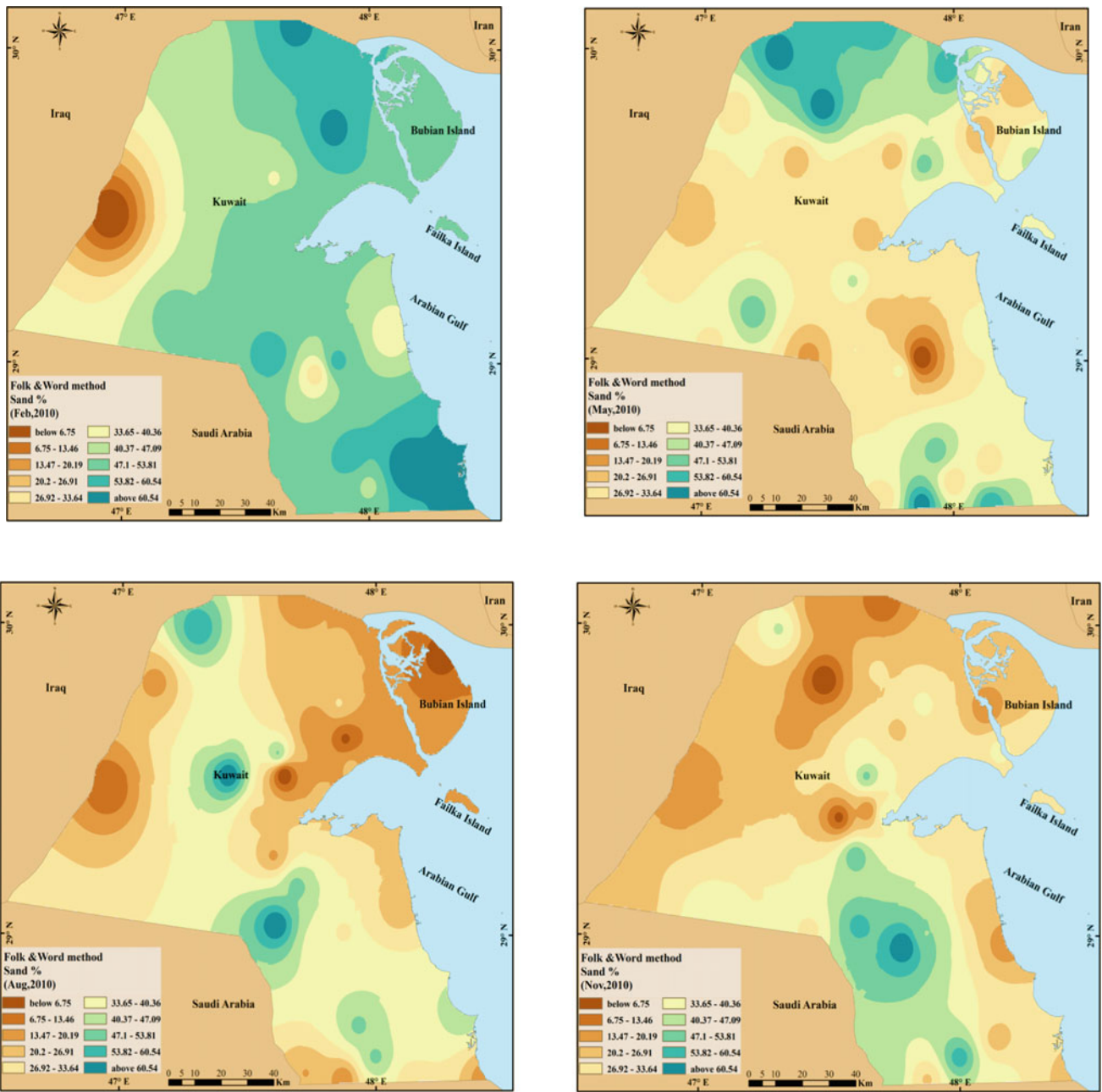


Fig. 3.22 Sand size fractions percentages in Feb, May, Aug, Nov 2010

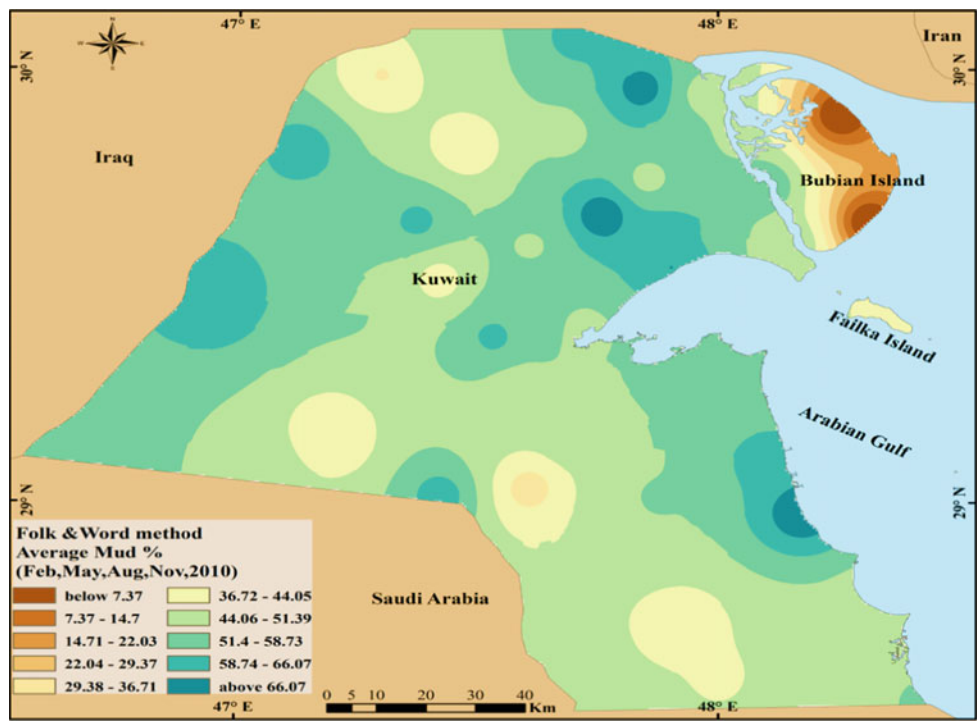


Fig. 3.23 Average percentages of mud in the deposited dust (February, May, August, November 2010)

Mud size fractions are less than 0.063 mm (4 phi). Mud contains two main size fractions: silt and clay. The northern parts of Kuwait had higher mud percentages than the south. February had the lowest mud percentages, while August and November had the highest percentage rates. The highest percentages were recorded within a corridor that extends from the Retqah toward Wafra, as these areas experienced the highest aeolian accumulation in Kuwait.

Areas with high particle size concentration	Areas with low particle size concentration
Ubayriq	Bubiyan Island
Abdulli	Failaka Island
Gudhi	Wafra Farms
Shuaiba	Ratqah

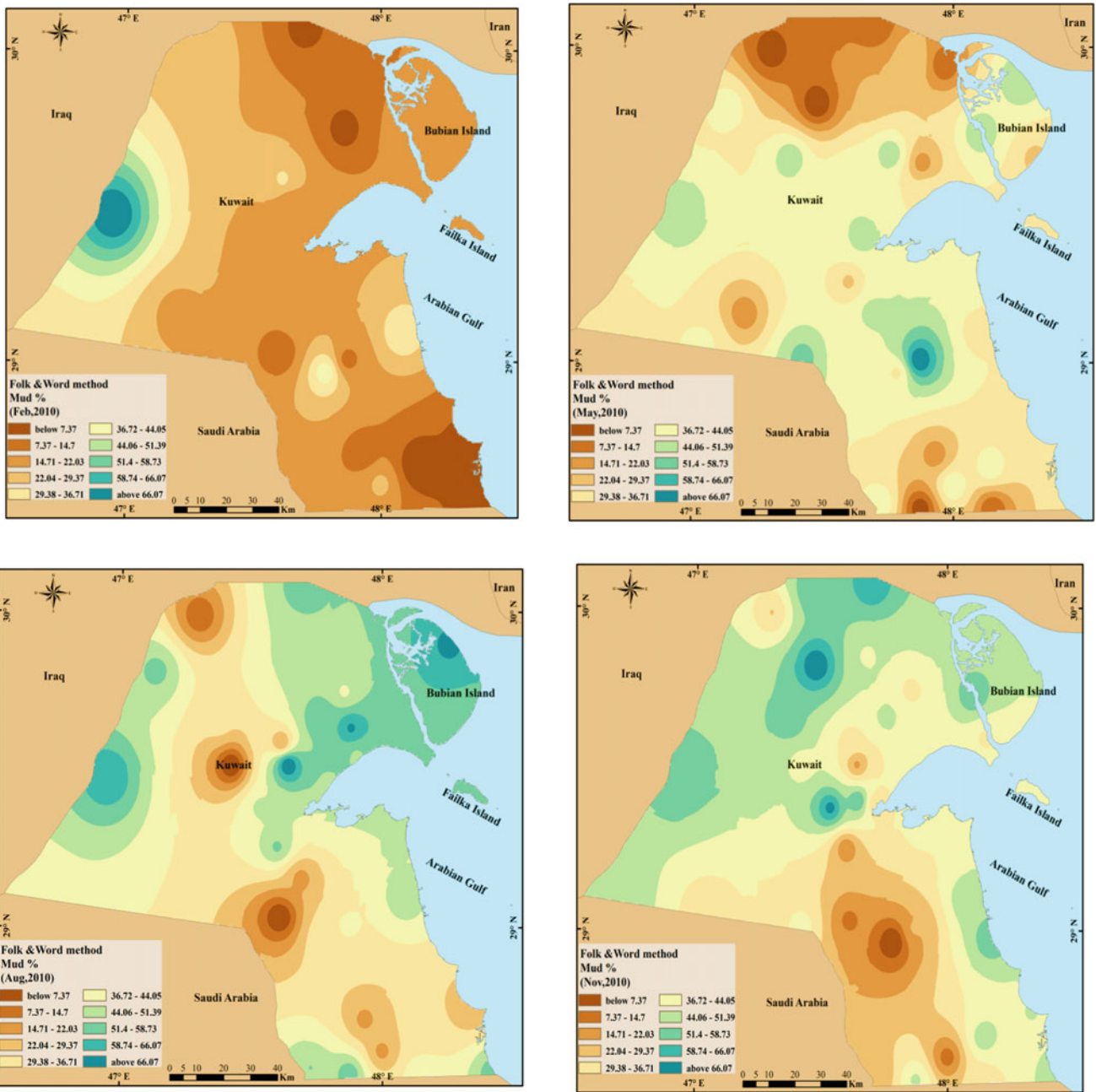


Fig. 3.24 Mud size fractions percentages in Feb, May, Aug, Nov 2010

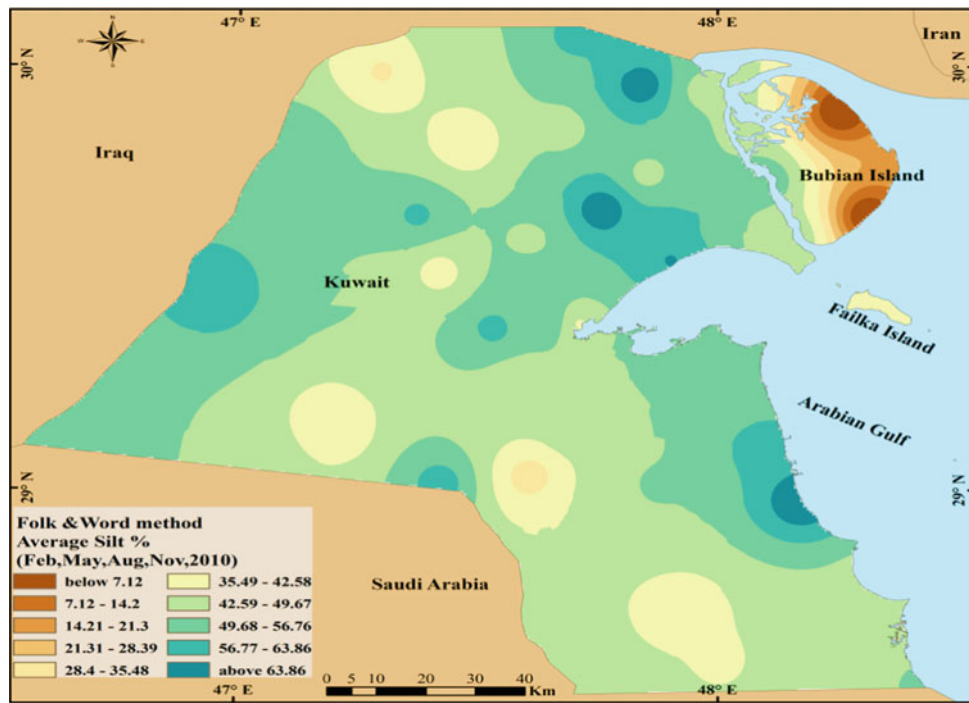


Fig. 3.25 Average percentages of silt in the deposited dust (February, May, August, November 2010)

Silt size fractions range in size from 0.002 mm to 0.063 mm (9–4 phi). Similar to mud, northern Kuwait had higher mud percentages than the south. February had the lowest mud percentages, while August and November had the highest rates. Preserved areas were more silt-dominant than other locations in Kuwait.

Areas with high particle size concentration	Areas with low particle size concentration
Ubayriq	Bubiyan Island
Abdulli	Failaka Island
Gudhi	Wafra Farms
Shuaiba	Ratqah

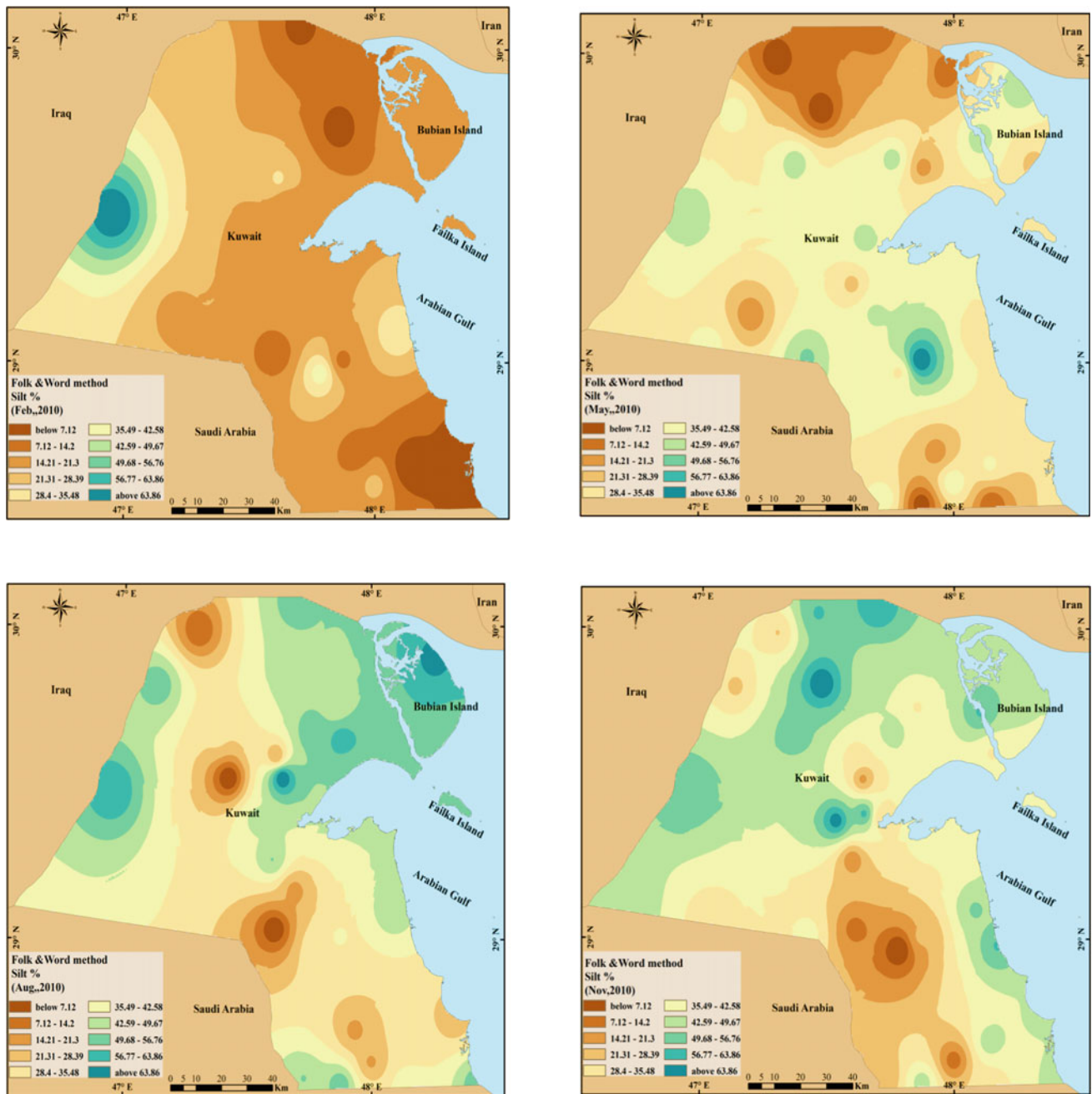


Fig. 3.26 Silt size fractions percentages in Feb, May, Aug, Nov 2010

Methodology

The parameters proposed by Folk And Ward (1957) have been widely used for quantitative comparisons between natural grain-size distribution and the log-normal

distribution that shows better-sorted sediments have lower values of σ_1 (Table 2).

Table 2 Terminology applied to graphical statistical parameter values (modified after Folk & Ward 1957)

Inclusive graphic standard deviation or (phi sorting) (σ)		Inclusive Graphic Skewness or (phi skewness) (Sk1)		Inclusive Graphic kurtosis or (phi kurtosis) (KG)	
Very well sorted	<0.35	Very positively skewed	+0.3– + 1.0	Very platykurtic	<0.67
Well sorted	0.35–0.50	Positively skewed	+0.1– + 0.3	Platykurtic	0.67 – 0.90
Well sorted moderately	0.50–0.70	Symmetrical	+0.1– – 0.1	Mesokurtic	0.90 – 1.11
Moderately sorted	0.70–1.00	negatively skewed	–0.1 to –0.3	Leptokurtic	1.11 – 1.50
Poorly sorted	1.00–2.00	Very negatively skewed	–0.3 to –1.0	Very leptokurtic	1.50 – 3.00
Very poorly sorted	2.00–4.00				

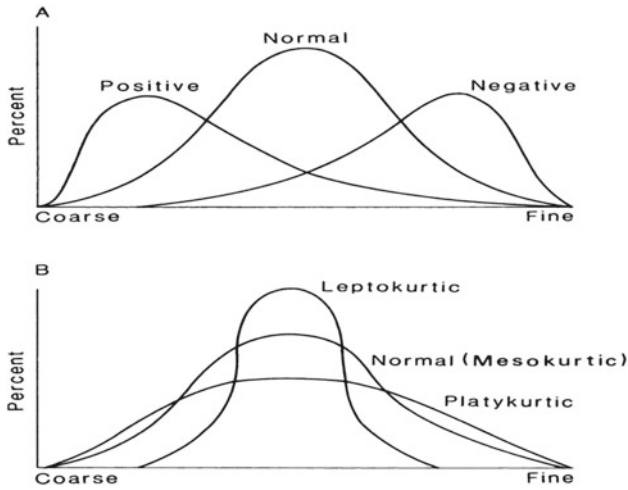


Fig. 3.27 Diagrams illustrating the nature of **a** skewness (asymmetry) and **b** kurtosis (peakedness) in grain-size distributions (Pye and Tsoar, 1990)

Positive values of Sk1 indicate that the distribution has a more evident trail of fine material compared with a log-normal distribution. In contrast, negative values of Sk1 announce an insufficiency of fine particles compared with the log-normal distribution (Fig. 3.27).

The ‘peakedness’ or kurtosis of a distribution is indicated by the inclusive graphic kurtosis:

Frequency distributions, which are flatter than a normal probability curve, are referred to as platykurtic, and strongly peaked curves are described as leptokurtic. Intermediate curves are referred to as mesokurtic (Table 2, Fig. 3.27).

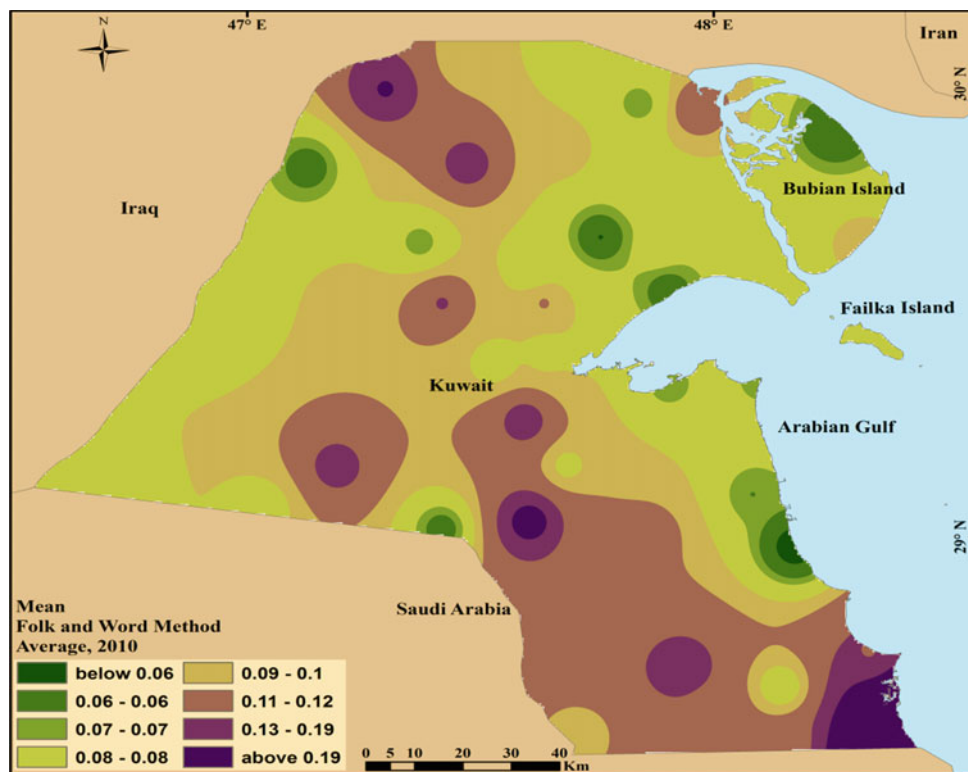


Fig. 3.28 Average statistical parameters (mean) for the deposited dust. (February, May, August, November 2010)

The mean particle size for dust fallout in Kuwait was coarser in the southern areas of Kuwait. The particle size ranges from very fine sand to very coarse silt. There was a zone of coarsening dust particle size that extends from the Ratqah, in northern Kuwait, to the south at Wafra Farms. During August, the mean size tended to be smaller, while it is finer during May and November.

Areas with high statistical parameter concentration	Areas with low statistical parameter concentration
Khiran Ratqah Dibdibah Kabd Wafra Farms	Bubiyan Island Salmi Shuaiba Ubayriq Gudhi

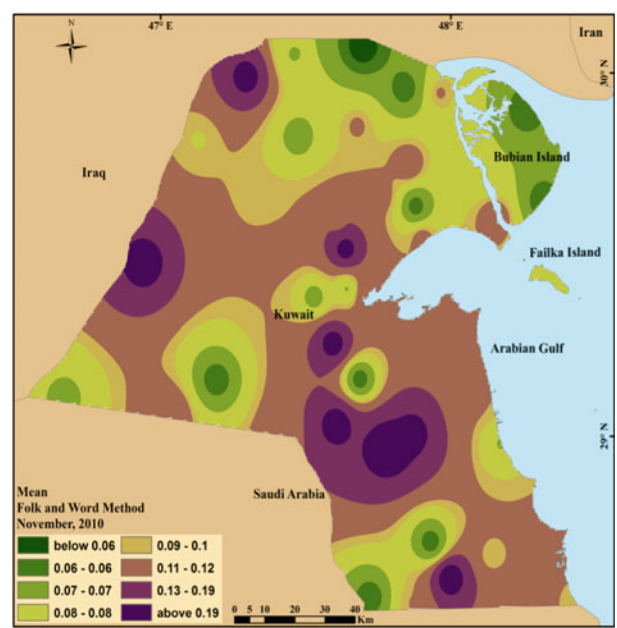
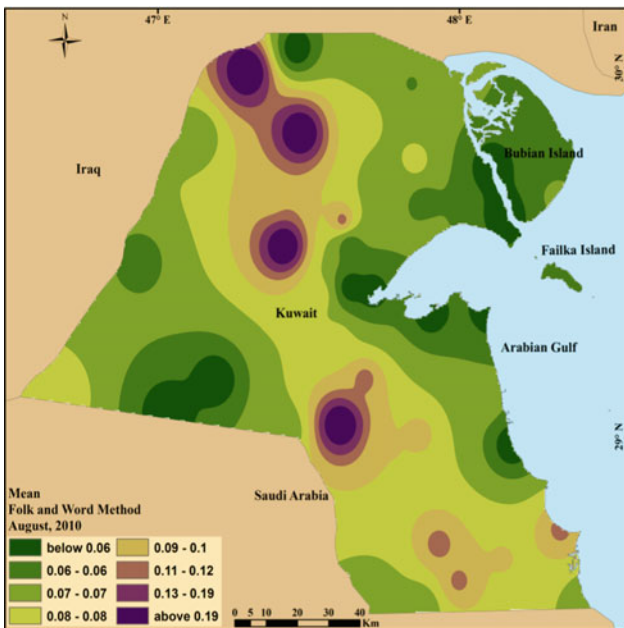
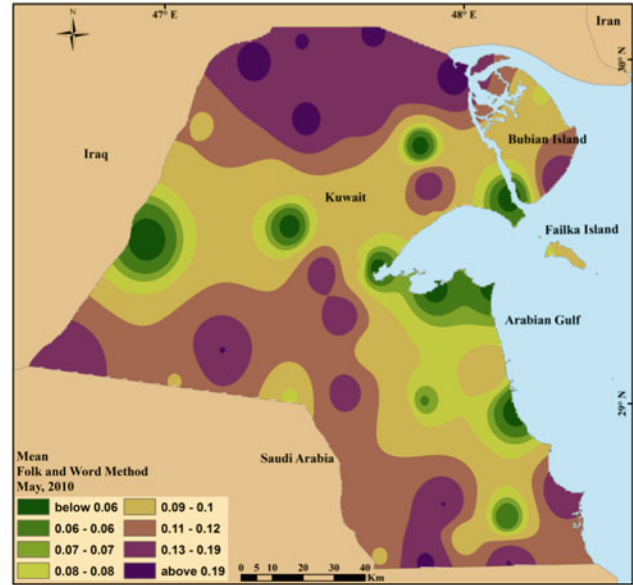
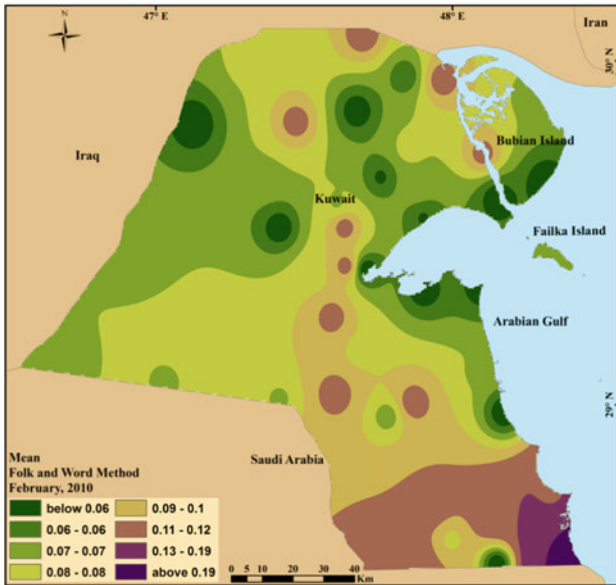


Fig. 3.29 Mean for the deposited dust February, May, August, November 2010

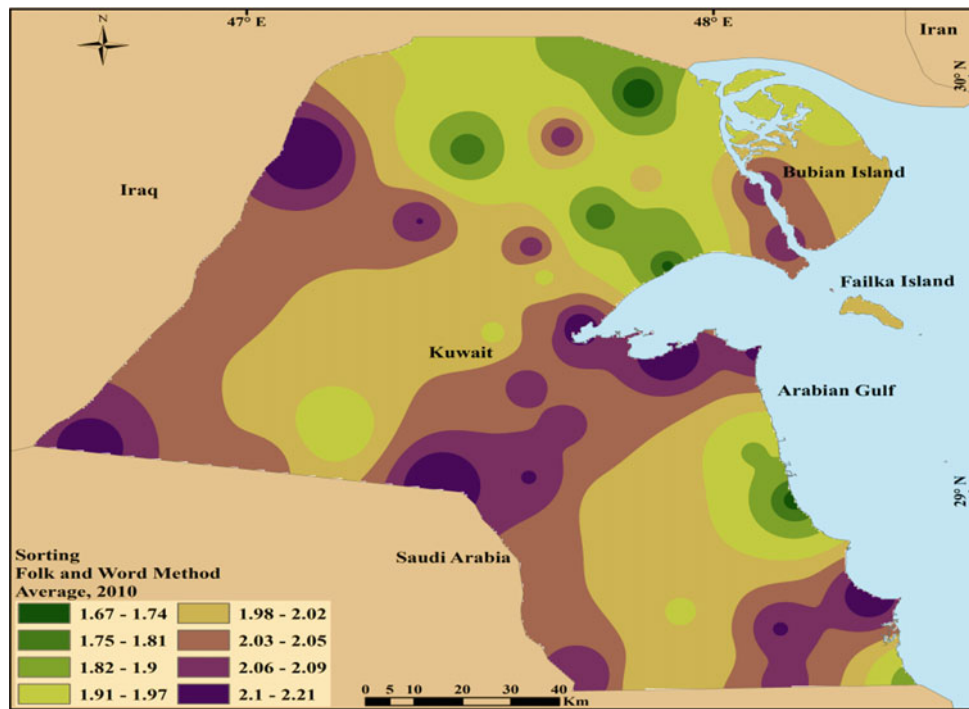


Fig. 3.30 Average statistical parameters (sorting) for the deposited dust. (February, May, August, November 2010)

The dust fallout particles in Kuwait are poorly to very poorly sorted. Particles are very poorly sorted in Wadi Al-Batin, the Jahra, and the southern areas of Kuwait. For all months, the dust fallout particles are better classified around Kuwait Bay.

Areas with high statistical parameter concentration	Areas with low statistical parameter concentration
Jreshan	Ratqah
Salmi	Dibdibah
Kabd	Um Niqa
Doha	Shuaiba
Khiran	Gudhi

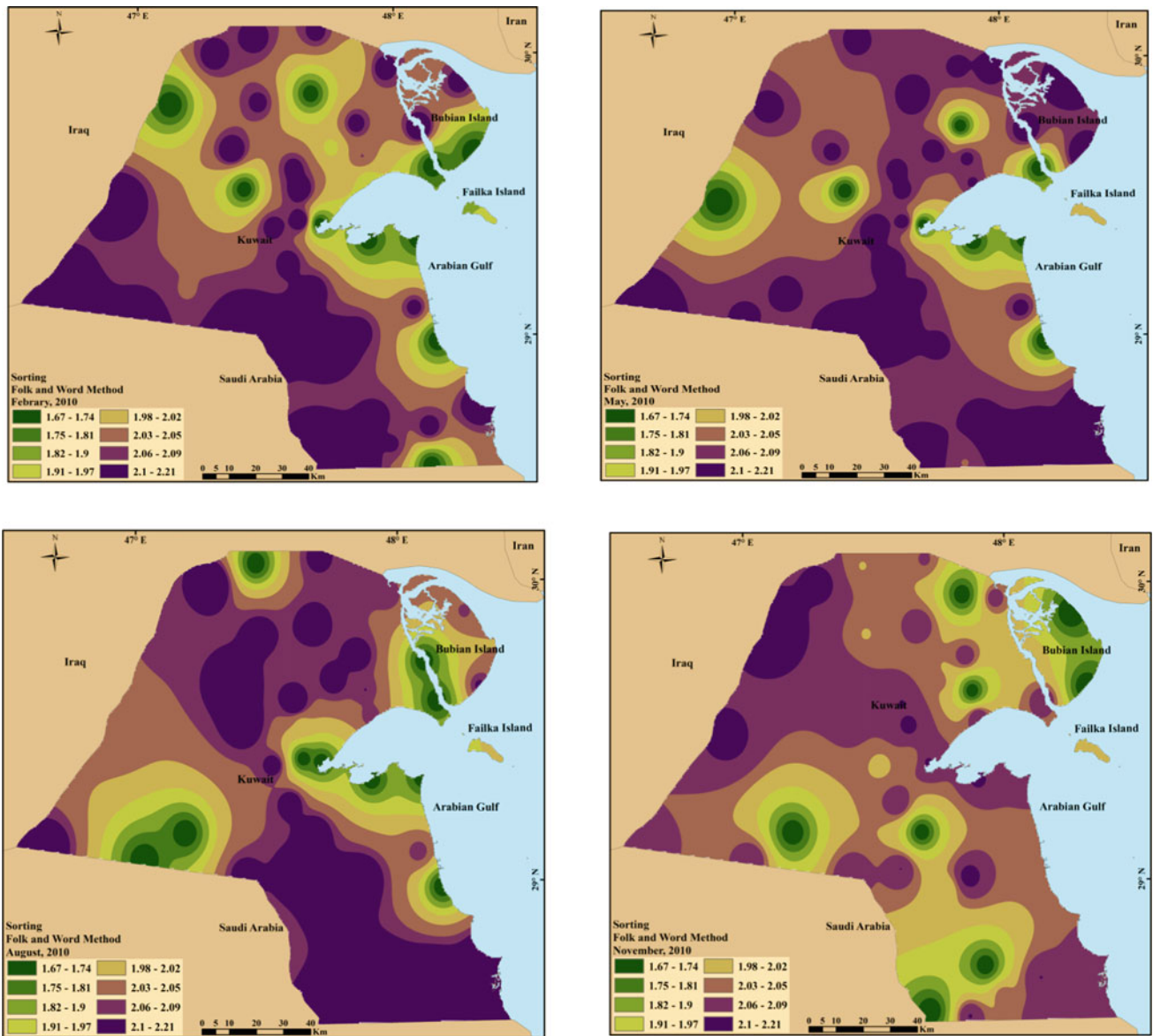


Fig. 3.31 Sorting for the deposited dust February, May, August, November 2010

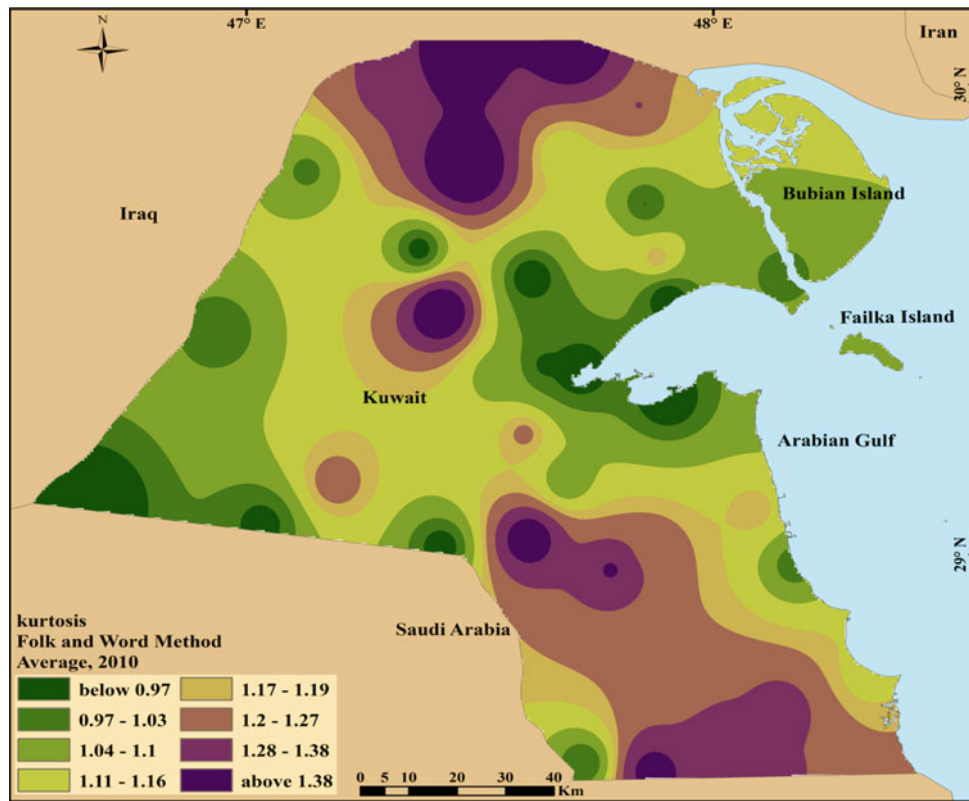


Fig. 3.32 Average statistical parameters (kurtosis) for the deposited dust. (February, May, August, November 2010)

The dust fallout in Kuwait is leptokurtic to mesokurtic. The fallout was leptokurtic in the southern and northern areas of Kuwait, and mesokurtic around coastal areas (mainly around Kuwait Bay) and Wadi Al-Batin at the western borders of Kuwait. Kuwaiti fallen dust tended to be more mesokurtic during February and May. Wadi Al-Batin was characterized by predominantly mesokurtic dust fallout throughout the year.

Areas with high statistical parameter concentration	Areas with low statistical parameter concentration
Abdulli	Bubiyan Island
Kabd	Salmi
Liyah	Shuaiba
Ratqah	Ubayriq
Wafra Farms	Mutla

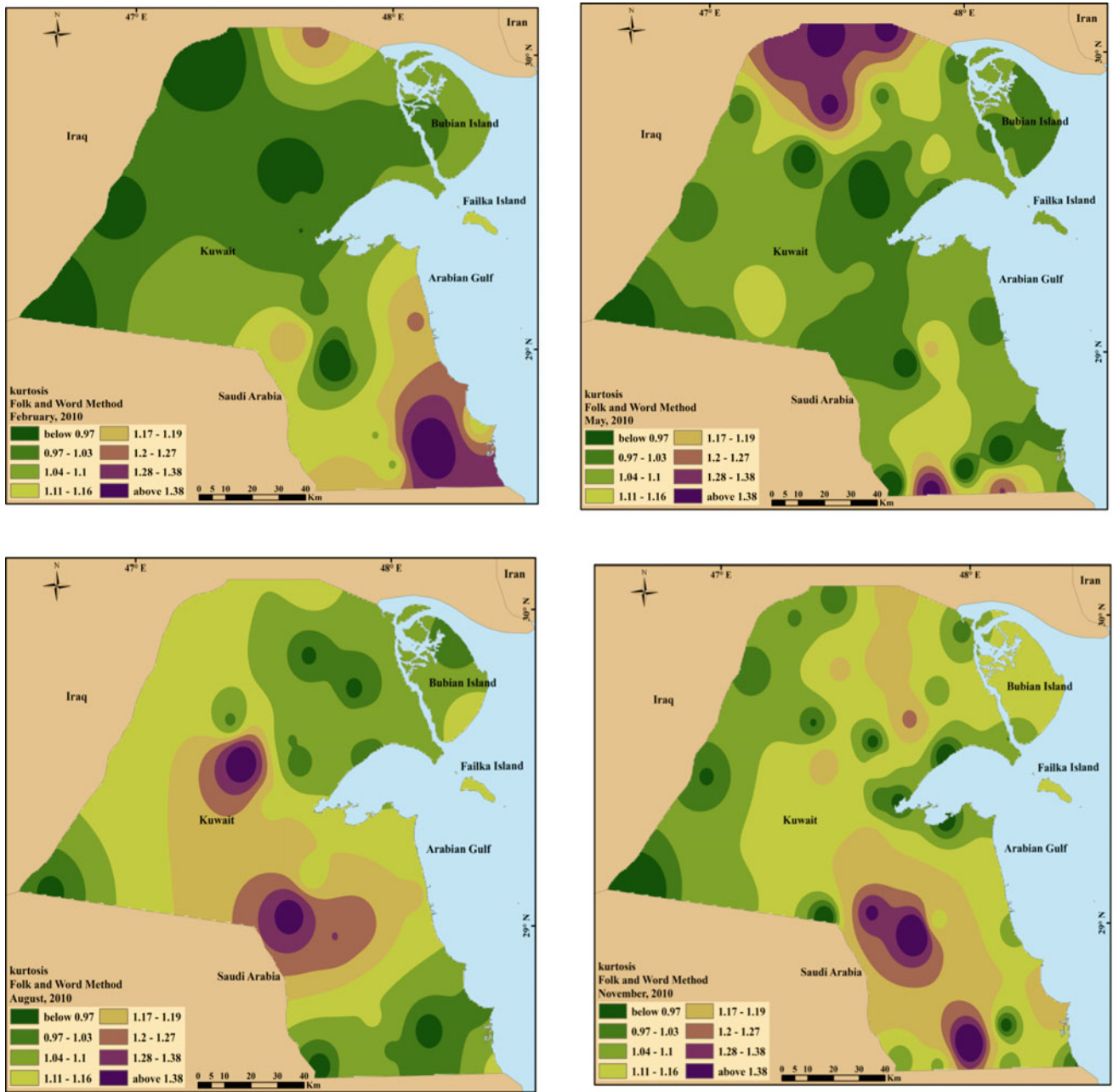


Fig. 3.33 Kurtosis for the deposited dust (February, May, August, November 2010)

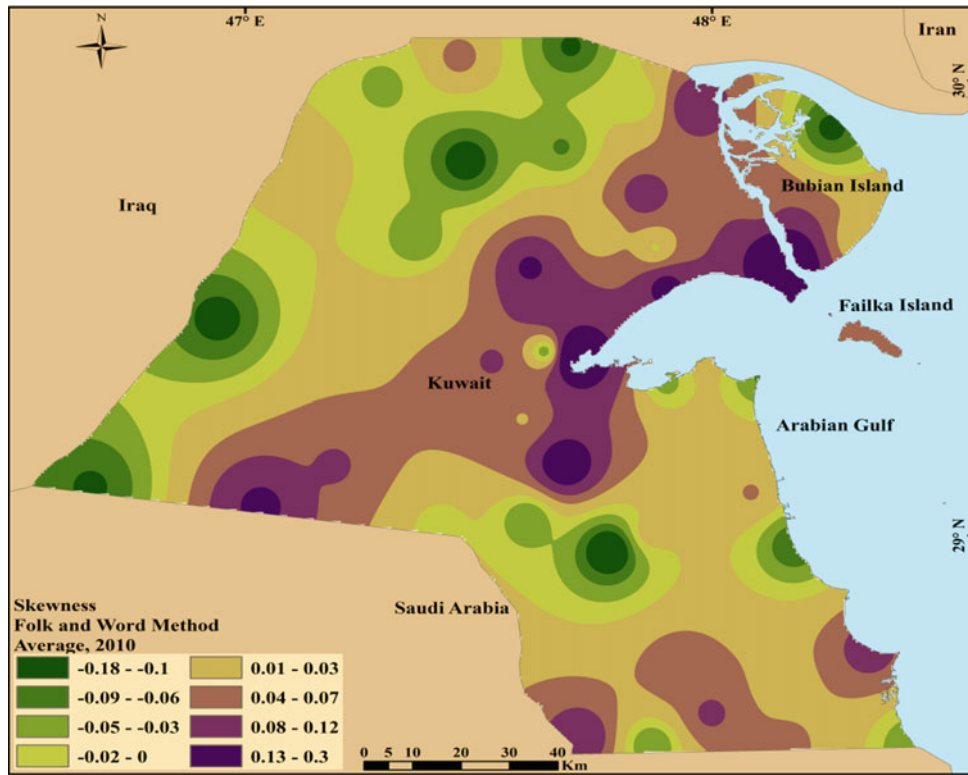


Fig. 3.34 Average statistical parameters (skewness) for the deposited dust. (February, May, August, November 2010)

The dust fallout in Kuwait varies in values from negatively skewed to positively skewed. There were two corridors with positive skewness, the first extends from the Sabiyah toward the Dibdibah, while the second is parallel to the first in the southern areas of Kuwait. Kuwaiti fallen dust tended to be more negatively skewed during August.

Areas with high statistical parameter concentration	Areas with low statistical parameter concentration
Subiyah	Ratqah
Dibdibah	Salmi
As Sulaiyah	Shuaiba
Doha	Kabd
Um Niqa	Um Al Madfi'

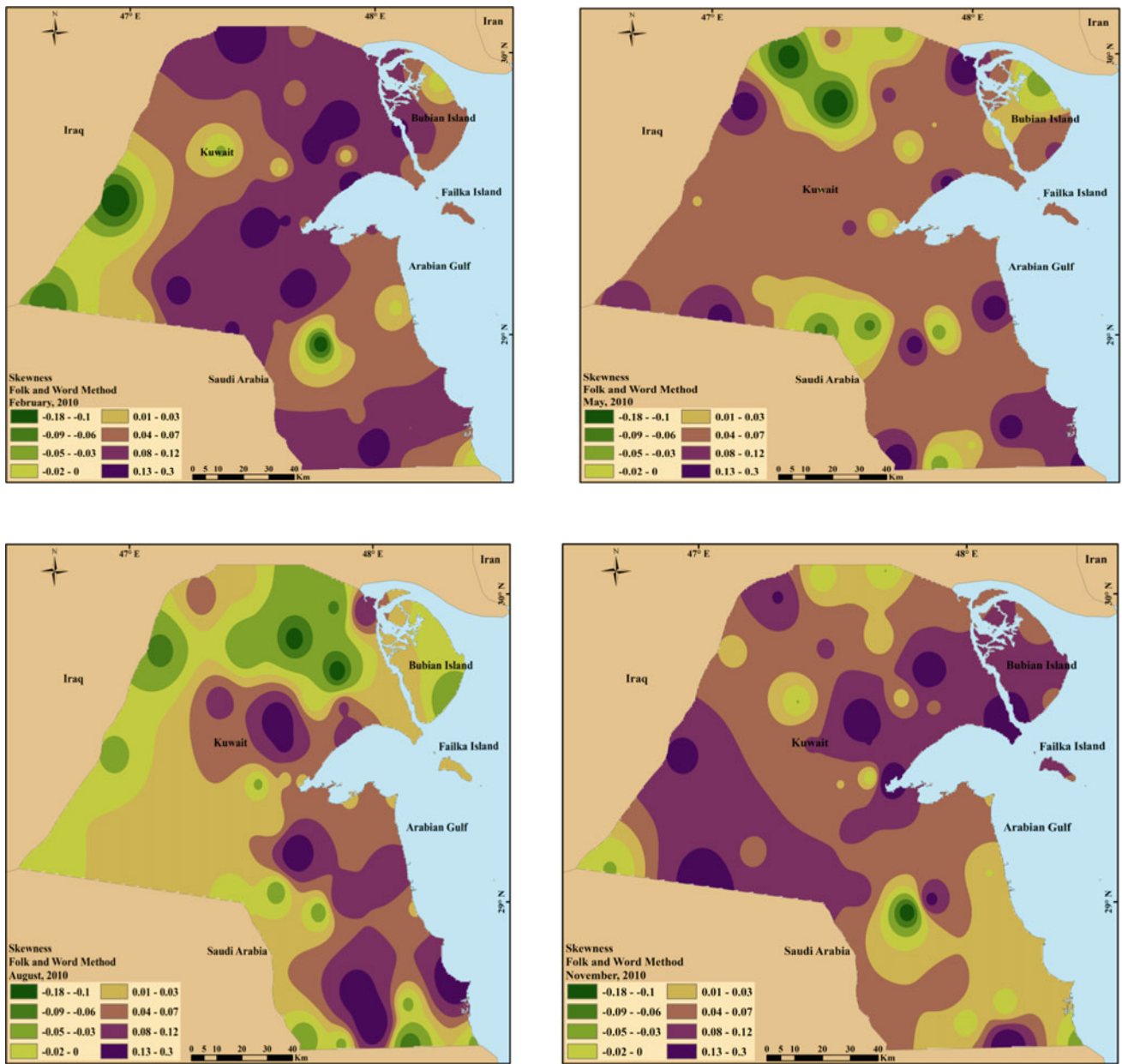


Fig. 3.35 Skewness for the deposited dust (February, May, August, November 2010)

References

- Carter, R. W. G. (1982). Some problems associated with the analysis and interpretation of mixed carbonate and quartz beach sand, illustrated by examples from north-west Ireland. *Sediment Geol*, 33, 35–56. [https://doi.org/10.1016/0037-0738\(82\)90026-4](https://doi.org/10.1016/0037-0738(82)90026-4).
- Folk, R. L., & Ward, W. C. (1957). Brazos river bar. A study in the significances of grain size parameters. *Journal of Sedimentary Petrology*, 27, 3–26. <https://doi.org/10.1306/74D70646-2B21-11D7-8648000102C1865D>.
- Friedman, G. M., & Sanders, F. E. (1978). Principles of sedimentology, Wiley and sons, New York. 792.
- Kennedy, S. K., Meloy, T. P., & Gurney, T. E. (1985). Sieve data—size and shape information. *Journal of Sedimentary Petrology*, 55, 356–360. <https://doi.org/10.1306/212F86CA-2B24-11D7-8648000102C1865D>.
- Komar, Paul D., & Cui, Bingquan. (1984). The analysis of grain-size measurements by sieving and settling-tube techniques. *Journal of Sedimentary Research*, 54, 2. <https://doi.org/10.1306/212F8481-2B24-11D7-8648000102C1865D>.
- Krumbein, W. C. (1934). Size frequency distributions of sediments. *Journal of Sedimentary Research*, 4, 2. <https://doi.org/10.1306/D4268EB9-2B26-11D7-8648000102C1865D>.
- Pye, K., & Tsoar, H. (1990). *Aeolian sand and sand dunes*. London: Unwin Hyman. p. 458. <http://dx.doi.org/10.1007/978-94-011-5986-9>. ISBN 978-94-011-5988-3.
- Udden, J. A. (1914). Mechanical composition of some clastic sediments. *Bulletin of the Geological Society*, 25, 655–744.
- Wentworth, C. K. (1922). A scale of grade and class terms for clastic sediments. *The Journal of Geology*, 30(5), 377–392. <https://doi.org/10.1086/622910>.

Open Access This chapter is licensed under the terms of the Creative Commons Attribution 4.0 International License (<http://creativecommons.org/licenses/by/4.0/>), which permits use, sharing, adaptation, distribution and reproduction in any medium or format, as long as you give appropriate credit to the original author(s) and the source, provide a link to the Creative Commons licence and indicate if changes were made.



The images or other third party material in this chapter are included in the chapter's Creative Commons licence, unless indicated otherwise in a credit line to the material. If material is not included in the chapter's Creative Commons licence and your intended use is not permitted by statutory regulation or exceeds the permitted use, you will need to obtain permission directly from the copyright holder.



Abstract

- The two main particle size components of the dust samples were subjected to mineralogical analysis to identify the mineral constituents and determine their frequency percentage in each textural class; the fine sand (particle size between 0.125 and 0.063 mm) and Mud (less than 0.063 mm).
- The average percentage of minerals was mapped out for each season i.e. March, June, September and December 2010 showing the high and low mineral concentration in areas in Kuwait covering the mineral concentrations of Calcite, Carbonate, clay minerals, dolomite, feldspars, and quartz.

Methodology

The two main particle-size components of the dust samples were subjected to mineralogical analysis, namely:

1. Very fine sand (particle size between 0.125 mm and 0.063 mm);
2. Mud (less than 0.063 mm).

The mineralogical analysis of dust particles was performed to identify the mineral constituents and to determine their frequency percentage in each textural class. The whole components of the dust samples were gently powdered and analyzed using XRD and a Philips PW-1830 Powder Diffractometer, and data were semi-quantitatively analyzed using X'Pert II software. Furthermore, to observe seasonal variations, the following four months' worth of samples was analyzed:

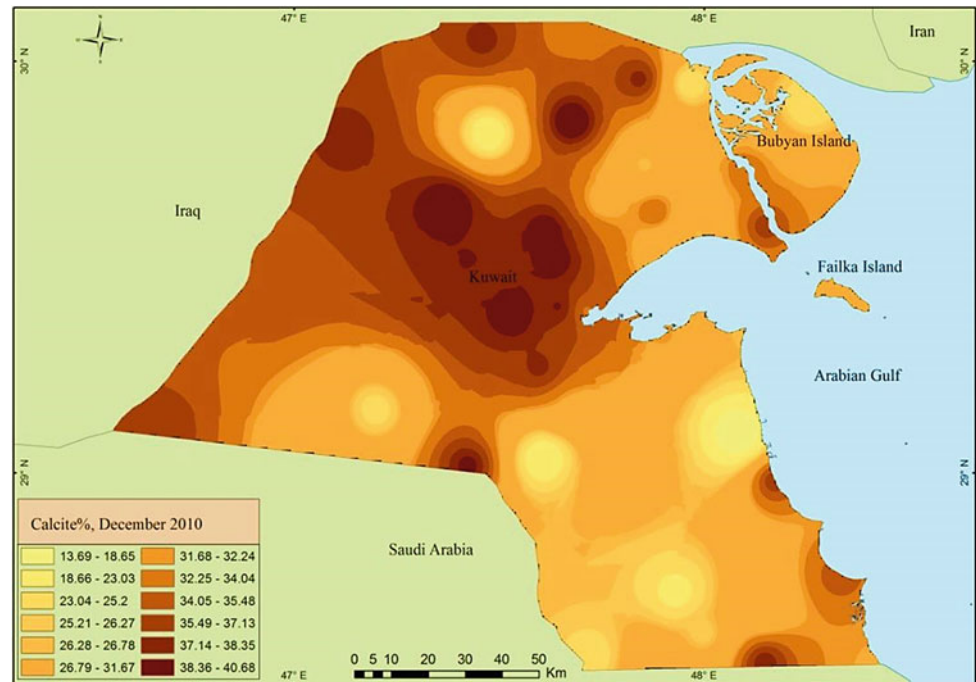
1. March 2010;
2. June 2010;
3. September 2010;
4. December 2010.

There were 47 site locations for the selected four months.

A. Al-Dousari (✉)
Crisis Decision Supports Program (CDS), Environment and Life Sciences Research Center (ELSRC), Kuwait Institute for Scientific Research (KISR), P.O. Box 24885 Safat, 13109, Kuwait
e-mail: adousari@kISR.edu.kw

M. Bahbahani
Environmental Pollution and Climate Program (EPCP), Environment and Life Sciences Research Center (ELSRC), Kuwait Institute for Scientific Research (KISR), P.O. Box 24885 Safat, 13109, Kuwait
e-mail: mbahbaha@kISR.edu.kw

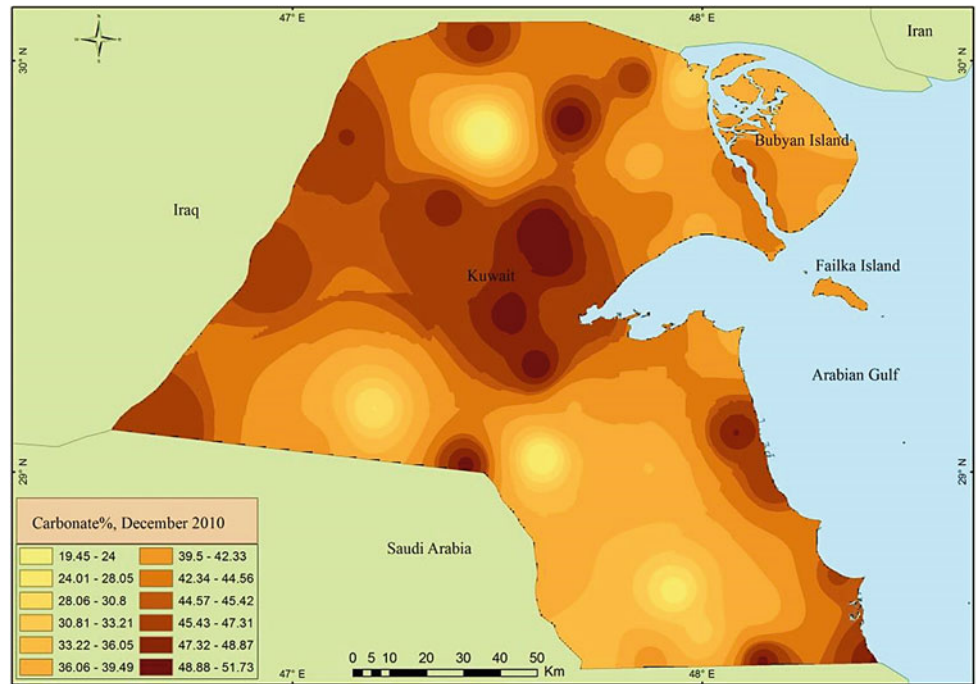
Fig. 4.1 Average percentages of calcite, December 2010



The mineralogy of dust fallout in Kuwait contains quartz, calcite, carbonates, dolomites, feldspars, and a small percentage of other minerals. Quartz and carbonates form the significant percentage of dust fallout mineralogy. The percentage of carbonates, in general, was highest during winter (October–April). Calcite, as a major constituent of carbonates in Kuwait, was higher in Liyah and coastal areas and extending toward the northwest. The Dibdibah Formation contains calcretes and dolcretes as a major source of carbonate dust.

Areas with high mineral concentration	Areas with low mineral concentration
Liyah	Northern Bubiyan Island
Huwaymilyah	Dibdibah
Abdulli	Ahmadi
Salmi	Quranis
Mutla	Khur Fawaris

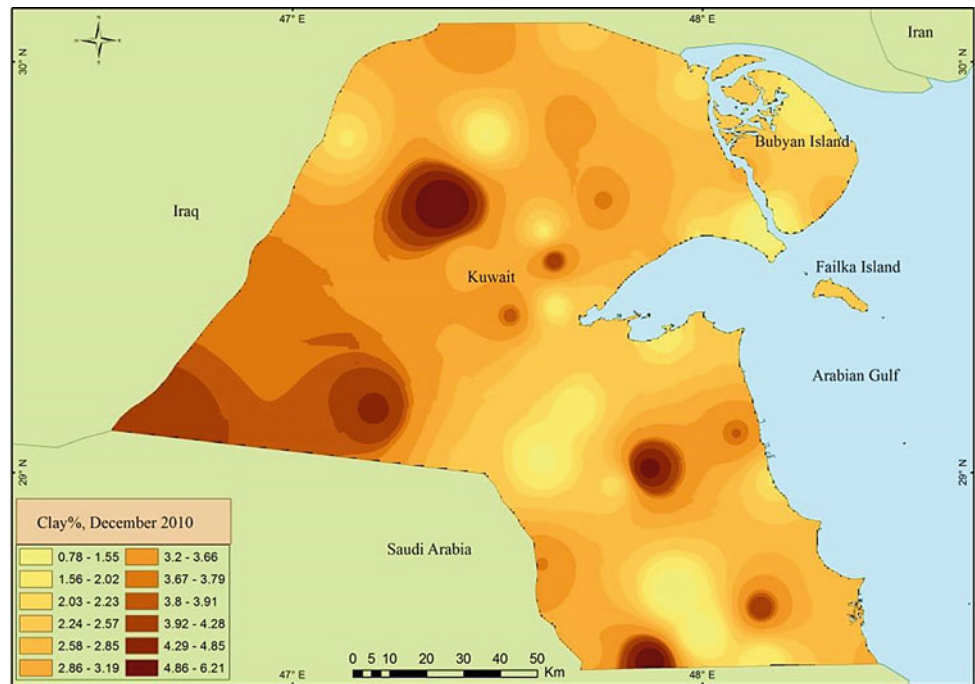
Fig. 4.2 Average percentages of carbonate, December 2010



The mineralogy of dust fallout in Kuwait constitutes carbonates as a main component. Quartz and carbonates form the major percentage of dust fallout mineralogy. The percentage rate of carbonates, in general, was highest in winter and springtime (October–April). Carbonates in Kuwait were greater in Liyah and in the coastal area that extends toward the northwest. The Dibdibah Formation contains calcretes and dolcretes as a major source of carbonate dust.

Areas with high mineral concentration	Areas with low mineral concentration
Liyah	Roudhatain
Huwaymilyah	Dibdibah
Abdulli	Ahmadi
Salmi	Qurain
Mutla	Khur Fawaris

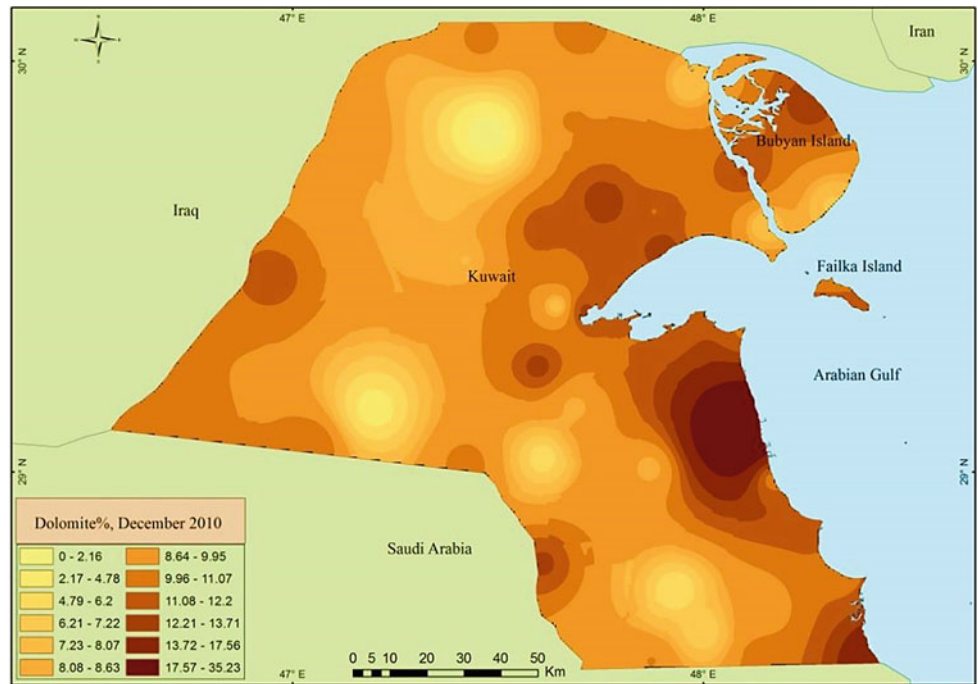
Fig. 4.3 Average percentages of clay, December 2010



The mineralogy of dust fallout in Kuwait contains a small percentage of clay minerals. This percentage, in general, was highest during wintertime (October–April). Clay minerals, as a minor constituent in Kuwait, were more present in Salmi, Dibdibah, and Liyah, as well as in the drainage systems, including “wadis” and “playas,” which are the primary local sources of dust in Kuwait.

Areas with high mineral concentration	Areas with low mineral concentration
Salmi	Roudhatain
Dibdibah	Bubiyah Island
Liyah	Kabd
Ahmadi	Qurain
Ubayriq	Wafra Farms

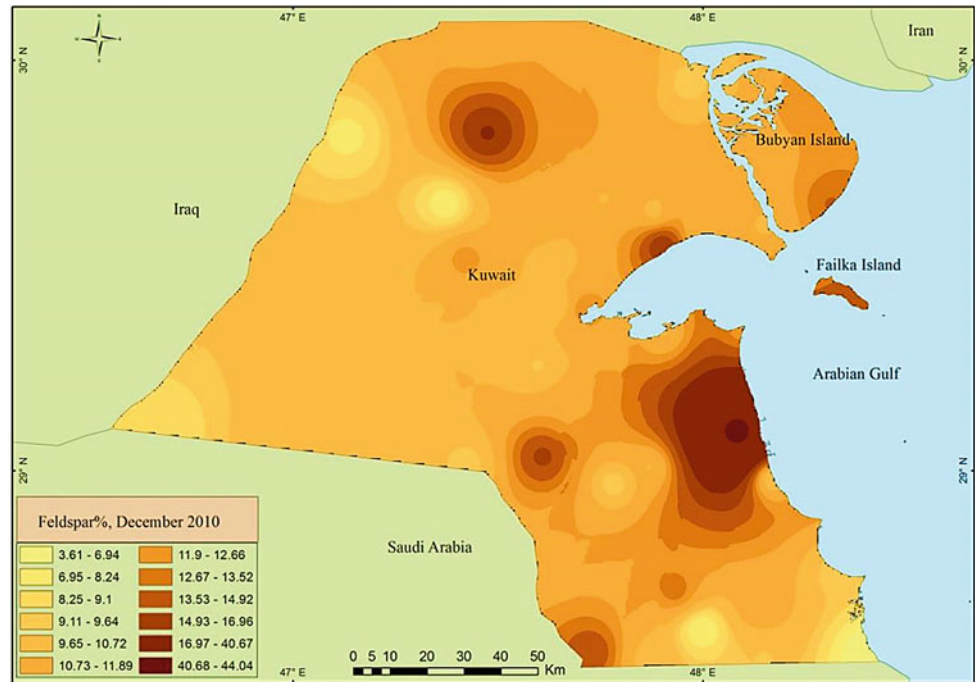
Fig. 4.4 Average percentages of dolomite, December 2010



Dust fallout in Kuwait contains appreciable amounts of dolomite. Quartz and carbonates form the major percentage of dust fallout mineralogy. The percentage of carbonates, in general, was highest during winter (October–April). Calcite, as a significant constituent of carbonates in Kuwait, was higher in Liyah and coastal areas and extends toward the northwest. The Dibdibah Formation contains calcretes and dolcretes as a major source of carbonate dust.

Areas with high mineral concentration	Areas with low mineral concentration
Parts of Bubiyan Island Jal Al Zur Shuaiba Ubayriq Khiran	Liyah Dibdibah Kabd Qurain Um Al Madafi*

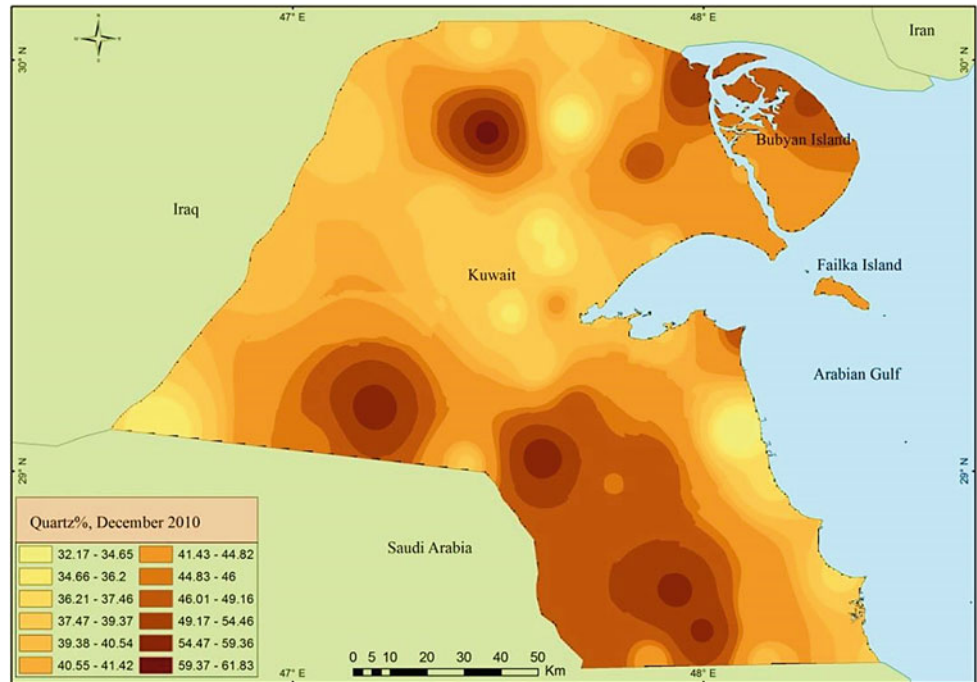
Fig. 4.5 Average percentages of feldspars, December 2010



Dust in Kuwait contains considerable amounts of feldspar minerals (alkali and plagioclase feldspars). The percentage of feldspar, in general, was highest in winter and spring (October–April). Feldspar content was as high as 44% in the Shuaiba area. Feldspars act as a primary component of rock-forming minerals and are classified as “soft” (6 on the Moho Hardness scale). Therefore, they disintegrate quickly and are transported in the form of dust for long distances, passing the Arabian Gulf from Iran toward Kuwait. Higher percentages were noted in Liyah and the coastal area and extend toward the northwest.

Areas with high mineral concentration	Areas with low mineral concentration
Shaiba Ahmadi Roudhatain Kabd Khur Fawaris	Salmi Khiran Wafra Farms Huwaymilyah Um Al Madafi'

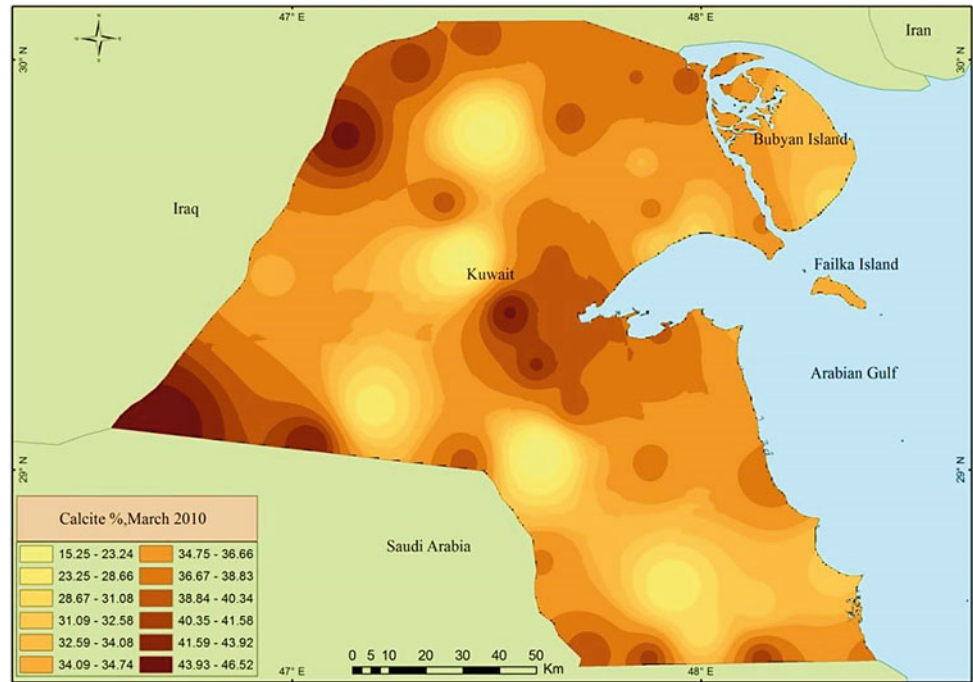
Fig. 4.6 Average percentages of quartz, December 2010



In December, fallen dust had lower quartz percentages than in summertime. The northeastern coastal areas (Bubiyan, Um Niqa) and southwestern border of Kuwait had the highest percentages (up to 61.8%). These percentages in these areas were thanks to the wind direction during these months. The southern coastal areas and major dunes corridor had the lowest percentage (as low as 32%). The higher percentages of quartz indicate high aeolian activity in the region.

Areas with high mineral concentration	Areas with low mineral concentration
Parts of Bubiyan Island	Salmi
Roudhatain	Um Rimam
Dibdibah	Mutla
Kabd	Shuaiba
Wafra Farms	Um Eish

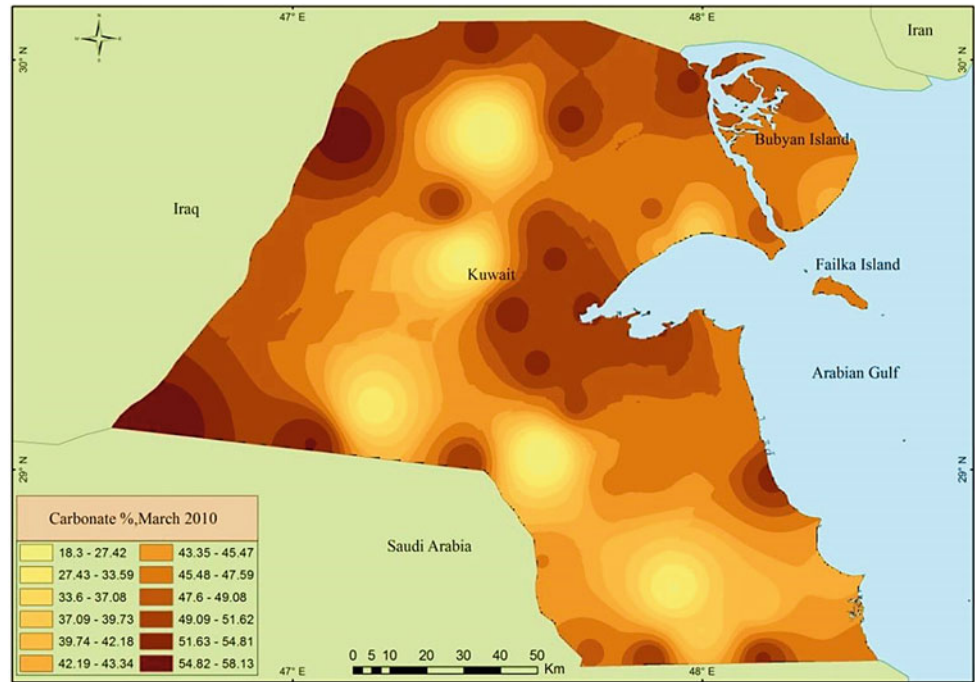
Fig. 4.7 Average percentages of calcite, March 2010



Fallen dust in Kuwait contains high percentages of carbonates and, more specifically, calcite. Quartz and carbonates form the large percentage of dust fallout mineralogy. The percentage rate of carbonates is usually highest in winter and springtime (October-April). Calcite, as a major constituent of carbonates in Kuwait, is higher in dust as a component in areas such as Salmi, Huwaymilyah, and Jahra due to the wind direction and speed in these months. The Dibdibah Formation contains calcretes and dolcretes as a major source of carbonate dust. Furthermore, the higher percentages of calcites and carbonates indicate lower aeolian activity in the area.

Areas with high mineral concentration	Areas with low mineral concentration
Salmi	Um Al Madafi'
Huwaymilyah	Dibdibah
Atraf	Kabd
Um Niqa	Wafra Farms
Khur Fawaris	Liyah

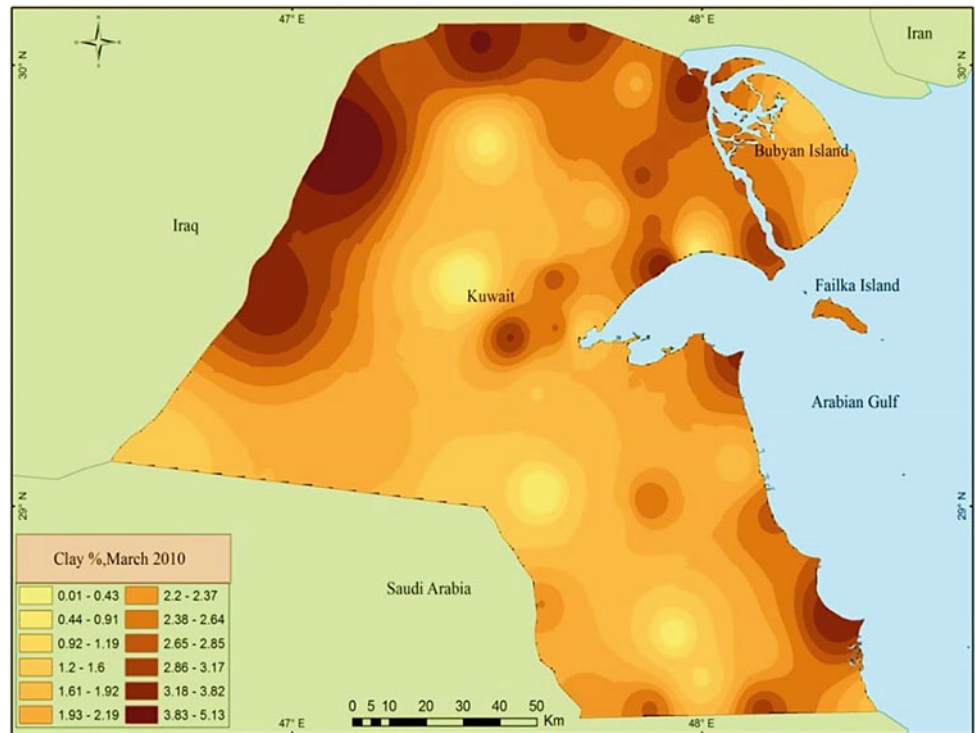
Fig. 4.8 Average percentages of carbonate, March 2010



Fallen dust in Kuwait contains high percentages of carbonates (up to 58%). Carbonates, as a major component of dust fallout mineralogy, are good indicators of low aeolian activity in the area during winter and springtime (October–April). Carbonates include dolomite and calcite. There were high percentages of carbonates within dust in Kuwait in areas such as Salmi, Huwaymilyah, and Atrah due to the wind directions and speed in these months. The Dibdibah Formation contains calcretes and dolcretes as a major source of carbonate dust.

Areas with high mineral concentration	Areas with low mineral concentration
Salmi	Um Al Madafi'
Huwaymilyah	Dibdibah
Atrah	Kabd
Um Niqa	Wafra Farms
Shuaiba	Liyah

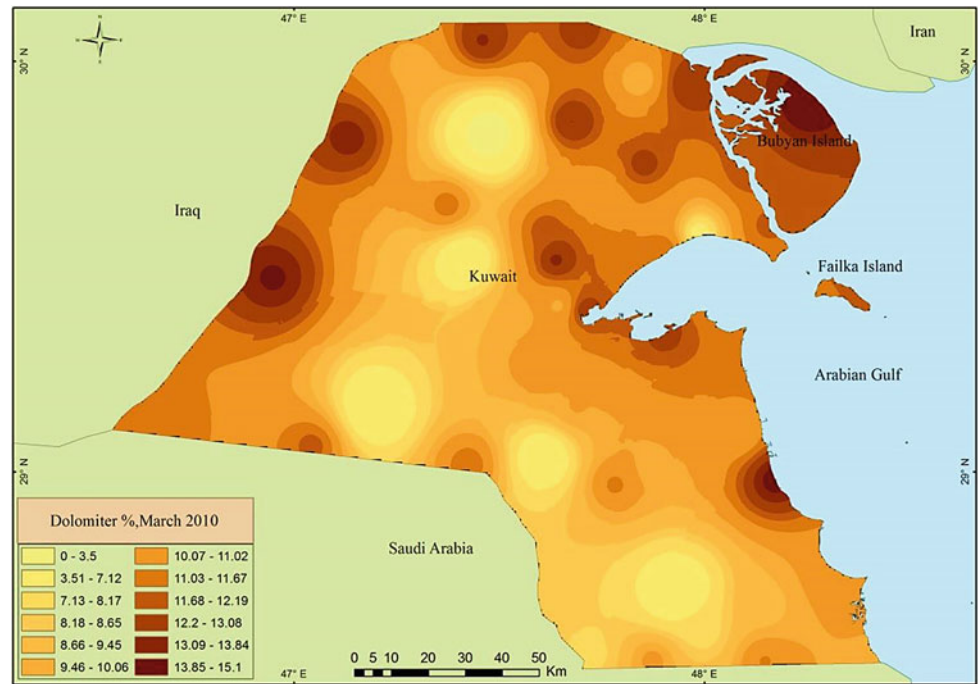
Fig. 4.9 Average percentages of clay, March 2010



High percentages of clay during March 2010 were restricted to major wadis such as Wadi Al-Batin, the Sabkha region, and the northeastern coastal areas in Kuwait, reaching up to 5.1%. Clay was higher also in densely vegetated areas, such as Al-Mutla, a protected habitat in northern Kuwait Bay, as clay mineral is lighter in weight, making it difficult to be captured by vegetation, as quartz and carbonates are. On the other hand, open desert areas in south-western areas had the lowest percentages.

Areas with high mineral concentration	Areas with low mineral concentration
Huwaymilyah	Salmi
Ubayriq	Roudhatain
Ratqah	Kabd
Um Niqa	Qurain
Khiran	Wafra Farms

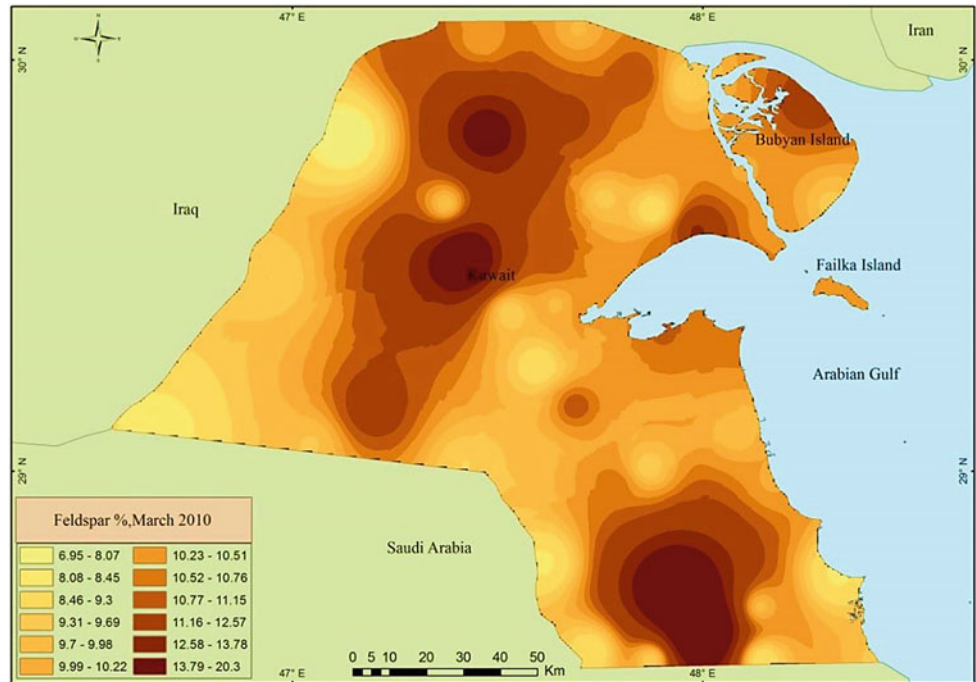
Fig. 4.10 Average percentages of minerals dolomite, March 2010



Fallen dust in Kuwait contains a considerable percentage of dolomite (up to 15%). Higher percentages of dolomite indicate lower aeolian activity in the area. The Dibdibah Formation contains calcretes and dolcretes as a major source of dolomite dust. During March, carbonates, including dolomite, were lowest in the five major areas indicated on the map. Dolomite, as a major constituent of carbonates in Kuwait, was higher in dust in areas such as Salmi, Huwaymilyah, and Bubiyan Island due to the wind directions and speed.

Areas with high mineral concentration	Areas with low mineral concentration
Salmi	Um Al Madafi'
Huwaymilyah	Dibdibah
Bubiyan Island	Kabd
Um Niqa	Wafra Farms
Shuaiba	Liyah

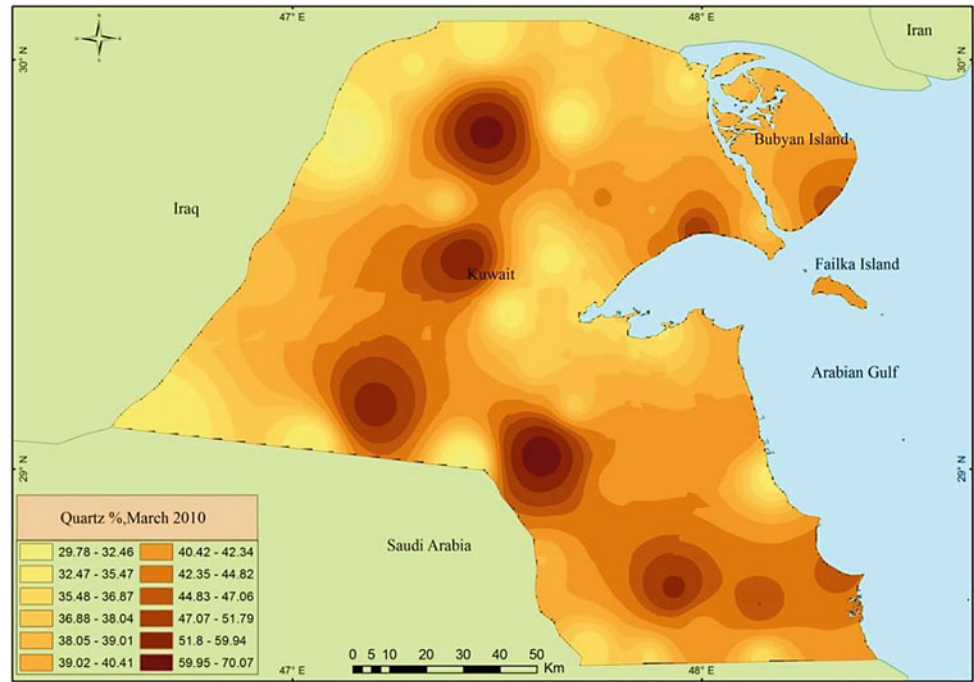
Fig. 4.11 Average percentages of feldspars, March 2010



Alkali and plagioclase feldspar minerals within fallen dust were present in considerable percentages (up to 20.3%) during March. Feldspars are soft (6 on the Moho Hardness scale) and are a major component of rock-forming minerals. Feldspars are easily disintegrated and transported in the form of dust over long distances. In March, higher percentages were noted in areas low in carbonates, such as Liyah, Wafra, and Bubiyan Island.

Areas with high mineral concentration	Areas with low mineral concentration
Roudhatain	Salmi
Dibdibah	Huwaymilyah
Bubiyan Island	Ubayriq
Qurain	Khur Fawaris
Liyah	Khiran

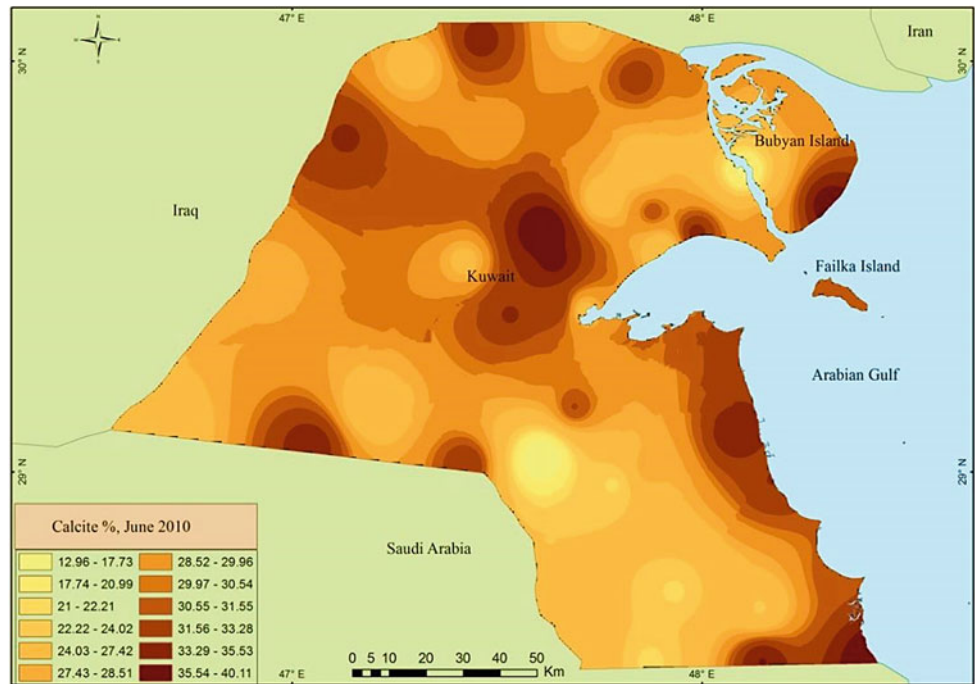
Fig. 4.12 Average percentages of quartz, March 2010



Quartz mineral in dust particles was present in high percentages of up to 70% during March, but lower than in summertime. Quartz is highly resistant to disintegration and is classified as hard on the Moho Hardness scale. Quartz is a major component of rock-forming minerals. During March, some areas, such as Liyah, Kabd, and Dibdibah, had higher percentages of quartz, which indicate higher aeolian activities in these regions compared with other regions. Furthermore, during March, fallen dust that contains a higher percentage of quartz indicates a low carbonate content.

Areas with high mineral concentration	Areas with low mineral concentration
Um Al Madafi'	Salmi
Dibdibah	Huwaymilyah
Kabd	Bubiyan Island
Wafra Farms	Um Niqa
Liyah	Shuaiba

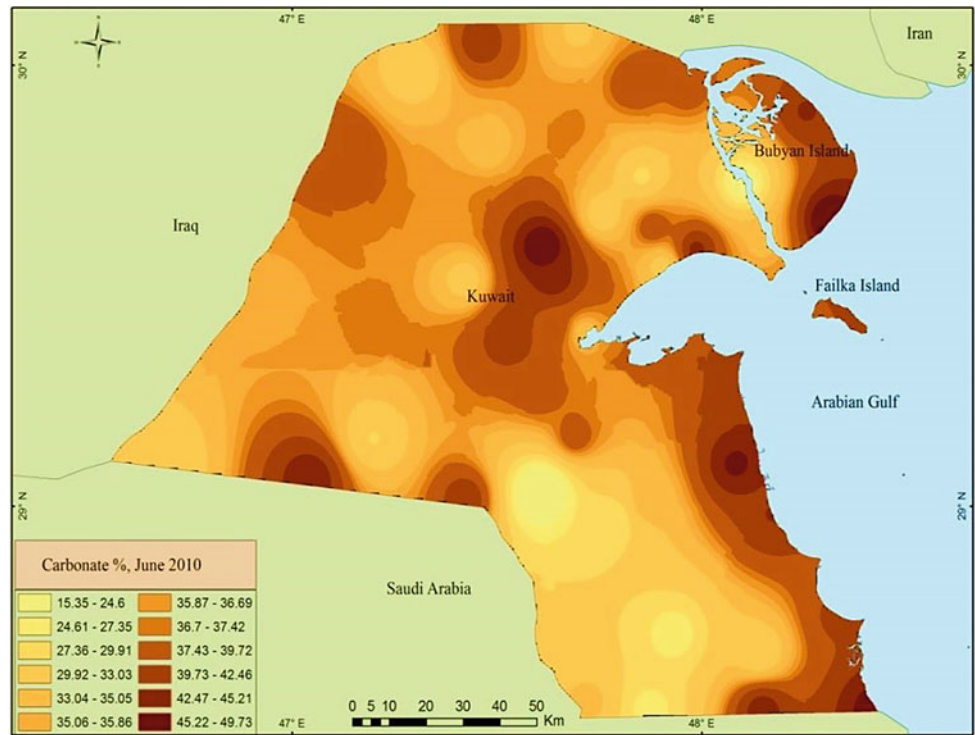
Fig. 4.13 Average percentages of calcite, June 2010



Calcite mineral concentrations in dust fallout during summer differed compared with winter and spring. Higher percentages of calcite were evident in the coastal areas and major wind corridor in Kuwait, reaching up to 40%. Calcite, in higher percentages, covered smaller areas than in winter. This difference is attributed to an increase in aeolian activity during summertime, which causes a decrease of calcite and carbonates in dust fallout content.

Areas with high mineral concentration	Areas with low mineral concentration
Liyah	Um Eish
Khiran	Salmi
Abdulli	Kabd
Huwaymilyah	Khur Fawaris
Shuaiba	Wafra Farms

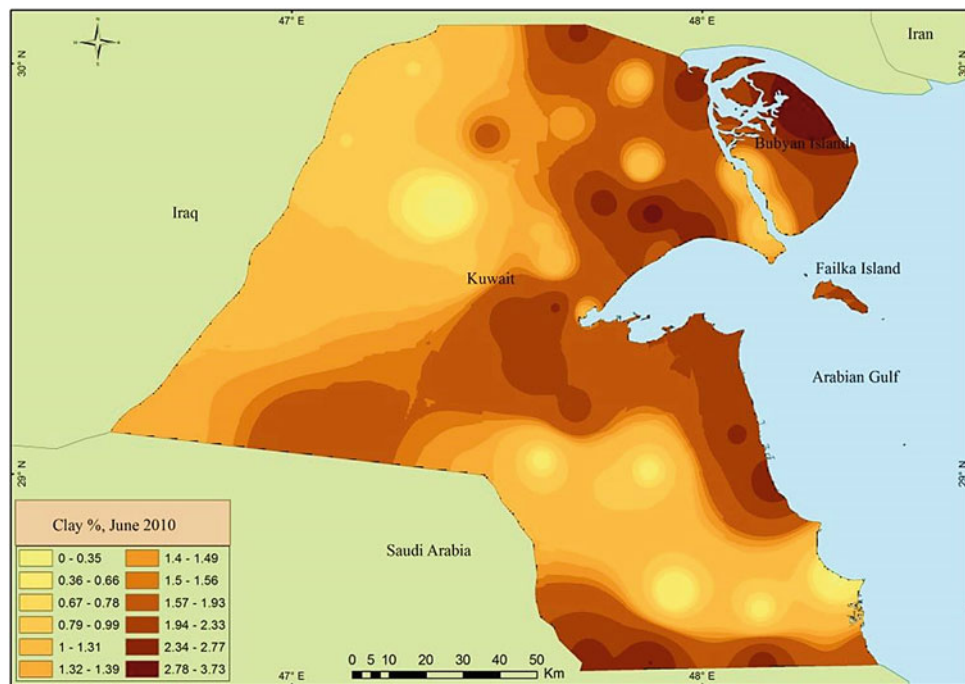
Fig. 4.14 Average percentages of carbonate, June 2010



Carbonate minerals are present in lower percentages of up to 49.7% in July. The low levels of carbonates in dust are good indicators of high aeolian activity in the area during summer. Higher percentages of carbonates within dust in Kuwait were found in areas such as Salmi, Huwaymilyah, and Atraf due to the wind direction and speed within this month, which was predominantly from the northwest. Calcretes and dolcretes within the Dibdibah Formation act as a major source of carbonate dust in the open desert of Kuwait.

Areas with high mineral concentration	Areas with low mineral concentration
Parts of Bubiyan Island Huwaymilyah Mutla Shuaiba Khiran	Wafra Farms Qurain Subiyah Burqan Kabd

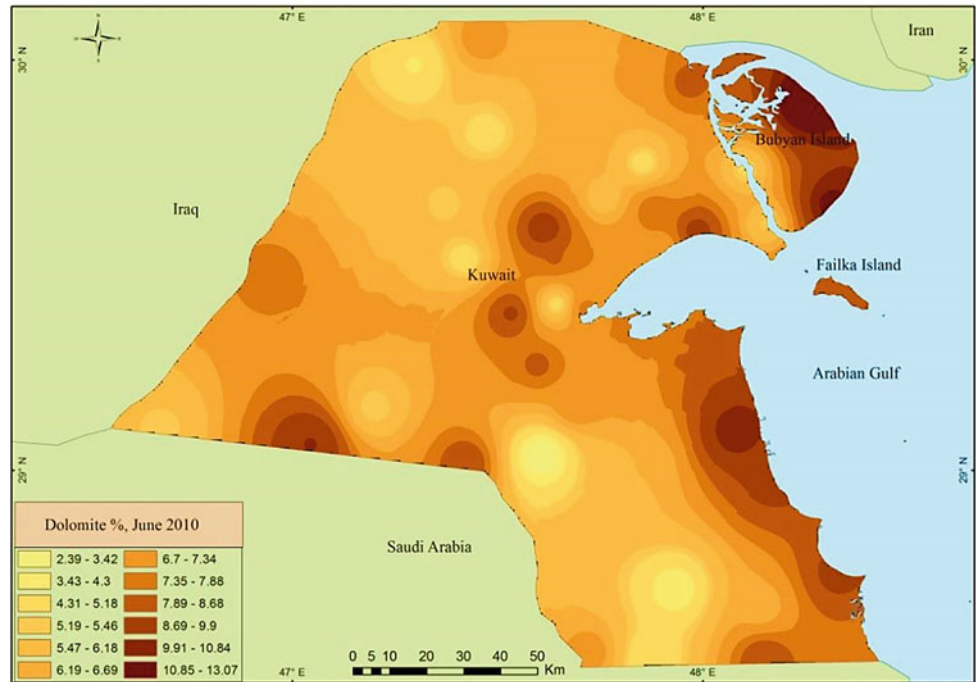
Fig. 4.15 Average percentages of clay, June 2010



There are small percentages of clay minerals within dust fallout in Kuwait. The percentage of clay minerals, in general, is lowest in June (up to 3.7%). Clay minerals, as a minor constituent of dust in Kuwait, are higher in percentage in the coastal area and around wadis, playas, and sabkhas, as these represent major local sources of dust in Kuwait.

Areas with high mineral concentration	Areas with low mineral concentration
Bubyan Island Jal Al Zur Abdulli Atraf Dibdibah	Ratqa Um Al Madafi' Urayfijan Burqan Liyah

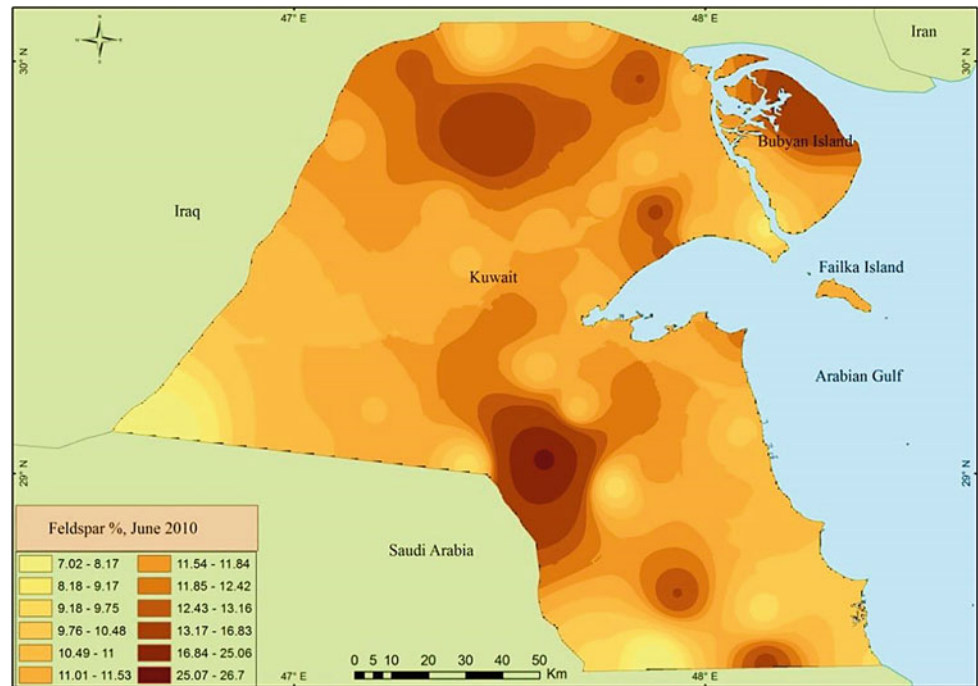
Fig. 4.16 Average percentages of dolomite, June 2010



There is a considerable percentage of dolomite within fallen dust in Kuwait (up to 13%). Higher percentages of dolomite indicate lower aeolian activity in the area. The Dibdibah Formation contains calcretes and dolcretes as a major source of dolomite dust. During summer, carbonates, including dolomite, are in low percentages within areas affected by active aeolian processes. Dolomite, as a significant constituent of carbonates in Kuwait, was higher in dust in areas such as Salmi, Subiyah, and Atrah due to wind directions and wind speed for these months.

Areas with high mineral concentration	Areas with low mineral concentration
Bubiyah Island	Ratqa
Salmiya	Roudhatain
Subiyah	Wafra Farms
Atrah	Burqan
Dibdibah	Um Eish

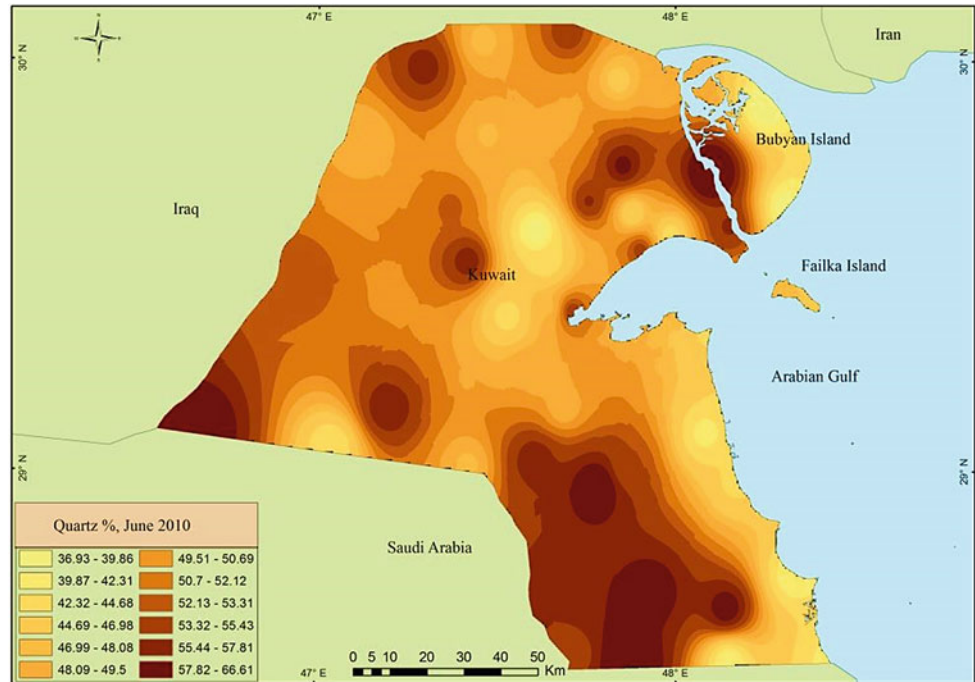
Fig. 4.17 Average percentages of feldspars, June 2010



Aeolian activities increase during summer, resulting in an increase in quartz percentages at the expense of other minerals, including alkali and plagioclase feldspar minerals. The dust in Kuwait contains considerable amounts of feldspar minerals. The percentage of feldspars, in general, is lowest during June. Feldspars reach up to 26.7% on Bubiyan Island and preserved areas such as Kabd, Um Rimam, and west Roudhtain. This level is attributed to the effect of native vegetation in controlling quartz but not feldspar minerals.

Areas with high mineral concentration	Areas with low mineral concentration
Parts of Bubiyan Island Roudhtain Kabd Um Rimam Qurain	Salmi Khur Fawaris Ubayriq Subiyah Dibdibah

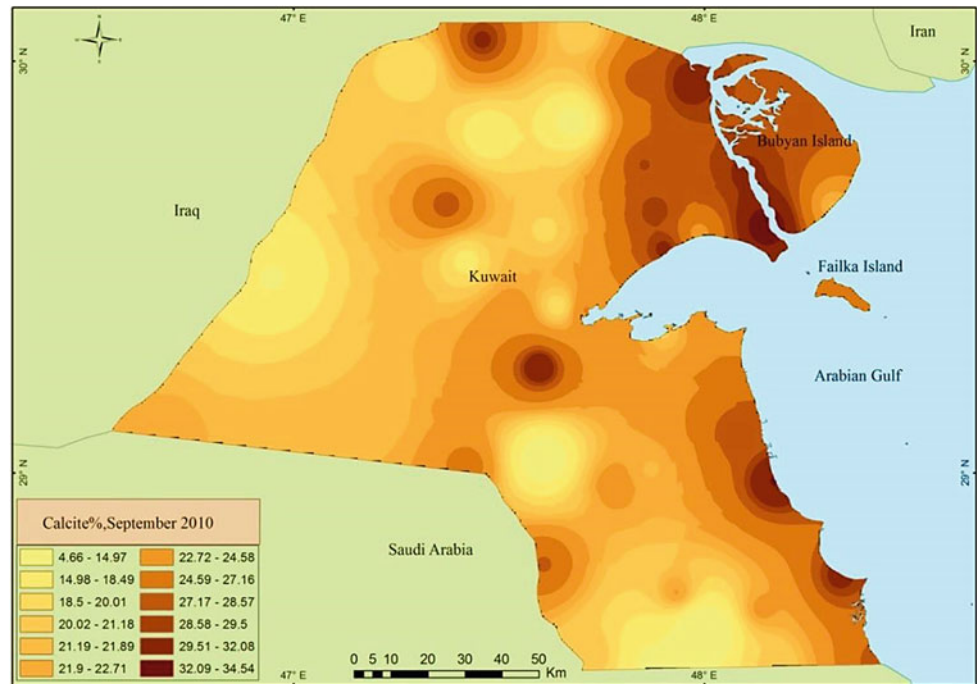
Fig. 4.18 Average percentages of quartz, June 2010



The western, northwestern, and southwestern areas of Kuwait had higher percentages of quartz (up to 66.6%). Furthermore, the wind corridor had a higher percentage of quartz among the dust samples. The coastal areas and Bubiyan Island had lower amounts of quartz within the dust samples. Active aeolian processes play a major role in increasing quartz percentages within Kuwait during June. Extensive areas during June and summertime experience higher percentages of quartz.

Areas with high mineral concentration	Areas with low mineral concentration
Salmi	Bubiyan Island
Ratqah	Um Rimam
Dibdibah	Shuaiba
Khur Fawaris	Khiran
Burqan	Mutla

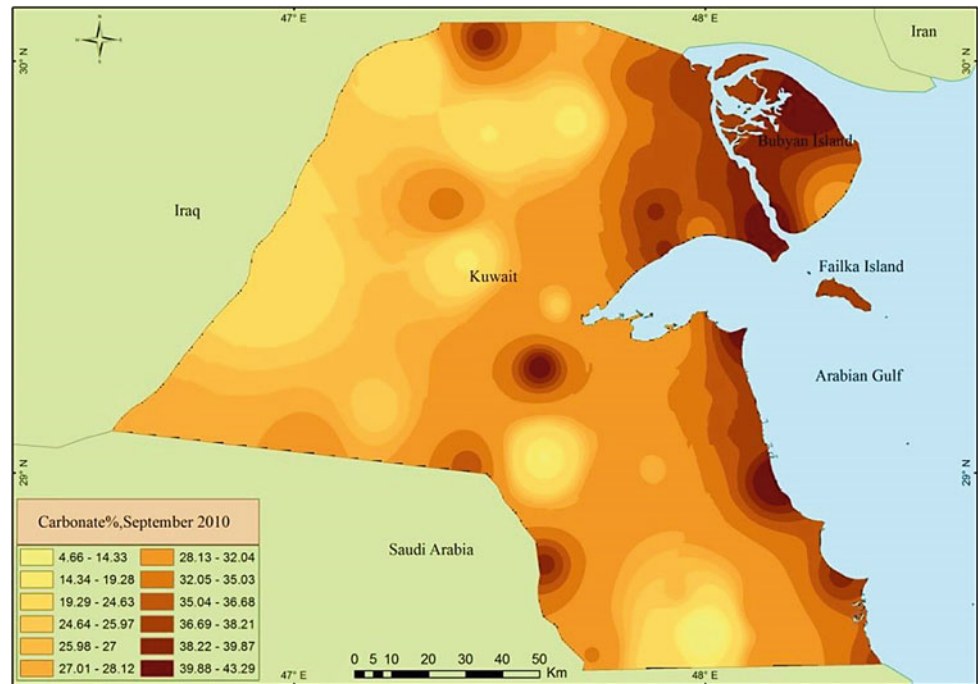
Fig. 4.19 Average percentages of calcite, September 2010



In September, calcite, as an essential carbonate mineral, had lower percentages along the northwestern sides of Kuwait and the major wind corridor. Higher percentage rates of up to 18% were evident in coastal areas and protected habitats. The reason for this presence of calcite with carbonates, feldspars, and clay minerals within protected habitats is due to calcite's light density, meaning it can easily be carried by the wind. Calcite is usually found more in smaller size fractions than quartz, which is predominantly found with medium and fine sand size fractions. Furthermore, the calcite map indicates three areas with higher percentages for all carbonates and clay minerals with dust samples in September, namely Shuaiba, Ritqa, and Liyah.

Areas with high mineral concentration	Areas with low mineral concentration
Bubian Island	Roudhatain
Ritqa	Ubayriq
Shuaiba	Wafra Farms
Khiran	Kabd
Abdulli	Khur Fawaris

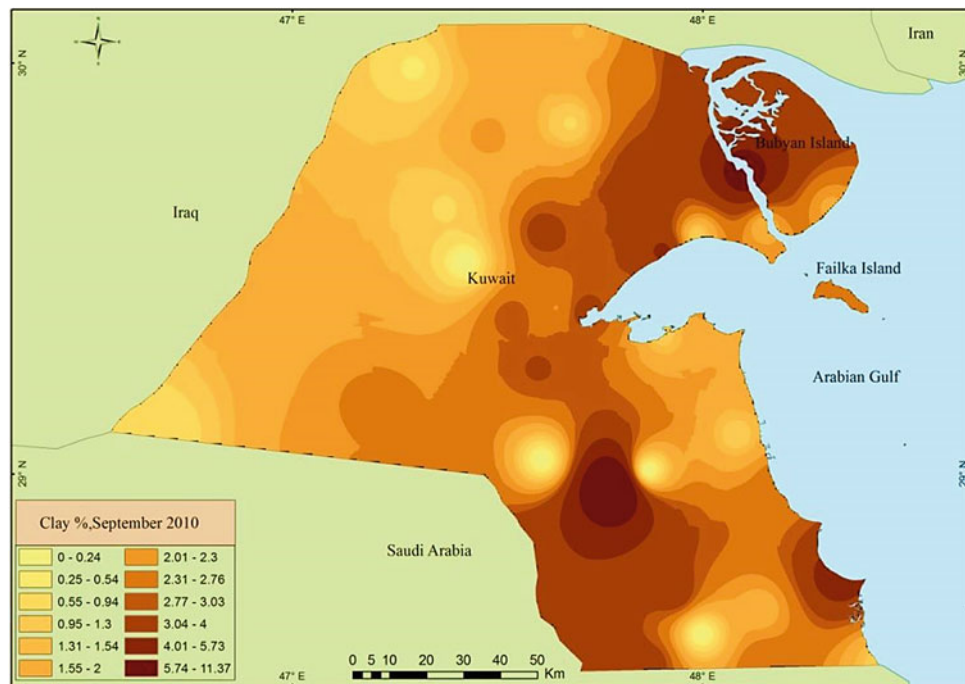
Fig. 4.20 Average percentages of carbonate, September 2010



The coastal areas, including Bubiyan Island, had the highest percentages of carbonates (up to 43.3%) of the total weight of dust samples during September. In September, large areas of Kuwait experienced lower percentage rates of carbonates. The wind corridor, western, and northwestern areas had the lowest percentages (as little as 5%) of the total weight of dust samples. The higher percentages of carbonates indicate higher percentages of low size fraction (mainly silt and clay), and higher BET-surface area for dust samples.

Areas with high mineral concentration	Areas with low dust fallout concentration
Bubiyan Island	Roudhatain
Jal Al Zur	Ubayriq
Shuaiba	Wafra Farms
Subiyah	Kabd
Abdulli	Khur Fawaris

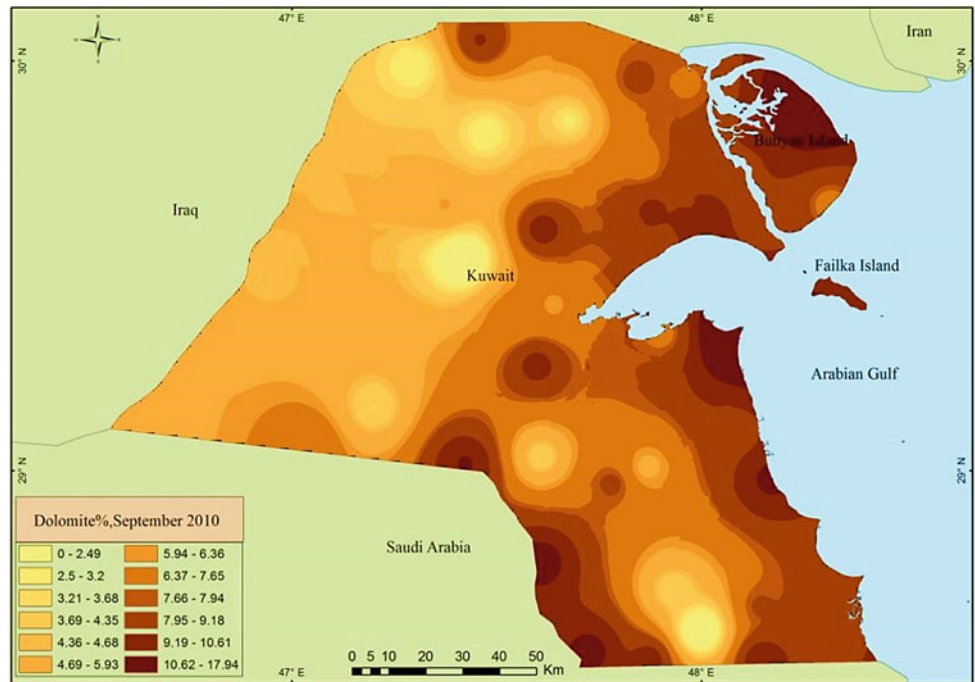
Fig. 4.21 Average percentages of clay, September 2010



The distribution map of clay minerals reveals that the higher percentages are nearly the same as for carbonate minerals during September 2010. The only exception is urban areas, such as Salmiya, which had lower quantities of clay minerals. Areas that experience high aeolian activities, such as the western and northwestern areas of Kuwait, had lower quantities of clay minerals. In September, clay reached up to 11.4% of the total weight of dust samples, mainly in areas such as Bubiyan Island, Um Niqa, and Um Eish.

Areas with high mineral concentration	Areas with low mineral concentration
Bubiyan Island	Roudhatain
Um Eish	Ubayriq
Um Niqa	Huwaymilyah
Khur Fawaris	Kabd
Um Qudayr	Salmiya

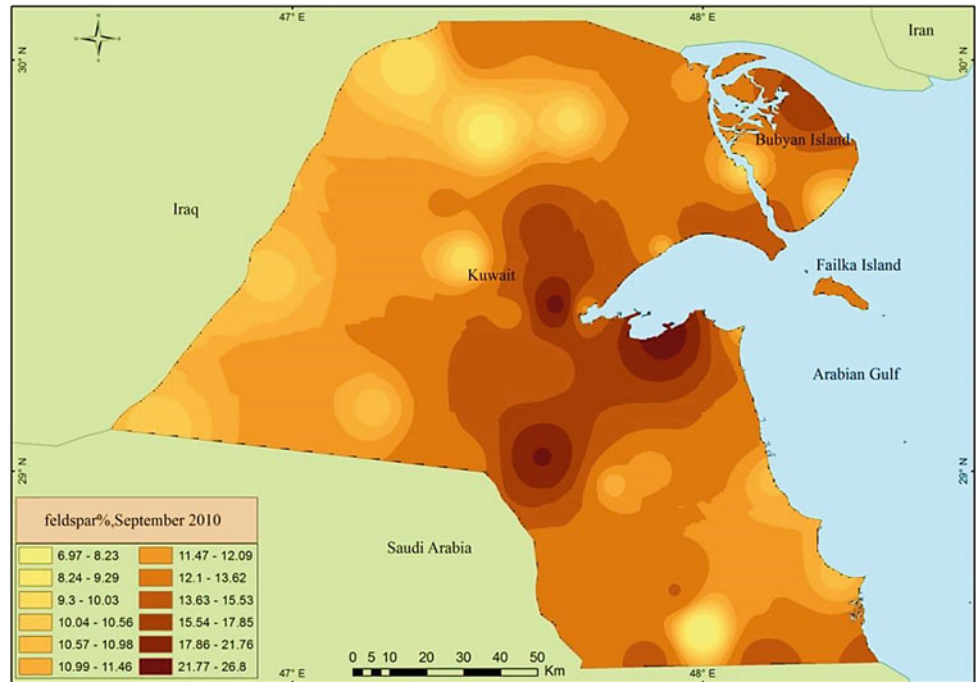
Fig. 4.22 Average percentages of dolomite, September 2010



In September, dolomite, like other carbonates and clay minerals, had lower percentages along the northwestern side of Kuwait and within the major wind corridor. Higher percentage rates of up to 18% were evident in the coastal and preserved areas. The reason for the presence of higher percentages of dolomite with carbonates, feldspars, and clay minerals within preserved areas is due to dolomite’s low density, meaning it can easily be carried by the wind, as it is usually found more within the smaller size fractions when compared with quartz, which is predominantly found with medium and fine sand size fractions.

Areas with high mineral concentration	Areas with low mineral concentration
Bubiyan Island	Roudhatain
Um Eish	Ratqah
Um Niqa	Huwaymilyah
Khur Fawaris	Wafra Farms
Shaiba	Liyah

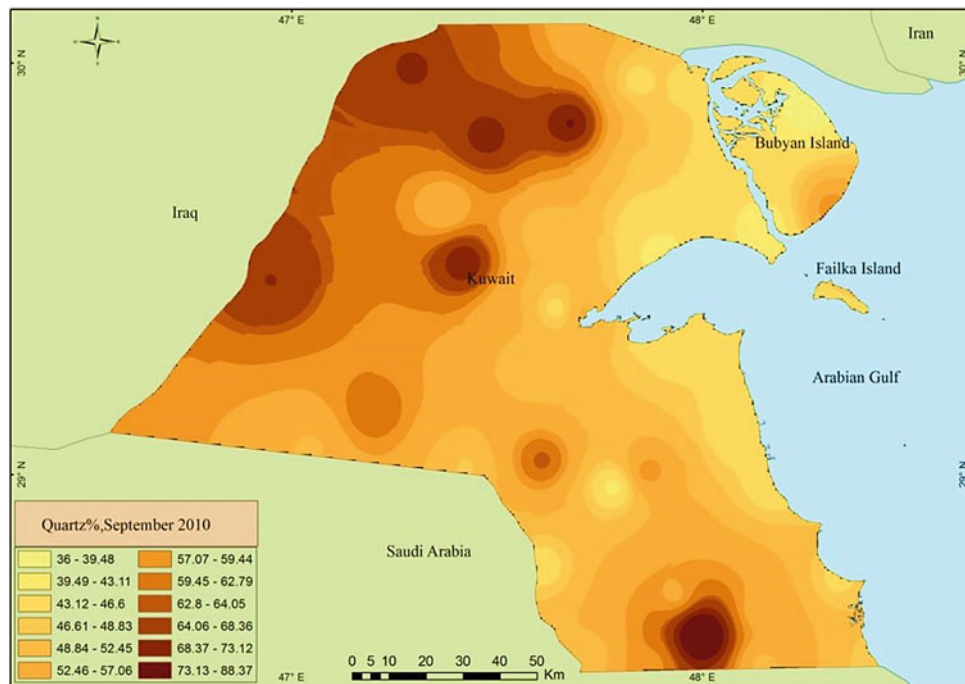
Fig. 4.23 Average percentages of feldspars, September 2010



The feldspar mineral percentages map for September 2010 is nearly opposite to the quartz percentages map for the same month. The feldspar mineral percentages were higher in coastal areas, mainly along the northeastern sides of Kuwait, including Bubiyan Island, Mutla, and around Kuwait Bay. The lowest quantities were along the north-western and western sides of Kuwait, mainly in Ratqa, Huwaymilyah. The percentages of feldspar reach up to 28.8%. Feldspar minerals disintegrate rapidly, with low hardness on the Moho scale. Therefore, feldspar usually comes from local sources and travels only short distances.

Areas with high mineral concentration	Areas with low dust fallout concentration
Bubiyan Island	Ratqa
Mutla	Roudhatain
Sulaybiyah	Salmi
Kabd	Huwaymilyah
Um Rimam	Ubayriq

Fig. 4.24 Average percentages of quartz, September 2010



During September, the quartz percentages were higher along the northwestern and western sides of Kuwait, mainly in Ratqa, Huwaymilyah, and Wafra. The lowest quantities were recorded along the coastal areas, Bubiyan Island, Salmiya, and Mutla. The percentages of quartz reached up to 88.4%, indicating that some areas experienced greater aeolian activity, especially those located within active wind corridors in Kuwait.

Areas with high mineral concentration	Areas with low mineral concentration
Ratqa Roudhatain Wafra Farms Huwaymilyah Ubayriq	Bubiyan Island Mutla Sulaybiyah Salmiya Um Rimam

Open Access This chapter is licensed under the terms of the Creative Commons Attribution 4.0 International License (<http://creativecommons.org/licenses/by/4.0/>), which permits use, sharing, adaptation, distribution and reproduction in any medium or format, as long as you give appropriate credit to the original author(s) and the source, provide a link to the Creative Commons licence and indicate if changes were made.

The images or other third party material in this chapter are included in the chapter’s Creative Commons licence, unless indicated otherwise in a credit line to the material. If material is not included in the chapter’s Creative Commons licence and your intended use is not permitted by statutory regulation or exceeds the permitted use, you will need to obtain permission directly from the copyright holder.



Ali Al-Dousari, Fatin Al-Mutawaa, Hanan Al-Mansour,
and Badreya Mandekar

Abstract

- The crushed powder from defined dust particle size fractions was analyzed using inductively coupled spectrometry plasma (ICP) for major and trace elements.
- The ICP was used for the determination of concentrations of trace elements and six major elements: (Al, Fe, Mg, Ca, Na, and K) and five minor elements (Ba, Cr, V, Ti, and Pb). They are quoted in part per million (ppm).
- Maps showing high and low concentrations of ICP among Kuwait.

ICP (Inductively Coupled Plasma) Spectrometry Analysis

The crushed powder from defined dust particle size fractions was analyzed using ICP to identify major and trace elements. The reason for using ICP to analyze major elements was

A. Al-Dousari (✉)
Crisis Decision Supports Program (CDS), Environment and Life Sciences Research Center (ELSRC), Kuwait Institute for Scientific Research (KISR), P.O. Box 24885 Safat, 13109, Kuwait
e-mail: adousari@kISR.edu.kw

F. Al-Mutawaa
Nanotechnology and Advanced Materials Program (NAM), Energy and Building Research Center (EBRC), Kuwait Institute for Scientific Research (KISR), P.O. Box 24885 Safat, 13109, Kuwait
e-mail: fmutawa@kISR.edu.kw

H. Al-Mansour
Environmental Pollution and Climate Program (EPCP), Environment and Life Sciences Research Center (ELSRC), Kuwait Institute for Scientific Research (KISR), P.O. Box 24885 Safat, 13109, Kuwait
e-mail: hsultan@kISR.edu.kw

B. Mandekar
Analytical Chemistry Division, General Department of Criminal Evidence, Criminal Secure, Ministry of Interior, P.O. Box 11 Safat, 13001, Kuwait
e-mail: bedraya.mandekar@moi.gov.kw

because some samples had less weight than needed (7 g) for analysis by XRF, while only 2 g (± 0.05) of powder is used in the ICP method. The method used for dissolved sediment samples for ICP involved open evaporation of the sample with hydrofluoric acid, together with nitric acid (HNO_3), in a platinum crucible.

The ICP was used to determine the concentrations of trace elements and six major elements: (Al, Fe, Mg, Ca, Na, and K) and five minor elements (Ba, Cr, V, Ti, and Pb). The amounts are quoted in parts per million (ppm) (Fig. 5.1).

Iron (Fe)

Iron (Fe) plays a major role in the biochemical reactions within a marine environment and acts as a major feeder to microorganisms (e.g., phytoplankton, cyanobacteria). The average amount of iron within fallen dust varies from 13,000 to 57,000 ppm. The distribution of areas with higher concentrations of iron indicates the effect of northeastern wind coming from the Zagros Mountains. The southern coastal areas had the highest concentrations of iron. There were some areas with high iron concentrations in a straight line from Bubiyan Island in the northeast toward Arafat in the southeast. The lowest concentration of iron in Kuwait was recorded in March and September, while the highest was in December (Figs. 5.1 and 5.2).

Areas with high ICP concentration	Areas with low ICP concentration
Um Eish	Um Niqa
Salmiya	Ratqah
Shuaiba	Dibdibah
Khiran	Sulaybiyah
Parts of Bubiyan Island	Wafra farms

Aluminum (Al)

Aluminum as an element is a major indication of higher concentrations of alkali and plagioclase feldspar minerals. The average amount of aluminum within fallen dust varies from 3000 ppm to more than 80,000 ppm (average: 41,246 ppm). The distribution of areas with higher concentrations of aluminum is sporadic and without trend. September was an exceptional case; the Western Desert areas had lower concentrations than the coastal areas. The lowest concentration in Kuwait was in September, while the highest was in December (Figs. 5.3 and 5.4).

Areas with high ICP concentration	Areas with low ICP concentration
Salmi Abdulli Um Niqa Um Rimam Shuaiba	Subiyah Abdulli Roudhatain Kabd Wafra farms

Barium (Ba)

Barium (Ba) as an element is a major indication of higher concentrations of alkali and plagioclase feldspar minerals. The average amount of aluminum within fallen dust varies from 3000 ppm to more than 80,000 ppm (average: 41,246 ppm). The distribution of areas with higher concentrations of Ba was found mainly in three locations: Abdulli, Shuaiba, and northern Kuwait Bay in Sabah Al-Ahmed National Reserve. The lowest concentration in Kuwait was

recorded in June, while the highest was in March and September (Figs. 5.5 and 5.6).

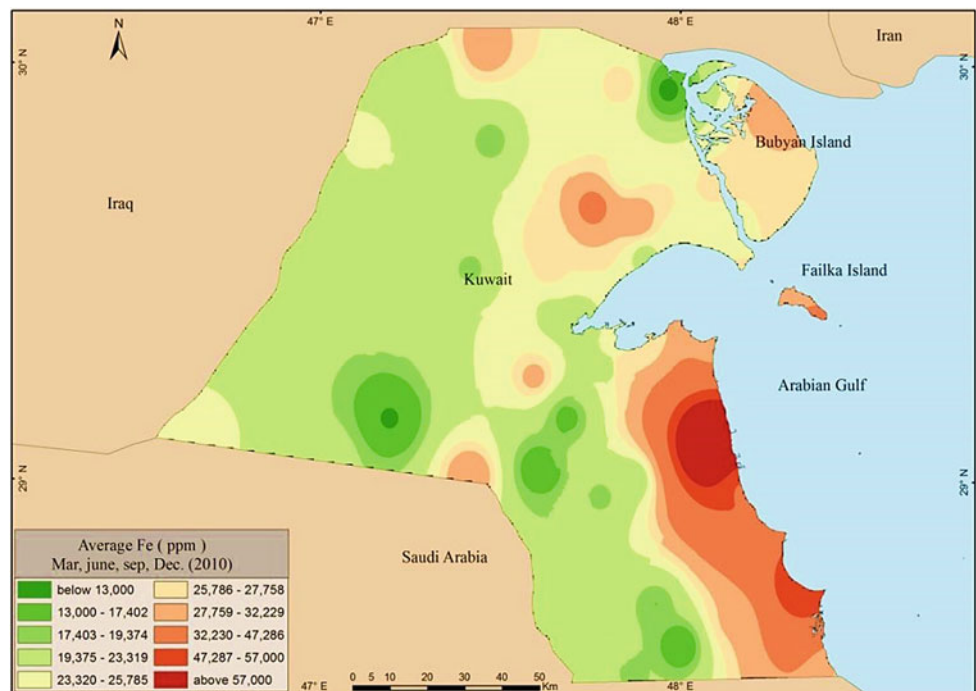
Areas with high ICP concentration	Areas with low ICP concentration
Abdulli Um Eish Salmiya Shuaiba Burqan	Bubiyah Island Ubayriq Dibdibah Khur Fawaris Khiran

Calcium (Ca)

Calcium (Ca) as an element is a major indication of higher concentrations of plagioclase feldspars and heavy minerals. The average amount of calcium within fallen dust varies from 1247 ppm to more than 115,500 ppm (average: 48,318 ppm). The higher distribution areas cover most of Kuwait, but, on average, the northern areas had higher concentrations than southern Kuwait. The lowest concentration in Kuwait was in June, while the highest was in December (Figs. 5.7 and 5.8).

Areas with high ICP concentration	Areas with low ICP concentration
Salmi Ratqah Bubiyah Island Khiran Um Eish	Jal Al Zur Ubayriq Kabd Ahmadi Wafra farms

Fig. 5.1 Average iron (Fe) content in ppm within fallen dust in Kuwait (2010)



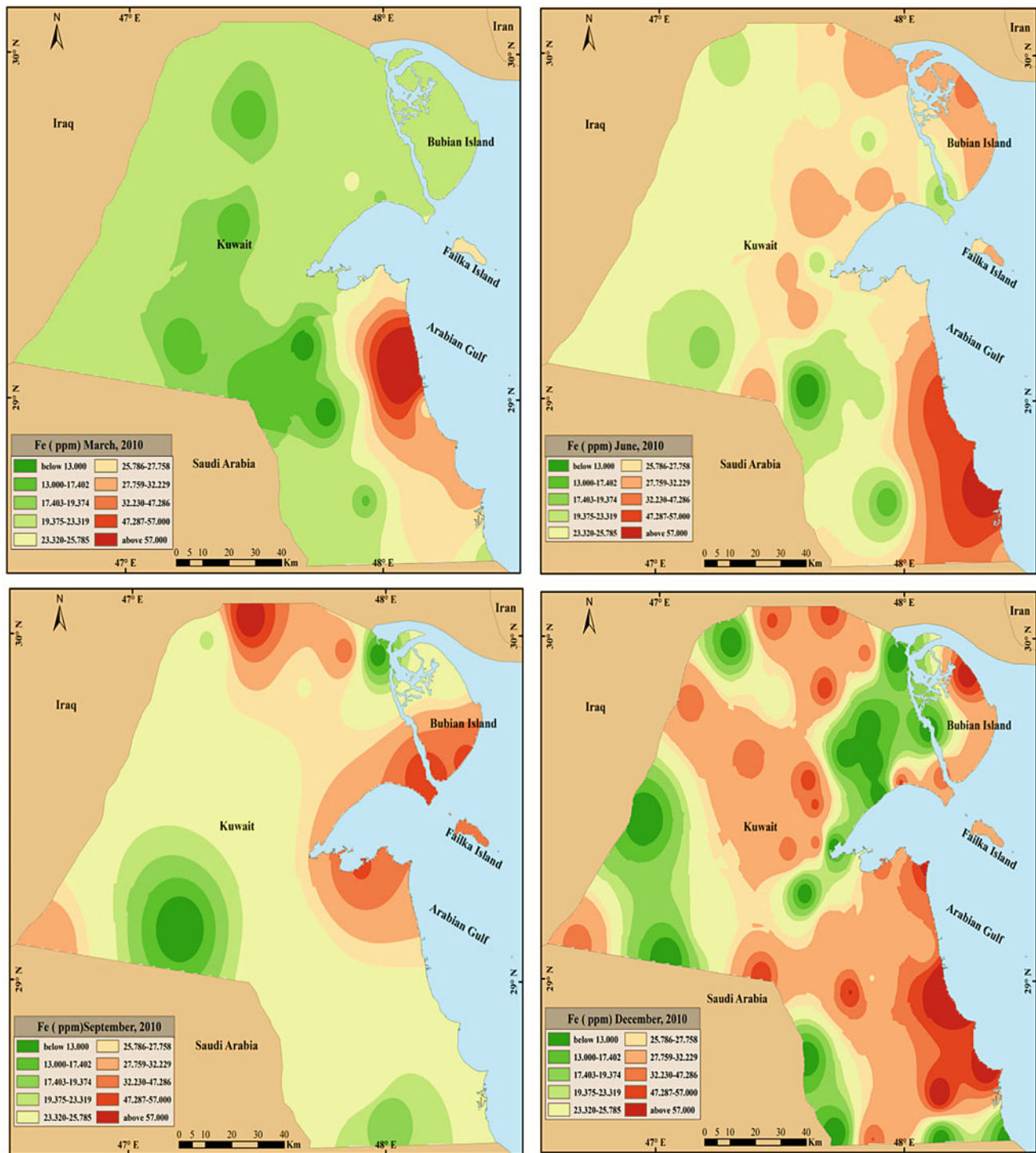


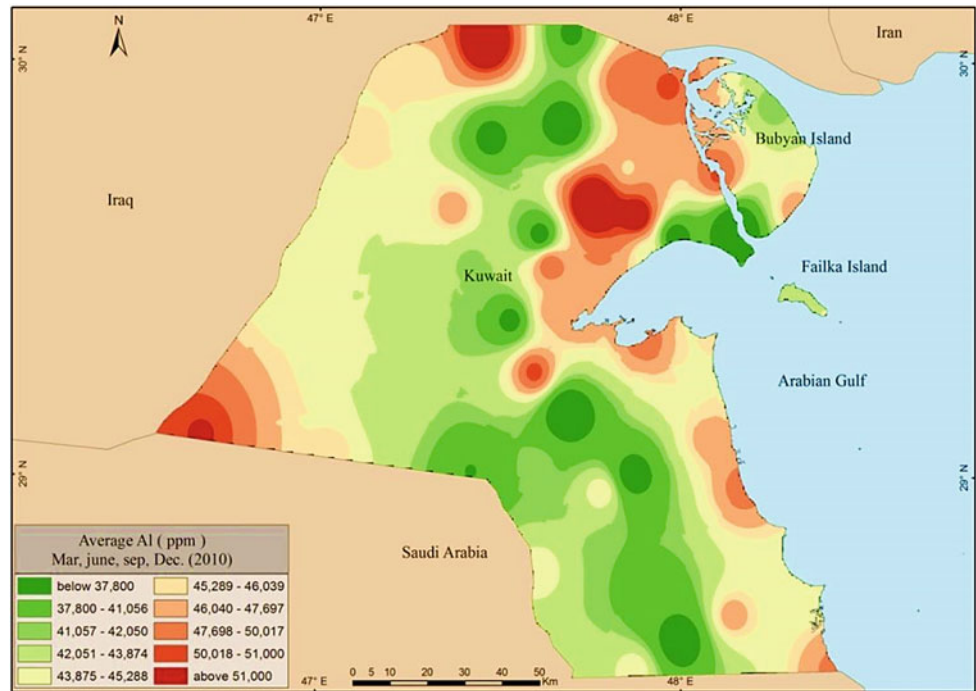
Fig. 5.2 Fe content in ppm within fallen dust in Kuwait (2010)

Chromium (Cr)

Chromium with iron plays a major role in the biochemical reactions within marine environments and acts as a major feeder to microorganisms (e.g., phytoplankton, cyanobacteria). The average amount of chromium within fallen dust

varies from 28 to 2128 ppm. The chromium higher distribution areas are similar to that of iron. Bubiyan Island and areas around Kuwait Bay were the highest areas of chromium. The lowest concentration in Kuwait was in December, while the highest was in September (Figs. 5.9 and 5.10).

Fig. 5.3 Average aluminum (Al) content in ppm within fallen dust in Kuwait (2010)



Areas with high ICP concentration	Areas with low ICP concentration
Bubiyan Island Abdulli Jal Al Zur Salmiya Atraf	Salmi Liyah Burqan Qurain Wafra farms

Potassium (K)

Potassium (K) as an element is a major indication of higher concentrations of alkali feldspar minerals. The average amount of potassium within fallen dust varies from 848 ppm to more than 178,600 ppm (average: 18,035 ppm). The higher distribution areas of potassium are associated with major wind corridors in western (Salmi) and northeastern areas (Bubiyan and Subiyah) in Kuwait. The lowest concentration in Kuwait was in June, while the highest was in September and December (Figs. 5.11 and 5.12).

Areas with high ICP concentration	Areas with low ICP concentration
Parts of Bubiyan Island Um Eish Salmi Kabd Khur Fawaris	Shuaiba Wafra farms Sulaybiyah Ratqah Liyah

Magnesium (Mg)

The presence of magnesium (Mg) as an element indicates higher concentrations of heavy minerals. The average amount of magnesium within fallen dust varies from 1247 ppm to more than 115,500 ppm (average: 48,318 ppm). Magnesium’s higher distribution areas are in the northern and northeastern sides of Kuwait more than in the south and far west. The lowest concentration in Kuwait was in September, while the highest was recorded in March (springtime with low wind activity) (Figs. 5.13 and 5.14).

Areas with high ICP concentration	Areas with low ICP concentration
Abdulli Subiyah Um Eish Atraf Kabd	Salmi Ubayriq Sulaybiyah Burqan Wafra farms

Sodium (Na)

The presence of sodium (Na) as an element indicates higher concentrations of alkali feldspar minerals and salt content within dust samples. The average amount of sodium within the fallen dust varies from 941 ppm to more than 62,700 ppm (average: 9091 ppm). The sodium higher

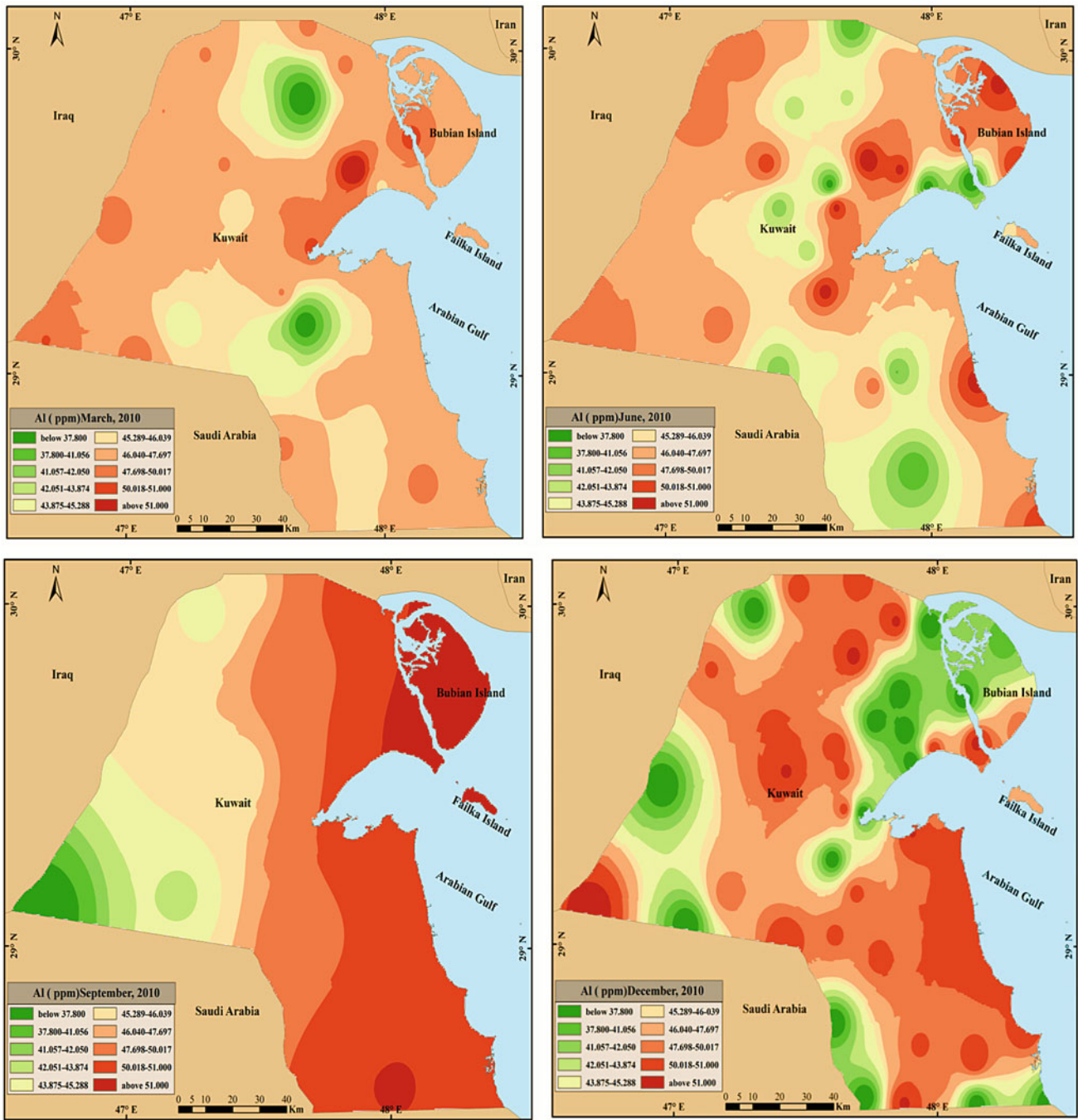
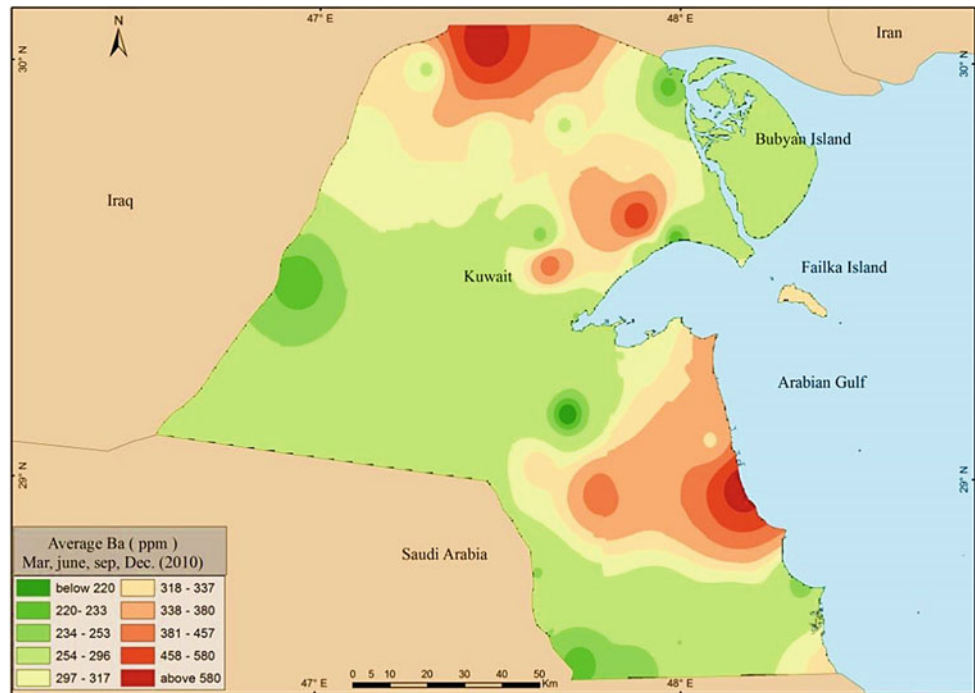


Fig. 5.4 Al content in ppm within fallen dust in Kuwait (2010)

distribution areas are associated with major wind corridors in northwestern areas (Um Al Madafi), with low concentrations in farms and preserved areas with dense vegetation. The lowest concentration in Kuwait was in March, while the highest was in June (Figs. 5.15 and 5.16).

Areas with high ICP concentration	Areas with low ICP concentration
Bubian Island	Salmi
Ratqah	Abdulli
Um Al Madafi'	Urayfijan
Liyah	Khur Fawaris
Salmiya	Wafra farms

Fig. 5.5 Average barium (Ba) content in ppm within fallen dust in Kuwait (2010)



Lead (Pb)

The presence of lead (Pb) and magnesium (Mg) as elements indicates higher concentrations of heavy minerals within the dust. The average amount of lead within fallen dust varies from 6 ppm to more than 8500 ppm (average: 2168 ppm). Lead’s higher distribution areas cover the northeastern sides of Kuwait more than the south and far west, which might offer some indications regarding the source areas, especially the Mesopotamian Floodplain and the Zagros Mountains. The lowest concentrations in Kuwait were in December and September, while the highest was in March. Furthermore, there is another trend: a high lead concentration that extends from Um Al Madafi toward Atraf in Kuwait (Figs. 5.17 and 5.18).

Areas with high ICP concentration	Areas with low ICP concentration
Bubiyan Island Subiyah Abdulli Um Al Madafi Atraf	Ratqah Ubayriq Dibdibah Burqan Wafra farms

Titanium (Ti)

The average amount of titanium within the fallen dust varies from 4 ppm to 8873 ppm (average: 2328 ppm). The presence of titanium as an element indicates higher concentrations of heavy minerals within dust. The titanium distribution was higher in areas around Kuwait Bay, western areas, and the southern coastal zone of Kuwait, indicating higher concentrations than in the northern and central areas of Kuwait. The lowest concentration in Kuwait was in summer, during September and June, while the highest was in December and March (Figs. 5.19 and 5.20).

Areas with high ICP concentration	Areas with low ICP concentration
Subiyah Um Rimam Salmiya Shuaiba Ubayriq	Bubiyan Island Abdulli Um Eish Burqan Wafra farms

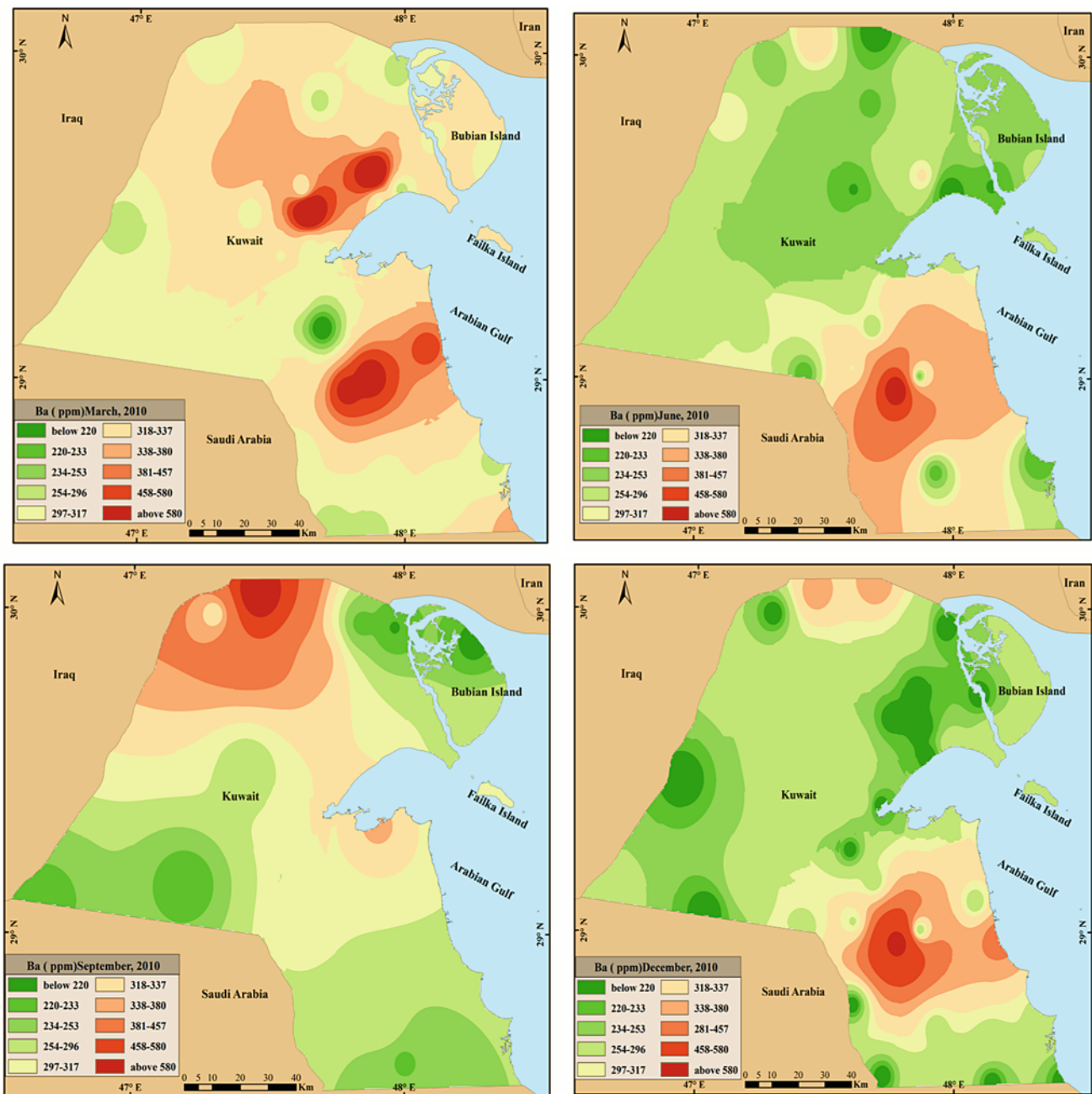


Fig. 5.6 Ba content in ppm within fallen dust in Kuwait (2010)

Vanadium (V)

The average amount of vanadium (V) within fallen dust varies from 11 to 153 ppm (average: 2328 ppm), which is the lowest concentration (in addition to thallium [TL]) of all the detected elements within dust fallout. The presence of vanadium as an element indicates higher concentrations of heavy minerals within dust. The highest distribution of vanadium was present around the coastal zone and north-eastern areas of Kuwait. The lowest concentration in Kuwait

was in December, while the highest was in March (Figs. 5.21 and 5.22).

Areas with high dust fallout concentration	Areas with low ICP concentration
Bubiyah Island	Ratqah
Subiyah	Ubayriq
Abdulli	Dibdibah
Salmiya	Burqan
Um Rimam	Wafra farms

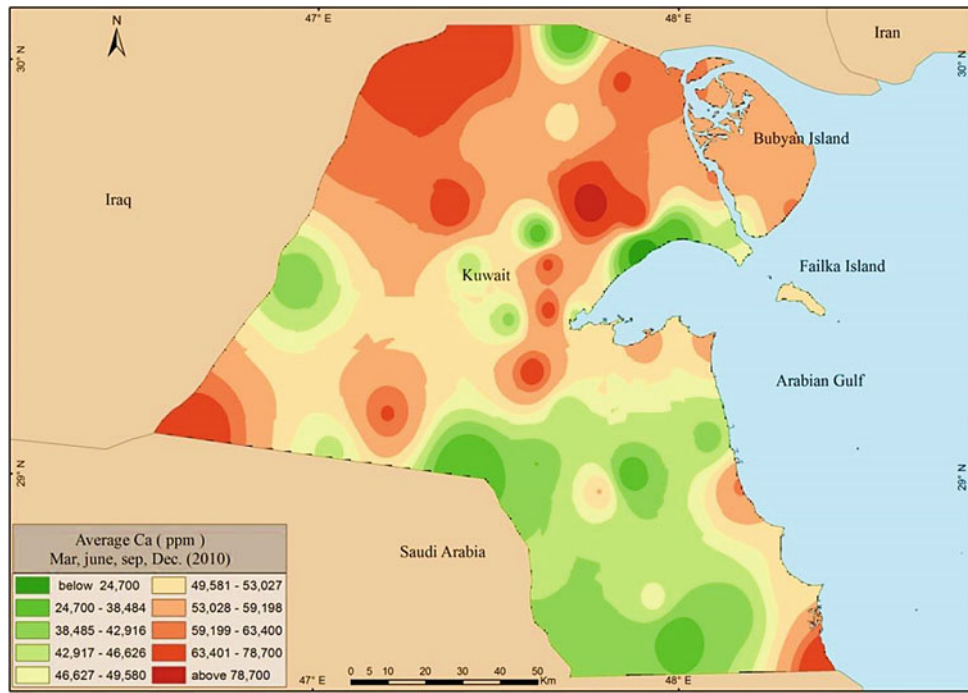


Fig. 5.7 Average calcium (Ca) content in ppm within fallen dust in Kuwait (2010)

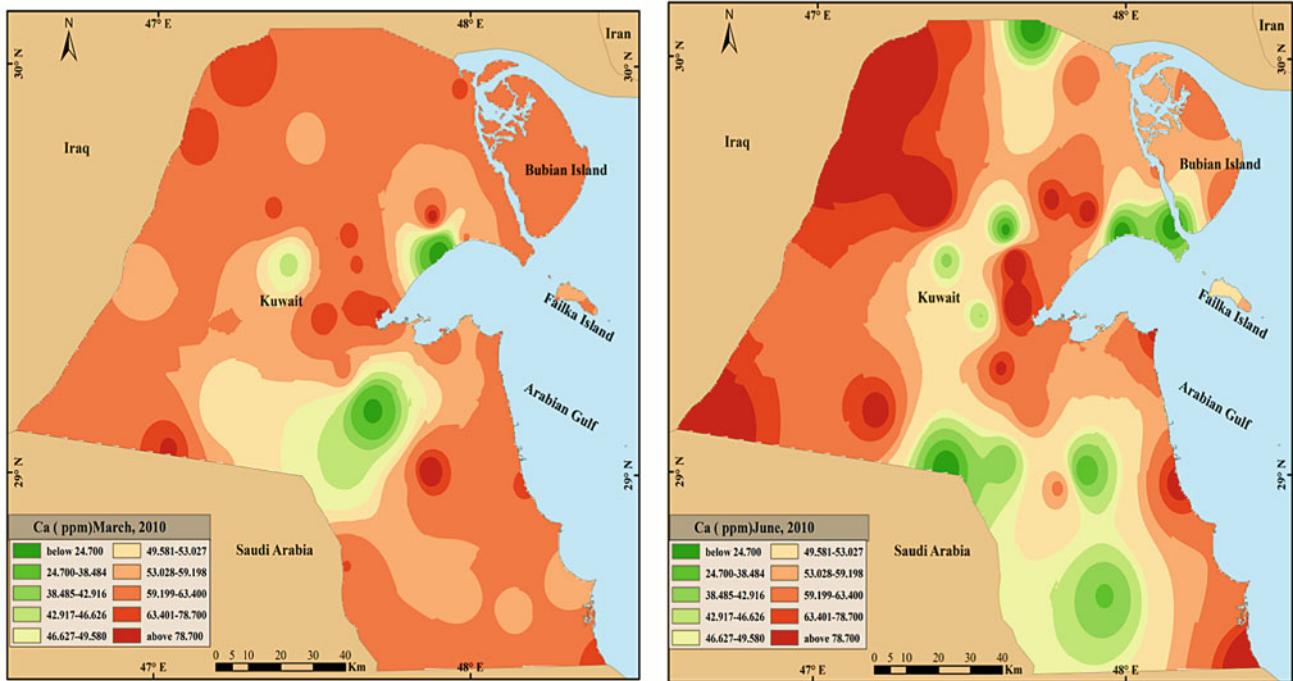


Fig. 5.8 Ca content in ppm within fallen dust in Kuwait (2010)

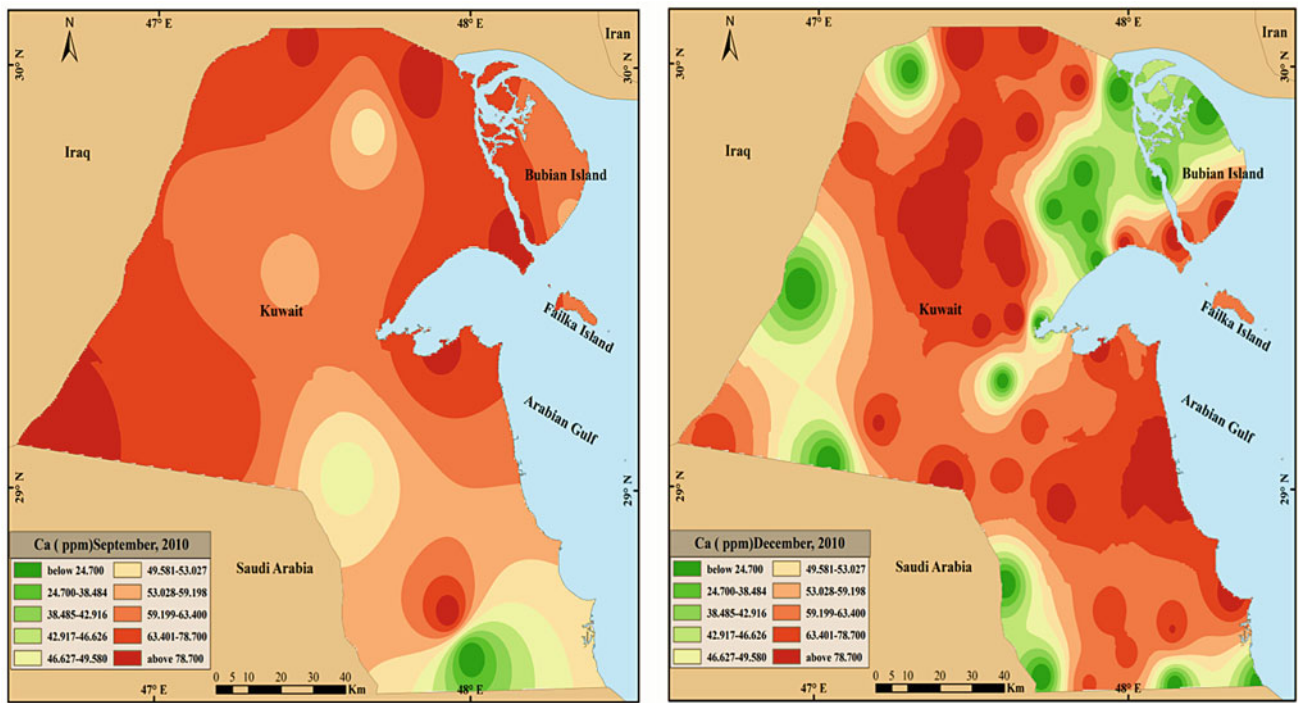


Fig. 5.8 (continued)

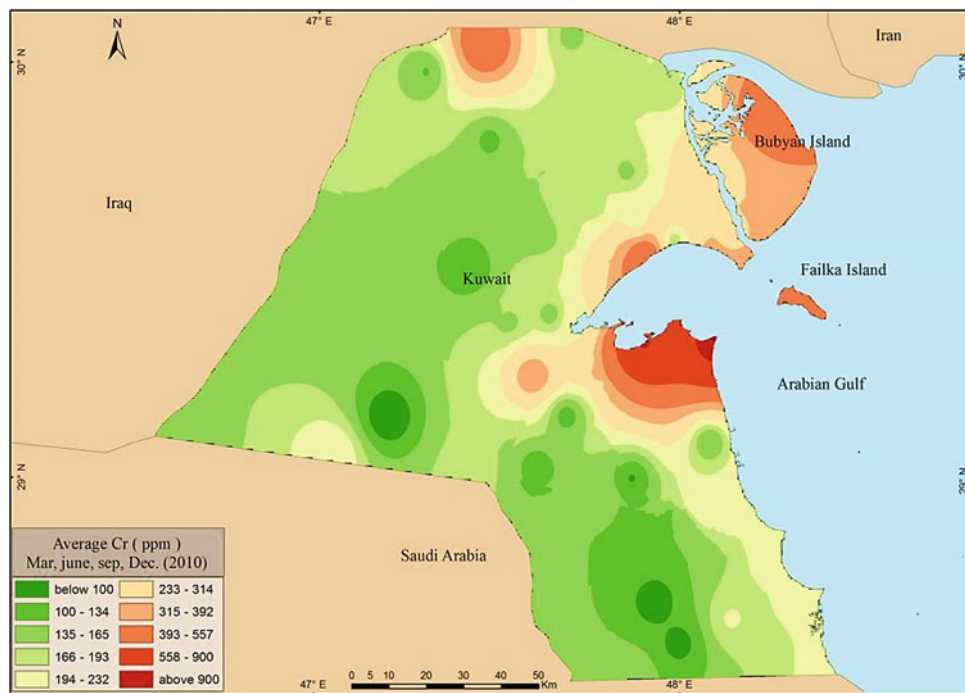


Fig. 5.9 Average chromium (Cr) content in ppm within fallen dust in Kuwait (2010)

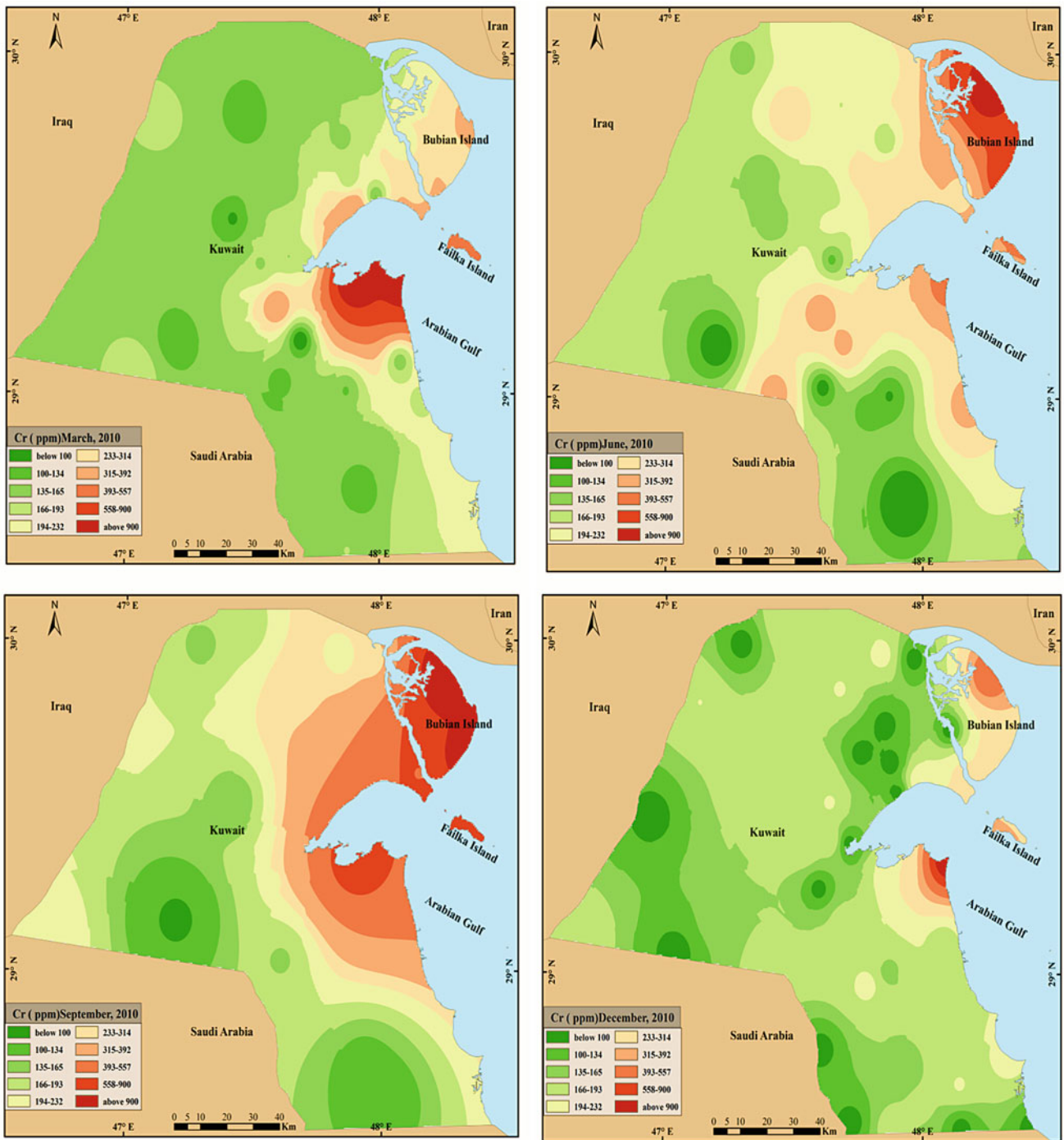


Fig. 5.10 Cr content in ppm within fallen dust in Kuwait (2010)

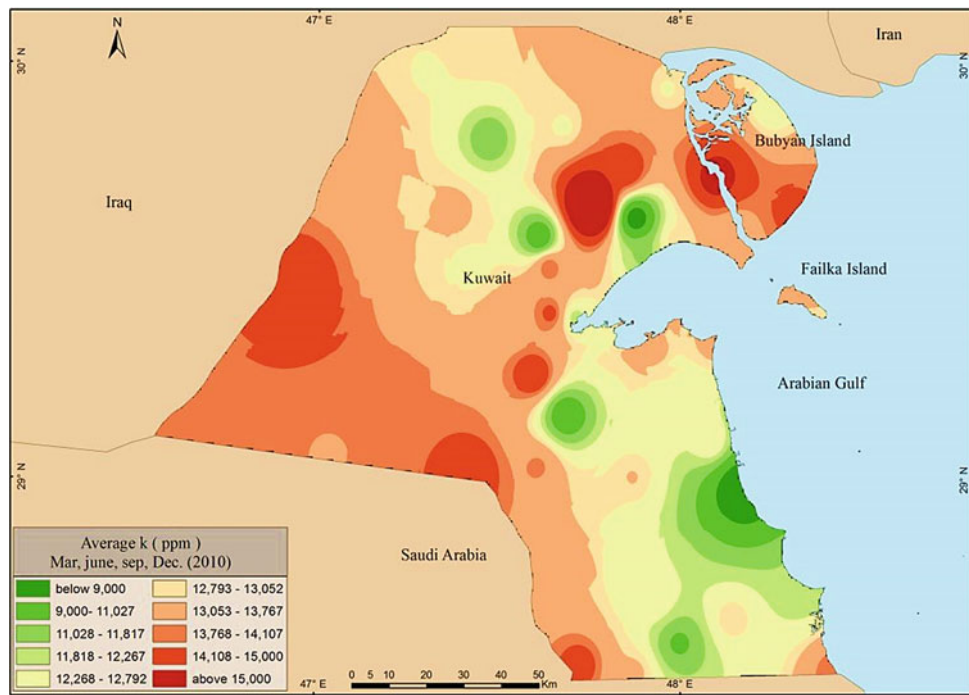


Fig. 5.11 Average potassium (K) content in ppm within fallen dust in Kuwait (2010)

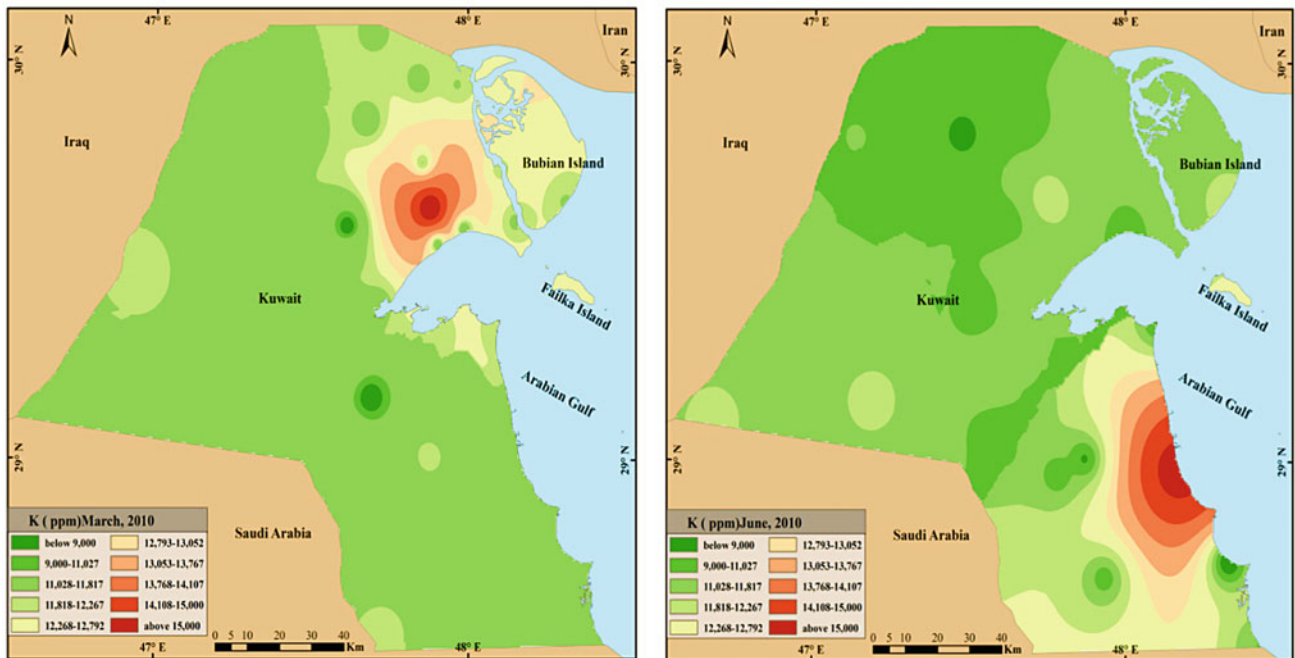


Fig. 5.12 K content in ppm within fallen dust in Kuwait (2010)

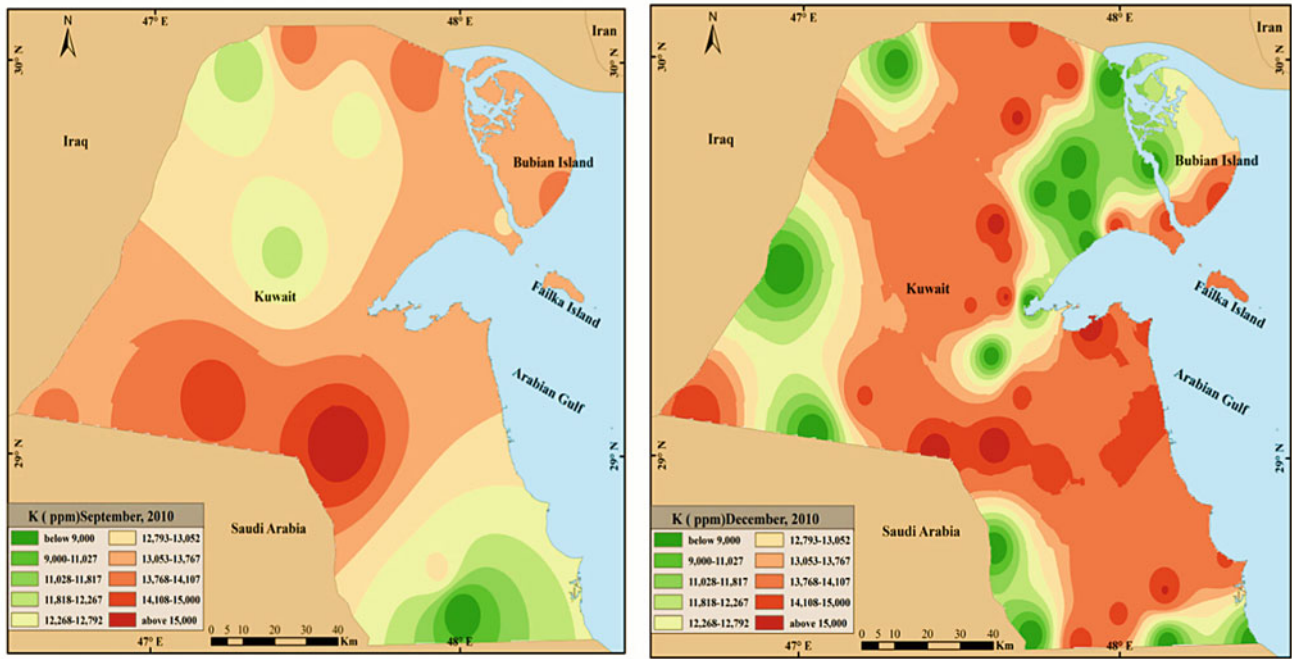
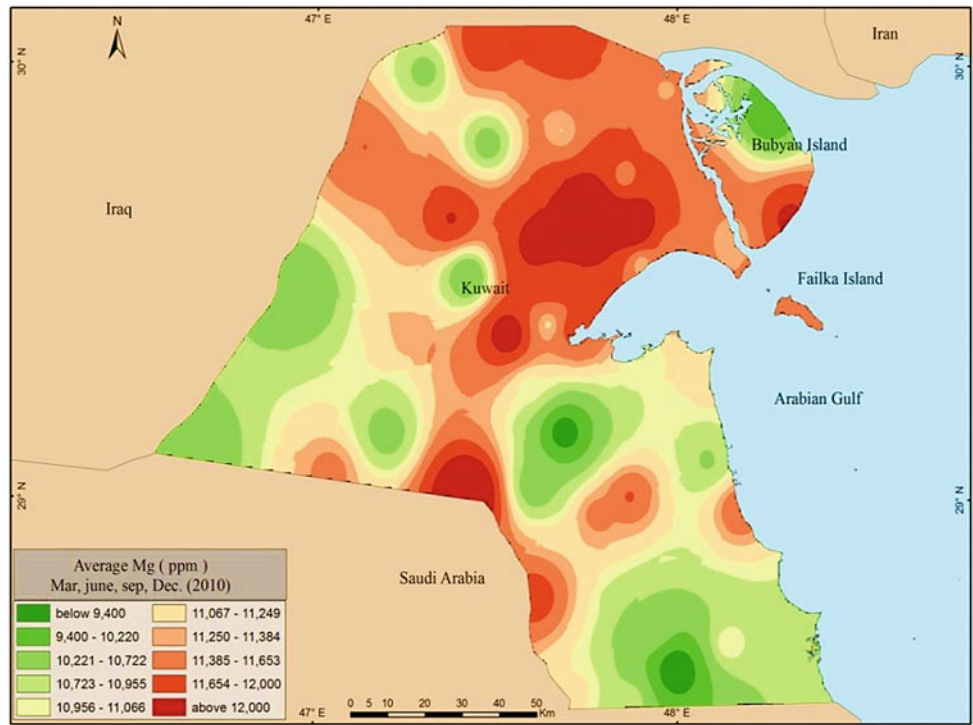


Fig. 5.12 (continued)

Fig. 5.13 Average magnesium (Mg) content in ppm within fallen dust in Kuwait (2010)



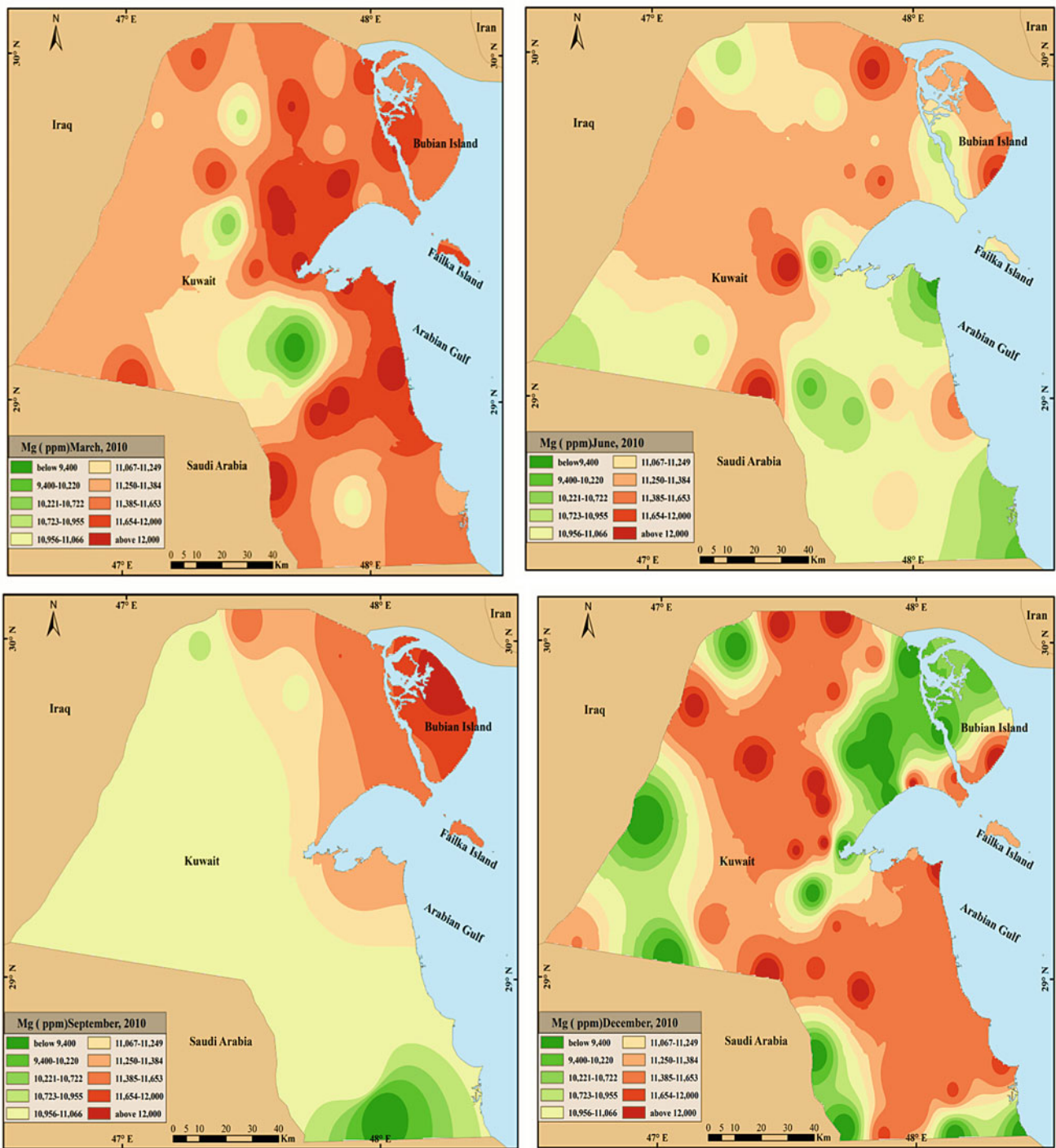


Fig. 5.14 Mg content in ppm within fallen dust in Kuwait (2010)

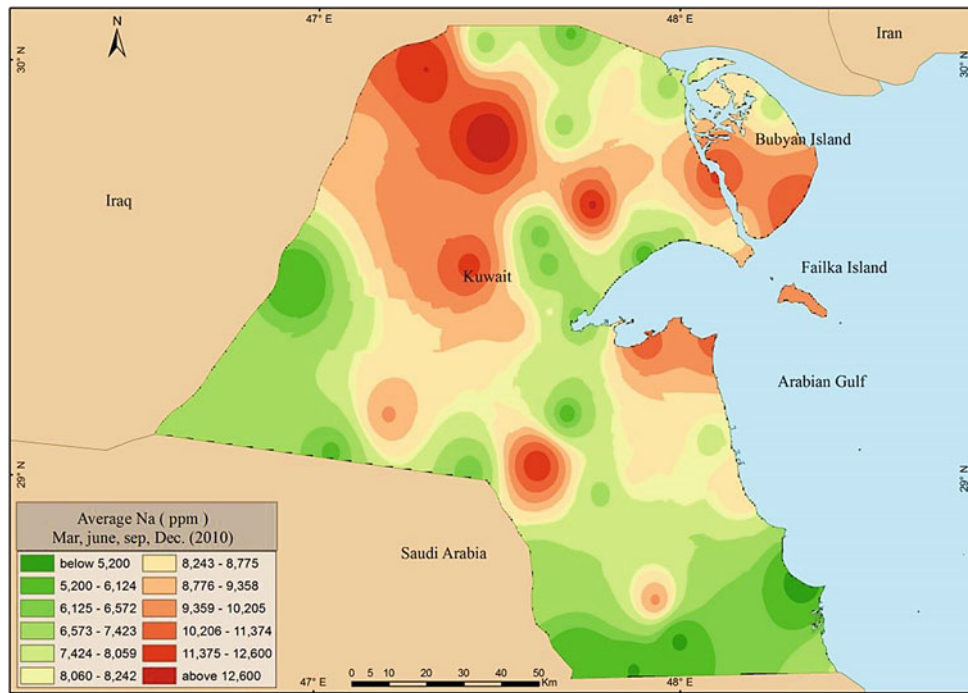


Fig. 5.15 Average sodium (Na) content in ppm within fallen dust in Kuwait (2010)

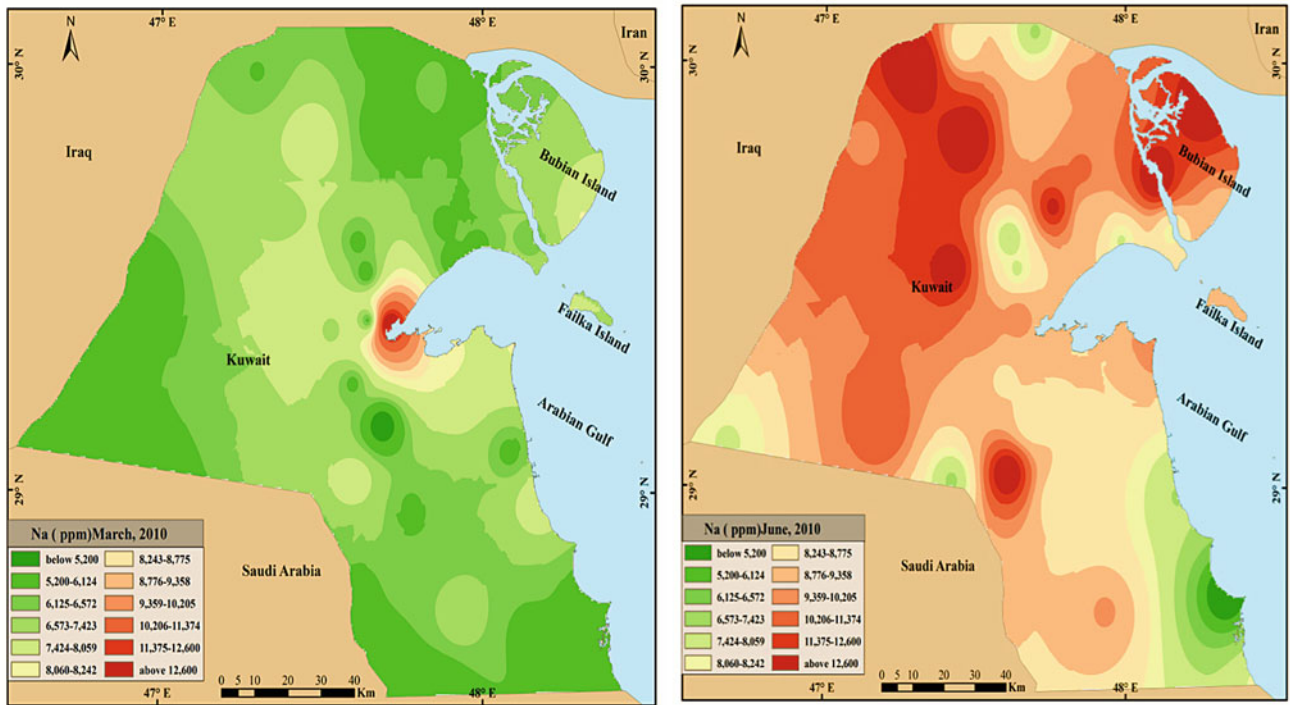


Fig. 5.16 Na content in ppm within fallen dust in Kuwait (2010)

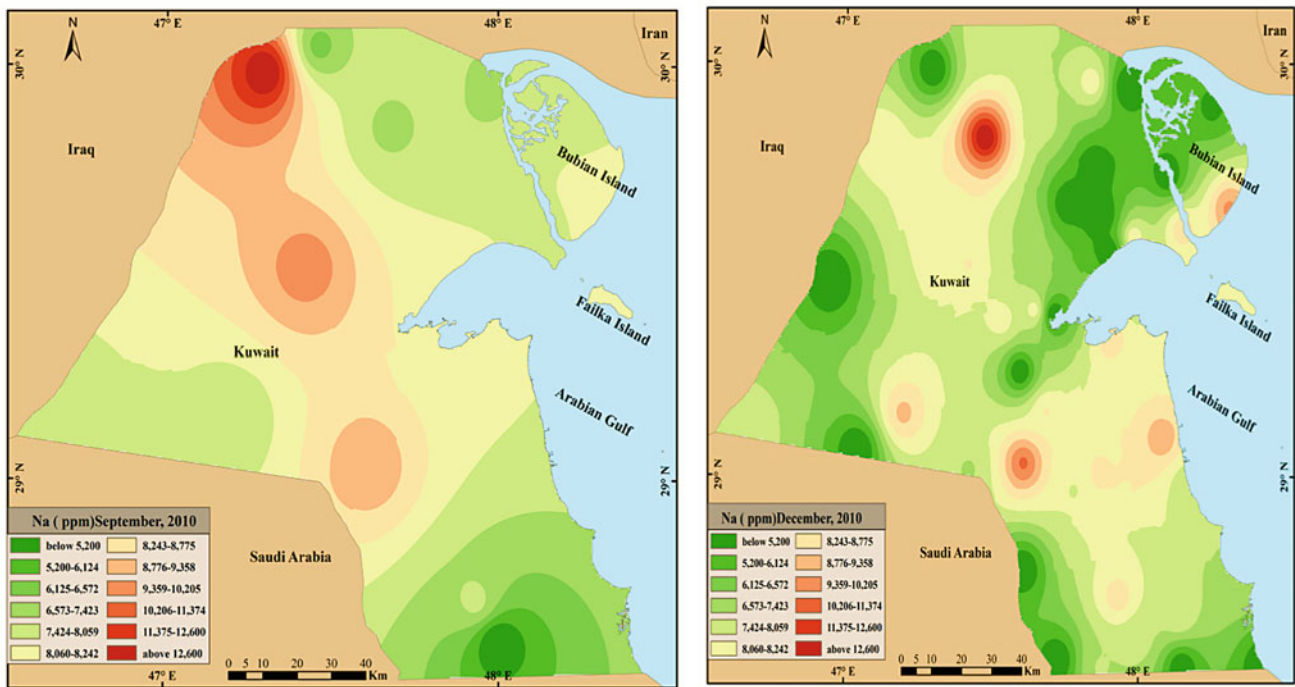


Fig. 5.16 (continued)

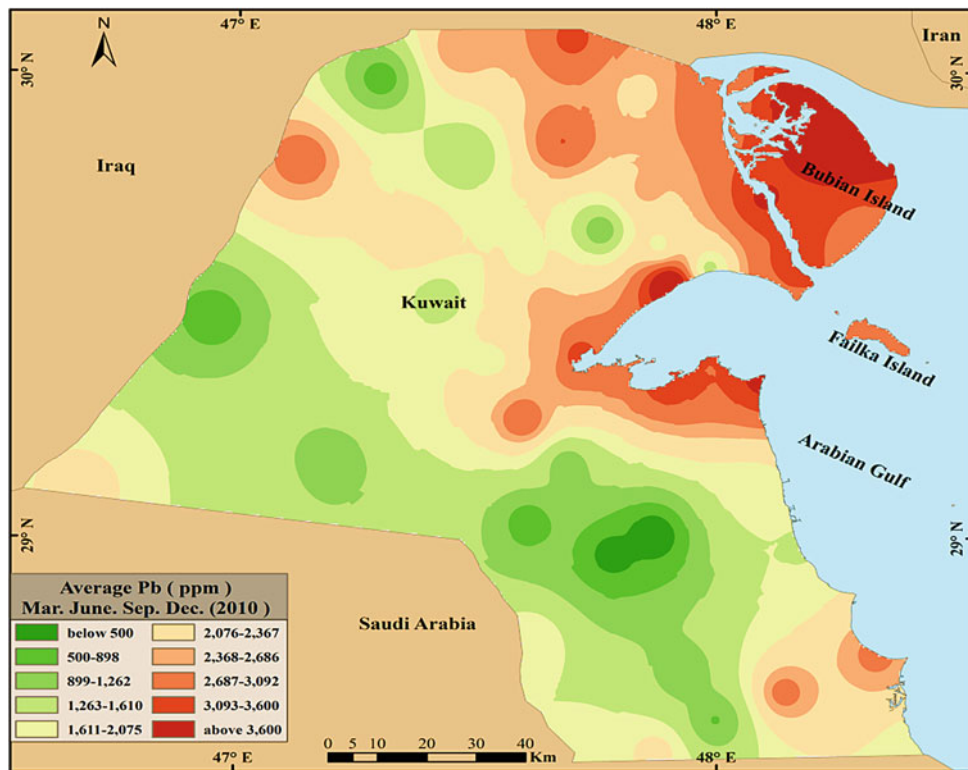


Fig. 5.17 Average lead (Pb) content in ppm within fallen dust in Kuwait (2010)

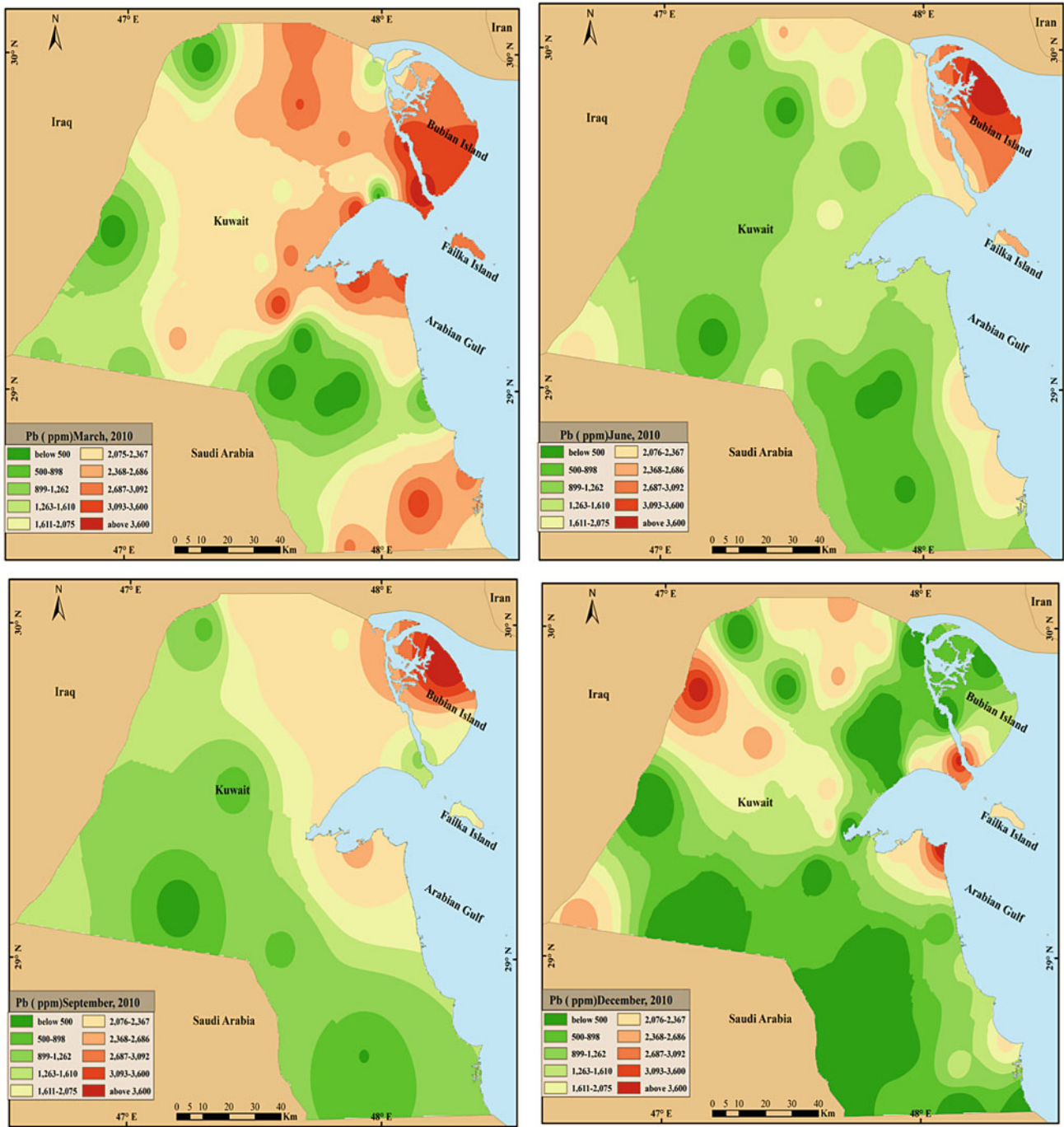


Fig. 5.18 Pb content in ppm within fallen dust in Kuwait (2010)

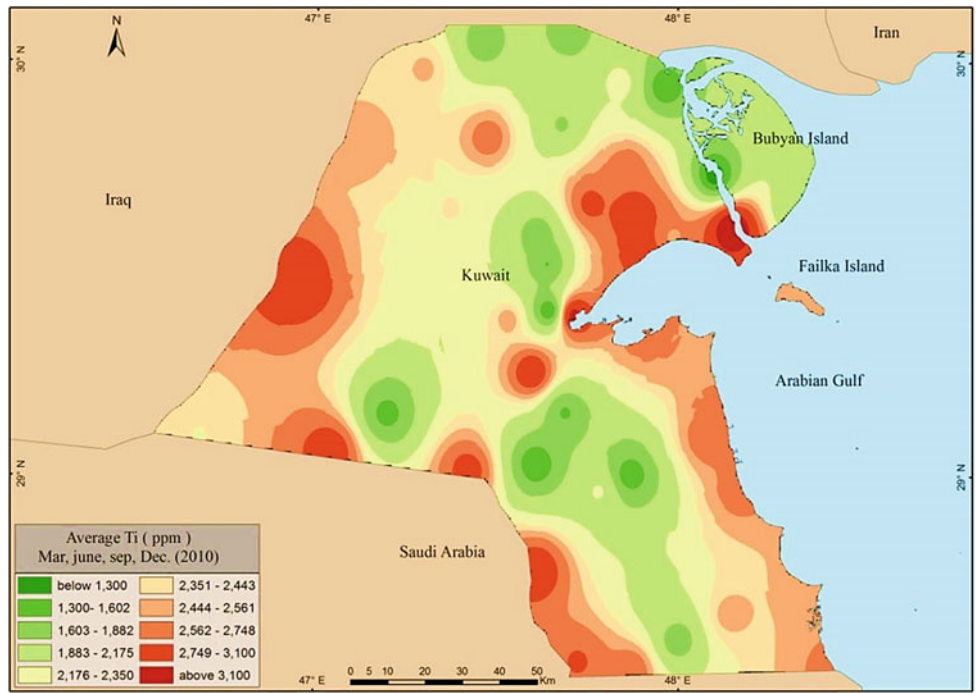


Fig. 5.19 Average titanium (Ti) content in ppm within fallen dust in Kuwait (2010)

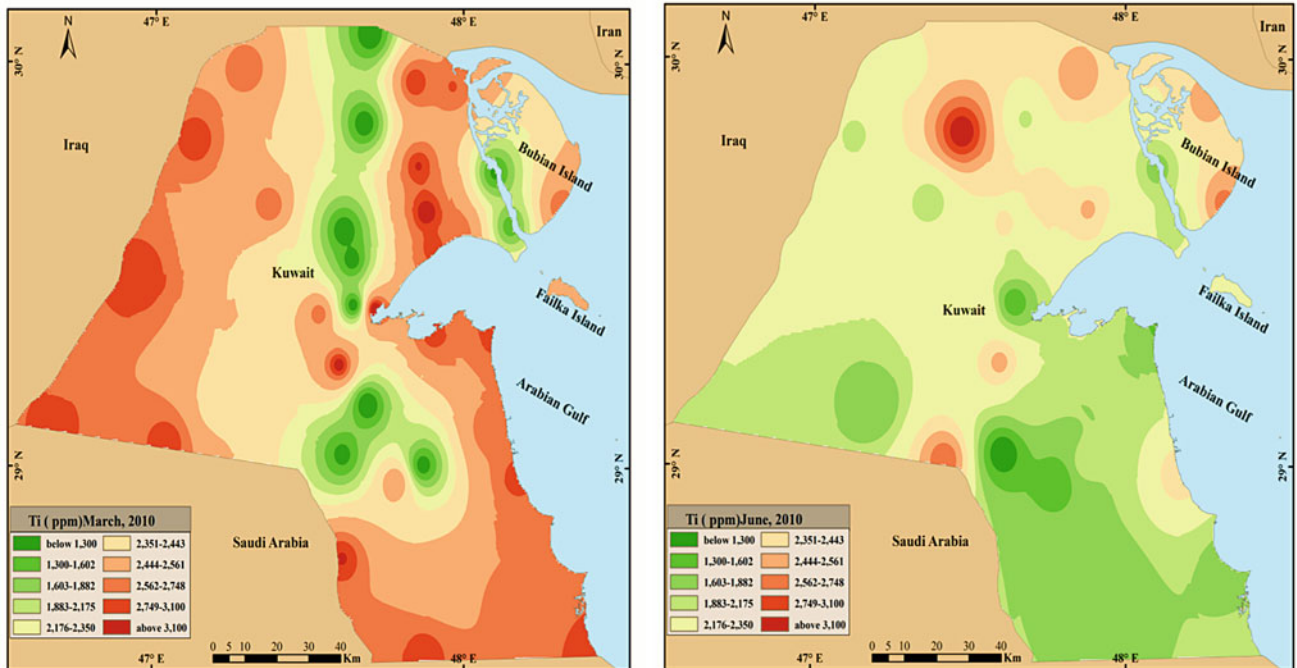


Fig. 5.20 Ti content in ppm within fallen dust in Kuwait (2010)

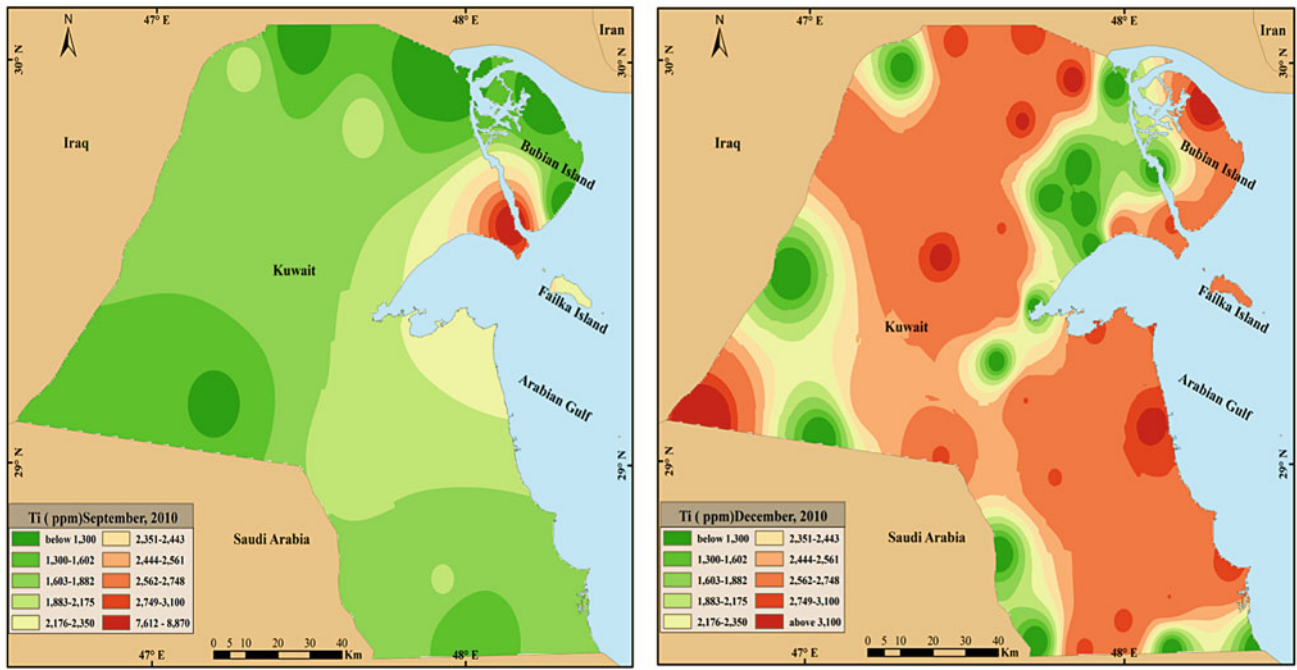


Fig. 5.20 (continued)

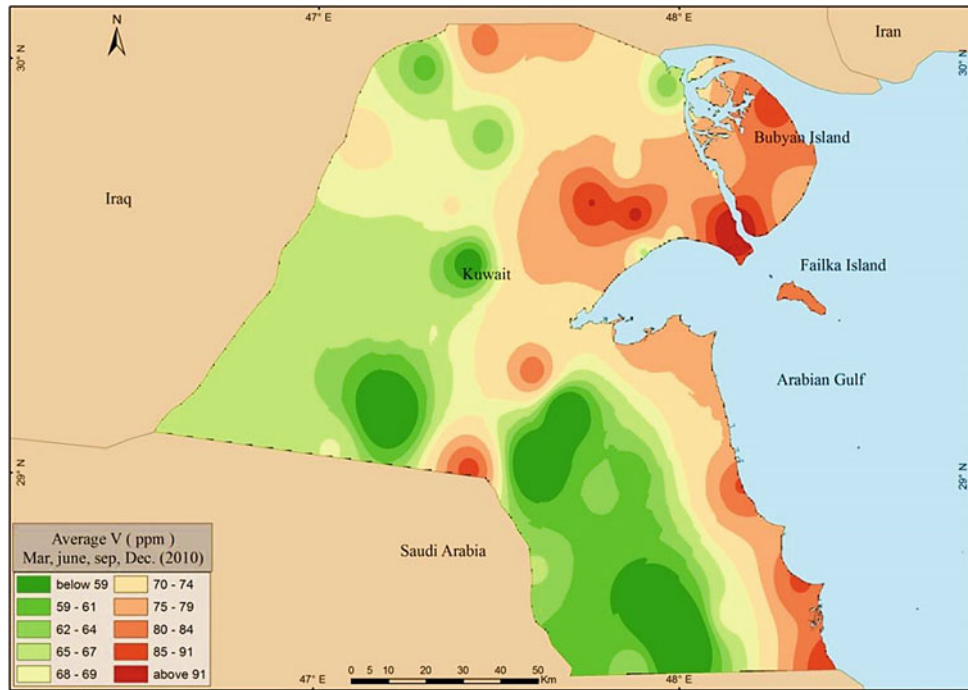


Fig. 5.21 Average vanadium (V) content in ppm within fallen dust in Kuwait (2010)

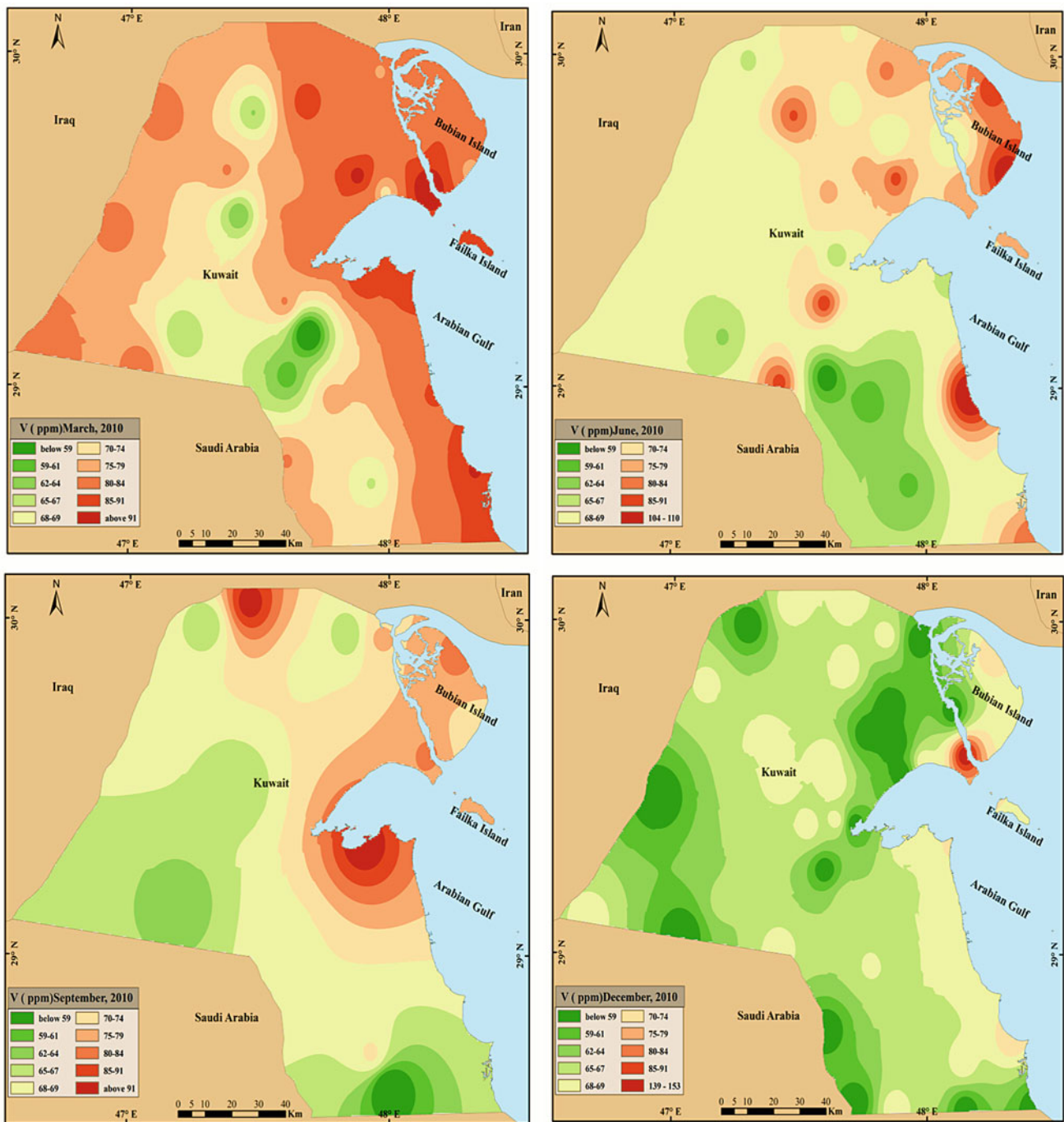
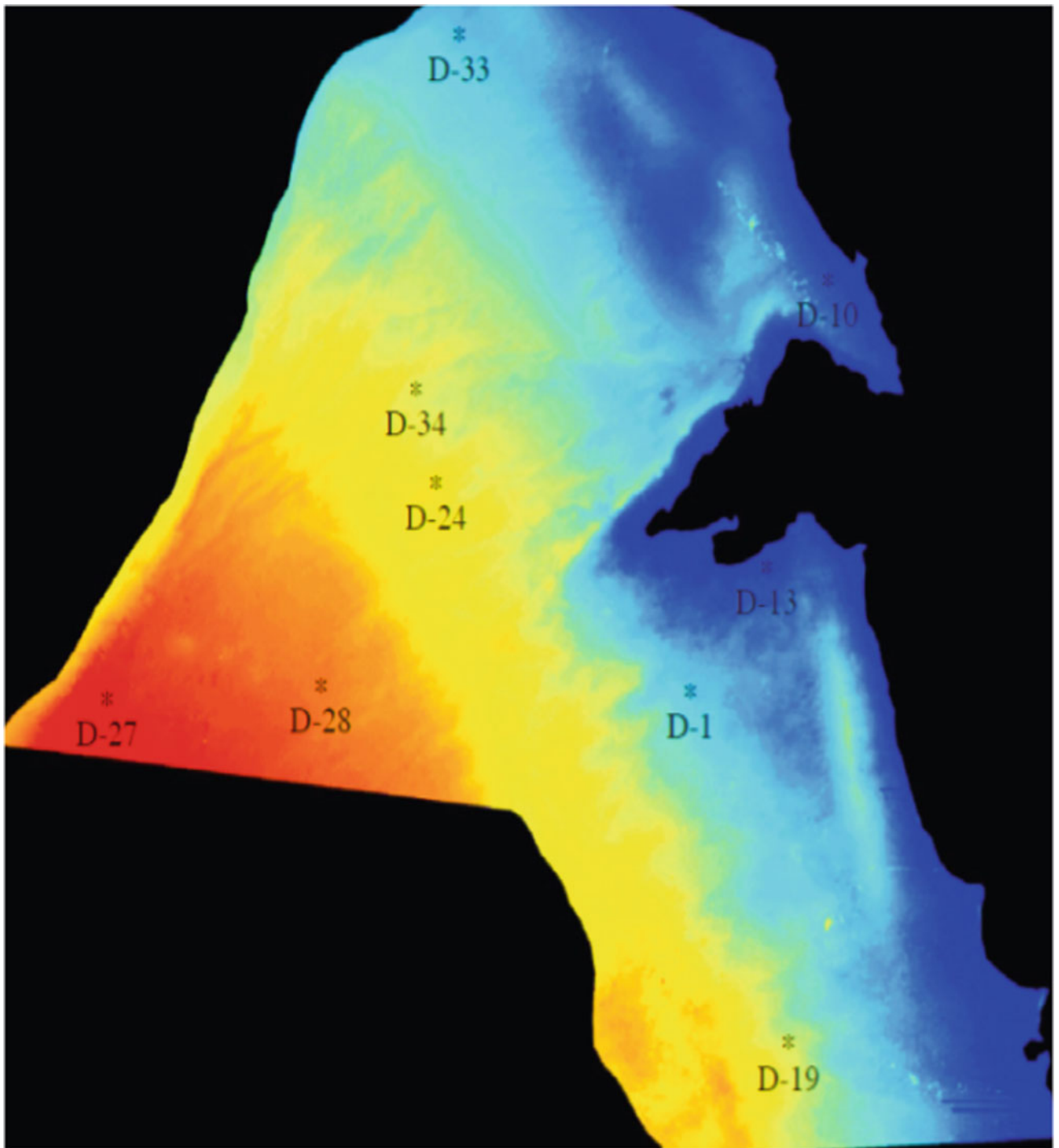


Fig. 5.22 V content in ppm within fallen dust in Kuwait (2010)

Open Access This chapter is licensed under the terms of the Creative Commons Attribution 4.0 International License (<http://creativecommons.org/licenses/by/4.0/>), which permits use, sharing, adaptation, distribution and reproduction in any medium or format, as long as you give appropriate credit to the original author(s) and the source, provide a link to the Creative Commons licence and indicate if changes were made.

The images or other third party material in this chapter are included in the chapter's Creative Commons licence, unless indicated otherwise in a credit line to the material. If material is not included in the chapter's Creative Commons licence and your intended use is not permitted by statutory regulation or exceeds the permitted use, you will need to obtain permission directly from the copyright holder.





Abdulaziz Aba, Anfal Ismaeel, Aisha Al-Boloushi, Hanadi Al-Shimary, and Omar Al-Boloushi

Abstract

- Temporal and Spatial Distribution of Radionuclides in Dust Fallout.
- The depositional fluxes of the natural radionuclides (^{40}K , ^{210}Pb , and ^7Be) and the man-made radionuclides (^{137}Cs) have been calculated using efficiency calibrated ultra-low background gamma spectrometry in nine sampling sites covering Kuwait.
- Maps showing high and low concentrations of radionuclides distribution among Kuwait.

Radionuclides

Methodology

Temporal and Spatial Distribution of Radionuclides in Dust Fallout

The depositional fluxes of the natural radionuclides (^{40}K , ^{210}Pb , and ^7Be) and the man-made radionuclides (^{137}Cs) were calculated using efficiency-calibrated ultralow

background gamma spectrometry in nine sampling sites covering Kuwait (Fig. 6.1). The dust fallout samples were collected on a monthly basis. Four collectors were installed in each sampling location to collect the adequate sample mass required for radioactivity analysis. The composite samples were subjected to long counting times regarding attaining an acceptable detection limit and to resolve very low-intensity peaks.

The collected gamma spectra were analyzed by Genie-2000 (Canberra Inc, USA) using the spectral lines of the most intense gamma energy lines. The decay correction and building-up factor of ^7Be during the sampling period (almost 30 days) were considered due to the relatively short half life of ^7Be . The concentration of radionuclides in dry deposition fluxes (Bq m^{-2}) per month was determined by multiplying their specific activities in Bq g^{-1} with the weight per unit area of the collector (g m^{-2}) during sampling time (30 days).

The variety of all of the calculated radionuclides and depositional fluxes revealed a temporal tendency (i.e., highest in the spring months [February, March, April], when the precipitation rates are highest, and hence, more dust is washed out and the lowest in October–November of each year) (Fig. 6.2). The correlation of depositional dust fallout and the radionuclides fluxes was in the order of ^{40}K ; ^{137}Cs ; ^{210}Pb and ^7Be . The strongest correlation was with the terrestrial origin ^{40}K (0.92), and the weakest was with the cosmogenic origin ^7Be (0.67).

On the other hand, the spatial distributions of radionuclide depositional fluxes showed a site-dependent relationship that is similar to the spatial dust fallout: highest in the interior areas and gradually decreasing along the coastal line. Nevertheless, an exception of the cosmogenic radionuclide ^7Be distribution was observed in some months because of possibly different climatologically conditions.

The averages of the depositional fluxes of similar months were gridded using the GIS (ArcGIS) software package and presented as averages on a monthly basis from October 2009 to August 2011.

A. Aba (✉) · A. Ismaeel · A. Al-Boloushi · H. Al-Shimary ·

O. Al-Boloushi

Crisis Decision Supports Program (CDS), Environment and Life Sciences Research Center (ELSRC), Kuwait Institute for Scientific Research (KISR), P.O. Box 24885 13109 Safat, Kuwait

e-mail: aaba@kisir.edu.kw

A. Ismaeel

e-mail: aismaeel@kisir.edu.kw

A. Al-Boloushi

e-mail: aboloushi@kisir.edu.kw

H. Al-Shimary

e-mail: hshammari@kisir.edu.kw

O. Al-Boloushi

e-mail: oboloushi@kisir.edu.kw

1. Monthly spatial distribution of ^7Be

Figures 6.3, 6.4, 6.5, 6.6, 6.7, 6.8, 6.9, 6.10, 6.11, 6.12, 6.13, 6.14 and 6.15 show the annual and monthly spatial deposition rates of the ^7Be radionuclide in dust fallout during October 2009–October 2011. The minimum monthly deposition fluxes (2.4 Bq m^{-2}) were observed in December, when the precipitation was the lowest. In contrast, the high concentration during the spring season (March–April–May) was due to rainfall during the period supporting the theory of wet precipitation commonly associated with the mixing of stratospheric and tropospheric air masses (Daish et al. 2005). In spring time, a rapid removal from lower polar troposphere to the troposphere at the northern hemisphere is well known (UNSCEAR 2000) and, possibly due to the folding of the troposphere during April and May at mid-latitude (30–50), enhances the removal of the stratospheric ^7Be into the troposphere (Viezee and Singh 1980; Kritz et al. 1991). However, in contrast, the spatial distribution in the fall months (September–October–November) might be due to the effect of southeasterly wind contribution. The highest monthly readings (76.5 and 184 Bq m^{-2}) were observed in January and April, respectively, due to the effect of a washout by precipitation.

2. Temporal, spatial distribution of ^{137}Cs

^{137}Cs is a human-made radionuclide with a half life of 30 years. It was produced during the atmospheric testing of thermonuclear weapons in the period extending from the mid-1950s to the 1980s. Global fallout of ^{137}Cs began in 1954, peaked in the early 1960s and subsequently decreased, reaching near-zero levels in the mid-1980s. Fallout levels were globally variable, reflecting both annual precipitation amount and location relative to the main weapons tests (Walling 2002). Smaller amounts of ^{137}Cs have been released into the atmosphere by catastrophes at nuclear power plants, notably the Chernobyl disaster in 1986, which resulted in additional outputs of ^{137}Cs fallout over large areas of Europe and adjacent regions. However, wide measurements of ^{137}Cs concentration have also been carried out in Kuwaiti aerosol, in cooperation with the Comprehensive Nuclear Test Ban Treaty (CTBT) from 1995 to 1999. The reported ^{137}Cs concentration in the air was between 1.44 and 107.84, with an average value of $10.6 \mu\text{Bq m}^{-3}$ (Biegalski et al. 2001).

Figures 6.16, 6.17, 6.18, 6.19, 6.20, 6.21, 6.22, 6.23, 6.24, 6.25, 6.26, 6.27 and 6.28 illustrate the annual and monthly spatial deposition rates of ^{137}Cs , which display similar behavior to ^{210}Pb and ^7Be variations. The correlation

coefficients of $^{137}\text{Cs}/^{210}\text{Pb}$ and $^{137}\text{Cs}/^7\text{Be}$ were 0.87 and 0.94, respectively. The average monthly deposition rates varied from 0.02 to 4.18 Bq m^{-2} , while the annual deposition rates varied from 0.2 to 50.21 Bq m^{-2} . Based on the previous observations (e.g., the influence of precipitation, wind direction, and depositional dust rates), the dominant source of ^{137}Cs fallout is the transportation of dust by the northwesterly wind, as the areas of northern Europe and eastern Mediterranean are most affected by ^{137}Cs fallout (nuclear bomb tests and Chernobyl accident), more so than the Gulf Region.

3. Temporal, spatial distribution of ^{40}K

Figures 6.29, 6.30, 6.31, 6.32, 6.33, 6.34, 6.35, 6.36, 6.37, 6.38, 6.39, 6.40 and 6.41 illustrate the annual and monthly spatial deposition rates of ^{40}K radionuclide in dust fallout. The highest ^{40}K concentrations were observed in spring months, when it reached a maximum in March 2011 (96.27 Bq m^{-2}) and the lowest in fall (1.8 Bq m^{-2}), which is quite consistent with the dust loadings of the corresponding months. The annual variations of ^{40}K concentration in dust fallout varied from 74 to 557 Bq m^{-2} , as presented in Fig. 6.29. This quantity of the ^{40}K deposition rate corresponds to about 412 Bq kg^{-1} and the average measured ^{40}K concentration in Kuwaiti soil is 365 Bq kg^{-1} , which is similar to the worldwide average concentration (420 Bq kg^{-1}) (UNSCEAR 2000). The distribution of ^{40}K monthly and seasonal variations displays similar behavior to the dust fallout trend. However, the site specificity of ^{40}K is very similar to the dust deposition distribution, which is very low in the coastal zone, significantly increasing in the southwest of the country.

4. Temporal, spatial distribution of ^{210}Pb

Figures 6.42, 6.43, 6.44, 6.45, 6.46, 6.47, 6.48, 6.49, 6.50, 6.51, 6.52, 6.53 and 6.54 illustrate the annual and monthly spatial deposition rates of ^{210}Pb radionuclide in dust fallout from October 2009 to October 2011. The highest ^{210}Pb concentrations were observed in spring (41.4 Bq m^{-2}) and the lowest in fall (1.8 Bq m^{-2}), which is quite consistent with the dust loadings of the corresponding months. However, the wet precipitation associated with Sarrayat and Koss played a major role in obtaining these high deposition fluxes (Aba et al. 2016, 2018; Al-Dousari et al. 2016). The monthly deposition ratios of ^7Be and ^{210}Pb are largely consistent with the dust loading in the corresponding months. However, an extreme deposition rate (63 Bq m^{-2}) was observed in March 2011, when an exotic storm hit Kuwait.

Samples Locations

Figure 6.1.

Temporal Variations of Radionuclides

Figure 6.2.

Annual Deposited Rates of ⁷Be

The average annual ⁷Be deposited rates in Kuwait from October 2009 to August 2011 varied from 339 to 481 Bq m⁻², with an average similar (422 Bq m⁻²) to the reported

data of the global model (400 Bq m⁻²). The maximum rates were found in a transect width of about 50 km from north to south. The minimum rates were shown along the transect from the middle of the country down to the southeastern part. The dominant annual wind direction is northwesterly (Fig. 6.3).

Areas with high radionuclide concentration	Areas with low radionuclide concentration
Abdulli	Sulaybiyah
Ratqah	Wafra Farms
Dibdibah	KhurFawaris
Um Al Madafi'	Khiran
Liyah	Qurain

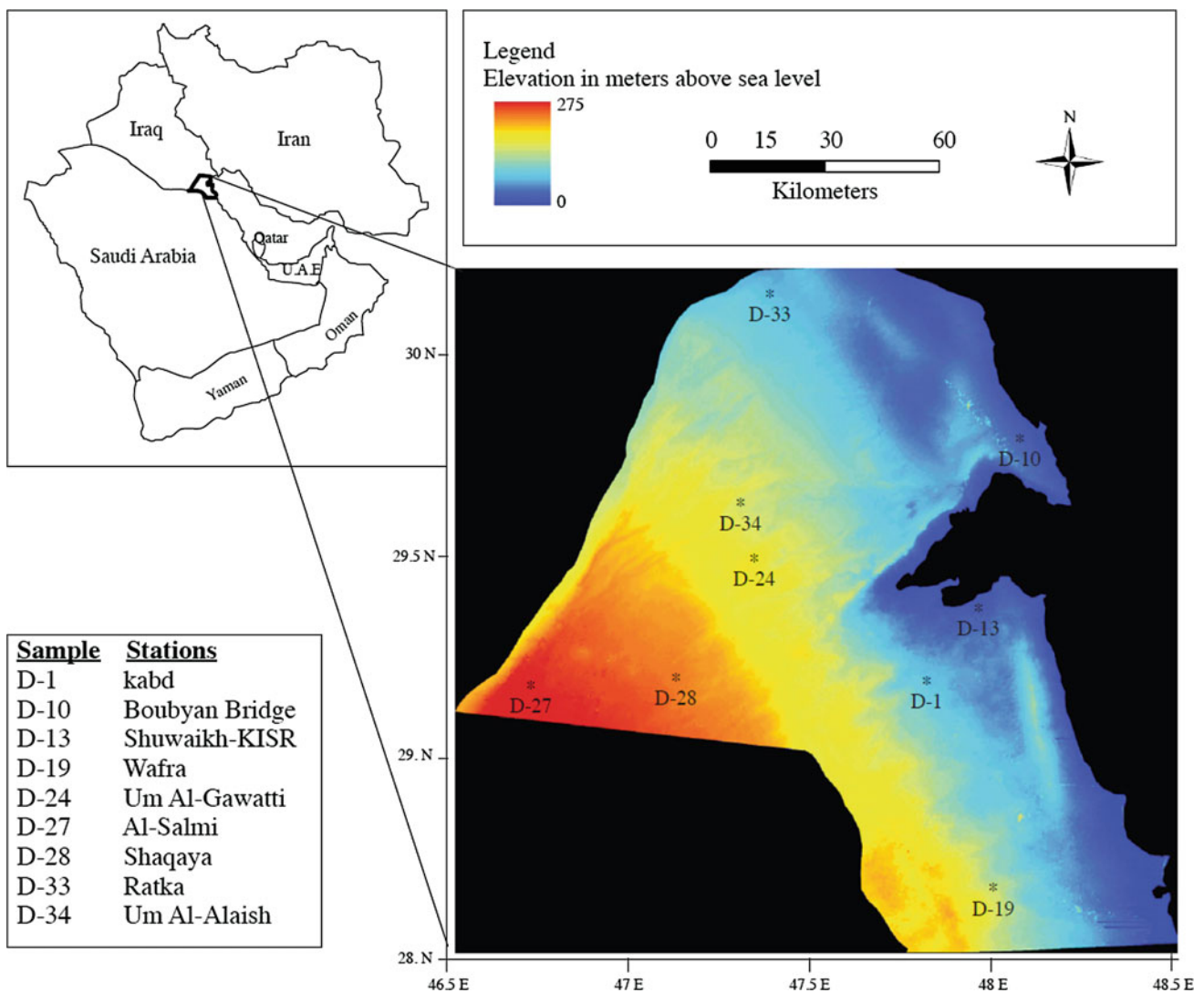


Fig. 6.1 Sampling locations of dust fallout and digital elevation model of Kuwait using ASTER stereo data

Fig. 6.2 Temporal variations of radionuclide depositional fluxes in Kuwait

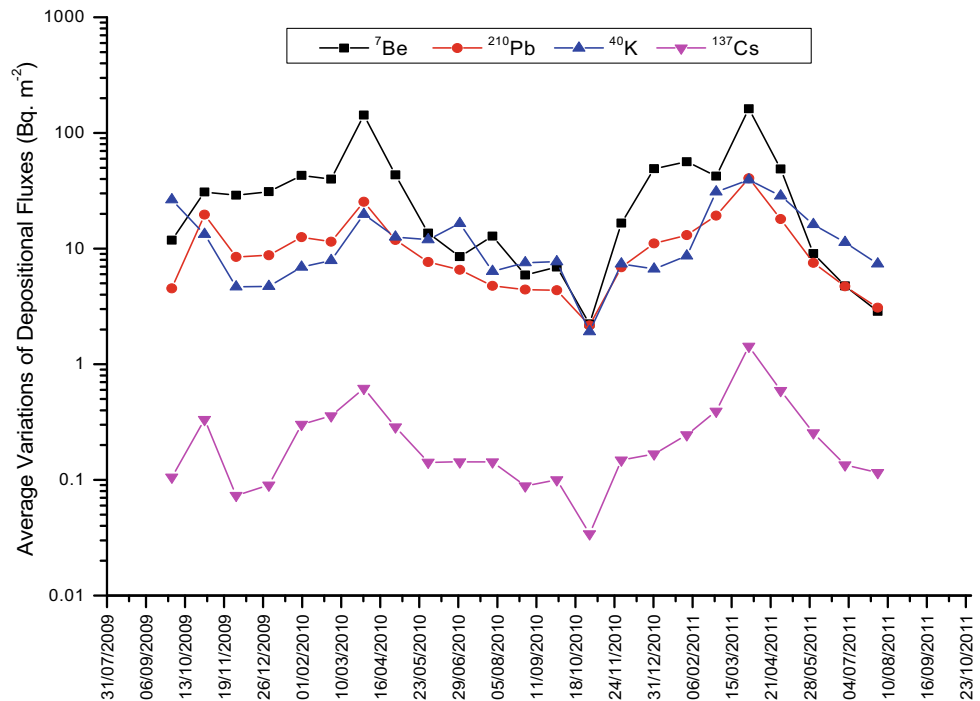
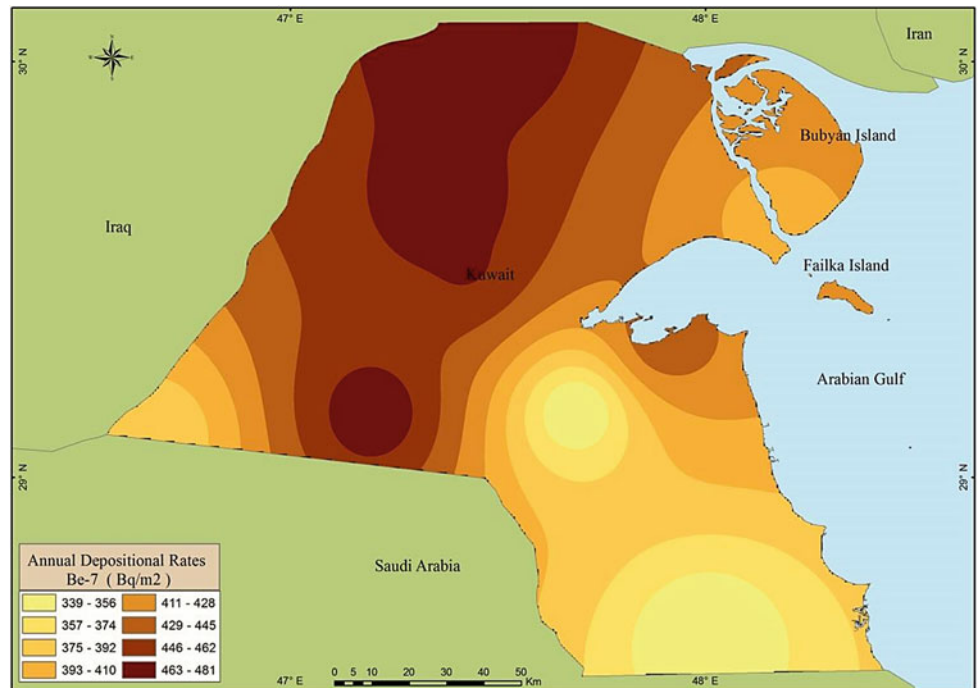


Fig. 6.3 Average deposited rates of ⁷Be

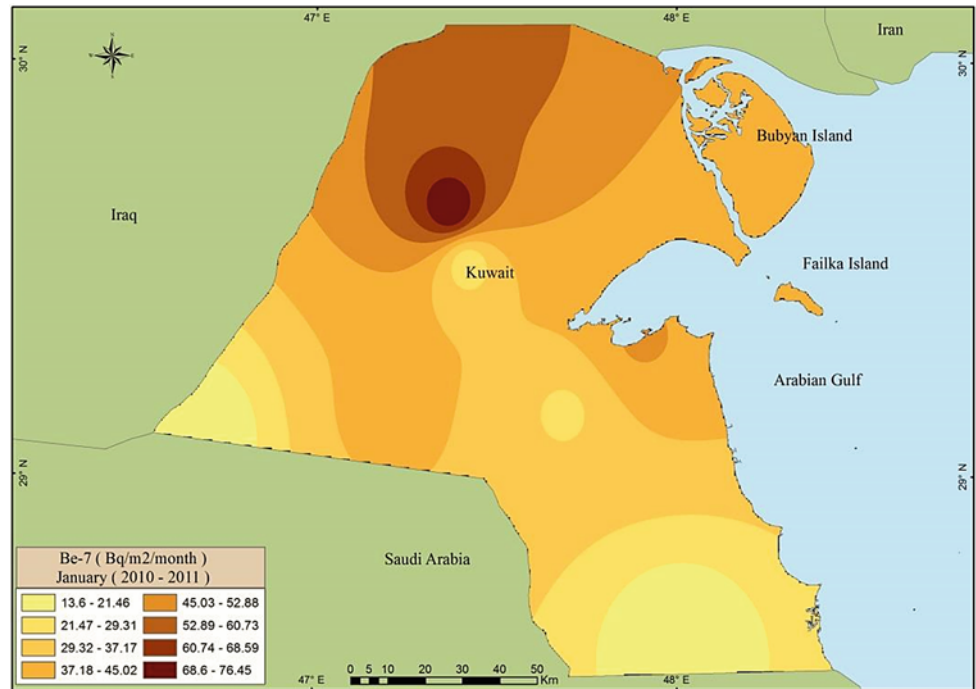


Monthly Deposited Rates of ⁷Be

The monthly ⁷Be deposited rates in Kuwait January 2010–2011 reveal a range from 13.6 to 76.5 Bq m⁻², with the maximum in northern areas and the lowest in southern areas. The predominant wind direction for this month was north-westerly (Fig. 6.4).

Areas with high radionuclide concentration	Areas with low radionuclide concentration
Abdulli	Salmi
Ratqah	Sulaybiyah
Um Eish	Wafra Farms
Raudhatain	KhurFawaris
Huwaymilyah	Khiran

Fig. 6.4 Average deposited rates of ⁷Be in January (2010–2011)



The monthly rates at which ⁷Be were deposited in Kuwait in February 2010–2011 which reveal a range from 36.08 to 63.83 Bq m⁻², with three maximum spots. This possibly happened because of the effect of dust storms this month. The predominant wind direction for this month was north-westerly (Fig. 6.5).

Areas with high radionuclide concentration	Areas with low radionuclide concentration
Bubiyah Bridge	Salmi
Dibdibah	Um Al Madafi'
Wafra Farms	Liyah
KhurFawaris	Shegaya
Subiyah	Um Eish

Fig. 6.5 Average deposited rates of ⁷Be in February (2010–2011)

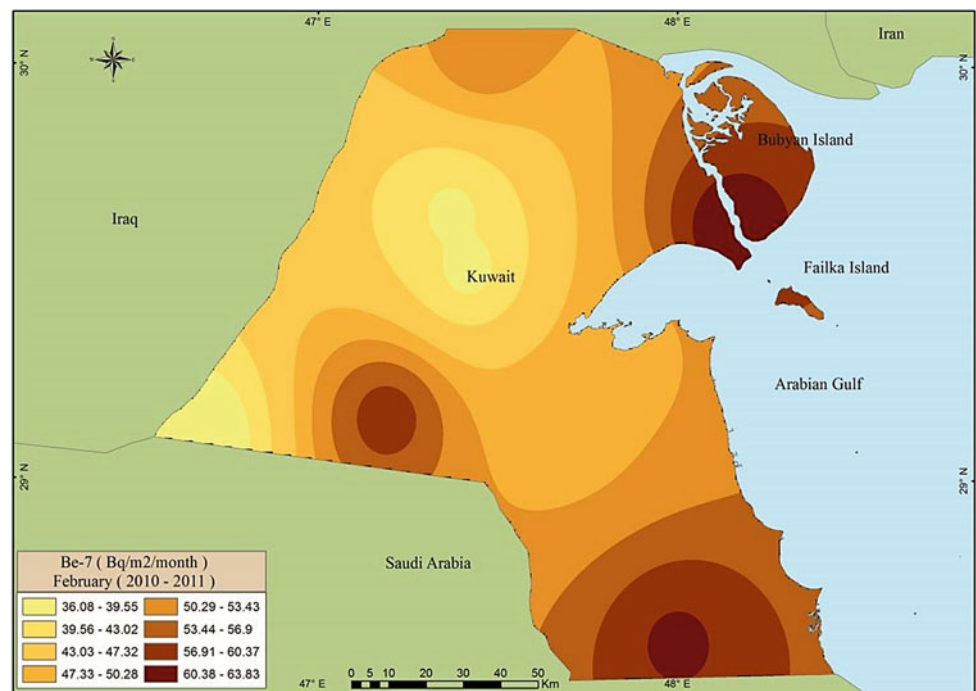
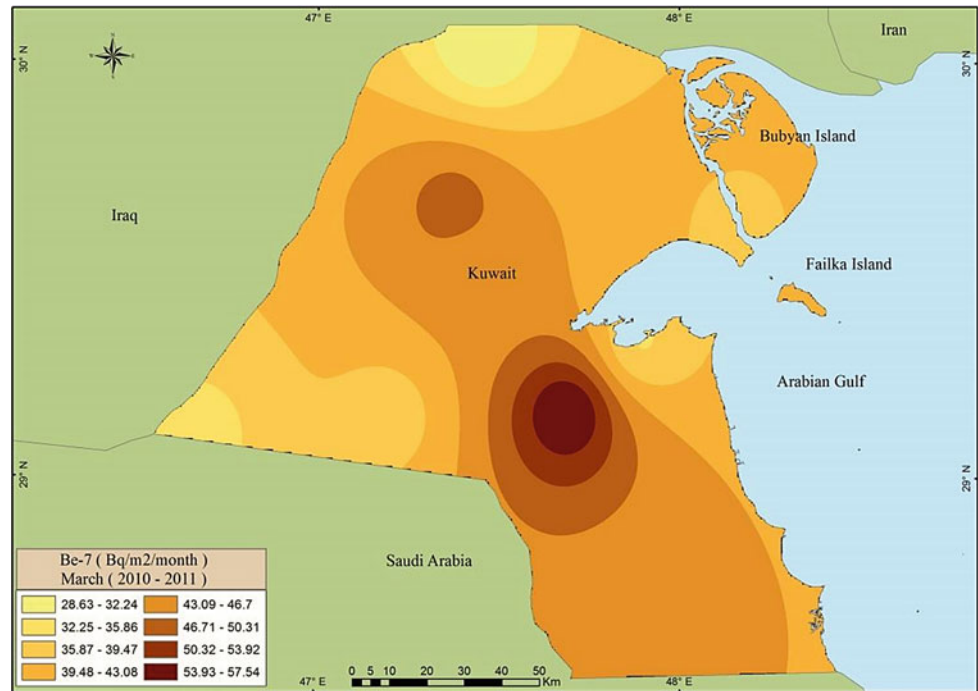


Fig. 6.6 Average deposited rates of ⁷Be in March (2010–2011)



The monthly ⁷Be deposited rates in Kuwait during March 2010–2011 reveal a range from 28.63 to 57.54 Bq m⁻², with a maximum in the central region with the northern, western wind corridor, and the lowest in the northern area. The predominant wind direction for this month was northwesterly, with high speeds sometimes. However, the occurrence of dust storms was lower in February, as well as precipitation. Nevertheless, the effect of the exotic storm that hit Kuwait in March 2011 led to critical dynamic weather that could probably have decreased the ⁷Be deposition flux (Fig. 6.6).

Areas with high radionuclide concentration	Areas with low radionuclide concentration
Abdulli Ratqah Roudhatain Liyah Salmiya	Salmi Atraf Kabd Sulaybiyah Wafra Farms

Areas with high radionuclide concentration	Areas with low radionuclide concentration
Atraf Um Al Madafi' Liyah Sulaybiyah Kabd	Abdulli Salmi Subiyah Shegaya Ratqah

The monthly ⁷Be deposited rates in Kuwait during April 2010–2011 reveal the highest deposited rates, with a range from 106 to 184 Bq m⁻², with a maximum in the northern and central areas and the lowest in eastern central areas. The major parameter affecting this high value was the higher precipitation rate in this month (Fig. 6.7).

The monthly ⁷Be deposited rates in Kuwait during May 2010–2011 reveal a range from 27 to 69 Bq m⁻², with a maximum in the southern, eastern and northern areas and the lowest in the southern areas. The high values are attributed to the high precipitation rates this month that increased the dust washout (Fig. 6.8).

Areas with high radionuclide concentration	Areas with low radionuclide concentration
Salmi Shegaya Dibdibah Huwaymilyah Ubayriq	Sulaybiyah Wafra Farms Salmiya Khiran KhurFawaris

The monthly ⁷Be deposited rates in Kuwait during June 2010–2011 reveal a lower rate than previous months, with a range from 4.23 to 17.32 Bq m⁻². The maximum rates were in the northern and western areas, while the lowest were in

Fig. 6.7 Average deposited rates of ⁷Be in April (2010–2011)

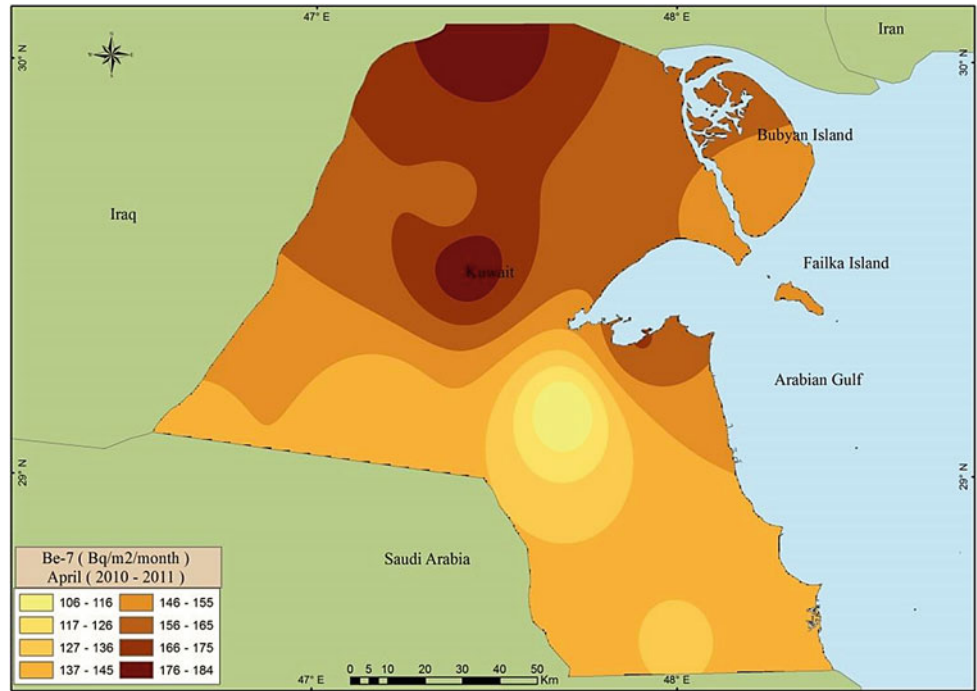


Fig. 6.8 Average deposited rates of ⁷Be in May (2010–2011)

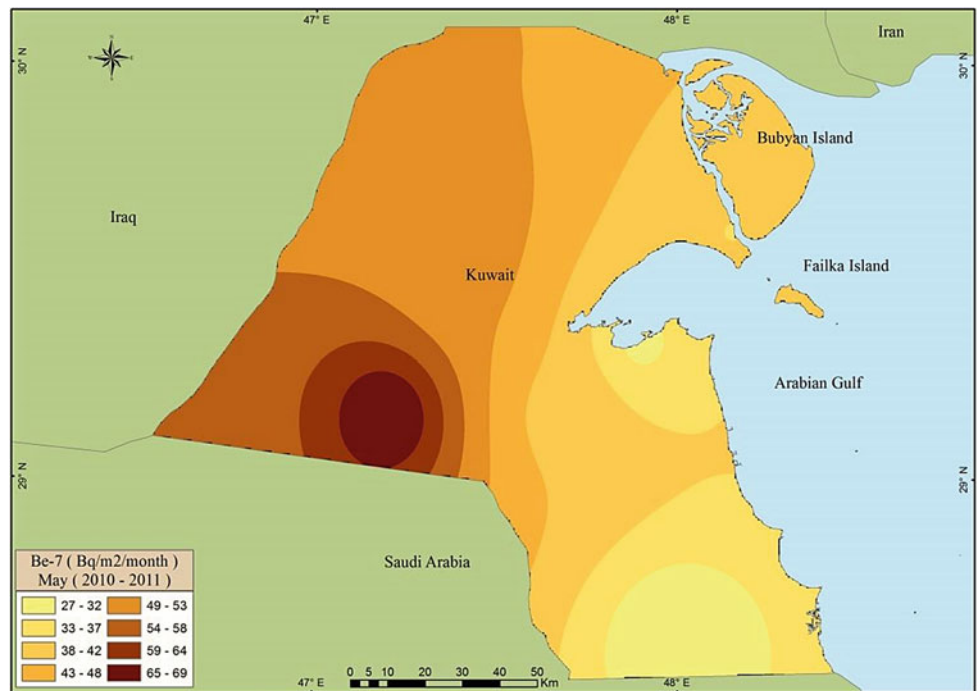
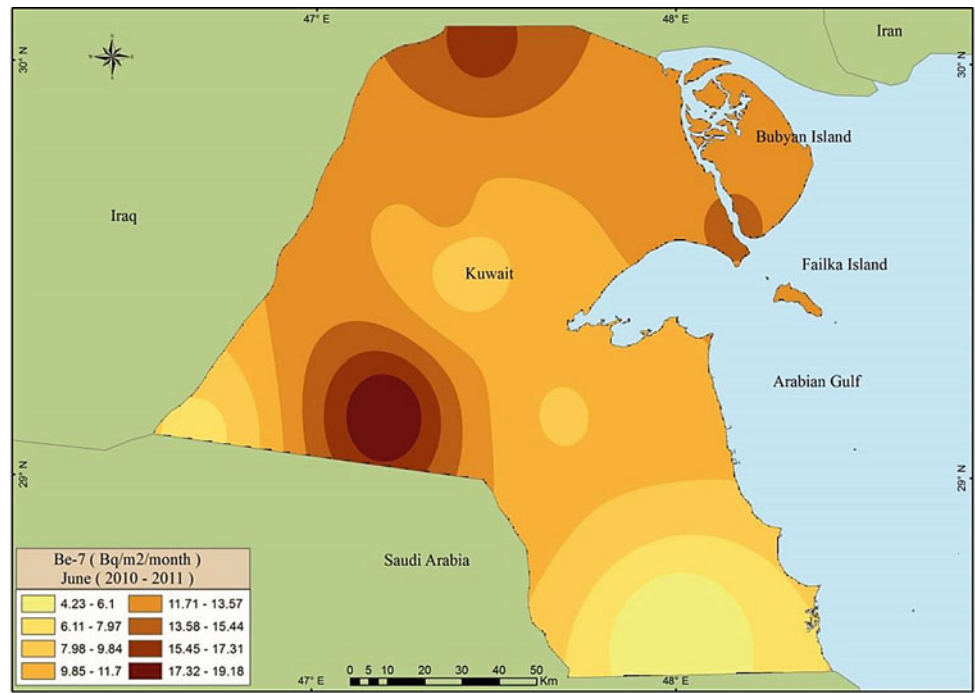


Fig. 6.9 Average deposited rates of ⁷Be in June (2010–2011)



the southern and eastern areas. The predominant wind direction for this month was northwesterly, with no precipitation events (Fig. 6.9).

Areas with high radionuclide concentration	Areas with low radionuclide concentration
Abdulli Ratqah Dibdibah Subiyah Ubayriq	Liyah Wafra Farms Salmi Khiran KhurFawaris

Similar to June, the monthly ⁷Be deposited rates in Kuwait during July 2010–2011 reveal lower rates than previous months, with a range from 3.71 to 11.78 Bq m⁻². The maximum rates were in the northern eastern areas and the lowest in the southern and northeastern areas. The predominant wind direction for this month was northwesterly, with no precipitation events to impact wind from other directions (Fig. 6.10).

Areas with high radionuclide concentration	Areas with low radionuclide concentration
Salmi Shegaya Dibdibah Ubayriq Bubiyah Island	Liyah Wafra Farms Huwaymilyah Khiran KhurFawaris

Similar to June and July, the monthly ⁷Be deposited rates in Kuwait during August 2010–2011 reveal a range from

3.66 to 29.49 Bq m⁻², with a maximum in the northern areas and the lowest in the southeastern area (Fig. 6.11).

Areas with high radionuclide concentration	Areas with low radionuclide concentration
Abdulli Ratqah Roudhatain Um Niqa Huwaymilyah	Um Madafi' Wafra Farms Subiyah Salmi Atraf

Similar to the summer months, the monthly ⁷Be deposited rates in Kuwait during September 2010–2011 reveal low rates, ranging from 2.44 to 11.6 Bq m⁻², with the maximum in the northern areas and the lowest in the southern and southeastern areas (Fig. 6.12).

Areas with high radionuclide concentration	Areas with low radionuclide concentration
Abdulli Ratqah Roudhatain Dibdibah Huwaymilyah	Salmi Wafra Farms Shegaya Khiran KhurFawaris

Similar to the summer months, the monthly ⁷Be rates deposited in Kuwait during October 2009–2010 reveal a lower rate, ranging from 5.59 to 16.09 Bq m⁻², with a maximum in northeast areas, and lowest in the southern areas (Fig. 6.13).

Fig. 6.10 Average deposited rates of ⁷Be for July (2010–2011)

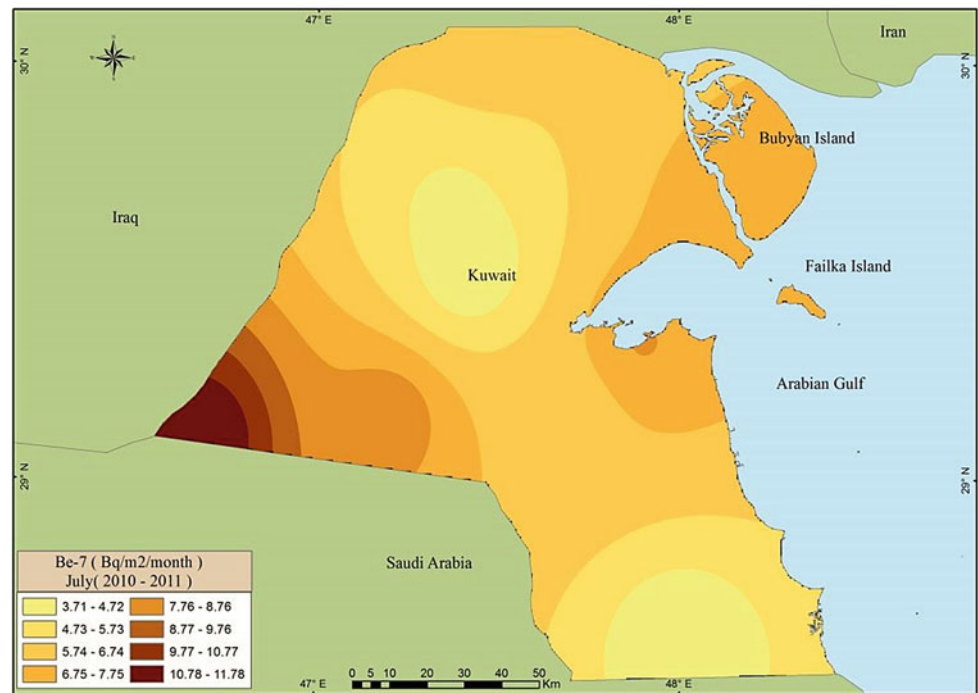
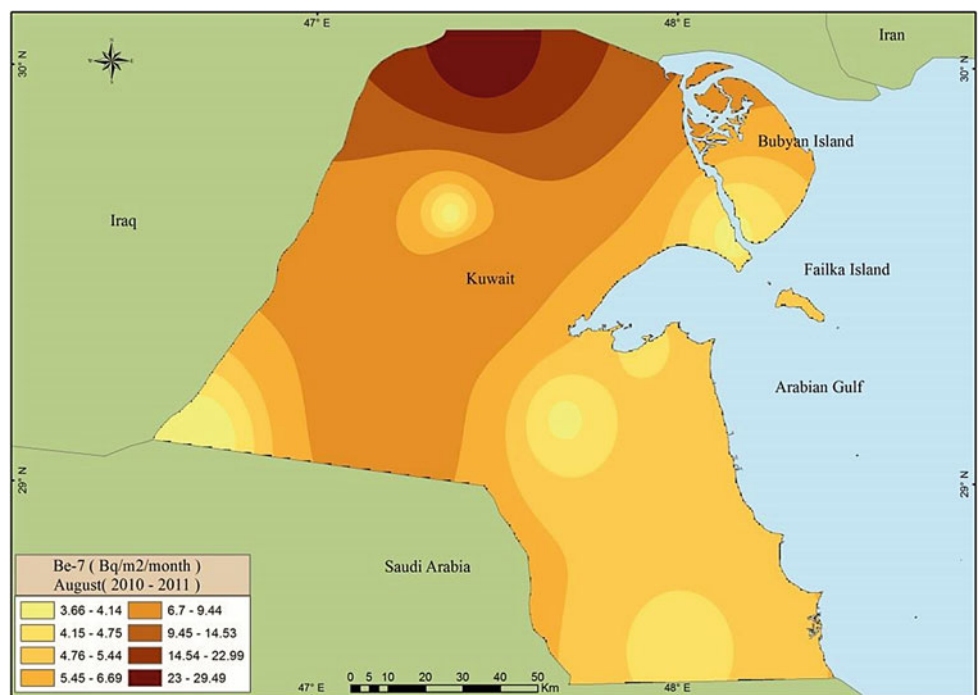


Fig. 6.11 Average deposited rates of ⁷Be in August (2010–2011)



Areas with high radionuclide concentration	Areas with low radionuclide concentration
Salmi	Liyah
Shegaya	Wafra Farms
Ubayriq	Urayfijan
Dibdibah	Khiran
Salmiya	KhurFawaris

The monthly ⁷Be deposited rates in Kuwait during November 2009–2010 reveal moderate rates that range from 4.53 to 48.04 Bq m⁻², with the maximum in the central areas and the lowest in the southern, northern, and north-western regions. The predominant wind direction was northwesterly at a minimum speed (Fig. 6.14).

Fig. 6.12 Average percentages of ⁷Be in September (2010–2011)

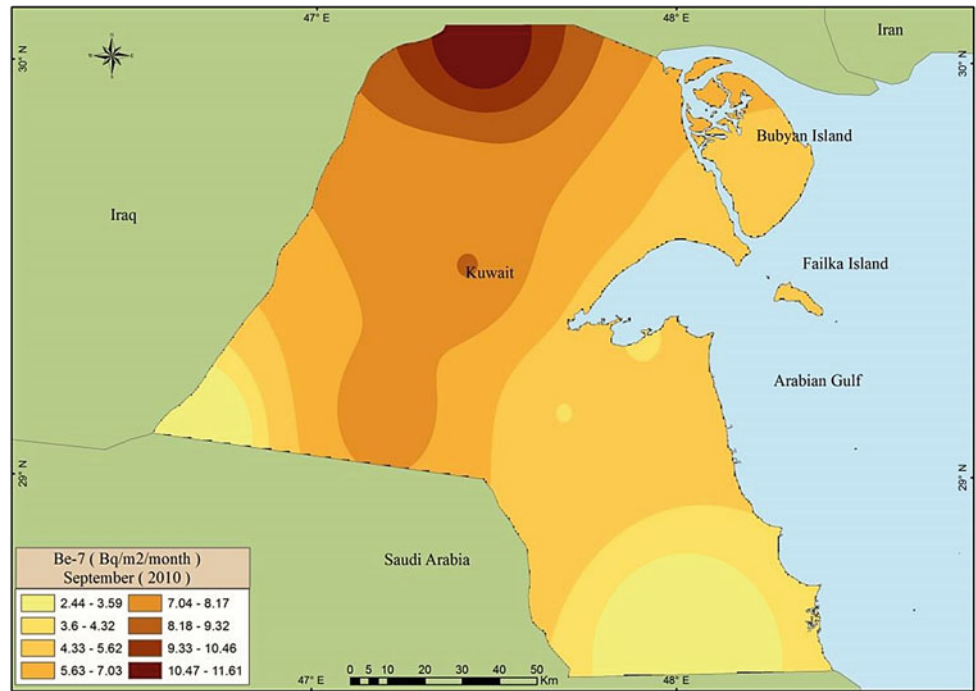
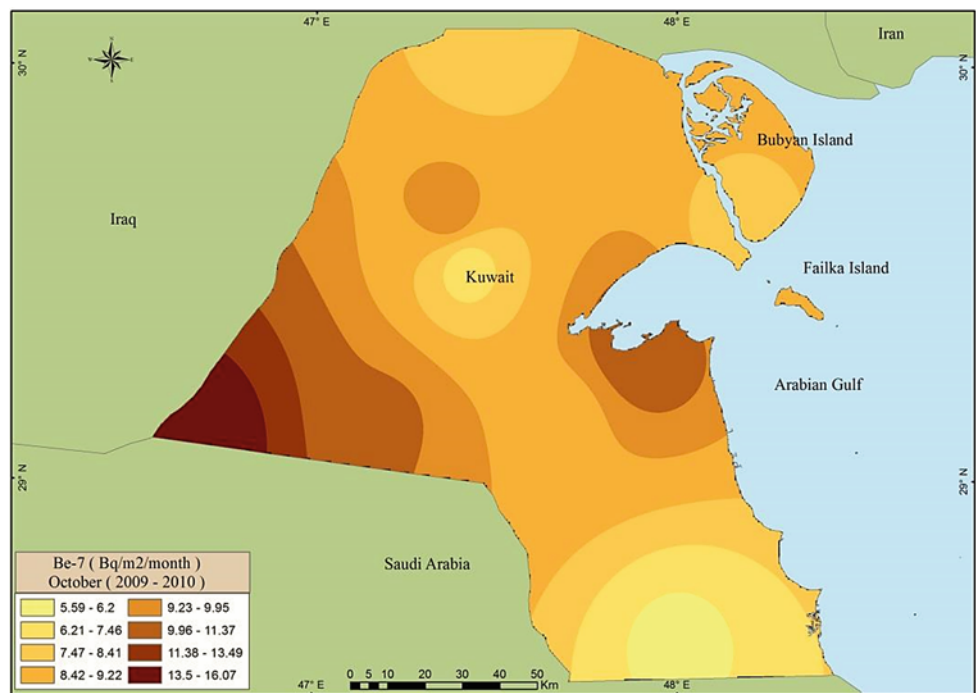


Fig. 6.13 Average deposited rates of ⁷Be in October (2009–2010)



Areas with high radionuclide concentration	Areas with low radionuclide concentration
Shegaya	Abdulli
Ubayriq	Subiyah
Dibdibah	Urayfjan
Liyah	Khiran
Atraf	KhurFawaris

The monthly ⁷Be rates deposited in Kuwait during December 2009–2010 reveal moderate rates that range from 3.69 to 46.96 Bq m⁻², with the maximum in the central and central western areas and the lowest in the central southern areas. The predominant wind direction was northwesterly at high speed (Fig. 6.15).

Fig. 6.14 Average deposited rates of ⁷Be in November (2009–2010)

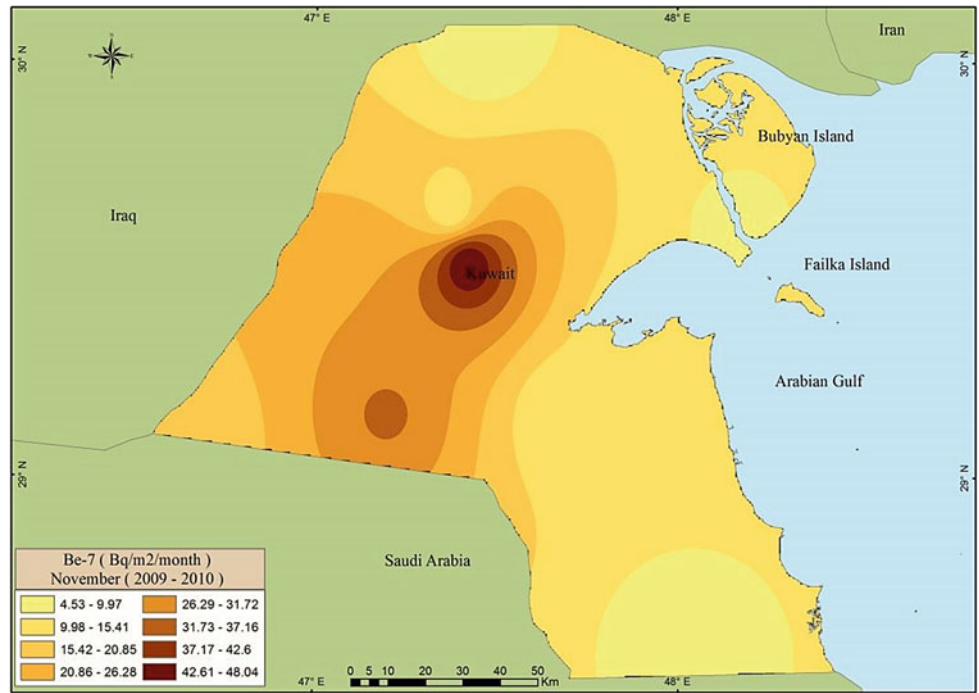
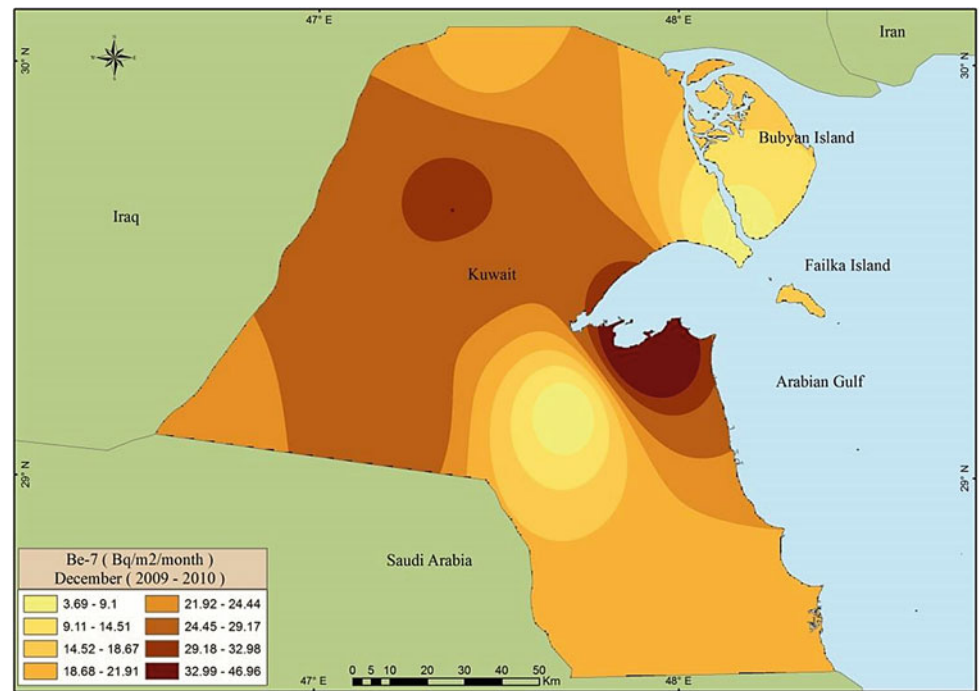


Fig. 6.15 Average deposited rates of ⁷Be in December (2009–2010)



Areas with high radionuclide concentration	Areas with low radionuclide concentration
Gudhi Ubayriq Dibdibah Liyah Salmiya	Bubiyah Island Subiyah Sulaybiyah Kabd Atraf

Monthly Deposited Rates of ¹³⁷Cs

The monthly ¹³⁷Cs rates deposited in Kuwait during January 2010–2011 reveal a range from 0.1 to 0.39 Bq m⁻², with the maximum in central and southwestern areas and the lowest in southern areas of the Wafra Farms. The predominant wind direction for this month was northwesterly, with high wind speed sometimes (Fig. 6.17).

Annual Deposited Rates of ¹³⁷Cs

The average annual ¹³⁷Cs rates deposited in Kuwait from October 2009 to August 2011 varied from 0.2 to 4.18 Bq m⁻², with an average of 4.76 Bq m⁻². The maximum rates were in southwestern areas. The ¹³⁷Cs rates deposited gradually decreased from the interior to the coastal areas, where they reached the minimum value. The predominant annual wind direction was northwesterly (Fig. 6.16).

Areas with high radionuclide concentration	Areas with low radionuclide concentration
Huwaymilyah Ubayriq Dibdibah Um Al Madafi' Ratqah	Salmi Subiyah Sulaybiyah Khiran KhurFawaris

The monthly ¹³⁷Cs deposited rates in Kuwait during February 2010–2011 varied from 0.21 to 0.54 Bq m⁻², with two high deposition rate spots. This possibly happened because of the effect of the dust storms in this month. The predominant wind direction for this month was northwesterly, and the precipitation rates were low (Fig. 6.18).

Areas with high radionuclide concentration	Areas with low radionuclide concentration
Salmi Shegaya Ubayriq Dibdibah Um Qudayr	Ratqa Sulaybiyah Bubiyah Island Subiyah Failaka Island

Areas with high radionuclide concentration	Areas with low radionuclide concentration
Salmi Shegaya	Ratqah Liyah

(continued)

Fig. 6.16 Average deposited rates of ¹³⁷Cs in (Oct 2009–Aug 2011)

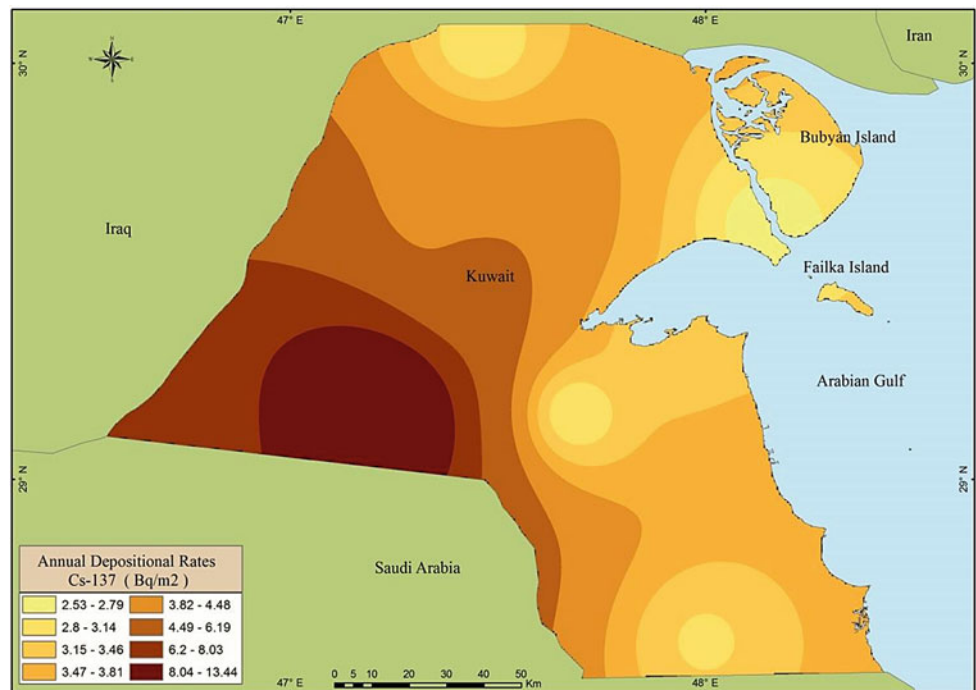


Fig. 6.17 Average deposited rates of ^{137}Cs in January (2010–2011)

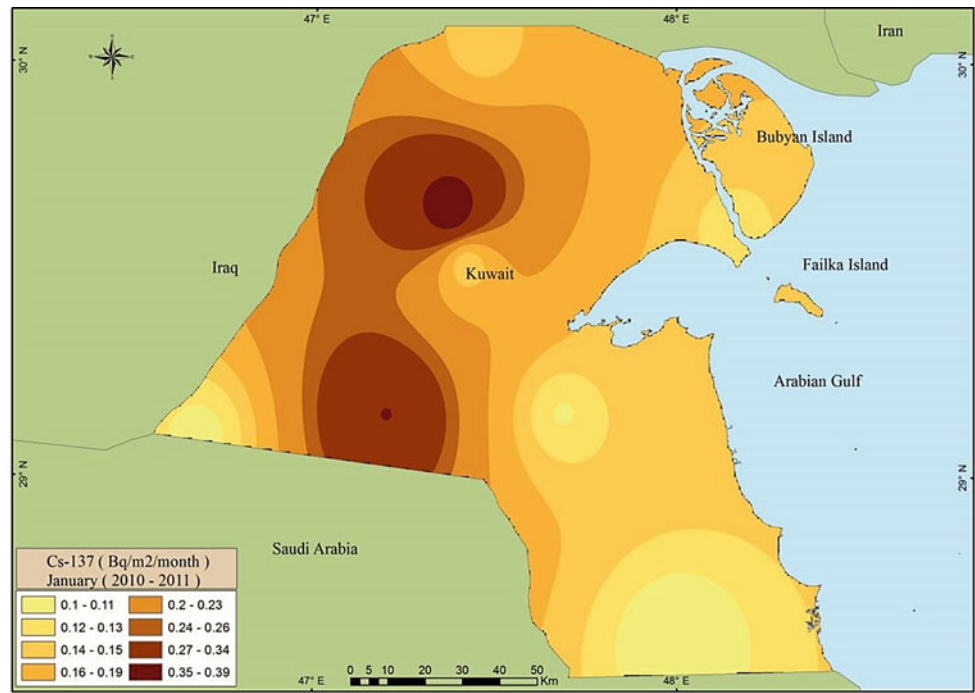


Fig. 6.18 Average deposited rates of ^{137}Cs in February (2010–2011)

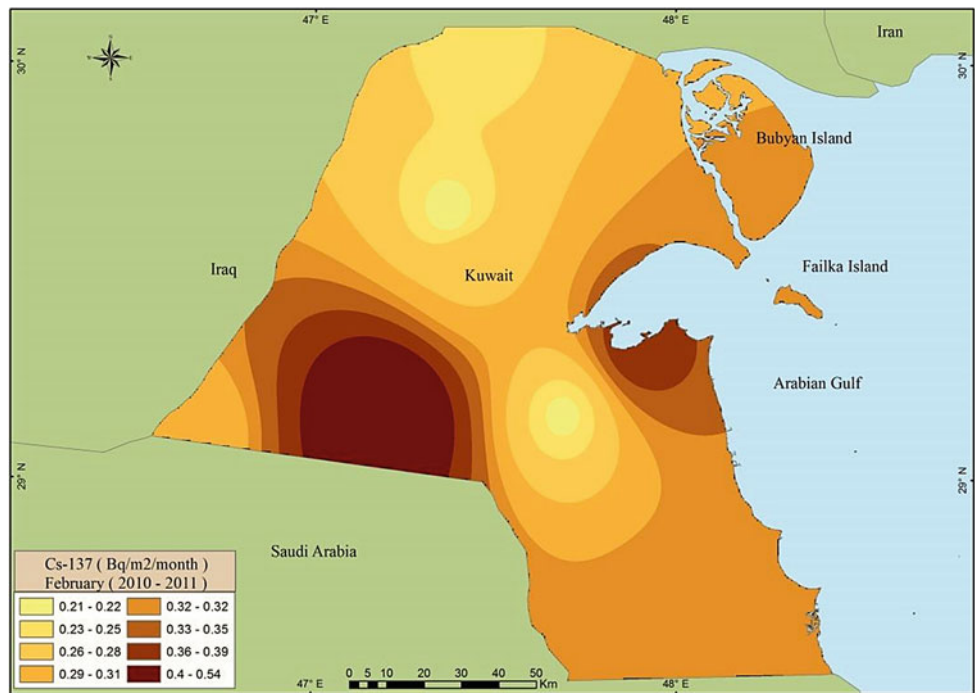
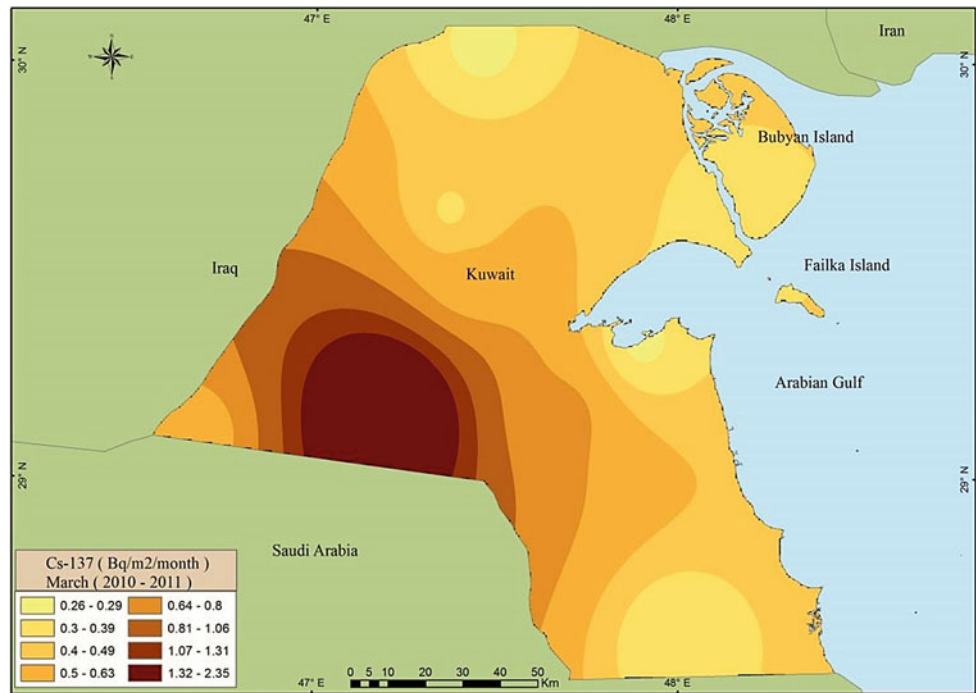


Fig. 6.19 Average deposited rates of ¹³⁷Cs in March (2010–2011)



Areas with high radionuclide concentration	Areas with low radionuclide concentration
Ubayriq Dibdibah Salmiya	Roudhatain Sulaybiyah Atraf

The monthly ¹³⁷Cs rates deposited in Kuwait during March 2010–2011 reveal a high range that varied from 0.26 to 2.35 Bq m⁻², with the maximum in the southwestern area and the lowest in the northern and southern regions. The predominant wind direction for this month was northwesterly, with high speed sometimes. However, the highest deposition flux was reported in this month due to the effect of the exotic storm that hit Kuwait, in addition to the high precipitation recorded (Fig. 6.19).

Areas with high radionuclide concentration	Areas with low radionuclide concentration
Kabd Shegaya Ubayriq Dibdibah Um Qudayr	Ratqa Subiyah Bubiyan Island Salmiya Wafra Farms

The monthly ¹³⁷Cs rates deposited in Kuwait during April 2010–2011 ranged from 0.67 to 1.4 Bq m⁻², which is considered high, but it is less than March due to lower precipitation. The predominant wind direction was northwesterly, with a high wind speed of northeasterly, easterly, and southeasterly direction (Fig. 6.20).

Areas with high radionuclide concentration	Areas with low radionuclide concentration
Shegaya Ubayriq Dibdibah Huwaymilyah Um Al Madafi'	Subiyah Bubiyan Island Sulaybiyah Kabd Jal Al Zur

The monthly ¹³⁷Cs rates deposited in Kuwait during May 2010–2011 ranged from 0.22 to 2.23 Bq m⁻², with the maximum in the southeastern and central regions. The lowest deposition fluxes were in the southern and eastern areas. However, the slightly high deposition flux in this month was due to the effect of the exotic storm that hit Kuwait on March 25, 2011 (Fig. 6.21).

Areas with high radionuclide concentration	Areas with low radionuclide concentration
Shegaya Ubayriq Dibdibah Huwaymilyah Liyah	Subiyah Bubiyan Island Salmiya Wafra Farms Shuaiba

The monthly ¹³⁷Cs deposited rates in Kuwait during June 2010–2011 display similar rates to previous months, but with lower minimum rates, the range varied from 0.06 to 1.3 Bq m⁻². The maximum rates were in southeast areas, and the lowest was in central areas. The predominant wind direction for this month was northwesterly, with no precipitation events (Fig. 6.22).

Fig. 6.20 Average deposited rates of ¹³⁷Cs in April (2010–2011)

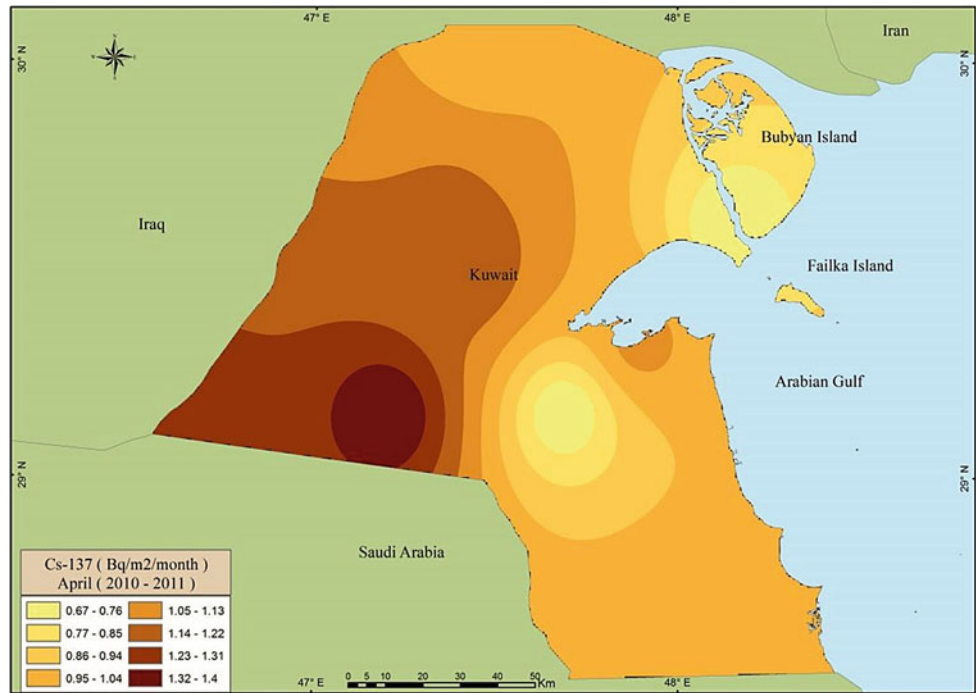
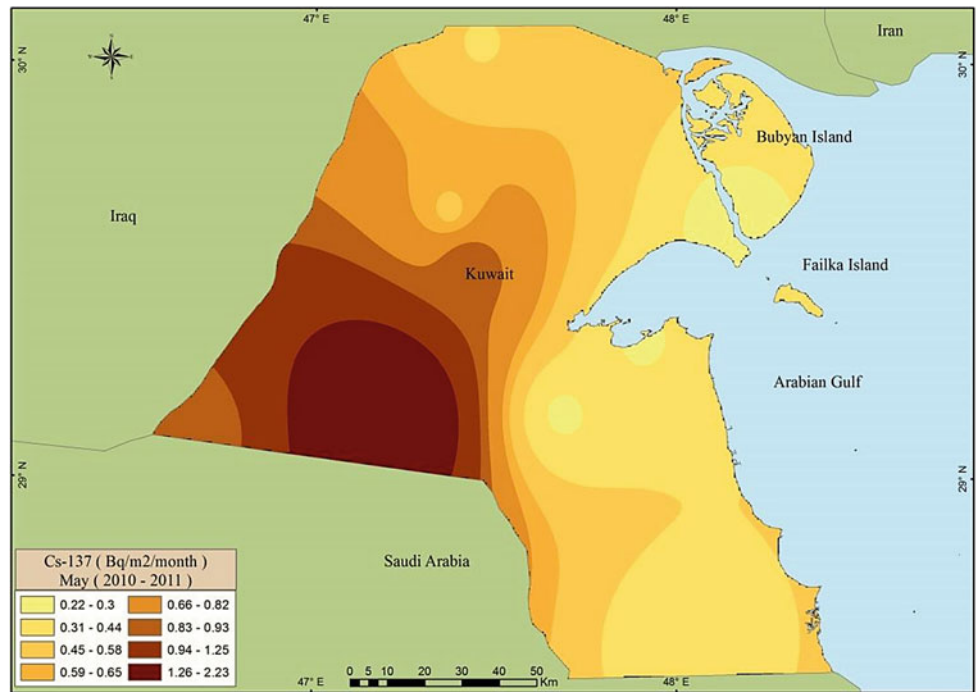


Fig. 6.21 Average deposited rates of ¹³⁷Cs in May (2010–2011)



Areas with high radionuclide concentration	Areas with low radionuclide concentration
Shegaya	Kabd
Ubayriq	Abdulli
Dibdibah	Atraf
Um Qudayr	Mutla
Liyah	Wafra Farms

The monthly ¹³⁷Cs rates deposited in Kuwait during July 2010–2011 showed similar rates to the other summer months. The range of deposition flux varied between 0.09 and 1.39 Bq m⁻². The maximum rates were in northeastern areas and the lowest in southern and northeastern areas. The predominant wind direction for this month was northwesterly, with no precipitation events that impact wind from other directions (Fig. 6.23).

Fig. 6.22 Average deposited rates of ^{137}Cs in June (2010–2011)

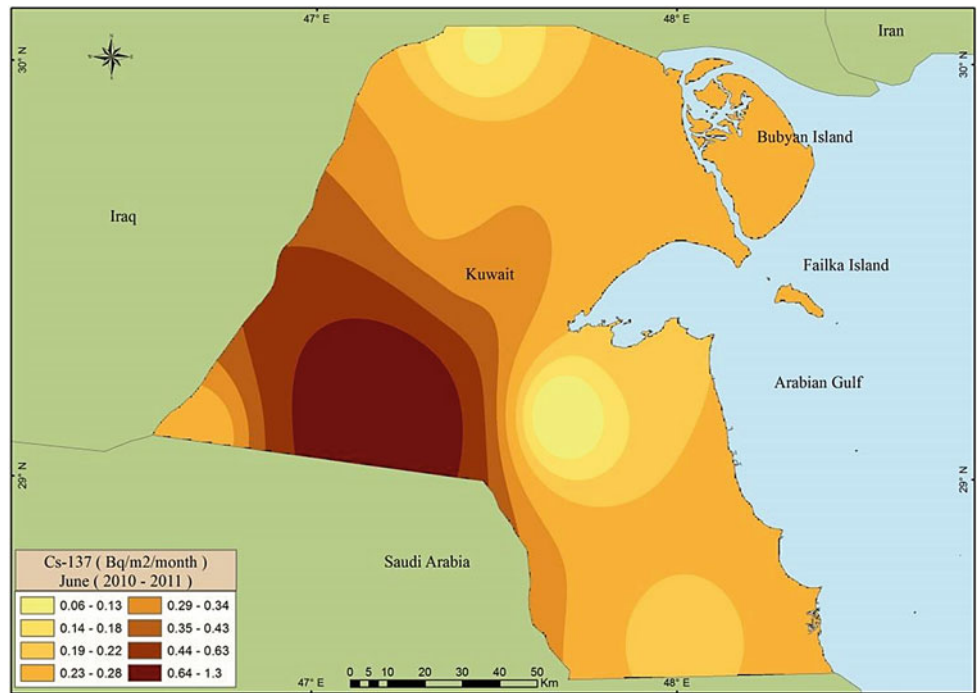


Fig. 6.23 Average deposited rates of ^{137}Cs in July (2010–2011)

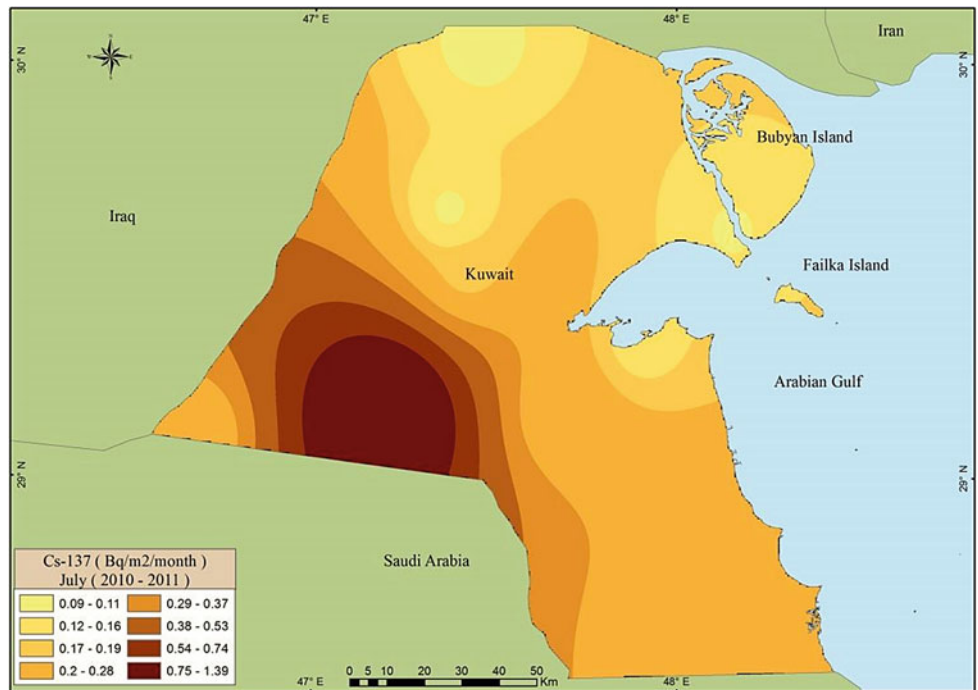
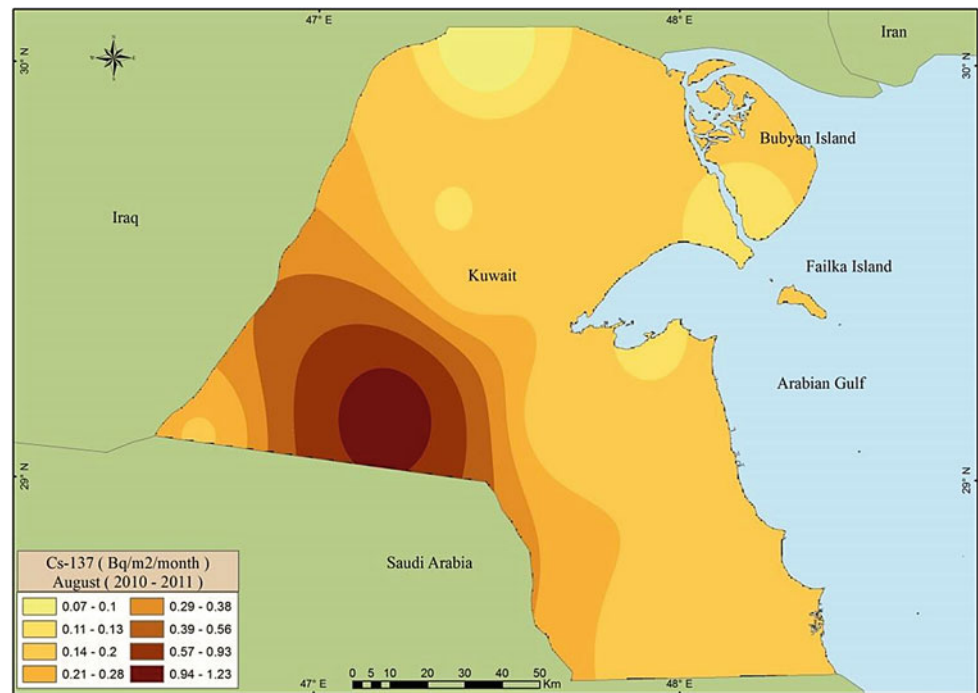


Fig. 6.24 Average deposited rates of ¹³⁷Cs in August (2010–2011)



Areas with high radionuclide concentration	Areas with low radionuclide concentration
Shegaya Ubayriq Dibdibah Um Qudayr Huwaymilyah	Abdulli Ratqah Um Al Madafi' Salmiya Bubiyah Island

The monthly ¹³⁷Cs rates deposited in Kuwait during August 2010–2011 showed similar rates in June and July, with a range that varied from 0.07 to 1.23 Bq m⁻², with the maximum in the southwestern areas and the lowest in the southern areas (Fig. 6.24).

Areas with high radionuclide concentration	Areas with low radionuclide concentration
Shegaya Ubayriq Dibdibah Um Qudayr Huwaymilyah	Abdulli Ratqah Um Al Madafi' Salmiya Bubiyah Island

Similar to the summer months, the monthly ¹³⁷Cs rates deposited in Kuwait during September 2010–2011 ranged from 0.05 to 0.87 Bq m⁻², with the maximum in southwestern areas and the lowest in northern and central areas. The predominant wind direction in this month was northwesterly, with no contribution from other directions (Fig. 6.25).

Areas with high radionuclide concentration	Areas with low radionuclide concentration
Huwaymilyah Ubayriq Dibdibah Um Qudayr Liyah	Abdulli Ratqah Um Al Madafi' Sulaybiyah Wafra Farms

Similar to the summer months, the monthly ¹³⁷Cs rates deposited in Kuwait during October 2010–2011 ranged from 0.07 to 0.72 Bq m⁻², with the maximum in southwestern areas and the lowest in northern and central eastern areas. The predominant wind direction in this month was northwesterly, with no contribution from other directions (Fig. 6.26).

Areas with high radionuclide concentration	Areas with low radionuclide concentration
Huwaymilyah Ubayriq Dibdibah Um Qudayr Salmi	Um Al Madafi' Sulaybiyah Wafra Farms Salmiya Bubiyah Island

The monthly ¹³⁷Cs rates deposited in Kuwait during November 2009–2010 showed moderate rates ranging from 0.06 to 1.54 Bq m⁻², with the maximum in the central and eastern areas and the lowest in southern areas. The predominant wind direction was northwesterly with minimum speed (Fig. 6.27).

Fig. 6.25 Average deposited rates of ¹³⁷Cs in September (2010)

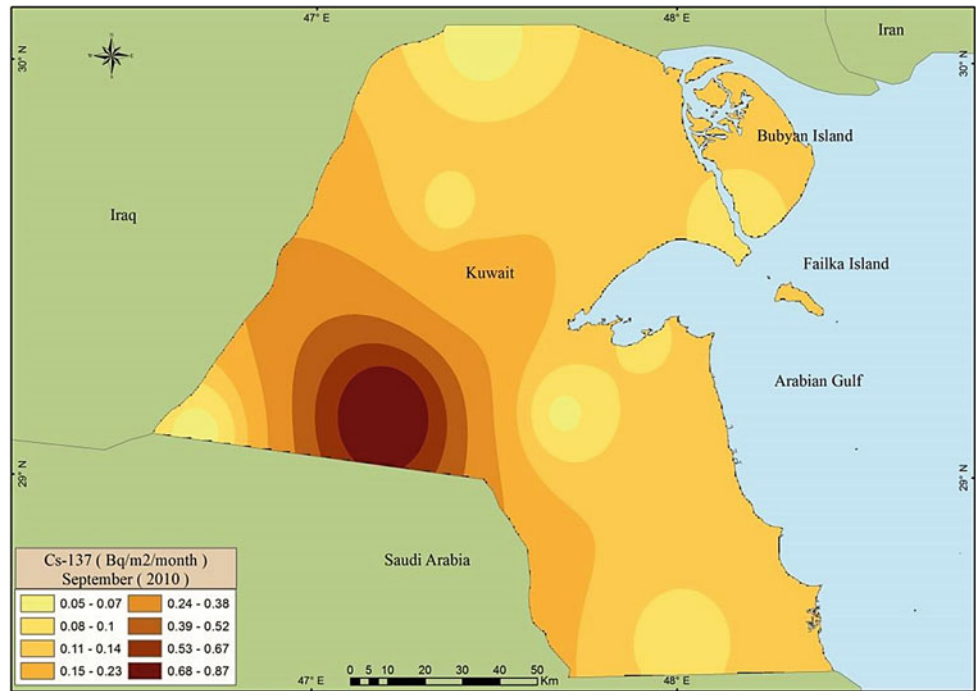
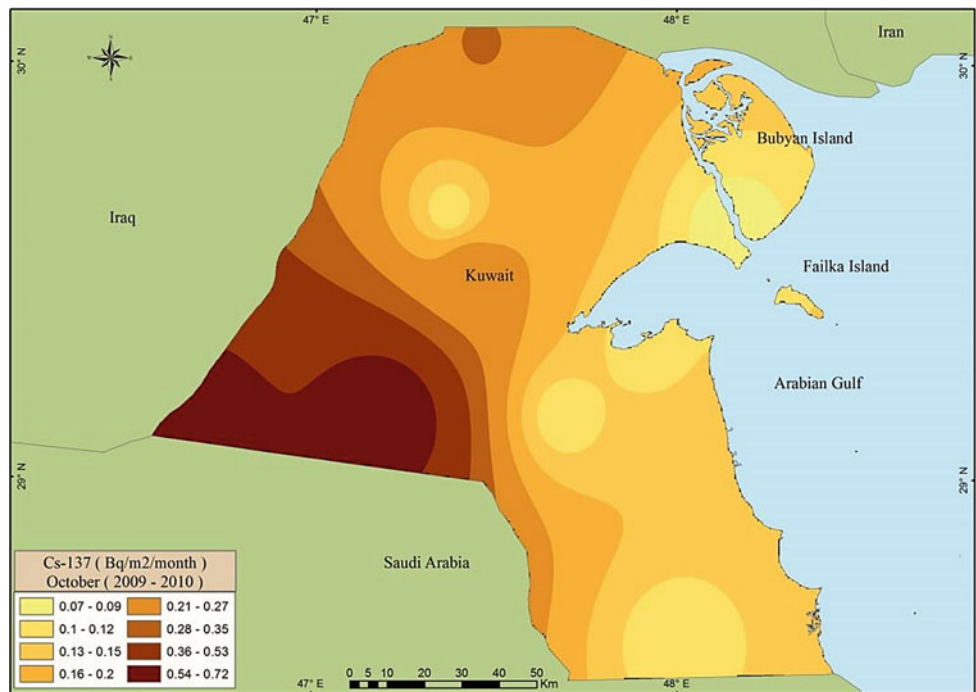


Fig. 6.26 Average deposited rates of ¹³⁷Cs in October (2009–2010)



Areas with high radionuclide concentration	Areas with low radionuclide concentration
Huwaymilyah	Ratqah
Ubayriq	Sulaybiyah
Dibdibah	Wafra Farms
Shegaya	Salmiya
Salmi	Bubiyan Island

The monthly ¹³⁷Cs rates deposited in Kuwait during December 2009–2010 reveals lower rates than during summer. The deposition rates varied from 0.04 to 0.17 Bq m⁻², with the maximum value observed along the transect from the central to southwestern areas. The predominant wind direction was northwesterly, with high speed at times (Fig. 6.28).

Fig. 6.27 Average deposited rates of ¹³⁷Cs in November (2009–2010)

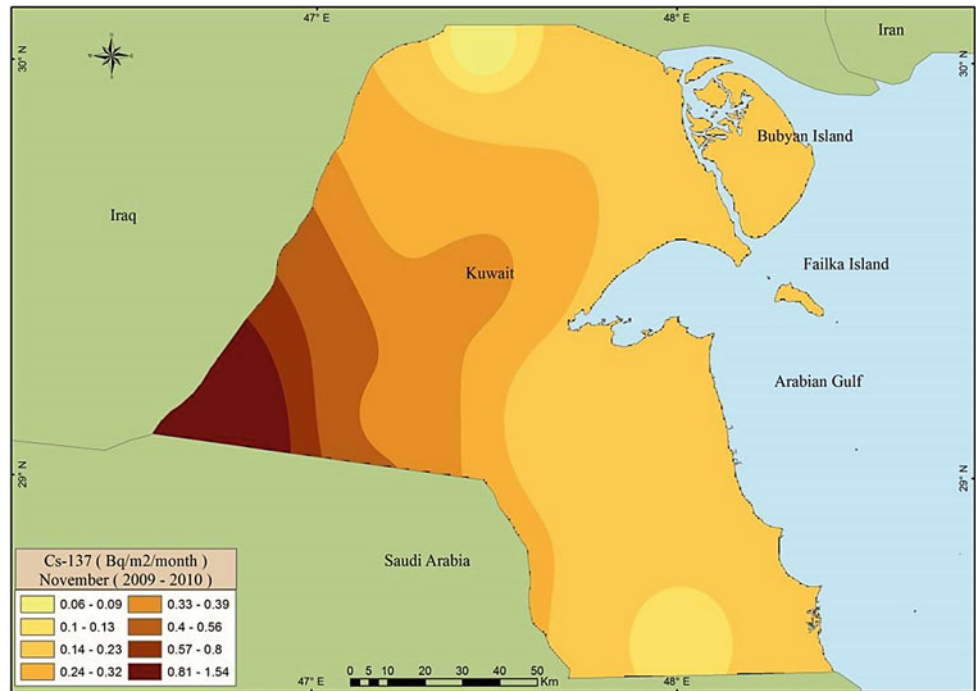
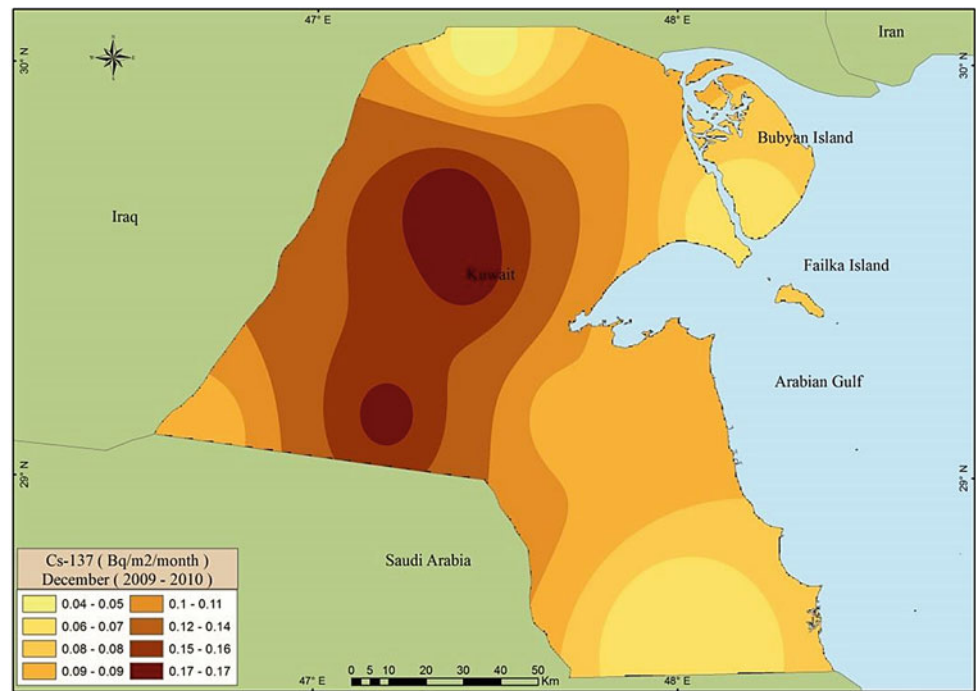


Fig. 6.28 Average deposited rates of ¹³⁷Cs in December (2009–2010)

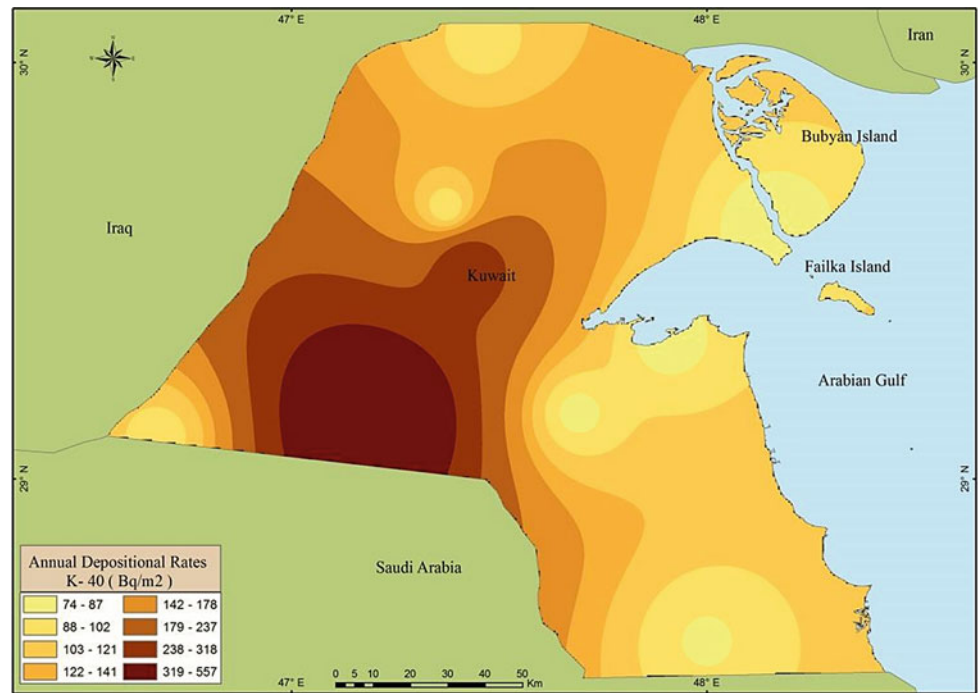


Areas with high radionuclide concentration	Areas with low radionuclide concentration
Huwaymilyah	Abdulli
Ubayriq	Subiyah
Dibdibah	KhurFawaris
Um Al Madafi'	Khiran
Liyah	Wafra Farms

Annual Deposited Rates of ⁴⁰K

The average annual ⁴⁰K deposited rates in Kuwait from October 2009 to August 2011 varied from 74 to 557 Bq m⁻², with an average of about 160 Bq m⁻². The maximum rates were found in the southwestern areas. The ⁴⁰K

Fig. 6.29 Average deposited rates of ⁴⁰K in (Oct 2009–Aug 2011)



deposited rates gradually decreased from the interior to the coastal areas, where it reached the minimum. The predominant annual wind direction was northwesterly (Fig. 6.29).

Areas with high radionuclide concentration	Areas with low radionuclide concentration
Huwaymilyah Ubayriq Dibdibah Um Eish Liyah	Abdulli Subiyah Atraf Salmiya Wafra Farms

Monthly Deposited Rates of ⁴⁰K

The monthly ⁴⁰K deposited rates in Kuwait during January 2010–2011 ranged from 1.14 to 15.62 Bq m⁻², with the maximum in southeastern and western areas, and the lowest was in the central areas. The predominant wind direction for this month was northwesterly, with high wind speed at times (Fig. 6.30).

Areas with high radionuclide concentration	Areas with low radionuclide concentration
Huwaymilyah Ubayriq Dibdibah Salmi Wafra Farms	Abdulli Subiyah Liyah Salmiya Sulaybiyah

The monthly ⁴⁰K rates deposited in Kuwait during February 2010–2011 varied from 3.13 to 23.0 Bq m⁻², with

a high deposition rate noted in southeastern areas. This possibly happened because of dust storms that occurred in this month. The predominant wind direction for this month was northwesterly, and the precipitation rates were low (Fig. 6.31).

Areas with high radionuclide concentration	Areas with low radionuclide concentration
Huwaymilyah Ubayriq Dibdibah Liyah Um Qudayr	Abdulli Subiyah Um Al Madafi' Salmiya Sulaybiyah

The monthly ⁴⁰K rates deposited in Kuwait during March 2010–2011 had a high range that varied from 5.19 to 96.27 Bq m⁻², with the maximum in the southwestern area and the lowest in the northern and southern areas. The predominant wind direction for this month was northwesterly, with high speed registered at times. However, the highest deposition flux was reported in this month because of the effect of the exotic storm that hit Kuwait, in addition to high precipitation (Fig. 6.32).

Areas with high radionuclide concentration	Areas with low radionuclide concentration
Huwaymilyah Ubayriq Dibdibah Liyah Um Qudayr	Abdulli Subiyah Wafra Farms Salmiya Bubiyah Island

Fig. 6.30 Average deposited rates of ^{40}K in January (2010–2011)

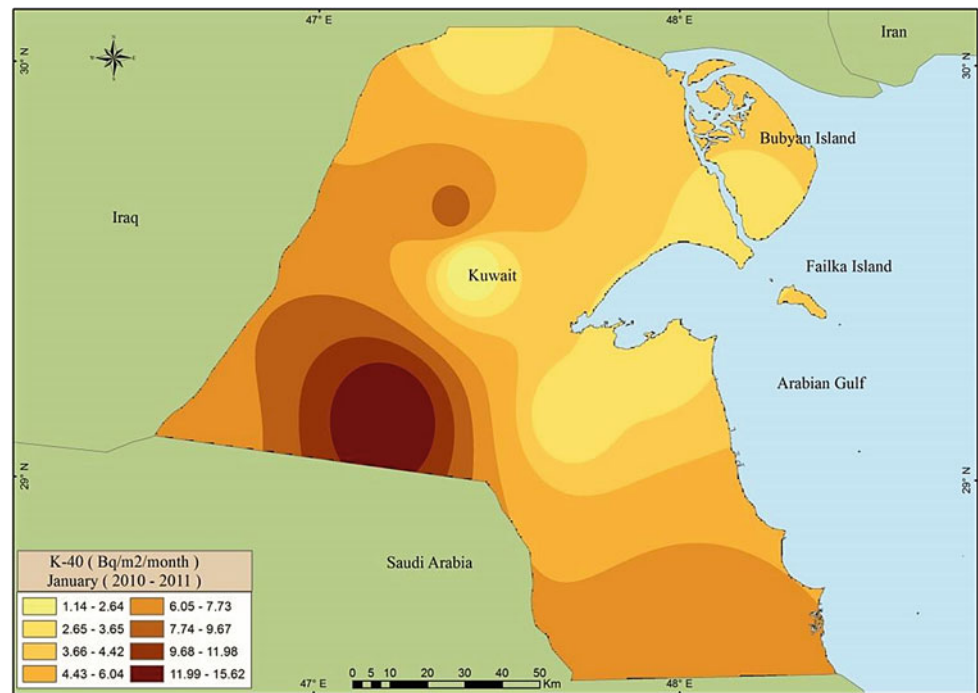
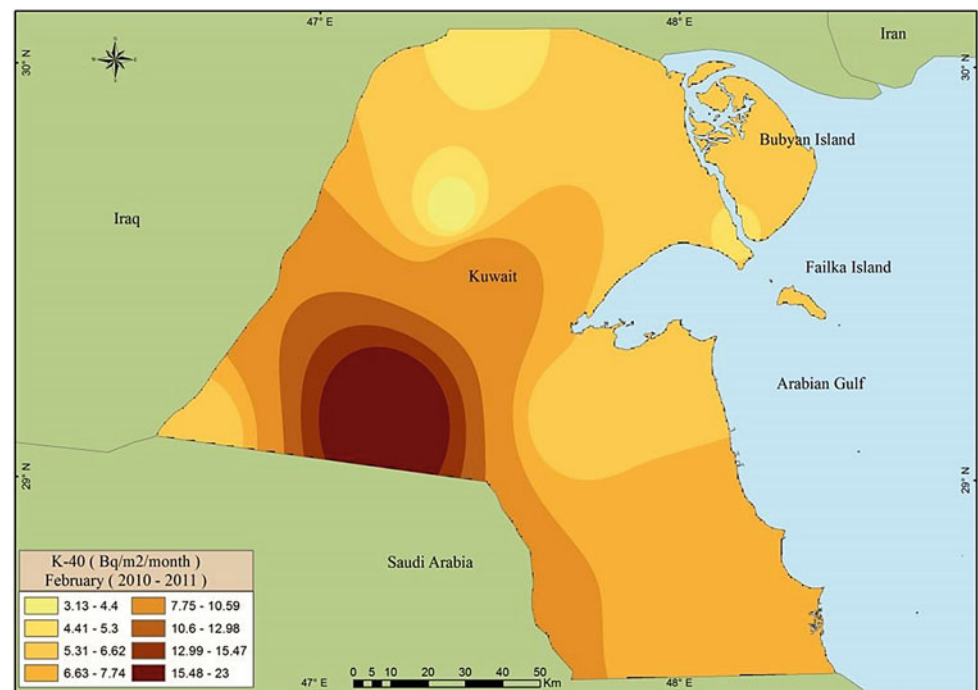


Fig. 6.31 Average deposited rates of ^{40}K in February (2010–2011)



The monthly ^{40}K rates deposited in Kuwait during April 2010–2011 ranged from 12.88 to 69.77 Bq m^{-2} , which is considered high but is lower than the rates in March due to lower precipitation rates. A spot with high deposition rates was found in the central areas. The predominant wind

direction was northwesterly, with a high wind speed of northeastern, eastern, and southeastern wind contribution. The critical dynamic weather due to Koss and Sarrayat that occurred in spring contributed toward the high deposition rates (Fig. 6.33).

Fig. 6.32 Average deposited rates of ⁴⁰K in March (2010–2011)

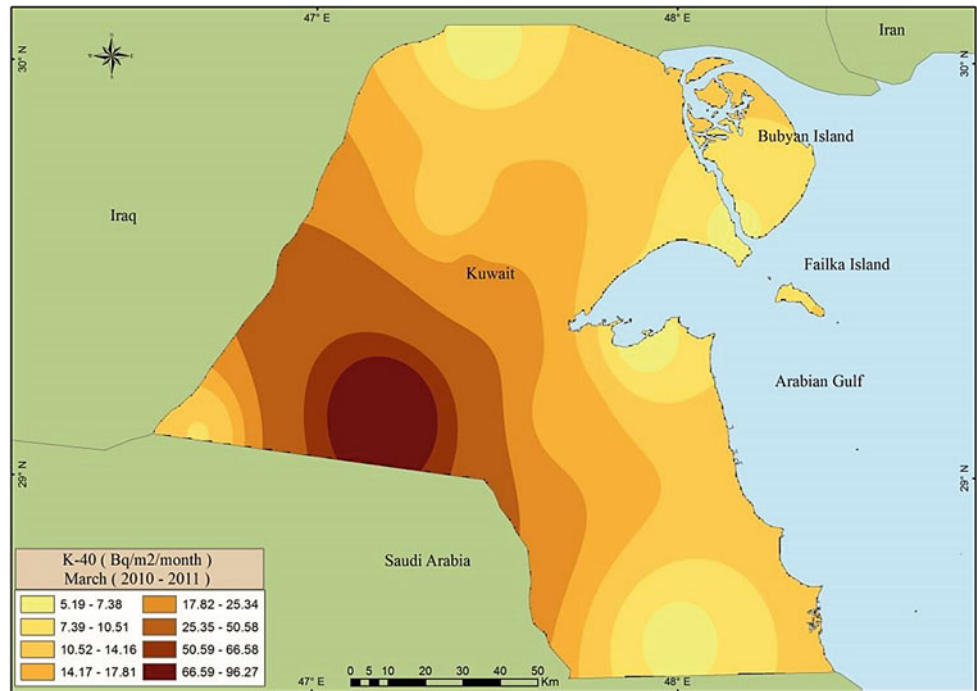
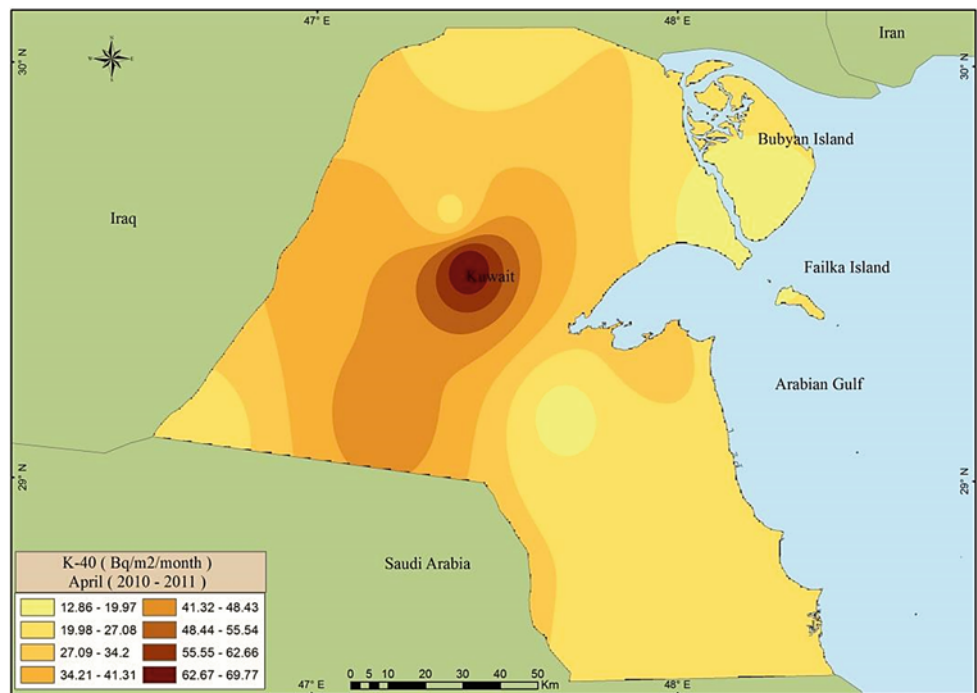


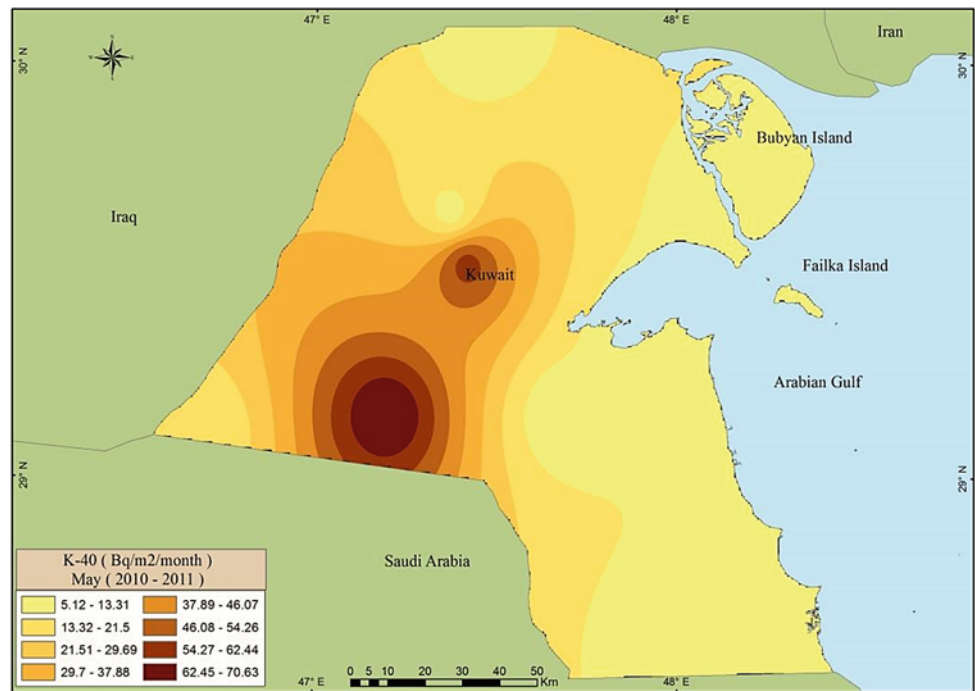
Fig. 6.33 Average deposited rates of ⁴⁰K in April (2010–2011)



Areas with high radionuclide concentration	Areas with low radionuclide concentration
Huwaymilyah	Abdulli
Ubayriq	Subiyah
Dibdibah	Wafra Farms
Liyah	Shuaiba
Gudhi	Bubiyah Island

The monthly ⁴⁰K rates deposited in Kuwait during May 2010–2011 ranged from 5.12 to 70.63 Bq m⁻², with the maximum in southeastern and central areas. This range is similar to the other spring months, in which the critical dynamics weather due to Koss and Sarrayat contributed toward high deposition rates. The lowest deposition fluxes were in southern and eastern areas. However, the high

Fig. 6.34 Average deposited rates of ⁴⁰K in May (2009–2010)



deposition flux this month was due to the effect of the exotic storm that hit Kuwait on March 25, 2011 (Fig. 6.34).

Areas with high radionuclide concentration	Areas with low radionuclide concentration
Huwaymilyah	Abdulli
Ubayriq	Jal Al Zur
Dibdibah	Wafra Farms
Liyah	Shuaiba
Kabd	Bubiyan Island

The monthly ⁴⁰K deposited rates in Kuwait during June 2010–2011 had similar rates as previous months, but with lower minimum rates, the range varied from 4.53 to 60.43 Bq m⁻². The maximum rates were in southeastern areas, and the lowest was in coastal areas. The predominant wind direction for this month was northwesterly, with no precipitation events (Fig. 6.35).

Areas with high radionuclide concentration	Areas with low radionuclide concentration
Huwaymilyah	Abdulli
Ubayriq	Salmi
Dibdibah	Salmiya
Liyah	Sulaybiyah
Um Qudayr	Kabd

The monthly ⁴⁰K rates deposited in Kuwait during July 2010–2011 were similar to the other summer months. The range of deposition varied between 2.31 and 61.76 Bq m⁻². The maximum rates were in southeastern areas, and the lowest rates were in southern and northeastern areas. The

predominant wind direction for this month was northwesterly, with no precipitation events or impact wind from other directions (Fig. 6.36).

Areas with high radionuclide concentration	Areas with low radionuclide concentration
Huwaymilyah	Abdulli
Ubayriq	Subiyah
Dibdibah	Salmiya
Liyah	Salmi
Um Qudayr	Bubiyan Island

The monthly ⁴⁰K rates deposited in Kuwait during August 2010–2011 had a similar trend to June and July, with a low range that varied from 2.23 to 27.63 Bq m⁻², with the maximum in southwestern areas. The predominant wind direction was northwesterly, with a minor contribution made by southeastern wind (Fig. 6.37).

Areas with high radionuclide concentration	Areas with low radionuclide concentration
Huwaymilyah	Abdulli
Ubayriq	Salmi
Dibdibah	Salmiya
Liyah	Sulaybiyah
Bubiyan Island	Wafra Farms

Similar to the summer months, the monthly ⁴⁰K rates deposited in Kuwait during September 2010–2011 ranged from 1.55 to 41.61 Bq m⁻², with the maximum recorded in southwestern areas and the lowest recorded in northern and central coastal areas. The predominant wind direction in this

Fig. 6.35 Average deposited rates of ^{40}K in June (2010–2011)

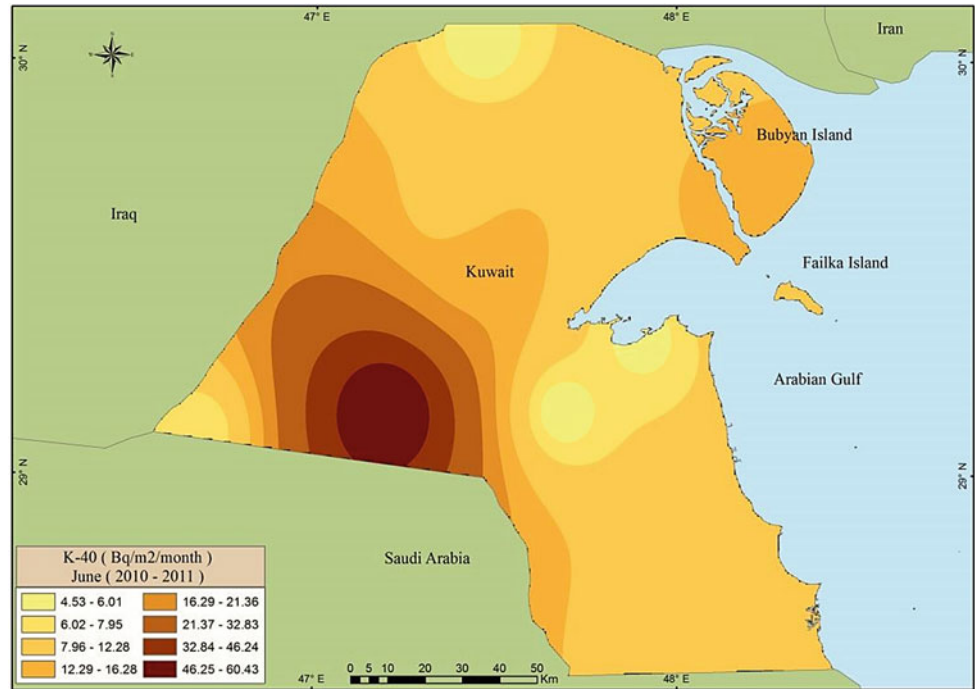


Fig. 6.36 Average deposited rates of ^{40}K in July (2010–2011)

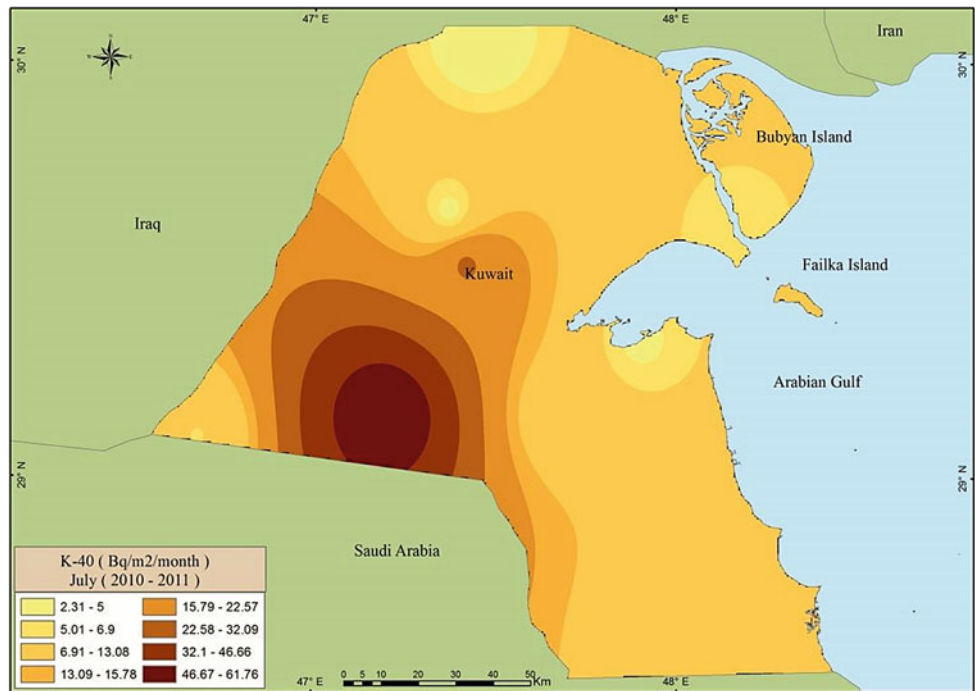
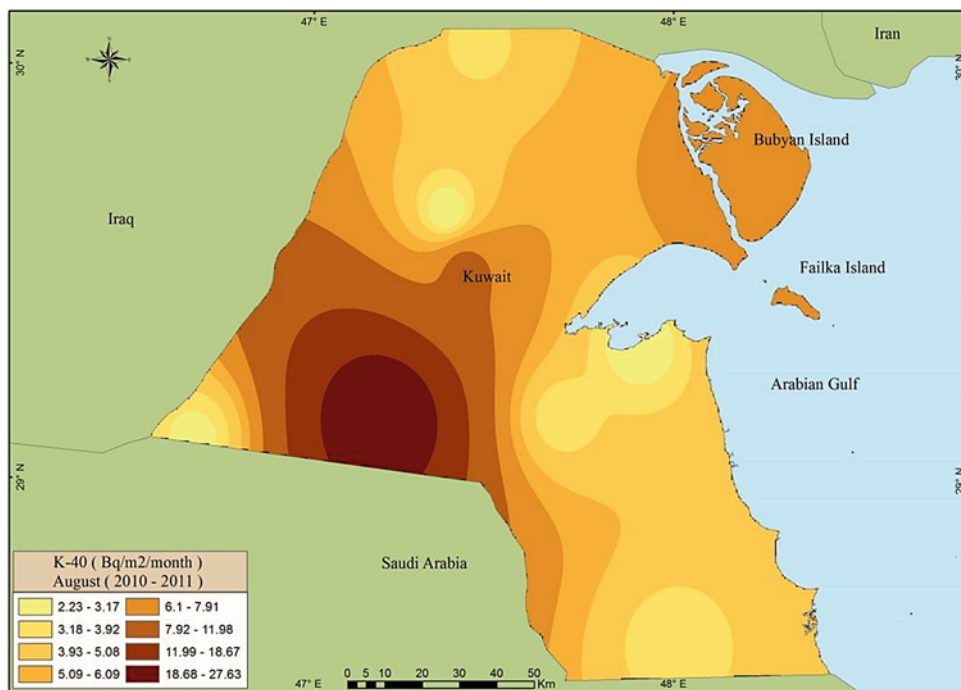


Fig. 6.37 Average deposited rates of ⁴⁰K in August (2010–2011)



month was northwesterly, with no contribution from other directions (Fig. 6.38).

Areas with high radionuclide concentration	Areas with low radionuclide concentration
Ubayriq Dibdibah Liyah Shegaya Huwaymilyah	Abdulli Salmi Salmiya Bubiyon Island Wafra Farms

Similar to summer, the monthly ⁴⁰K rates deposited in Kuwait during October 2010–2011 ranged from 1.56 to 61.32 Bq m⁻², with the maximum in southwestern areas and the lowest in northern and central eastern areas. The predominant wind direction of this month was northwesterly, with no contribution from other directions (Fig. 6.39).

Areas with high radionuclide concentration	Areas with low radionuclide concentration
Ubayriq Dibdibah Liyah Ratqah Huwaymilyah	Subiyah Salmi Salmiya Bubiyon Island Wafra Farms

The monthly ⁴⁰K rates deposited in Kuwait during November 2009–2010 were low, ranging from 1.28 to

21.28 Bq m⁻², with the maximum in the central and southwestern areas and the lowest in the southern and northern areas. The predominant wind direction was northwesterly, with high speed recorded at times (Fig. 6.40).

Areas with high radionuclide concentration	Areas with low radionuclide concentration
Ubayriq Dibdibah Liyah Shegaya Huwaymilyah	Abdulli Subiyah Salmiya Bubiyon Island Wafra Farms

The monthly ⁴⁰K rates deposited in Kuwait during December 2009–2010 were moderate and ranged from 1.91 to 31.12 Bq m⁻², with the maximum in the southwestern areas and the lowest in the southern areas. The predominant wind direction was northwesterly, with high speed at times (Fig. 6.41).

Areas with high radionuclide concentration	Areas with low radionuclide concentration
Ubayriq Dibdibah Liyah Shegaya Huwaymilyah	Abdulli Subiyah Salmi Bubiyon Island Wafra Farms

Fig. 6.38 Average deposited rates of ^{40}K in September (2010)

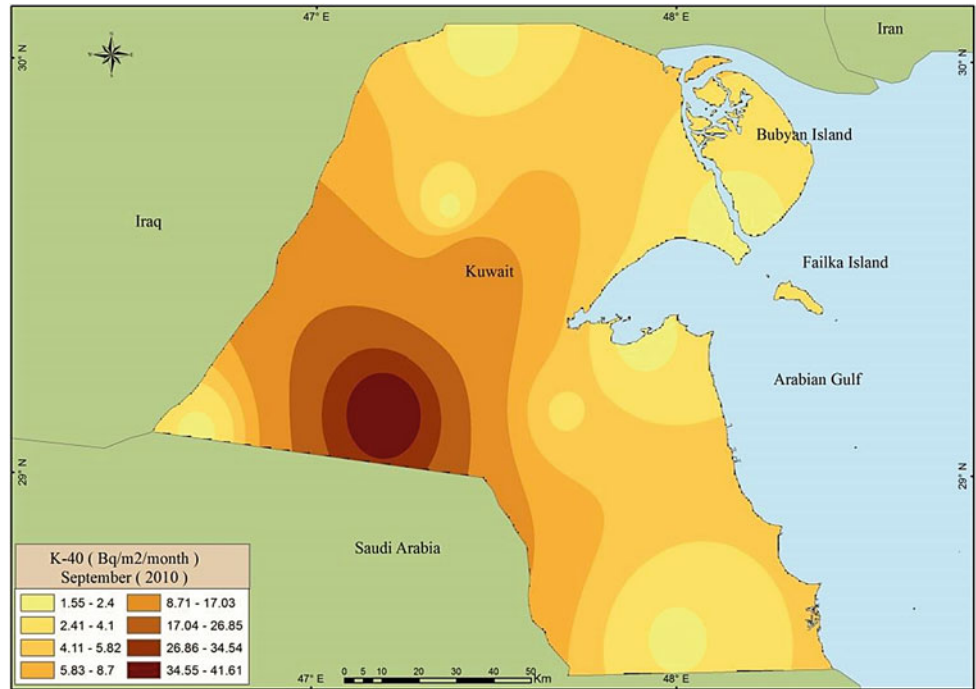


Fig. 6.39 Average deposited rates of ^{40}K in October (2009–2010)

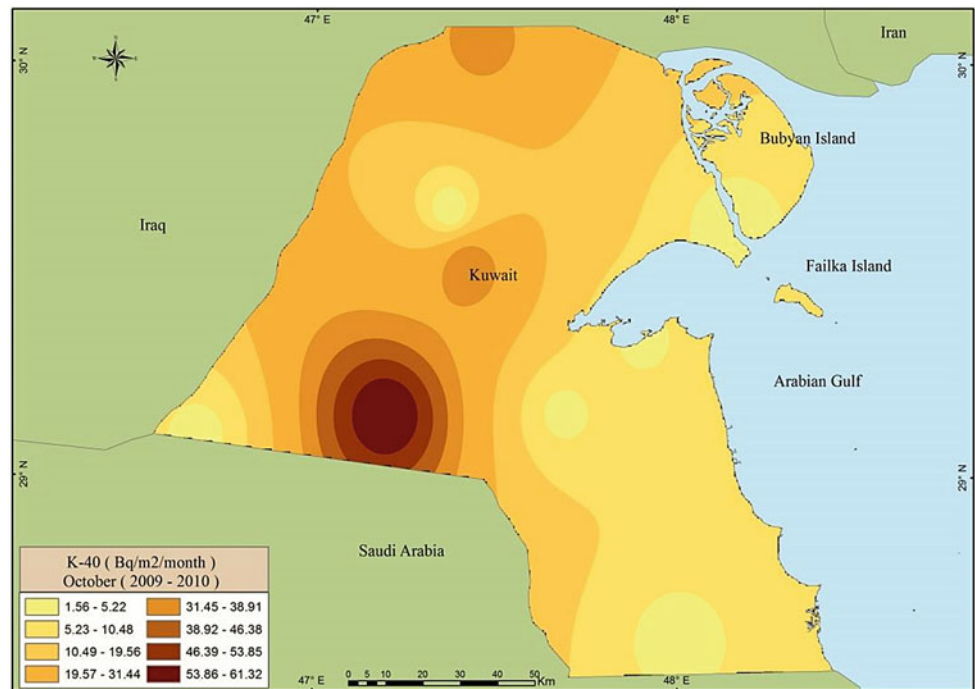


Fig. 6.40 Average deposited rates of ^{40}K in November (2009–2010)

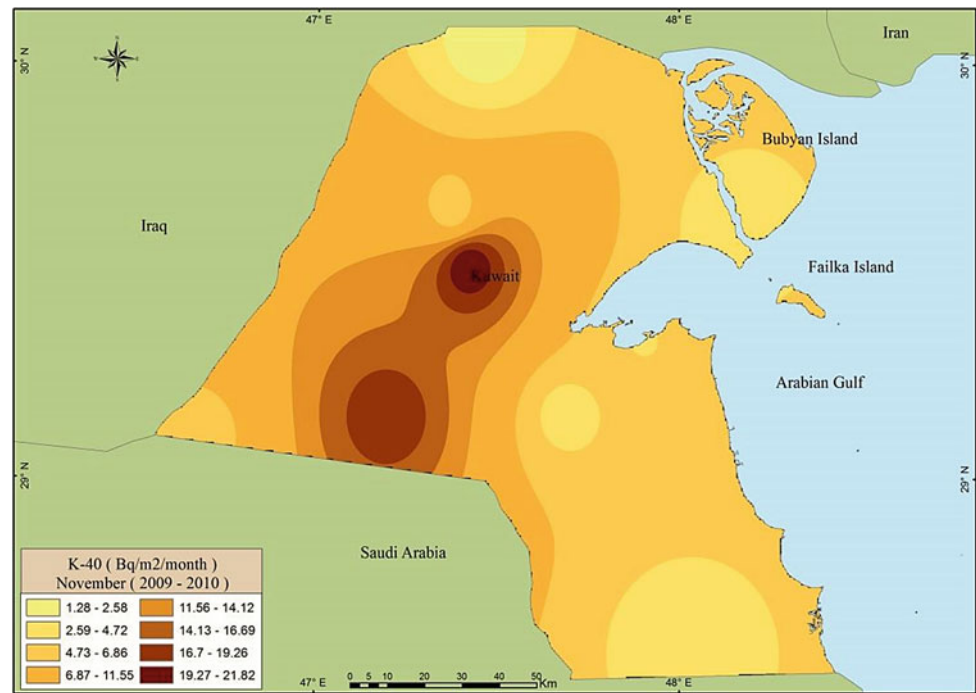
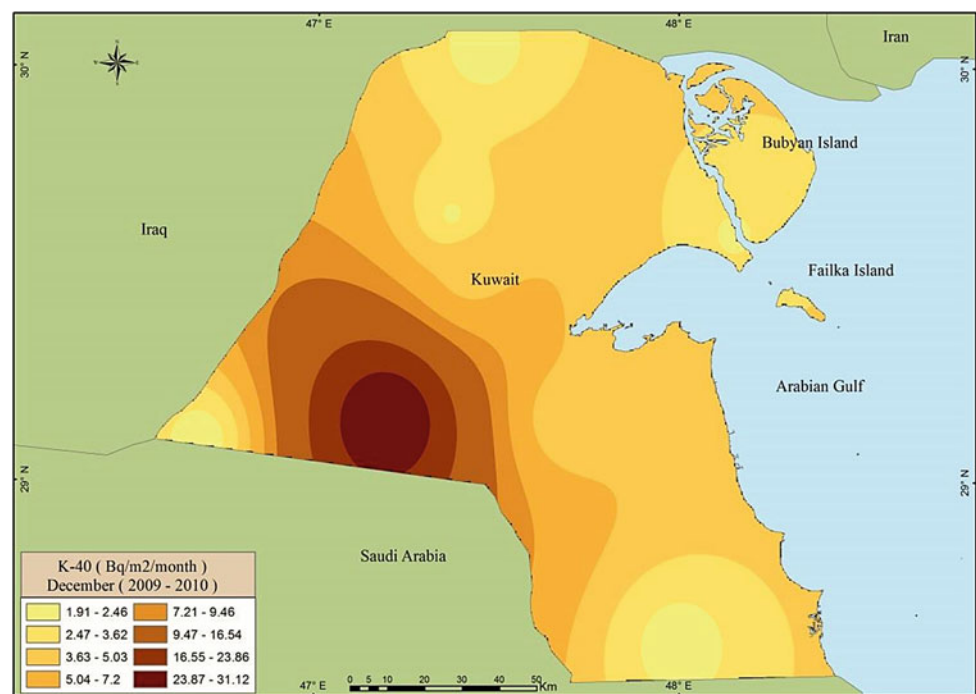


Fig. 6.41 Average deposited rates of ^{40}K in December (2009–2010)

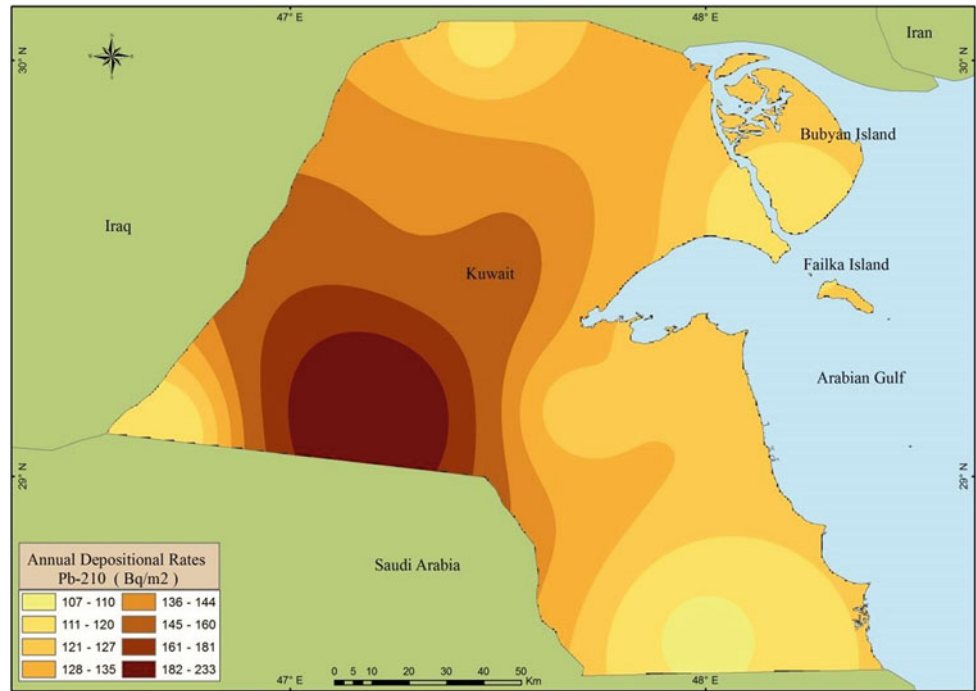


Annual Deposited Rates of ^{210}Pb

The average annual ^{210}Pb rates deposited in Kuwait from October 2009 to August 2011 varied from 107 to 233 Bq m^{-2} , with an average of about 134 Bq m^{-2} , which is close to the reported ^{210}Pb annual deposition rates on the continent between

10° and 30° N latitude (160 Bq m^{-2}). The maximum rates were in the southeastern part of the country (Shaqaaya). The minimum rates were along the coastal areas. A maximum of ^{210}Pb deposition flux was revealed in the spring months; when the precipitation was high, the predominant annual wind direction was northwesterly (Fig. 6.42).

Fig. 6.42 Average deposited rates of ²¹⁰Pb in (October 2009–August 2011)



Areas with high radionuclide concentration	Areas with low radionuclide concentration
Ubayriq Dibdibah Liyah Shegaya Huwaymilyah	Abdulli Subiyah Salmi Bubiyan Island Wafra Farms

direction for this month was northwesterly, and the precipitation rates were lower (Fig. 6.44).

Areas with high radionuclide concentration	Areas with low radionuclide concentration
Bubiyan Island Dibdibah Liyah Ratqah Subiyah	Salmi Sulaybiyah Liyah Atraf Kabd

Monthly Deposited Rates of ²¹⁰Pb

The monthly ²¹⁰Pb deposited rates in Kuwait during January 2010–2011 ranged from 4.9 to 16.73 Bq m⁻², with the maximum in central areas and the lowest in southern areas. The predominant wind direction for this month was northwesterly (Fig. 6.43).

Areas with high radionuclide concentration	Areas with low radionuclide concentration
Huwaymilyah Dibdibah Liyah Ratqah Um Al Madafi'	Salmi Sulaybiyah KhurFawaris Khiran Wafra Farms

The monthly ²¹⁰Pb rates deposited in Kuwait during February 2010–2011 ranged from 9.39 to 16.6 Bq m⁻², with three maximum spots. This is possibly visible because of the effect of dust storms this month. The predominant wind

The monthly ²¹⁰Pb deposited rates in Kuwait during February 2010–2011 ranged from 9.39 to 16.6 Bq m⁻², with three maximum spots. This is possibly visible because of the effect of dust storms this month. The predominant wind direction for this month was northwesterly, and the precipitation rates were lower (Fig. 6.45).

Areas with high radionuclide concentration	Areas with low radionuclide concentration
Huwaymilyah Dibdibah Liyah Ubayriq Um Al Madafi'	Salmi Subiyah Ratqah Salmiya Wafra Farms

The monthly ²¹⁰Pb deposited rates in Kuwait during April 2010–2011 ranged from 22.36 to 41.38 Bq m⁻². The major parameter affecting this high value was the high precipitation rate. The predominant wind direction was northwesterly,

Fig. 6.43 Average deposited rates of ^{210}Pb in January (2010–2011)

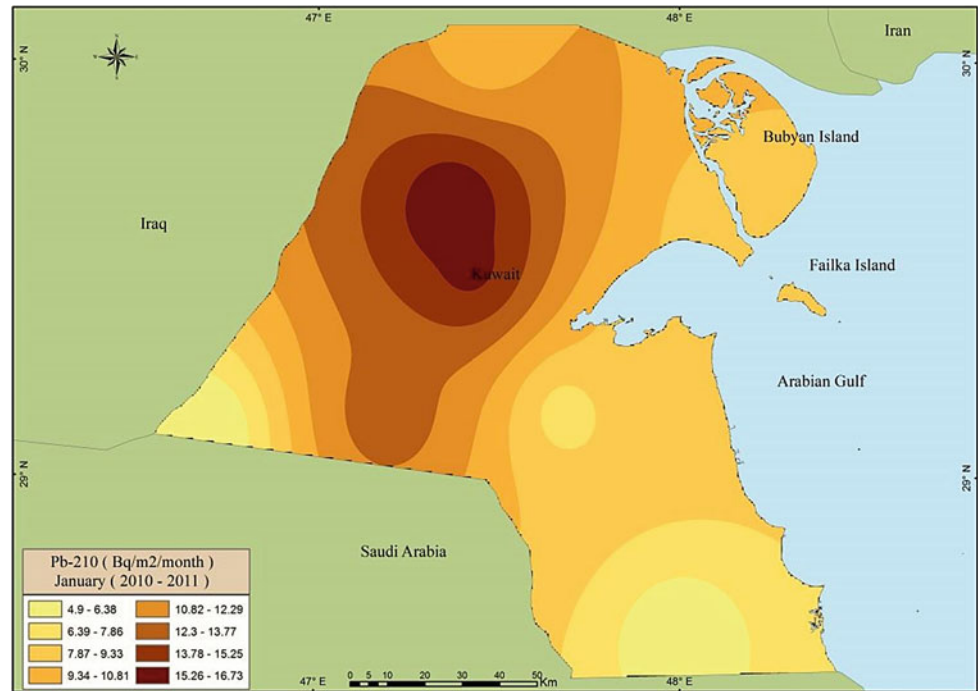


Fig. 6.44 Average deposited rates of ^{210}Pb in February (2010–2011)

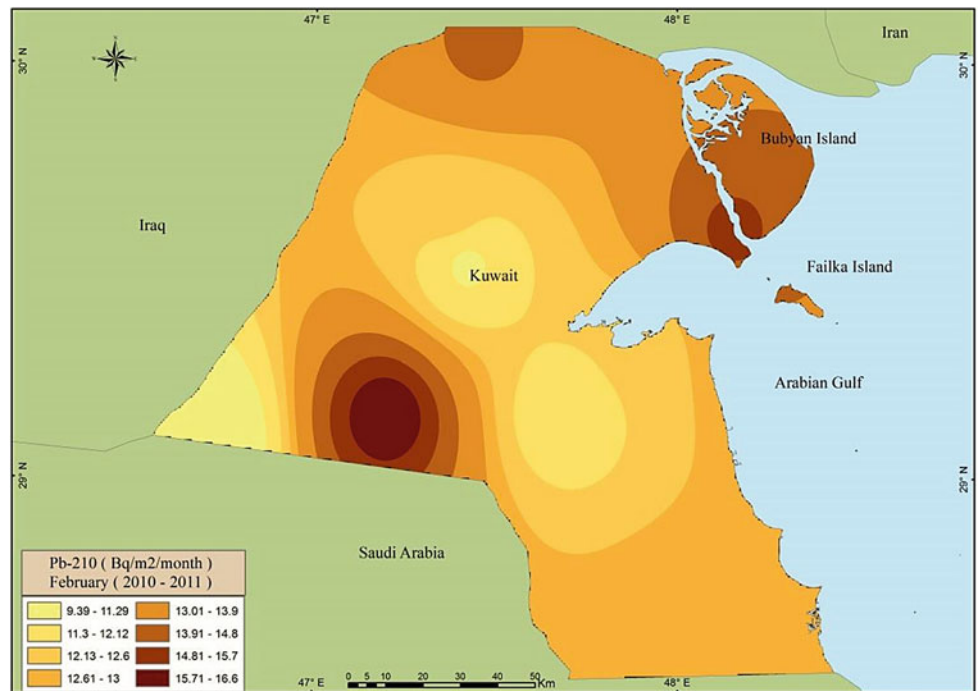
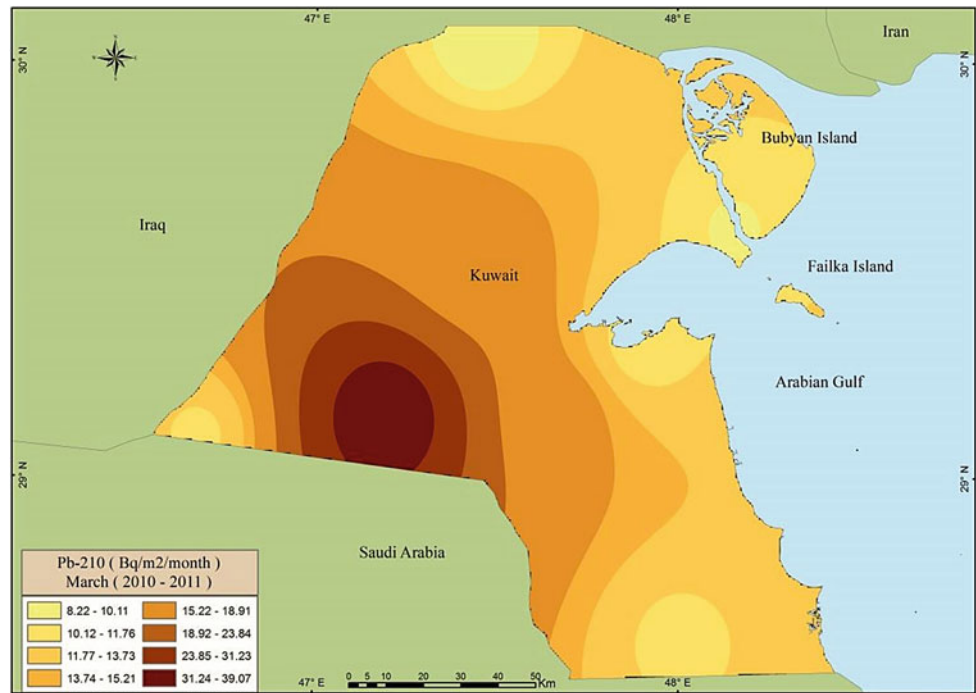


Fig. 6.45 Average deposited rates of ²¹⁰Pb in March (2010–2011)



with a high wind speed of northeastern, eastern, and south-eastern wind contribution (Fig. 6.46).

Areas with high radionuclide concentration	Areas with low radionuclide concentration
Liyah Huwaymilyah	Salmi Sulaybiyah

Areas with high radionuclide concentration	Areas with low radionuclide concentration
Dibdibah Ratqah Doha	Subiyah Kabd Bubiyan Island

(continued)

The monthly ²¹⁰Pb rates deposited in Kuwait during May 2010–2011 ranged from 8.19 to 30.44 Bq m⁻², with the

Fig. 6.46 Average deposited rates of ²¹⁰Pb in April (2010–2011)

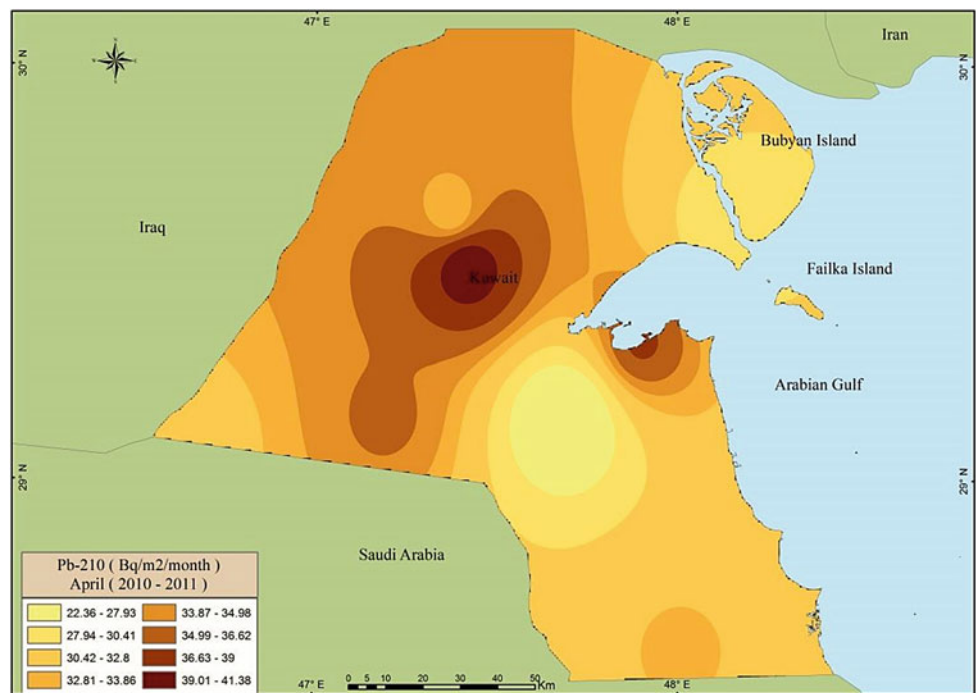
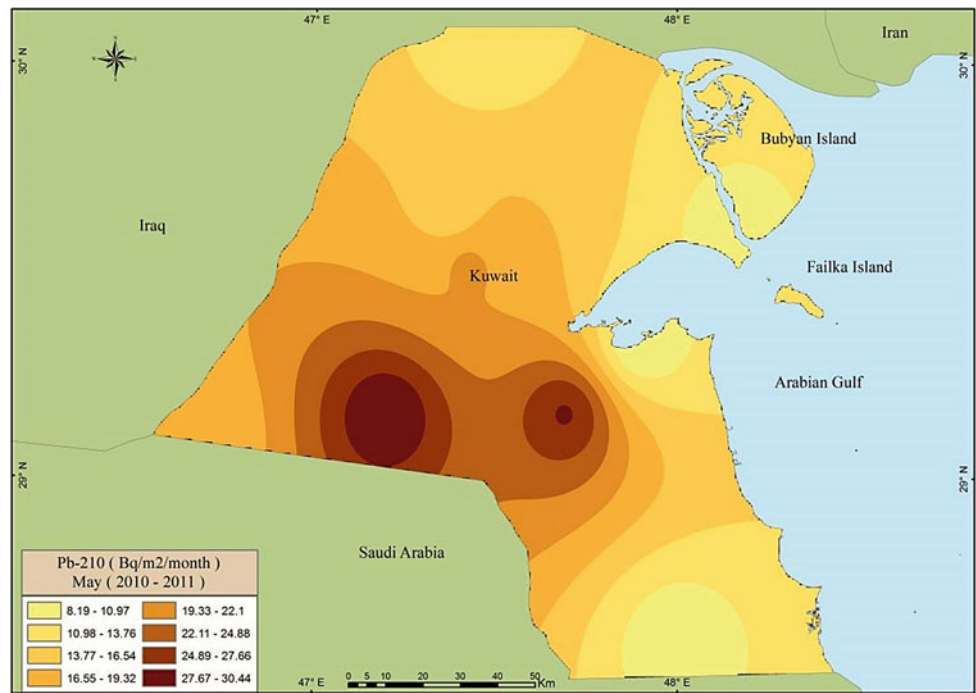


Fig. 6.47 Average deposited rates of ²¹⁰Pb in May (2010–2011)



maximum in the southeastern and central areas. The lowest deposition fluxes were in the southern and eastern areas. However, the slightly high deposition flux in this month was because of the effect of the exotic that storm hit Kuwait on March 25, 2011 (Fig. 6.47).

between 3.09 and 15.48 Bq m⁻². The maximum rates were in the northeastern areas and the lowest in the southern and northeastern areas. The predominant wind direction for this month was northwesterly, with no precipitation events or impact wind from other directions (Fig. 6.49).

Areas with high radionuclide concentration	Areas with low radionuclide concentration
Huwaymilyah Dibdibah Liyah Ubayriq Kabd	Doha Subiyah Ratqah Salmiya Wafra Farms

Areas with high radionuclide concentration	Areas with low radionuclide concentration
Huwaymilyah Dibdibah Liyah Ubayriq Kabd	Doha Subiyah Ratqah Salmiya Bubiyah Island

The monthly ²¹⁰Pb rates deposited in Kuwait during June 2010–2011 were lower compared with previous months, with a range from 4.17 to 20.2 Bq m⁻². The maximum rates were in the southeastern areas and the lowest in the central areas. The predominant wind direction for this month was northwesterly, with no precipitation events (Fig. 6.48).

The monthly ²¹⁰Pb deposited rates in Kuwait during August 2010–2011 were lower than in June and July, with a range that varied from 2.16 to 9.72 Bq m⁻², with the maximum in the northern and southwestern areas, and the lowest within the transect along the northwesterly wind corridor (Fig. 6.50).

Areas with high radionuclide concentration	Areas with low radionuclide concentration
Huwaymilyah Dibdibah Liyah Ubayriq Bubiyah Island	Doha Sulaybiyah Ratqah Salmi Wafra Farms

Areas with high radionuclide concentration	Areas with low radionuclide concentration
Huwaymilyah Dibdibah Ratqah Ubayriq Bubiyah Island	Doha Sulaybiyah Um Al Madafi' Salmi Wafra Farms

Similar to June, the monthly ²¹⁰Pb deposited rates in Kuwait during July 2010–2011 were lower when compared with previous months. The range of deposition fluxes varied

Similar to the summer months, the monthly ²¹⁰Pb deposited rates in Kuwait during September 2010–2011 had low rates that ranged from 1.8 to 10.64 Bq m⁻², with the

Fig. 6.48 Average deposited rates of ^{210}Pb in June (2010–2011)

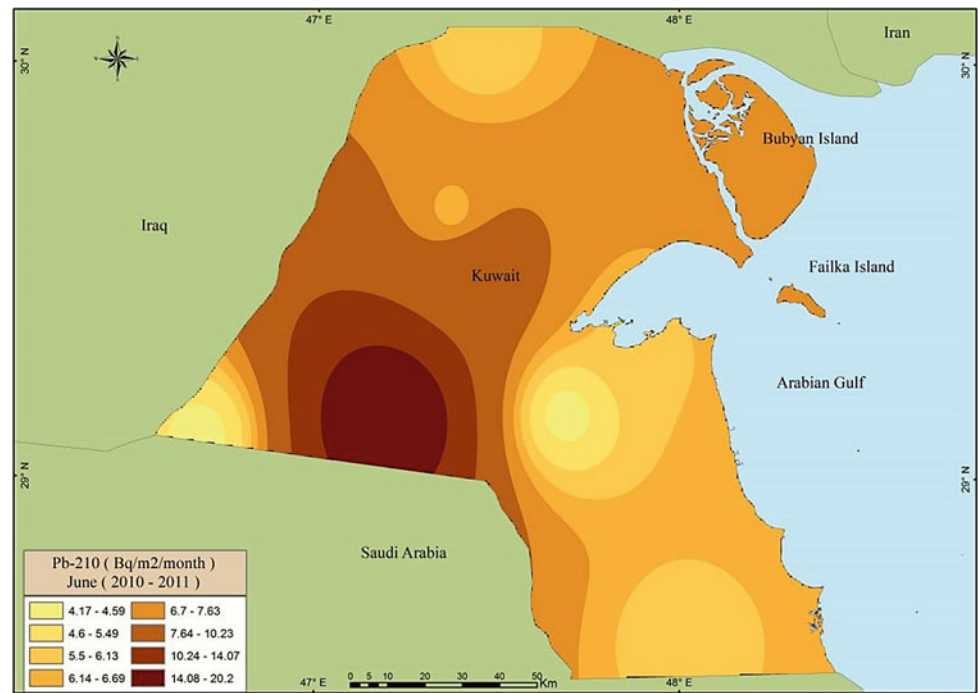


Fig. 6.49 Average deposited rates of ^{210}Pb in July (2010–2011)

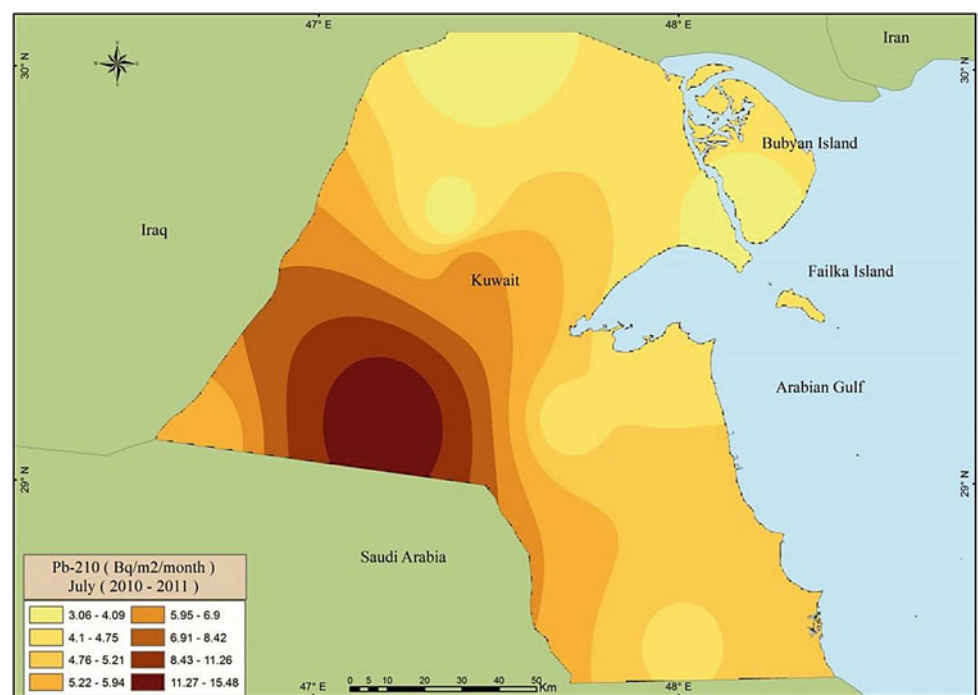
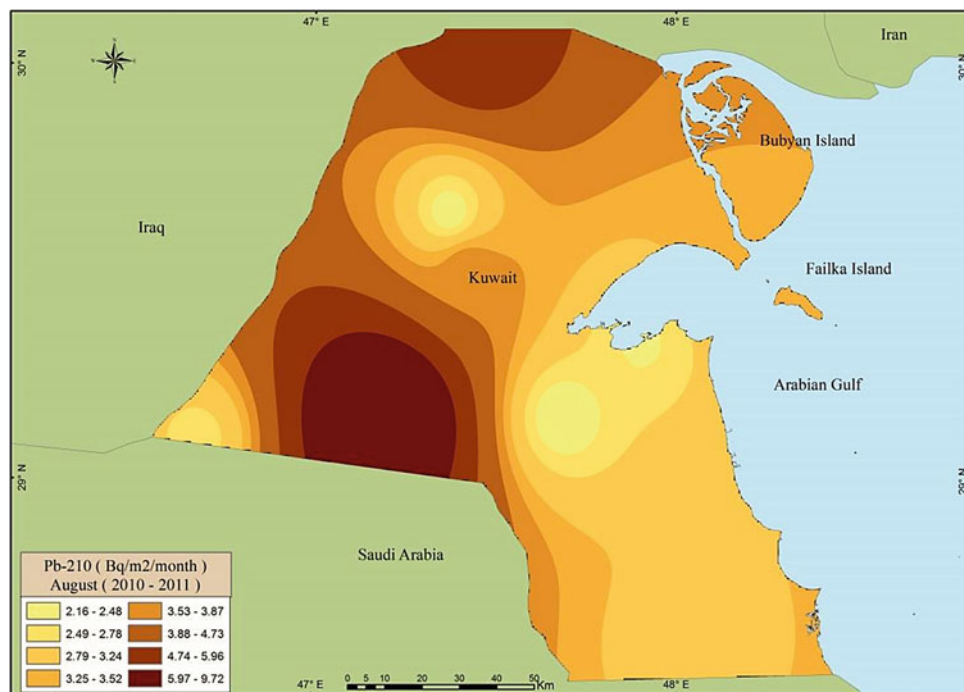


Fig. 6.50 Average deposited rates of ²¹⁰Pb in August (2010–2011)



maximum in the northwestern areas and the lowest in the southern and southwestern areas. The predominant wind direction in this month was northwesterly, with no contribution from other directions (Fig. 6.51).

Areas with high radionuclide concentration	Areas with low radionuclide concentration
Huwaymilyah Dibdibah Liyah Ubayriq Kabd	Doha Sulaybiyah Failaka Island Salmi Wafra Farms

Similar to the summer months, the monthly ²¹⁰Pb deposited rates in Kuwait during October 2009–2010 showed low rates, with a range that varied from 2.52 to 8.74 Bq m⁻², with the maximum in the southeastern and northern areas and the lowest along the northwesterly wind corridor (Fig. 6.52).

Areas with high radionuclide concentration	Areas with low radionuclide concentration
Abdulli Dibdibah Ratqah Ubayriq Shegaya	Doha Sulaybiyah Um Al Madafi' Khiran Wafra Farms

The monthly ²¹⁰Pb deposited rates in Kuwait during November 2009–2010 were moderate, ranging from 5.25 to

14.2 Bq m⁻², with the maximum in the central and south-eastern areas and the lowest in the southern areas. The predominant wind direction was northwesterly at a minimum speed (Fig. 6.53).

Areas with high radionuclide concentration	Areas with low radionuclide concentration
Huwaymilyah Dibdibah Doha Ubayriq Bubiyah Island	Abdulli Sulaybiyah Ratqah Salmi Wafra Farms

The monthly ²¹⁰Pb rates deposited in Kuwait during December 2009–2010 were similar to November. The rates varied from 4.74 to 14.06 Bq m⁻², with the maximum in the southwestern and central eastern areas. The predominant wind direction was northwesterly, with high speed at times (Fig. 6.54).

Areas with high radionuclide concentration	Areas with low radionuclide concentration
Doha Dibdibah Ratqah Ubayriq Um Al Madafi'	Ratqah Sulaybiyah Salmi Khiran Wafra Farms

Fig. 6.51 Average deposited rates of ^{210}Pb in September (2010)

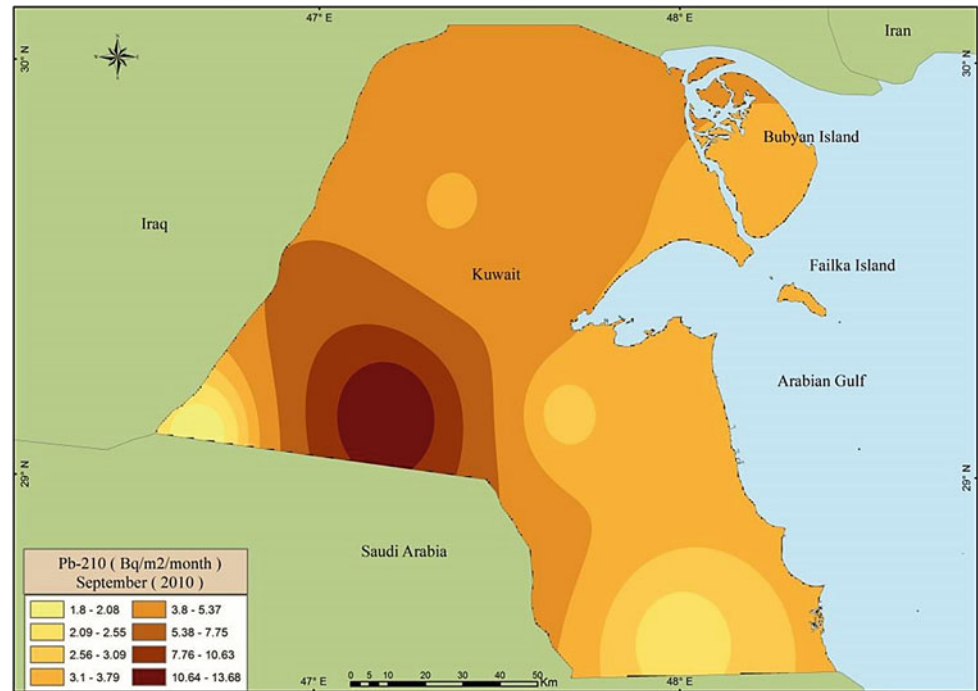


Fig. 6.52 Average deposited rates of ^{210}Pb in October (2009–2010)

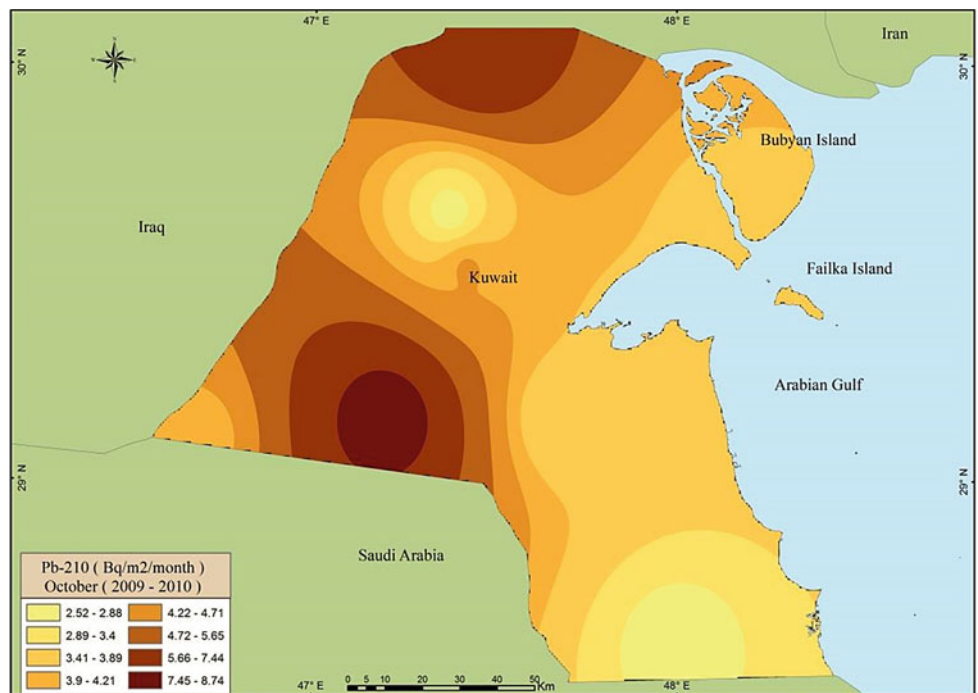


Fig. 6.53 Average deposited rates of ^{210}Pb in November (2009–2010)

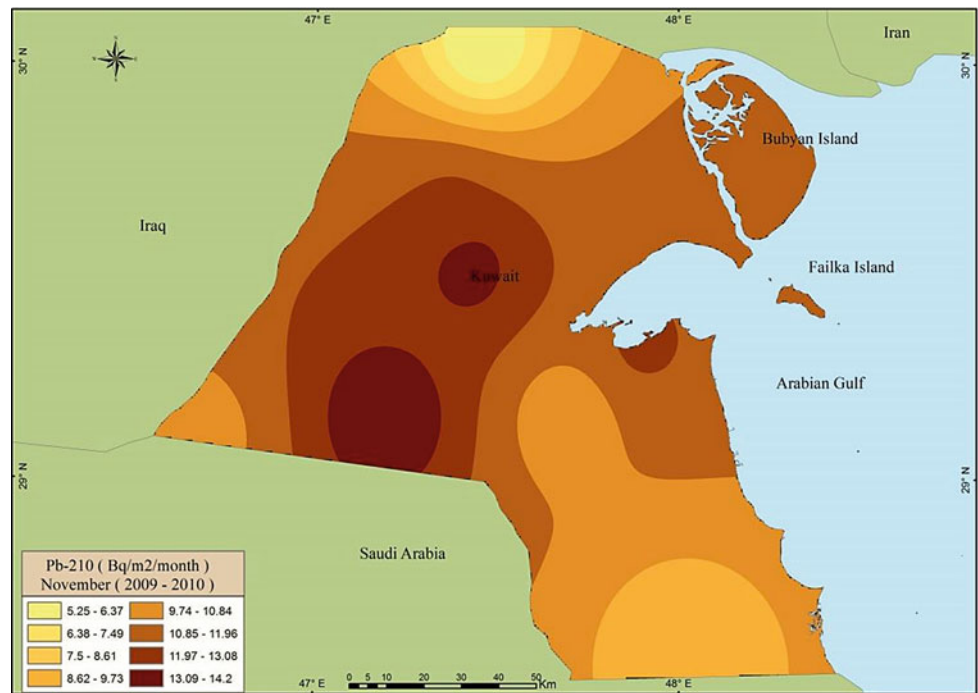
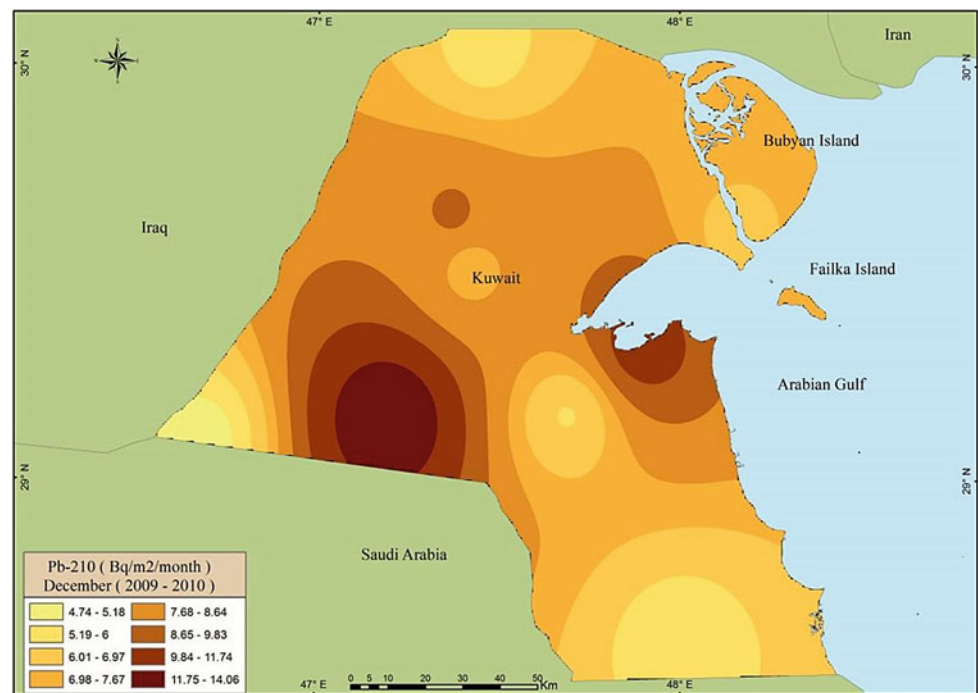


Fig. 6.54 Average deposited rates of ^{210}Pb in December (2009–2010)



References

- Aba, A., Al-Dousari, A. M., & Ismaeel, A. (2016). Depositional characteristics of ^7Be and ^{210}Pb in Kuwaiti dust. *Journal of Radioanalytical and Nuclear Chemistry*, 307(1), 15–23. <https://doi.org/10.1007/s10967-015-4129-y>.
- Aba, A., Al-Dousari, A. M., & Ismaeel, A. (2018). Atmospheric deposition fluxes of ^{137}Cs associated with dust fallout in the northeastern Arabian Gulf. *Journal of Environmental Radioactivity*, 192, 565–572. <https://doi.org/10.1016/j.jenvrad.2018.05.010>.
- Al-Dousari, A. M., Aba, A., Al-Awadhi, S., Ahmed, M., & Al-Dousari, N. (2016). Temporal and spatial assessment of pollen, radionuclides, minerals and trace elements in posited dust within Kuwait. *Arabian Journal of Geosciences*. <https://doi.org/10.1007/s12517-015-2182-z>.
- Biegalski, S., Hosticka, B., & Mason, L. (2001). Cesium-137 concentrations, trends, and sources observed in Kuwait city,

- Kuwait. *Journal of Radioanalytical and Nuclear Chemistry*, 248(3), 643–649. <https://doi.org/10.1023/A:1010676208657>.
- Daish, S., Dale, A., Dale, C., May, R., & Rowe, J. (2005). The temporal variations of ^7Be , ^{210}Pb and ^{210}Po in air in England. *Journal of Environmental Radioactivity*, 84, 457–467. <https://doi.org/10.1016/j.jenvrad.2005.05.003>.
- Kritz, M. A., Rosner, S. W., Danielsen, E. F., & Selkirk, H. B. (1991). Air mass origins and troposphere-to-stratosphere exchange associated with mid-latitude cyclogenesis and tropopause folding inferred from ^7Be measurements. *Journal of Geophysical Research: Atmospheres (1984–2012)*, 96, 17405–17414. <https://doi.org/10.1029/91JD01358>.
- UNSCEAR. (2000). *Sources and effects of ionizing radiation: Sources Annex X C: A exposures to the public from man-made sources of radiation*.
- Viezee, W., & Singh, H. B. (1980). The distribution of beryllium-7 in the troposphere: Implications on stratospheric/tropospheric air exchange. *Geophysical Research Letters*, 7. <https://doi.org/10.1029/gl007i010p00805>. ISSN: 0094-8276.
- Walling, D. E. (2002). Recent advances in the use of environmental radionuclides in soil erosion investigations. In *Nuclear techniques in integrated plant nutrient, water and soil management* (pp. 279–301). RN:33034207.

Open Access This chapter is licensed under the terms of the Creative Commons Attribution 4.0 International License (<http://creativecommons.org/licenses/by/4.0/>), which permits use, sharing, adaptation, distribution and reproduction in any medium or format, as long as you give appropriate credit to the original author(s) and the source, provide a link to the Creative Commons licence and indicate if changes were made.

The images or other third party material in this chapter are included in the chapter's Creative Commons licence, unless indicated otherwise in a credit line to the material. If material is not included in the chapter's Creative Commons licence and your intended use is not permitted by statutory regulation or exceeds the permitted use, you will need to obtain permission directly from the copyright holder.



Abstract

- Twenty-eight pairs of pollen and aeolian dust traps covering the State of Kuwait were used to obtain seasonal pollen counts of the most eight dominant families during 2009–2011 i.e. Chenopodiaceae, Poaceae (Gramineae), Cyperaceae, Leguminosae (Fabaceae), Cyperaceae, Brassicaceae, Malvaceae, Compositae, and Plantaginaceae.
- The sampling site locations were chosen to cover all the geomorphological sectors and native vegetation areas in Kuwait.
- Generally, pollen counts show us a remarkable distinction between the year 2009–2010 and 2010–2011, It is also evident that pollen counts (concentration) vary from season to season. Pollen counts over four seasons for two years (October 2009–August 2011) reveal the presence of two peaks in spring (April–May) and autumn (October–November).
- Map distribution of pollens in each of the dominant plant families in Kuwait is generated according to seasons showing higher and lower concentrations of dust pollen counts.

M. I. Ibrahim (✉)
 Faculty of Science, Alexandria University, 1 Baghdad Street,
 Moharam Bek, P.O. Box: 21511 Alexandria, Egypt
 e-mail: m.ibrahim@alexu.edu.eg

A. Al-Dousari · A. H. Al-Saleh
 Crisis Decision Supports Program (CDS), Environment and Life
 Sciences Research Center (ELSRC), Kuwait Institute for Scientific
 Research (KISR), P.O. Box: 24885 13109 Safat, Kuwait
 e-mail: adousari@kISR.edu.kw

A. H. Al-Saleh
 e-mail: ahsaleh@kISR.edu.kw

Samples Collection and Preparation

Twenty-eight pairs of pollen and eolian dust traps covering the State of Kuwait (Fig. 7.1) were used. The pollen trap is a simple cylindrical container with 40 cm depth and 20 cm radius fixed at 0 cm and 240 cm from the ground level. The traps were designed to capture bouncing and suspended particles from all directions (Fig. 7.1). The sampling site locations were chosen to cover all the geomorphological sectors and native vegetation areas in Kuwait. The samples within the traps were collected on a monthly basis for a period of 23 months. The weight of the collected samples from all the dust traps was measured. Fifty grams of sand (collected from pollen trap at 0 cm from ground level) was weighted from each station and treated as follows:

1. 50 grams of sand was sieved using a 150 μm sieve.
2. 10 grams of the fine fraction ($\leq 150 \mu\text{m}$) was washed with distilled water to remove the unwanted organic material, which was then dried.
3. The dried fine dust was soaked in diluted HCl (10%) to remove any carbonates present. Occasional agitation with a polypropylene stirring rod allowed the acid to penetrate the entire sample. If the reaction did not stop before several hours had elapsed, the depleted acid was replaced with fresh acid until all reactions ceased. Heating the sample can speed up the reaction, but only low heat should be used ($<95^\circ\text{C}$).
4. The acid was decanted when the residue had settled.
5. The residue was washed three times with distilled water to assure that the residue was in a neutral medium, which can be determined with calibrated litmus paper.
6. 40–60% hydrofluoric acid was used to remove any silicates present. In this step, the samples were put in polypropylene beakers and, using polypropylene rods, the mixture was left for at least 48 h. Sometimes heating in a water bath can occur.



Fig. 7.1 Dust tarp fixed at 240 cm above ground level (left), and pollen traps before and after fixing (right)

7. The residue was washed with distilled water, as described above in step (5).
8. Concentrated hydrochloric acid was added to the residue to remove any fluorides that may have been precipitated in the post HF water washes. After settling, the acid was decanted.
9. The residue was washed with distilled water, as described in step (5).
10. The residue was left in a glass vial to dry.
11. Glycerin jelly was used as a mounting medium for permanent slides.
12. The pellet of jelly was transferred to a slide; the slide was warmed to allow the jelly to melt. The pollen residue was dispersed in the jelly using a needle.
13. The jelly was allowed to cool slightly. A cover glass was placed on the jelly and pressed slightly using a needle.
14. The cover glass was cleaned in direct tap water and then labeled.

Microscopic Identification

Each sample slide was analyzed for pollen particle and spore content. Each identified particle or spore was counted as the prepared slide was traversed on a mechanical stage under the high-power microscope. Then, a pollen diagram and graphical expression of pollen analysis were constructed.

A seasonal pollen diagram and/or map illustrating the pollen distribution in Kuwait was then prepared according to the following seasons:

- (a) Fall (October–November 2009 and 2010)
- (b) Winter (January–February 2010 and 2011)
- (c) Spring (April–May 2010 and 2011)
- (d) Summer (July–August 2010 and 2011).

Climate and Vegetation

The climate of Kuwait is characterized by very hot, dry summers and cool to mild rainy winters. The rainfall pattern follows that of arid environments, being erratic and inconsistent, and showing great temporal and spatial fluctuations (Ahmed and Al-Dousari 2013). Records reveal that the average seasonal rainfall (October to April) total is 115 mm, with wide fluctuations between 29 mm and 262.7 mm. Rainfall usually occurs between November and May, while occasional showers may fall during May (Al-Dousari et al. 2020a). The mean temperature reaches its maximum during July–August (about 44°C) and its minimum during January (about 8 °C). Mean values of RH range between 90% in January and 31% in June, while the mean number of dusty days is 23 during July and nine during December (Al-Dousari et al. 2020b).

Kuwait's vegetation comprises eight units, which are described by Omar (2000) as follows:

1. HALOXYLETUM (Chenopodiaceae): It covers about 23% of the total area of Kuwait. It is dominated by the species *Haloxylon salicornicum*, a low shrub that grows

up to 60 cm in height. The community type covers large areas in the northern and western parts of Kuwait.

2. RHANTERIETUM (Compositae): The total area covered by the community is about 7% of Kuwait. It is dominated by the species *Rhanterium epapposum* in association with *Convolvulus oxyphyllus*, *Molkiopsis ciliate*, *Helianthemum lippi*, *Centropodia forsskalii*, and *Stipagrostis plumosa*. It occurs in small patches in the northern, central, and southern parts of Kuwait.
3. CYPERETUM (Cyperaceae): It is one of the most extensive vegetation units in Kuwait, covering approximately 26% of the country. The sedge *Cyperus conglomeratus* dominates it.
4. STIPAGROSTIETUM (Gramineae/Poaceae): It is dominated by *Stipagrostis plumosa*. It extends in the west and southwest of Kuwait, with few clusters in the north and northwest. The Stipagrostietum map unit covers 39% of Kuwait.
5. ZYGOPHYLLETUM (Zygophyllaceae): This type is dominated by *Zygophyllum qatarense*, which is a medium-sized shrub commonly found in coastal areas and depressions. The total distribution of the community is 1% of the total vegetation.
6. CENTROPODIETUM (Gramineae/Poaceae): This map unit is dominated by the species *Centropodia forsskalii*, a perennial grass that has recently become abundant in the southwest of Kuwait. The *Centropodietum* map unit covers approximately 1% of Kuwait.
7. PANICETUM (Gramineae/Poaceae): It is dominated by *Panicum turgidum*, a perennial desert grass forming tangled bunches up to 1 m tall. The distribution of the plant is very limited: estimated at < 1% of Kuwait.
8. HALLOPHYLETUM (Tamaricaceae): This map unit is dominated by many halophytic plant communities, such

as *Tamarix aucheriana*, *Nitraria Retusa*, *Halocnemum strobilaceum*, and *Seidlitzia rosmarinus*. It is found in the northern and southern coastal areas of Kuwait. The total area is about 1.5% of Kuwait.

Results

Total Pollen Count

Generally, pollen counts reveal a remarkable distinction between the year 2009–2010 and 2010–2011: the pollen particle concentration in 2009–2010 was higher in percentage than that of 2010–2011 (Figs. 7.4, 7.5). It is evident also that pollen counts (concentration) vary from season to season. Pollen counts over four seasons for two years (October 2009–August 2011) reveal the presence of two peaks in spring (April–May) and fall (October–November). The first peak is higher and is due to the greater number of pollen particle species that flower during the spring season, such as *Chenopodiaceae*, *Poaceae* (Gramineae), *Cyperaceae*, *Leguminosae* (Fabaceae), and *Plantaginaceae*. The second peak in fall (October–November) is lower and is characterized by the abundance of *Chenopodiaceae* and *Leguminosae* (Fig. 7.3).

On the other hand, two troughs are apparent during summer (July–August) and winter (January–February) due to summer drought, dust storms, and winter wind and rainfall. The summer lows are characterized by higher counts than the winter lows. In summer and fall, *Chenopodiaceae* dominates, followed by *Leguminosae* (Fig. 7.2).

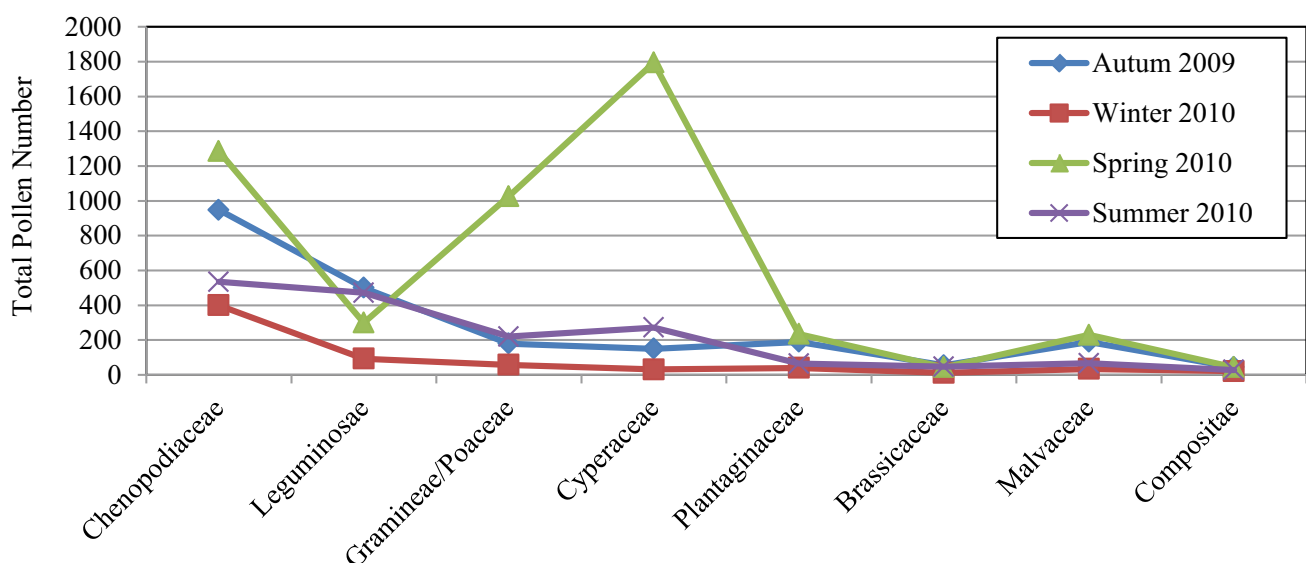


Fig. 7.2 Seasonal pollen counts of the most dominant families during 2009–2010

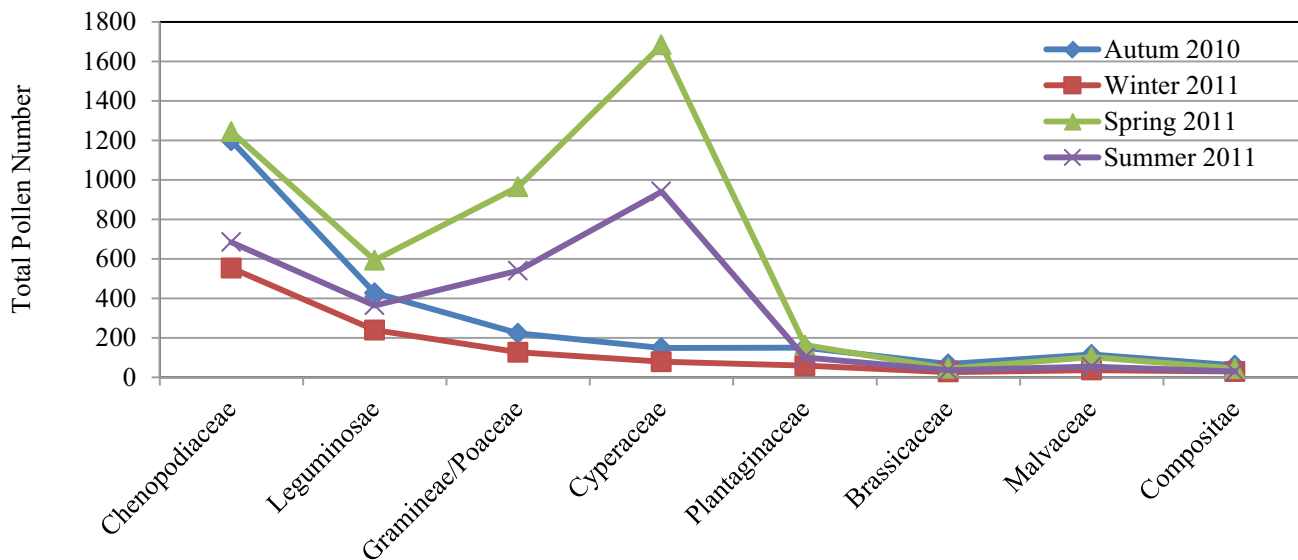


Fig. 7.3 Seasonal pollen counts of the most dominant families during 2010–2011

Among the 28 sites, the highest counts over the two years of study were recorded at sites 13, 15, 14, and 7, in descending order, especially in fall and spring (Fig. 7.4).

Chenopodiaceae and *Leguminosae* together comprise over 70% of the total pollen during fall.

Local flora is the main source of the pollen load, and the concentration depends on the amount of vegetation around each station, except for a very low percentage (2–3%) of *Pinaceae* pollen recorded in the north and northwest of Kuwait, which could be interpreted as being transported by the northwesterly wind. *Chenopodiaceae* had a high percentage (90%) during fall 2009. The spring peaks are higher because of the greater number of *Cyperaceae* and *Gramineae*. Generally, the pollen count for the period 2009–2010 is higher than 2010–2011.

Twenty-eight pairs of pollen and eolian dust traps were used throughout Kuwait. The pollen trap distribution was based on two parameters:

1. The dominant native desert plant dispersal in Kuwait and the surrounding region were selected in accordance with vegetation maps prepared by Dickson (1955), Kernick (1966), Ergun (1969), Macksad (1969), Halwagy and Halwagy (1974), and Omar (2000). These plants are *Cyperus conglomeratus*, *Haloxylon salicornicum*, *Rhanterium epapposum*, *Astragalus spinosus*, *Lycium shawii*, *Citrullus colocynthis*, *Panicum turgidum*, *Calligonum polygonoides*, *Nitraria retusa*, *Tamarix aucheriana*, *Halocnemum strobilaceum*, *Salicornia europaea*, *Heliotropium bacciferum*, *Arnebia decumbens*, and *Convolvulus oxyphyllus*.
2. The geomorphology of the area, because there is a positive relationship between the types of native plants

present, in which most of the plants are present within drainage systems such as water, wadis, playas, and sabkhas.

According to the above-mentioned parameters, the pollen traps were selected.

Mohamed et al. (1983) found a highly significant correlation between the concentration of *Cyperus*, *Plantago*, and *Brassicaceae* pollen. *Brassicaceae* is a large family of plants with four-petaled flowers. For spring 2011, the pollen distribution and abundance indicate the same trend as in spring 2010, with an abundance of *Cyperaceae* (33.7%) followed by *Chenopodiaceae* (24.9%), *Gramineae* (19.3%), *Leguminosae* (12%), *Plantaginaceae* (3.2%), *Malvaceae* (1.9%), *Ephedraceae* (1.2%), and *Brassicaceae* (1.1%). The highest of all pollen noted in Kuwait during springtime was *Brassicaceae*, which appears mostly around farms and cultivated urban areas, such as in Wafra Farms, Liyah, and Qurain (Fig. 7.5).

Areas with high pollen in dust concentration	Areas with low pollen in dust concentration
Qurain	Abdulli
Liyah	Ratqah
Salmiya	Salmi
Kabd	Burqan
Wafra Farms	Subiyah

Al-Dousari et al. (2018) found a highly significant correlation between the concentration of *Cyperus*, *Plantago*, and *Brassicaceae* pollen. *Brassicaceae* is a large family of plants with four-petaled flowers. For spring 2011, the pollen distribution and abundance indicate the same trend as in

Fig. 7.4 Kuwait image showing the location of the pollen and dust sampling sites

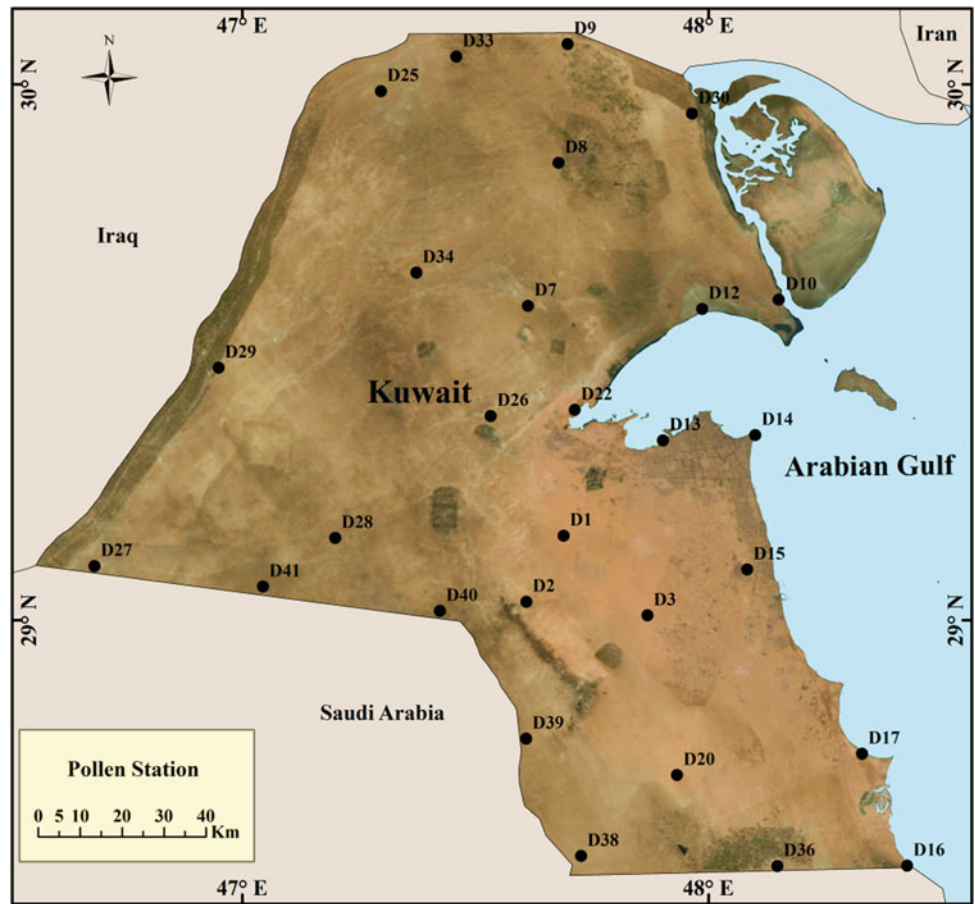


Fig. 7.5 Average percentages of *Brassicaceae* pollen in dust. Spring (April–May 2010 and 2011)

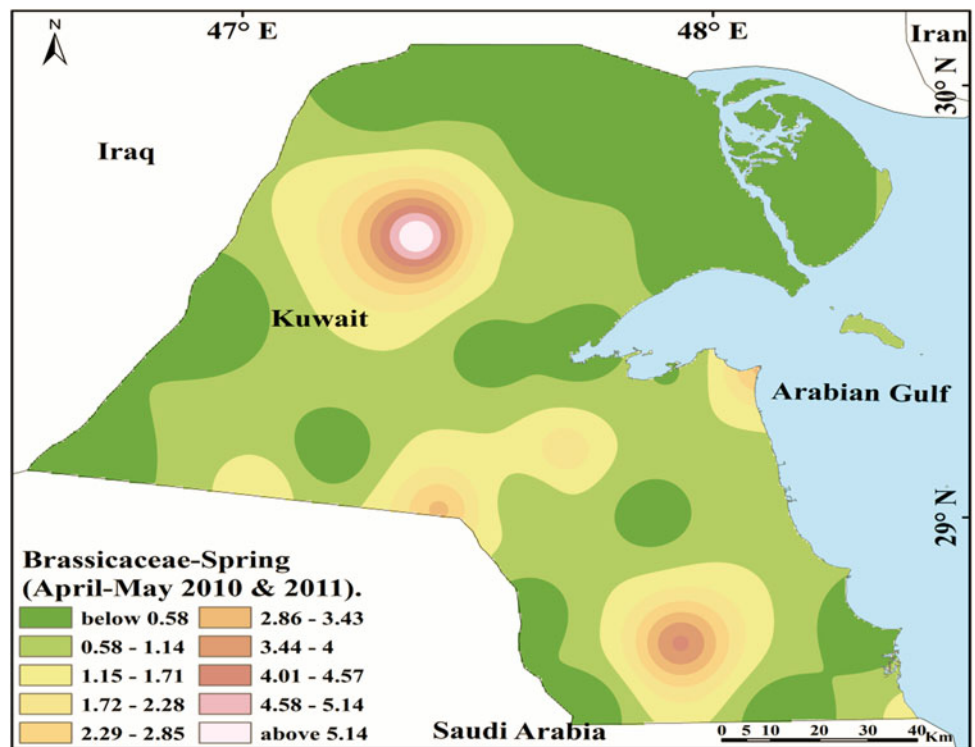
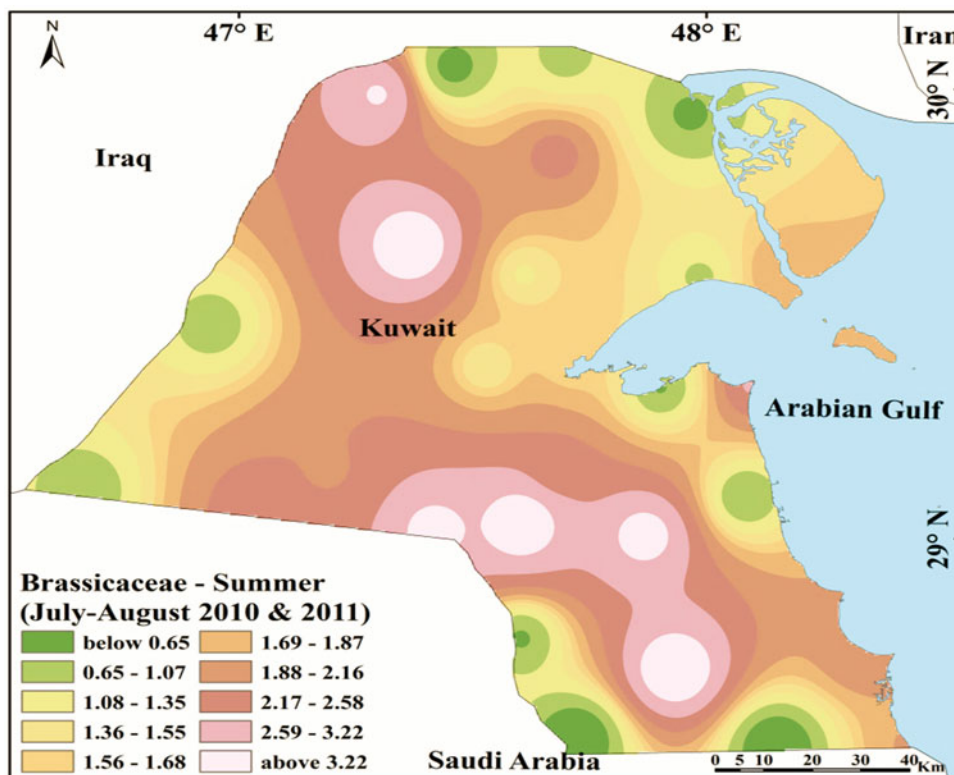


Fig. 7.6 Average percentages of *Brassicaceae* pollen in dust. Summer (July–August 2010 and 2011)



spring 2010, with an abundance of *Cyperaceae* (33.7%) followed by *Chenopodiaceae* (24.9%), *Gramineae* (19.3%), *Leguminosae* (12%), *Plantaginaceae* (3.2%), *Malvaceae* (1.9%), *Ephedraceae* (1.2%), and *Brassicaceae* (1.1%). The highest of all pollen noted in Kuwait during springtime was *Brassicaceae*, which appears mostly in farms and other cultivated urban areas, such as in Kabd, Liyah, and Qurain. The distribution of *Brassicaceae* is similar to the distribution of other pollen during summer (Fig. 7.6).

Areas with high pollen in dust concentration	Areas with low pollen in dust concentration
Qurain	Um Niqa
Burqan	Ratqah
Jreshan	Ubayriq
Liyah	Salmi
Kabd	Wafra Farms

The highest percentages of *Brassicaceae* pollen were noted during fall. The pollen appeared mostly around farms and cultivated urban areas, such as in Wafra Farms, Salmiya, and Qurain. The distribution of *Brassicaceae* is completely different from the distribution of other pollen during fall. The high distribution takes the form of a corridor that extends from Huwaymilyah to northern Kuwait Bay. There are two major wind corridors in Kuwait, one showing higher

concentrations up to 48% in Huwaymilyah and the other with very low concentrations in Um Niqa. This result indicates that *Brassicaceae*'s dominant source area is the Western Desert of Iraq, and it is rarely found in the Mesopotamian Floodplain upwind of the Um Niqa wind corridor (Fig. 7.7).

Areas with high pollen in dust concentration	Areas with low pollen in dust concentration
Um Al Madafi'	Ratqah
Huwaymilyah	Abdulli
Subiyah	Um Niqa
Ratqah	Salmi
Qurain	Burqan

Chenopodiaceae covers about 23% of the total area of Kuwait. The most dominant pollen family reached its maximum abundance (90%) during fall 2009. The highest pollen concentrations were recorded in fall 2009 around Kuwait City, and in the southeast, northwest, and northeast of Kuwait; whereas, the lowest concentrations were recorded during winter 2010 and 2011. The most common genera are *Bienertia*, *Brassia*, *Chenopodium*, *Cornulaca*, *Halocnemum*, *Hammada*, *Salsola*, *Seidlitzia*, and *Schanginia*. *Haloxylon salicornicum* is a low dominant shrub that grows up to 60 cm in height. The community type covers large areas in the

Fig. 7.7 Average percentages of *Brassicaceae* pollen in dust. Autumn (October–November 2009 and 2010)

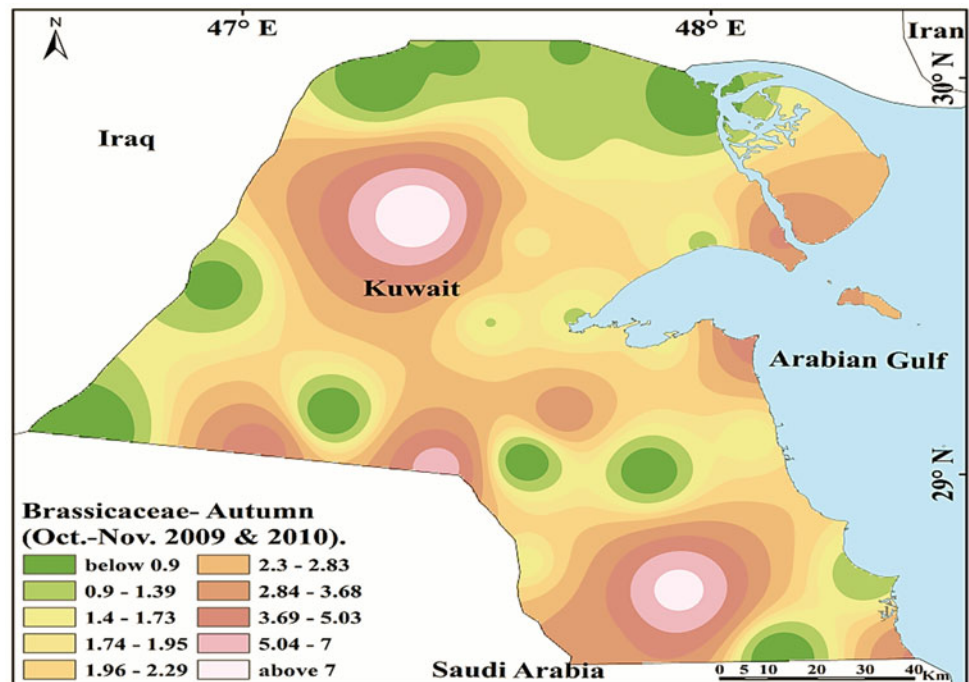
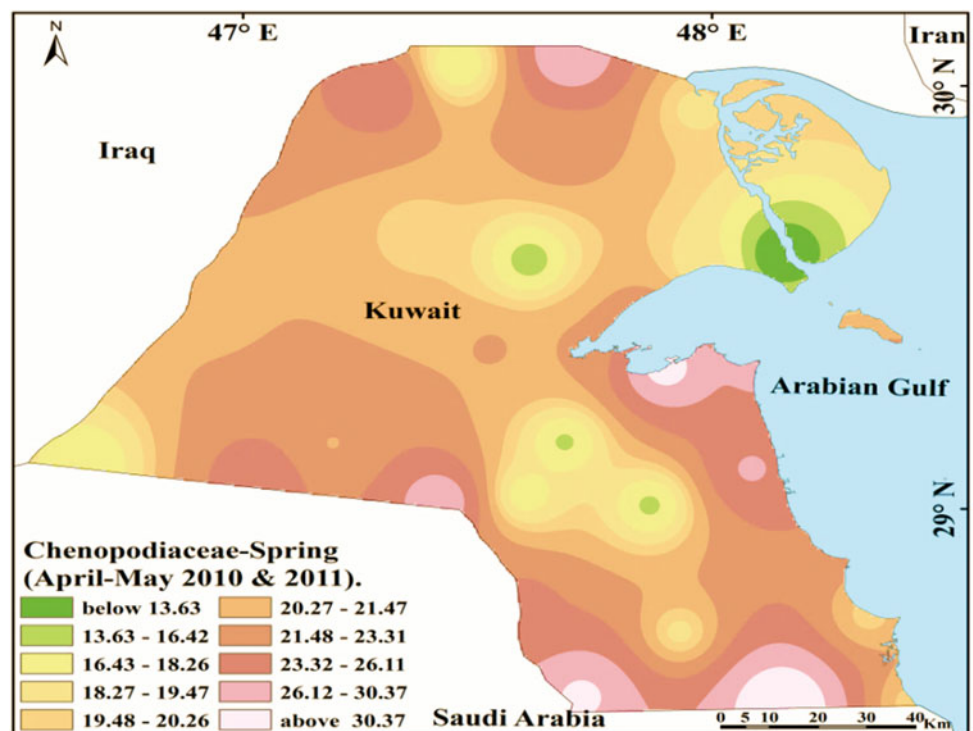


Fig. 7.8 Average percentages of *Chenopodiaceae* pollen in dust. Spring (April–May 2010 and 2011)



northern and western parts of Kuwait. The average counts of *Chenopodiaceae* pollen in the dust during spring (April–May 2010 & 2011) reveal a similar distribution density to that of *Cyperaceae* pollen, which indicates a close distribution between the two dominant native plants, namely *Haloxylon*

salicornicum from the *Chenopodiaceae* family and *Cyperus conglomeratus* from the *Cyperaceae* vegetation family. *Haloxylon salicornicum* flourished from October until December. *Haloxylon salicornicum* pollen is heavy when compared with other native plants, and its pollen largely

comes from local and nearby regional sources. Therefore, *Haloxylon salicornicum* pollen's maximum counts were in areas such as Shuaiba, Subiyah, Liyah, and Abdulli. In spring 2010 and 2011, the most abundant pollen families belonged to *Cyperaceae* (33.6% and 33.7%, respectively) and *Chenopodiaceae* (24% and 24.9%, respectively) (Fig. 7.8).

Areas with high pollen in dust concentration	Areas with low pollen in dust concentration
Abdulli	Ratqah
Khur Fawaris	Um Eish
Wafra Farms	Subiyah
Shuaiba	Sulaybiyah
Shuwaikh	Salmi

The average counts of the *Chenopodiaceae* pollen in the dust during summer (July–August 2010 and 2011) show similar distribution density to that in spring with *Cyperaceae* pollen. Summer had the lowest counts for most of the native plants' pollen. Mutla had the highest counts, as it is surrounded by preserved and protected areas that are densely vegetated by *Haloxylon salicornicum*. *Haloxylon salicornicum* pollen had the maximum counts in areas such as Shuaiba, Shuwaikh, Wafra Farm, and Um Rimam. Most of the northern borders with Iraq, the southern areas of Kuwait,

and the areas around Kuwait Bay show no counts of *Chenopodiaceae*. *Chenopodiaceae* and *Leguminosae* together comprise over 70% of the total pollen during fall. In summer 2010 and 2011, the highest counts were from *Chenopodiaceae* (32.8% and 33% respectively) (Fig. 7.9).

Areas with high pollen in dust concentration	Areas with low pollen in dust concentration
Abdulli	Ratqah
Khur Fawaris	Liyah
Wafra Farm	Subiyah
Shuaiba	Qurain
Shuwaikh	Salmi

The total area covered by the pollen community is about 7% of Kuwait. The pollen is dominated by the species *Rhanterium epapposum* in association with *Convolvulus oxyphyllus*, *Moltkiopsis ciliata*, *Helianthemum lippi*, *Centropodia forsskalii*, and *Stipagrostis plumosa*. It occurs in small patches in the northern, central, and southern parts of Kuwait. The average percentages of the composite pollen in dust during spring (April–May 2010 and 2011) are the lowest distribution within most areas in Kuwait. This finding is a good indication of two important notes:

Fig. 7.9 Average percentages of *Chenopodiaceae* pollen in dust. Summer (July–August 2010 and 2011)

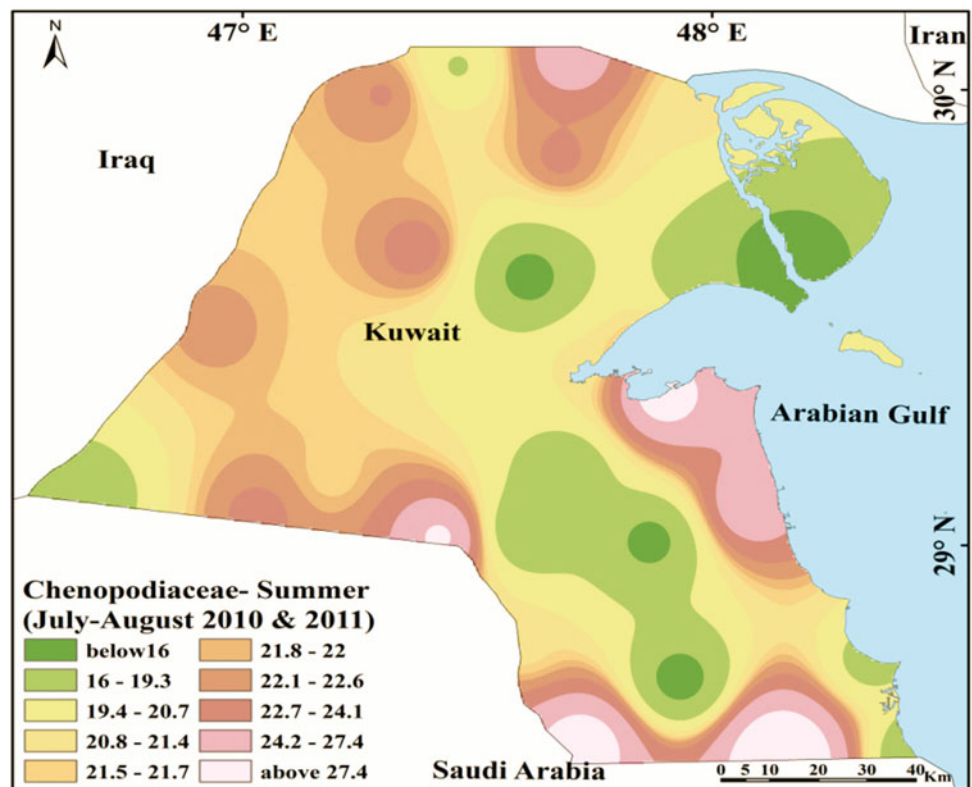


Fig. 7.10 Average percentages of *Compositae* pollen in dust. Spring (April–May 2010 and 2011)

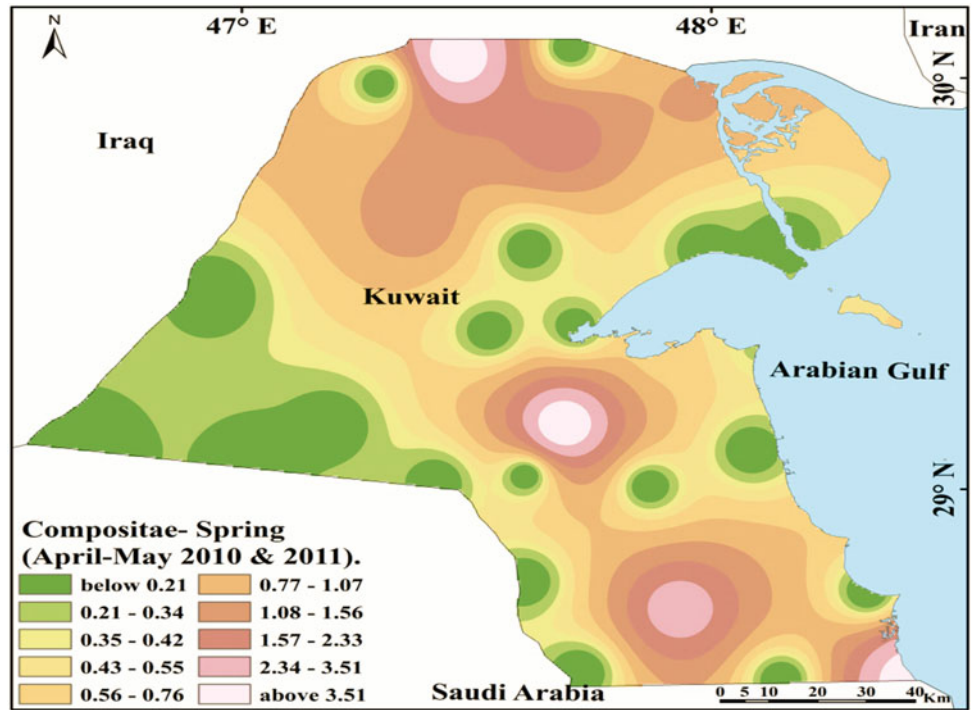
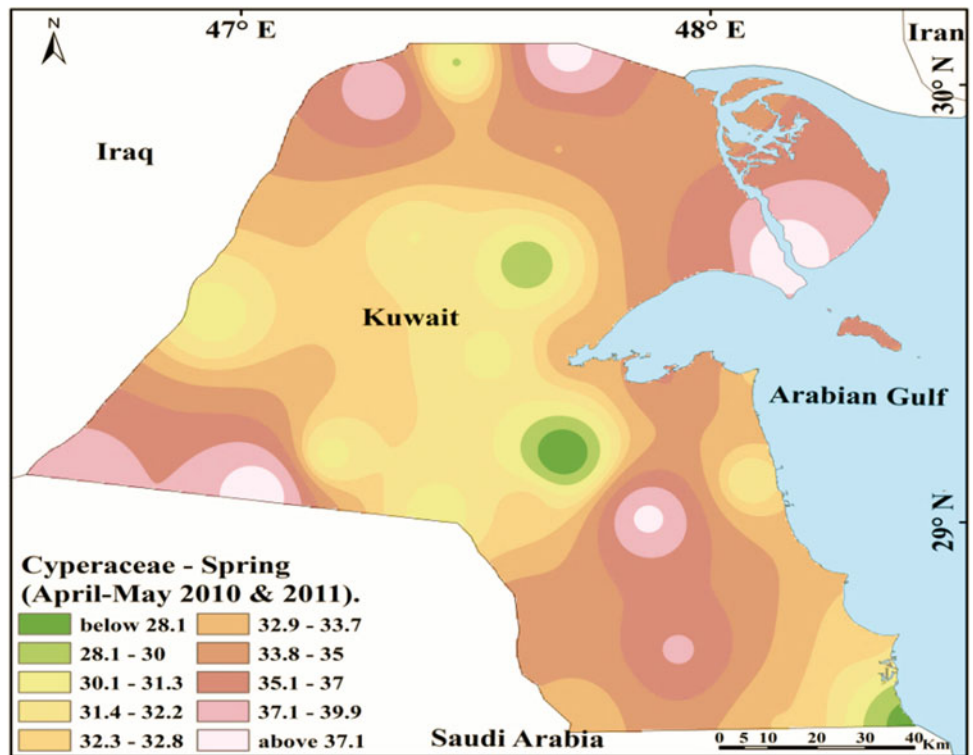


Fig. 7.11 Average percentages of *Cyperaceae* pollen in dust. Spring (April–May 2010 and 2011)



1. The deterioration of the *Rhanteium epapposum* native plant in Kuwait.
2. Dust storm trajectories from the east play a major role in transporting *Rhanteium* pollen from regional sources; there are high counts present in Ratqah, Sulaybiyah, and Burqan (Fig. 7.10).

Areas with high pollen in dust concentration	Areas with low pollen in dust concentration
Ratqah Sulaybiyah Burqan Khiran Um Al- Madafi'	Ratqah Huwaymilyah Um Niqa Jal Al Zur Khiran

Cyperaceae pollen in dust predominantly originates from *Cyperus conglomeratus*, a native plant species in the region. It is one of the most extensive vegetation units in Kuwait, covering approximately 26% of the country. In spring 2010 and 2011, the abundant pollen families belonged to *Cyperaceae* (33.6% and 33.7%, respectively). *Cyperus conglomeratus* flourished in two major times:

1. November–February
2. May–July

The plant is found within mobile sand corridors and away from the preserved areas with dense vegetation. The dense pollen of *Cyperus conglomeratus* appears during wintertime

as there are other, more palatable plant species for grazing animals. Therefore, *Cyperus conglomeratus* pollen's maximum counts were in areas such as Subiyah, Dibdibah, and Abdulli. The maximum counts of *Cyperus conglomeratus* in Salmiya could have originated from regional sources from dust storm trajectories that come from the coast (Fig. 7.11).

Areas with high pollen in dust concentration	Areas with low pollen in dust concentration
Abdulli Dibdibah Subiyah Burqan Qurain	Ratqah Um Eish Sulaybiyah Liyah Khiran

Cyperus conglomeratus flourished in summertime in May–July. The low counts for pollen of *Cyperus conglomeratus* during summer are evident as there are no other palatable plant species for grazing animals. Therefore, *Cyperus conglomeratus* is severely grazed by grazing animals (goats, sheep and camels), and this is reflected in the pollen counts, which were much lower than in winter. The maximum counts were in the same areas during winter, such as Subiyah, Um Qudayr, and Abdulli, which might indicate that *Cyperus conglomeratus* pollen is heavy compared with other native plant pollen and largely comes from local and nearby regional sources.

In summer 2010, the highest counts were from *Chenopodiaceae* (32.8%), followed by *Leguminosae* (23.2%), *Cyperaceae* (18.7%), and *Gramineae* (11.5%). In

Fig. 7.12 Average percentages of *Cyperaceae* pollen in dust. Summer (July–August 2010 and 2011)

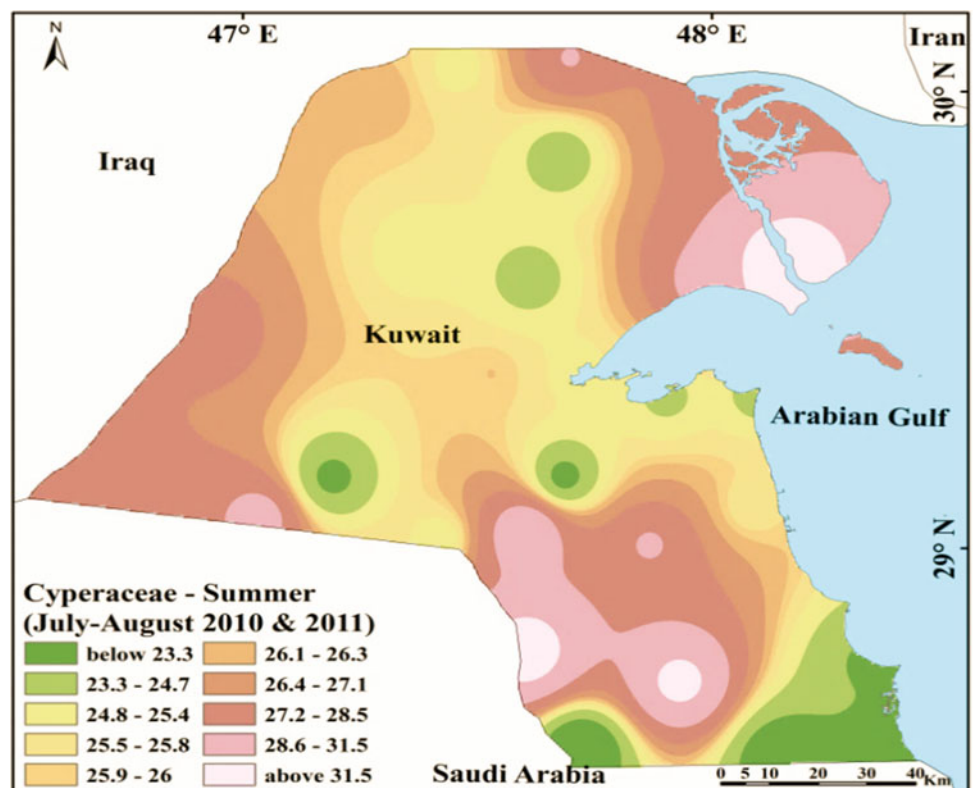
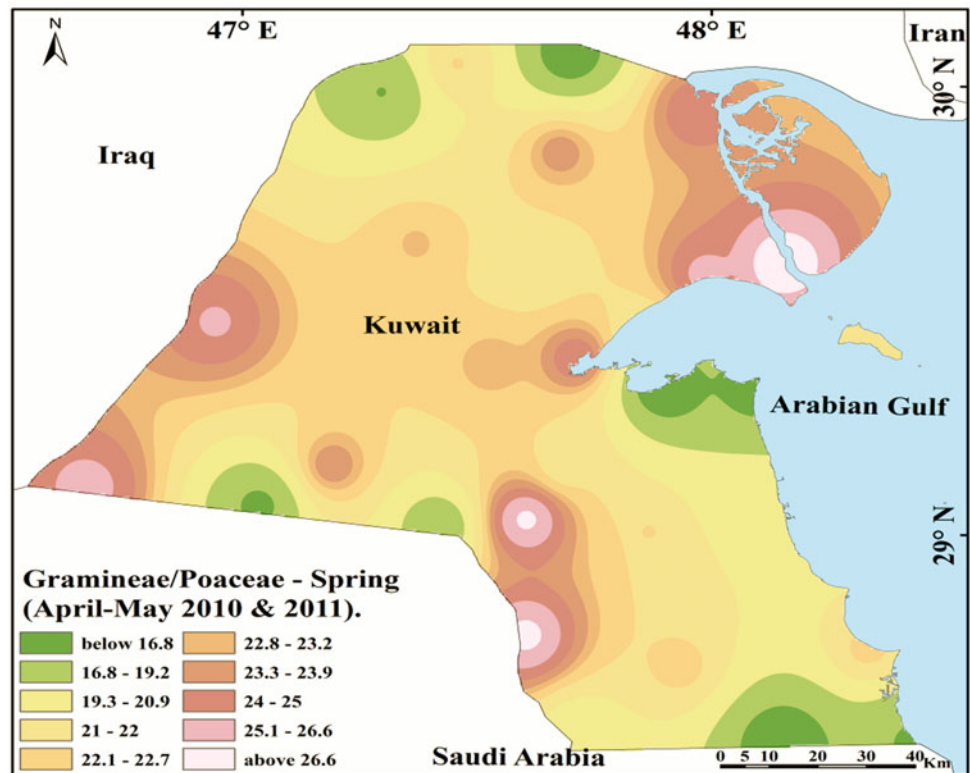


Fig. 7.13 Average percentages of *Gramineae/Poaceae* pollen in dust. Spring (April–May 2010 and 2011)



summer 2011, a similar tendency is apparent, with nearly the same dominance percentage (*Chenopodiaceae*, 33%; *Leguminosae*, 24%; and *Cyperaceae*, 19.4%) (Fig. 7.12).

Areas with high pollen in dust concentration	Areas with low pollen in dust concentration
Abdulli	Khur Fawaris
Qurain	Dibdibah
Subiyah	Um Eish
Salmi	Salmiya
Um Qudayr	Khiran

Gramineae/Poaceae is dominated in Kuwait by *Stipagrostis* species, such as *plumosa*, *obtusa*, *drarii*, and *ciliata*. It extends to the west and southwest of Kuwait, with a few clusters to the north and northwest. The *Stipagrostietum* map unit covers 39% of Kuwait, including huge areas in the desert environment, and presents densely in dust in areas such as Kabd, Liyah, Subiyah, and Um Qudayr, reaching up to 26.6 counts during spring. The *Stipagrostis* species flourishes from March until May. In spring 2010, the abundant pollen families belonged to *Cyperaceae* (33.6%), followed by *Chenopodiaceae* (24%), and *Gramineae*

(19.6%). The same was observed in spring 2011 with *Gramineae* (19.3%) (Fig. 7.13).

Areas with high pollen in dust concentration	Areas with low pollen in dust concentration
Kabd	Ratqah
Um Qudayr	Huwaymilyah
Subiyah	Salmiya
Ubayriq	Dibdibah
Salmi	Khiran

Gramineae/Poaceae is dominated in Kuwait by the *Stipagrostis* species, which are dominant from March to May. The *Stipagrostis* species during summer reached the maximum counts and were present only in preserved areas such as the border areas, Liyah, and Jal Al Zur, all of which are preserved areas. The maximum and minimum counts of *Gramineae/Poaceae* distribution were similar in spring, summer, and winter, the only difference being in the numbers of detection, as it was the highest in winter and spring but the lowest in summer. In summer 2010, the highest counts were for families of *Chenopodiaceae* (32.8%), followed by *Leguminosae* (23.2%), *Cyperaceae* (18.7%), and

Fig. 7.14 Average percentages of *Gramineae/Poaceae* pollen in dust. Summer (July–August 2010 and 2011)

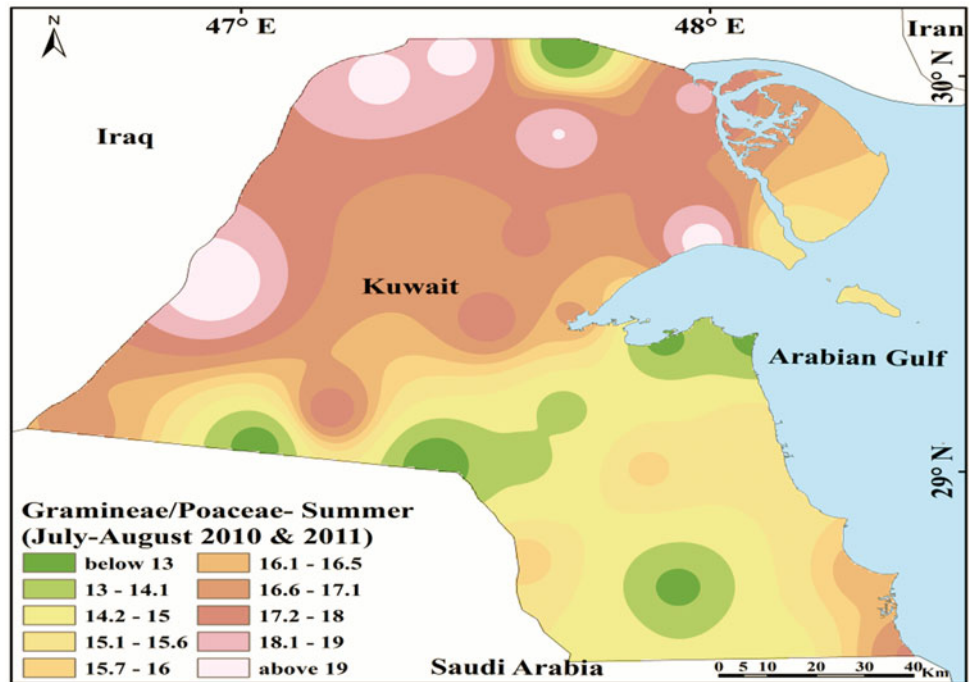
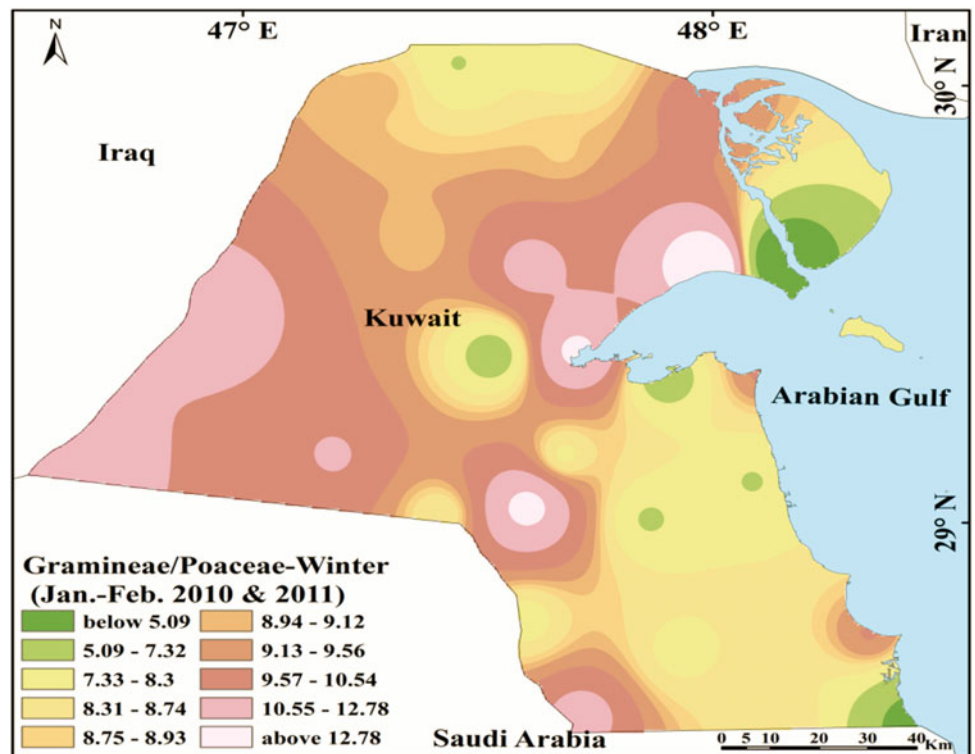


Fig. 7.15 Average percentages of *Gramineae/Poaceae* pollen in dust. Winter (January–February 2010 and 2011)



Gramineae (11.5%). In summer 2011, nearly the same dominance percentage occurred (*Chenopodiaceae*, 33%; *Leguminosae*, 24%; *Cyperaceae*, 19.4%; and *Gramineae*, 18.9%) (Fig. 7.14).

Areas with high pollen in dust concentration	Areas with low pollen in dust concentration
Ubayriq Ratqah Jal Al Zur Liyah Khiran	Dibdibah Abdulli Qurain Kabd Shuwaikh

Gramineae/Poaceae dominated in most desert areas but was maximum in areas such as Liyah, Gudhi, and Kabd. The maximum and minimum counts of *Gramineae/Poaceae* distribution were similar in spring and summer, the only difference being the number of detections, as it was the highest in winter, when these plants cover huge areas in Kuwait and in upwind regional areas in Iraq. The maximum counts reached up to 12.78 during winter, even before the flourishing of the dominating plant species. In the winters of 2010 and 2011, *Gramineae/Poaceae* reached 7.6% and 10%, respectively, in counts (Fig. 7.15).

Areas with high pollen in dust concentration	Areas with low pollen in dust concentration
Gudhi Mutla Kabd Khur Al-Fawaris Shegaya	Ratqah Subiyah Jal Al-Atraf Burqan Khiran

Leguminosae (Fabaceae) was the second most abundant family that flourished during autumn and spring. The highest distribution was recorded during fall 2009 and 2010 (up to 54%) in the extreme western side of the country, and the lowest pollen concentrations were recorded in the west of Kuwait (fall 2009), eastern Kuwait (winter 2010), and southern Kuwait (spring 2011 and summer 2011). The dominant genera in Kuwait are *Acacia*, *Astragalus*, *Coronilla*, *Lotus*, *Medicago*, *Prosopis*, *Scorpiurus*, *Trigonella* and *Astragalus* in Liyah, while *Coronilla* dominates in open, deteriorated desert, such as in Shegaya and Salmi. *Chenopodiaceae* and *Leguminosae* together comprise over 70% of the total pollen during fall. In spring 2010 and 2011, the *Leguminosae* pollen families had higher percentages, with 11.7% and 12%, respectively (Fig. 7.16).

Areas with high pollen in dust concentration	Areas with low pollen in dust concentration
Um Niqa Khiran Ubayriq Shegaya Gudhi	Dibdibah Kabd Um Qudayr Qurain Um Eish

Leguminosae (Fabaceae) had the highest pollen count in small areas in summer, extending from Abdulli to Liyah. As most of the native plant species within this family flourish during fall and spring, summer may also contain appreciable amounts of pollen. The lowest pollen concentrations were recorded in southern Kuwait (spring 2011 and summer 2011). *Acacia*, *Astragalus*, *Coronilla*, *Lotus*, *Medicago*, *Prosopis*, *Scorpiurus*, *Trigonella*, and *Astragalus* are the dominant

Fig. 7.16 Average percentages of *Leguminosae* pollen in dust. Spring (April–May 2010 and 2011)

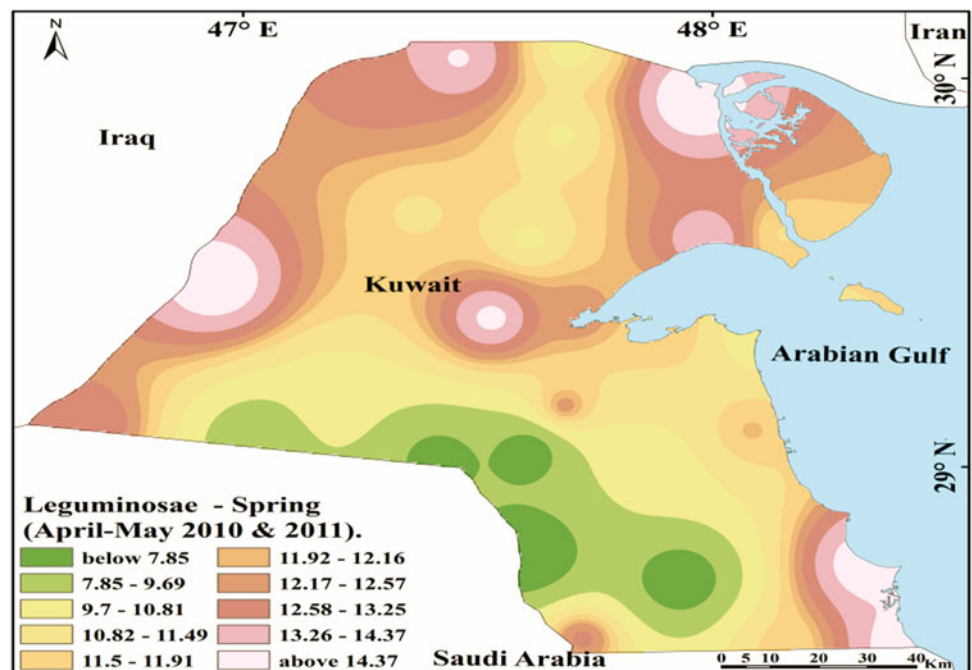
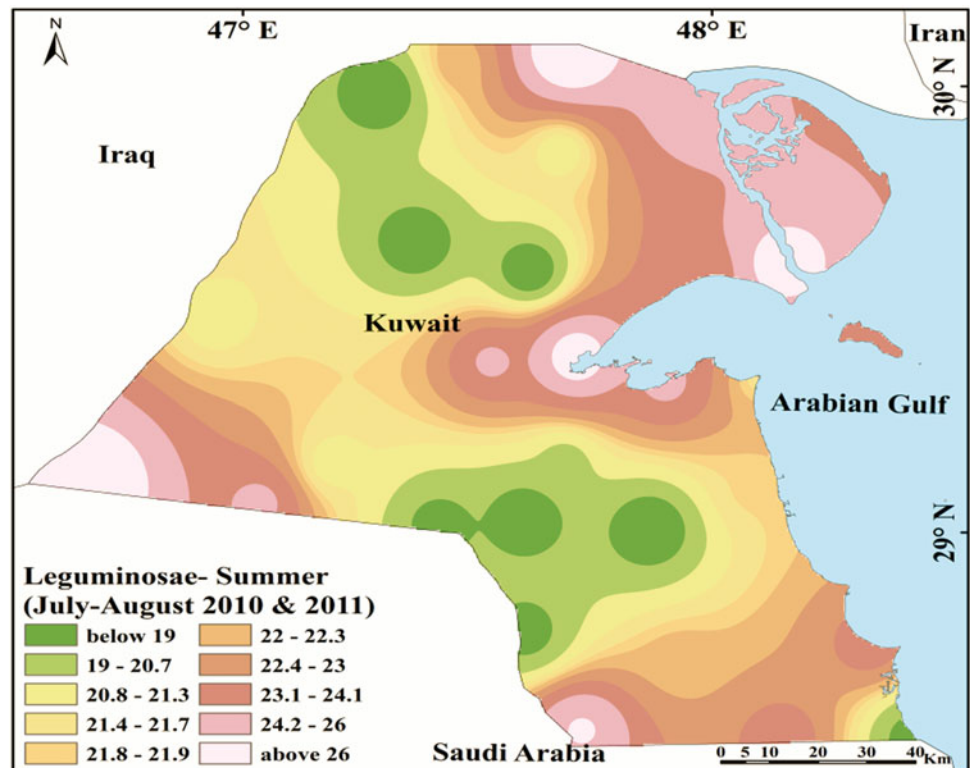


Fig. 7.17 Average percentages of *Leguminosae* pollen in dust. Summer (July–August 2010 and 2011)



genera from this plant family and dominated in Abdulli, Shegaya, and Salmi. In summer and fall, *Chenopodiaceae* dominated, followed by *Leguminosae*. In summer 2010, the highest counts were of *Chenopodiaceae* (32.8%) and *Leguminosae* (23.2%). The same trend was observed in summer 2011, with nearly the same dominance percentage (*Chenopodiaceae*, 33%; *Leguminosae*, 24%) (Fig. 7.17).

Areas with high pollen in dust concentration	Areas with low pollen in dust concentration
Mutla	Ratqah
Subiyah	Huwaymilyah
Abdulli	Kabd
Khur Al-Fawaris	Burqan
Shegaya	Khiran

Leguminosae (*Fabaceae*) in winter had a similar distribution to summer and springtime. The highest counts were in an area that extends from Abdulli to Liyah. As most of the native plant species within this family flourish during autumn and spring, summer may also contain appreciable amounts of pollen. The lowest pollen concentrations were recorded in the Liyah area (spring 2011 and summer 2011). The *Acacia*, *Astragalus*, *Coronilla*, *Lotus*, *Medicago*, *Prosopis*, *Scorpiurus*, and *Trigonella*. *Astragalus* species are the dominant genera in this plant family, and it is dominant in Wafra Farm, Shegaya, and Salmi. In winter 2010 and 2011, *Chenopodiaceae* dominated the counts (52% and 43%,

respectively), followed by *Leguminosae* (12.2% and 18.8%, respectively) (Fig. 7.18).

Areas with high pollen in dust concentration	Areas with low pollen in dust concentration
Salmi	Ras Ezur
Wafra Farm	Liyah
Dibdibah	Doha
Ratqah	Jreshan
Shegaya	Sulaybiyah

The *Malvaceae* family contains nearly 243 genera and at least 4,225 species of trees, shrubs, and herbs. Kuwait is home to three herbs from the *Malvaceae* family, namely *Althaea ludwigii*, *Malva nicaeensis*, and *Malva parviflora*. All the flowers bloom in April. During spring 2010 and 2011, the abundant pollen families belonging to *Cyperaceae* (33.6%) are followed by *Chenopodiaceae* (24%), *Gramineae* (19.6%), *Leguminosae* (11.7%), *Plantaginaceae* (4.4%), *Malvaceae* (2.1%), and *Ephedraceae* (1.2%). In spring 2011, the pollen distribution and abundance showed the same trend as in spring 2010, with an abundance of *Cyperaceae* (33.7%), followed by *Chenopodiaceae* (24.9%), *Gramineae* (19.3%), *Leguminosae* (12%), *Plantaginaceae* (3.2%), *Malvaceae* (1.9%), *Ephedraceae* (1.2%), and *Brassicaceae* (1.1%). In the map, above, *Malvaceae* pollen is absent from the northern Kuwait desert but appears with maximum counts in Dibdibah and Ratqah (Fig. 7.19).

Fig. 7.18 Average percentages of *Leguminosae* pollen in dust. Winter (January–February 2010 and 2011)

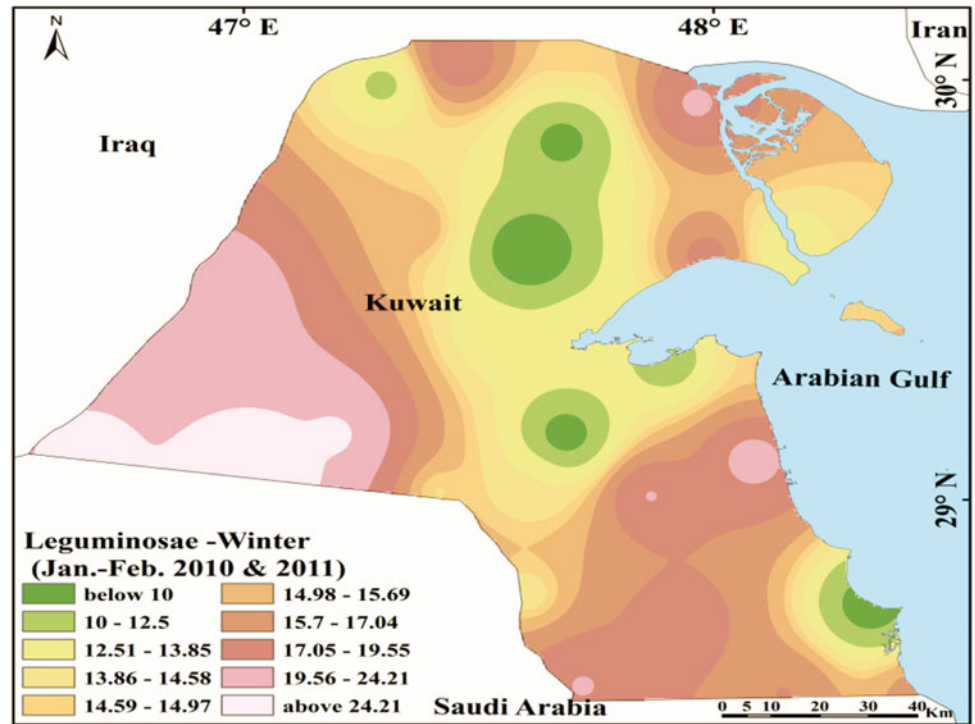


Fig. 7.19 Average percentages of *Malvaceae* pollen in dust. Spring (April–May 2010 and 2011)

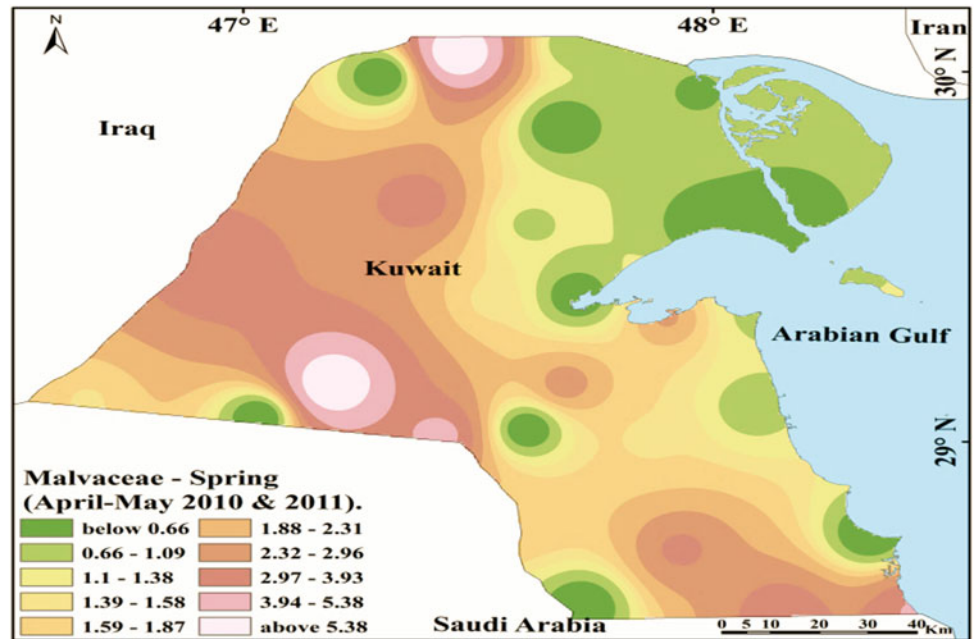
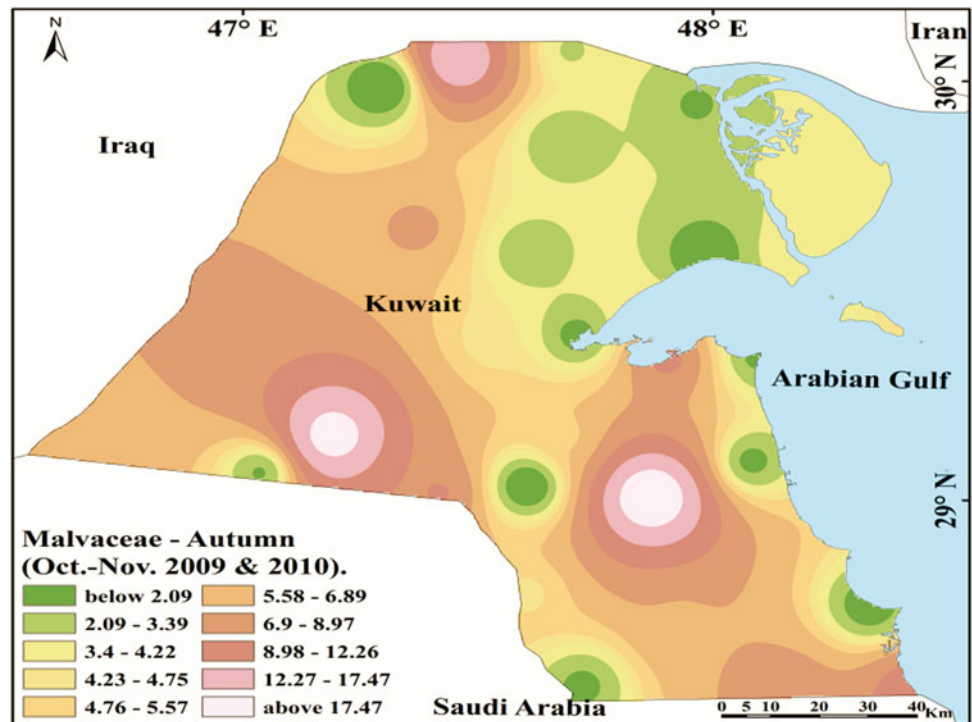


Fig. 7.20 Average percentages of *Malvaceae* pollen in dust. Autumn (October–November 2009 & 2010)



Areas with high pollen in dust concentration	Areas with low pollen in dust concentration
Ratqah	Subiyah
Dibdibah	Shuaiba
Um Al Madafi'	Doha
Ubayriq	Kur Al-Fawaris
Wafra Farm	Shuaiba

The three major herbs from the *Malvaceae* family present in the region are *Althaea ludwigii*, *Malva nicaeensis*, and *Malva parviflora*. The *Malvaceae* family contains about 243 genera and at least 4,225 species of trees, shrubs, and herbs. In Kuwait, All flowers bloom during April. In fall 2010, the highest pollen counts were of *Chenopodiaceae* (57%), followed by *Leguminosae* (22%), *Plantaginaceae* (7%), *Malvaceae* (7%), and *Gramineae* (6.5%). The distribution map for *Malvaceae* pollen during fall shows an abundance level around farms (Abdulli and Wafra Farms) and is still present in Salmiya, coming from regional sources from the coast (Fig. 7.20).

Areas with high pollen in dust concentration	Areas with low pollen in dust concentration
Ratqah	Khur Fawaris
Dibdibah	Ratqah
Salmi	Gudhi
Burqan	Um Niqa
Wafra Farm	Jal Al Zur

The *Malvaceae* three major herbs present in the region are *Althaea ludwigii*, *Malva nicaeensis*, and *Malva*

parviflora. In summer 2010, the highest counts were of *Chenopodiaceae* (32.8%), followed by *Leguminosae* (23.2%), *Cyperaceae* (18.7%), *Gramineae* (11.5%), *Plantaginaceae* (4.3%), and *Malvaceae* (2.3%). The same trend was observed in summer 2011, with nearly the same dominance percentage (*Chenopodiaceae*, 33%; *Leguminosae*, 24%; *Cyperaceae*, 19.4%; *Gramineae*, 18.9%; *Plantaginaceae*, 3.5%; and *Malvaceae*, 1.8%). In the map, above, *Malvaceae* pollen appears with the maximum count in the northern Kuwait desert but is absent from urban areas Subiyah and Abdulli (Fig. 7.21).

Areas with high pollen in dust concentration	Areas with low pollen in dust concentration
Ratqah	Salmiya
Huwaymilyah	Subiyah
Salmi	Abdulli
Dibdibah	Um Niqa
Khiran	Kabd

Plantaginaceae pollens were majorly present in the pollen traps and originate primarily from *Plantago* species (*amplexicaulis*, *boissieri*, *ciliata*, *coronopus*, *lanceolata*, *notate*, *ovata*, and *psammophila*). The most-detected *Plantaginaceae* pollens were found in spring. In spring 2010 and 2011, the pollen families belonging to *Plantaginaceae* reached up to 4.4% and 3.2%, respectively. The pollen appeared only in preserved areas such as Sabiyah, Liyah, and Kabd (Fig. 7.22).

Fig. 7.21 Average percentages of *Malvaceae* pollen in dust. Summer (July–August 2010 and 2011)

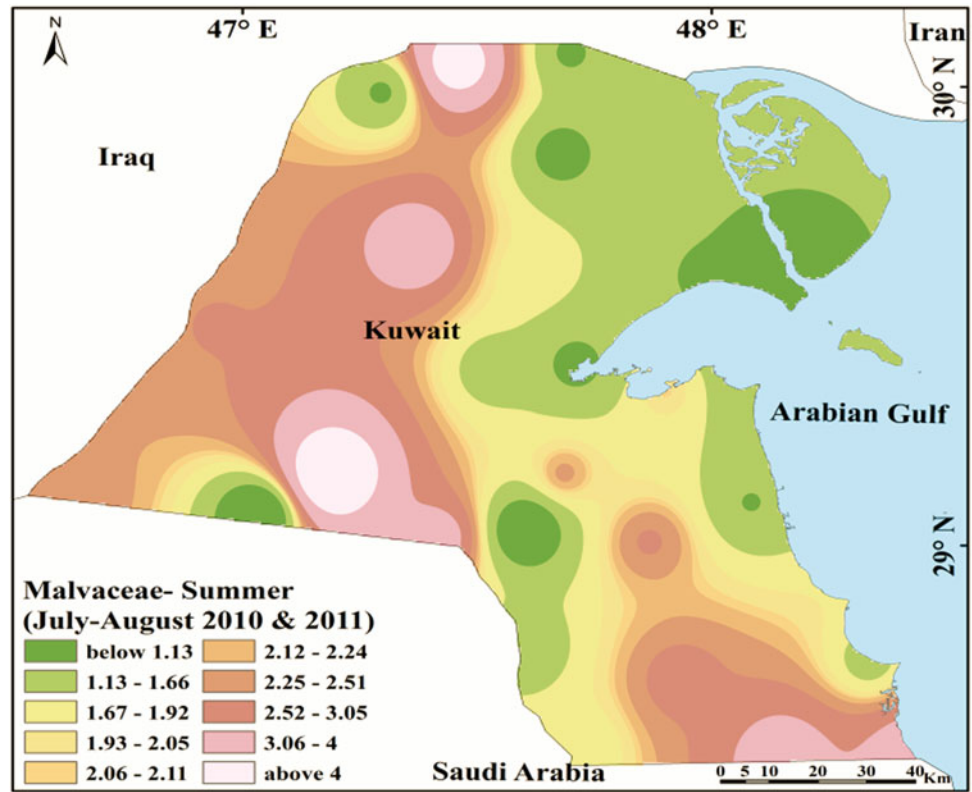
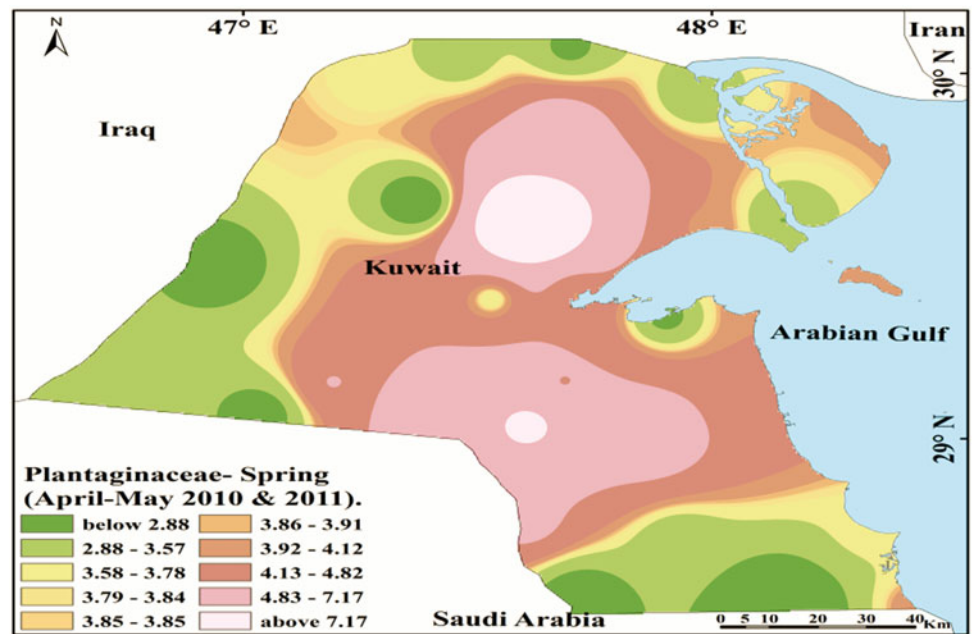


Fig. 7.22 Average percentages of *Plantaginaceae* pollen in dust. Spring (April–May 2010 and 2011)



Areas with high pollen in dust concentration	Areas with low pollen in dust concentration
Liyah Sulaybiyah Liyah Dibdibah Kabd	Ratqah Huwaymilyah Salmi Um Niqa Khiran

Plantaginaceae pollen originates mainly from *Plantago* species (*amplexicaulis*, *boissieri*, *ciliata*, *coronopus*, *lanceolata*, *notata*, *ovata*, and *psammophila*). In summer 2010, the highest counts were recorded for *Chenopodiaceae* (32.8%), followed by *Leguminosae* (23.2%), *Cyperaceae* (18.7%), *Gramineae* (11.5%), and *Plantaginaceae* (4.3%). The same trend was observed in summer 2011, with nearly the same dominance percentage (*Chenopodiaceae*, 33%; *Leguminosae*, 24%; *Cyperaceae*, 19.4%; *Gramineae*, 18.9%; and *Plantaginaceae*, 3.5%). The distribution of *Plantaginaceae* pollen was similar to that in spring. The highest counts were around Sabah Al-Ahmed National Reserve (a preserved area) (Fig. 7.23).

Areas with high pollen in dust concentration	Areas with low pollen in dust concentration
Liyah Kabd Um Eish Sulaybiyah Gudhi	Ratqah Salmi Abdulli Mutla Wafra Farm

Plantaginaceae pollens were majorly present in traps mainly containing *Plantago* species (*amplexicaulis*, *boissieri*, *ciliata*, *coronopus*, *lanceolata*, *notata*, *ovata*, and *psammophila*). In fall (October to November) 2010 and 2011, low pollen counts were observed for *Plantaginaceae* (7% and 5.7%, respectively). The lowest counts of *Plantaginaceae* were noted during fall, and it appeared only in preserved areas, such as Liyah, Kabd, and Shuaiba (Fig. 7.24).

Areas with high pollen in dust concentration	Areas with low pollen in dust concentration
Liyah Huwaymilyah Kabd Um Qudayr Shuaiba	Ratqah Abdulli Burqan Um Niqa Salmi

The local flora are the main source of the pollen load, and the concentration depends on the amount of vegetation around each station, except for very low percentages (2–3%) of *Pinaceae* pollen recorded in the north and northwest of Kuwait, which can be interpreted as being transported by the dominant northwesterly winds from regional sources. The nearest pine trees on the regional scale are situated in northern Iraq and Syria, and in Lebanon and Turkey (Fig. 7.25).

Fig. 7.23 Average percentages of *Plantaginaceae* pollen in dust. Summer (July–August 2010 and 2011)

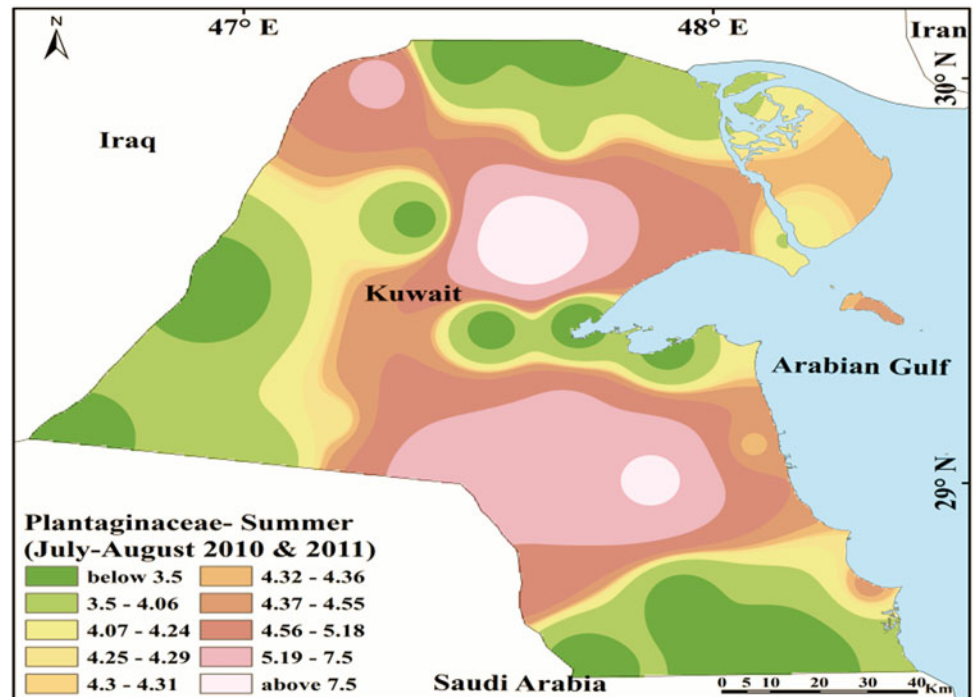


Fig. 7.24 Average percentages of *Plantaginaceae* pollen in dust, Autumn (October–November 2009 and 2010)

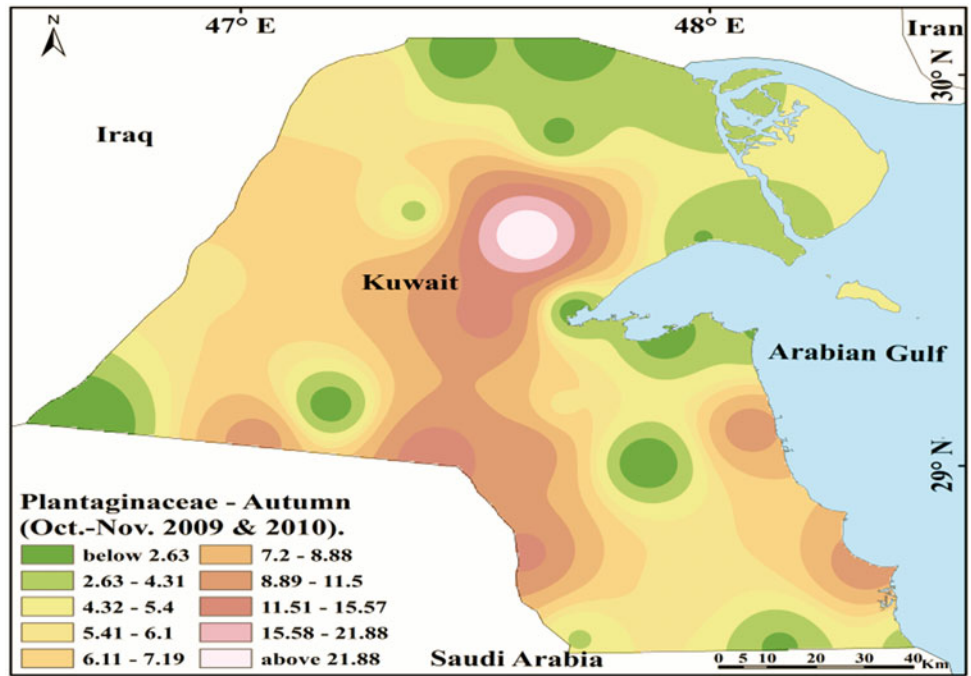
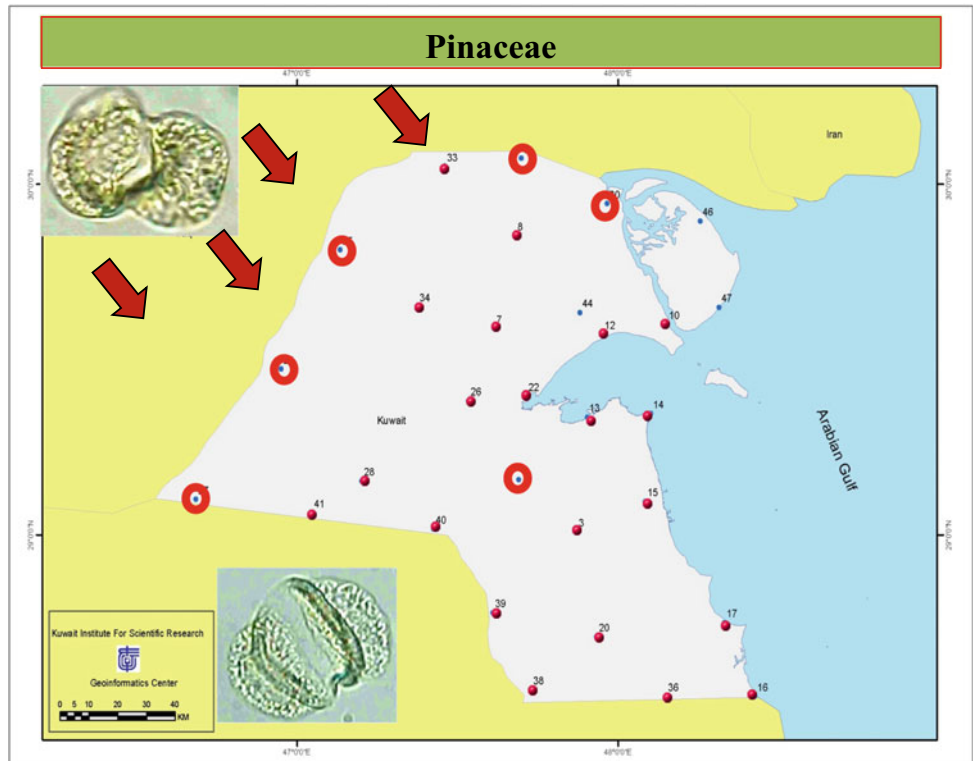


Fig. 7.25 Map showing the sites of *Pinaceae* pollen



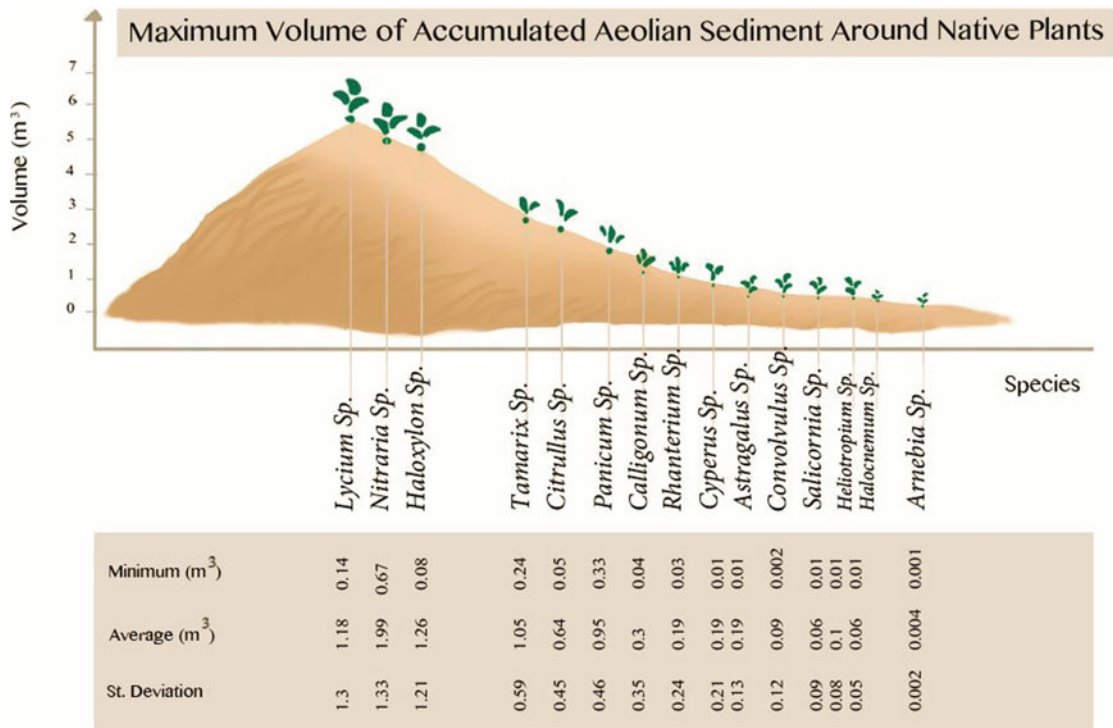
References

- Ahmed, M., & Al-Dousari, A. (2013). Geomorphological characteristics of the Um-Rimam depression in northern Kuwait. *Kuwait Journal of Science*, 40(1), 165–178.
- Al-Dousari, A. M., Ibrahim, M. I., Al-Dousari, N., Ahmed, M., & Al-Awadhi, S. (2018). Pollen in aeolian dust with relation to allergy and asthma in Kuwait. *Aerobiologia*, 34(3), 325–336. <https://doi.org/10.1007/s10453-018-9516-8>.
- Al-Dousari, A., Pye, K., Al-Hazza, A., et al. (2020). Nanosize inclusions as a fingerprint for aeolian sediments. *Journal of Nanoparticle Research*, 22, 94. <https://doi.org/10.1007/s11051-020-04825-7>.
- Al-Dousari et al. (2020b). Cost and effect of native vegetation change on aeolian sand, dust, microclimate and sustainable energy in Kuwait. *Journal of Taibah University for Science*. 14(1). <https://doi.org/10.1080/16583655.2020.1761662>.
- Dickson, V. (1955). *The wild flowers of Kuwait and Bahrain*. London: Allen and Unwin.
- Ergun, H. (1969). *Reconnaissance soil survey*. FAO/Ku/Tf, Kuwait: Report to the Government of Kuwait.
- Halwagy, R., & Halwagy, M. (1974). Ecological studies on the desert of Kuwait. II. The vegetation. *Journal of the University of Kuwait (Science)*, 1, 87–95.
- Kernick, M.D. (1966). Plant resources, range ecology and fodder plant introduction. Report to the Government of Kuwait, FAO, TA 181, Mimeograph. Kuwait.
- Macksad, A. M. (1969). The desert flowers of Kuwait. *Al-Arabi*, 132, 94–103. (in Arabic).
- Omar, S.A.S. (2000). *Vegetation of Kuwait—A comprehensive illustrative guide to the flora and ecology of the desert of Kuwait*. Kuwait Institute for Scientific Research. First edition, p. 159.
- Mohamed, D., Abdul, H. M., Kazmy, K. (1983). Descriptive analysis of asthma and their allergic diseases in Kuwait. In: Proceedings of 18th Middle East Regional Conference on International Union Against Tuberculosis, Ministry of Public Health, Kuwait (pp. 272–279).

Open Access This chapter is licensed under the terms of the Creative Commons Attribution 4.0 International License (<http://creativecommons.org/licenses/by/4.0/>), which permits use, sharing, adaptation, distribution and reproduction in any medium or format, as long as you give appropriate credit to the original author(s) and the source, provide a link to the Creative Commons licence and indicate if changes were made.

The images or other third party material in this chapter are included in the chapter's Creative Commons licence, unless indicated otherwise in a credit line to the material. If material is not included in the chapter's Creative Commons licence and your intended use is not permitted by statutory regulation or exceeds the permitted use, you will need to obtain permission directly from the copyright holder.







Other Properties (BET Surface Area, Conductivity, Organic Matter, and pH)

8

Modi Ahmed and Khaliq Beg

Abstract

- Brunauer, Emmett, and Teller (BET) test were applied to dust samples in which samples (BET) surface area is highly related to the roundness of dust particles. The higher angularity and low roundness of the dust particles show a higher (BET) surface area. The roundness is also related to the particle size distribution and mineralogical composition.
- The electrical conductivity test relates very well with the chemical and physical properties of dust samples in the transmission of an electrical current.
- The organic matter content was measured using the ignition method and the pH of the samples was recorded.
- Maps of the distribution of high and low BET concentrations, electrical conductivity EC, organic matter content, pH.

Methods

BET Surface Area

The BET surface area is a specific measurement of the area of the dust particle surface. BET surface area resolute BET through gas physical adsorption of the dust particle surface by calculating the mass of adsorbed gas corresponding to a monomolecular layer on the particle surface. The gas physical adsorption results from weak van der Waals forces between the adsorbent surface area of the tested dust particles and the adsorbed nitrogen gaseous molecules. The determination is frequently carried out at the temperature of liquid nitrogen. The mass of gas adsorbed can be determined by either a volumetric or continuous flow process. The measurement of the BET surface area for dust particles was made using a COULTER-SA 3100 (Fig 8.1).

M. Ahmed (✉) · K. Beg
Crisis Descision Supports Program (CDS), Environment & Life
Sciences Research Center (ELSRC), Kuwait Institute for Scientific
Research (KISR), P.O. Box: 24885 Safat, 13109, Kuwait
e-mail: mmahmed@kISR.edu.kw

K. Beg
e-mail: krbeg@kISR.edu.kw

© The Author(s) 2021
A. Al-Dousari (ed.), *Atlas of Fallen Dust in Kuwait*,
https://doi.org/10.1007/978-3-030-66977-5_8



Fig. 8.1 COULTER-3100 for measuring the BET surface area for dust particles

Electrical Conductivity

Electrical conductivity is a measurement that relates very well with the chemical and physical properties of dust samples. Electrical conductivity is the capability of a sample to transmit an electrical current, and it is normally expressed in units of deciSiemens per meter (dS/m). The electrical conductivity measurements can be expressed in milliSiemens per meter (mS/m) also, which is 100 times less than deciSiemens per meter.

pH

The dust samples were mixed in 125 ml of distilled water. The mixture was shaken in an electrical shaker for one hour and then left to settle for one hour. The resulting suspension was used for pH determination (Fig 8.2).



Fig. 8.2 Conductivity and pH meter used for dust samples

Organic Matter

The organic matter was measured using the ignition method, in which the dust sample was weighed, dried in an oven at 60 C for 24 h, weighed again, and then washed in a muffle

furnace at 400 °C for four hours. The organic matter was calculated by using the difference of the initial weight and the final weight multiplied by 100/58. Organic matter % = organic carbon % \times 11/58.

BET-Surface Area

The BET surface area is highly related to the roundness of dust particles. The higher angularity and low roundness of the dust particles reveal a higher BET surface area. The roundness is also related to the particle size distribution and mineralogical composition. Dust samples with smaller size fractions and lower quartz percentages have higher values of BET surface area. The dust samples in the northeastern part of Kuwait and near the coastal area have higher BET surface areas, with values of more than 12 m²/g. This result is attributed to geographical reasons, as those areas with high BET surface area are close to the Mesopotamian Floodplain and Al-Ahwar areas in Iraq, as dust coming from those areas is low in quartz and high in carbonates, feldspars, clay, and heavy minerals. Furthermore, the dust samples in summertime are expected to have a low BET surface area compared with winter (Fig. 8.3).

Areas with high BET concentration	Areas with low BET concentration
Abdulli Subiyah Jal Al Zur Khiran Sulaybiyah	Warba Island Khur Fawaris Shegaya Dibdibah Mutla

Conductivity

Electrical conductivity (EC) is a measurement of the dissolved material associated with or attached to dust samples, which relates to the ability of the material to conduct an electrical current. More salt or evaporated minerals, such as halite, gypsum, and anhydrite, cause higher values of EC. High conductivity is present on Bubiyan Island and the southern sector of Kuwait, as most sabkhas are present. Sabkhas contain salt minerals that cause an increase in conductivity. The areas extending from Jirashan in the northwest, near the Iraqi border, to northern Kuwait Bay displayed minimum values of conductivity readings (Fig. 8.4).

Areas with high conductivity concentration	Areas with low conductivity concentration
Bubiyan Island Failaka Island Kabd Um Qudayr Khur Fawaris	Warba Island Liyah Shegaya Jal Al Zur Mutla

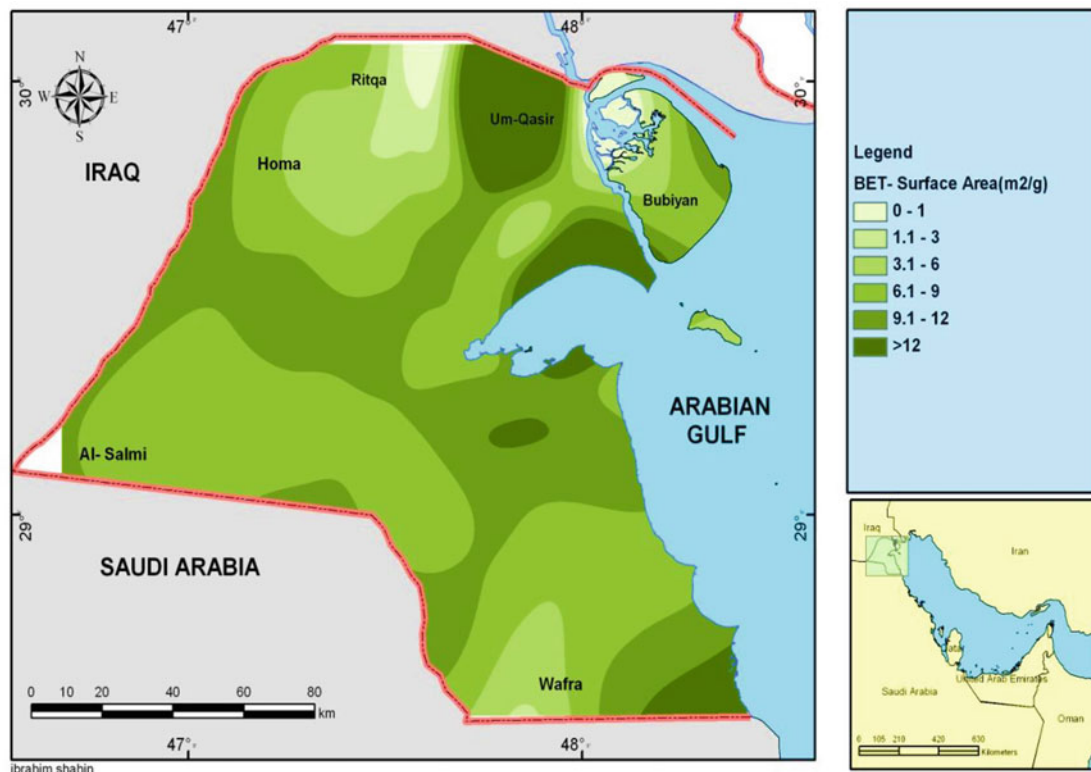


Fig. 8.3 Surface area distribution of dust in Kuwait

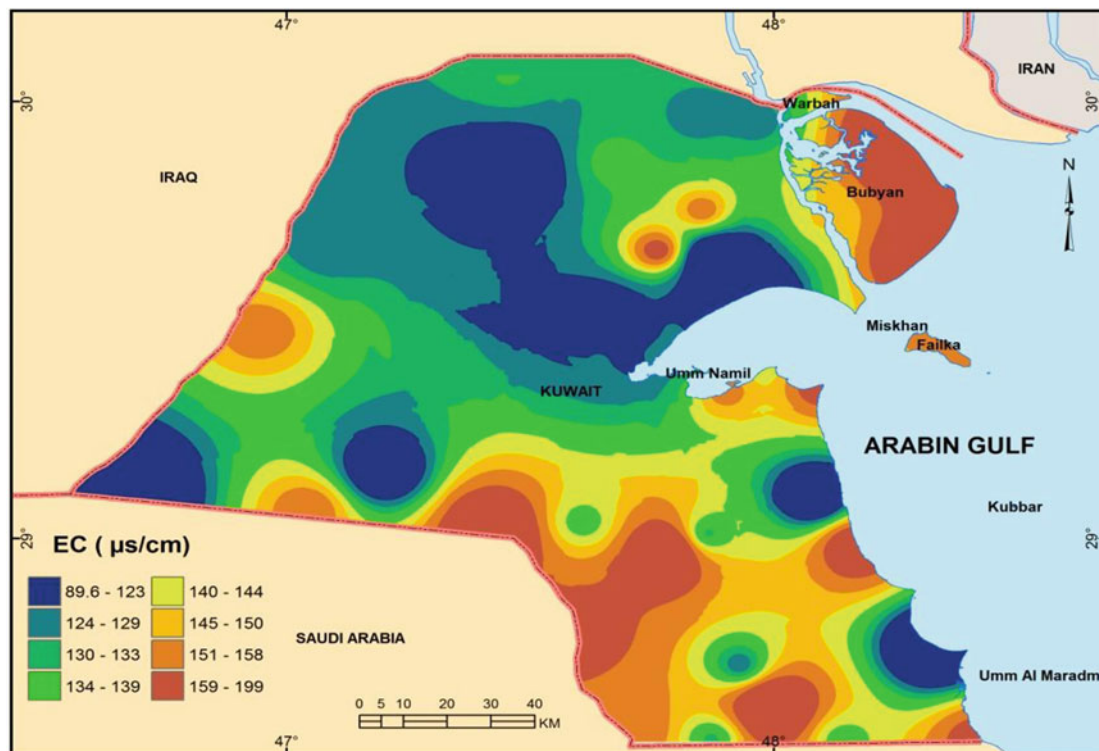


Fig. 8.4 Conductivity area distribution for dust in Kuwait

Organic Matter

Organic matter is measured with reference to the total weight percentage for the dust samples. The values were restricted, from 1.38% to about 9%. The highest percentages of dust values containing organic matter within the dust samples were in the northeastern part of Kuwait and around farms. The presence of high organic matter percentages in dust samples collected in the northeastern parts of Kuwait is attributed to the type of dust, which mostly originates from the Mesopotamian Floodplain. Lower percentages were in the west and northwest of Kuwait. Compared with other dust

in the world, deposited dust in Kuwait can be classified as being rich in organic matter. Therefore, dust plays a major role in maintaining the ecological system in the region, and the organic matter in dust is essential, mainly to the marine environment (Fig. 8.5).

Areas with high organic matter concentration	Areas with low organic matter concentration
Bubiyan Island	Ubayriq
Dibdibah	Khur Fawaris
Um Niqa	Salmi
Failaka Island	Shegaya
Wafra Farms	Burqan

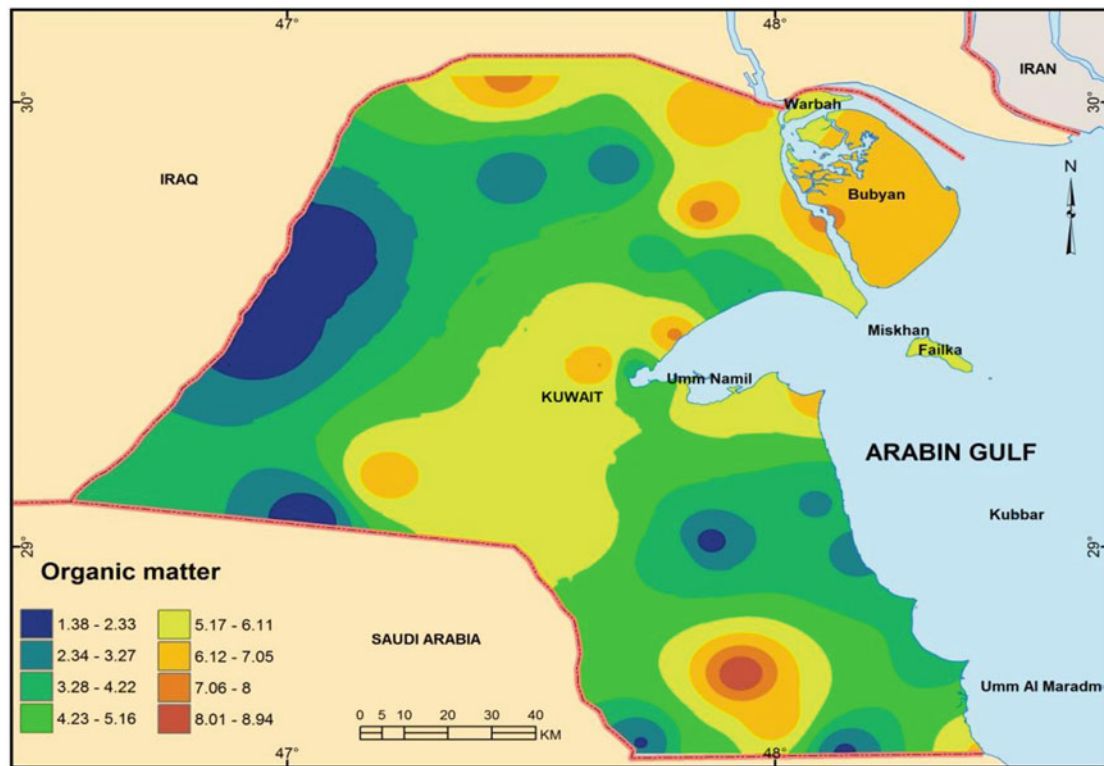


Fig. 8.5 Organic matter area distribution for dust in Kuwait

pH

The dust is more basic than acidic. The variation in pH values is from 7.4 to 8.1. The highest values are present in three areas, namely Huwamilyah, Um Al-Qawatti, and Atrah, while the lowest are present in Jirashan, Shuaiba, Khur Fawaris, and Um Niqa.

These results might indicate that dust occurring in the northwest, from the Western Desert of Iraq, is more basic than the dust coming from other directions, mainly the

Mesopotamian Foodplain, Iran, and Saudi sides. The pH level might be related to humidity, as Saudi source areas of dust are more humid (Fig. 8.6).

Areas with high Ph concentration	Areas with low Ph concentration
Bubiyah Island	Shuaiba
Huwaymilyah	Khur Fawaris
Khiran	Ratqah
Atrah	Dibdibah
Um Al-Qawatti	Um Niqa

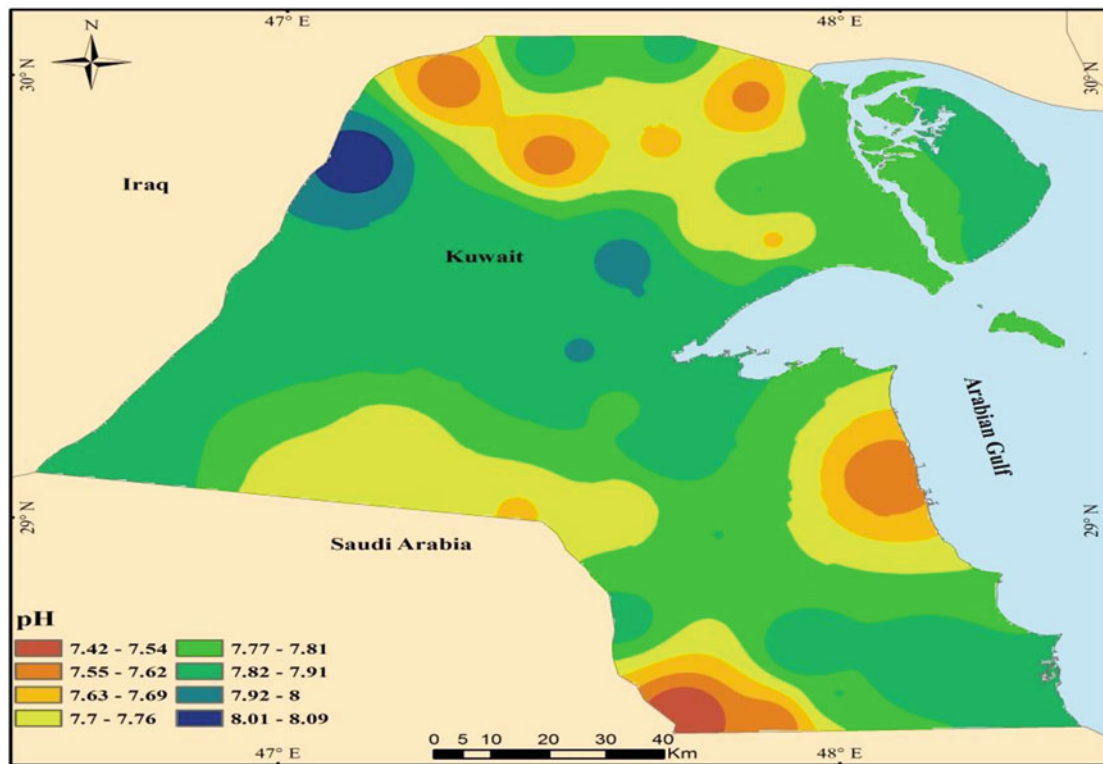
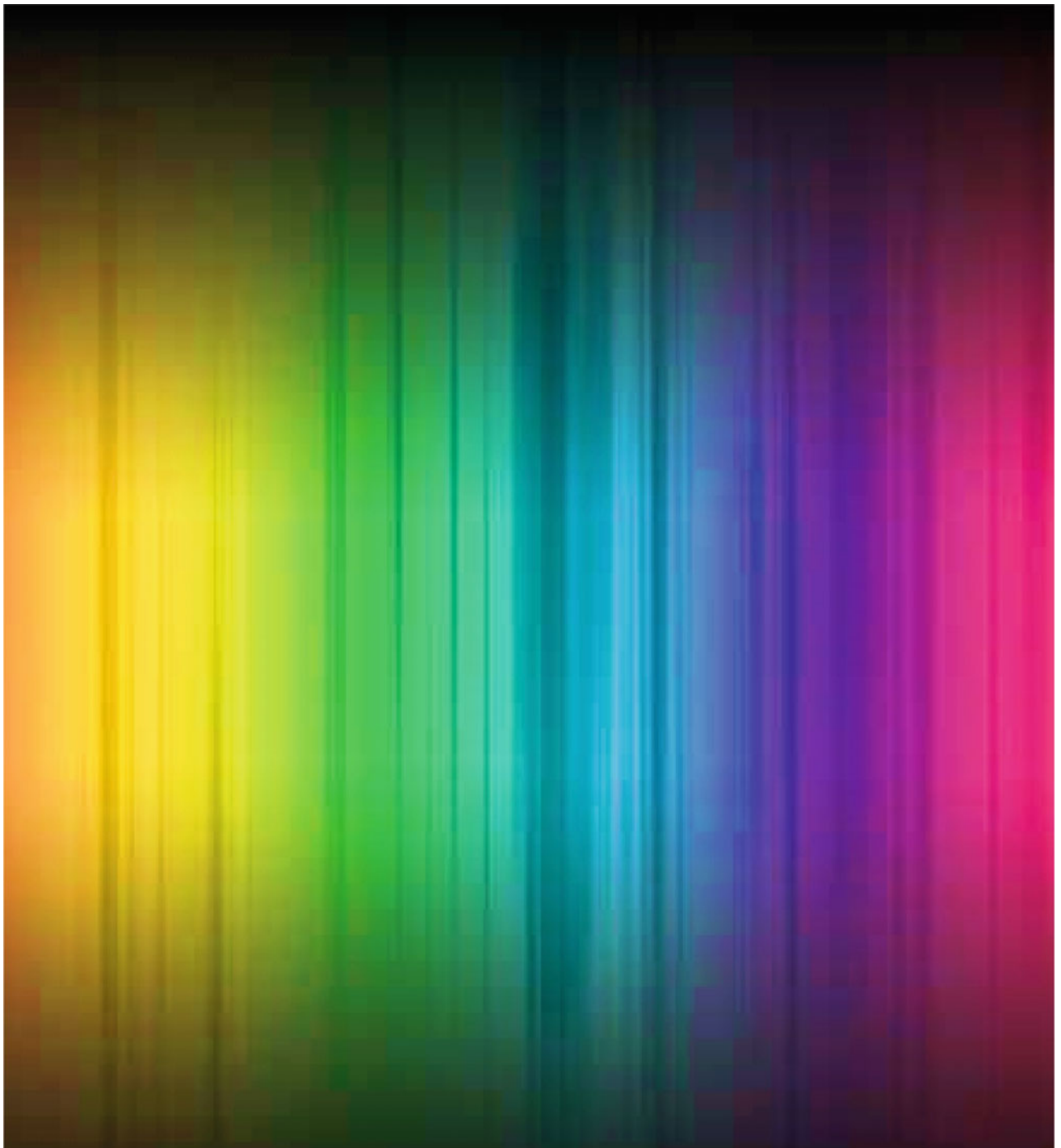


Fig. 8.6 Ph distribution for dust in Kuwait

Open Access This chapter is licensed under the terms of the Creative Commons Attribution 4.0 International License (<http://creativecommons.org/licenses/by/4.0/>), which permits use, sharing, adaptation, distribution and reproduction in any medium or format, as long as you give appropriate credit to the original author(s) and the source, provide a link to the Creative Commons licence and indicate if changes were made.

The images or other third party material in this chapter are included in the chapter's Creative Commons licence, unless indicated otherwise in a credit line to the material. If material is not included in the chapter's Creative Commons licence and your intended use is not permitted by statutory regulation or exceeds the permitted use, you will need to obtain permission directly from the copyright holder.





Abstract

- Ultraviolet–visible UV-VIS. Varian Bio Cary 100 UV–VIS instrument was used for measuring the spectrum of dust samples.
- The certified materials according to Lab sphere SRS. 99–020 were used and the dust samples were placed in a cuvette (10 mm) and placed on the diffuse reflectance accessory.
- Measurement was done with respect to the reference. The UV–VIS spectra cover the regions from 900 to 190 nm which includes the near-infrared region, visible light regions, and ultraviolet regions.
- The FT-IR data shows the different chemical content of dust in the scanning of what possible compounds can be found in dust particles for required further analysis.
- The dust absorption of the light spectrum in Kuwait was revealed in maps according to seasons showing higher and lower concentrations of light absorption of ultraviolet, violet, blue, cyan, green, yellow, orange, red, infrared.

S. Al-Awadhi (✉)
 Crisis Decision Supports Program (CDS), Environment and Life Sciences Research Center (ELSRC), Kuwait Institute for Scientific Research (KISR), P. O. Box. 24885 Kuwait City, Safat 13109, Kuwait
 e-mail: smawadhi@kISR.edu.kw

M. Al-Shemali
 Environmental Pollution and Climate Program (EPCP), Environment and Life Sciences Research Center (ELSRC), Kuwait Institute for Scientific Research (KISR), Kuwait City, Kuwait
 e-mail: mshamali@kISR.edu.kw

Introduction

Sun produces different types of radiation that travel through space to the earth, as well as to other planets in the solar system. The atmospheric layers protect the earth from much of this radiation. Some radiation penetrates the atmosphere to reach the earth, however, such as infrared, visible light, ultraviolet rays, and etc.

A small amount of solar radiation is essential for many chemical life reactions for humans; however, when animals and plants are exposed to high doses of radiation, this is harmful. For example, sunstroke occurs when humans are exposed to long periods of solar radiation, and it can cause death. In other cases, such exposure causes skin burns and cancer. Drying plants occur when plants are exposed to the sun for long periods, in addition to facing hot winds during the summer (Al-Enezi et al. 2014; Al-Dousari et al. 2016).

Dust helps to protect the earth by absorbing and reflecting some of the sun's radiation, which explains why, when a dust storm is heavy and lasts for a long period, the temperature is reduced. The absorbance of light depends on the constituent compounds of dust. The dust compound depends on the culture of the areas the carrier wind crosses. Although dust causes many problems, such as reduced vision sight and breathing issues (Al-Dousari et al. 2014; Subramaniam et al. 2015; Subramaniam and Al-Dousari 2014), it reduces the sun's heat and direct interaction with objects on earth. Below are maps that illustrate dust absorption of the sunlight during different seasons in Kuwait.

Methodology

Ultraviolet–visible UV–VIS. The Varian Bio Cary 100 UV–VIS instrument was used to measure the spectrum of dust samples. First, the certified material's (Lab sphere SRS. 99–020) background was taken. Second, the dust samples were put in a cuvette (10 mm) and placed on the diffuse

reflectance accessory. Finally, the measurement was made with respect to the reference. The UV–VIS spectra cover the regions from 900 to 190 nm, which include the near-infrared region, visible light regions, and ultraviolet regions. The data were analyzed using Microsoft Excel to extract the maximum absorption of light radiation frequency.

Furrier Transformer Mid-Infrared FT-MID. The Victor 22 BRUKER instrument was used for this experiment. First, the KBr powder was ground and transferred to the diffuse reflectance holder, then the powder was pressed with a flat plate. Second, the holder was placed inside the experiment accessory installed inside the instrument. Third, the background experiment was run on KBr. Fourth, a very small portion of dust was mixed with ground KBr powder. Finally, the mixture was transferred to the experiment holder and pressed to be measured against the KBr background spectrum. The spectra covered the normal MID-infrared region, from 4000 cm^{-1} to 400 cm^{-1} .

UV Absorption Summer 2010

The ultraviolet light absorbed in summer varies throughout Kuwait. The dust shows a high absorption to UV light near the coast of Kuwait Bay (collector D22 in Kathma) and at Sabah Al-Ahmad Nature Reserve (collector D44 and D45). Along the border with Iraq, the absorption of UV light was very low at dust collector D25 and South Buffer zone D32 (Homa) and D33 (Ritqa). Similarly, the borderline with Saudi Arabia in the southeast border at collector D20 Wafra animal farm, D18 Ras Zur-Wafra, D16 Nuwaisieb, D27 Salmi border zone, and D28 Poultry mid-way Salmi road Abraq all displayed low absorption of UV. In general, the area near Kuwait Bay, which covers Kuwait City and Hawalli City, had a high absorption of UV. The absorbance rate began to reduce toward Jahra City in the north and Ahmadi in the south. The chemical content of the dust near Kuwait Bay has the ability in summer to absorb more UV light than the dust in areas farther away (Fig. 9.1).

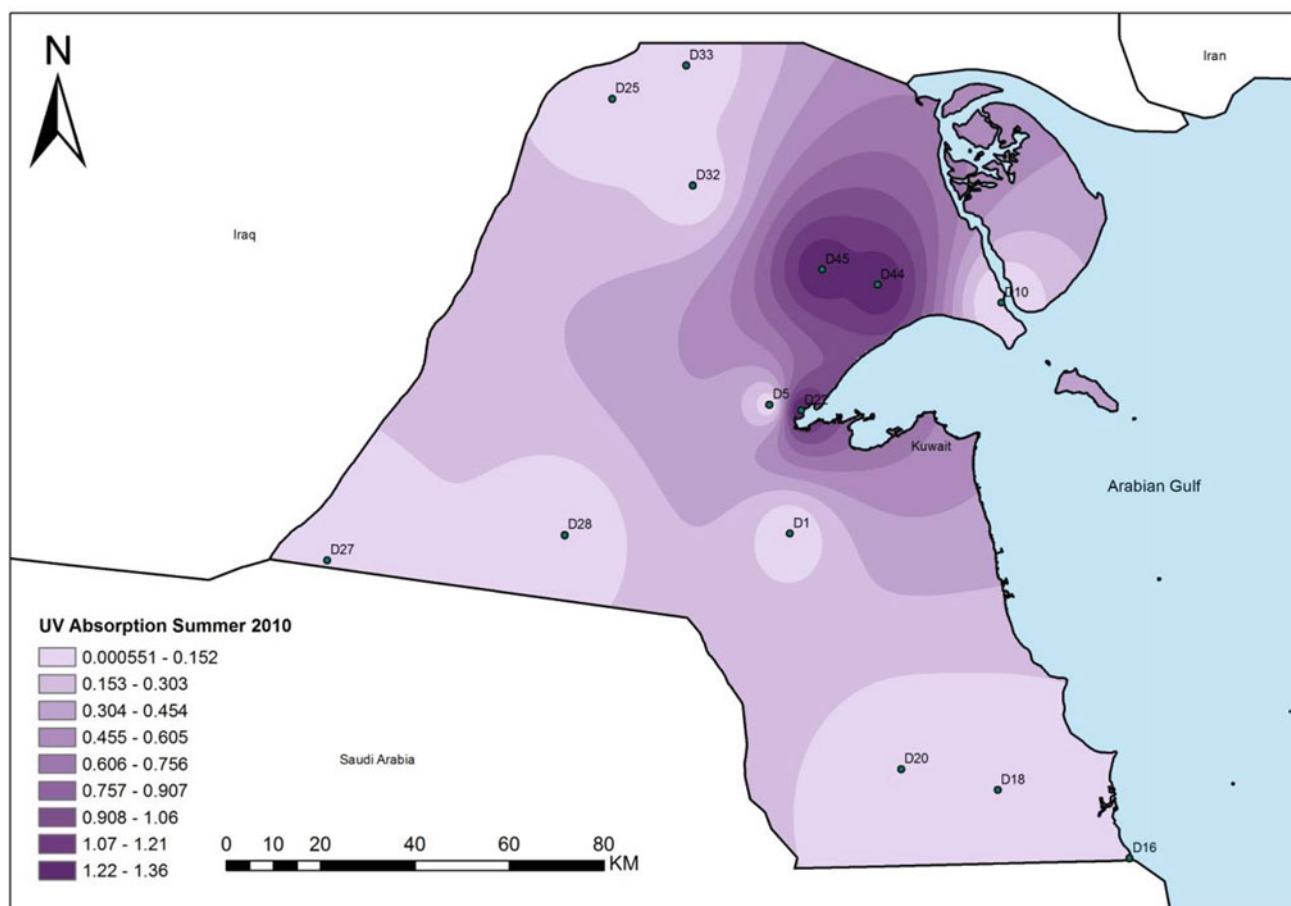


Fig. 9.1 Dust absorption of ultraviolet light in summer 2010

Violet Absorption Summer

The absorbed violet light in summer varies throughout Kuwait. The dust shows high absorption to violet light at Sabah Al-Ahmad Nature Reserve (collectors D44 and D45) and begins to reduce near the coast at Kuwait Bay (collector D22 in Kathma). On the border with Iraq, the absorption of violet light was very low at dust collector D25, the South Buffer zone, D32 Homa, and D33 Ritqa, and on the borderline with Saudi Arabia

in the southeast borders at collector D20 Wafra animal farm, D18 Ras Zur-Wafra, D16 Nuwaissieb, D27 Salmi border zone, D28 Poultry mid-way Salmi road Abra. In general, the area near Kuwait Bay, which covers Kuwait City and Hawalli City, had high absorption of UV. This absorbance capacity begins to reduce toward Jahra City in the north and Ahmadi in the south. The chemical content of the dust near Kuwait Bay has the ability in summer to absorb more violet light than the dust in areas that are situated farther away (Fig. 9.2).

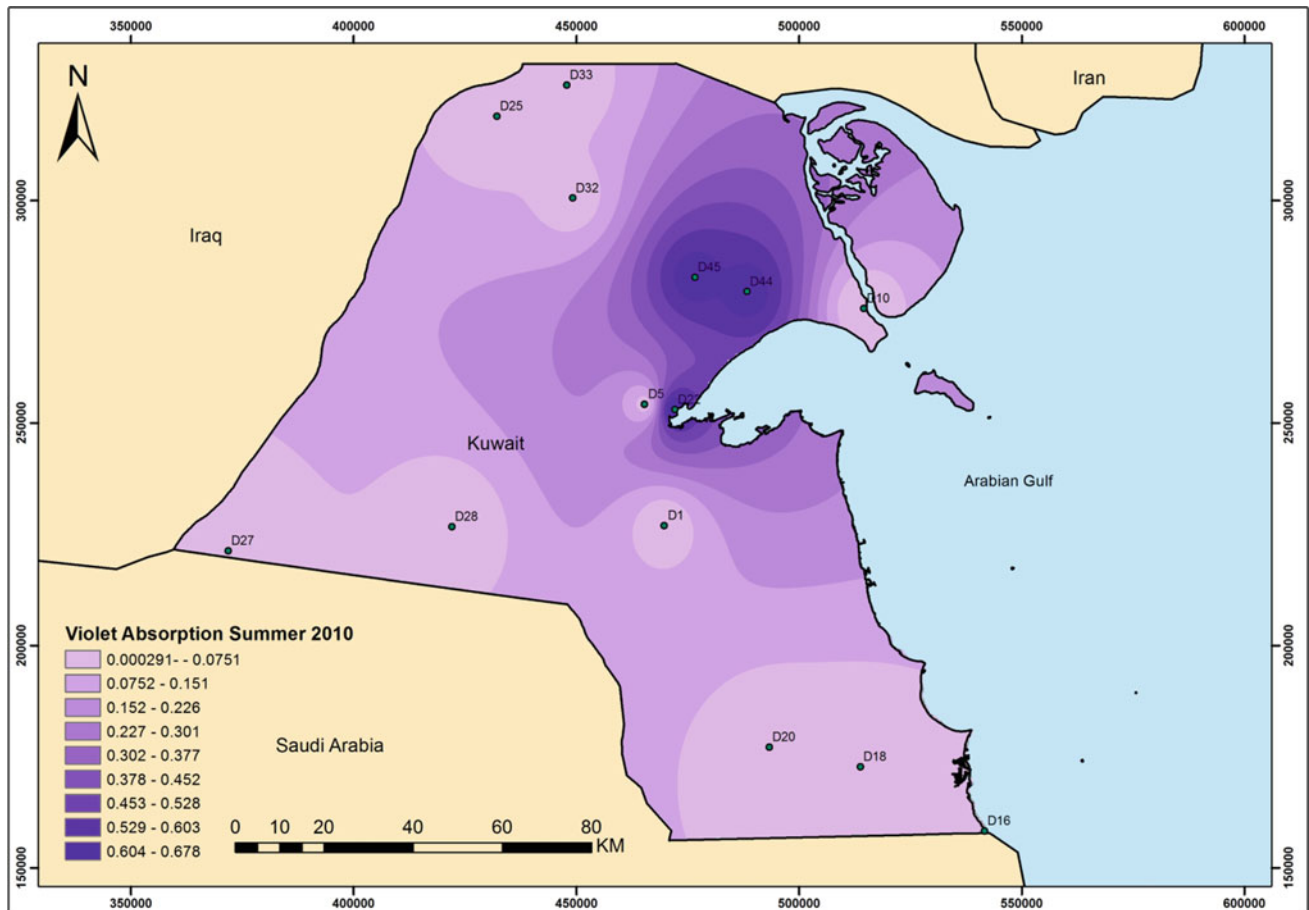


Fig. 9.2 Dust absorption of violet light in summer 2010

Blue Absorption Summer

The blue light in absorbed summer varies throughout Kuwait. The dust shows high absorption of the blue light at Sabah Al-Ahmad Nature Reserve (collectors D44 and D45) and begins to reduce near the coast at Kuwait Bay (collector D22 in Kathma). On the border with Iraq, the absorption of blue light was very low at collector D25 South Buffer zone, D32 Homa, and D33 Ritqa, and along the border with Iraq.

The southeast borders at collector D20 Wafra animal farm, D18 Ras Zur-Wafra, D16 Nuwaissieb, D27 Salmi border zone, D28 Poultry mid-way Salmi road Abraç all had low absorption of blue light also. In general, the area near Kuwait Bay, including Kuwait City and Hawalli, had high absorbance, which begins to reduce toward Jahra in the north and Ahmadi in the south. The chemical content of the dust near Kuwait Bay has the ability in summer to absorb more blue light in the dust than areas farther away (Fig. 9.3).

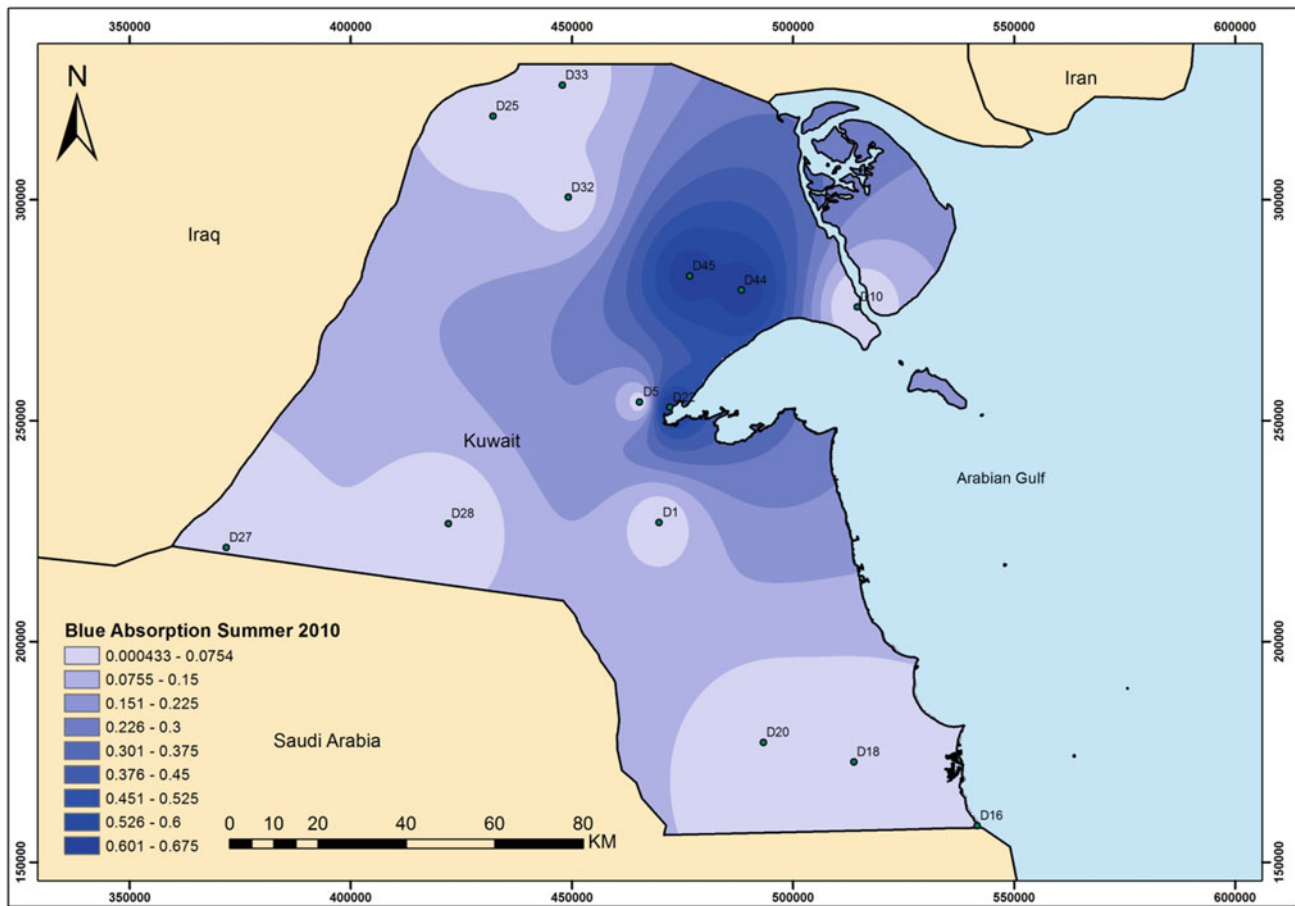


Fig. 9.3 Dust absorption of blue light in summer 2010

Cyan Absorption Summer 2010

The cyan light absorbed in summer varies throughout Kuwait. The dust shows high absorption of cyan light at Sabah Al-Ahmad Natural Reserve (collectors D44 and D45), and it begins to reduce near the coastal side of Kuwait Bay (collector D22 in Kathma). On the border with Iraq, the absorption of cyan light was very low at collector D25 South Buffer zone, D32 Homa, and D33 Ritqa. The same tendency is apparent on the borderline with Saudi

Arabia along southeast borders at collector D20 Wafra animal farm, D18 Ras Zur-Wafra, D16 Nuwaissieb, D27 Salmi border zone, and D28 Poultry mid-way Salmi road Abraaq. In general, the area near Kuwait Bay, which covers Kuwait City and Hawalli, had a high absorbance of cyan light. The absorbance capacity starts to reduce toward Jahra City in north and Ahmadi in the south. The chemical content of the dust near Kuwait Bay has the ability to absorb more cyan light in the summer than in areas that are farther away (Fig. 9.4).

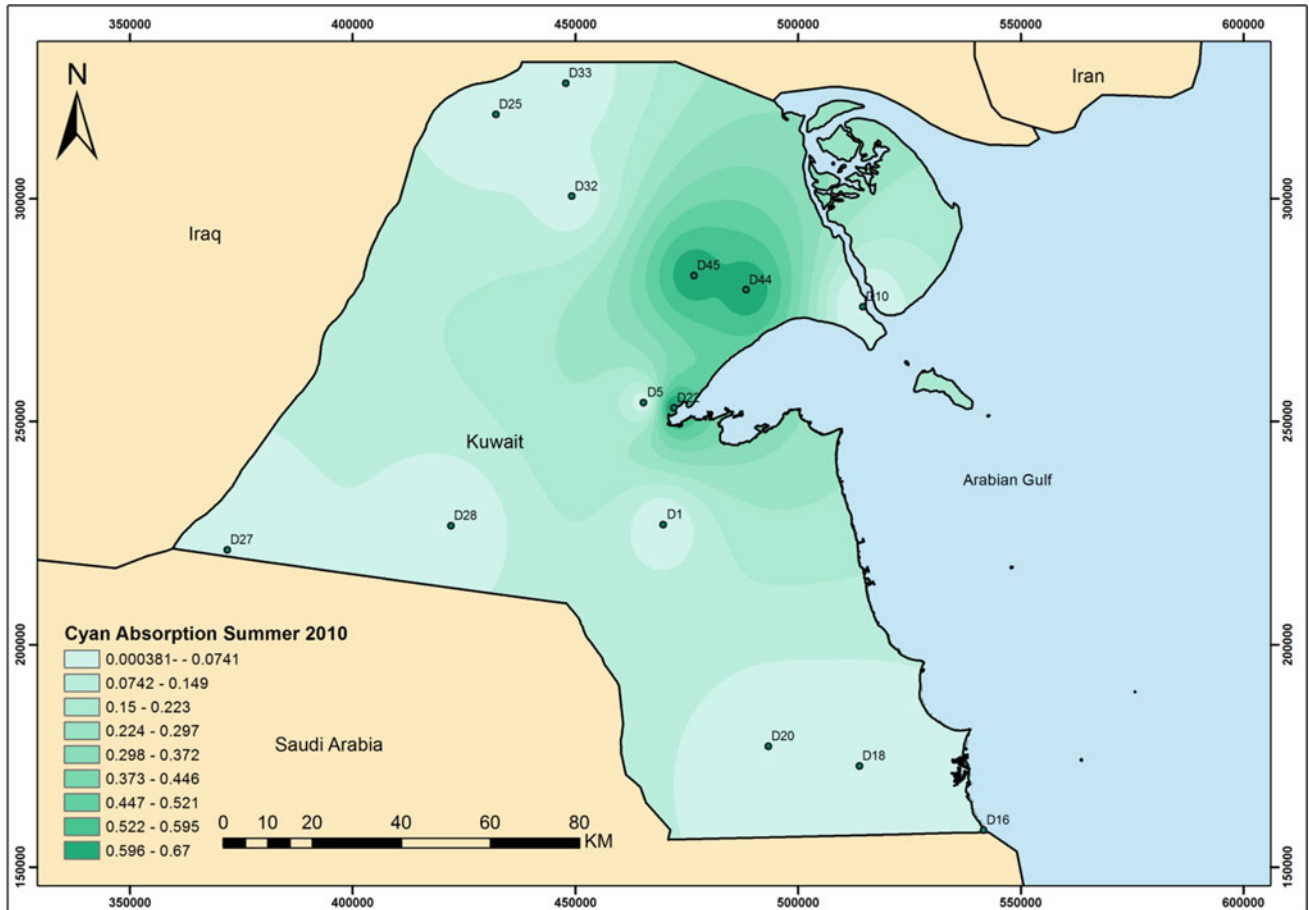


Fig. 9.4 Dust absorption of cyan light in summer 2010

Green Absorption Summer 2010

The green light absorbed in summer varies throughout Kuwait. The dust shows a high absorption of green light at Sabah Al-Ahmad Nature Reserve (collectors D44 and D45) and begins to reduce near the coastal side Kuwait Bay (collector D22 in Kathma). On the border with Iraq, the absorption of green light was very low at collector D25 South Buffer zone, D32 Homa, and D33 Ritqa, as well as on the borderline with Saudi Arabia along the southeast

borders at collector D20 Wafra animal farm, D18 Ras Zur-Wafra, D16 Nuwaissieb, D27 Salmi border zone, and D28 Poultry mid-way Salmi road Abra. In general, the area near Kuwait Bay, which covers Kuwait City and Hawalli, had a high absorbance of green light. The absorbance capacity starts to reduce toward Jahra City in north and Ahmadi in the south. The chemical content of the dust near Kuwait Bay has the ability to absorb more green light in the summer than in areas that are farther away (Fig. 9.5).

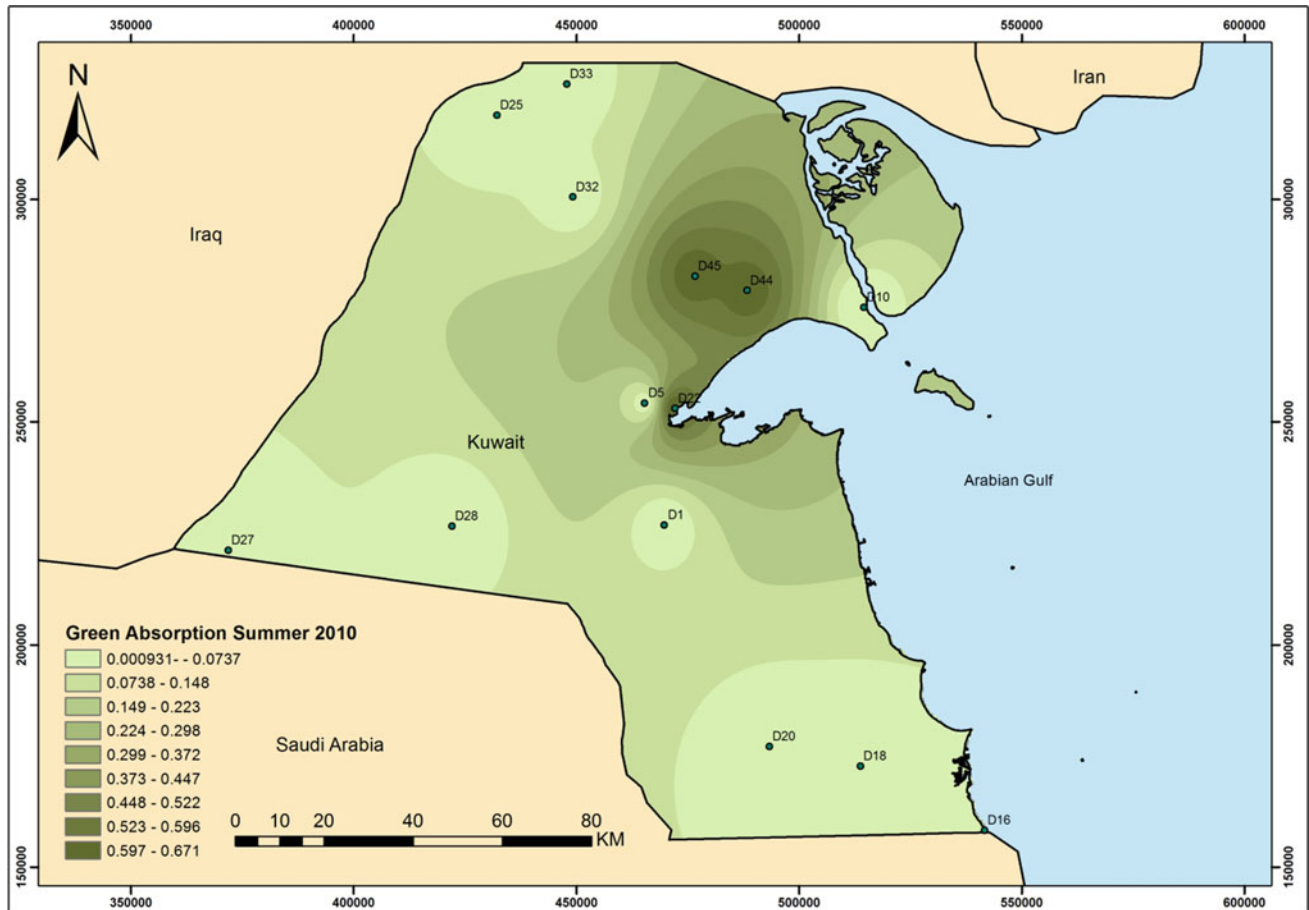


Fig. 9.5 Dust absorption of green light in summer 2010

Yellow Absorption Summer 2010

The yellow light absorbed in summer varies throughout Kuwait. The dust particles show a high absorption of yellow light at Sabah Al-Ahmad Nature Reserve (collectors D44 and D45) that begins to reduce near the coastal side Kuwait Bay (collector D22 in Kathma). On the border with Iraq, the absorption of yellow light was very low at collector D25 South Buffer zone, D32 Homa, and D33 Ritqa, as well as on the borderline with Saudi Arabia along the

southeast borders at collector D20 Wafra animal farm, D18 Ras Zur-Wafra, D16 Nuwaissieb, D27 Salmi border zone, D28 Poultry mid-way Salmi road Abra. In general, the area near Kuwait Bay, which covers Kuwait City and Hawalli, had a high absorbance of yellow light. The absorbance capacity starts to reduce toward Jahra City in north and Ahmadi in the south. The chemical content of the dust near Kuwait Bay has the ability to absorb more yellow light in the summer than in areas that are farther away (Fig. 9.6).

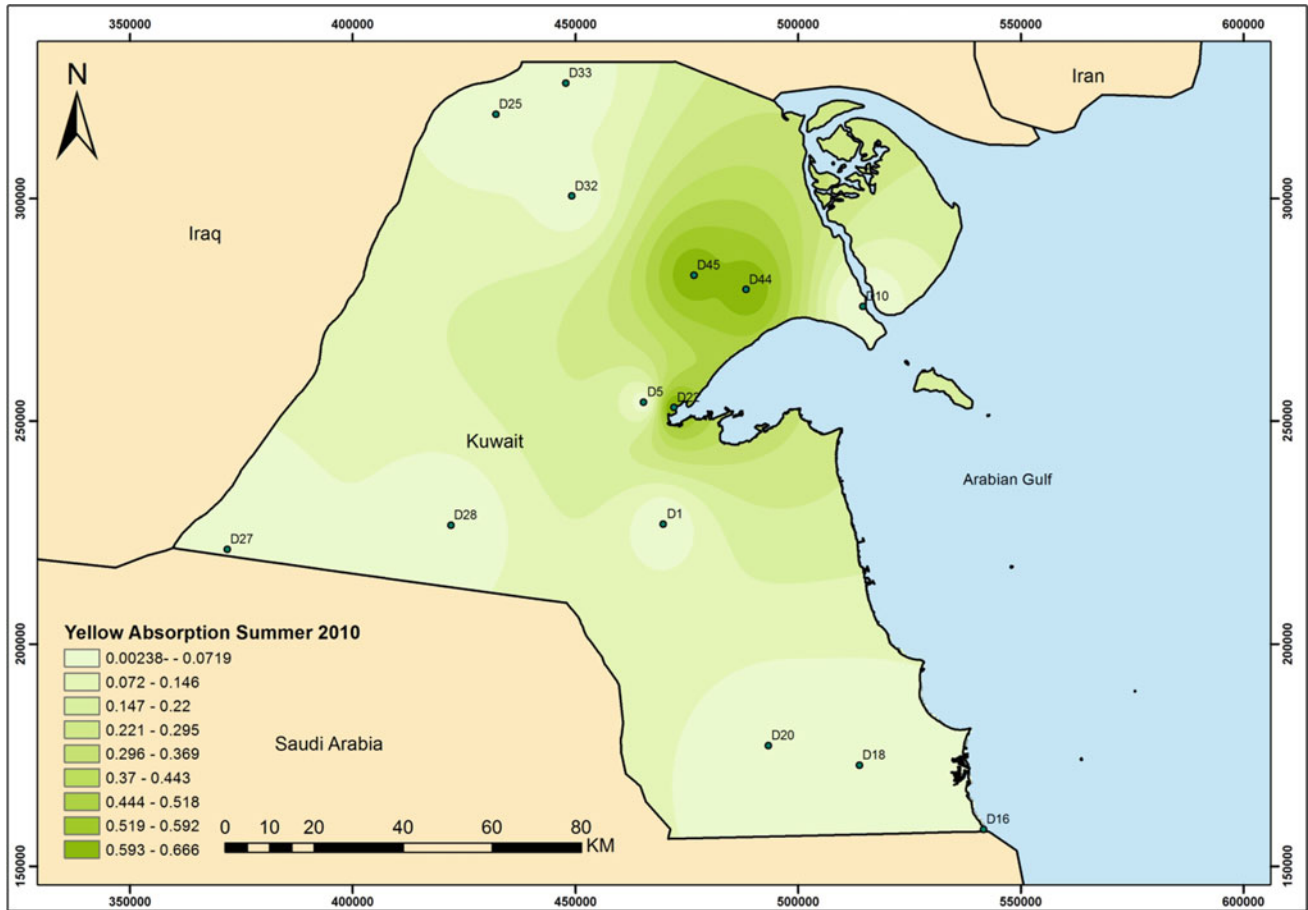


Fig. 9.6 Dust absorption of yellow light in summer 2010

Orange Absorption Summer 2010

The orange light absorbed in summer varies throughout Kuwait. The dust shows high absorption of orange light at Sabah Al-Ahmad Nature Reserve (collectors D44 and D45) and it begins to reduce near the coastal side of Kuwait Bay (collector D22 in Kathma). On the border with Iraq, the absorption of orange light was very low at collector D25 South Buffer zone, D32 Homa, and D33 Ritqa, as well as on the borderline with Saudi Arabia along the southeast

borders at collector D20 Wafra animal farm, D18 Ras Zur-Wafra, D16 Nuwaissieb, D27 Salmi border zone, and D28 Poultry mid-way Salmi road Abraaq. In general, the area near Kuwait Bay, which covers Kuwait City and Hawalli, had a high absorbance of orange light. The absorbance capacity starts to reduce toward Jahra City in north and Ahmadi in the south. The chemical content of the dust near Kuwait Bay has the ability to absorb more orange light in the summer than in areas that are farther away (Fig. 9.7).

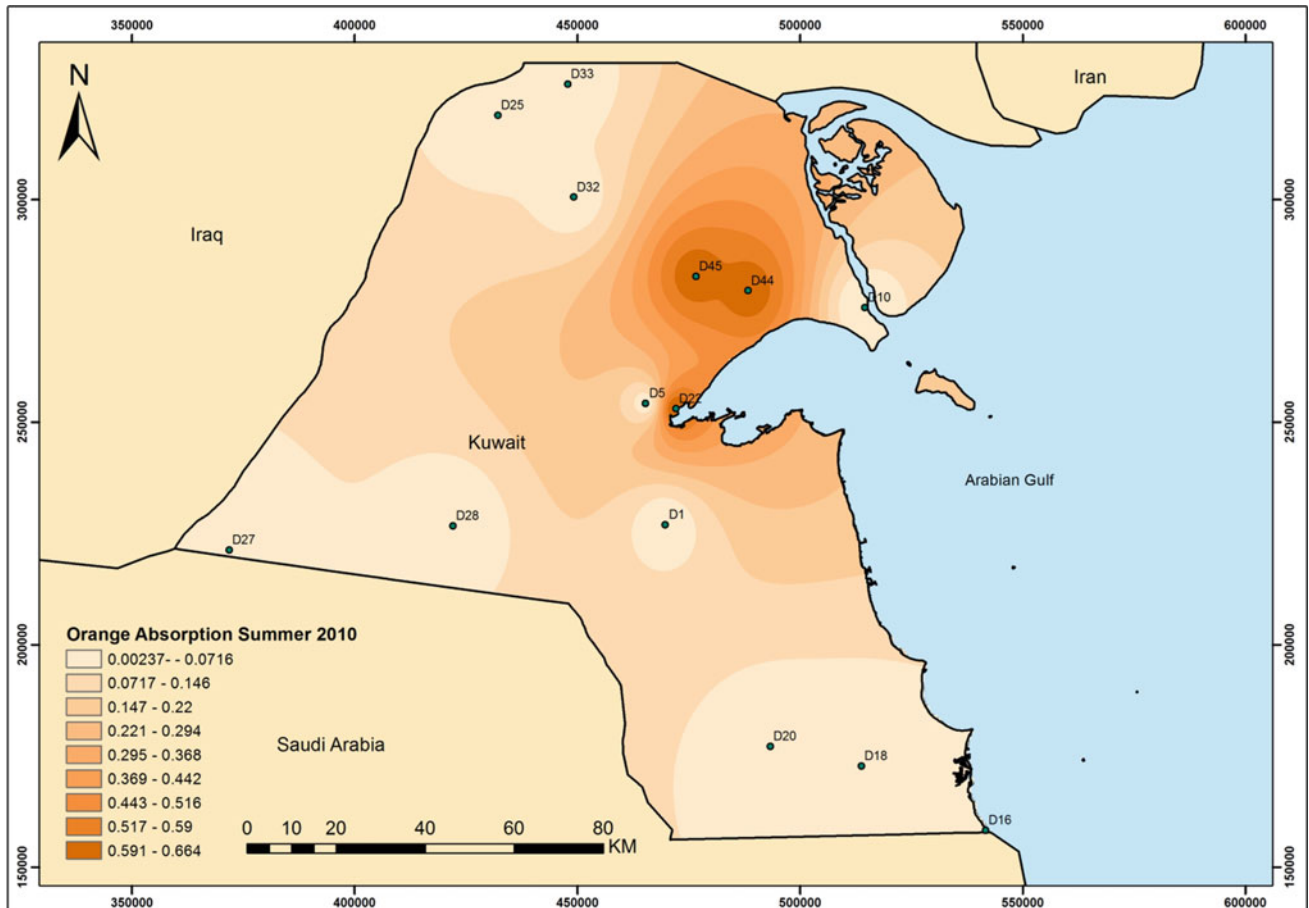


Fig. 9.7 Dust absorption of orange light in summer 2010

Red Absorption Summer 2010

The red light absorbed in summer varies throughout Kuwait. The dust shows high absorption of red light at Sabah Al-Ahmad Nature Reserve (collectors D44 and D45) and begins to reduce near the coastal side Kuwait Bay (collector D22 in Kathma). On the border with Iraq, the absorption of red light was very low at collector D25 South Buffer zone, D32 Homa, and D33 Ritqa, as well as on borderline with Saudi

Arabia along the southeast borders at collector D20 Wafra animal farm, D18 Ras Zur-Wafra, D16 Nuwaissieb, D27 Salmi border zone, and D28 Poultry mid-way Salmi road Abraaq. In general, the area near Kuwait Bay, which covers Kuwait City and Hawalli, had a high absorbance of red light. The absorbance capacity starts to reduce toward Jahra City in north and Ahmadi in the south. The chemical content of the dust near Kuwait Bay has the ability to absorb more red light in the summer than in areas that are farther away (Fig. 9.8).

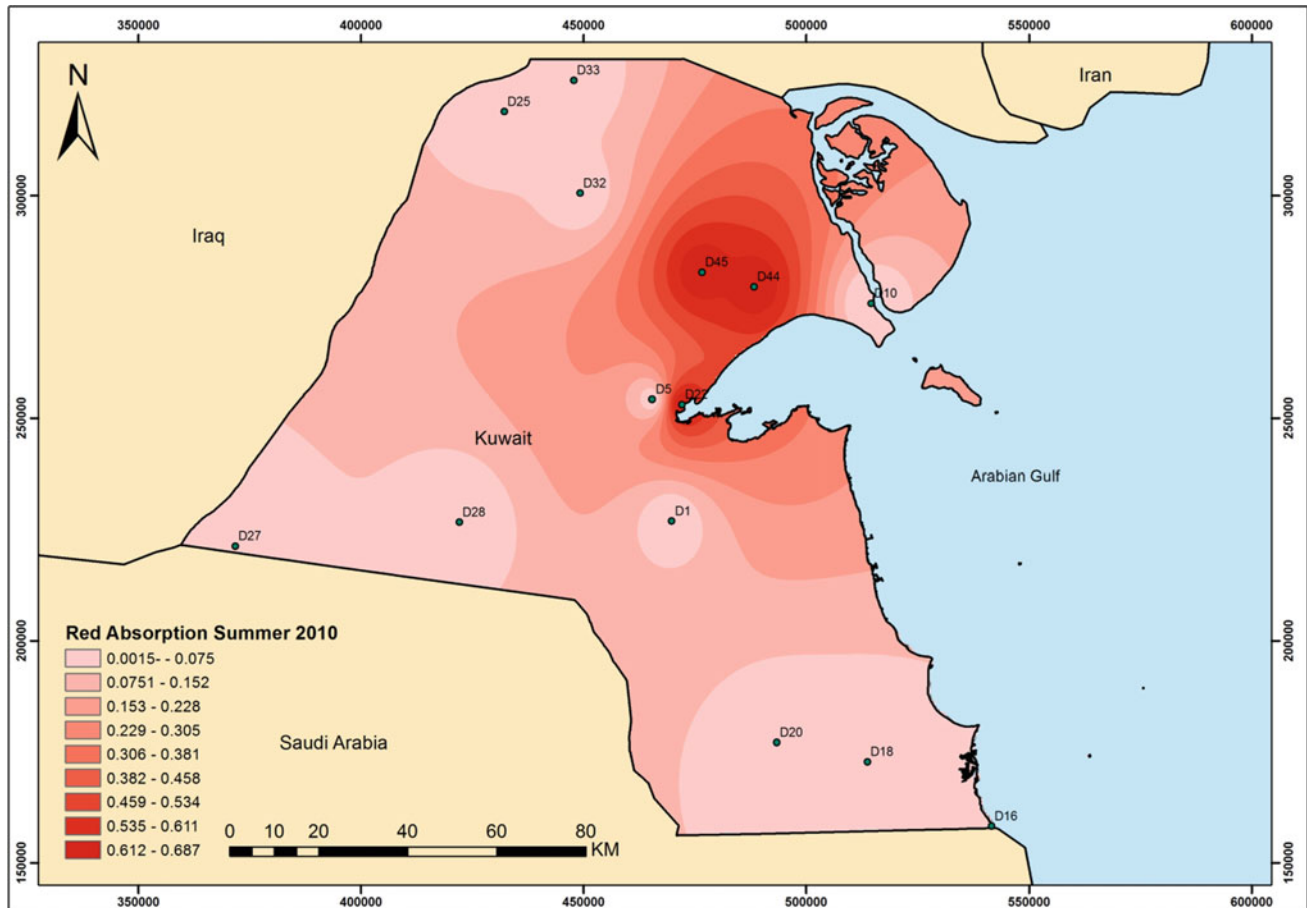


Fig. 9.8 Dust absorption of red light in summer 2010

Infrared Absorption Summer 2010

The absorbed infrared light in summer varies throughout Kuwait. The dust shows high absorption of infrared light at Sabah Al-Ahmad Nature Reserve (collectors D44 and D45) and begins to reduce near the coastal side Kuwait Bay (collector D22 in Kathma). On the border with Iraq, the absorption of infrared light was very low at collector D25 South Buffer zone, D32 Homa, and D33 Ritqa, as well as on the borderline with Saudi Arabia along the southeast

borders at collector D20 Wafra animal farm, D18 Ras Zur-Wafra, D16 Nuwaissieb, D27 Salmi border zone, and D28 Poultry mid-way Salmi road Abraaq. In general, the area near Kuwait Bay, which covers Kuwait City and Hawalli, had a high absorbance of infrared light. The absorbance capacity starts to reduce toward Jahra City in north and Ahmadi in the south. The chemical content of the dust near Kuwait Bay has the ability to absorb more infrared light in the summer than in areas that are farther away (Fig. 9.9).

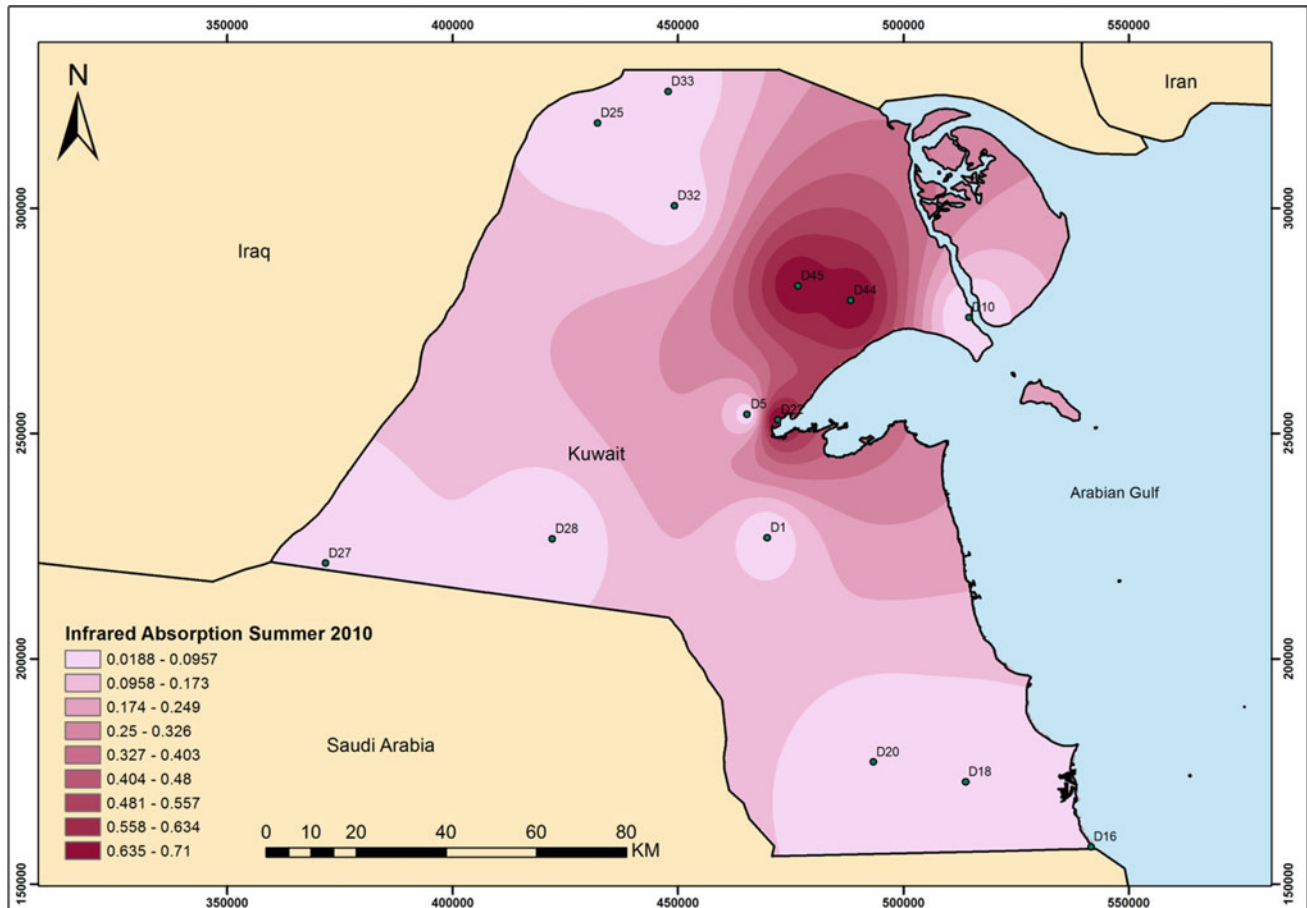


Fig. 9.9 Dust absorption of infrared light in summer 2010

UV Absorption Fall 2010

The ultraviolet light absorbed in autumn varies throughout Kuwait. The dust shows high absorption of ultraviolet light at Sabah Al-Ahmad Nature Reserve (collector D44), at Sabiya close to the Bubiyan bridge (collector D10), near Saudi Arabia at Um Jethathil (collector D41), at Nuwaisieb (collector D16), and at Wafra animal farm (collector D20). The absorption of

ultraviolet light was very low at Abdulia-Managish Road (collector D2), at Poultry mid-way Salmi road (collector D28), and at Sabah Al-Ahmad Nature Reserve (collector D42). In fall, the ultraviolet light absorption varies from high to low in Kuwait Bay. The southern borderline with Saudi Arabia (collector D19) and Salmi border zone (collector D27) had medium ultraviolet light absorbance, while the northern part of Kuwait at Ritqa (collector D33) had mid-high absorption (Fig. 9.10).

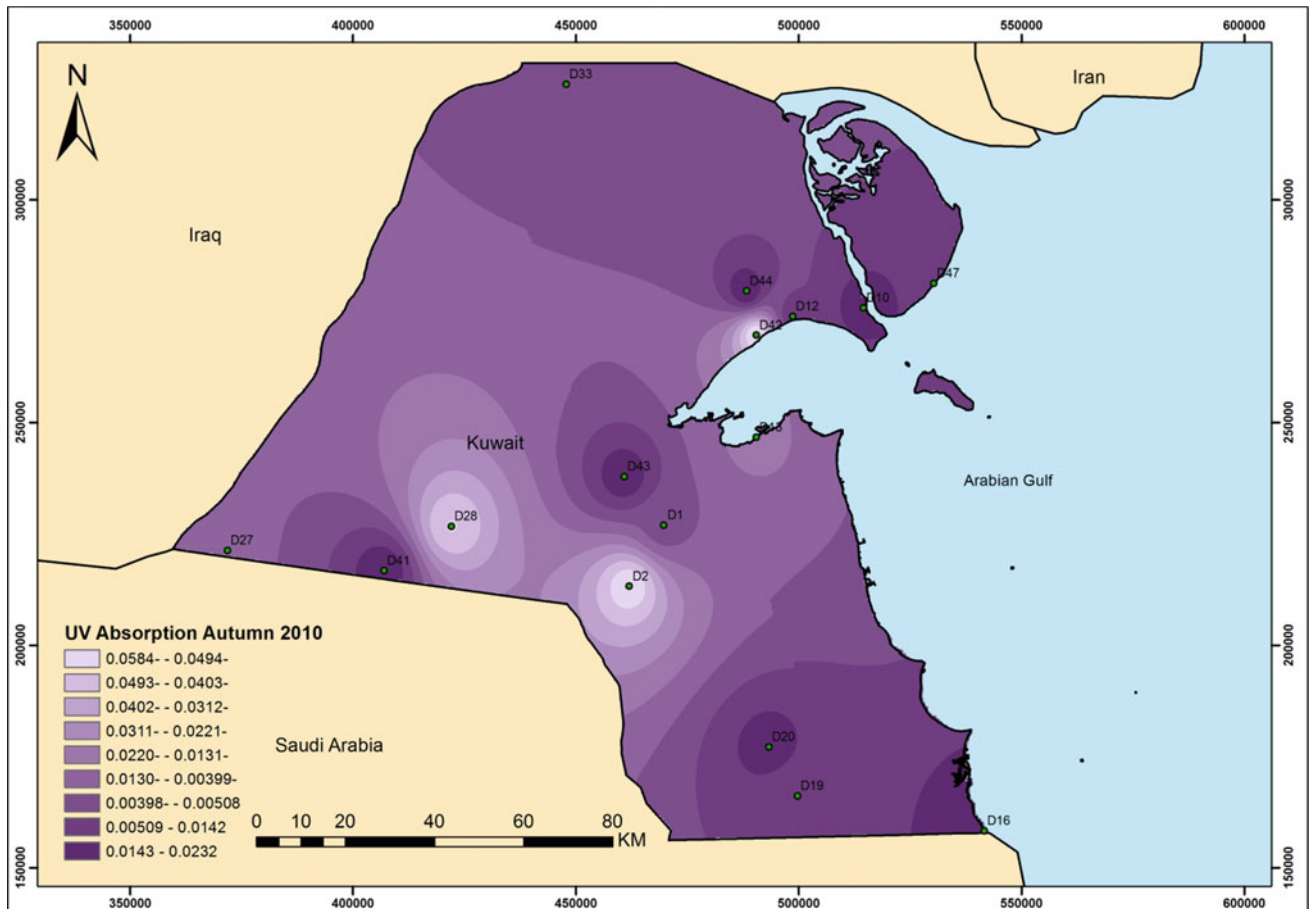


Fig. 9.10 Dust absorption of ultraviolet light in fall 2010

Violet Absorption Fall 2010

The absorbed violet light in fall varies throughout Kuwait. The dust shows high absorption of violet light at Sabah Al-Ahmad Nature Reserve (collector D44), at Sabiya close to the Bubiyan bridge (collector D10), near Saudi Arabia at Um Jethathil (collector D41), at Nuwaissieb (collector D16), and at Wafra animal farm (collector D20). The

absorption of the violet light was very low at Abdulia-Managish Road (collector D2), at Poultry mid-way Salmi road (collector D28), and at Sabah Al-Ahmad Nature Reserve (collector D42). The southern borderline with Saudi Arabia (collector D19) and Salmi border zone (collector D27) had medium violet light absorbance, while the northern part of Kuwait at Ritqa (collector D33) had mid-high absorption (Fig. 9.11).

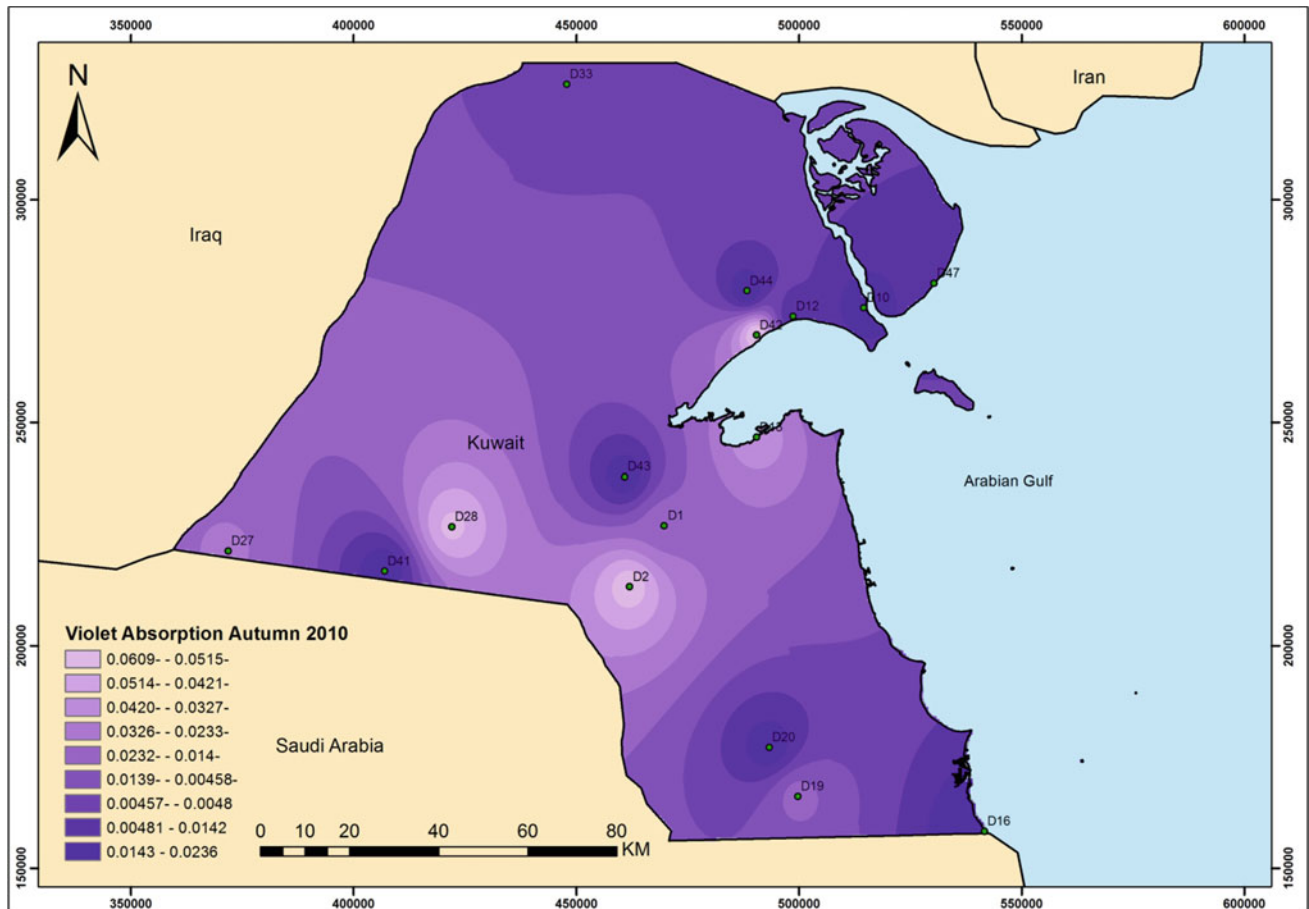


Fig. 9.11 Dust absorption of violet light in fall 2010

Blue Absorption Fall 2010

The blue light absorbed in fall varies throughout Kuwait. The dust shows a high absorption of the blue light at Sabah Al-Ahmad Nature Reserve (collector D44), at Sabiya close to the Bubiyan bridge (collector D10), near Saudi Arabia at Um Jethathil (collector D41), at Nuwaissieb (collector D16), and at Wafra animal farm (collector D20). The absorption of blue

light was very low at Abdulia-Managish Road (collector D2), at Poultry mid-way Salmi road (collector D28), and at Sabah Al-Ahmad Nature Reserve (collector D42). In fall, blue light absorption varies from high to low in Kuwait Bay. The southern borderline with Saudi Arabia (collector D19) and Salmi border zone (collector D27) had medium blue light absorbance, while the northern part of Kuwait at Ritqa (collector D33) had mid-high absorption (Fig. 9.12).

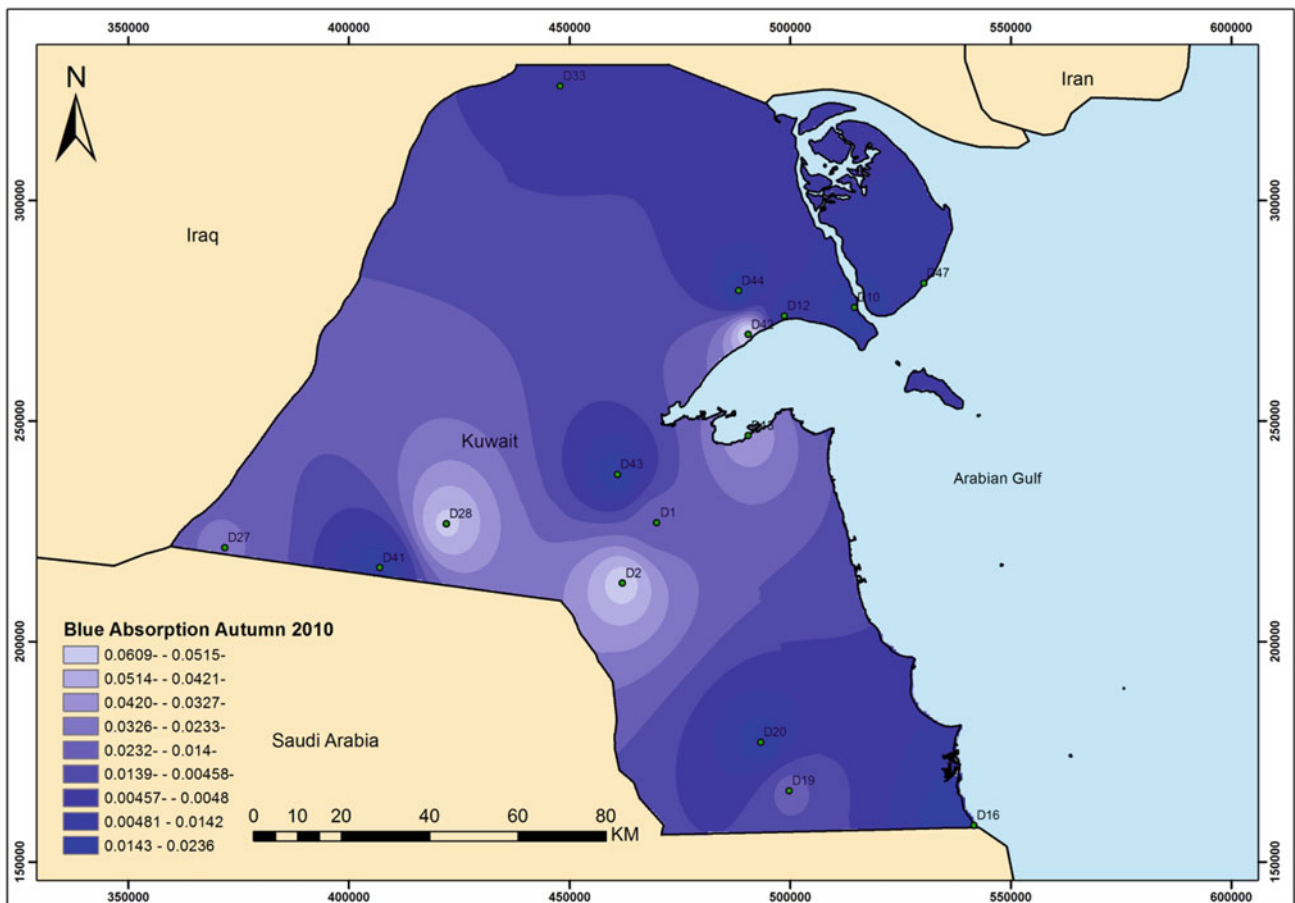


Fig. 9.12 Dust absorption of blue light in fall 2010

Cyan Absorption Fall 2010

The cyan light absorbed in fall varies throughout Kuwait. The dust shows high absorption of cyan light at Sabah Al-Ahmad Nature Reserve (collector D44), at Sabiya close to the Bubiyan bridge (collector D10), near Saudi Arabia at Um Jethathil (collector D41), at Nuwaisieb (collector D16), and at Wafra animal farm (collector D20). The absorption of

cyan light was very low at Abdulia-Managish Road (collector D2), at Poultry mid-way Salmi road (collector D28), and at Sabah Al-Ahmad Nature Reserve (collector D42). In fall, cyan light absorption varies from high to low in Kuwait Bay. The southern borderline with Saudi Arabia (collector D19) and Salmi border zone (collector D27) had medium cyan light absorbance, while the northern part of Kuwait at Ritqa (collector D33) had mid-high absorption (Fig. 9.13).

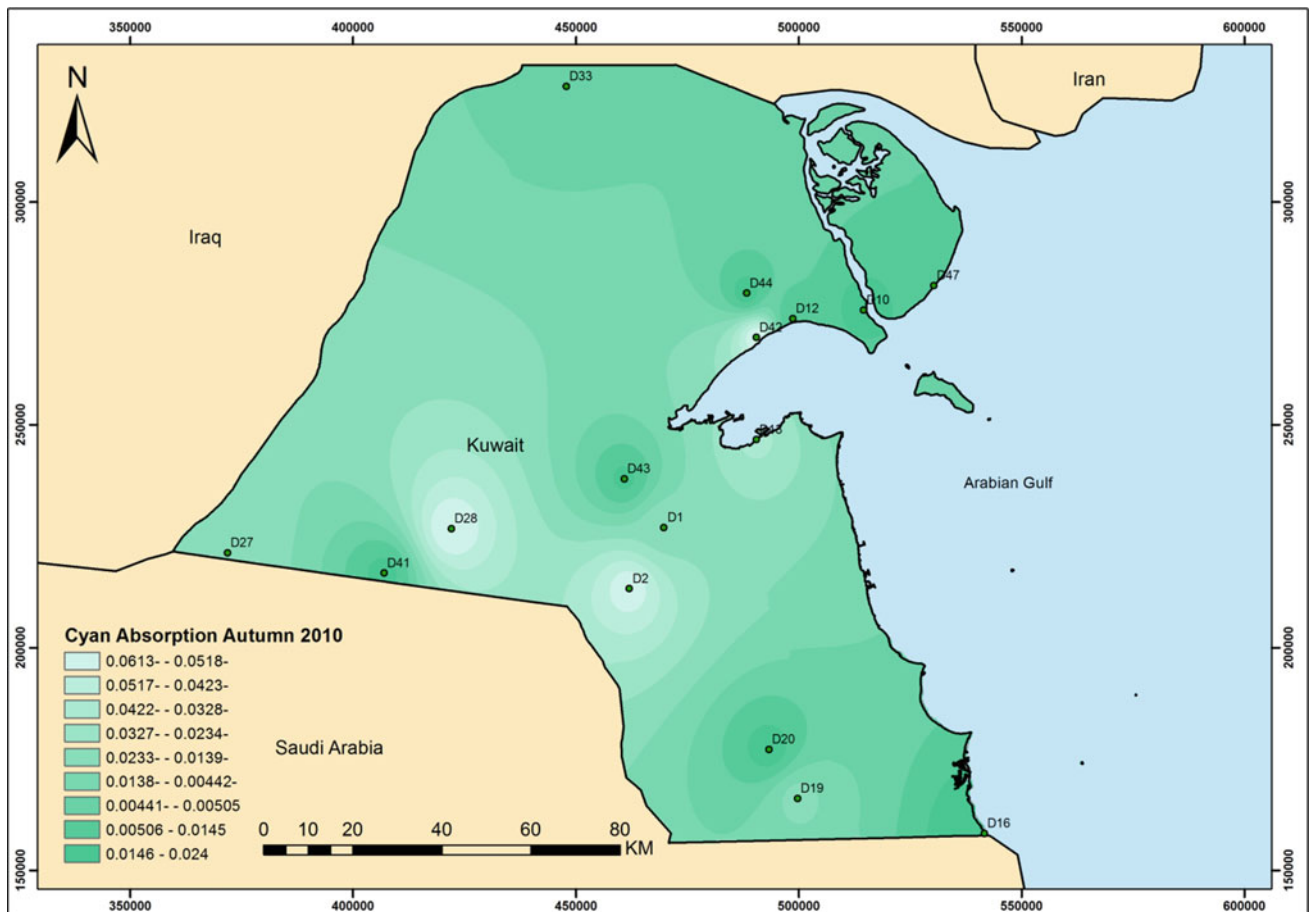


Fig. 9.13 Dust absorption of cyan light in fall 2010

Green Absorption Fall 2010

The green absorbed light in fall varies throughout Kuwait. The dust shows a high absorption of green light at Sabah Al-Ahmad Nature Reserve (collector D44), at Sabiya close to the Bubiyan bridge (collector D10), near Saudi Arabia at Um Jethathil (collector D41), at Nuwaissieb (collector D16), and at Wafra animal farm (collector D20). The absorption of green

light was very low at Abdulia-Managish Road (collector D2), at Poultry mid-way Salmi road (collector D28), and at Sabah Al-Ahmad Nature Reserve (collector D42). In fall, green light absorption varies from high to low in Kuwait Bay. The southern borderline with Saudi Arabia (collector D19) and Salmi border zone (collector D27) had medium green light absorbance, while the northern part of Kuwait at Ritqa (collector D33) had mid-high absorption (Fig. 9.14).

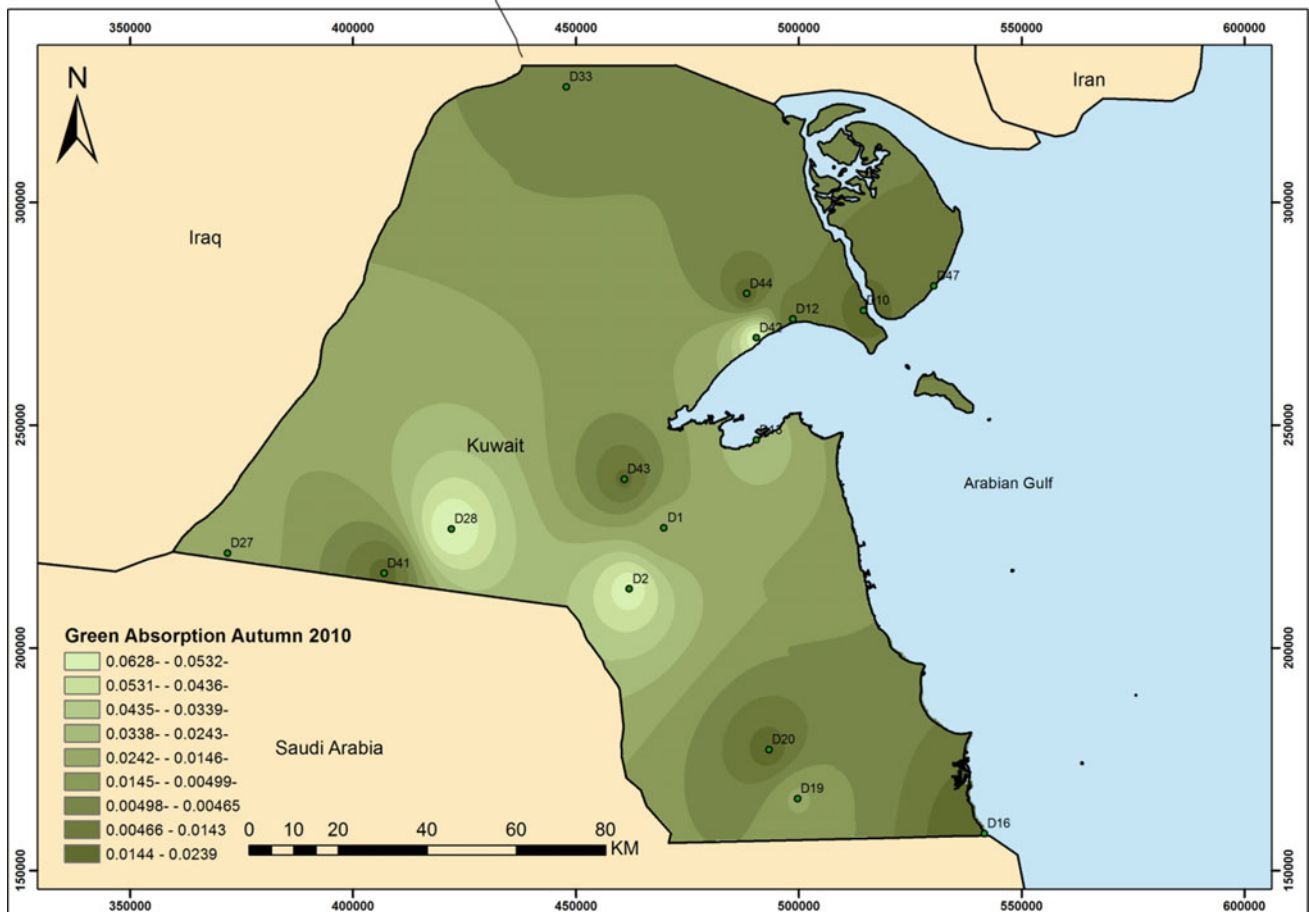


Fig. 9.14 Dust absorption of green light in fall 2010

Yellow Absorption Fall 2010

The yellow light absorbed in fall varies throughout Kuwait. The dust shows a high absorption of yellow light at Sabah Al-Ahmad Nature Reserve (collector D44), at Sabiya (close to the Bubiyan bridge) (collector D10), near Saudi Arabia at Um Jethathil (D41), at Nuwaissieb (collector D16), and at Wafra animal farm (collector D20). The absorption of yellow

light was very low at Abdalia-Managish Road (collector D2), at Poultry mid-way Salmi road (collector D28), and at Sabah Al-Ahmad Nature Reserve (collector D42). In fall, yellow light absorption varies from high to low in Kuwait Bay. The southern borderline with Saudi Arabia (collector D19) and Salmi border zone (collector D27) had medium yellow light absorbance, while the northern part of Kuwait at Ritqa (collector D33) had mid-high absorption (Fig. 9.15).

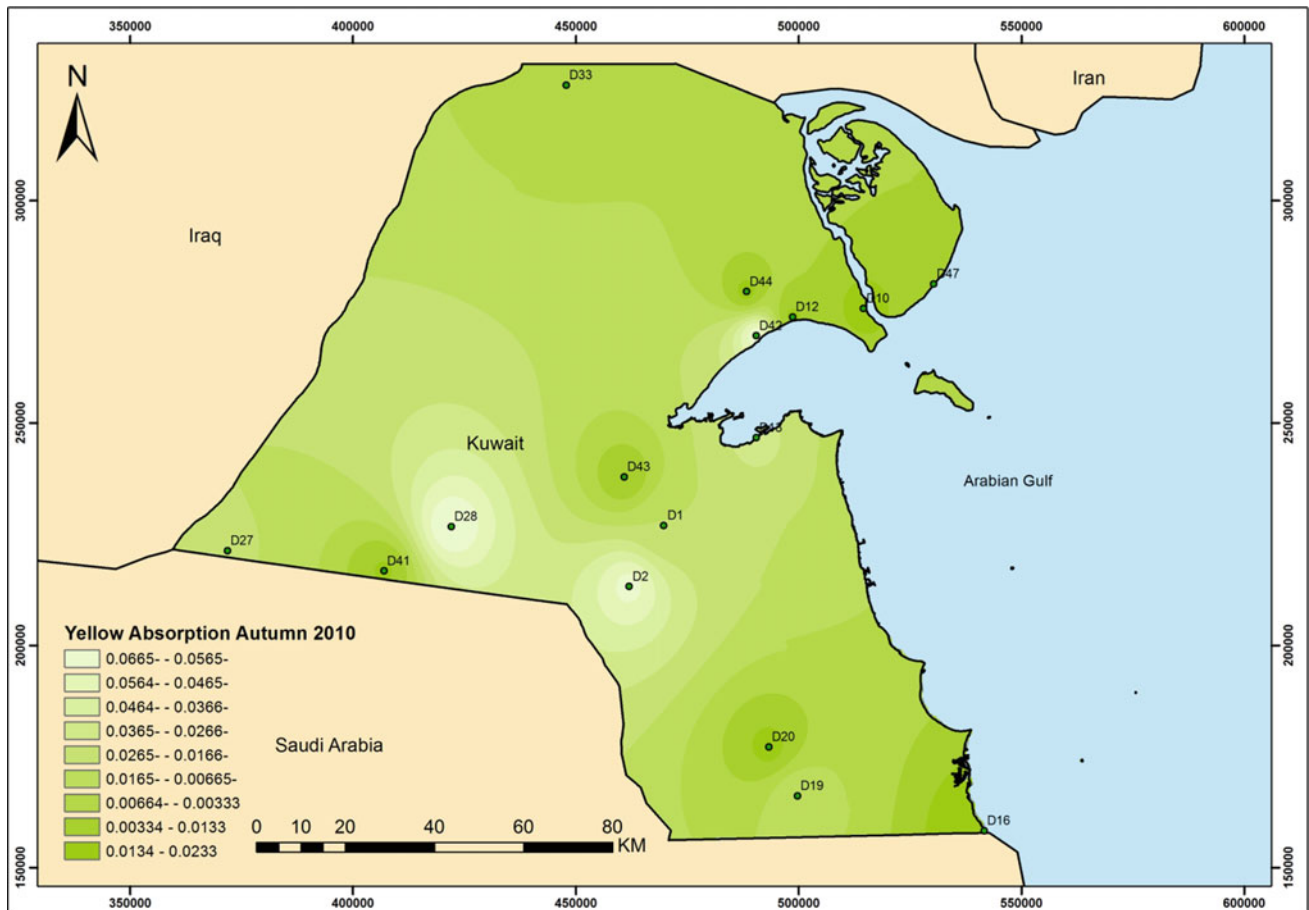


Fig. 9.15 Dust absorption of yellow light in fall 2010

Orange Absorption Fall 2010

The orange light absorbed in fall varies throughout Kuwait. The dust shows high absorption of orange light at Sabah Al-Ahmad Nature Reserve (collector D44), at Sabiya close to the Bubiyan bridge (collector D10), near Saudi Arabia at Um Jethathil (collector D41), at Nuwaisieb (collector D16), and at Wafra animal farm (collector D20). The absorption of

orange light was very low at Abdulia-Managish Road (collector D2), at Poultry mid-way Salmi road (collector D28), and at Sabah Al-Ahmad Nature Reserve (collector D42). In fall, orange light absorption varied from high to low in Kuwait Bay. The southern borderline with Saudi Arabia (collector D19) and Salmi border zone (collector D27) had medium orange light absorbance, while the northern part of Kuwait at Ritqa (collector D33) had mid-high absorption (Fig. 9.16).

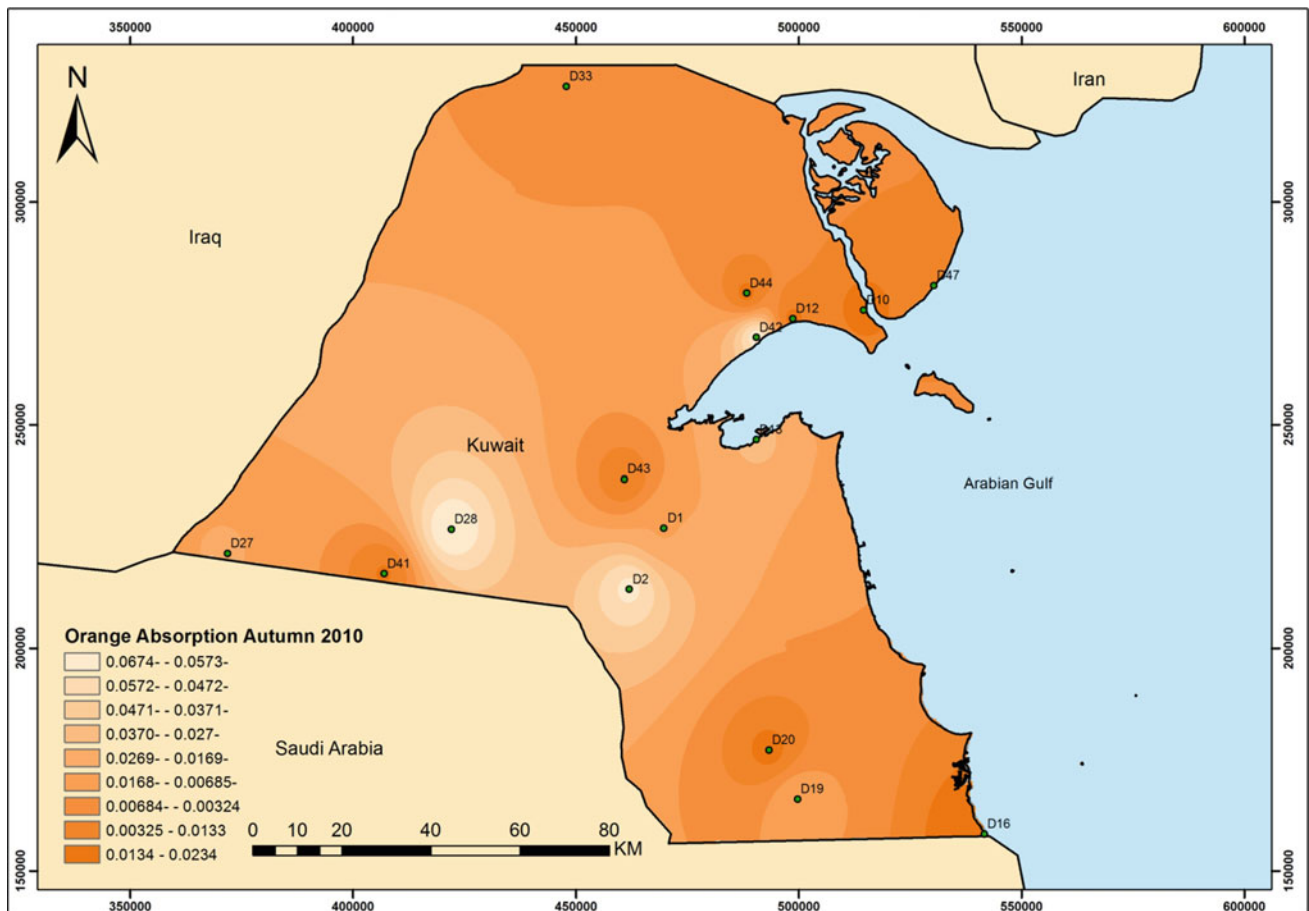


Fig. 9.16 Dust absorption of orange light in fall 2010

Red Absorption Fall 2010

The red light absorbed in fall varies throughout Kuwait. The dust shows high absorption of red light in Sabah Al-Ahmad Nature Reserve (collector D44), at Sabiya close to the Bubiyan bridge (collector D10), near Saudi Arabia at Um Jethathil (collector D41), at Nuwaissieb (collector D16), and at Wafra animal farm (collector D20). The absorption of red

light was very low at Abdulia-Managish Road (collector D2), at Poultry mid-way Salmi road (collector D28), and at Sabah Al-Ahmad Nature Reserve (collector D42). In fall, red-light absorption varies from high to low in Kuwait Bay. The southern borderline with Saudi Arabia (collector D19) and Salmi border zone (collector D27) had medium red-light absorbance, while the northern part of Kuwait at Ritqa (collector D33) had mid-high absorption (Fig. 9.17).

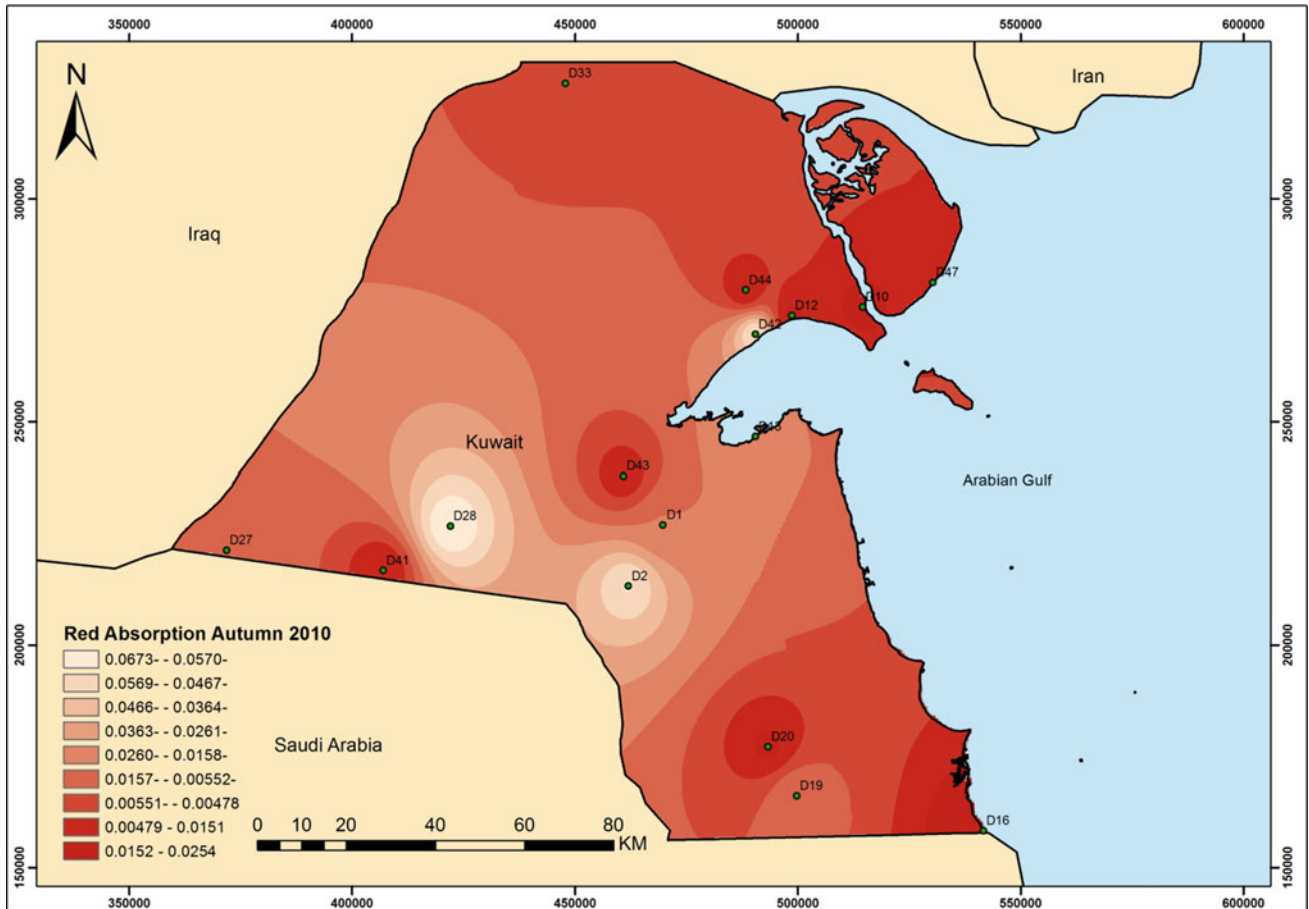


Fig. 9.17 Dust absorption of red light in fall 2010

IR Absorption Fall 2010

The infrared light absorbed in fall varies throughout Kuwait. The dust shows high absorption of infrared light at Sabah Al-Ahmad Nature Reserve (collector D44), at Sabiya close to the Bubiyan bridge (collector D10), near Saudi Arabia at Um Jethathil (collector D41), at Nuwaissieb (collector D16), and at Wafra animal farm (collector D20). The absorption of

infrared light was very low at Abdulia-Managish Road (collector D2), at Poultry mid-way Salmi road (collector D28), and at Sabah Al-Ahmad Nature Reserve (collector D42). In fall, infrared light absorption varied from high to low in Kuwait Bay. The southern borderline with Saudi Arabia (collector D19) and Salmi border zone (collector D27) had medium infrared light absorbance, while the northern part of Kuwait at Ritqa (collector D33) had mid-high absorption (Fig. 9.18).

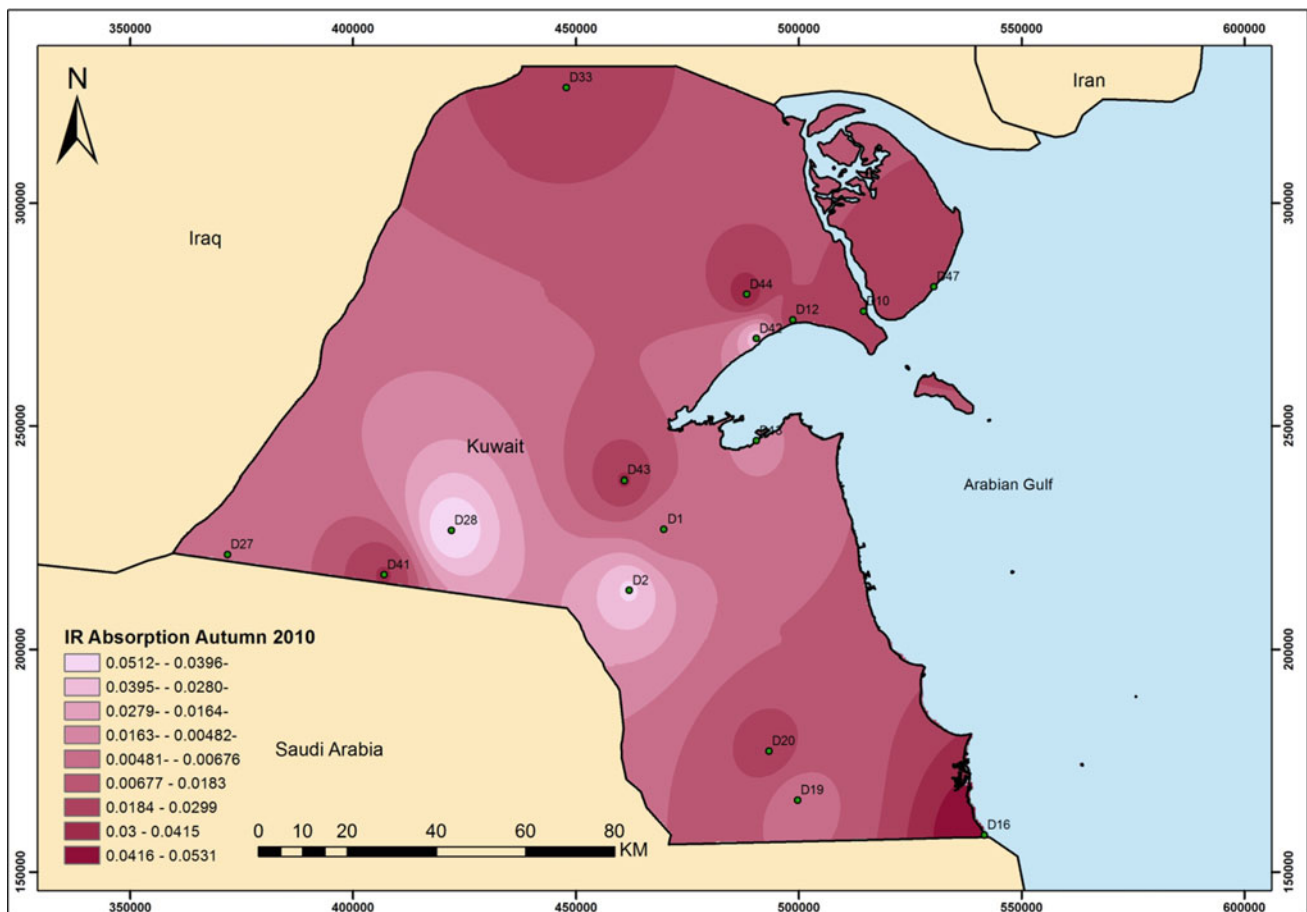


Fig. 9.18 Dust absorption of infrared light in fall 2010

UV Absorption Winter 2010

The absorbed ultraviolet light by dust particles in winter varies throughout Kuwait. The dust shows high absorption of ultraviolet light on the northeastern borders with Saudi Arabia at Abraq (collector D29). The dust shows mid-high absorption of ultraviolet light at various places in Kuwait, including the southern Kuwait-Saudi Arabia border zone (collector D38), as well as on Um Bubiyan Island (collector D46), and the southeast area of Kuwait (collectors 41 and 28). The dust shows medium absorption of ultraviolet light in various places in Kuwait, including Sabah Al-Ahmad Nature Reserve (collectors D42 and D44), in the KISR main

building location in Kuwait Bay (collector D13), in Kathma (collector D22), in the northern area in Um Qasir/Bahaith (collector D30), and along the western borders with Saudi Arabia (collector D37). However, the dust shows a low absorption of ultraviolet light in many areas, such as the northern side of Kuwait Bay at Bahra coastal zone (collector D12), in the KISR petroleum center in Ahmadi in the east (collector 15), along the northern borders with Iraq at Ritqa (collector D33), at Homa (collector D32), at gate Sabriya oil field (collector D23), at Kabd station (collector D1), at Abdulia-Managish Road (collector D2), and along the western borders with Saudi Arabia at the Salmi border zone (collector 27) (Fig. 9.19).

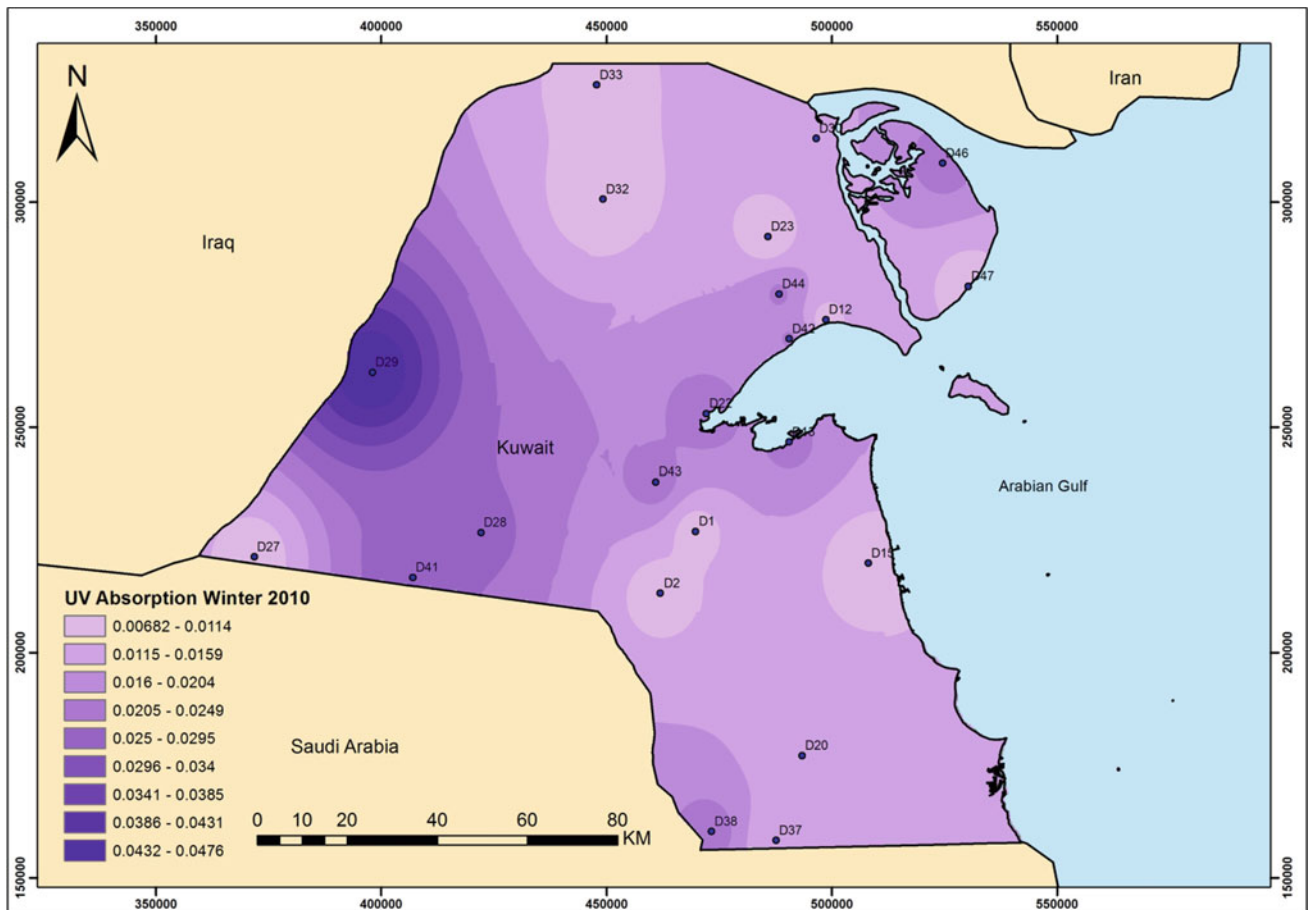


Fig. 9.19 Dust absorption of ultraviolet light in winter 2010

Violet Absorption Winter 2010

The violet light absorbed by dust particles in winter varies throughout Kuwait. The dust shows high absorption of violet light on the northeastern borders with Saudi Arabia at Abraq (collector D29). The dust shows mid-high absorption of violet light at various places in Kuwait, including the southern Kuwait-Saudi Arabia border zone (collector D38), on Bubiyan Island (collector D46), and at the mid-western area of Kuwait (collectors 28 and 41). The dust shows medium absorption of violet light at various places, including Sabah Al-Ahmad Nature Reserve (collectors D42 and D44),

in the KISR’s main building location in Kuwait Bay (collector D13), in Kathma (collector D22), and in the northern area in Um Qasir/Bahaith (collector D30). However, the dust shows low absorption of violet light in the north of Kuwait Bay at the Bahra coastal zone (collector D12), in the KISR’s petroleum center in Ahmadi (collector 15), on the northern borders with Iraq at Ritqa (collector D33), at Homa (collector D32), at gate Sabriya oil field (collector D23), along the western borders with Saudi Arabia (collector D37), at Kabd station (collector D1), at Abdulia-Managish Road (collector D2), and at the western border with Saudi Arabia at Salmi border zone (collector 27) (Fig. 9.20).

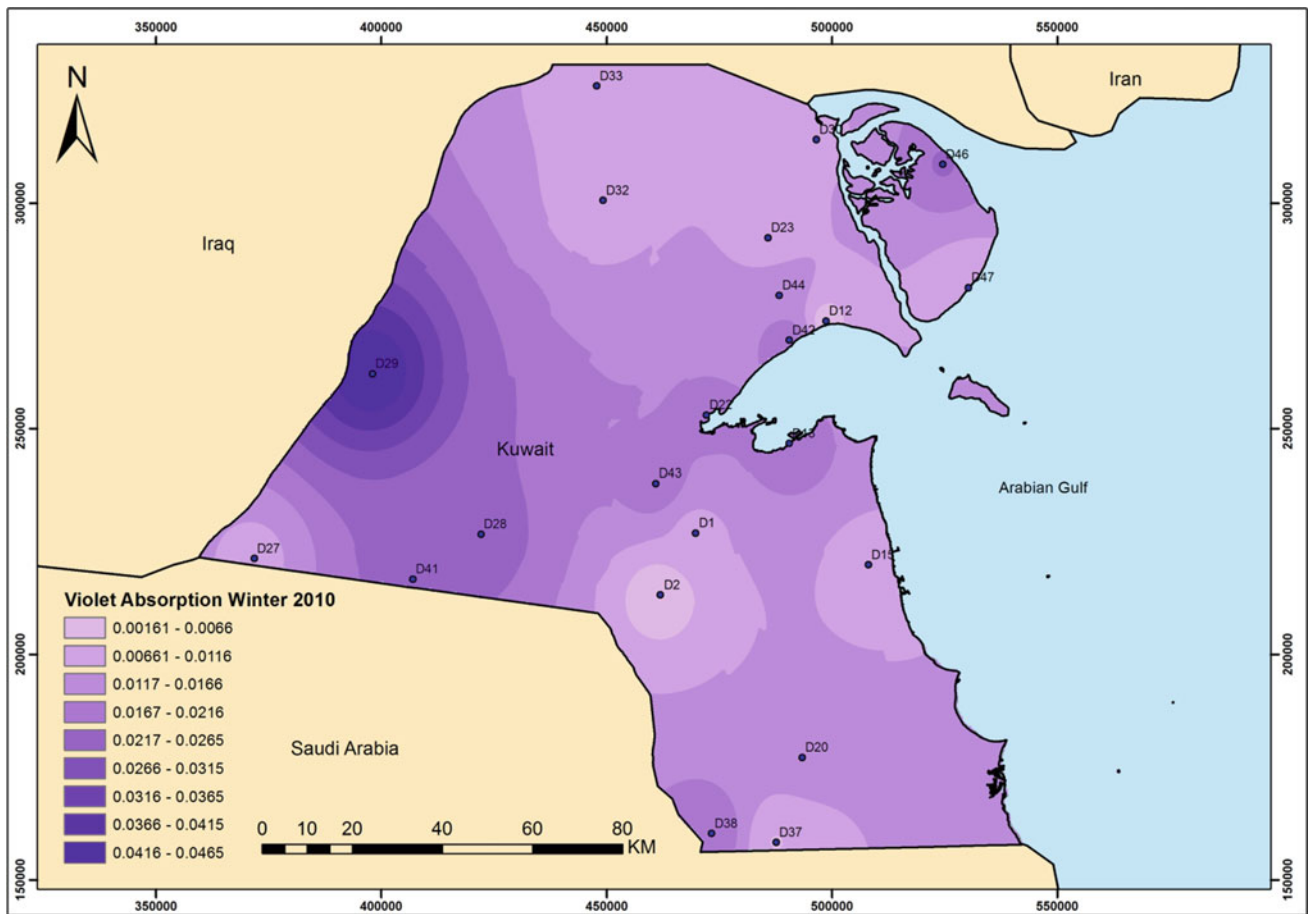


Fig. 9.20 Dust absorption of violet light in winter 2010

Blue Absorption Winter 2010

The blue light absorbed by dust particles in winter varies throughout Kuwait. The dust shows high absorption of blue light on the northeastern border with Saudi Arabia at Abraq (collector D29). The dust shows mid-high absorption of blue light at various places in Kuwait, including the southern Kuwait-Saudi Arabia border zone (collector D38), on Bubiyan Island (collector D46), and at the mid-western area of Kuwait (collectors 28). The dust shows medium absorption of blue light across various places, including Sabah Al-Ahmad Nature Reserve (collectors D42 and D44), in the KISR's main building location in Kuwait Bay

(collector D13), in Kathma (collector D22), and in the northern area in Um Qasir/Bahaith (collector D30). However, the dust shows low absorption of blue light in the KISR's petroleum center in Ahmadi (collector 15), on the northern borders with Iraq at Ritqa (collector D33), at Homa (collector D32), at gate Sabriya oil field (collector D23), at Kabd station (collector D1), and at the western borders with Saudi Arabia at Salmi border zone (collector 27). Finally, the dust shows very low absorption at three main areas in Kuwait: north of Kuwait Bay at Bahra coastal zone (collector D12), along the western border with Saudi Arabia (collector D37), and at Abdulia-Managish Road (collector D2) (Fig. 9.21).

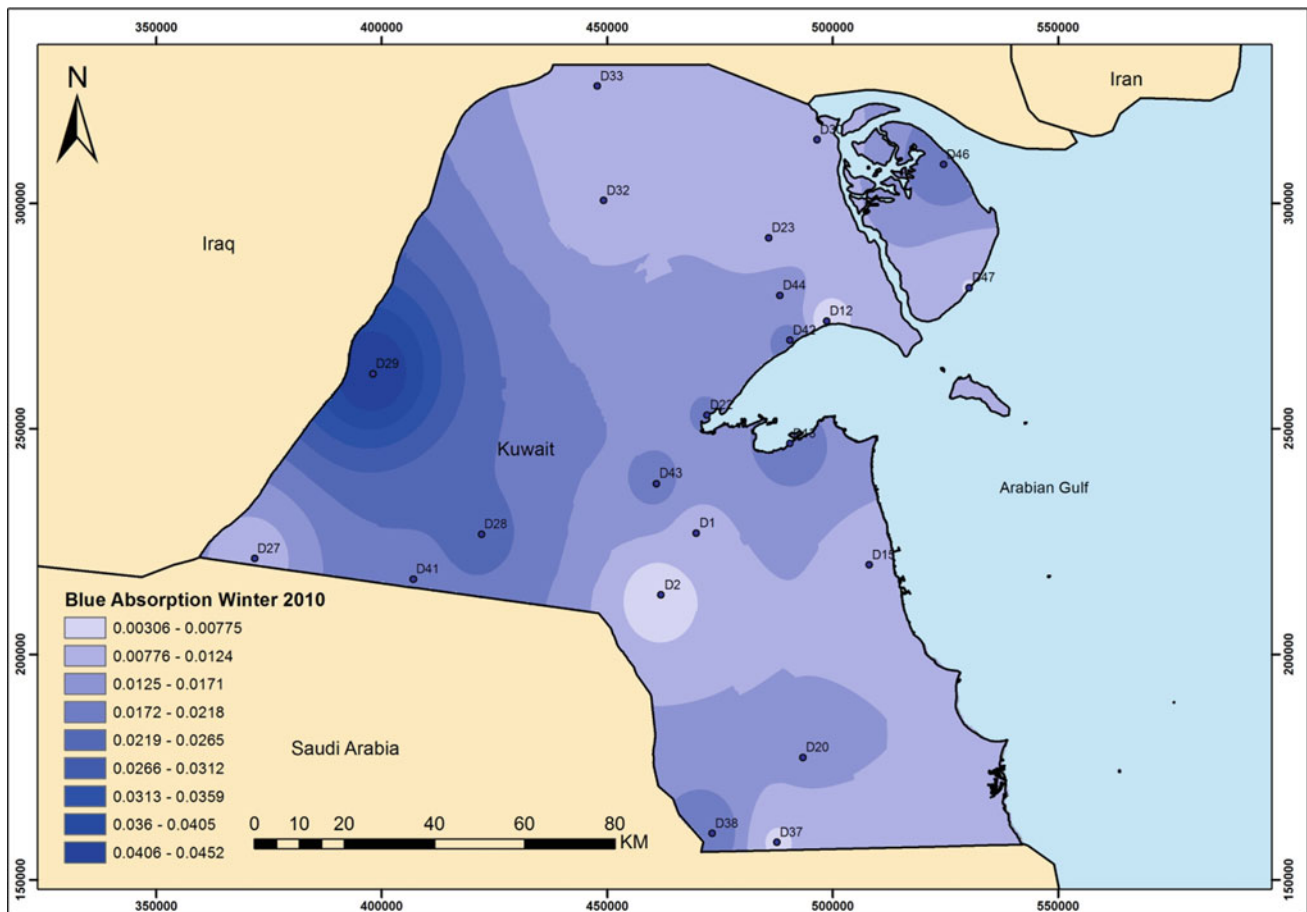


Fig. 9.21 Dust absorption of blue light in winter 2010

Cyan Absorption Winter 2010

The cyan light absorbed by dust particles in winter varies throughout the State of Kuwait. The dust shows high absorption of cyan light on the northeastern border with Saudi Arabia at Abraç (collector D29). The dust shows mid-high absorption of cyan light at various places in Kuwait, including the southern Kuwait-Saudi Arabia border zone (collector D38), on Bubiyan Island (collector D46), and at the mid-western area of Kuwait (collectors 28). The dust shows a medium absorption of cyan light at various other places, including Sabah Al-Ahmad Nature Reserve (collectors D42 and D44), at the KISR's main building location in

Kuwait Bay (collector D13), in Kathma (collector D22), and in the northern area in Um Qasir/Bahaith (collector D30). However, the dust shows low absorption of cyan light in the KISR's petroleum center in Ahmadi (collector 15), on the northern border with Iraq at Ritqa (collector D33), at Homa (collector D32), at gate Sabriya oil field (collector D23), at Kabd station (collector D1), and at the western border with Saudi Arabia at Salmi border zone (collector 27). The dust shows very low absorption at three main locations in Kuwait: north of Kuwait Bay at Bahra coastal zone (collector D12), on the western border with Saudi Arabia (collector D37), and at Abdulia-Managish Road (collector D2) (Fig. 9.22).

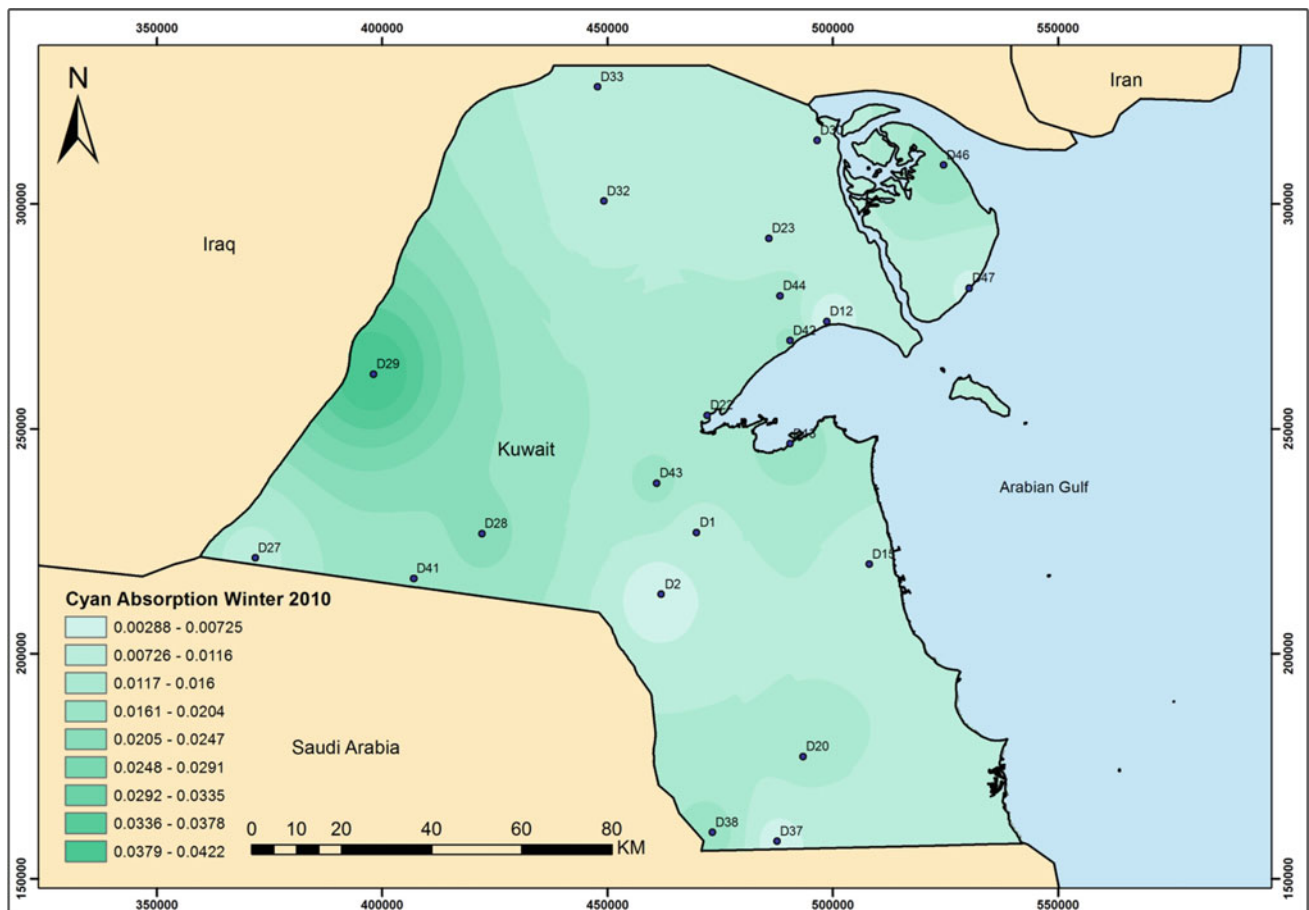


Fig. 9.22 Dust absorption of cyan light in winter 2010

Green Absorption Winter 2010

The green light absorbed by dust particles in winter varies throughout the State of Kuwait. The dust shows high absorption of green light on the northeastern border with Saudi Arabia at Abraç (collector D29). The dust shows mid-high absorption of green light at various places in Kuwait, including the southern Kuwait-Saudi Arabia border zone (collector D38), on Bubiyan Island (collector D46), and at the mid-western area of Kuwait (collectors 28). The dust shows medium absorption of green light at various other places, including Sabah Al-Ahmad Nature Reserve (collectors D42 and D44), at the KISR's main building location in

Kuwait Bay (collector D13), in Kathma (collector D22), and in the northern area in Um Qasir/Bahaith (collector D30). However, the dust shows a low absorption of green light in the KISR's petroleum center in Ahmadi (collector 15), on the northern border with Iraq at Ritqa (collector D33), at Homa (collector D32), at gate Sabriya oil field (collector D23), and at Kabd station (collector D1). The dust shows very low absorption of green light across four main locations in Kuwait: north of Kuwait Bay at Bahra coastal zone (collector D12), on the western border with Saudi Arabia (collector D37), at Abdulia-Managish Road (collector D2), and at the western border with Saudi Arabia at Salmi border zone (collector 27) (Fig. 9.23).

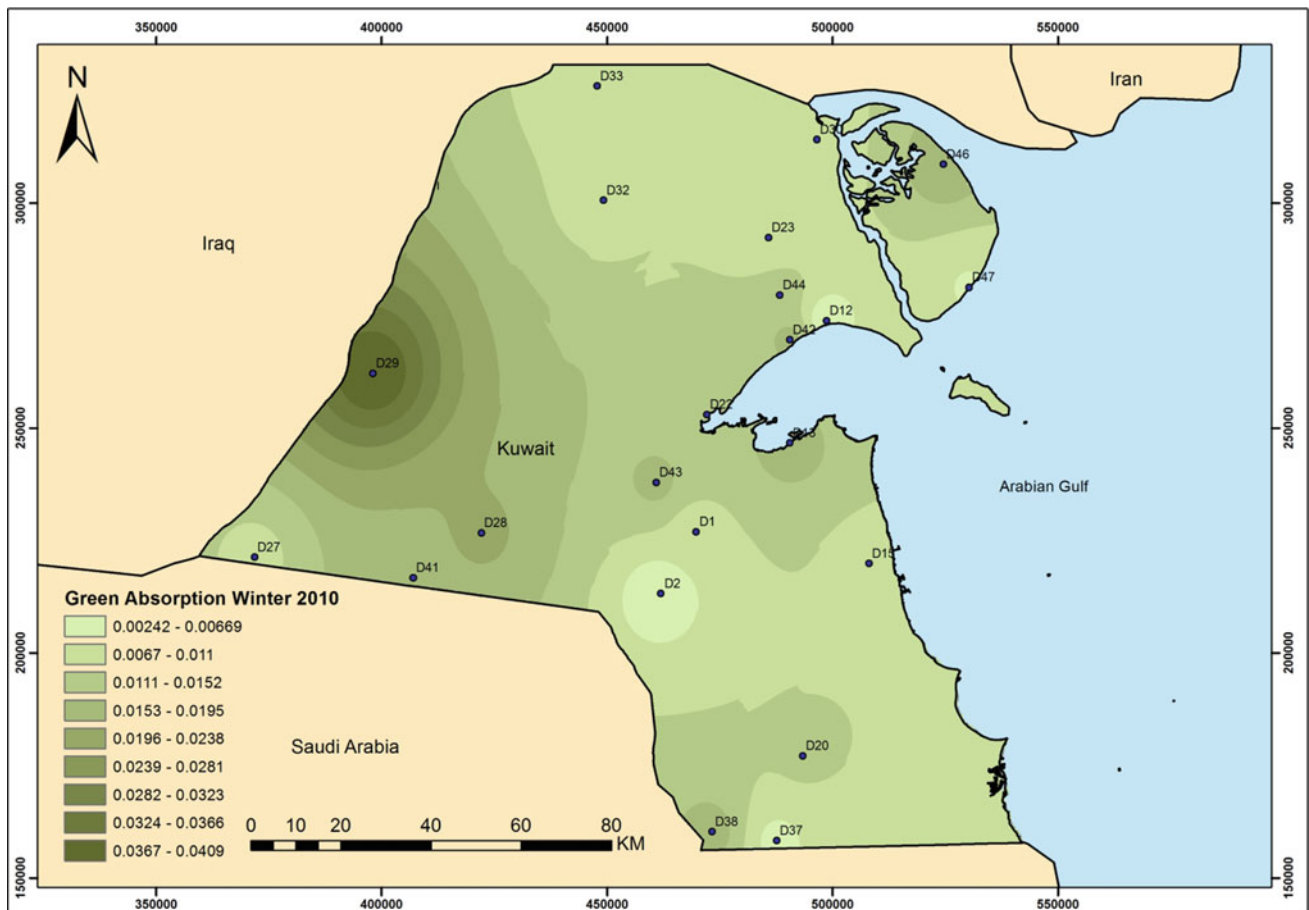


Fig. 9.23 Dust absorption of green light in winter 2010

Yellow Absorption Winter 2010

The yellow light absorbed by dust particles in winter varies throughout Kuwait. The dust shows high absorption of yellow light on the northeastern border with Saudi Arabia at Abra q (collector D29). The dust shows mid-high absorption of yellow light at various places in Kuwait, including the southern Kuwait-Saudi Arabia border zone (collector D38), on Bubiyan Island (collector D46), and at the mid-western area of Kuwait (collectors 28). The dust shows medium absorption of yellow light at various other places, including Sabah Al-Ahmad Nature Reserve (collectors D42 and D44), in the KISR’s main building location in Kuwait Bay

(collector D13), in Kathma (collector D22), and in the northern area in Um Qasir/Bahaith (collector D30). However, the dust shows low absorption of yellow light in the KISR’s petroleum center in Ahmadi (collector 15), on the northern border with Iraq at Ritqa (collector D33), at Homa (collector D32), at gate Sabriya oil field (collector D23), and at Kabd station (collector D1). The dust shows very low absorption of yellow light at four main locations in Kuwait: north of Kuwait Bay at Bahra coastal zone (collector D12), on the western border with Saudi Arabia (collector D37), at Abdulia-Managish Road (collector D2), and on the western border with Saudi Arabia at Salmi border zone (collector 27) (Fig. 9.24).

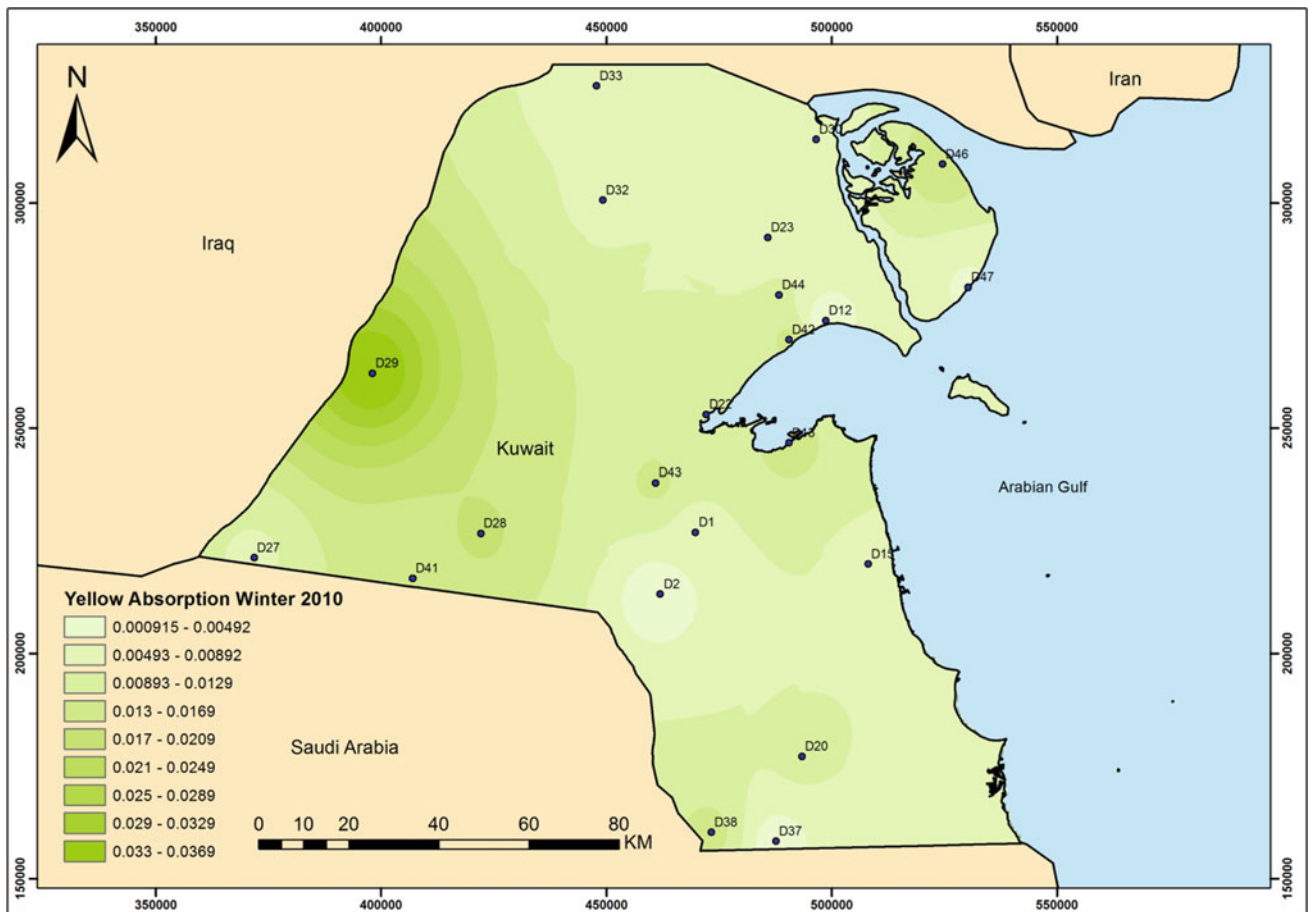


Fig. 9.24 Dust absorption of yellow light in winter 2010

Orange Absorption Winter 2010

The orange light absorbed by dust particles in winter varies throughout the State of Kuwait. The dust shows high absorption of orange light on the northeastern border with Saudi Arabia at Abraç (collector D29). The dust shows mid-high absorption of orange light at various places in Kuwait, including the southern Kuwait-Saudi Arabia border zone (collector D38), on Bubiyan Island (collector D46), and at the mid-western area of Kuwait (collectors 28). The dust shows medium absorption of orange light at various other places, including Sabah Al-Ahmad Nature Reserve (collectors D42 and D44), in the KISR's main building

location in Kuwait Bay (collector D13), in Kathma (collector D22), and in the northern area in Um Qasir/Bahaith (collector D30). However, dust shows low absorption of orange light in the KISR's petroleum center in Ahmadi (collector 15), on the northern border with Iraq at Ritqa (collector D33), at Homa (collector D32), at gate Sabriya oil field (collector D23), and at Kabd station (collector D1). The dust shows very low absorption of orange light across four main locations in Kuwait: north of Kuwait Bay at Bahra coastal zone (collector D12), in the western border with Saudi Arabia (collector D37), at Abdulia-Managish Road (collector D2), and on Bubyan Island (collector 47) (Fig. 9.25).

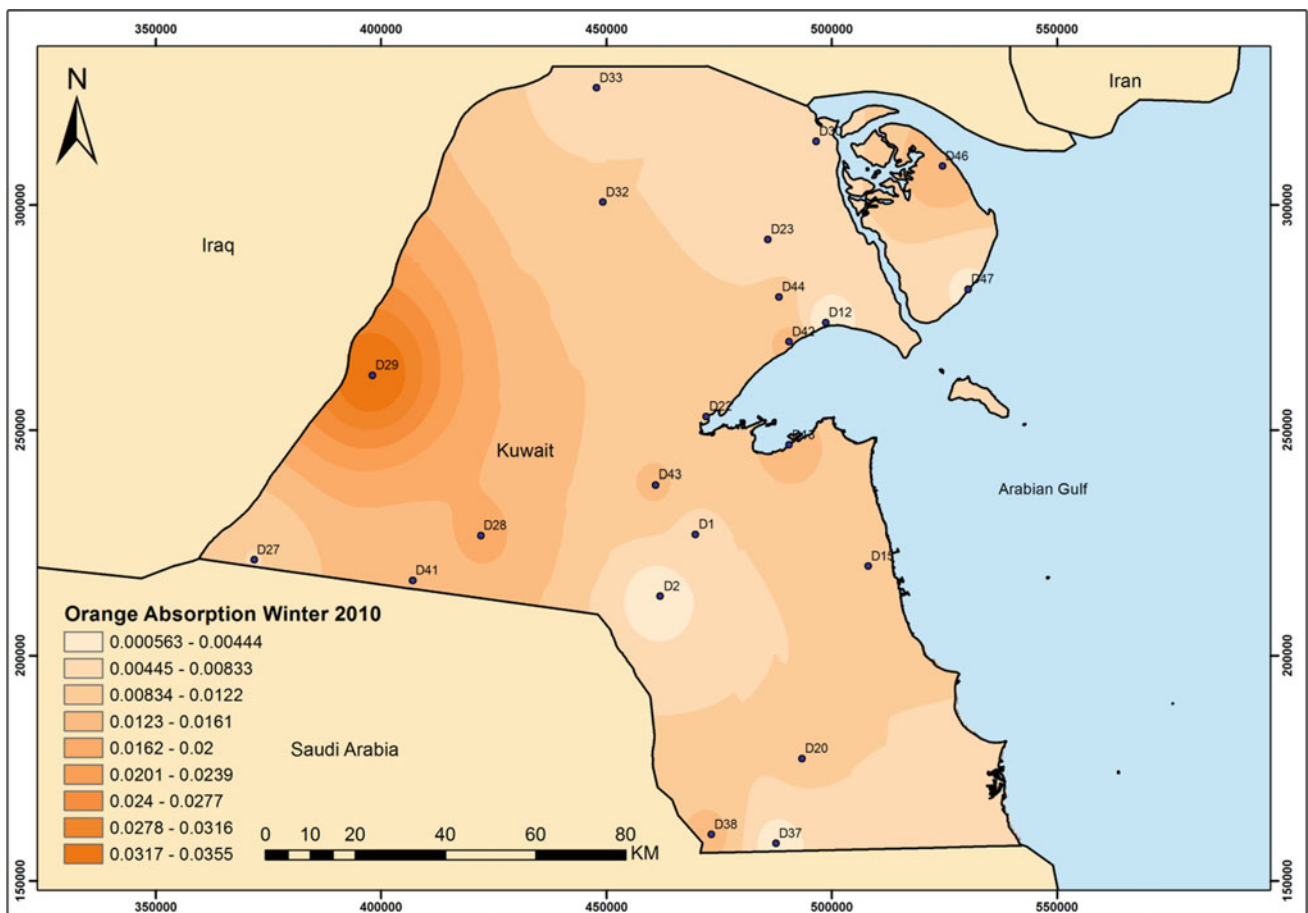


Fig. 9.25 Dust absorption of orange light in winter 2010

Red Absorption Winter 2010

The red light absorbed by dust particles in winter varies throughout Kuwait. The dust shows high absorption of red light on the northeastern border with Saudi Arabia at Abraq (collector D29). The dust shows mid-high absorption of red light across various places of Kuwait, including the southern Kuwait-Saudi Arabia border zone (collector D38), on Bubiyan Island (collector D46), and at the mid-western area of Kuwait (collectors 28). The dust shows medium absorption of red light across various other places, including Sabah Al-Ahmad Nature Reserve (collectors D42 and D44), in the

KISR's main building location in Kuwait Bay (collector D13), in Kathma (collector D22), and in the northern area in Um Qasir/Bahaith (collector D30). However, the dust shows a low absorption of red light at the KISR's petroleum center in Ahmadi (collector 15), on the northern border with Iraq at Ritqa (collector D33), at Homa (collector D32), at gate Sabriya oil field (collector D23), and at Kabd station (collector D1). The dust shows very low absorption of red light across four main locations in Kuwait: north of Kuwait Bay at Bahra coastal zone (collector D12), on the western border with Saudi Arabia (collector D37), at Abdulia-Managish Road (collector D2), and on Bubiyan Island (collector 47) (Fig. 9.26).

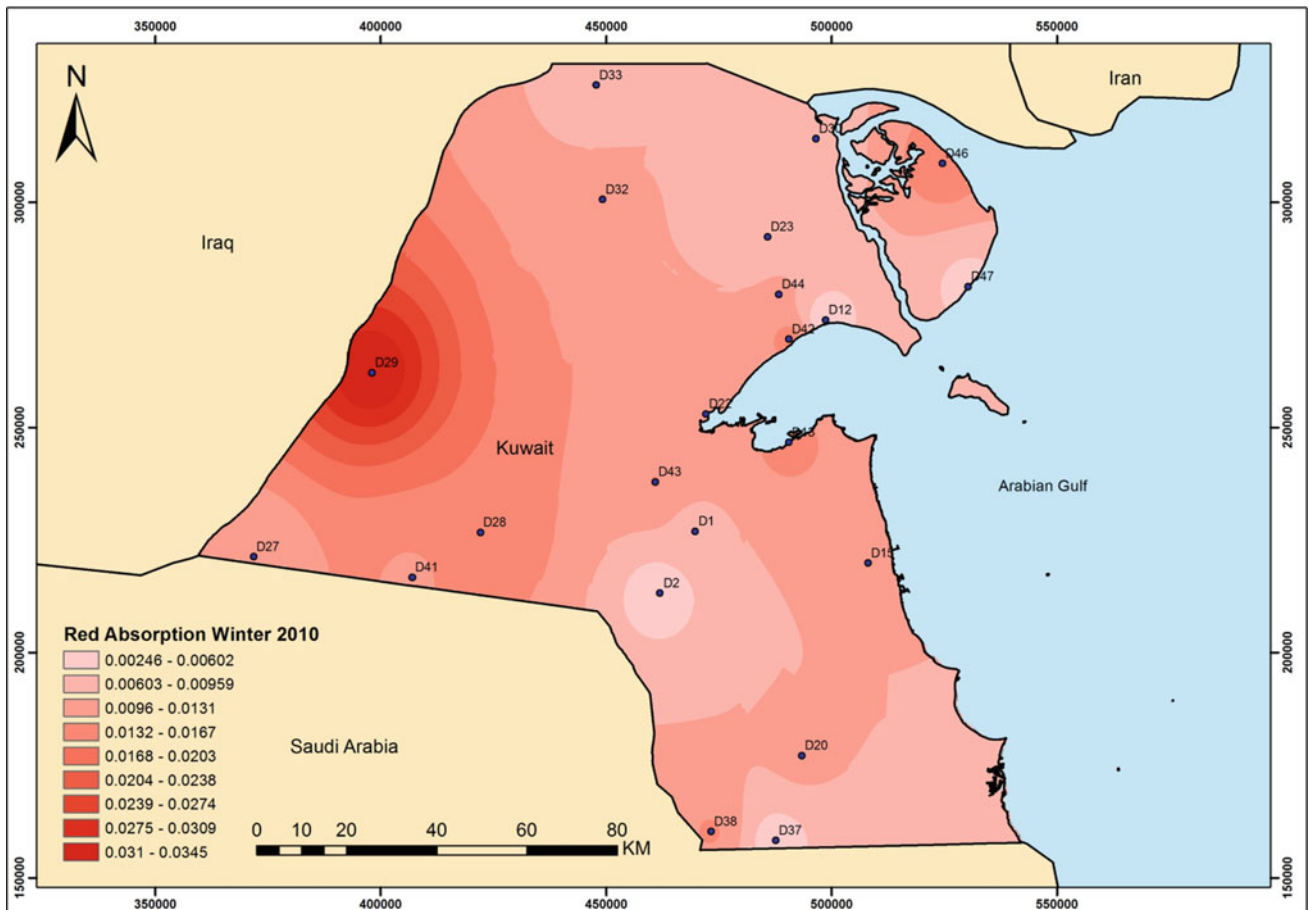


Fig. 9.26 Dust absorption of red light in winter 2010

IR Absorption Winter 2010

The red light absorbed by dust particles in winter varies throughout the State of Kuwait. The dust shows high absorption of red light across three main locations: the northeastern border with Saudi Arabia at Abraaq (collector D29), Abdulia-Managish Road (collector D2), and at the border with Saudi Arabia at Um Jethathil (collector D41). The dust shows mid-high absorption of red light at various places in Kuwait, including Kathma (collector D22), north of Kuwait Bay at Bahra coastal zone (collector D12), and the western border with Saudi Arabia (collector D37). The dust shows medium absorption of red light at various other places, including the southern Kuwait-Saudi Arabia border

zone (collector D38), on Bubiyan Island (collector D46), at the mid-western area of Kuwait (collectors 28), at Sabah Al-Ahmad Nature Reserve (collectors D42 and D44), and at the KISR’s main building location in Kuwait Bay (collector D13). However, the dust shows low absorption of red light at the northern area in Um Qasir/Bahaith (collector D30), on the northern border with Iraq at Ritqa (collector D33), and at Homa (collector D32). Finally, the dust shows very low absorption of red light across six main locations in Kuwait: on Bubiyan Island (collector 47), at gate Sabriya oil field (collector D23), at Kabd station (collector D1), in the KISR’s petroleum center in Ahmadi (collector 15), and in the southern part of Kuwait (collector D20) (Fig. 9.27).

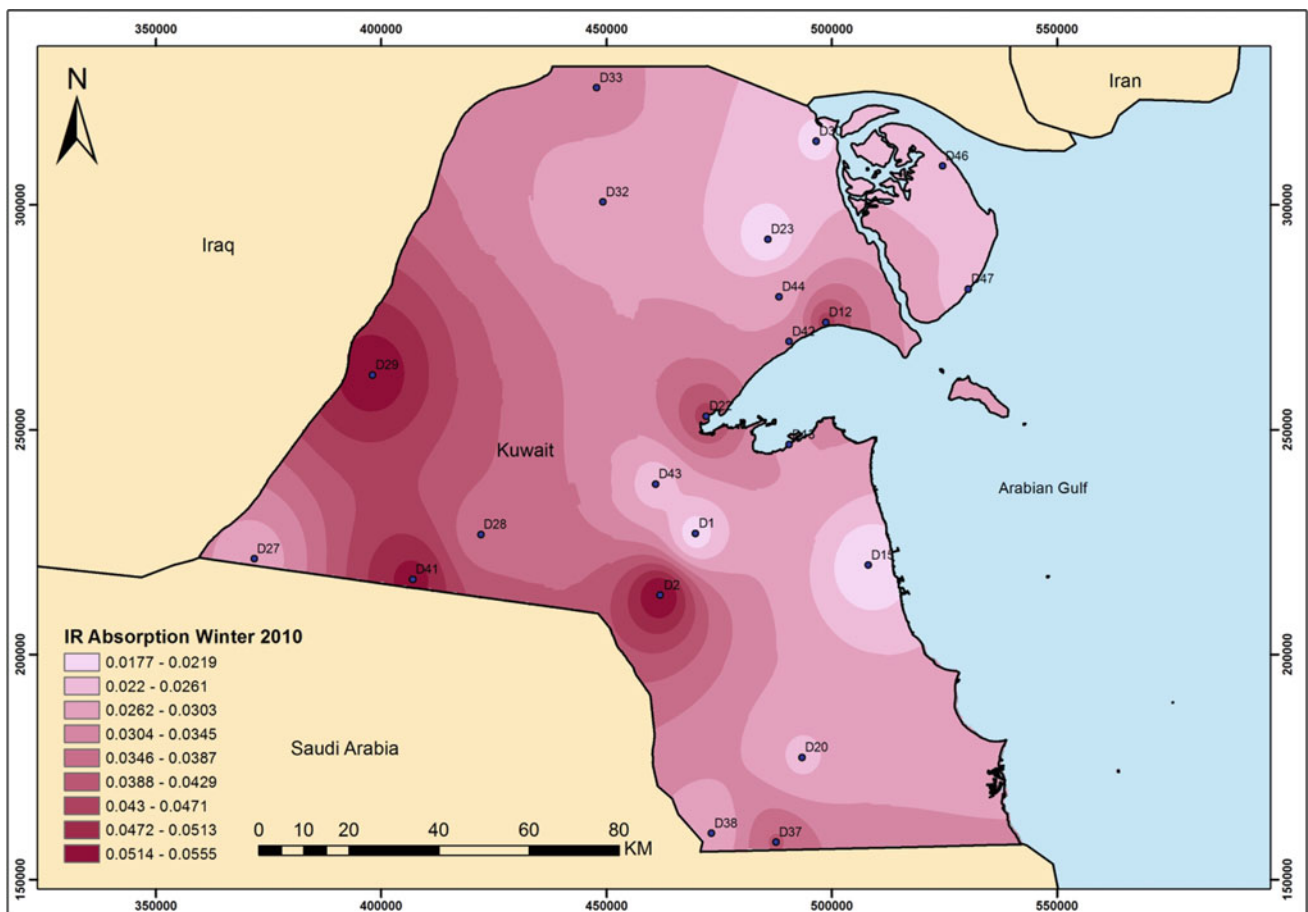


Fig. 9.27 Dust absorption of infrared light in winter 2010

UV Absorption Spring 2010

The absorbed ultraviolet light in spring varies throughout Kuwait. The absorption of ultraviolet light was high across four main locations in Kuwait that are represented by dark violet on the above map. These locations are in the north at Um Nega area (collector D31) and at North Um Qawati (collector D34), and along the northwestern border with Iraq (collector 35), as well as the southern border with Saudi Arabia (collector D39).

The dust shows mid-high absorption across various areas in Kuwait. These areas are North Ahmad Al-Jaber Air Base (collector D4), at Mutla (collector D5), at North Mutla (collector D6), at Raudhatain gate (D8), at North Sabiya (collector D11), at Ras Zur-Wafra (collector D18), et al. Wafra (collector D19), at Kathma (collector D22), at Salmi border zone (collector D27), at Sabah Al-Ahmad Nature Reserve (collectors D42 and D44), at Bubiyan-Northeast (collector D46), at Ritqa (collector D33), at Huwaimiliyah (collector D35), and at the Kuwait-Saudi Arabia border zone (collector D39).

The dust shows medium absorption of ultraviolet at the western side of Burgan oil field (collector D3), at Liyah (collector D7), et al. Wafra (collector D19), at Wafra animal farm (collector D20), at Um Qawati (collector D24), at Poultry mid-way Salmi road (collector D38), and at the Kuwait-Saudi Arabia border zone (collector D40).

The dust shows low absorption of ultraviolet light in five locations in Kuwait. These locations are Abdulia-Managish Road (collector D2), the western side of Burgan oil field (collector D3), the Kuwait-Saudi Arabia border zone (collector D36), Um Jethathil (collector D41), and Sabah Al-Ahmad Nature Reserve (collector D43). Finally, the dust shows very low absorption of ultraviolet light across five various locations in Kuwait: the South Buffer zone at (collector D25), at Poultry mid-way Salmi road (collector D28), at the KISR's Salmiya station (Collector D14), at the KISR's main building Shuwaikh (Collector D13), and at Um Qasir/Bahaith (collector D30) (Fig. 9.28).

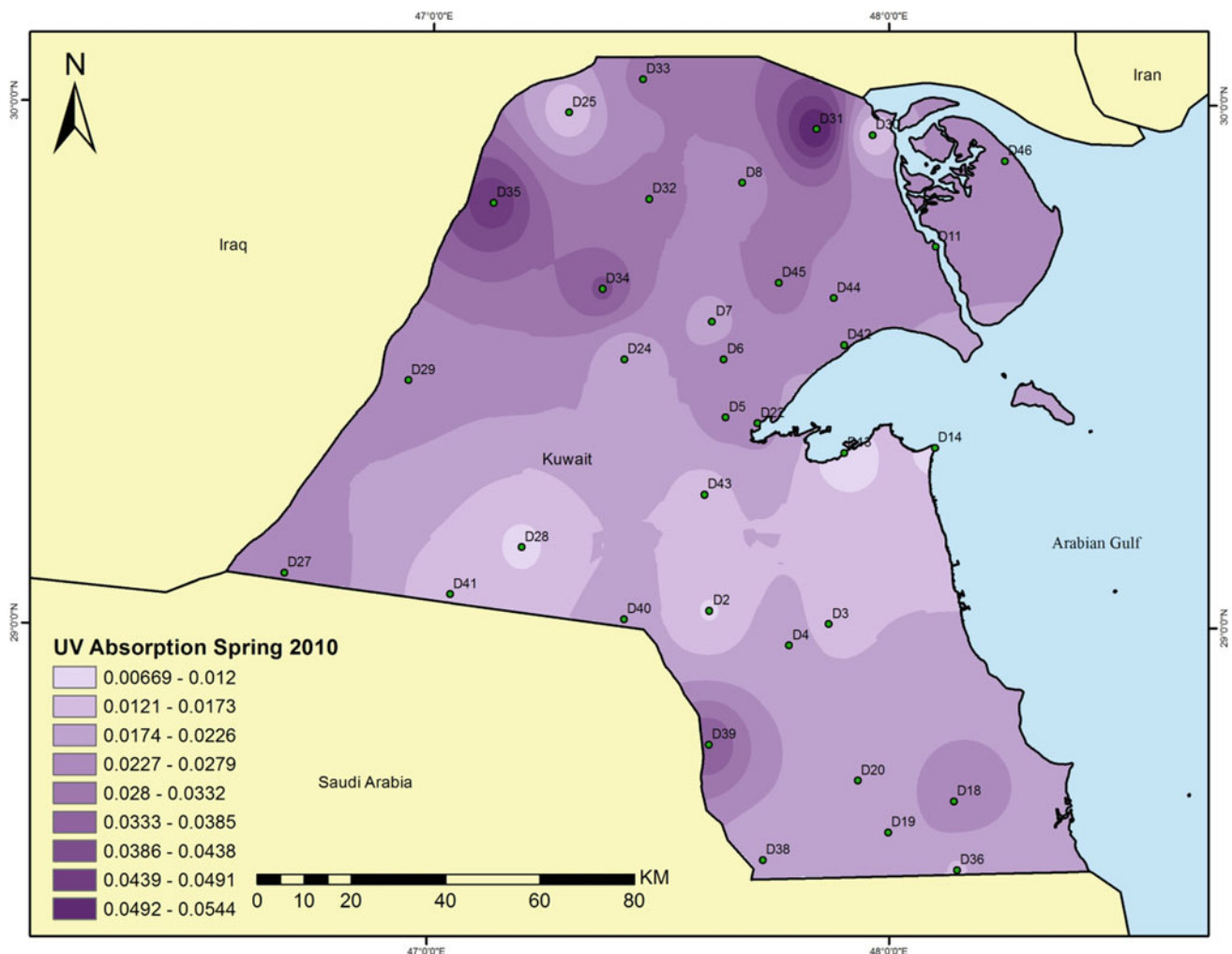


Fig. 9.28 Dust absorption of ultraviolet light in spring 2010

Violet Absorption Spring 2010

The violet light absorbed in spring varies throughout Kuwait. The absorption of violet light was high at four main locations in Kuwait represented by dark violet on the above map. These locations are in the north at Um Nega (collector D31) and at North Um Qawati (collector D34), and along the northwestern border with Iraq (collector 35), as well as the southern border with Saudi Arabia (collector D39).

The dust shows mid-high absorption across various areas in Kuwait. These areas are North Ahmad Al-Jaber Air Base (collector D4), Mutla (collector D5), North Mutla (collector D6), Raudhatain gate (D8), North Sabiya (collector D11), Ras Zur-Wafra (collector D18), Al Wafra (collector D19), Kathma (collector D22), Salmi border zone (collector D27), Sabah Al-Ahmad Nature Reserve (collectors D42 and D44), Bubiyan-Northeast (collector D46), Ritqa (collector D33), Huwaimiliyah (collector D35), and the Kuwait-Saudi Arabia border zone (collector D39).

The dust shows medium absorption of violet at the western side of Burgan oil field (collector D3), at Liyah (collector D7), at Wafra animal farm (collector D20), at Poultry mid-way Salmi road (collector D38), and at the Kuwait-Saudi Arabia border zone (collector D40).

The dust shows low absorption of violet light across four locations in Kuwait: the western side of Burgan oil field (collector D3), Um Jethathil (collector D41), the KISR's Salmiya station (Collector D14), Um Qasir/Bahaith (collector D30), and Um Qawati (collector D24).

The dust shows very low absorption of violet lights across seven various locations in Kuwait, represented by very light violet on the map. These locations are the Abdulia-Managish Road (collector D2), the Sabah Al-Ahmad Nature Reserve (collector D43), the South Buffer zone (collector D25), the Poultry mid-way Salmi road (collector D28), the Kuwait-Saudi Arabia border zone (collector D36), Al Wafra (collector D19), and the KISR's main building Shuwaikh (Collector D13) (Fig. 9.29).

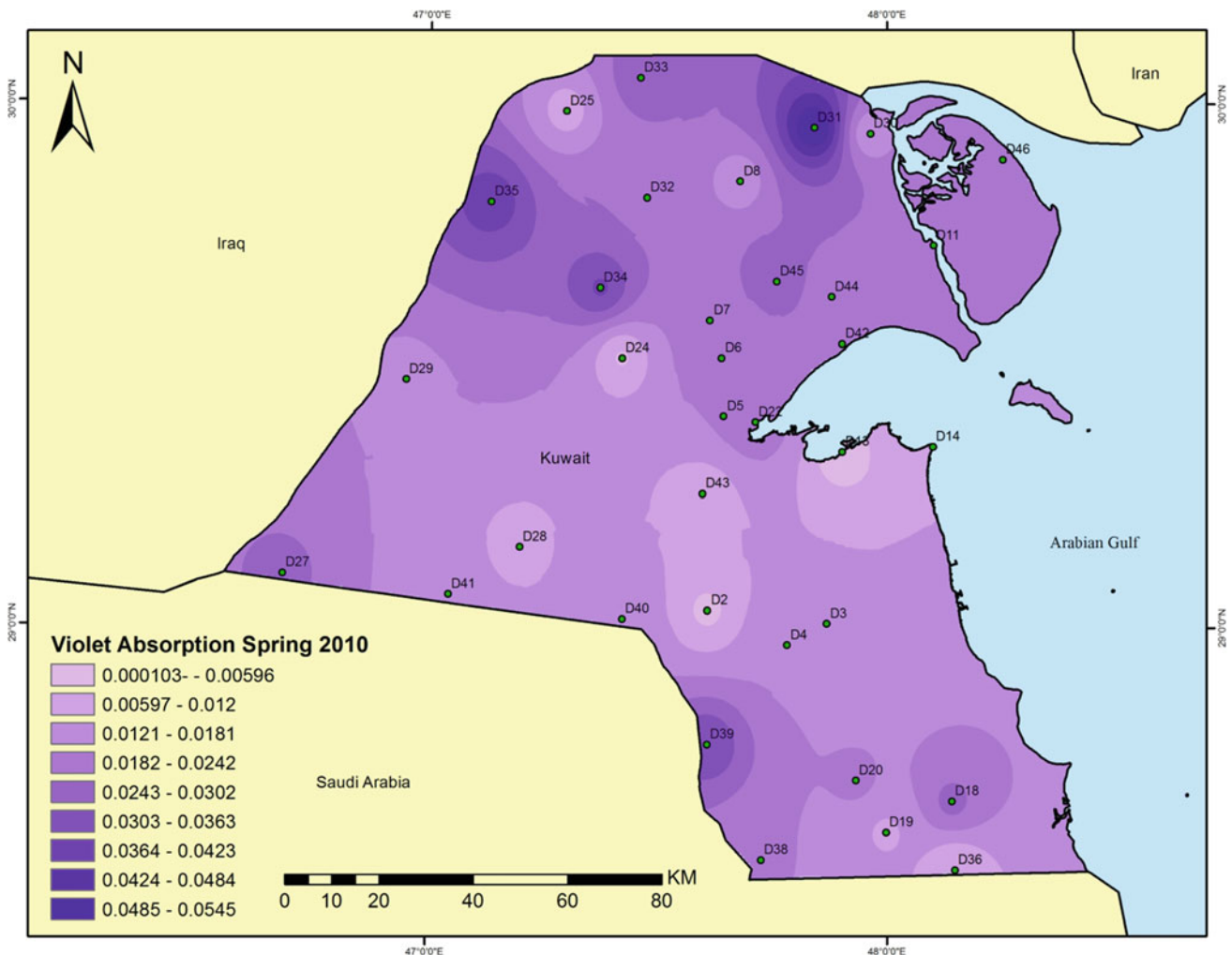


Fig. 9.29 Dust absorption of violet light in spring 2010

Blue Absorption Spring 2010

The absorbed blue light in spring varies throughout Kuwait. The absorption of blue light was high at four main locations in Kuwait represented by dark blue on the above map. These locations are in the north at Um Nega (collector D31) and at North Um Qawati (collector D34), and along the northwestern border with Iraq (collector 35), as well as the southern border with Saudi Arabia (collector D39).

The dust shows mid-high absorption various areas across Kuwait. These areas are North Ahmad Al-Jaber Air Base (collector D4), Mutla (collector D5), North Mutla (collector D6), Raudhatain gate (D8), North Sabiya (collector D11), Ras Zur-Wafra (collector D18), Al Wafra (collector D19), Kathma (collector D22), Salmi border zone (collector D27), Sabah Al-Ahmad Nature Reserve (collectors D42 and D44), Bubiyan-Northeast (collector D46), Ritqa (collector D33), Huwaimiliyah (collector D35), and the Kuwait-Saudi Arabia border zone (collector D39).

The dust shows medium absorption of blue at the western side of Burgan oil field (collector D3), at Liyah (collector D7), at Wafra animal farm (collector D20), at Poultry mid-way Salmi road (collector D38), and at the Kuwait-Saudi Arabia border zone (collector D40).

The dust shows low absorption of blue light across five locations in Kuwait: the western side of Burgan oil field (collector D3), Um Jethathil (collector D41), the KISR's Salmiya station (Collector D14), Um Qawati (collector D30), and the northeastern border with Saudi Arabia at Abraq (collector D29).

The dust shows very low absorption of blue lights across eight locations in Kuwait, represented by very light blue on the map. These locations are the Abdulia-Managish Road (collector D2), Sabah Al-Ahmad Nature Reserve (collector D43), Um Qawati (collector D24), the South Buffer zone (collector D25), Poultry mid-way Salmi road (collector D28), the Kuwait-Saudi Arabia border zone (collector D36), Al Wafra (collector D19), and the KISR's main building Shuwaikh (Collector D13) (Fig. 9.30).

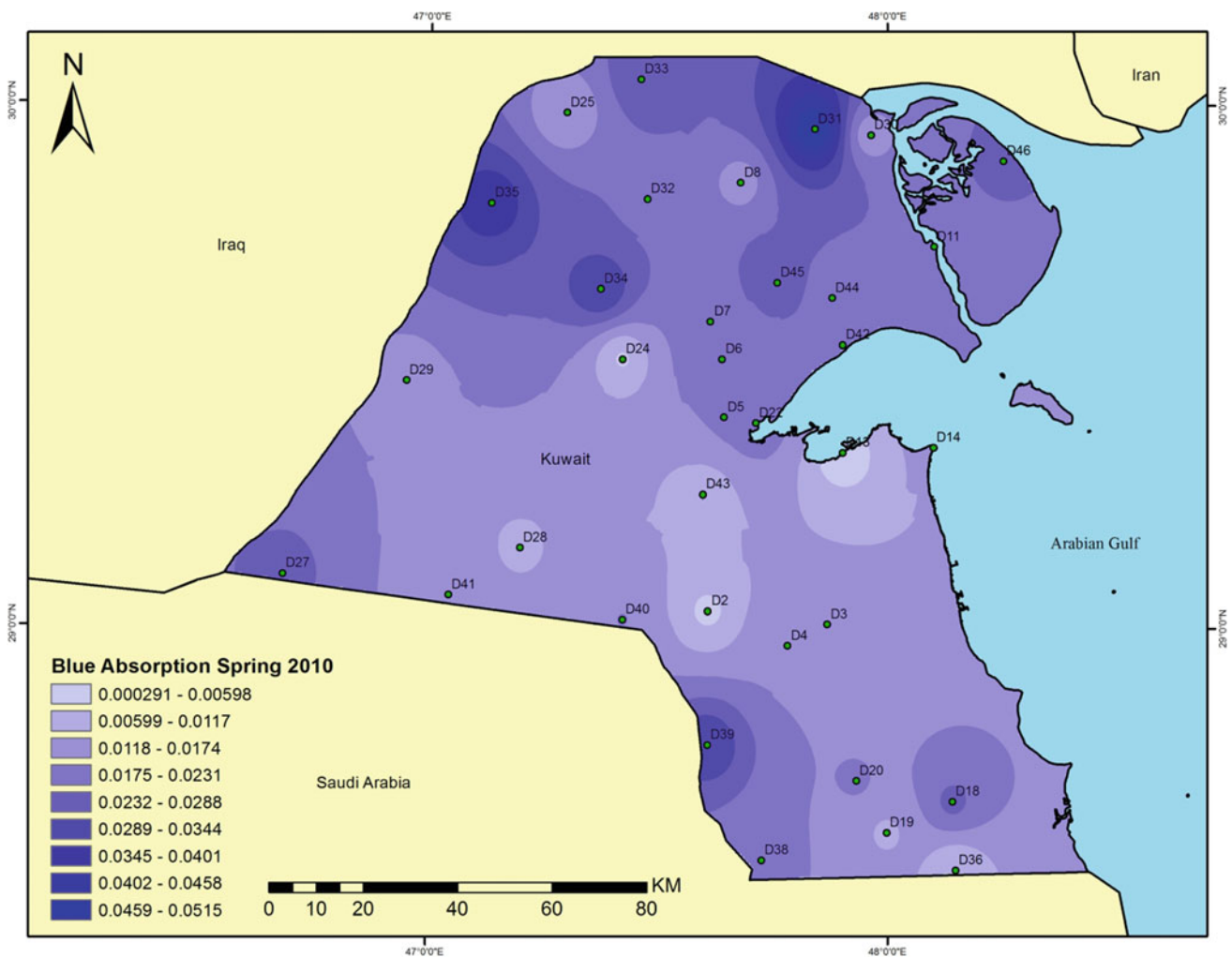


Fig. 9.30 Dust absorption of blue light in spring 2010

Cyan Absorption Spring 2010

The cyan light absorbed in spring varies throughout Kuwait. The absorption of cyan light is high at four main locations in Kuwait, represented by dark cyan on the above map. These locations are in the north at Um Nega (collector D31) and North Um Qawati (collector D34), and along the north-western border with Iraq (collector 35), as well as the southern border with Saudi Arabia (collector D39).

The dust shows mid-high absorption in various areas across Kuwait. These areas are North Ahmad Al-Jaber Air Base (collector D4), Mutla (collector D5), North Mutla (collector D6), Raudhatain gate (D8), North Sabiya (collector D11), Ras Zur-Wafra (collector D18), Al Wafra (collector D19), Kathma (collector D22), Salmi border zone (collector D27), Sabah Al-Ahmad Natural Reserve (collectors D42 and D44), Bubiyan-Northeast (collector D46), Ritqa (collector D33), Huwaimiliyah (collector D35), and the Kuwait-Saudi Arabia border zone (collector D39).

The dust shows medium absorption of cyan at the western side of Burgan oil field (collector D3), at Liyah (collector D7), at Wafra animal farm (collector D20), at Poultry mid-way Salmi road (collector D38), and at the Kuwait-Saudi Arabia border zone (collector D40).

The dust shows low absorption of cyan light across five locations in Kuwait: the western side of Burgan oil field (collector D3), Um Jethathil (collector D41), the KISR’s Salmiya station (Collector D14), Um Qasir/Bahaith (collector D30), and the northeastern border with Saudi Arabia at Abraq (collector D29).

The dust shows very low absorption of cyan light across eight various locations in Kuwait, represented by the very light cyan on the map. These locations are the Abdulia-Managish Road (collector D2), Sabah Al-Ahmad Nature Reserve (collector D43), Um Qawati (collector D24), the South Buffer zone (collector D25), Poultry mid-way Salmi road (collector D28), the Kuwait-Saudi Arabia border zone (collector D36), Al Wafra (collector D19), and the KISR’s main building Shuwaikh (collector D13) (Fig. 9.31).

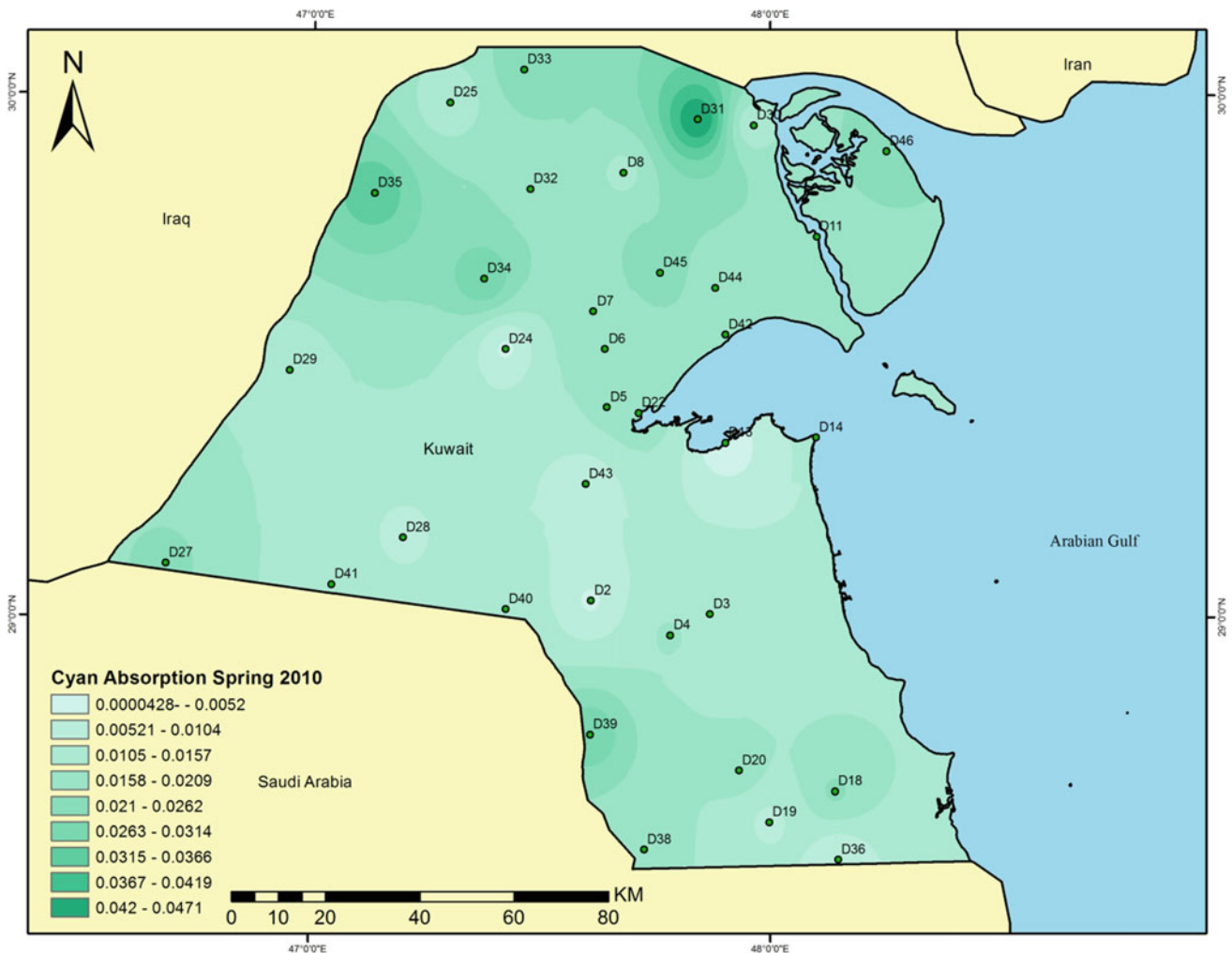


Fig. 9.31 Dust absorption of cyan light in spring 2010

Green Absorption Spring 2010

The green light absorbed in spring varies throughout Kuwait. The absorption of green light is high across four main locations in Kuwait, represented by dark green on the above map. These locations are in the north at Um Nega (collector D31) and North Um Qawati (collector D34), and along the northwestern border with Iraq (collector 35), as well as the southern border with Saudi Arabia (collector D39).

The dust shows mid-high absorption across various areas in Kuwait. These areas are North Ahmad Al-Jaber Air Base (collector D4), Mutla (collector D5), North Mutla (collector D6), Raudhatain gate (D8), North Sabiya (collector D11), Ras Zur-Wafra (collector D18), Al Wafra (collector D19), Kathma (collector D22), Salmi border zone (collector D27), Sabah Al-Ahmad Nature Reserve (collectors D42 and D44), Bubiyan-Northeast (collector D46), Ritqa (collector D33), Huwaimilyah (collector D35), and the Kuwait-Saudi Arabia border zone (collector D39).

The dust shows medium absorption of green at the western side of Burgan oil field (collector D3), at Liyah (collector D7), at Wafra animal farm (collector D20), at Poultry mid-way Salmi road (collector D38), and at the Kuwait-Saudi Arabia border zone (collector D40).

The dust shows low absorption of green light in five locations in Kuwait: the western side of Burgan oil field (collector D3), Um Jethathil (collector D41), the KISR’s Salmiya station (Collector D14), Um Qasir/Bahaith (collector D30), and the northeastern border with Saudi Arabia at Abraq (collector D29).

The dust shows very low absorption of green lights across eight locations in Kuwait, represented by very light green on the map. These locations are Abdulia-Managish Road (collector D2), Sabah Al-Ahmad Nature Reserve (collector D43), Um Qawati (collector D24), the South Buffer zone (collector D25), Poultry mid-way Salmi road (collector D28), the Kuwait-Saudi Arabia border zone (collector D36), Al Wafra (collector D19), and the KISR’s main building Shuwaikh (collector D13) (Fig. 9.32).

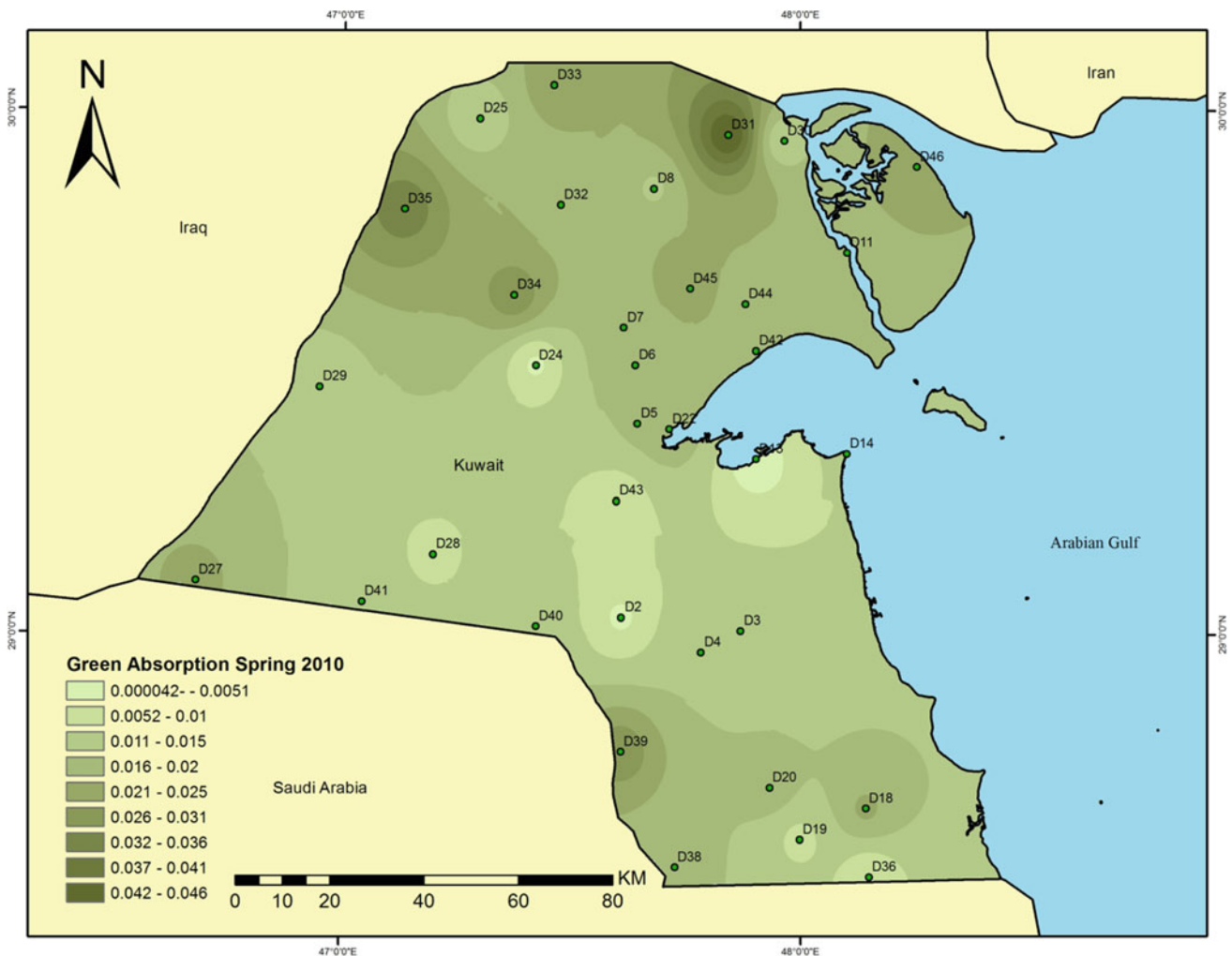


Fig. 9.32 Dust absorption of green light in spring 2010

Yellow Absorption Spring 2010

The yellow light absorbed in spring varies throughout Kuwait. The absorption of yellow light was high at four main locations in Kuwait, represented by dark yellow on the above map. These locations are in the north at Um Nega (collector D31) and North Um Qawati (collector D34), and along the northwestern border with Iraq (collector 35), as well as the southern border with Saudi Arabia (collector D39).

The dust shows mid-high absorption in various areas across the State of Kuwait. These areas are North Ahmad Al-Jaber Air Base (collector D4), Mutla (collector D5), North Mutla (collector D6), Raudhatain gate (D8), North Sabiya (collector D11), Ras Zur-Wafra (collector D18), Al Wafra (collector D19), Kathma (collector D22), Salmi border zone (collector D27), Sabah Al-Ahmad Nature Reserve (collectors D42 and D44), Bubiyan-Northeast (collector D46), Ritqa (collector D33), Huwaimiliyah (collector D35), and the Kuwait-Saudi Arabia border zone (collector D39).

The dust shows medium absorption of yellow at the western side of Burgan oil field (collector D3), at Liyah (collector D7), at Wafra animal farm (collector D20), at Poultry mid-way Salmi road (collector D38), and at the Kuwait-Saudi Arabia border zone (collector D40).

The dust shows low absorption of yellow light across five locations in Kuwait: the western side of Burgan oil field (collector D3), Um Jethathil (collector D41), the KISR's Salmiya station (collector D14), Um Qasir/Bahaith (collector D30), and the northeastern border with Saudi Arabia at Abraha (collector D29).

The dust shows very low absorption of yellow light across eight locations in Kuwait, represented by the very light yellow on the map. These locations are Abdulia-Managish Road (collector D2), Sabah Al-Ahmad Nature Reserve (collector D43), Um Qawati (collector D24), the South Buffer zone (collector D25), Poultry mid-way Salmi road (collector D28), the Kuwait-Saudi Arabia border zone (collector D36), Al Wafra (collector D19), and the KISR's main building Shuwaikh (collector D13) (Fig. 9.33).

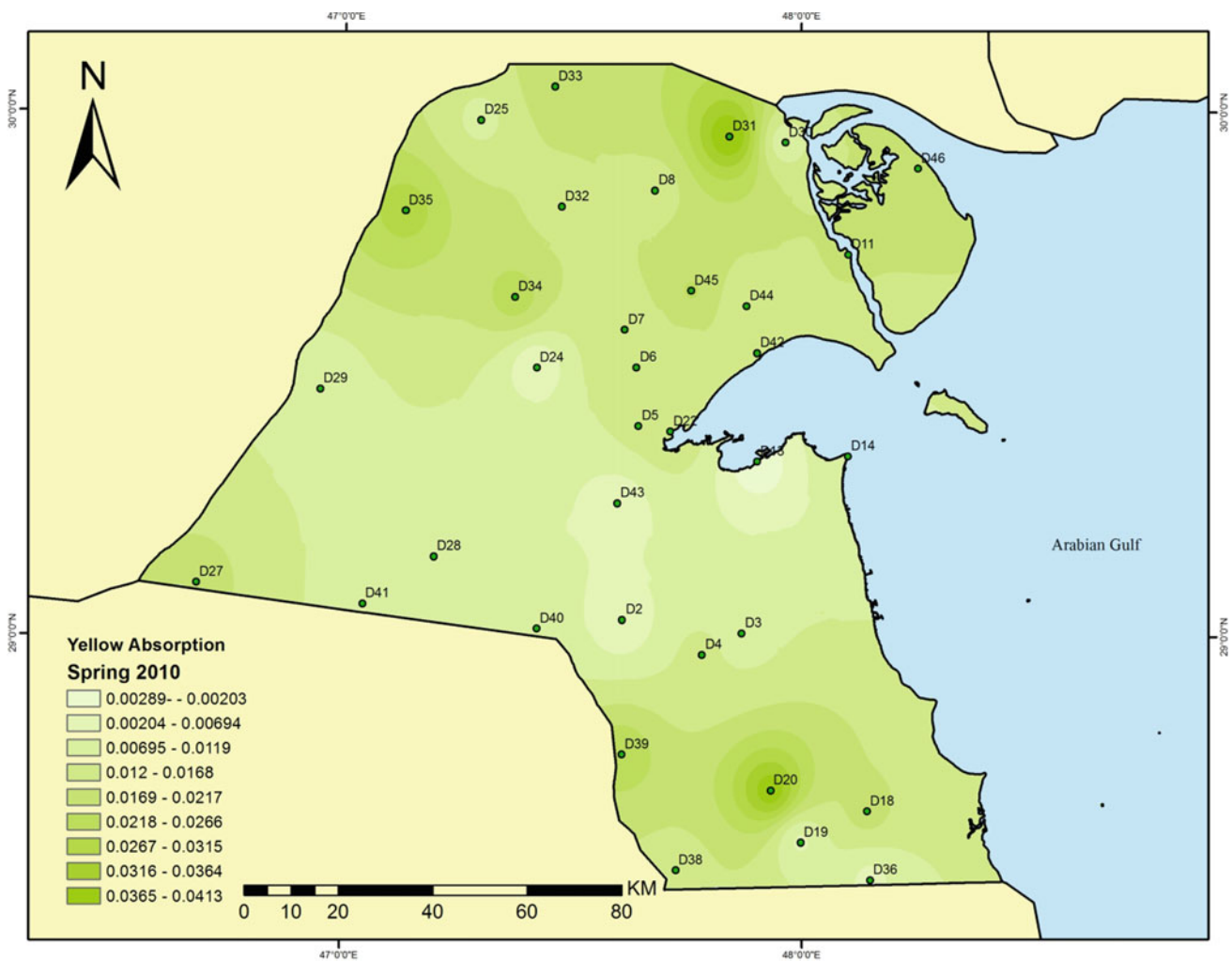


Fig. 9.33 Dust absorption of yellow light in spring 2010

Orange Absorption Spring 2010

The orange light absorbed in spring varies throughout Kuwait. The absorption of orange light was high across four main locations in Kuwait, represented by dark orange on the above map. These locations are the in north at Um Nega (collector D31) and North Um Qawati (collector D34), and along the northwestern border with Iraq (collector 35), as well as the southern border with Saudi Arabia (collector D39).

The dust shows mid-high absorption across various areas in Kuwait. These areas are North Ahmad Al-Jaber Air Base (collector D4), Mutla (collector D5), North Mutla (collector D6), Raudhatain gate (D8), North Sabiya (collector D11), Ras Zur-Wafra (collector D18), et al. Wafra (collector D19), at Kathma (collector D22), at Salmi border zone (collector D27), at Sabah Al-Ahmad Nature Reserve (collectors D42 and D44), at Bubiyan-Northeast (collector D46), at Ritqa (collector D33), at Huwaimilyah (collector D35), and at the Kuwait-Saudi Arabia border zone (collector D39).

The dust shows medium absorption of orange at the western side of Burgan oil field (collector D3), at Liyah (collector D7), at Wafra animal farm (collector D20), at Poultry mid-way Salmi road (collector D38), and at the Kuwait-Saudi Arabia border zone (collector D40).

The dust shows low absorption of orange light in five locations in Kuwait: the western side of Burgan oil field (collector D3), Um Jethathil (collector D41), the KISR’s Salmiya station (collector D14), Um Qasir/Bahaith at (collector D30), and the northeastern border with Saudi Arabia at Abraq (collector D29).

The dust shows very low absorption of orange light across eight locations in Kuwait, represented by the very light orange on the map. These locations are Abdulia-Managish Road (collector D2), Sabah Al-Ahmad Nature Reserve (collector D43), Um Qawati (collector D24), the South Buffer zone (collector D25), Poultry mid-way Salmi road (collector D28), the Kuwait-Saudi Arabia border zone (collector D36), Al Wafra (collector D19), and the KISR’s main building Shuwaikh (collector D13) (Fig. 9.34).

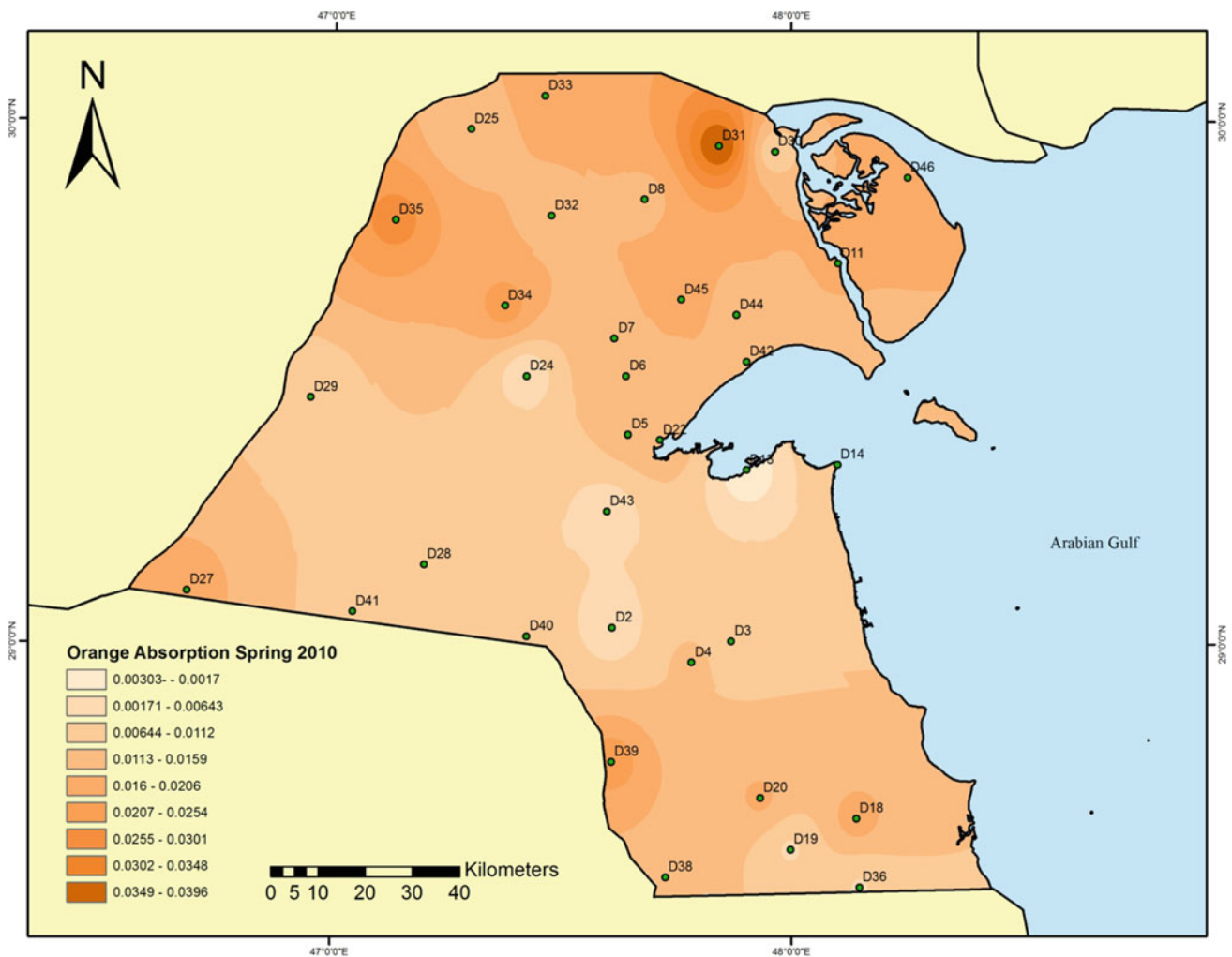


Fig. 9.34 Dust absorption of orange light in spring 2010

Red Absorption Spring 2010

The red light absorbed in spring varies throughout Kuwait. The absorption of red light was high at four main locations in Kuwait, represented by dark red on the above map. These locations are in the north at Um Nega (collector D31) and North Um Qawati (collector D34), and along the north-western border with Iraq (collector 35), as well as the southern border with Saudi Arabia (collector D39).

The dust shows mid-high absorption in various areas across the State of Kuwait. These areas are North Ahmad Al-Jaber Air Base (collector D4), Mutla (collector D5), North Mutla (collector D6), Raudhatain gate (D8), North Sabiya (collector D11), Ras Zur-Wafra (collector D18), Al Wafra (collector D19), Kathma (collector D22), Salmi border zone (collector D27), Sabah Al-Ahmad Nature Reserve (collectors D42 and D44), Bubiyan-Northeast (collector D46), Ritqa (collector D33), Huwaimilyah (collector D35), and the Kuwait-Saudi Arabia border zone (collector D39).

The dust shows medium absorption of red at Liyah (collector D7), at Wafra animal farm (collector D20), at the southern border with Saudi Arabia (collector D38), and at the Kuwait-Saudi Arabia border zone (collectors D40 and 41).

The dust shows low absorption of red light in five locations in Kuwait: the western side of Burgan oil field (collector D3), Um Jethathil (collector D41), the KISR's Salmiya station (Collector D14), the northeastern border with Saudi Arabia at Abraq (collector D29), the Kuwait-Saudi Arabia border zone (collector D36), Al Wafra (collector D19), Poultry mid-way Salmi road (collector D28), and the South Buffer zone (collector D25).

The dust shows very low absorption of red light across five locations in Kuwait, represented by the very light red on the map. These locations are Abdulia-Managish Road (collector D2), Sabah Al-Ahmad Nature Reserve (collector D43), Um Qawati (collector D24), Um Qasir/Bahaith (collector D30), and the KISR's main building Shuwaikh (collector D13) (Fig. 9.35).

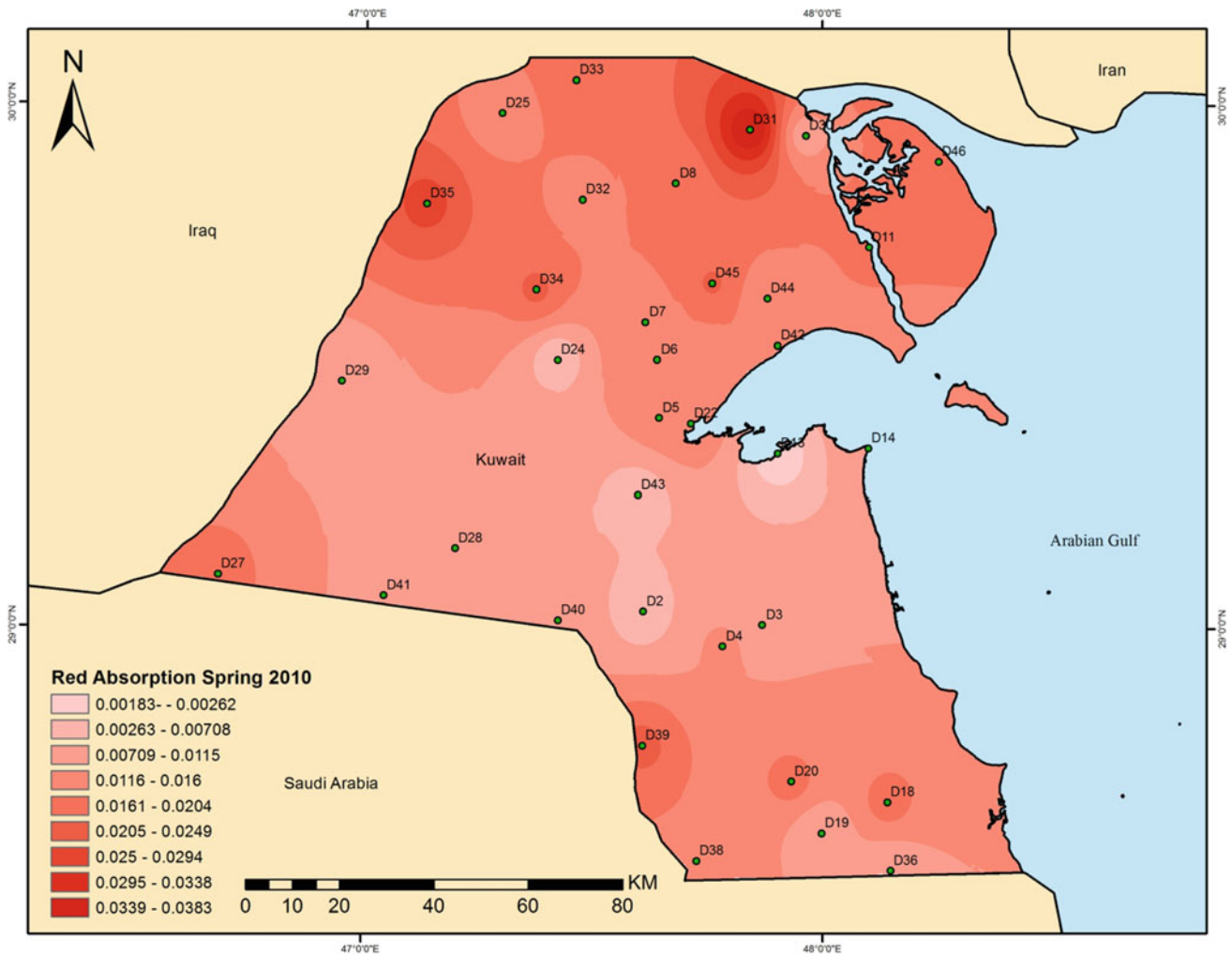


Fig. 9.35 Dust absorption of red light in spring 2010

Infrared Absorption Spring 2010

The absorbed red light in spring varies throughout Kuwait. The dust shows high absorption at five main locations across Kuwait, represented by the dark red on the above map. These locations are at Um Nega (collector D31), at the South Buffer zone (collector D25), at Raudhatain gate (D8), at Um Jethathil (collector D41), and at Salmi border zone (collector D27).

The dust absorbs mid-high infrared light at several locations: Sabah Al-Ahmad Nature Reserve (collector D43), Poultry mid-way Salmi road (collector D38), Ras Zur-Wafra (collector D18), the western side of Burgan oil field (collector D3), Ritqa (collector D33), North Um Qawati (collector D34), Huwaimilyah (collector D35), the Kuwait-Saudi Arabia border zone (collector D39), North Ahmad Al-Jaber Air Base (collector D4), Mutla (collector D5), North Mutla (collector D6), North Sabiya (collector D11),

Al Wafra (collector D19), Kathma (collector D22), Salmi border zone (collector D27), Sabah Al-Ahmad Nature Reserve (collectors D42 and D44), and Bubiyan-Northeast (collector D46).

The dust shows medium absorption at the western side of Burgan oil field (collector D3), at Liyah (collector D7), et al. Wafra (collector D19), at Wafra animal farm (collector D20), at Um Qawati (collector D24), at Um Qasir/Bahaith (collector D30), and at the Kuwait-Saudi Arabia border zone (collector D40).

The dust shows a very low absorption at four main locations, represented by the light red on the map in Fig. 9.36. These locations are Abdulia- Managish Road (collector D2), Poultry mid-way Salmi road (collector D28), the Kuwait-Saudi Arabia border zone (collector D36), and the KISR's main building location in Kuwait Bay (collector D13).

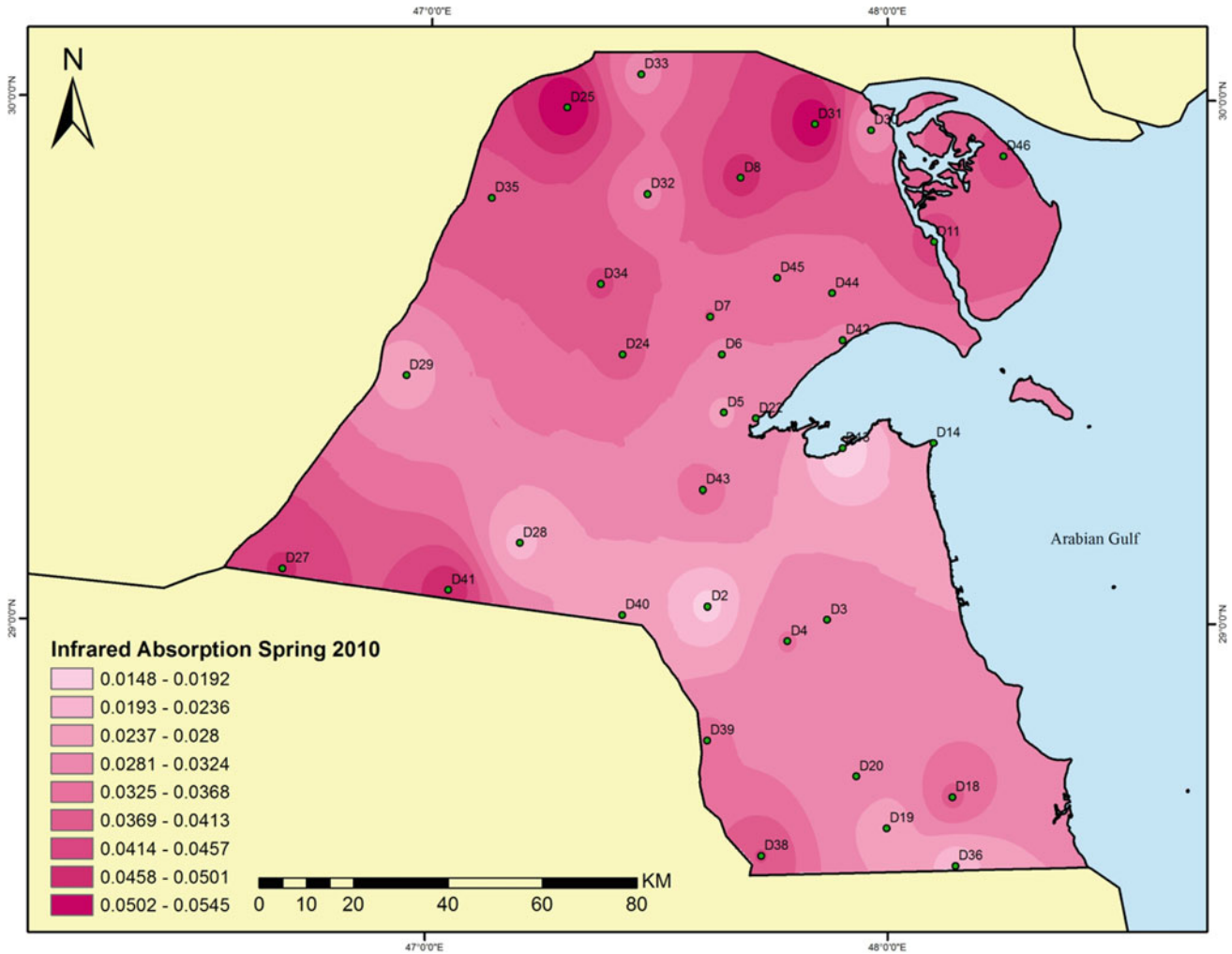


Fig. 9.36 Dust absorption of infrared light in spring 2010

From the UV–VIS maps of absorption in different seasons across Kuwait, it is clear that the dust absorption for the UV–VIS light radiation varies from month to month and season to season. The Fourier transformer infrared data clarify these phenomena in the following section.

Furrier Transformer Infrared (FT-IR (MID))

The collectors showed that the chemical functional group, chemical bounding, and chemical elements vary for the same collectors in different seasons. The dust for the same collector contained the same functional groups; however, it contained different structures, such as the silicon group. In December, the D3 collector had Si₂O only; whereas, in September, the same collector had more silicon functional

groups, such as Si–OH, Si–F, and Si₂O. Some chemicals appeared during some seasons and disappeared during others, such as the nitrite functional group R–O–N=O, which was found in the December collector; however, it disappeared from the March and September collectors.

From the study of the collectors for the four seasons, the dust chemicals in the collectors changed depending on the weather conditions and the nature of the area. Dust content that has a nitrogen compound, such as the amide, the amine, or the nitro, appeared in a few collectors. The dust mostly contained silicon (Si) compounds, hydrocarbons (CH), sulfur (sulphur) (S), phosphorus (P), and halogens (F, Cl, Br, I). The three tables for the D-3 collector (Tables 9.1, 9.2, and 9.3) show how the chemical compound varies from season to season. Seasonal Color Spectrophotometric Variations of Dust Samples within Kuwait, April 2014.

Table 9.1 Collector D-3
December 2010

No	Function Group	Compound	Bounds	Peak Regions (cm ⁻¹)	
				From	To
1	Alkanes	R–CH ₂ –R''	CH	2936	2916
			CH	2863	2843
			CH	1485	1445
		R(CH ₂) ₄ –C	CH	2936	2916
			CH	2863	2843
			CH	1485	1445
			CC	750	720
		RCH ₃	CH	2972	2952
			CH	2882	2862
CH	1475		1435		
CH	1380		1385		
2	Ketones	RCO–Ph#NH ₂	C=O	1655	1635
		4C ring K	C=O	1785	1765
		Fused ring	C=O	1655	1635
3	Nitrite	R–O–N =O	N=O	1681	1648
			N=O	1625	1605
			N–O	814	751
4	Phosphorus	P=S	P=S	800	580
5	Silicon	Si–OH	O–H	3700	3200
			Si–OH	1040	1020
			Si–O	910	830
		Si–O–Si	Si–O–Si	1020	1010
		Si–O–C	Si–O–C	1100	1000
Si–O–C	Si–O–C	990	945		
Si–Cl	Si–Cl	550	470		
7	Sulfur	S=S	S=S	500	400
		R–SO ₃ H ₃ O	H ₃ O	2800	1650
			SO ₃	1230	1120

Table 9.2 Sample D-3
28-3-2010

No	Function group	Compound	Bounds	Peak regions (cm ⁻¹)	
				From	To
1	Ethers	4-Ring ETH	C–O–C C–O–C	1035 990	1020 975
		6-Ring ETH	C–O–C C–O–C	1110 820	1090 805
2	Halogens	C–Br	C–Br	600	500
		C–I	C–I	610	485
3	Ketones	Ph–CO–Ph	C=O	1670	1660
		RCO–Ph#NH ₂	C=O	1655	1635
		C=C–CO–C=C	C=O	1670	1663
		Quinones	C=O	1655	1635
4	Phosphorus	P=S	P=S	800	580
5	SILICONS	Si–O–Si	Si–O–Si	1020	1010
6	Sulfur	C=S	C=S	1200	1050
		S–S	S–S	500	400
		R–SOOH	O–H S=O S–O	2790 1090 870	2340 990 810

Table 9.3 Sample D-3
28-9-2010

No	Function group	Compound	Bounds	Peak regions (cm ⁻¹)	
				From	To
1	Alkanes	Ph–CH ₃	CH CH	2930 2870	2920 2860
		R'–CH ₂ –R''	CH CH CH	2936 2863 1485	2916 2843 1445
2	Ethers	4-Ring ETH	C–O–C C–O–C	1035 990	1020 975
		6-Ring ETH	C–O–C C–O–C	1110 820	1090 805
3	Halogens	C–Br	C–Br	600	500
		C–I	C–I	610	485
4	Ketones	Ph–CO–Ph	C=O	1670	1660
		RCO–Ph#NH ₂	C=O	1655	1635
		C=C–CO–C=C	C=O	1670	1663
		Quinones	C=O	1655	1635
5	SILICONS	Si–O–Si	Si–O–Si	1100	1000
		Si–F	Si–F	920	820
		Si–OH	O–H Si–OH Si–O	3700 1040 910	3200 1020 830
6	Sulfur	C=S	C=S	1200	1050
		S–S	S–S	500	400
		R–SOOH	O–H S=O S–O	2790 1090 870	2340 990 810

Conclusion

From the UV–VIS study and FT-IR study, it is clear that the absorbance of UV–VIS light varies from season to season and from month to month. The difference in absorbance is related to the change in the chemical content of dust. The FT-IR data are very important for revealing the different chemical content of dust and for quickly scanning what possible compounds can be found in dust particles when further analysis is required.

References

- Al-Dousari A.M., N. Al-Dousari, A. Ramadhan, M. Ahmed, A. Aba. 2014. Assessments of dust fallout within Kuwait. ProScience- 1st international conference on atmospheric dust (DUST-14). 1: 149–155. DOI: <https://doi.org/10.14644/dust.2014.024>
- Al-Dousari, A., Aba, A., Al-Awadhi, S., Ahmed, M., & Al-Dousari, N. (2016). Temporal and spatial assessment of pollen, radionuclides, minerals and trace elements in deposited dust within Kuwait. *Arabian Journal of Geosciences*, 9(2), 95. <https://doi.org/10.1007/s12517-015-2182-z>.
- Al-Enezi, E., Al-Dousari, A. M., Pokavanich, T., & Al-Shammari, F. M. (2014). Modeling adsorption of inorganic phosphorus on dust fallout in Kuwait bay. *Journal of Engineering Research*, 2(2), 1–14. <https://doi.org/10.7603/s40632-014-0001-4>.
- Neelamani, S., & Al-Dousari, A. (2016). A study on the annual fallout of the dust and the associated elements into the Kuwait Bay. *Kuwait. Arabian Journal of Geosciences.*, 9(3), 210. <https://doi.org/10.1007/s12517-015-2236-2>.
- Subramaniam, N., Al-Sudairawi, M., Al-Dousari, A., & Al-Dousari, N. (2015). Probability distribution and extreme value analysis of total suspended particulate matter in Kuwait. *Arabian Journal of Geosciences.*, 8(12), 11329–11344. <https://doi.org/10.1007/s12517-015-2008-z>.

Open Access This chapter is licensed under the terms of the Creative Commons Attribution 4.0 International License (<http://creativecommons.org/licenses/by/4.0/>), which permits use, sharing, adaptation, distribution and reproduction in any medium or format, as long as you give appropriate credit to the original author(s) and the source, provide a link to the Creative Commons licence and indicate if changes were made.

The images or other third party material in this chapter are included in the chapter's Creative Commons licence, unless indicated otherwise in a credit line to the material. If material is not included in the chapter's Creative Commons licence and your intended use is not permitted by statutory regulation or exceeds the permitted use, you will need to obtain permission directly from the copyright holder.



Summary

The satellite images show seven major source areas of dust storm trajectories in the world:

- (I) The Western and Southern Sahara Desert (Western Libya toward Morocco or south toward Nigeria and Ghana).
- (II) The Eastern Sahara Desert (Eastern Libya toward Egypt and Palestine).
- (III) Ethiopia-Southern Arabia (East Sudan and Ethiopia toward Southern Arabia).
- (IV) Northern Arabia (Jordan toward Mesopotamia, Kuwait, and Bahrain).
- (V) The Gobi Desert (Gobi Desert toward North China, Korea, and Japan).
- (VI) The Taklimakan Desert (Taklimakan Desert toward east China or south to Afghanistan, Pakistan, and Baluchistan).
- (VII) The Australian Desert (Northern Australia toward the West and Southern Australia toward the East).

This present study indicates that each zone of global dust storm trajectories has unique dust fallout characteristics regarding depositional rates, grain size, mineralogy, particle surface area, and variations between upwind and downwind. Dust fallout rates tend to diminish downwind, except in Zone IV, where the midpoint of the dust storm trajectory shows a higher amount of dust than the borders.

On average, mud particles represent 74% of dust samples, while the rest is formed by sand particles (26%). The average samples of the world's fallen dust are negatively skewed, trimodal, with a dominance of silt size fractions (61%). The grain-size trimodality might indicate multiple sources. All of the world's dust storm trajectories are fining downwind due to rapid deposition of sand size fractions. Zone IV is an exceptional case, in which the main trajectory passes from the Western Desert of Iraq through the Mesopotamian Floodplain, loading the wind with mud size fractions (97%), toward Kuwait (desert area), where fallen dust

contains 37% sand particles (UNEP 2016; Al-Dousari et al. 2017; Al-Dousari and Al-Hazza 2013; Al-Ghadban et al. 2008).

The mineralogical and surface area comparison between collected dust in this study and mud particles from surface sediments surrounding the traps shows large variations, which indicate that the mud size particles predominantly originated from regional and global sources (Figs. 3 and 4). Other researchers support the long-distance origination of mud particles. Most of the exposed bedrock in Hawaii (USA) is basalt with little or no quartz, but the overlying soil contains considerable quartz, which is believed to be blown as dust particles from North America across the Pacific Ocean (Péwé et al. 1981). Long-distance traveling dust is commonly composed of very fine particles, with the predominant sizes between 0.068 and 0.02 mm (Walker and Costing 1971).

Regarding the dust in Kuwait, the northwestern, western, and northern winds play major roles in the origin of dust storms to the study area. Regional areas represent the dominant sources of dust fallout, while local sources contribute appreciable amounts. The very fine and fine sand particles originate from local sources as they move in the form of saltation or short-term suspension for a short distance, representing 37% of the average dust fallout percentages in Kuwait. There is a trend of fining in Mean size for dust particles toward the east and the northeast. Carbonates and quartz are the major components of dust in Kuwait, and feldspars are found in appreciable amounts. Other minerals in the dust are gypsum, anhydrite, bassanite, and heavy minerals. The muddy playas, depressions, sabkhas, and intertidal zone (Bubiyan and Warba islands) are the major sources of local dust. Natural vegetation plays a major role in minimizing and reducing fallen dust. Open desert areas show an increase in the quantities of dust fallout by at least two-thirds more than in the National Park in Kuwait. Further studies should concentrate on other aerosols associated with dust (pollen, organic matter, hydrocarbons) rather than dust-control measures.

The continuous monitored pollen and deposited dust in the State of Kuwait from August 2009 to August 2011 lead us to conclude that local and close regional flora are the main source of the pollen load. Except for very low percentages (2–3%) of *Pinaceae* pollen recorded in the north and north-west borders of Kuwait with Iraq (D9, 25, 27, 29, and 30), the remainder could be interpreted as being transported by the northwesterly wind from long-distance regional sources. The closest pine trees in the regional scale are in northern Iraq and Syria, Lebanon, and Turkey. It can also be concluded that areas that experience low depositional dust have a higher concentration of pollen. The years 2009–2010 experienced a high concentration of pollen but lower in the deposited dust compared with 2010–2011. This finding indicates the decrease in native vegetation in the regional and local areas, which caused the increase in deposited dust rates. The pollen counts can be taken as a good indicator of vegetation density deterioration rate. The pollen distribution reached its maximum peak at the end and the beginning of the rainy season in spring (April–May) and fall (October–November), which indicates that the pollen concentration is highly related to climatic conditions and the distribution of drainage system (wadis). Spring marked the highest pollen distribution because of the flowering of a great number of *Chenopodiaceae*, *Gramineae* (*Poaceae*), *Cyperaceae*, *Leguminosae*, and *Plantaginaceae*. Summer (July–August) and winter (January–February) recorded a graph with a

lower distribution of pollen due to the severe drought, dust storms, winter wind, and rainfall. Winter had the lowest pollen count. *Chenopodiaceae* are the most common trigger of allergies in Kuwait, but no correlations so far were noted between pollen and the number of asthma patients in Kuwait (Al-Dousari et al. 2016, 2018b).

Tamarix aphyllae, *Prosopis juliflora* and *Moringa pterigosperma* were found to be effective in controlling the eolian processes. The average sand accumulation around each tree within green belts is equivalent to 10 m³, while it is equivalent to 1.92 m³ for the dominant native plants in Kuwait. Although the trees are much larger in size, some native plants display better capability in controlling eolian sediments. The maximum volumes of sand accumulation were observed around *Nitraria retusa* (21.9 m³), *Lycium shawii* (15.5 m³), and *Haloxylon salicornium* (14.5 m³), which is significant to consider them the most efficient native plants in controlling eolian sediments. Correspondingly, each native plant has its distinctive morphological properties (Ahmed et al. 2016; Ahmed and Al-Dousari 2013; Al-Awadhi and Al-Dousari 2013; Al-Dousari et al. 2018b, c). The green belts and native plants were found to be effective solutions in controlling eolian accumulations, and they have the potential to reduce costs. Therefore, green belts and native plants are recommended as potential future applications to control the sand encroachment problem and resuspended dust particles.

Index

- A**
Absorption, 6, 207–244
Abu Dhabi, 7
Afghanistan, 247
AOD, 6–10
Arabia, 1, 14–20, 24, 27, 28, 31, 32, 36, 43, 47, 208, 209, 211–243, 247
Arabian, 1, 13–40, 100
Australia, 47, 247
- B**
Bahrain, 7, 30, 247
Baluchistan, 247
BET surface area, 202
Bubiyah, 14, 22, 23, 48, 49, 57, 59, 61, 63, 65, 67, 69, 71, 73, 75, 77, 79, 81, 83, 86, 89, 96, 98, 99, 101, 105–107, 109–119, 121–127, 145, 148, 152, 154, 157, 158, 160, 162, 163, 165, 168, 170, 171, 173, 202–204, 217–243, 247
- C**
Calcite, 96, 99, 102, 103, 108, 114
Carbonates, 13–18, 20–23, 25–35, 43, 96, 97, 99, 102–109, 111, 114–117, 177, 202, 247
China, 247
Clay, 13–18, 20–23, 25–33, 43, 47, 57, 58, 77, 78, 81, 98, 104, 110, 114–117, 202
Conductivity, 199–203
- D**
Dolomite, 96, 99, 103, 105, 111, 117
- E**
Egypt, 247
Element, 1, 2, 47, 121, 122, 124, 126, 127, 244
Ethiopia, 247
- F**
Feldspar, 18, 31, 96, 100, 106, 112, 114, 117, 118, 122, 124, 202, 247
- G**
Gulf, 1, 7, 13–40, 100, 142
- H**
Heavy minerals, 35, 122, 124, 126, 127, 202, 247
- I**
Image, 1, 2, 5, 6, 12–14, 16–43, 48, 58, 181, 247
Inductively Coupled Plasma (ICP), 121, 122, 124–127
Iraq-Iran, 18
- J**
Jordan, 24, 247
- K**
Kurtosis, 85, 89, 90
Kuwait, 1–3, 5–7, 10, 12–43, 47–49, 59, 61, 63, 65, 67, 69, 71, 73, 75, 77, 79, 81, 83, 86, 87, 89, 91, 96–105, 108–119, 121–139, 141–146, 148–150, 152, 154, 155, 157–163, 165, 167, 168, 170, 171, 173, 177–184, 186, 187, 189, 190, 192, 194, 202–205, 207–244, 247, 248
- L**
Leguminosae, 177, 179, 180, 182, 184, 186, 187, 189–192, 194, 248
Libya, 247
- M**
Malvaceae, 177, 180, 182, 190–193
Mean, 2, 4–6, 10, 17, 57, 85, 86, 178, 247
Mesopotamian, 1, 14–19, 21–23, 25, 28, 29, 31–33, 43, 57, 126, 182, 202–204, 247
Mineral, 14–23, 25–33, 43, 47, 95–119, 122, 124, 202, 247
Morocco, 247
- N**
NASA, 6, 7

- O**
Organic matter, 15–33, 43, 199, 201, 203, 204, 247
- P**
Pakistan, 247
Palestine, 24, 247
Parameters, 2, 6, 48, 84–87, 89, 91, 146, 168, 180
Particle, 1, 6, 7, 9–13, 15–35, 43, 47–49, 57–59, 61, 63, 65, 67, 69, 71, 73, 75, 77, 79, 81, 83, 85–87, 95, 107, 121, 177–179, 199, 200, 202, 207, 213, 226–234, 246–248
Particulate, 1, 6, 7, 10
Particulate Matter (PM), 1, 5–13, 47
pH, 199, 200, 201, 204, 205
Pollen, 1, 2, 20, 27, 47, 177–195, 247, 248
- Q**
Quartz, 13–21, 25, 26, 28–35, 43, 58, 96, 97, 99, 101, 102, 104, 107, 112–114, 117–119, 202, 247
- R**
Radionuclide, 1, 141–146, 148–150, 152, 154, 155, 157–160, 162, 163, 165, 168, 170, 171, 173
Relative humidity, 3
Remote sensing, 1, 3, 6
- S**
Sahara, 14, 15, 24, 247
Satellite, 1, 5, 6, 11–14, 28, 41–43, 48, 247
Saudi, 1, 14, 47, 204, 208, 209, 211–243
Size, 1, 6, 7, 10–26, 29–34, 43, 47–49, 57–86, 95, 114, 115, 117, 121, 199, 202, 247, 248
Skewness, 85, 91, 92
Spectro, 207
Standard deviation, 85
Statistical, 2, 10, 58, 85–87, 89, 91
Sudan, 247
- T**
Taklimakan, 14, 15, 247
Temperature, 5, 6, 10, 178, 207
- W**
Warba, 3, 13, 14, 20, 29, 30, 40, 43, 48, 98, 102, 178, 180, 199, 202, 211, 236, 239, 247